

HIGH TEMPERATURE SUPERCONDUCTIVITY

Editor: Charles M. Rief

Stewart E. Bolger
Joseph Ashkenazi
Joseph E. Guen
Philip Zurek

19991122 110

AIP CONFERENCE PROCEEDINGS 483

REPORT DOCUMENTATION PAGE

Form Approved
OMB No. 0704-0188

Public reporting burden for this collection of information is estimated to average 1 hour per response, including the time for reviewing instructions, searching data sources, gathering and maintaining the data needed, and completing and reviewing the collection of information. Send comments regarding this burden estimate or any other aspect of this collection of information, including suggestions for reducing this burden to Washington Headquarters Service, Directorate for Information Operations and Reports, 1215 Jefferson Davis Highway, Suite 1204, Arlington, VA 22202-4302, and to the Office of Management and Budget, Paperwork Reduction Project (0704-0188) Washington, DC 20503.

PLEASE DO NOT RETURN YOUR FORM TO THE ABOVE ADDRESS.

1. REPORT DATE (DD-MM-YYYY) 15-11-1999		2. REPORT DATE FINAL		3. DATES COVERED (From - To) 7-1-1999 → 30-6-1999	
4. TITLE AND SUBTITLE HIGH-TEMPERATURE SUPERCONDUCTIVITY AIP CONFERENCE PROCEEDINGS, VOL. 483				5a. CONTRACT NUMBER	
				5b. GRANT NUMBER N00014-99-1-0272	
				5c. PROGRAM ELEMENT NUMBER	
6. AUTHOR(S) STEWART E. BARNES, JOSEPH ASHKENAZI, JOSHUA L. COHN, FULIN ZUO				5d. PROJECT NUMBER	
				5e. TASK NUMBER	
				5f. WORK UNIT NUMBER	
7. PERFORMING ORGANIZATION NAME(S) AND ADDRESS(ES) UNIVERSITY OF MIAMI DEPARTMENT OF PHYSICS P.O. Box 248046 CORAL GABLES, FL 33124-0530				8. PERFORMING ORGANIZATION REPORT NUMBER	
9. SPONSORING/MONITORING AGENCY NAME(S) AND ADDRESS(ES) OFFICE OF NAVAL RESEARCH PROGRAM OFFICER: JOHN PAZIK, ONR 331 BALLSTON CENTRE TOWER ONE 800 N. QUINCY ST. ARLINGTON, VA 22217-5660				10. SPONSOR/MONITOR'S ACRONYM(S) ONR	
				11. SPONSORING/MONITORING AGENCY REPORT NUMBER	
12. DISTRIBUTION AVAILABILITY STATEMENT APPROVED FOR PUBLIC RELEASE					
13. SUPPLEMENTARY NOTES					
14. ABSTRACT This volume contains the proceedings of the 1999 University of Miami Conference on High Temperature Superconductivity. In addition to addressing physical properties, microscopic theory and mechanisms for high-temperature superconductivity, included are related topics (e.g. ladders, manganites, nickelates). The reader will find in this volume a series of papers discussing the most important experimental and theoretical developments as of spring 1999. Despite more than ten years of intensive research on high-T _c materials, there remains considerable controversy both with respect to the interpretation of experiment and even more so in connection with the construction of an appropriate theory. In this regard, conferences such as this, gathering scientists with many viewpoints and varying specializations, and fostering constructive discussions, are important in the development of a common ground. Of major concern in the present context were the basic physical processes involved in high-temperature superconductivity. The conference was held at the James L. Knight Physics Building on the campus of the University of Miami, Coral Gables, January 7-13, 1999. More than 100 scientists from more than a dozen countries attended this workshop, most of whom presented either invited or contributed papers.					
15. SUBJECT TERMS HIGH-TEMPERATURE SUPERCONDUCTIVITY, MAGNETISM, OXIDES					
16. SECURITY CLASSIFICATION OF:			17. LIMITATION OF ABSTRACT	18. NUMBER OF PAGES	19a. NAME OF RESPONSIBLE PERSON
a. REPORT	b. ABSTRACT	c. THIS PAGE			JOSHUA L. COHN
U	U	U	UU	440	19b. TELEPHONE NUMBER (Include area code) 305 284-2325 X9

DISTRIBUTION STATEMENT A
Approved for Public Release
Distribution Unlimited

HIGH TEMPERATURE SUPERCONDUCTIVITY

Coral Gables, Florida January 1999

EDITORS

Stewart E. Barnes
Joseph Ashkenazi
Joshua L. Cohn
Fulin Zuo

University of Miami, Coral Gables

1999/122 110

AIP

American Institute of Physics

**AIP CONFERENCE
PROCEEDINGS 483**

Woodbury, New York

DTIC QUALITY INSPECTED 4

Editors:

Stewart E. Barnes

Joseph Ashkenazi

Joshua L. Cohn

Fulin Zuo

University of Miami

Department of Physics

Box 248046

Coral Gables, FL 33124

U.S.A.

E-mail: barnes@physics.miami.edu

ashkenazi@physics.miami.edu

cohn@physics.miami.edu

zuo@physics.miami.edu

This work relates to Department of Navy grant N00014-99-1-0272 issued by the Office of Naval Research. The United States Government has a royalty-free license throughout the world in all copyrightable material contained herein.

The articles on pp. 79–84, 336–340, and 359–365 were authored by U. S. Government employees and are not covered by the below mentioned copyright.

Authorization to photocopy items for internal or personal use, beyond the free copying permitted under the 1978 U.S. Copyright Law (see statement below), is granted by the American Institute of Physics for users registered with the Copyright Clearance Center (CCC) Transactional Reporting Service, provided that the base fee of \$15.00 per copy is paid directly to CCC, 222 Rosewood Drive, Danvers, MA 01923. For those organizations that have been granted a photocopy license by CCC, a separate system of payment has been arranged. The fee code for users of the Transactional Reporting Service is: 1-56396-880-0/99/\$15.00.

© 1999 American Institute of Physics

Individual readers of this volume and nonprofit libraries, acting for them, are permitted to make fair use of the material in it, such as copying an article for use in teaching or research. Permission is granted to quote from this volume in scientific work with the customary acknowledgment of the source. To reprint a figure, table, or other excerpt requires the consent of one of the original authors and notification to AIP. Reproduction or systematic or multiple reproduction of any material in this volume is permitted only under license from AIP. Address inquiries to Office of Rights and Permissions, 500 Sunnyside Boulevard, Woodbury, NY 11797-2999; phone: 516-576-2268; fax: 516-576-2499; e-mail: rights@aip.org.

L.C. Catalog Card No. 99-64710

ISBN 1-56396-880-0

ISSN 0094-243X

DOE CONF- 990129

Printed in the United States of America

CONTENTS

Preface	xi
Group Photo	xiii

THEORY HIGH T_c CUPRATES

RVB Revisited.....	3
P. W. Anderson	
Stripes, Carriers, and High T_c in the Cuprates.....	12
J. Ashkenazi	
A BCS—Bose-Einstein Crossover Theory and its Application to the Cuprates.....	22
Q. Chen, I. Kosztin, B. Jankó, and K. Levin	
Theory of Pairing in the Cu-O Plane: Three-Band Hubbard Model and Beyond	26
M. Cini, G. Stefanucci, and A. Balzarotti	
Resonant Neutron Scattering on the High T_c Cuprates and π and η Excitations of the t-J and Hubbard Models.....	30
E. Demler and S.-C. Zhang	
Local Electronic Structure and High Temperature Superconductivity	37
V. J. Emery and S. A. Kivelson	
Metallic Stripes in Doped Hubbard Model.....	45
M. Fleck, A. I. Lichtenstein, and A. M. Oleś	
Orbital Occupancy and Atom Charge States in $\text{R}\text{Ba}_2\text{Cu}_3\text{O}_x$ High Temperature Superconductors.....	49
V. E. Gusakov	
Quasi-Particle Spectrum around a Single Vortex in s-wave Superconductors.....	53
M. Kato and K. Maki	
Pseudogap Phenomena in the Superconducting Phase of the Cuprates.....	57
I. Kosztin, Q. Chen, B. Jankó, and K. Levin	
Forward Electron-Phonon Scattering and HTS.....	63
M. L. Kulić and O. V. Dolgov	
SO(6)-Generalized Pseudogap Model of the Cuprates	69
R. S. Markiewicz, C. Kusko, and M. T. Vaughn	
Stripe Disorder Transition.....	75
R. S. Markiewicz and M. T. Vaughn	
Suppression and Restoration of Superconductivity in $\text{Pr}\text{Ba}_2\text{Cu}_3\text{O}_7$ (A Mini-Review).....	79
I. I. Mazin	
Microscopic Theory for High T_c Superconductivity	85
I. Panas	
Influence of Ionic Dielectricity on the Dynamic Superconducting Order Parameter	90
M. Peter and M. Weger	

Filamentary Dopant Condensation in $\text{HgBa}_2\text{CuO}_{4+\delta}$	104
J. C. Phillips	
Thermodynamics of the van Hove BCS Model: Mixed Gap Symmetries	110
D. Quesada, R. Peña, and C. Trallero-Giner	
Role of the Long-Range Coulomb Interaction on the Formation of Striped Phases in the Two-dimensional Hubbard Model	114
G. Seibold, C. Castellani, C. Di Castro, and M. Grilli	
Spontaneous Ferroelectric State Induced by External Fields in a High T_c Superconductor	118
S. E. Shafranjuk	
The Fermion-Lochon Model and the Pseudogap in Cuprate Superconductors	122
K. P. Sinha	
Canonical BCS Approximation for the Attractive Hubbard Model	126
K. Tanaka and F. Marsiglio	
Theory of the Photoemission Spectral Function in High T_c Cuprates	130
T. Tohyama, S. Nagai, Y. Shibata, and S. Maekawa	
Surface Roughness, NIS Tunneling, and the Zero Bias Conductance Peak	136
M. B. Walker and P. Pairor	
On the Coexistence in $\text{RuSr}_2\text{GdCu}_2\text{O}_8$ of Superconductivity and Ferromagnetism	141
R. Weht, A. B. Shick, and W. E. Pickett	
Why T_c is too High When Antiferromagnetism is Underestimated?—An Understanding Based on the Phase-String Effect	147
Z. Y. Weng	
Magnetic Scattering; Pair-Breaking Effect and Anomalous Diamagnetism Above H_{c2} and T_c	153
S. Wolf, Yu. Ovchinnikov, and V. Kresin	

EXPERIMENT HIGH T_c CUPRATES

NMR Studies of the Original Magnetic Properties of the Cuprates:	
Effect of Impurities and Defects	161
H. Alloul, J. Bobroff, A. Mahajan, P. Mendels, and Y. Yoshinari	
Incommensurate Spin Dynamics of Superconductor $\text{YBa}_2\text{Cu}_3\text{O}_{6+x}$	172
M. Arai, T. Nishijima, Y. Endoh, S. Tajima, K. Tomimoto, Y. Shiohara, M. Takahashi, A. Garrett, and S. M. Bennington	
Decreasing Superconductivity Suppression of Pr in RE:123 Compounds by Isolating the Same from Cu-O Conduction Band	176
V. P. S. Awana, O. F. de Lima, S. K. Malik, W. B. Yelon, and A. V. Narlikar	
Lattice-Charge Stripes and Spectral Weight Near the Fermi Surface	180
A. Bianconi, N. L. Saini, and A. Lanzara	
High Temperature Superconductivity is Charge-Reservoir Superconductivity	187
H. A. Blackstead and J. D. Dow	

Superconductivity in $\text{Pr}_{2-z}\text{Ce}_z\text{Sr}_2\text{Cu}_2\text{NbO}_{10}$ and in $\text{Gd}_{2-z}\text{Ce}_z\text{Sr}_2\text{Cu}_2\text{RuO}_{10}$	191
H. A. Blackstead, J. D. Dow, I. Felner, D. D. Jackson, and D. B. Pulling	
Superconductivity in $\text{PrBa}_2\text{Cu}_3\text{O}_7$	195
H. A. Blackstead and J. D. Dow	
Investigations of the Vortex Matter in $\text{Bi}_2\text{Sr}_2\text{Ca}_1\text{Cu}_2\text{O}_{8+\delta}$ Single Crystals	201
T. Blasius, C. Niedermayer, J. Schiessling, U. Bolz, J. Eisenmenger, B.-U. Runge, P. Leiderer, J. L. Tallon, D. M. Pooke, A. Golnik, C. T. Lin, and C. Bernhard	
Spin Dynamics in High T_c Superconductors	207
P. Bourges, Y. Sidis, H. F. Fong, B. Keimer, L. P. Regnault, J. Bossy, A. S. Ivanov, D. L. Milius, and I. A. Aksay	
1/8 Doping Anomalies and Oxygen Vacancies in Underdoped Superconducting Cuprates	213
J. L. Cohn	
Low-Energy Electronic Structure in $\text{Y}_{1-x}\text{Ca}_x\text{Ba}_2\text{Cu}_3\text{O}_{7-\delta}$: Comparison of Time-Resolved Optical Spectroscopy, NMR, Neutron and Tunneling Data	219
J. Demsar, K. Zagar, V. V. Kabanov, and D. Mihailovic	
Study of Superfluid Condensation in the Cuprates by Andreev Reflections	225
G. Deutscher	
Low Temperature Anomaly of LO Phonons in $\text{La}_{1.85}\text{Sr}_{0.15}\text{CuO}_4$ and $\text{YBa}_2\text{Cu}_3\text{O}_7$	231
T. Egami, R. J. McQueeney, Y. Petrov, M. Yethiraj, G. Shirane, and Y. Endoh	
Direct and Continuous Measurements of the Irreversibility Line of High T_c Superconductors Using an Automatic PID Controller	237
L. E. Flores, C. Noda, C. Abascal, E. Altshuler, and J. L. Gonzales	
Where Do the Doped Holes Go in $\text{La}_{2-x}\text{Sr}_x\text{CuO}_4$? A Close Look by XAFS	241
D. Haskel, V. Polinger, and E. A. Stern	
C-Axis Penetration Depth in Single Crystal $\text{La}_{2-x}\text{Sr}_x\text{CuO}_4$	247
J. R. Kirtley, K. A. Moler, M. Nohara, and H. Takagi	
Pinning Strength of Cuprate Superconductors and Pseudo-Gap in the Normal State	253
K. Kitazawa, J. Shimoyama, T. Hanaguri, T. Sasagawa, and K. Kishio	
C-Axis Twist $\text{Bi}_2\text{Sr}_2\text{CaCu}_2\text{O}_{8+\delta}$ Josephson Junctions: A New Phase-Sensitive Test of Order Parameter Symmetry	259
R. A. Klemm, C. T. Rieck, and K. Scharnberg	
High Pressure X-ray Diffraction Studies of Rare Earth Doped Bi 2212 System	265
R. S. Kumar, A. Sekar, N. V. Jaya, and S. Natarajan	
Violation of the Ambegaokar-Baratoff Relation in the c-Axis Transport in Bi-2212 High Quality Stacks	268
Y. I. Latyshev and T. Yamashita	

Superconductivity-induced Effect on c-Axis Electronic Raman Scattering in $\text{Bi}_2\text{Sr}_2\text{CaCu}_2\text{O}_{8+\delta}$ Single Crystals	272
H. L. Liu, G. Blumberg, M. V. Klein, P. Guptasarma, and D. G. Hinks	
Evidence for Strong Electron-Lattice Coupling in $\text{La}_{2-x}\text{Sr}_x\text{NiO}_4$	278
R. J. McQueeney and J. S. Sarrao	
Photoinduced Infrared Absorption in $(\text{La}_{1-x}\text{Sr}_x\text{Mn})_{1-\delta}\text{O}_3$: Observation of Anti-Jahn-Teller Polarons	284
T. Mertelj, D. Kušcer, and D. Mihailovic	
Fermi Surface Geometry and the Ultrasonic Attenuation of a Clean d-wave Superconductor	288
E. J. Nicol, I. Vekhter, and J. P. Carbotte	
Hole Doping Dependence of the Antiferromagnetic Correlations in $\text{La}_{2-x}\text{Sr}_x\text{CuO}_4$ and $\text{Y}_{1-x}\text{Ca}_x\text{Ba}_2\text{Cu}_3\text{O}_6$	292
C. Niedermayer, T. Blasius, C. Bernhard, A. Golnik, A. Moodenbaugh, and J. I. Budnick	
Fermi Surfaces, Fermi Patches, and Fermi Arcs in High T_c Superconductors	298
M. R. Norman	
Doping Dependence of Electronic Structure in $\text{Bi}_2\text{Sr}_2\text{CaCu}_2\text{O}_{8+x}$	304
M. Onellion, S. Christensen, B. Frazer, R. Gatt, R. J. Kelley, S. Misra, T. Schmauder, H. Berger, M. Grioni, G. Margaritondo, I. Vobornik, F. Zwick, M. Möble, R. Kleiner, and P. Müller	
The Specific Heat of $\text{La}_{1.85}\text{Sr}_{0.15}\text{CuO}_4$: Evidence for d-Wave Pairing	310
N. E. Phillips, R. A. Fisher, A. Schilling, B. Buffeteau, T. E. Hargreaves, C. Marcenat, R. Calemczuk, A. S. O'Connor, K. W. Dennis, and R. W. McCallum	
Pressure Dependence of Flux Dynamics in High Temperature Superconductors	314
M. P. Raphael, M. E. Reeves, E. F. Skelton, and C. Kendziora	
Phase Separation in Overdoped $\text{Y}_{1-0.8}\text{Ca}_{0-0.2}\text{Ba}_2\text{Cu}_3\text{O}_{6.96-6.98}$	320
J. Röhler, C. Friedrich, T. Granzow, E. Kaldis, and G. Böttger	
Vortex Motion in YBCO Thin Films	324
V. Shapiro, A. Verdyan, I. Lapsker, and J. Azoulay	
Electronic Raman Scattering in High T_c Superconductors	328
T. Strohm, M. Cardona, and A. A. Martin	
Experimental Evidence for Topological Doping in the Cuprates	336
J. M. Tranquada	
Quasiparticle Properties of d-Wave Superconductors in the Vortex State	341
I. Vekhter, J. P. Carbotte, P. J. Hirschfeld, and E. J. Nicol	
Observations of YBCO Superconductor Under Low-Temperature Scanning Electron Microscope	347
A. Vyas, C. C. Lam, P. C. W. Fung, S. H. Li, and H. S. Lam	
Quasiparticle Tunneling and Andreev Reflection Study of the Pairing Symmetry in $\text{YBa}_2\text{Cu}_3\text{O}_{7-\delta}$	351
J. Y. T. Wei, N.-C. Yeh, D. F. Garrigus, M. Strasik, and R. P. Vasquez	

RELATED COMPOUNDS THEORY

Possibility of High Temperature Superconductivity in C_{36} and $C_{24}N_{12}$ Solids	359
M. L. Cohen	
Electronic Characteristics of Quasi-2D Metallochlonitrides:	
Na_xHfNCl ($T_c=25$ K)	366
R. Weht, A. Filippetti, and W. E. Pickett	
p-Wave Superconductivity in Sr_2RuO_4	372
H. Won, K. Maki, E. Puchkaryov, and G. F. Wang	

RELATED COMPOUNDS EXPERIMENT

X-Ray Scattering Studies of Charge Stripes in Manganites and Nickelates	383
C.-H. Du, Y. Su, P. D. Hatton, S. Brown, and S-W. Cheong	
Electron-Lattice Interactions in Nickel-Oxide Perovskites	388
J. B. Goodenough, J.-S. Zhou, and B. Dabrowski	
Electronic Raman Scattering in the Perovskite Manganese Oxides	394
H. L. Liu, S. Yoon, S. L. Cooper, S.-W. Cheong, and P. D. Han	
Local Lattice Effects in Oxides	400
D. Louca and G. H. Kwei	
Measurement of the Spin-Polarization of $LaSrMnO$	407
M. S. Osofsky, B. Nadgorny, R. J. Soulen, Jr., P. Broussard, M. Rubinstein, J. Byers, G. Laprade, Y. M. Mukovskii, D. Shulyatev, and A. Arsenov	
Anomalous Linear Resistivity from ~ 1 to 10^3 K in $Sr_2RuO_{4-\delta}$	412
D. Pavuna, L. Forró, and H. Berger	
Charge, Spin, and Lattice Excitations in Double-layer Manganites	418
D. B. Romero, Y. Moritomo, J. F. Mitchell, and H. D. Drew	
Universal Behavior of Magnetization Curves in Rb_3C_{60} Fullerene	424
M.-F. Tai, J.-B. Shi, and C.-J. Wu	
Interlayer Magnetoresistance Peak in the ET-based Organic Superconductors	429
F. Zuo	
Author Index	437

PREFACE

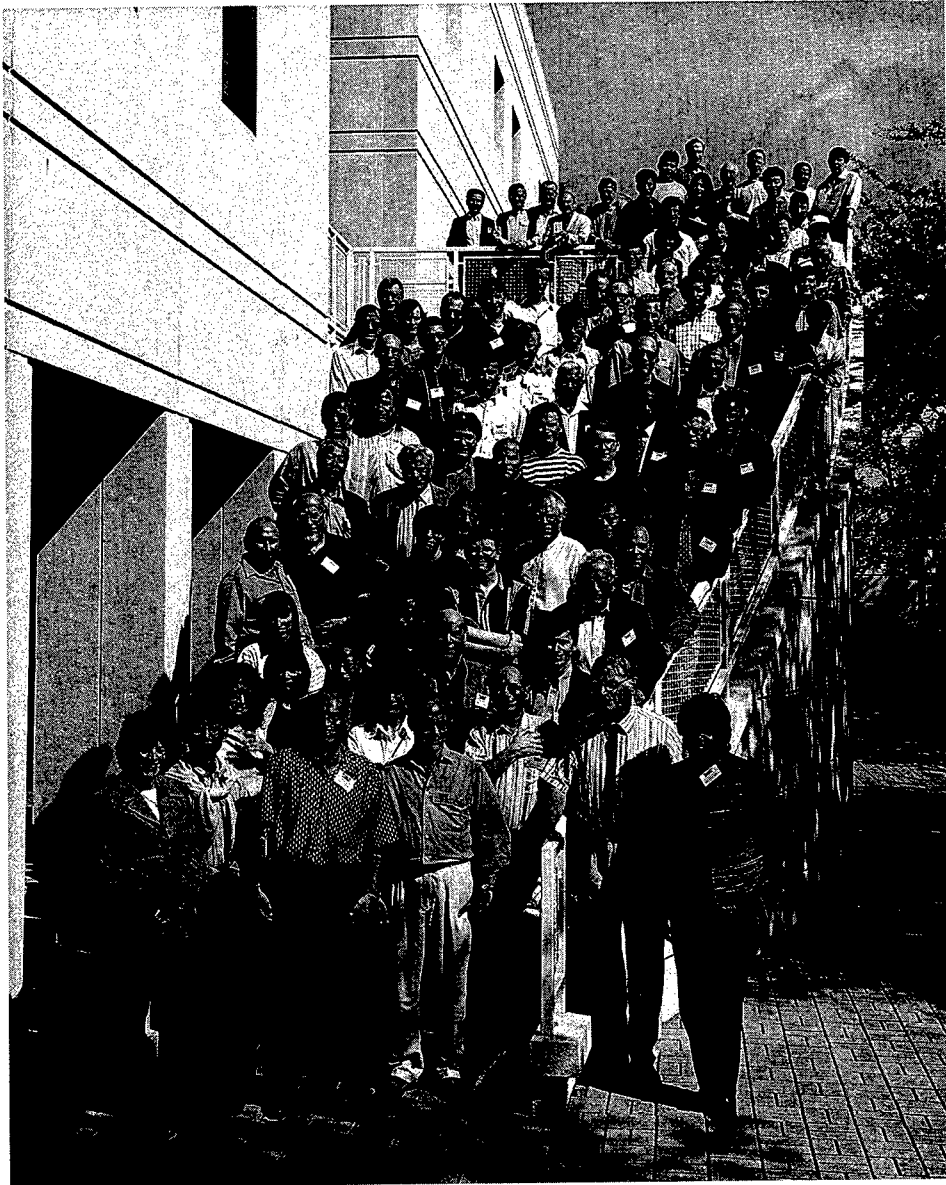
This volume contains the proceedings of the 1999 University of Miami Conference on High Temperature Superconductivity. This conference followed two similar successful conferences on High Temperature Superconductivity in January, 1991 and 1995. In addition to addressing physical properties, microscopic theory and mechanisms for high-temperature superconductivity, included are related topics (e.g. ladders, manganites, nickelates). The general goal of the conference was to provide a forum for engaging researchers in a focused dialog directed at exploring and distilling the latest experimental and theoretical results in the field likely to have a significant influence on the understanding of the normal-state properties and origin of superconductivity in this class of materials.

The conference was held at the James L. Knight Physics Building on the campus of the University of Miami, Coral Gables, January 7-13, 1999. More than 100 scientists from more than a dozen countries attended this workshop, most of whom presented either invited or contributed papers.

The reader will find in this volume a series of papers discussing the most important experimental and theoretical developments as of spring 1999. Despite more than ten years of intensive research on high- T_c materials, there remains considerable controversy both with respect to the interpretation of experiment and even more so in connection with the construction of an appropriate theory. In this regard, conferences such as this, gathering scientists with many viewpoints and varying specializations, and fostering constructive discussions, are important in the development of a common ground. Of major concern in the present context were the basic physical processes involved in high-temperature superconductivity.

The conference organizing committee, J. Ashkenazi, S. E. Barnes, J. L. Cohn, and F. Zuo, wishes to thank all of the participants for their contributions to what was an animated, enjoyable, and very informative experience. They wish to extend their thanks to the International Advisory Committee: O. K. Andersen, B. Batlogg, A. Bianconi, J. Bok, J. P. Carbotte, M. Cardona, G. Deutscher, V. L. Ginzburg, J. B. Goodenough, A. Kapitulnik, J. Kirtley, K. Kitazawa, M. V. Klein, M. Lagues, D. Pavuna, W. E. Pickett, C.N.R. Rao, G. A. Sawatzky, J. R. Schrieffer, Z.-X. Shen, J. L. Tallon, J. Tranquada, Y. Tokura, E. Zeldov, S.-C. Zhang, Z. Zhao for their suggestions which were instrumental in determining the conference program. The organizers are indebted to the University of Miami and its Physics Department faculty and staff and, in particular, DARPA through ONR Grant N00014-99-1-0272, for their financial support. We gratefully acknowledge Ms. Rosa Epstein, Carletta Hatcher Johnston, Judy Mallory and Lourdes Castro for their organization of accommodations and excursions, and for providing secretarial and other technical assistance.

The Editors



THEORY HIGH T_c CUPRATES

RVB Revisited

Philip W. Anderson

Joseph Henry Laboratories of Physics Princeton University, Princeton, NJ 08544

Abstract. We propose that early speculations on the nature of the normal state of the CuO_2 planes in high T_c superconductors can be revised and brought into agreement with more modern theories, simulations and experimental observations.

The early speculations proposed an "RVB" state which is an incompressible liquid of singlet pairs in which the magnetic excitations are spin 1/2 fermion-like objects called spinons, the charge exhibiting a separate dynamics (charge-spin separation.) The revisions proposed are the following:

- (1) At finite concentrations x of holes there are two non-Fermi liquid, charge-spin separated states, (I) a metal with a full Fermi surface (the "Luttinger Liquid") and no spin gap, and below a crossover, (II) a spin-gapped RVB state of "d" symmetry with spinons at gap nodes ("nodons").
- (2) Since spinons have no phase—no charge—the gap parameter in the second phase must be real, $d_{x^2-y^2}$, as proposed by Affleck and Kotliar.
- (3) Both are based on a large Fermi surface satisfying Luttinger's theorem.
- (4) Phase I is a good metal in the ab direction, phase II is a poor metal. There appear to be two types of transition into the superconducting state, depending on whether it takes place from phase I or II. Whether there are two mechanisms causing superconductivity remains unclear as also is the relationship between the two.

In the first months after the discovery of high T_c superconductivity the close connection of this phenomenon with the one-band Hubbard model in two dimensions was realized [1,2]. An old speculation called "resonating valence bonds", about a possible non-symmetry-breaking solution of the antiferromagnetic Heisenberg model in two dimensions (to which the Hubbard model reduces at half filling), was revived [1], and used to motivate a scenario for explaining the high T_c phenomenon.

Zou and Baskaran, along with others [3], showed that the RVB state naturally led to the idea of charge-spin separation and to the concept of the "spinon", a spin 1/2 object which can be thought of as half of a spin wave or half of an electron (the idea of Fermionic spin 1/2 excitations of an antiferromagnet dates back in fact to Landau.) The one-dimensional Hubbard model has non-classical soliton-like

excitations carrying a spin of $1/2$, and it was thought that they could appear in 2D also. The “RVB” state is a ground (“vacuum”) state made up of singlet pairs of electrons, and the spinon soliton is thought of as a single spin moving freely through the background gas of singlets, displacing the singlet correlations but not the charge. In 1D it can also be thought of as a π phase singularity in a spin density wave. The RVB state is an incompressible spin liquid, in the sense that the one-electron compressibility (the density of states) vanishes, $\frac{\partial \Sigma}{\partial k}$ and $\frac{\partial \Sigma}{\partial \omega}$ both diverge, and v_F and hence the true compressibility remains finite but $Z \equiv 0$.

The most accurate characterization of the spinon has come from studies of exactly soluble one-dimensional models, the Lieb-Wu solution of the Hubbard model and the Haldane-Shastry solution of the $1/r^2$ model, as well as from tomographic bosonization of the 2D interacting electron gas. The spinon can be defined in terms of non-Abelian bosonization of the spin fluctuations of a Fermi sea at any interaction and for any density, and is necessarily a semion in Haldane’s sense rather than an anyon or a true Fermion. For any case where renormalized perturbation theory (Fermi Liquid Theory) remains valid, its velocity is degenerate with that of the charge fluctuations and it is merely half of a quasiparticle. It is also useful to think of it as moving on a “squeezed” Heisenberg model from which the holes have been removed; at the Fermi surface particles move non-diffractively and the spin degrees of freedom are like those in the 1D model because removing holes does not alter the spin ordering.

While the spinon, at least in 2D, is rigorous only as a Fermi surface excitation, visualization in terms of the RVB type of state as a Gutzwiller-projected electron, as in Ref. 2, is a useful guide to our thinking. Of course, a similar caveat about the Fermi surface exists for the quasi-particle concept, for that matter.

It soon became clear that the RVB idea in its original form was not sophisticated enough to account for high T_c . While other authors, most notably Lee and co-workers [4], continued with modified versions of the original scheme, a number of authors beginning with R.B. Laughlin [5] and including Wilczek [6] and others have emphasized the “flux phase” version of RVB and its relation to anyon theory, while I have retained the idea of spinons and spin-charge separation, but focussed on the non-Fermi Liquid metallic state [7], and on the effect of spin-charge separation in modifying transport processes, and neglected the “pairing” aspect of the theory. In fact, I postulated that the single 2D plane was not superconducting by itself [7]

It was in connection with RVB theory that the idea of a d-wave order parameter first arose, in work of Affleck and of Kotliar, [8] since in a simple square lattice Heisenberg model “d wave” is a natural solution of the mean field equations using nearest-neighbor antiferromagnetic exchange

$$\sum_{(ij)=nn} J_{ij} S_i \cdot S_j \quad (1)$$

as a 4-spinon interaction, where

$$\vec{S}_i = \sum_{\sigma\sigma'} s_{\sigma}^+ \vec{S}_{\sigma\sigma'} s_{\sigma'}. \quad (2)$$

The s 's are spinon operators, which we shall define later.

The basic derivation of (1) was put forward by Rice, adapted from my own derivation of "superexchange" in Mott insulators. A modern version to which we will later refer was given by Zou. In the presence of a strong repulsive interaction "U", the amplitude of doubly occupied states is renormalized to zero by a projective canonical transformation which is perturbative in t/U , where t is the hopping kinetic energy. This projective transformation cannot be continued smoothly to a perturbation theory in positive powers of the interaction U because it is projective. Thus when an antiferromagnetic "J" is postulated, Fermi liquid theory has per se been abandoned. The signal for this is that the kinetic energy term "T" in the $t-J$ Hamiltonian is projected onto a subspace with zero double occupancy, so that the fluctuations are algebraically distinct from conventional quasiparticles.

We observe that the spin fluctuations can be expressed in terms of spinons, and that the exchange interaction affects only the spinons directly, since the two sites " i " and " j " must both be occupied in order for the superexchange effect to act. In most theories of the cuprates, conventional exchange (which is always ferromagnetic) is neglected. Thus we follow custom in assuming that the true interaction is $S_i \cdot S_j - \frac{n_i n_j}{4}$ and no interaction affects parallel spins, in our first crude survey of the problem.

The original RVB hypothesis was that a good variational ground state of (1) could be attained by the Ansatz

$$\psi_0 = P_G^A \psi_{MF} \quad (3)$$

where P_G^A is the $n = 1$ projector

$$P_G^A = \prod_i (n_{i\uparrow} + n_{i\downarrow} - 2n_{i\uparrow} n_{i\downarrow}) \quad (4)$$

and ψ_{MF} is a mean field BCS or Hartree-Fock solution of the problem of N electrons on N sites. My original hypothesis was a BCS solution with a symmetrical energy gap going to zero at a Fermi surface, with kinetic energy,

$$\Delta_k = \gamma_k = J(\cos k_x + \cos k_y) \quad (5)$$

which is called an "extended s " solution, and is equivalent, as I showed (following Rice) to a half-filled tight-binding band of noninteracting electrons, projected on $n_i = 1$.

Affleck soon pointed out that an equivalent solution was the ' d -wave' with

$$\Delta_k^d = J(\cos k_x - \cos k_y) \quad (6)$$

and shortly thereafter Kotliar, as well as Zhang et al, suggested " $s + id$ " where

$$\Delta_k = \gamma_k + i\Delta_k^d \quad (7)$$

which is variationally better and has nodes of the one-spinon energy rather than a Fermi surface. This in turn was equivalent, essentially, to another choice, the so-called “flux phase”, in which the Hartree-Fock solution is for electrons with kinetic energy $\epsilon_k = \gamma_k$ and a flux of $\Phi_{0/2} = “\pi”$ natural units through each plaquette of the lattice.

All of these “RVB” solutions of the Heisenberg Hamiltonian (1) could be variationally improved and their energies compared, but all turned out to be slightly inferior to the Néel state with antiferromagnetic long range order, which also turned out to be the actual physical state of the cuprate CuO_2 planes when doped to Cu^{++} , where (1) is an appropriate Hamiltonian. Hsu showed that one could consider the Néel state as a somewhat weak symmetry-breaking perturbation of the flux phase, and understand its experimental high-energy spectrum in terms of flux phase spinons, but otherwise the “flux phase” has receded somewhat into the background as a result of the fact that it seems not to be easily generalized to the doped 2D case with mobile holes, which is thought to be a good model for the superconducting cuprates. The most straightforward such attempt is to change the flux from π , giving a state which is not time-reversal invariant, contrary to all experimental tests.

As a result of this failure, the flux phase solution has tended to be ignored, even though it has the nodal structure which is so conspicuous in the observations, and which shows up fairly clearly in numerical calculations on the 2D Hubbard model [9]. A purpose of the present paper is to suggest that the correct generalization of the “ $s + id$ ” or flux phase does not involve time-reversal and that the apparent dependence upon the introduction of “i” or a π flux is illusory. This was indicated very early by constructing actual real space wave functions for the flux phase, which turned out to be entirely real.

In the early work spinons were treated as full-fledged Fermions. In order to satisfy the projective constraints it was necessary to introduce an $SU(2)$ gauge field. With fuller understanding of the process of non-Abelian bosonization from which they arise, and of exact one-dimensional models where they are elementary excitations, it can be demonstrated that spinons can be described as semions, and that their algebraic character and statistics do not change all the way from the noninteracting electron case to the Mott insulator. The spinon propagator remains asymptotically $(x - v_s t)^{-1/2}$, and spinon amplitudes are $SO(2)$ matrices with real determinant. Thus in a Hartree-Fock factorization of the exchange term (1) it is not consistent to allow complex self-energies for spinons to arise. The self-energy can contain an anomalous (pairing) term, but this term cannot be complex: the self-energy is a real, orthogonal matrix, not a Hermitian one.

$$\tilde{\Sigma} = \begin{pmatrix} \Sigma & \Delta \\ \Delta & \Sigma \end{pmatrix} \quad (8)$$

where Δ like Σ , is real. [Another way of seeing this is that the two possible zero-momentum, zero-spin pairings of spinons are $\langle s_{k\sigma}^+ s_{k\sigma} \rangle$ and $\langle s_{k\sigma}^+ s_{-k-\sigma}^+ \rangle$, but

$s_{k\sigma}$ and $s_{-k-\sigma}^+$ are equivalent under a $U(1)$ gauge group of Abelian rotations, which allows only one extra degree of freedom.]

Thus the spinons can have a conventional self-energy (γ_k) and a single real anomalous one Δ_k^d , but not a third, since no such degree of freedom exists. The existence of an anomalous self-energy generated from the exchange term does not, therefore, in any sense imply superconductivity, since a spinon gap has no phase.

We can, thus, envisage two types of RVB, non-superconducting states: one in which the spinons form a Fermi surface, with $\Delta = 0$; and one in which the spinons would have nodal points with Dirac-like excitations about the nodes. The latter would form below some critical temperature of the order of J given by a BCS-like equation. Neither is stable at low T because the umklapp terms force a magnetic order on the half-filled case; but they do have a definable order parameter in the sense that the Fermi surface, or Dirac points, are an order parameter [10].

Now let us move away from the half-filled case and dope the system. Let us assume that spin-charge separation remains valid—for example, we can use the Zou transformation, suitably modified to work with spinon semions and not Fermions, and from it derive a superexchange interaction via the $t - J$ transformation. It is important to realize that the exchange interaction involves only spinons, so that any energy derived from it still does not directly effect superconductivity; it causes an energy gap, for spin excitations, which is intrinsically real. (For a practical illustration of this possibility, see the analysis in my interlayer theory of the spin gap, which is applicable in modified form here.) [11]

We shall make an arbitrary but reasonable (and I suspect provable) assumption about charge-spin separation using spinons. This is that as the system is doped away from half-filling, the Fermi surface for spinons as defined by the self-energy Σ_k continues to enclose a number of momentum states equal to twice the number of particles. There are several ways to justify this. First, the number of spin degrees of freedom = the number of spinons = twice the number of particles, and independent spinons comprise the interior of the Fermi surface only. Second, when eventually the charge attaches itself to the spinons and makes quasiparticle degrees of freedom, it will be the spinons, with their fixed statistics, which determine the Fermi surface; charge degrees of freedom in the Luttinger liquid as in anyon theory or the dual theories of Fisher et al have no fixed statistics.

In the Zou derivation of the $t - J$ Hamiltonian, or in fact in any reasonable treatment of the kinetic energy term

$$T = P_G \sum_{k,\sigma} \epsilon_k n_{k\sigma} P_G \quad (9)$$

the $n_{k\sigma}$ may be factorized into a product of bilinear operators in charge and spin variables; in Zou and Baskaran's approach as quoted in (1), (after projecting out double occupancy):

$$\mathcal{H} = t \sum_{\langle ij \rangle} e_i^+ e_j s_{i\sigma}^+ s_{j\sigma} + J \sum_{\langle ij \rangle} (s_{i\uparrow}^+ s_{j\downarrow} - s_{i\downarrow}^+ s_{j\uparrow}) \times (cc) \quad (10)$$

Cuprates: Science beyond High T_c

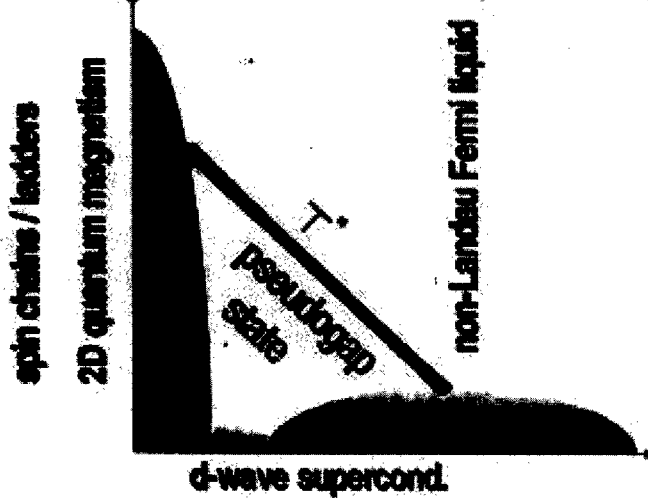


FIGURE 1. Phase Diagram

As we learn in the tomographic bosonization approach, e , the “holon” operator, is not an elementary excitation with any conventional statistics, in the same way that s_{σ} is, and its dynamics need to be further analyzed. Nonetheless $t < e_i^+ e_j >$ must be proportional to the mean kinetic energy of hole motion, proportional roughly to x , the number of holes. This will provide an addition to the diagonal self-energy which at half-filling is solely due to exchange.

The charge-correlation sum rule controlling the magnitude of the “Drude” peak is empirically, in the cuprates, and theoretically, in 1D, roughly linearly proportional to x ; we believe the same is to be expected for this term in the spinon kinetic energy. Thus the spinon’s velocity, i.e., the inverse of the density of states, given by the diagonalized self-energy, will grow proportionally to $J + \text{const} \times tx$, while J itself will become smaller as x increases, because the fraction of nearest neighbor sites which are both occupied decreases as $(1 - x)^2$.

We can schematize these conclusions in a phase diagram of temperature vs doping percentage x (Fig 1). [12] The lines are not true phase boundaries but crossovers, since because of local gauge degrees of freedom actual broken symmetry can only occur at absolute zero. We place the hypothesized transition for $x = 0$ at $\sim J$, leaving out of account the ordered antiferromagnetic state, and recognize that here the “extended s ” and “d-wave” gaps will appear together. But as the spinon velocity rises proportionally to x , we will have an increasing regime where the spinon Fermi surface is established while at a lower temperature will appear the

d -wave gap Δ_k^d . This lower temperature scale will be

$$T^* = J_{\text{eff}}(x) e^{-\frac{t_{\text{eff}}(x)}{J_{\text{eff}}(x)}} \quad (11)$$

where $J_{\text{eff}}(x)$ will decrease as $(1-x)^2$ and $t_{\text{eff}}(x)$ will increase with x . This is presumably the energy scale " T^* " seen in ARPES and other measurements in the underdoped regime. The resulting smearing and gapping of the Fermi surface is observed in the computations of Puttিকা et al [9] using series extrapolations.

Thus we have a basic phase diagram for the two-dimensional Hubbard model which is divided into two regions, both of which are charge-separated non-Fermi liquids. (For the two-dimensional case, I have shown that the true Fermi liquid without separate spinons occurs only for zero coupling or density.) In the cuprates, as charge-spin separation becomes weaker we will begin to get coherent interlayer coupling and a true Fermi liquid will set in somewhere in the overdoped region.

In the Fig (1) phase diagram, the NFL (Luttinger liquid) regime extends over an increasingly wide region as x increases.

Fig (1) is the phase diagram of the isolated plane. What I do not presume to speculate on is whether or not this actually contains a region of true superconductivity. The arguments of Lee Nagaosa and Wen at least make it plausible that this may be the case. If so, the region where superconductivity may appear is the crosshatched area of Fig. (1). As observed both by Nagaosa and Lee, and by the "nodon" arguments of Nayak et al, T_c for the superconductors is very seriously limited by the low stiffness (high mass) which is implied for gap fluctuations in the small- x regime, by straightforward sum rule arguments. Nonetheless, it appears that superconductivity may be possible in the isolated CuO_2 plane, without interlayer enhancement; several compounds seem to support this possibility experimentally—highly doped BISCO "2201", and TI 2201; in particular. (Not NdCCO , which is apparently an s -wave superconductor.)

Optimally doped compounds, however, seem in general to develop directly from the NFL region without an intervening d -wave RVB phase (i.e., an intervening pseudogap). However, invariably—for the truly high T_c cases—the superconductivity occurs in the d -wave state favored by RVB arguments. Also, in the superconducting state, as opposed to the spin gap state, the nodes experimentally are mathematically sharp, in contradiction to the expectations of theories relying exclusively on interlayer tunneling as expressed, for instance, in Ref. (7). This fact seems to require that some component of the attractive interaction have d -wave symmetry, i.e., that it be of long range in k -space. Our working concept that the intralayer interaction only involves spinons would be sufficient, if at the optimum this intralayer interaction is above or near its natural T_c^* . But as yet it seems not clear what the admixture of interactions responsible for the higher T_c may be.

It is, however, possible to make the following statement: attractive interactions between opposite-spin electrons such as are necessary to cause a singlet superconductor are invariably the result of frustrated kinetic energy; and if the mechanism is to be purely electronic (as it surely is in the cuprates) it must be frustrated

electronic kinetic energy. In a true Landau (quasiparticle) Fermi liquid, the Fermi surface is by definition determined in such a way as to minimize the electronic kinetic energy as renormalized by interactions: there is no frustrated kinetic energy. Thus there can be no attractive interactions for opposite spins. Superexchange as in the $t - J$ model, as well as interlayer tunneling interactions, requires frustration: the elementary excitations must not be true quasiparticles, but projected entities of different algebraic and possibly topological character. We may make a small table of possible attractive interactions:

	Intralayer	Interlayer
Exchange	Superexchange	IL Superexchange (Millis-Monien)
Josephson	Pair Hopping ?? (charge stiffness)	IL Pair Hopping (PWA-Hsu-Wheatley)

Note that pair hopping within the plane (coherent charge motion) is not frustrated in the NFL state, only in the RVB state: hence we can apparently get superconductivity in one layer if we go first into the RVB state. But any 2D NFL frustrates interlayer hopping, hence the IL mechanisms work from the NFL state.

One final remark needs to be made. The antiferromagnetic insulator gains extra energy from umklapp processes, hence is a downward cusp in energy *vs* x at $x = 0$. (As can be seen by the indeterminacy of $\mu = (\frac{dE}{dx})^{-1}$). The metallic state has screening of the long-range Coulomb interaction, which means that low density x has negative curvature $\frac{\partial^2 F}{\partial x^2} < 0$. Hence small x is not a stable homogeneous thermodynamic state. On some, presumably microscopic but occasionally macroscopic, scale it will phase separate. Yoshimori's XPS measurements clearly illustrate that this is happening in $(\text{LaSr})_2 \text{CuO}_4$. This phase separation which causes "stripes" is however clearly over by the optimally doped concentration in every case. Hence it is an interesting phenomenon, but somewhat irrelevant to our major concerns. It seems likely to inhibit superconductivity by trapping the charge fluctuations, except insofar as one obtains quasimacroscopic superconducting droplets of near optimal concentration.

It is not possible for me to acknowledge all the colleagues with whom I have had useful discussions during the past 12 years. A list must include M. Norman, S. Chakravarty, G. Baskaran, S. Strong, S. Kivelson, A. Adbo, W. Puttika, R. Laughlin, T. Hsu, T. M. Rice, N.-P. Ong, but also many others. I also most acknowledge the Aspen Center for Physics.

REFERENCES

1. P. W. Anderson, *Science*, **235**, 1196 (1987)
2. P. W. Anderson. Proceedings of the Enrico Fermi International School of Physics, Varenna, Italy, July 1987, *Frontiers and Borderlines in Many Particle Physics*, (North-Holland, Amsterdam 1987)
3. G. Baskaran, Z. Zou, P. W. Anderson, *Sol. St. Comm.* **63**, 973 (1987)
4. X.-G. Wen and P. A. Lee, *Phys. Rev. Lett.*, **76**, 503 (1996); N. Nagaosa and P.A. Lee, *Phys. Rev. Lett.*, **79**, 3577 (1997); P. A. Lee, and X.-G. Wen, *Phys. Rev. Lett.*, **80**, 2193 (1998)
5. V. Kalmeyer and R. B. Laughlin, *Phys. Rev. Lett.*, **59**, 2095 (1987); I. Affleck and J. B. Marston, *Phys. Rev.* **37**, 3664 (1988)
6. F. Wilczek, *Phys. Rev.*, **B 39**, 11413 (1989)
7. P. W. Anderson, *The Theory of Superconductivity in the High T_c Cuprates* Princeton University Press, Princeton (1997)
8. I. Affleck, Z. Zou, T. Hsu and P. W. Anderson, *Phys. Rev.* **B38**, 745 (1988); G. Kotliar, *Phys. Rev.* **B37**, 3664 (1998); see also F. C. Zhang, C. Gros, T. M. Rice and H. Shiba, *Supercond. Sci., Tech.*, **1**, 36 (1988). For a good review of much of the material, see T. M. Rice, in *Strongly-Interacting Fermions and High- T_c Superconductivity*, (Les Houches Summer School 1991), B. Doucot and J. Zinn-Justin, eds., p. 19, Elsevier, Amsterdam, 1995.
9. W. O. Puttika, M. U. Luchini, R. Singh, *Phys. Rev. Lett.*, **81**, 2966 (1998); D. Scalapino and S. White, *Phys. Rev. Lett.*, **80**, 1271; *Phys. Rev. Lett.*, **81**, 3222 (1998)
10. F. D .M. Haldane, "Luttinger's Theorem and Bosonization of the Fermi Surface", in *Perspectives in Many-Particle Physics*, eds. R. Broglia and J. R. Schrieffer. (North Holland, Amsterdam 1994, pp. 5-30)
11. P. W. Anderson, in SNS 1997, A. Bansil, Y. Fujii, R.N. Shelton etc., *J. Phys. Chem. Solids*, **59**, 1675 (1998)
12. A Phase Diagram like Fig. 1 is implicit in Refs. 1-2 but is clearly set out in V. J. Emery and S. Kivelson, *Nature* **374** 434 (1995)

Stripes, Carriers, and High- T_c in the Cuprates

Josef Ashkenazi

Physics Department, University of Miami, P.O. Box 248046, Coral Gables, FL 33124, U.S.A.

Abstract. Considering both “large- U ” and “small- U ” orbitals it is found that the high- T_c cuprates are characterized by a striped structure, and three types of carriers: polaron-like “stripions” carrying charge, “quasielectrons” carrying charge and spin, and “svivons” carrying spin and lattice distortion. It is shown that this electronic structure leads to the anomalous physical properties of the cuprates, and specifically the systematic behavior of the resistivity, Hall constant, and thermoelectric power. High- T_c pairing results from transitions between pair states of quasielectrons and stripions through the exchange of svivons. A pseudogap phase occurs when pairing takes place above the temperature where stripions become coherent, and this temperature determines the Uemura limit.

INTRODUCTION

The existence of static stripes in the CuO_2 planes has been observed in some superconducting cuprates [1,2], and there is growing evidence on the existence of dynamic stripes in others [3]. Many experimental observations have been pointing to the presence of both itinerant and almost localized (or polaron-like) carriers in these materials.

Though one-band theoretical models have been quite popular, and easier to treat, first-principles calculations [4] indicate that such models are probably oversimplified. Here an approach is proposed to the cuprates, taking into account the existence of both “large- U ” and “small- U ” orbitals in the vicinity of the Fermi level (E_F).

AUXILIARY PARTICLES

The large- U orbitals are treated using the “slave-fermion” method [5]. An electron of these orbitals at site i and of spin σ is then created by $d_{i\sigma}^\dagger = e_i^\dagger s_{i,-\sigma}$, if it is in the “upper-Hubbard-band”, and by $d_{i\sigma}^\dagger = \sigma s_{i\sigma}^\dagger h_i$, if it is in a Zhang-Rice-type

“lower-Hubbard-band”. Here e_i and h_i are “excession” and “holon” fermion operators, and $s_{i\sigma}$ are “spinon” boson operators. These auxiliary particle operators should satisfy in each site the constraint $e_i^\dagger e_i + h_i^\dagger h_i + \sum_\sigma s_{i\sigma}^\dagger s_{i\sigma} = 1$.

The constraint can be imposed on the average by introducing a chemical-potential-like Lagrange multiplier. But the Hilbert space (referred to as the auxiliary space) then contains many non-physical states. However, since the time evolution of Green’s functions is determined by the Hamiltonian which obeys the constraint rigorously, expressing Physical observables in term of Green’s functions results in a correct treatment of the physical subspace. This can be violated by applying inappropriate approximations to the Green’s functions.

Within the “spin-charge separation” approximation two-particle spinon-holon Green’s functions are decoupled into products of one-(auxiliary)-particle Green’s functions. Such an approximation has been shown to be appropriate in one dimension.

The Bogoliubov transformation $s_\sigma(\mathbf{k}) = \cosh(\xi_{\sigma\mathbf{k}})\zeta_\sigma(\mathbf{k}) + \sinh(\xi_{\sigma\mathbf{k}})\zeta_{-\sigma}^\dagger(-\mathbf{k})$ is applied to diagonalize the spinon states. The diagonalized operators $\zeta_\sigma^\dagger(\mathbf{k})$ create spinons of “bare” energies $\epsilon_\sigma(\mathbf{k})$. These energies have a V-shape zero minimum at $\mathbf{k} = \mathbf{k}_0$, where \mathbf{k}_0 is either $(\frac{\pi}{2a}, \frac{\pi}{2a})$ or $(\frac{\pi}{2a}, -\frac{\pi}{2a})$. Bose condensation results in antiferromagnetism (AF), and the spinon reciprocal lattice is extended over the basic reciprocal lattice by adding the vector $\mathbf{Q} = 2\mathbf{k}_0$.

STRIPES AND CARRIERS

It has been shown [6,7] that a lightly doped AF plane tends to phase-separate into “charged” and AF regions (gaining both hopping and exchange energies). A preferred structure under long-range Coulomb repulsion is of stripes of these phases, at least on the short range. Such a scenario is supported by experiment [1–3]. A structure of narrow charged stripes forming antiphase domain walls between wider AF stripes, has been confirmed for at least some cuprates, and there exists growing evidence indicating that such a structure probably exists, at least dynamically on the short range, in all the superconducting cuprates.

Spin-charge separation applies along the charged stripes (being one dimensional). Holons (excessions) within these stripes are referred to as “stripons”. They carry charge, but not spin. Their fermion creation operators are denoted by $p_\mu^\dagger(\mathbf{k})$, and their bare energies by $\epsilon_\mu^p(\mathbf{k})$. Note that \mathbf{k} here corresponds to an approximate periodicity determined by the stripes structure.

It has been observed [3] that the stripes in the cuprates are quite “frustrated”, and consist of disconnected segments. Since itinerancy in one-dimension requires perfect order, it is assumed here that an appropriate starting point is of localized stripon states.

The effect of the small- U orbitals is the existence of other carriers (of both charge and spin) whose states are hybridized small- U states and those coupled holon-spinon and excersion-spinon states which are orthogonal to the stripon states.

These carriers as referred to as "Quasi-electrons" (QE's). Their fermion creation operators are denoted by $q_{i\sigma}^\dagger(\mathbf{k})$. Their bare energies $\epsilon_i^q(\mathbf{k})$ form quasi-continuous ranges of bands crossing E_F over ranges of the Brillouin zone (BZ).

COUPLING VERTEX

The auxiliary space fields are coupled to each other due to hopping and hybridization terms of the original Hamiltonian. This coupling can be expressed in terms of the following effective Hamiltonian term whose parameters could be, in principle, derived self-consistently:

$$\begin{aligned} \mathcal{H}' = \frac{1}{\sqrt{N}} \sum_{i\mu\lambda\sigma} \sum_{\mathbf{k}, \mathbf{k}'} \{ & \sigma \epsilon_{i\mu\lambda\sigma}^{qp}(\mathbf{k}', \mathbf{k}) q_{i\sigma}^\dagger(\mathbf{k}) p_\mu(\mathbf{k}') \\ & \times [\cosh(\xi_{\lambda\sigma, (\mathbf{k}-\mathbf{k}')}) \zeta_{\lambda\sigma}(\mathbf{k}-\mathbf{k}') \\ & + \sinh(\xi_{\lambda\sigma, (\mathbf{k}-\mathbf{k}')}) \zeta_{\lambda, -\sigma}^\dagger(\mathbf{k}'-\mathbf{k})] + h.c. \}, \end{aligned} \quad (1)$$

Let us denote the QE, stripon, and spinon Green's functions by \mathcal{G}^q , \mathcal{G}^p , and \mathcal{G}^s , respectively. The propagators corresponding to them are presented diagrammatically in Fig. 1. \mathcal{H}' introduces a coupling vertex between these propagators, as shown in Fig. 1 too. As will be discussed below, the stripon bandwidth turns out to be at least an order of magnitude smaller than the QE and spinon bandwidths. Consequently one gets using a generalized Migdal theorem that "vertex corrections" are negligible.

In Fig. 2 are presented diagrammatically the self-energy corrections Σ^q , Σ^p , and Σ^s , obtained for the QE's, stripions, and spinons, respectively.

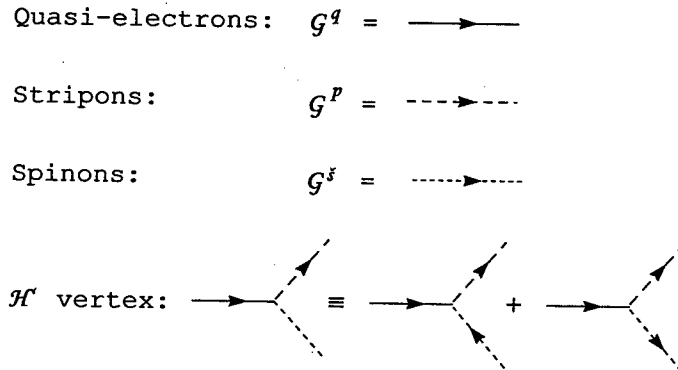


FIGURE 1. Diagrams for the auxiliary space propagators and the coupling vertex between them.

The auxiliary space spectral functions $A(\mathbf{k}, \omega) \equiv \Im \mathcal{G}(\mathbf{k}, \omega - i0^+)/\pi$, and scattering rates $\Gamma(\mathbf{k}, \omega) \equiv 2\Im \Sigma(\mathbf{k}, \omega - i0^+)$ are denoted by A^q , A^p , and A^s , and by Γ^q , Γ^p , and Γ^s , for the QE's, stripons, and spinons, respectively.

QUASIPARTICLES

For sufficiently doped cuprates the self-consistent self-energy corrections determine quasiparticles of the following features:

Spinons

One gets spinon spectral functions behaving as: $A^s(\mathbf{k}, \omega) \propto \omega$ for small ω . Consequently $A^s(\mathbf{k}, \omega) b_T(\omega) \propto T$ for $\omega \ll T$, where $b_T(\omega)$ is the Bose distribution function (at temperature T). Thus there is no long-range AF order (associated with the divergence in the number of spinons at $\mathbf{k} = \mathbf{k}_0$).

Stripons

The energies of the localized stripon states are renormalized to a very narrow range around zero, thus getting polaron-like states. Some hopping via QE-spinon states results in the onset of coherent itineracy at low temperatures, with a bandwidth of ~ 0.02 eV. The stripon scattering rates can be expressed as:

$$\Gamma^p(\mathbf{k}, \omega) \propto A\omega^2 + B\omega T + CT^2. \quad (2)$$

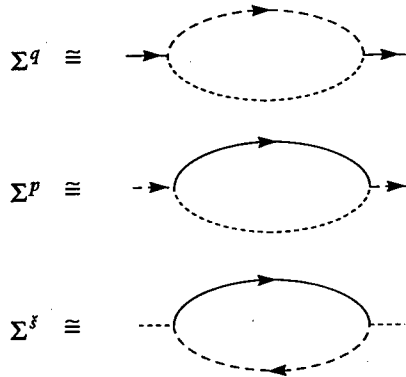


FIGURE 2. Diagrams for the self-energy corrections of the auxiliary space fields

Quasi-electrons

The QE scattering rates, can be approximately expressed as:

$$\Gamma^q(\mathbf{k}, \omega) \propto \omega [b_T(\omega) + \frac{1}{2}], \quad (3)$$

becoming $\Gamma^q(\mathbf{k}, \omega) \propto T$ in the limit $T \gg |\omega|$, and $\Gamma^q(\mathbf{k}, \omega) \propto \frac{1}{2}|\omega|$ in the limit $T \ll |\omega|$, in agreement with “marginal Fermi liquid” phenomenology [8].

Phonon-dressed spinons (svivons)

It was found [1] that the charged stripes are characterized by LTT structure, while the AF stripes are characterized by LTO structure. The result would be that in any physical process induced by the \mathcal{H}' vertex [see Eq. (1) and Fig. 1], the transformation of a stripon into a QE, or vice versa, through the emission/absorption of a spinon, is followed also by the emission/absorption of phonons. Thus the stripions have also lattice features of polarons, and the spinons are “dressed” by phonons in processes induced by the \mathcal{H}' vertex. We refer to such a phonon-dressed spinon as a “svivon”, and its propagator can be expressed as a spinon propagator multiplied by a power series of phonon propagators, as shown diagrammatically in Fig. 3. The svivons carry spin, but not charge, however they also “carry” lattice distortion.

SOME ANOMALOUS PHYSICAL PROPERTIES

Optical conductivity

The optical conductivity of the doped cuprates can be expressed [9] as a combination of a Drude term and mid-IR peaks. Within the present approach the Drude term results from transitions between low energy QE states, while excitations of stripon states result in the mid-IR peaks. Such excitations can either leave a stripon in the same stripe segment, exciting spinon and phonon states, or transform it through \mathcal{H}' into a QE and a svivon.

Phonon propagator:

Svivon propagator:

$$\text{.....} \equiv \text{.....} (1 + \text{.....} + \text{.....} + \text{.....} + \dots)$$

FIGURE 3. Diagrams for a phonon propagator and a svivon propagator (expressed in terms of spinon and phonon propagators).

Spectroscopic anomalies

Experiments like photoemission give information about the electronic spectral function, which is expressed as a combination of QE and stripon-svicon contributions. Thus it has a "coherent" part, due to the contributions of few QE bands, and an "incoherent" part of a comparable weight, due to the contributions of other quasi-continuous QE bands, and stripon-svicon states.

The frequently observed $\sim|E - E_F|$ bandwidth is consistent with Eq. (3). The spectroscopic "signature" of stripsons is smeared over few tenths of an eV around E_F due to the accompanying svicon excitations. The observed "Shadow bands" and "extended" van Hove singularities result from the effect of the striped superstructure on the QE bands [10].

Transport properties

Within the present approach the electric current is expressed as a sum: $\mathbf{j} = \mathbf{j}^q + \mathbf{j}^p$, where the QE and stripon contributions \mathbf{j}^q and \mathbf{j}^p are presented diagrammatically in Fig. 4. Since stripsons transport occurs through transitions to intermediate QE-spinon states, one gets $\mathbf{j}^p \cong \alpha \mathbf{j}^q$, where α is approximately T -independent. In order for this condition to be satisfied gradients $\nabla\mu^q$ and $\nabla\mu^p$ of the QE and stripon chemical potentials must be formed in the presence of an electric field or a temperature gradient, where $N^q \nabla\mu^q + N^p \nabla\mu^p = 0$ (N^q and N^p are the contributions of QE's and stripsons to the electrons density of states at E_F).

Expressions for the dc conductivity and Hall constant are derived using the Kubo formalism. Within the present approach they are expressed in term of diagonal and non-diagonal conductivity QE terms σ_{xx}^{qq} and σ_{xy}^{qq} , stripon terms σ_{xx}^{pp} and σ_{xy}^{pp} , and mixed terms σ_{xy}^{qpp} . The diagrams for these terms are shown in Fig. 5.

It has been shown elsewhere [11] that the electrical resistivity can then be expressed as:

$$\rho_x = \frac{1}{(N^q + N^p)(1 + \alpha)} \left(\frac{N^q}{\sigma_{xx}^{qq}} + \frac{\alpha N^p}{\sigma_{xx}^{pp}} \right), \quad (4)$$

and the Hall constant as:



FIGURE 4. Diagrams for quasi-particles contributions to the electric current.

$$R_H = \frac{\rho_x}{\cot \theta_H}, \quad \cot \theta_H = (1 + \alpha) \left[\frac{\sigma_{xy}^{qqq} + \sigma_{xy}^{qqpp}}{\sigma_{xx}^{qq}} + \frac{\alpha(\sigma_{xy}^{ppp} + \sigma_{xy}^{qqpp})}{\sigma_{xx}^{pp}} \right]^{-1}. \quad (5)$$

The temperature dependencies of these transport quantities are determined by those of the scattering rates Γ^q and Γ^p , given in Eqs. (2), (3), to which temperature-independent impurity scattering terms are added. Consequently one can express them in terms of parameters A, B, C, D, N , and Z , as follows:

$$\begin{aligned} \sigma_{xx}^{qq} &\propto \frac{1}{D + CT}, & \sigma_{xx}^{pp} &\propto \frac{1}{A + BT^2}, \\ \sigma_{xy}^{qqq} &\propto \frac{1}{(D + CT)^2}, & \sigma_{xy}^{ppp} &\propto \frac{1}{(A + BT^2)^2}, & \sigma_{xy}^{qqpp} &\propto \frac{1}{(D + CT)(A + BT^2)}. \end{aligned} \quad (6)$$

Resulting in the following expressions for ρ_x and $\cot \theta_H$:

$$\rho_x = \frac{D + CT + A + BT^2}{N}, \quad \cot \theta_H = \left(\frac{Z}{D + CT} + \frac{1}{A + BT^2} \right)^{-1}. \quad (7)$$

These expressions reproduce the systematic behavior of the transport quantities in different cuprates, as has been demonstrated elsewhere [11]. Note that one can get at the same time linear temperature dependence of ρ_x and quadratic temperature dependence of $\cot \theta_H$, and that the temperature dependence of ρ_x can change to quadratic, and that of $\cot \theta_H$ to linear, as has been observed [12].

Comparing the present analysis to that of Anderson [13], who first suggested that ρ and $\cot \theta_H$ are determined by different scattering rates (attributing the T^2 term to spinons), it has been observed in ac Hall effect results [14] that the energy scale corresponding to the T^2 term is of ~ 120 K, which is in agreement with energies of stripions (suggested here) and not of spinons.

It has also been shown elsewhere [11] that the thermoelectric power (TEP) S can be expressed in terms of QE and stripon terms S^q and S^p , as: $S = (N^q S^q + N^p S^p) / (N^q + N^p)$, where $S^q \propto T$, while the stripon term saturates at $T \simeq 200$ K to $S^p = (k_B/e) \ln [(1 - n^p)/n^p]$, where n^p is the fractional occupation of the stripon band.

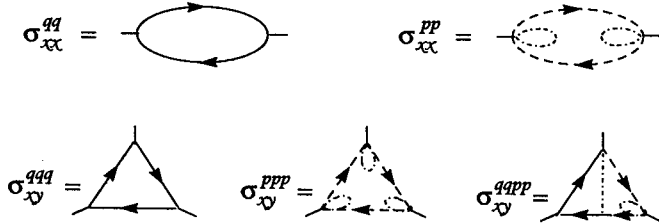


FIGURE 5. Diagrams for the QE, stripon, and mixed conductivity terms.

This result is consistent with the typical behavior of the TEP in the cuprates, and has been [15] parametrized as: $S = AT + BT^\alpha/(T + \Theta)^\alpha$. It was found [16,17] that $S^p = 0$ (namely the stripon band is half full) for slightly overdoped cuprates.

The effect of the doping is [2] both to change the density of the charged stripes within a CuO_2 plane, and to change the density of carriers (stripions) within a charged stripe. It is the second type of doping effect that changes n^p .

PAIRING MECHANISM

The \mathcal{H}' vertex provides a pairing mechanism which is suggested here to drive high- T_c superconductivity as well as the normal-state pseudogap in the cuprates. This mechanism involves transitions between pair states of QE's and stripions through the exchange of svivons, as demonstrated diagrammatically in Fig. 6. It is conceptually similar to the interband pair transition mechanism proposed by Kondo [18]. The symmetry of the superconducting gap is affected by \mathbf{k} -space symmetry which maximizes pairing.

A condition for superconductivity is that the narrow stripon band maintains coherence between different stripe segments. The diagram described in Fig. 6 can, however, drive pairing even when the stripions are incoherent. If this occurs, the carriers do not carry supercurrent, but a gap for pair breaking is still expected to exist. Such condensate is interpreted here as the pseudogap phase found in underdoped cuprates.

Thus a normal-state pseudogap is expected to have a similar size and symmetry to that of the superconducting gap, as has been observed [19]. Also the opening of the pseudogap should account for most of the pair-condensation energy, as has been observed.

If the BCS-like pairing temperature (below which the gap opens) is denoted by T_{pair} and the stripon coherence temperature is denoted by T_{coh} , one expects superconducting transition at:

$$T_c = \min(T_{\text{pair}}, T_{\text{coh}}). \quad (8)$$

Thus $T_c = T_{\text{coh}} < T_{\text{pair}}$ in underdoped cuprates, and $T_c = T_{\text{pair}} < T_{\text{coh}}$ in overdoped cuprates, in agreement with the observed behavior of the gap [20].

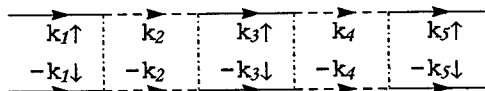


FIGURE 6. Diagram for transitions between pair states of QE's and stripions, leading to pairing.

Stripon coherence is energetically favorable at temperatures where there is a clear distinction between occupied and unoccupied stripon band states. Thus, an estimate for T_{coh} for an almost empty (full) stripon band is given by the distance \mathcal{E}_F of the Fermi level from the bottom (top) of the band at $T = 0$. Using a two-dimensional parabolic approximation one can express:

$$k_B T_{\text{coh}} \simeq \mathcal{E}_F = 2\pi\hbar^2(n^*/m^*), \quad (9)$$

where m^* in the stripions effective mass and n^* is their density per unit area of a CuO_2 plane (note that the stripions are spinless).

This result agrees with the "Uemura plots" [21] if the n^*/m^* ratio for stripions is approximately proportional to that for the supercurrent carriers, appearing in the expression for the London penetration depth. The "boomerang-type" behavior of the Uemura plots in overdoped cuprates [22] is consistent with as a transition from a band-top $T_c = T_{\text{coh}}$ to a band-bottom $T_c = T_{\text{pair}}$ behavior, as discussed above.

CONCLUSIONS

The existence of high- T_c superconductivity in the cuprates has been a challenge for both experimentalists and theorists over the last 13 years. These complex materials have been found to be anomalous in almost any physical property, and the traditional methods developed for simple materials may be inadequate dealing with them.

Here these materials are approached going beyond the "standard" models, and considering the effect of both large- U and small- U orbitals. A locally inhomogeneous striped structure is obtained, as well as a non-standard existence of three types of carriers: polaron-like stripions carrying charge, quasielectrons carrying charge and spin, and svivons carrying spin and lattice distortion.

Anomalous normal-state properties of the cuprates, and specifically transport properties, are clarified, and a pairing mechanism based on transitions between pair states of stripions and quasielectrons through the exchange of svivons is derived, leading to high- T_c superconductivity and to the normal-state pseudogap.

REFERENCES

1. A. Bianconi *et al.*, *Phys. Rev. B* **54**, 12018, (1996); *Phys. Rev. Lett.* **76** 3412 (1996); this issue.
2. J. M. Tranquada *et al.*, *Phys. Rev. B* **54**, 7489, (1996); *Phys. Rev. Lett.* **78**, 338 (1997); this issue.
3. Papers in this issue, and in the Proceedings of the 1996 and 1998 Rome Conferences on Stripes and High- T_c superconductivity, *J. Supercond.* **10**, #4 (1997), and *ibid.* (1999).
4. O. K. Andersen *et al.*, *J. Phys. Chem. Solids* **56**, 1573 (1995).

5. S. E. Barnes, *Adv. Phys.* **30**, 801 (1980).
6. J. Zaanen, and O. Gunnarsson, *Phys. Rev. B* **40**, 7391 (1989).
7. V. J. Emery, and S. A. Kivelson, *Physica C* **209**, 597 (1993); this issue.
8. C. M. Varma *et al.*, *Phys. Rev. Lett.* **63**, 1996 (1989).
9. D. B. Tanner, and T. Timusk, *Physical Properties of High Temperature Superconductors III*, edited by D. M. Ginsberg (World Scientific, 1992), p. 363.
10. M. I. Salkola, *et al.*, *Phys. Rev. Lett.* **77**, 155 (1996).
11. J. Ashkenazi, *J. Supercond.* **10**, 379 (1997); *ibid.*, (1999).
12. T. R. Chien, *et al.*, *Phys. Rev. Lett.* **67**, 2088 (1991); Y. Kubo and T. Manako, *Physica C* **197**, 378 (1992); H. Takagi, *et al.*, *Phys. Rev. Lett.* **69**, 2975 (1992); H. Y. Hwang, *et al.*, *ibid.* **72**, 2636 (1994).
13. P. W. Anderson, *Phys. Rev. Lett.* **67**, 2092 (1991).
14. H. D. Drew, S. Wu, and H.-T. S. Linh, preprint.
15. S. Tanaka, *et al.*, *J. Phys. Soc. Japan* **61**, 1271 (1992).
16. B. Fisher, *et al.*, *J. Supercond.* **1**, 53 (1988); J. Genossar, *et al.*, *Physica C* **157**, 320 (1989).
17. K. Matsuura, *et al.*, *Phys. Rev. B* **46**, 11923 (1992); S. D. Obertelli, *et al.*, *ibid.*, p. 14928; C. K. Subramaniam, *et al.*, *Physica C* **203**, 298 (1992).
18. J. Kondo, *Prog. Theor. Phys.* **29**, 1 (1963).
19. D. S. Marshall, *et al.*, *Phys. Rev. Lett.* **76**, 4841 (1996); H. Ding, *et al.*, *Phys. Rev. Lett.* **78**, 2628 (1997); M. R. Norman, this issue.
20. J. Demsar, K. Zagar, V. V. Kabanov, and D. Mihailovic, this issue.
21. Y. J. Uemura, *et al.*, *Phys. Rev. Lett.* **62**, 2317 (1989).
22. Ch. Niedermayer, *et al.*, *Phys. Rev. Lett.* **71**, 1764 (1993).

A BCS–Bose-Einstein Crossover Theory and its Application to the Cuprates

Qijin Chen, Ioan Kosztin, Boldizsár Jankó, and K. Levin

James Franck Institute, University of Chicago, 5640 South Ellis Avenue, Chicago, IL 60637

Abstract. We use a “pairing fluctuation” approach to address the behavior of T_c and pseudogap in d -wave superconductors. This theory yields a BCS–Bose-Einstein crossover description of the superconducting transition, which reduces to BCS in the weak coupling (small g) limit and to a Bose-Einstein description at large g . We investigate the effects of quasi-two dimensionality, lattice bandstructure and d -wave symmetry, and obtain a cuprate phase diagram, in quantitative agreement with experiment.

INTRODUCTION

BCS–Bose-Einstein condensation (BEC) crossover theories have been applied to the high T_c problem since the discovery of cuprate superconductors in 1986 [1]. Interest in these theories is based on the fact that these materials have short coherence lengths. Moreover, as a function of doping the system evolves smoothly from BCS-like behavior in the overdoped regime to the underdoped regime, where BCS theory manifestly fails as a consequence of an excitation gap at T_c [2]. Uemura’s plot [3] has also been used to suggest that the cuprates are intermediate between BCS and BEC systems. However, the application of crossover theories to the cuprates is made complex by the high anisotropy, lattice periodicity and d -wave pairing symmetry of these materials. Here we investigate these effects on the BCS-BEC crossover, and address pseudogap phenomena in cuprate superconductors.

THEORETICAL FORMALISM

Our system is composed of fermions with dispersion $\epsilon_{\mathbf{k}}$ in the presence of an effective pairing interaction $V_{\mathbf{k},\mathbf{k}'} = g\varphi_{\mathbf{k}}\varphi_{\mathbf{k}'}$, where the coupling strength $g < 0$. In a jellium gas, $\epsilon_{\mathbf{k}} = k^2/2m$ and the symmetry factor $\varphi_{\mathbf{k}} = (1 + (k/k_0)^2)^{-1/2}$; On a lattice, $\epsilon_{\mathbf{k}} = \sum_i^d 2t_i(1 - \cos k_i) - \mu$, and $\varphi_{\mathbf{k}} = 1$ (s -wave) or $\varphi_{\mathbf{k}} = \cos k_x - \cos k_y$ (d -wave). In quasi-2d cases, the hopping integrals satisfy $t_{\perp} \equiv t_z \ll t_{\parallel} \equiv t_x = t_y$.

At small g , the system is fermionic, and undergoes a BCS superconducting transition at T_c . At large g , composite bosons form above T_c , and the system undergoes

BEC at T_c . The effective *pair* chemical potential is identically zero for $T \leq T_c$. In the intermediate regime, both single fermions and (metastable) pairs exist above T_c and similarly, below T_c , the excitations consist of quasiparticles and finite momentum pair excitations (i.e., pairons). These new excitations, not present in BCS theory, are responsible for the pseudogap.

We first calculate T_c following the T-matrix approach, of Kadanoff and Martin [4]. We have for the self-energy $\Sigma(K) = G_0^{-1}(K) - G^{-1}(K) = \sum_Q t(Q) G_0(Q - K) \varphi_{\mathbf{k}-\mathbf{q}/2}^2$, and T-matrix $t(Q) = [g^{-1} + \sum_K G(K) G_0(Q - K) \varphi_{\mathbf{k}-\mathbf{q}/2}^2]^{-1}$, where $G_0(K)/G(K)$ are the bare/full Green's functions in the four-vector notation, $K \equiv (\mathbf{k}, i\omega)$, etc. At T_c , finite \mathbf{q} pairs are long lived for small \mathbf{q} , and the T-matrix can be approximated by $t_{\mathbf{q},\Omega} \approx a_0^{-1}/(\Omega - \Omega_{\mathbf{q}})$, with pair dispersion $\Omega_{\mathbf{q}} \approx \sum_i q_i^2/2M_i^*$. a_0 can be obtained by expanding $t^{-1}(Q)$.

The BEC condition requires the effective *pair* chemical potential $-\Omega_{\mathbf{q}=0} = 0$. This is equivalent to the superconducting instability condition $t^{-1}(0) = 0$ from the fermionic perspective. Because of the divergence of $t(Q)$ at $Q = 0$, $\Sigma(K) \approx G_0(-K) \varphi_{\mathbf{k}}^2 \sum_Q t(Q) \equiv -G_0(-K) \Delta_{pg}^2 \varphi_{\mathbf{k}}^2$, where $\Delta_{pg}^2 \equiv -\sum_Q t(Q)$ defines the pseudogap. Including the particle number equation, we obtain

$$\text{BEC condition} \quad 1 + g \sum_{\mathbf{k}} \frac{1 - 2f(E_{\mathbf{k}})}{2E_{\mathbf{k}}} \varphi_{\mathbf{k}}^2 = 0, \quad (1)$$

$$\text{Number equation} \quad \sum_{\mathbf{k}} \left[1 - \frac{\epsilon_{\mathbf{k}}}{E_{\mathbf{k}}} + 2 \frac{\epsilon_{\mathbf{k}}}{E_{\mathbf{k}}} f(E_{\mathbf{k}}) \right] = n, \quad (2)$$

$$\text{Pseudogap Equation} \quad \Delta_{pg}^2 \approx \frac{1}{a_0} \sum_{\mathbf{q}} b(\Omega_{\mathbf{q}}). \quad (3)$$

where $E_{\mathbf{k}} = \sqrt{\epsilon_{\mathbf{k}} + \Delta^2 \varphi_{\mathbf{k}}^2}$, $a_0 = \frac{1}{2\Delta^2} \sum_{\mathbf{k}} \left[[1 - 2f(\epsilon_{\mathbf{k}})] - \frac{\epsilon_{\mathbf{k}}}{E_{\mathbf{k}}} [1 - 2f(E_{\mathbf{k}})] \right]$, $\Delta = \Delta_{pg}$ at T_c , and $f(x)/b(x)$ is the Fermi/Bose function.

Below T_c , the superconducting order parameter Δ_{sc} adds to the excitation gap $\Delta = \sqrt{|\Delta_{sc}|^2 + \Delta_{pg}^2}$. As can be easily seen from Eq. (3), at $T = 0$, Δ_{pg} vanishes, and we recover Leggett's ground state [5].

NUMERICAL RESULTS

Figure 1 shows typical T_c behavior obtained by solving Eqs. (1)-(3), as a function of g at low densities. While at small g , T_c follows the BCS functional form, as g increases, μ decreases and simultaneously Δ_{pg} increases. The system becomes bosonic as μ becomes negative. At large g , T_c approaches the BEC temperature ($T_c \approx 0.218 E_F$) in the jellium case or vanishes asymptotically in the lattice case. The effective pair mass M^* increases with g in the presence of the lattice. In both cases, the figure shows $T_c \propto 1/M^*$ for large g , characteristic of BEC.

By contrast, at high densities, T_c decreases to zero at finite g reflecting the behavior of M^* . The pairs become too heavy to move and Bose condense.

Figure 2(a) plots T_c , μ , and Δ_{pg} for d -wave superconductors on a quasi-2d lattice

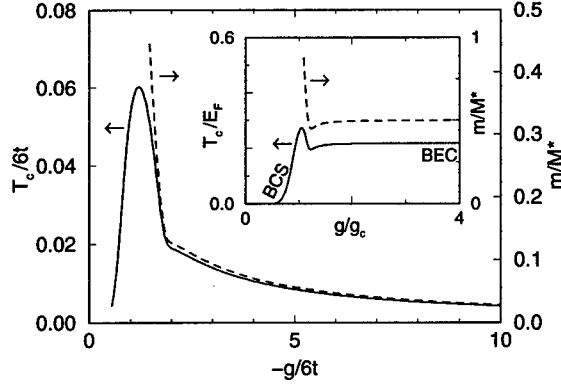


FIGURE 1. BCS-BEC crossover of T_c (solid lines) on a 3d lattice (main figure, $n = 0.1$) and in a 3d jellium gas (inset, $k_0 = 4k_F$) with an s -wave pairing symmetry in the low density or short range interaction case. Also plotted are the inverse effective pair mass m/M^* (dashed lines).

for densities relevant to the cuprates. T_c vanishes at a nearly universal value of g , well before the bosonic regime is reached; μ is still close to E_F . This is attributable to the finite pair size due to the d -wave symmetry. It indicates that there is no bosonic (or preformed pair) regime in d -wave superconductors.

Figure 2(b) shows the effect of mass anisotropy on T_c on a quasi-2d lattice. As $t_\perp/t_\parallel \rightarrow 0$, the system changes from 3d to 2d, and T_c is suppressed logarithmically to zero. In this way, pseudogap effects are enhanced by the low dimensionality.

To address the cuprates, we include Mott-insulator effect behavior near half filling. This leads to a renormalization of the in-plane hopping integral t_0 to $t_\parallel(x) \approx t_0(1 - n) = t_0x$. For lack of further information we assume g is x independent and calculate T_c , T^* , $\Delta(0)$, and $\Delta(T_c)$ as a function of x , as shown

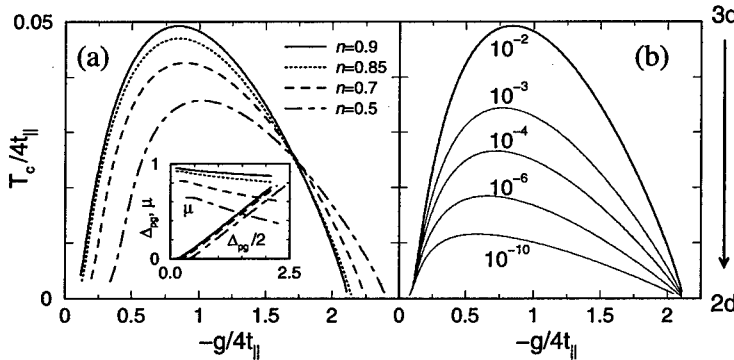


FIGURE 2. (a) T_c (main figure) and μ and Δ_{pg} (inset) as a function of coupling g on a quasi-2d lattice ($t_\perp/t_\parallel = 0.01$) with a d -wave pairing symmetry. (b) Effects on T_c of the mass anisotropy ($n = 0.9$). t_\perp/t_\parallel is labeled on the T_c curves.

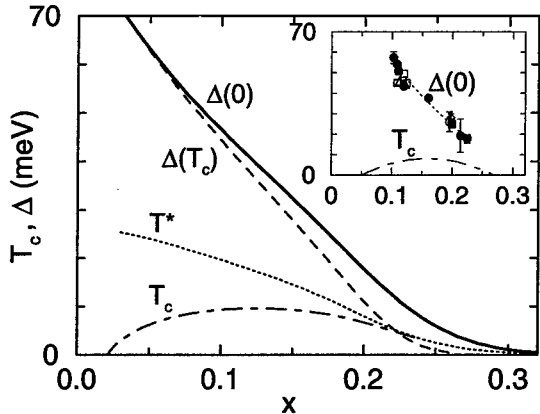


FIGURE 3. Calculated cuprate phase diagram for $t_{\perp}/t_{\parallel} = 0.01$. The gaps plotted here are the magnitude at $(\pi, 0)$, twice those in Eqs. (1-3). Experimental data from ref. [6] are plotted (inset).

in Fig. 3. T^* is estimated from the mean-field solution of Eqs. (1-2). To optimize agreement between the theoretical and measured phase diagram, we choose $-g/4t_0 = 0.045$. Taking $t_0 = 0.6$ eV (consistent with photoemission data) yields quite good agreement with experiment.

CONCLUSIONS

In constructing a BCS-BEC crossover theory, we find it necessary to include finite momentum pair excitations. These pair excitations lead to the pseudogap effects, which are enhanced by low dimensionality. When lattice effects and d -wave symmetry are included, T_c will vanish well before the bosonic regime is reached. A phase diagram is obtained, in quantitative agreement with cuprate experiments.

ACKNOWLEDGMENTS

This work was supported by the National Science Foundation under grant DMR No. 91-20000 through the Science and Technology Center for Superconductivity.

REFERENCES

1. For a review, see Randeria, M. in *Bose-Einstein Condensation*, ed. Griffin, A., Snoke, D. W., and Stringari, S., New York, Cambridge Press, 1995, pp. 355-392.
2. Ding, H. *et al.*, *Nature (London)* **382**, 51-54 (1996).
3. Uemura, Y. J., *Physica C* **282**, 194-197 (1997).
4. Kadanoff, L. P., and Martin, P. C., *Phys. Rev.* **124**, 670-697 (1961).
5. Leggett, A. J., *J. Phys. (Paris)* **41**, C7/19-26 (1980).
6. Miyakawa, N. *et al.*, *Phys. Rev. Lett.*, **80**, 157-160 (1998); cond-mat/9809398.

Theory of pairing in the Cu-O Plane: Three-Band Hubbard Model and Beyond

Michele Cini, Gianluca Stefanucci and Adalberto Balzarotti

*Istituto Nazionale di Fisica della Materia and Dipartimento di Fisica,
Università di Roma Tor Vergata, Via della Ricerca Scientifica 1- 00133 Roma, Italy*

Abstract. We calculate the effective interaction W_{eff} between two holes added to the ground state of the repulsive three-band Hubbard model. To make contact with Cooper theory and with earlier Hubbard model cluster studies. We first use a perturbative canonical transformation, to generate a two-body Hamiltonian. Then, we extend the results to all orders. The approach is exact in principle, and we obtain a closed analytic expression including explicitly the effects of all virtual transitions to 4-body intermediate states. Our scheme naturally lends itself to embody off-site, inter-planar, phonon-mediated and other interactions which are not considered in the Hubbard model but may well be important. The result depends qualitatively on the symmetry of the two-hole state: 1B_2 and 1A_2 pairs are special, because the bare holes do not interact by the on-site repulsion ($W=0$ pairs). The effective interaction in these channels is attractive and leads to a Cooper-like instability of the Fermi liquid; however W_{eff} is repulsive for triplet pairs. Bound two-hole states of the same nature were reported earlier in small cluster calculations by exact diagonalisation methods; only symmetric clusters are good models of the plane. Once W_{eff} is known, the pair eigenfunction is determined by an integral equation. We present numerical estimates of the binding energy $|\Delta|$ of the pairs, which is in the physically interesting range of tens of meV if unscreened on-site repulsion parameters are used.

The most fundamental question about high T_C superconductivity is: what is the quasiparticle? We have strong evidence now that the quasi-particle we want is a novel kind of singlet, the $W=0$ pair. We introduced them in cluster calculations from CuO_4 up to Cu_5O_{16} ; we pointed out [1] that these pairs arise from degenerate states having $e(x, y)$ symmetry, and are two-hole eigenstates of the kinetic energy H_0 that are also eigenstates of the on-site repulsion term W with eigenvalue 0. In the three-band Hubbard model Hamiltonian $H = H_0 + W$,

$$W = \sum_i U_i n_{i+} n_{i-}, \quad (1)$$

with $U_i = U_d$ for a Cu site, $U_i = U_p$ for an Oxygen site. The symmetry is an essential ingredient, because such solutions exist in the plane, and also in clusters provided that they have the same symmetry as the plane around a Cu site. The

planar lattice structure is also essential, because no $W=0$ pairs occur in 3D or in a continuous model. These calculations [2] showed that $W=0$ pairs are the "bare" quasiparticles that, when "dressed", become a bound state, with the characteristic superconducting flux-quantization [3]. Remarkably, CuO_4 , the smallest unit having the correct symmetry, already displays both effects; the reason why the $W=0$ pair which is realized there was not discovered before is probably that one needs 4 holes in such a small unit, and that is far from the experimental concentration. However, at lower filling n one gets no pairing. The main indirect attractive interaction through the background particles arises from the second-order contributions to the two-hole amplitude [3].

Recently [4] we extended the theory to the full plane. Omitting the band indices, let

$$d[k] = ||k_+, -k_-|| = c_{k_+,+}^+ c_{-k,-}^+ |vac> \quad (2)$$

be a two-hole determinantal state derived from the k eigenfunctions. The point symmetry Group of the Cu-O plane is C_{4v} . We introduce the determinants $Rd[k] = d[Rk]$, $R \in C_{4v}$, and the projected states

$$\Phi_\eta[k] = \frac{1}{\sqrt{8}} \sum_{R \in C_{4v}} \chi^{(\eta)}(R) Rd[k] \quad (3)$$

where $\chi^{(\eta)}(R)$ is the character of the operation R in the Irreducible Representation η . One finds that $\eta = 1 A_2$ and $\eta = 1 B_2$ yields $W=0$ pairs, like those studied previously [3]. One necessary condition for pairing in clusters is that the least bound holes form such a pair, and this dictates conditions on the occupation number. In the full plane, however, $W=0$ pairs exist at the Fermi level for any filling.

Suppose the Cu-O plane is in its ground state with chemical potential E_F and a couple of extra holes are added. We have shown that, by a canonical transformation, one can obtain an effective Hamiltonian which describes the propagation of a pair of dressed holes, and includes all many-body effects. The exact many-body ground state with two added holes can be expanded in terms of excitations over the vacuum (the non-interacting Fermi *sphere*) by a configuration interaction:

$$|\Psi_0> = \sum_m a_m |m> + \sum_\alpha b_\alpha |\alpha> + \sum_\beta c_\beta |\beta> + \dots \quad (4)$$

here m runs over pair states, α over 4-body states (2 holes and 1 e-h pair), β over 6-body ones (2 holes and 2 e-h pairs), and so on. The effects of the operators on the terms of $|\Psi_0>$ is:

$$H_0|m> = E_m|m>, H_0|\alpha> = E_\alpha|\alpha>, \dots \quad (5)$$

and since W can create or destroy up to 2 e-h pairs,

$$W|m> = \sum_{m'} V_{m',m} |m'> + \sum_\alpha |\alpha> W_{\alpha,m} + \sum_\beta |\beta> W_{\beta,m}, \quad (6)$$

and so on.

Directly from the many-body Schrödinger equation one can show that the a amplitudes obey an exact two-hole Schrödinger equation of the form

$$(E_0 - E_m'') a_m = \sum_{m'} a_{m'} \{ V_{m,m'}'' + \langle m | S[E_0] | m' \rangle \}, \quad (7)$$

where

$$\langle m | S[E_0] | m' \rangle = \sum_{\alpha} \frac{\langle m | W'' | \alpha \rangle \langle \alpha | W'' | m' \rangle}{E_0 - E_{\alpha}''}. \quad (8)$$

Here, E_0 is the interacting ground state energy, W'' and E_{α}'' can be obtained from W and E_{α} by a suitable renormalisation procedure, which corresponds to solving a system of equations that we have detailed [4]. So, a_m is the wave function of the dressed pair, which is acted upon by an effective hamiltonian \tilde{H} . The change from the full many-body H to \tilde{H} is a canonical transformation. The scattering operator S is of the form $S = W_{eff} + F$, where W_{eff} is the effective interaction between dressed holes, while F is a forward scattering operator, diagonal in the pair indices m, m' which accounts for the self-energy corrections of the one-body propagators: it just redefines the dispersion law E_m , and, essentially, renormalizes the chemical potential. F must be dropped, as the Cooper theory, where an effective interaction involving phonons is introduced via an (approximate) canonical transformation. Therefore the effective Schrödinger equation for the pair reads

$$(H_0 + V + W_{eff}) |a\rangle = E_0 |a\rangle \quad (9)$$

Writing the ground state energy $E_0 = 2E_F + \Delta$, where E_F is the chemical potential, it is clear that $\Delta < 0$ implies a positive binding energy $|\Delta|$ of the pair and a Cooper-like instability of the Fermi liquid in the Cu-O plane. The V interaction just adds to W_{eff} , and this feature allows to include in our model the effects of other pairing mechanisms, like phonons, off-site interactions, inter-planar coupling and so on. Since actually $V = 0$ in the Hubbard model, we drop it in the following.

In the computations we calculate W_{eff} neglecting 6-body and higher excitations, that is, we compute the *bare* quantities. This is a reasonable approximation if we compute small corrections to a Fermi liquid background, like in Cooper theory. Near half filling, when an antiferromagnetic background is more appropriate, a fuller solution of the system may be necessary, but the structure of the solution

TABLE 1. Dependence of Δ (meV) on hole concentration n and on the scale s

Pairs	$n = 1.3$		$n = 1.4$	
	$s = 1.4$	$s = 2.1$	$s = 1.4$	$s = 2.1$
1B_2	-8.8	-131	-35.6	-170.8
1A_2	-8.4	-34	-1.5	-2.6

is exact when expressed in terms of renormalized matrix elements. We obtain the effective interaction between $W=0$ pairs:

$$\begin{aligned} & \langle \Phi_\eta[p] | W_{eff} | \Phi_\eta[s] \rangle = \\ & 4 \sum_{R \in C_{4v}} \chi^{(\eta)}(R) \sum_{k_2: \varepsilon(Rs+p+k_2) > E_F}^o \frac{U(p, k_2, Rs+p+k_2, -Rs) U(Rs+p+k_2, -p, Rs, k_2)}{\varepsilon(Rs+p+k_2) + \varepsilon(s) + \varepsilon(p) - \varepsilon(k_2) - E_0} \end{aligned} \quad (10)$$

The sum is over occupied k_2 with empty $Rs+p+k_2$. Note that W_{eff} does not depend on the sign of U , because each excitation which is emitted must be reabsorbed. The m and m' indices run over the projected eigenstates $\Phi_\eta[k]$ of the kinetic energy, and the k labels run over $1/8$ of the BZ. We denote such a set of empty states $e/8$, and cast the result in the form of a (Cooper-like) Schrödinger equation

$$2\varepsilon(k) a(k) + \sum_{k'}^{e/8} W_{eff}(k, k') a(k') = E_0 a(k) \quad (11)$$

for a self-consistent calculation of E_0 (since W_{eff} depends on the solution). For numerical estimates, we used as parameters the current values (in eV) $t=1.3$, $\varepsilon_p=3.5$, $\varepsilon_d=0$, $U_p=6s$, $U_d=5.3s$, where s is a scale factor induced by renormalization.

Some results for the infinite plane are shown in Table I. We get negative Δ for both symmetry types; this is in line with perturbation theory approaches [5] and shows that electronic mechanisms alone can open a gap. With increasing doping, the 1B_2 gap widens while the 1A_2 tends to close. The gap increases in size rapidly with s . The reason for $s > 1$ could be that the current estimates of U 's are a bit low; however, since the screening excitations are explicitly accounted for in the Hamiltonian, it is reasonable that the input U 's must be somewhat larger than the fully screened interaction. Moreover, contributions from phonons and other mechanisms can be included by a non zero V , and must be relevant for a detailed comparison with experiment. This is just the beginning of a long way.

REFERENCES

1. M. Cini and A. Balzarotti, *Il Nuovo Cimento D* **18**, 89 (1996).
2. M. Cini and A. Balzarotti, *Solid State Commun.* **101**, 671 (1997).
3. M. Cini and A. Balzarotti, *Phys. Rev.* **B56**, 1, 14711 (1997).
4. M. Cini, G. Stefanucci and A. Balzarotti, *Solid State Commun.*, **109**, 229 (1998), and to be published.
5. See, e.g., G. Esirgen and N. E. Bickers, *Phys. Rev.* **B57**, 5376 (1998) and references therein.

Resonant neutron scattering on the high Tc cuprates and π and η excitations of the t - J and Hubbard models

Eugene Demler¹ and Shou-Cheng Zhang²

¹*Institute for Theoretical Physics, University of California, Santa Barbara, CA 93106*

²*Department of Physics, Stanford University Stanford, CA 94305*

Abstract. We review the explanation for resonant neutron scattering experiments in $\text{YBa}_2\text{Cu}_3\text{O}_{6+\delta}$ and $\text{Bi}_2\text{Sr}_2\text{Ca}_2\text{O}_{8+\delta}$ materials from the point of view of triplet excitation in the particle-particle channel, the π excitation. Relation of these resonances to the superconducting condensation energy and their role in stabilizing the superconducting state is discussed. Due to the superconducting fluctuations, the π resonance may appear as a broad peak above Tc. The analogue problem to the π excitation for the case of s -wave pairing, the η excitation, is considered in the strong coupling limit with an emphasis on the resonance precursors in a state with no long range order.

Inelastic neutron scattering (INS) on optimally doped $\text{YBa}_2\text{Cu}_3\text{O}_7$ revealed a striking resonance at the commensurate wavevector $Q = (\pi/a, \pi/a)$ and energy 41 meV [1]. This resonance appears in the spin-flip channel only, therefore it is of magnetic origin and not due to scattering by phonons. The most remarkable feature of this resonance is that it appears only below Tc and therefore tells us about enhanced antiferromagnetic fluctuations in the superconducting state of this material. Similar resonances have later been found for the underdoped $\text{YBa}_2\text{Cu}_3\text{O}_{6+\delta}$ at smaller energies but the same wavevector of commensurate antiferromagnetic fluctuations $(\pi/a, \pi/a)$ [2]. A new feature of the resonances in underdoped materials is that they no longer disappear above Tc but have precursors appearing at some temperature above the superconducting transition temperature. Recently, resonant peaks below Tc have also been observed in INS experiments on $\text{Bi}_2\text{Sr}_2\text{Ca}_2\text{O}_{8+\delta}$ materials [3].

Several theories have been suggested to explain the observed resonances [4]. One of the proposals [5] was to identify them with a π -excitation, a triplet excitation at momentum $(\pi/a, \pi/a)$ in the particle-particle channel : $\pi^\dagger = \sum_p (\cos p_x - \cos p_y) c_{p+Q\uparrow}^\dagger c_{-p\uparrow}^\dagger$. This excitation is a well-defined collective mode for a wide range of lattice Hamiltonians, including the Hubbard Hamiltonian [6] and the t - J model

[5,7,8]. A simple way to visualize the π -excitation is to think of a spin-triplet pair of electrons sitting on the nearest sites, having the center of mass momentum $(\pi/a, \pi/a)$ and the same relative wavefunction as a d -wave Cooper pair. When the system acquires a long-range superconducting order the d -wave Cooper pairs may be resonantly scattered into the π pairs and this gives rise to the sharp resonance seen in neutron scattering. Motivated by a recent proposal of Scalapino and White [9], we showed that last argument may be enhanced and we argued that it may be energetically favorable for the system to become superconducting, so that the π channel may contribute to the spin fluctuations and the system can lower its antiferromagnetic exchange energy [10]. In this way, the π excitation may be "promoted" from being a consequence of the d -wave superconductivity to being its primary cause. This argument is similar to the argument for the stabilization of the A phase of superfluid helium-3, where spin fluctuations are enhanced in the A phase relative to the B-phase [11]. So the effect of the spin fluctuation feedback may lead to stabilization of the A phase relative to the B base, which would always be favored in weak coupling BCS analysis. The hypothesis of the π excitation being the major driving force of the superconducting transition is supported by comparison of the superconducting condensation energy and the change in the antiferromagnetic exchange energy due to the appearance of the resonance. For optimally doped $\text{YBa}_2\text{Cu}_3\text{O}_7$ the resonance lowers the exchange energy by 18 K per unit cell [10], whereas the condensation energy for this material is 12 K per unit cell [12]. So the resonance by itself is sufficient to account for the superconducting condensation energy. At finite temperature there also seems to be a connection between the resonance intensity and the electronic specific heat, giving another indication of the important role played by the resonance in the thermodynamics of superconducting transition. Another important aspect of the π excitation is that it allows the unification of the spin $SU(2)$ and charge $U(1)$ symmetries into a larger $SO(5)$ symmetry and suggests a new effective low energy Lagrangian for the description of the high T_c cuprates [13]. From the point of view of $SO(5)$ symmetry the π operator is one of the generators of the symmetry and resonances observed in neutron scattering are pseudo-Goldstone bosons of broken symmetry.

Discussion of the π excitation in the state with long range superconducting order has been given within gauge invariant RPA formalism in [7] and from the point of view of $SO(5)$ symmetry in [13]. However an understanding of precursors of this excitation in the normal state of underdoped materials is still lacking. In reference [14] it was pointed out that the most likely origin of these precursors is the existence of strong superconducting fluctuations in the pseudogap regime of underdoped cuprates [15], an assumption phenomenologically supported by correlations between the temperature at which the resonance precursors appear and broadening of the singularity in the electronic specific heat above T_c . In weak coupling precursor of the π resonance have been identified with a process in which a π -pair and a preformed Cooper pair propagate in opposite directions [14] (see Figure 1), however quantitative analysis of such process is very difficult.

In this article we would like to point out that there is an analogue problem to

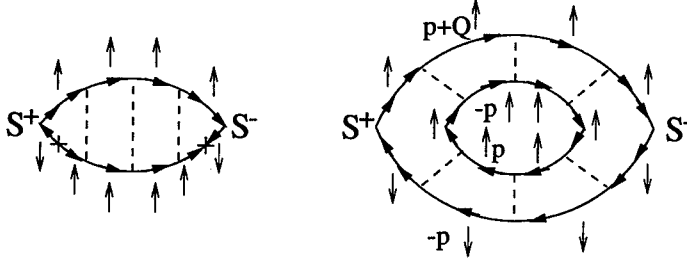


FIGURE 1. Feynmann diagram for the π resonance below T_c contrasted with the diagram above T_c .

the π -excitation, namely η excitation of the negative U Hubbard model [16,17], which allows a detailed study in the strong coupling limit, including the analysis of resonance precursors in a state without long range order. So in the remaining part of this article we will review the η excitation and the pseudospin $SU(2)$ symmetry that it gives rise to [18] and discuss the strong coupling limit of the negative U Hubbard model.

As originally suggested by Yang and Zhang [18] the negative U Hubbard model (we consider $d = 3$ case)

$$\mathcal{H} = -t \sum_{\langle ij \rangle \sigma} c_{i\sigma}^\dagger c_{j\sigma} + U \sum_i (n_{i\uparrow} - \frac{1}{2})(n_{i\downarrow} - \frac{1}{2}) - \mu \sum_{i\sigma} c_{i\sigma}^\dagger c_{i\sigma} \quad (1)$$

at half filling has $SO(4)$ symmetry where in addition to the usual spin $SU(2)$ symmetry the system possesses pseudospin $SU(2)$ symmetry, generated by operators $\eta^\dagger = \sum_p c_{p+Q\uparrow}^\dagger c_{-p\downarrow}^\dagger$, $\eta_0 = \frac{1}{2}(N_e - N)$, and $\eta = (\eta^\dagger)^\dagger$, where N_e is the total number of electrons and N is the total number of sites. The η operator that was introduced is similar to the π operator that we discussed earlier in that it acts in the particle-particle channel and has momentum $Q = (\pi/a, \pi/a)$, however it is spin singlet operator and creates pairs of electrons where electrons sitting on the same site. While the $SO(5)$ symmetry of the t - J model is related to the competition between the antiferromagnetic and d-wave superconducting orders in this system, the pseudospin $SU(2)$ symmetry relates CDW and s-wave superconductivity in the negative U Hubbard model. At half filling when $\mu = 0$ the symmetry is exact and there is a degeneracy between the CDW state and state with superconducting order. Away from half-filling the symmetry is explicitly broken and superconducting state is energetically more favorable than the CDW state. The η operator no longer commutes with the Hamiltonian but satisfies $[\mathcal{H}, \eta^\dagger] = -2\mu\eta^\dagger$. Therefore, when it acts on the ground state it creates an exact excited state at the energy of -2μ . In the normal state such η excitation does not contribute to the density fluctuation spectrum, since it is a charge 2 operator, however when the system becomes superconducting and there is a finite probability of converting particles into holes the η resonance appears as a resonance in the density fluctuation spectrum (one

can also think of this as resonant scattering of s-wave Cooper pairs into η pairs). Another way to see how the η channel gets coupled to the density channel below T_c is to notice that there is an exact commutation relation $[\eta^\dagger, \rho_Q] = \Delta$ where $\rho_Q = \sum_{p\sigma} c_{p+Q\sigma} c_{p\sigma}$ is density operator at momentum Q and Δ is a superconducting s-wave order parameter. In the superconducting state the right hand side of this relation acquires an expectation value, so ρ_Q and Δ become conjugate variables and resonant peak in one of them shows up as a resonance in the other [16].

The question that we want to address is what happens if we do not have long range order but only strong superconducting fluctuations. Can they lead to precursors of the η resonance in the density-density correlation function and what is the form of such precursors. The limit that we want to consider is strong coupling limit when $U \gg t$. We perform a particle-hole transformation on a bipartite lattice

$$c_{i\uparrow} \rightarrow c_{i\uparrow} \quad c_{i\downarrow} \rightarrow \begin{cases} c_{i\downarrow}^\dagger, i \in A, \\ -c_{i\downarrow}^\dagger, i \in B \end{cases} \quad (2)$$

where A and B denote two sublattices. This transformation maps the negative U Hubbard model at finite doping (i.e. finite μ) into positive U Hubbard model at half-filling but in the presence of magnetic field along z -axis. Pseudospin $SU(2)$ symmetry goes into the spin $SU(2)$ symmetry and η resonance becomes a Larmor resonance in the transverse spin channel. Particle-hole transformation maps superconducting order parameter into antiferromagnetic order parameter in the x - y plane and a CDW order parameter into antiferromagnetic order parameter in z direction. The advantage of doing such particle-hole transformation is that strong coupling limit of the positive U Hubbard model at half filling is well known. It is the Heisenberg model with the nearest neighbor exchange interaction $J = 4t^2/U$ [19]. So the effective Hamiltonian in strong coupling is

$$\mathcal{H} = J \sum_{\langle ij \rangle} \mathbf{S}_i \mathbf{S}_j + H_z \sum_i S_i^z \quad (3)$$

with $H_z = 2\mu$. At $T = 0$ Heisenberg model in external field will develop a long range antiferromagnetic order in the plane perpendicular to the direction of the applied field (xy plane in our case, which corresponds to the superconducting order in the original negative U model). When this happens, N_\pm get expectation values and we can use the commutation relation $[S_\pm, N_z] = \pm N_\pm$ to show that Larmor resonance, which was originally present in S_\pm channels only, will appear in the N_z - N_z correlation function as well. However we are interested in the regime when we have only finite range antiferromagnetic correlations (although strong) and we want to find possible precursors of the Larmor resonance in the N_z channel.

This effect is conveniently studied by using Schwinger boson representation of the Heisenberg model [19]. On a bipartite lattice one represents spin operators as $S_i^+ = a_i^\dagger b_i$ and $S_i^z = 1/2 (a_i^\dagger a_i - b_i^\dagger b_i)$ on sublattice A , and $S_i^+ = -b_i^\dagger a_i$ and $S_i^z = 1/2 (b_i^\dagger b_i - a_i^\dagger a_i)$ on sublattice B . Provided that constraint $a_i^\dagger a_i + b_i^\dagger b_i = 1$

is satisfied at each site and a and b obey the usual bosonic commutation relation we easily recover the proper commutation relations for spin $SU(2)$ algebra at each site. In terms of a and b operators Hamiltonian (3) can be written as

$$\mathcal{H} = -\frac{J}{2} \sum_{\langle ij \rangle} A_{ij}^\dagger A_{ij} + \frac{H_z}{2} \sum_i (-)^i (a_i^\dagger a_i - b_i^\dagger b_i) + \sum_i \lambda_i (a_i^\dagger a_i + b_i^\dagger b_i - 1) \quad (4)$$

where $A_{ij} = a_i a_j + b_i b_j$ and the last terms enforces the constraint at each site. In the mean field approximation the last Hamiltonian may be diagonalized by quasiparticles $\alpha_{a\mu,k}$ ($a = 1, 2$, $\mu = \pm$, and momentum k runs in the magnetic zone only) with dispersion $\omega_{a\pm,k} = \omega_k \pm H_z/2$, where $\omega_k = \sqrt{\lambda^2 - 4Q^2\gamma_k^2}$ and $\gamma_k = \cos k_x + \cos k_y$. Mean-field parameters λ and Q have to be found from minimizing the free energy $F = \frac{2}{\beta} \sum_{\mu k} \ln \left\{ \sinh \left[\frac{\beta \omega_{\mu,k}}{2} \right] \right\} - 2\lambda N + \frac{4Q^2}{J} N$. In terms of α operators the uniform and staggered spin operators can be written as

$$\begin{aligned} M_+ &= \frac{1}{N} \sum_k \left(\alpha_{1+,k}^\dagger \alpha_{2-,k} - \alpha_{2+,k}^\dagger \alpha_{1-,k} \right) \quad M_z = \frac{1}{N} \sum_{a,k} \left(\alpha_{a+,k}^\dagger \alpha_{a+,k} - \alpha_{a-,k}^\dagger \alpha_{a-,k} \right) \\ N_z &= \frac{1}{N} \sum_{a\mu k} (-)^a \left\{ \cosh(2\theta_k) \alpha_{a\mu,k}^\dagger \alpha_{a\mu,k} + \frac{1}{2} \sinh(2\theta_k) [\alpha_{a\mu,k}^\dagger \alpha_{a\mu,-k}^\dagger + \alpha_{a\mu,k} \alpha_{a\mu,-k}] \right\} \\ N_x &= \frac{1}{N} \sum_{\mu k} \left\{ \cosh(2\theta_k) \alpha_{1\mu,k}^\dagger \alpha_{2\bar{\mu},k} + \frac{1}{2} \sinh(2\theta_k) [\alpha_{1\mu,k}^\dagger \alpha_{2\bar{\mu},-k}^\dagger + \alpha_{1\mu,k} \alpha_{2\bar{\mu},-k}] \right\} \end{aligned} \quad (5)$$

where $\tanh(2\theta_k) = -2Q\gamma_k/\lambda$. From equations (5) we notice that the M_+ operator has the exact energy of H_z due to the fact that the mean-field approximation on Schwinger bosons does not break spin symmetry. The correlation function for N_z is given by

$$\begin{aligned} D(\omega > 0) &= \text{Im} \int dt e^{i\omega t} \theta(t) \langle N_z(t) N_z(0) \rangle \\ &= \frac{1}{N} \sum_k (1 + N(\omega_{+,k}) + N(\omega_{-,k})) \delta(\omega - \omega_{+,k} - \omega_{-,k}) \end{aligned} \quad (6)$$

where $N(\omega) = 1/(e^{\beta\omega} - 1)$. At $T < T_c$, bosons $\alpha_{1-,k=0}$ and $\alpha_{2-,k=0}$ are condensed so there is a δ -function resonance in $D(\omega)$ at frequency $H_z = 2\mu$ with the weight $\sinh^2(2\theta_{k=0}) = \langle N_z^2 \rangle / \langle M_z \rangle$ as dictated by the $SU(2)$ symmetry [18,16,17]. There is also an additional broad peak due to $\alpha_{a-,k \neq 0}$ that starts at energy 2μ and then extends in a frequency range of around T with an integrated weight proportional to $T^{3/2}$. Above the Neel ordering temperature the δ -peak in $D(\omega)$ is absent, however there is a broadened peak at the energy slightly larger than 2μ (the lower energy threshold is given by $\omega_{min} = \omega_{-,k=0} + \omega_{+,k=0} = 2\mu + 2\omega_{-,k=0}$, and $\omega_{-,k=0}$ is small since it vanishes at T_c). The width of this broad feature is T and the total spectral weight is proportional to $T^{3/2} e^{-\omega_{-,k=0}/T}$. As the temperature is lowered and the system approaches Bose condensation at T_c , the energy $\omega_{-,k=0}$ becomes

smaller leading to a smooth increase of the integrated intensity of the peak. So the intensity of the resonance changes continuously across T_c but as may be shown by a detailed analysis there is a jump in the derivative. On Figure 2 we show a sketch of $D(\omega)$ for temperatures below and above T_c .

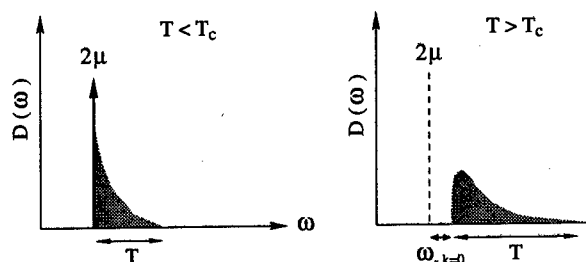


FIGURE 2. Density response function at momentum $Q = (\pi/a, \pi/a)$ for the negative- U Hubbard model in the large U limit. For $T < T_c$ $D(\omega)$ has a δ -peak at $\omega = 2\mu$ (η resonance) and a broad feature starting at the same energy. For $T > T_c$ there is only a broad peak at the energy slightly higher than 2μ .

Before concluding we would like to remark that many features of the precursors of the η excitations that we discussed here, such as temperature dependent shift to higher energies and considerable broadening are likely to be present for the π -excitation of the t - J model as well. INS on underdoped $YBa_2Cu_3O_{6+\delta}$ reveals considerable broadening of the resonance above T_c , however the current accuracy of experiments does not allow to see any changes in the energy of the resonance above the superconducting transition.

This work is partially supported by the NSF at ITP (ED) and by the NSF grant DMR-9814289. We acknowledge useful discussions with A. Auerbach and D.J. Scalapino.

REFERENCES

1. H. Mook *et al.*, *Phys. Rev. Lett.* **70**, 3490 (1993); J. Rossat-Mignod *et al.*, *Physica C*, **235** 59 (1994); H. Fong *et al.*, *Phys. Rev. Lett.* **75**, 316 (1995);
2. P. Dai *et al.*, *Phys. Rev. Lett.* **77**, 5425 (1997); H. Fong *et al.*, *Phys. Rev. Lett.* **78**, 713 (1997);
3. H. Mook *et al.*, cond-mat/9811100; H. Fong *et al.*, cond-mat/9902262.
4. N. Bulut and D. Scalapino, *Phys. Rev. B* **53**, 5149 (1996); I. Mazin and V. Yakovenko, *Phys. Rev. Lett.* **75**, 4134 (1995); D.Z. Liu *et al.*, *Phys. Rev. Lett.* **75**, 4130 (1995); F. Onufrieva *et al.*, *Physica (Amsterdam)* **251C**, 348 (1995); G. Blumberg *et al.*, *Phys. Rev. B* **52**, 15741 (1995); Y. Zha *et al.*, *Phys. Rev. B* **54**, 7561 (1996); A.J. Millis and H. Monien, cond-mat/9606008; L. Yin *et al.*, cond-mat/9606139; P.W. Anderson, *J. Phys. Condens. Matter* **8**, 10083 (1996); A. Abrikosov, preprint.
5. E. Demler and S. C. Zhang, *Phys. Rev. Lett.*, **75**:4126, 1995.
6. S. Meixner *et al.*, *Phys. Rev. Lett.* **79**, 4902 (1997).

-
7. E. Demler, H. Kohno and S. C. Zhang, *Phys. Rev. B* **58**, 5719 (1998).
 8. R. Eder, W. Hanke and S. C. Zhang, *Phys. Rev. B* **57**, 13781 (1998).
 9. D. J. Scalapino and S. White, *Phys. Rev. B* **58**, 8222 (1998).
 10. E. Demler and S. C. Zhang, *Nature* **396**, 733 (1998).
 11. P. W. Anderson and W. F. Brinkman, *Phys. Rev. Lett.* **30**, 1108 (1973).
 12. J. Loram *et al*, *Physica C* **171**, 243-256 (1990); J. Loram *et al*, *Journal of Superconductivity* **7**, 243 (1994).
 13. S. C. Zhang, *Science*, **275** 1089-1096 (1997).
 14. Shou-Cheng Zhang, cond-mat/9808309.
 15. S. Doniach and M. Inui, *Phys. Rev. B* **41**, 6668 (1990); V. Emery and S. Kivelson, *Nature* **374**, 434 1995; M. Randeria, *J. Phys. Chem. Solid* **59**, 10 (1998).
 16. S. C. Zhang, *Phys. Rev. Lett.* **65**, 120 (1990).
 17. E. Demler, S. C. Zhang, N. Bulut, and D. J. Scalapino, *Int. Journal of Modern Physics B*, **10**, 2137 (1996)
 18. C. N. Yang and S. C. Zhang, *Mod. Phys. Lett. B* **4**, 759 (1990).
 19. A. Auerbach, Interacting electrons and quantum magnetism, *Springer-Verlag, New York*, (1994)

Local Electronic Structure and High Temperature Superconductivity.

V. J. Emery¹ and S. A. Kivelson²

¹*Dept. of Physics Brookhaven National Laboratory Upton, NY 11973-5000*

²*Dept. of Physics University of California at Los Angeles Los Angeles, CA 90095*

Abstract.

It is argued that a new mechanism and many-body theory of superconductivity are required for doped correlated insulators. Here we review the essential features of and the experimental support for such a theory, in which the physics is driven by the kinetic energy.

I INTRODUCTION

High temperature superconductivity [1] is obtained by adding charge carriers into a highly-correlated antiferromagnetic insulating state. Despite the fact that there is a large "Fermi surface" containing all of the pre-existing holes and the doped holes, [2] it is impossible to understand the behavior of the system and, in particular, the origin of high temperature superconductivity unless the nature of the doped-insulating state is incorporated into the theory. In particular, the Fermi liquid theory of the normal state and the BCS theory of the superconducting state, which are so successful for conventional metals, were not designed for doped insulators, and they do not apply to the high temperature superconductors. (Section II.) Consequently it is necessary to develop a new mechanism and many-body theory of high temperature superconductivity.

In our view, the physics of the insulator and the doped insulator, including antiferromagnetism and superconductivity, is driven by a lowering of the zero-point kinetic energy. [3] This is well known for the antiferromagnetic state but, in addition, the motion of a single hole in an antiferromagnet is frustrated because it stirs up the spins and creates strings of ferromagnetic bonds. Consequently, a finite density of holes forms self-organized structures, designed to lower the zero-point kinetic energy. This is accomplished in three stages: a) the formation of charge inhomogeneity (stripes), b) the creation of local spin pairs, and c) the establishment of a phase-coherent high-temperature superconducting state. The zero-point kinetic

energy is lowered along a stripe in the first stage, and perpendicular to the stripe in the second and third stages.

Static or dynamical charge inhomogeneity, [4-8] or "topological doping" [9] is quite common for doped correlated insulators. In d dimensions, the charge forms one-dimensional arrays of $(d-1)$ -dimensional structures that are also antiphase domain walls for the background spins. In $d = 1$ there is an array of charge solitons, [10] whereas, in $d = 2$, there are linear "rivers of charge" (stripes) threading through the antiferromagnetic background. [5-7] In $d = 3$ there are arrays of charged planes [7,8], as observed in the manganates. [11] These self-organized structures, which may be fluctuating or form ordered or glass phases, are a consequence of the tendency of the correlated antiferromagnet to expel the doped holes, and they lead to a lowering of the zero-point kinetic energy. The theoretical arguments that lead to this picture will be summarized in Sec. III.

It is clear that any new many-body theory must be based on the local electronic structure and there are strong indications of a link to high temperature superconductivity. First of all, in LSCO and YBCO the value of T_c is inversely proportional to the spacing between stripes in underdoped and optimally doped materials. [12,13] Secondly, μ SR experiments [14,15] have found evidence for a phase in which superconductivity coexists with a cluster spin glass. In $\text{YBa}_2\text{Cu}_3\text{O}_{7-\delta}$, the spin freezing temperature goes to zero when the superconducting T_c is more than 50K. It is difficult to see how these two phases could coexist unless there is a glass of metallic stripes dividing the CuO_2 planes into randomly-coupled antiferromagnetic regions. A new mechanism and many-body theory of superconductivity, based on local charge inhomogeneity has been developed, [16-19] and there is substantial experimental support for the overall picture, as described in subsequent sections.

II BCS MANY-BODY THEORY

There are several reasons why the Fermi liquid theory of the normal state and the BCS theory of the superconducting state do not apply to the high temperature superconductors:

1) In BCS theory, the superfluid density n_s is given by all electrons in the Fermi sea, whereas, in the high temperature superconductors, n_s is proportional to the density of doped holes.

2) The outstanding success of BCS theory stems from the existence of sharp quasiparticles. However, an analysis of the temperature dependence of the resistivity shows that the quasiparticle concept does not apply to many synthetic metals, including the high temperature superconductors. [16,20] This idea is supported by angular resolved photoemission spectroscopy (ARPES) which shows no sign of a normal-state quasiparticle peak near the points $(0, \pm\pi)$ and $(\pm\pi, 0)$ where high temperature superconductivity originates. [21,22]

3) If there are no quasiparticles, there is no Fermi surface in the usual sense of a discontinuity in the occupation number $n_{\mathbf{k}}$ at $T = 0$. This undermines the very

foundation of the BCS mean-field theory, which is a Fermi surface instability.

4) In BCS theory, pairing and phase coherence take place at the same temperature T_c , and a good estimate of T_c is given by $\Delta_0/2$, where Δ_0 is the energy gap measured at zero temperature. However, this criterion does not give a good estimates of T_c for the high temperature superconductors, especially for underdoped materials: $\Delta_0/2T_c$ varies with doping and can be much greater than one. Rather, the value of T_c is determined by the onset of phase coherence [17,19] and is governed by the zero-temperature value of the "phase stiffness", $V_0 \equiv (\hbar c)^2 a / 16\pi (e\lambda(0))^2$, which sets the energy scale for the spatial variation of the superconducting phase. Here $\lambda(T)$ is the penetration depth and a is a microscopic length scale that depends on the dimensionality of the material. [17]

5) A major problem for any mechanism of high temperature superconductivity is how to achieve a high pairing scale in the presence of the repulsive Coulomb interaction, especially in a doped Mott insulator in which there is poor screening. In the high temperature superconductors, the coherence length is no more than a few lattice spacings, so neither retardation nor a long-range attractive interaction is effective in overcoming the bare Coulomb repulsion. Nevertheless ARPES [22] shows that the major component of the gap function is proportional to $\cos k_x - \cos k_y$. It follows that, in real space, the gap function and hence, in BCS theory, the net pairing force, is a maximum for holes separated by one lattice spacing, where the bare Coulomb interaction is very large (~ 0.5 eV, allowing for atomic polarization). It is not easy to find a source of an attraction that is strong enough to overcome the Coulomb force at short distances and achieve a high transition temperature *in a natural way* by the usual Cooper pairing.

Clearly there is a need for a new mechanism and many-body theory to explain high temperature superconductivity.

III TOPOLOGICAL DOPING

It is well known that the motion of a single hole in an antiferromagnet is frustrated by the creation of strings of broken bonds. [23] This idea is supported by ARPES, which found that the bandwidth of a single hole is controlled by the exchange integral J , rather than the hopping amplitude t . [24]

When there is a finite density of holes, the system strives to relieve this frustration and lower its kinetic energy. If the holes were neutral the system would separate into a hole-free antiferromagnetic phase and a hole-rich (magnetically disordered or possibly ferromagnetic) phase, in which the holes are mobile and the cost in exchange energy is less than the gain in kinetic energy. [25-27] In practice the holes are charged, but macroscopic phase separation can take place whenever the dopants are mobile, as in oxygen-doped and photo-doped materials. We have reviewed the experimental evidence for this behavior elsewhere. [28,5] More recent experiments exploring oxygen doping in detail have been carried out by Wells *et al.* [29]

When the dopants are immobile, charged holes can do no more than phase separate locally, by forming arrays of linear metallic stripes [5–7] which are “topological” in nature, since they are antiphase domain walls for the antiferromagnetic background spins. [9,30] This structure lowers the kinetic energy along the stripe but makes it more difficult, if anything, for a *single* hole to move perpendicular to the stripe direction. A hop transverse to a stripe takes the hole far above Fermi energy. [18] However, as we shall see, *pairs of holes* can move more easily transverse to a stripe, and they lower their kinetic energy first by forming spin pairs and, at a lower temperature, by making the system a high temperature superconductor.

It has been argued that charge stripes are energetically impossible because the driving energies are unable to overcome the Coulomb repulsion. [31] However, charge modulation is *inevitable* if the short-range interactions give a negative compressibility, κ , as they do between the spinodals of a system that, otherwise, would undergo phase separation. A general expression for the Debye screening length is $\lambda_D = \sqrt{\epsilon/4\pi e^2 n^2 \kappa}$, where ϵ is the dielectric constant, e is the charge and n is the density. When $\kappa < 0$, λ_D is imaginary, which indicates that the ground state is unstable to a density modulation. [32,33] Of course it requires a more detailed microscopic calculation to obtain the physical length scale.

The existence of charge and spin stripes in the $\text{La}_{2-x}\text{Sr}_x\text{CuO}_4$ family was established in an elegant series of experiments on $\text{La}_{1.6-x}\text{Nd}_{0.4}\text{Sr}_x\text{CuO}_4$ by Tranquada and co-workers. [34] In a Landau theory of the phase transition, [30] the spin order parameter $\vec{S}_{\vec{q}}$ and the charge order parameter $\rho_{-\vec{Q}}$ first couple in third order ($\vec{S}_{\vec{q}} \cdot \vec{S}_{\vec{q}} \rho_{-\vec{Q}}$), so the ordering vectors must satisfy $\vec{Q} = 2\vec{q}$ or, in other words, the wavelength of the spin modulation is twice that of the charge modulation. This relation is found to be satisfied experimentally, [34] and it implies that the charge stripes also form antiphase domain walls in the magnetic order, which gives the precise meaning of the concept of topological doping. [9] The observation of essentially ordered stripes allowed a study of the evolution of the spin and charge order parameters, which not only provided input into the mechanism of stripe formation by showing that they are charge driven, but also established that *inelastic incommensurate magnetic* peaks observed previously [35] in $\text{La}_{2-x}\text{Sr}_x\text{CuO}_4$ were produced by fluctuating stripes. Recently, inelastic incommensurate magnetic peaks have been observed in underdoped $\text{YBa}_2\text{Cu}_3\text{O}_{7-\delta}$ by neutron scattering experiments, [36] thereby establishing that $\text{YBa}_2\text{Cu}_3\text{O}_{7-\delta}$ and the $\text{La}_{2-x}\text{Sr}_x\text{CuO}_4$ family have a common spin structure.

By now, the prediction of metallic stripes [5,6] has been confirmed in all families of materials in which extensive neutron scattering experiments have been performed (LSCO and YBCO). There is growing evidence of similar behavior in $\text{Bi}_2\text{Sr}_2\text{CaCu}_2\text{O}_{8+\delta}$: preliminary neutron scattering experiments show incommensurate magnetic peaks, and there is ARPES evidence [37] of spectral weight transfer associated with stripes. Also, a calculation of the effects of stripes in ARPES experiments [38] produced regions of degenerate states and a flat section of the “Fermi surface” near $(0, \pm\pi)$ and $(\pm\pi, 0)$, as observed experimentally. [39,40,21]

IV SPIN PAIRING

The existence of a cluster spin-glass state for a substantial range of doping in the high temperature superconductors [14,15] implies that the stripe dynamics is slow and that the motion of holes along the stripe is much faster than the fluctuation dynamics of the stripe itself. Thus an individual stripe may be regarded as a finite piece of one-dimensional electron gas (1DEG) located in an active environment of the undoped spin regions between the stripes. Then it is appropriate to start out with a discussion of an extended 1DEG in which the singlet pair operator P^\dagger may be written

$$P^\dagger = \psi_{1\uparrow}^\dagger \psi_{2\downarrow}^\dagger - \psi_{1\downarrow}^\dagger \psi_{2\uparrow}^\dagger, \quad (1)$$

where $\psi_{i,\sigma}^\dagger$ creates a right-going ($i = 1$) or left-going ($i = 2$) fermion with spin σ . In one dimension, the fermion operators of a 1DEG may be expressed in terms of Bose fields and their conjugate momenta $(\phi_c(x), \pi_c(x))$ and $(\phi_s(x), \pi_s(x))$ corresponding to the charge and spin collective modes respectively. In particular, the pair operator P^\dagger becomes [10]

$$P^\dagger \sim e^{i\sqrt{2\pi}\theta_c} \cos(\sqrt{2\pi}\phi_s), \quad (2)$$

where $\partial_x \theta_c \equiv \pi_c$. In other words, there is an *operator* relation in which the amplitude of the pairing operator depends on the spin fields only and the (superconducting) phase is a property of the charge degrees of freedom. Now, if the system acquires a spin gap, the amplitude $\cos(\sqrt{2\pi}\phi_s)$ acquires a finite expectation value, and superconductivity will appear when the charge degrees of freedom become phase coherent. Clearly, in one dimension, the temperature at which the spin gap forms is generically distinct from the phase ordering temperature because phase order is destroyed by quantum fluctuations, even at zero temperature. [10]

We emphasize that we are *not* dealing with a *simple* 1DEG, for which a spin gap occurs only if there is an attractive interaction in the the spin degrees of freedom. [10] The 1DEG on the stripe is in contact with an active (spin) environment, and we have shown that pair hopping between the 1DEG and the environment will generate a spin gap in both the stripe and the environment, even for purely repulsive interactions. [18] The same mechanism gives rise to spin gaps in spin ladders. Also, although the theory was worked out for an *infinite* 1DEG in an active environment, it is known from numerical calculations on finite-size systems that the conclusions are correct for any property that has a length scale small compared to the size of the system. Here, we use the theory only to establish the existence of a spin gap, which corresponds to a length scale of a few lattice spacings. Once a spin gap has been formed, the problem is reduced to the physics of the superconducting phase and its quantum conjugate (the number density), and high temperature superconductivity emerges when phase order is established. [16,17,19]

Experimentally the formation of an amplitude of the order parameter is indicated by a peak in $(T_1 T)^{-1}$ (where T_1 is the spin-lattice relaxation rate), [41] and by

ARPES, [42] both of which are consistent with spin pairing. A drop in the specific heat [43] and a pseudogap in the c -axis optical conductivity, [44] both of which indicate that the charge is involved, occur at a higher temperature in underdoped materials, and are symptoms of the onset of stripe correlations. [18]

V PHASE COHERENCE

High temperature superconductivity is established when there is coherent motion of a pair from stripe to stripe. [18] This final step in the reduction of the zero-point kinetic energy is equivalent to establishing phase order, and it determines the value of T_c , especially in underdoped and optimally doped materials. [16,17,19]

It is sometimes argued that thermal phase fluctuations are excluded because the Coulomb interaction moves them up to the plasma frequency, ω_p , via the Anderson-Higgs mechanism. This argument, if correct, also would imply that critical phenomena near to T_c cannot display 3d-XY behavior. An explicit calculation shows why this objection is incorrect. The Fourier transform of the Lagrangian density in the long wavelength limit has the form [16,45]

$$\mathcal{L}(\vec{k}, \omega) = \frac{1}{2} \vec{k}^2 a^2 [V_0(\omega) + V_1 \omega^2 \epsilon(\omega)] \theta^2(\vec{k}, \omega) \quad (3)$$

where $\epsilon(\omega)$ is the dielectric function at $\vec{k} = 0$, $V_1 = \hbar^2 a / 16 \pi e^2$, and $V_0(0) \equiv V_0$ is the classical phase stiffness, defined above. At high frequency

$$\epsilon(\omega) = \epsilon_\infty - \frac{\omega_p^2}{\omega^2}. \quad (4)$$

Note that $V_0(\omega)$ vanishes at high frequency and, in general, it does not contribute to the plasma frequency. Then phase fluctuations occur at a frequency $\omega_p / \sqrt{\epsilon_\infty}$. At the same time, for $\omega = 0$, the Lagrangian has the form $\mathcal{L} = \text{const.} \vec{k}^2$, as required for classical phase fluctuations. In general, it is necessary to do a renormalization group calculation to obtain the zero-frequency limit, and we have shown that, for sufficiently good screening (large dielectric function), the behavior of the system is given by the classical (V_0) part of the Lagrangian. [16] The unusual form of the Lagrangian stems from the use of the dual phase-number representation, in which the V_0 term represents the kinetic energy (pair hopping) and the V_1 term is the potential energy (Coulomb interaction).

We have solved the following model of classical phase fluctuations [17,19]:

$$H = -J_\parallel \sum_{\langle ij \rangle_\parallel} \{ \cos(\theta_{ij}) + \delta \cos(2\theta_{ij}) \} - \sum_{\langle kl \rangle_\perp} \{ J_\perp^{kl} \cos(\theta_{kl}) \}, \quad (5)$$

where the first sum is over nearest neighbor sites within each plane, and the second sum is over nearest neighboring planes. The values of the constants J_\parallel and δ are taken to be isotropic within each plane and the same for every plane. The coupling

between planes, J_{\perp}^{kl} , is different for crystallographically distinct pairs of neighboring planes.

The results of this final stage of the calculation are in good agreement with experiment. For a reasonable range of parameter values (as constrained by the magnitudes of the penetration depths in different directions) the model gives a good estimate of T_c and its evolution with doping. It also explains [19] the temperature dependence of the superfluid density, obtained for a range of doping by microwave measurements. [46]

The phase diagram itself is consistent with this picture. The physics evolves in three stages. Above the superconducting transition temperature there are two crossovers, which are quite well separated in at least some underdoped materials. The upper crossover is indicated by the onset of short-range magnetic correlations and by the appearance of a pseudogap [44] in the c -axis optical conductivity (perpendicular to the CuO_2 planes) which might possibly indicate the establishment of a stripe glass phase. The lower crossover is where a spin gap or pseudogap (which is essentially the amplitude of the superconducting order parameter) is formed. Finally, superconducting phase order is established at T_c and, in fact, determines the value of T_c . [17,19]

Acknowledgements: We acknowledge frequent discussions with J. M. Tranquada. This work was supported at UCLA by the National Science Foundation grant number DMR93-12606 and, at Brookhaven, by the Division of Materials Sciences, U. S. Department of Energy under contract No. DE-AC02-98CH10886.

REFERENCES

1. J. G. Bednorz and K. A. Müller, *Z. Phys. B* **64**, 189 (1986).
2. Z.-X. Shen *et al.*, *Science* **267**, 343 (1995).
3. For a perspective on the circumstances in which physics is driven by the kinetic energy see P. W. Anderson, *Adv. in Phys.* **46**, 3 (1997).
4. J. Zaanen and O. Gunnarson, *Phys. Rev. B* **40**, 7391 (1989); H. Schultz, *Phys. Rev. Lett.* **64**, 1445 (1990).
5. S. A. Kivelson and V. J. Emery in *Strongly Correlated Electronic Materials: The Los Alamos Symposium 1993*, edited by K.S. Bedell, Z. Wang, D.E. Meltzer, A.V. Balatsky, and E. Abrahams, (Addison-Wesley, Reading, Massachusetts, 1994) p. 619.
6. U. Löw, V. J. Emery, K. Fabricius, and S. A. Kivelson, *Phys. Rev. Lett.* **72**, 1918 (1994).
7. L. Chayes, V. J. Emery, S. A. Kivelson, Z. Nussinov, and J. Tarjus, *Physica A* **225**, 129 (1996).
8. E. W. Carlson, S. A. Kivelson, Z. Nussinov, and V. J. Emery, *Phys. Rev. B* **57**, 14704 (1998).
9. S. A. Kivelson and V. J. Emery, *Synth. Met.* **80**, 151 (1996).
10. V. J. Emery in *Highly Conducting One-Dimensional Solids*, edited by J. T. Devreese, R. P. Evrard, and V. E. van Doren, (Plenum, New York, 1979) p. 327; J. Solyom, *Adv. Phys.* **28**, 201.

11. S. Mori, C. H. Chen, and S. W. Cheong, *Nature* **392**, 473 (1998).
12. K. Yamada *et al.* Phys. Rev. B **57**, 6165 (1998).
13. A. V. Balatsky and P. Bourges, preprint; cond-mat/9901294.
14. A. Weidinger *et al.* Phys. Rev. Lett. **62**, 102 (1989).
15. Ch. Niedermayer *et al.* Phys. Rev. Lett. **80**, 3843 (1998) and this conference.
16. V. J. Emery and S. A. Kivelson, Phys. Rev. Lett. **74**, 3253 (1995).
17. V. J. Emery and S. A. Kivelson, *Nature* **374**, 4347 (1995).
18. V. J. Emery, S. A. Kivelson, and O. Zachar, Phys. Rev. B **56**, 6120 (1997).
19. E. W. Carlson, S. A. Kivelson, V. J. Emery, and E. Manousakis, to be published.
20. V. J. Emery, S. A. Kivelson, and V. N. Muthukumar, preprint; cond-mat/9901270
21. M. R. Norman, this conference.
22. Z.-X. Shen *et al.*, Phys. Rev. Lett. **70**, 1553 (1993); H. Ding *et al.* Phys. Rev. B **54**, R9678 (1996).
23. L. N. Bulaevskii and D. I. Khomskii, Zh. Eksp. Teor. Fiz. **52**, 1603 (1967) [Sov. Phys. JETP **25**, 1067 (1967)]; Fiz. Tverd. Tela **9**, 3070 (1967) [Sov. Phys. Solid State **9**, 2422 (1968)]; W. Brinkman and T. M. Rice, Phys. Rev. B **2**, 1324 (1970).
24. B. O. Wells *et al.*, Phys. Rev. Lett. **74**, 964 (1995).
25. V. J. Emery, S. A. Kivelson, and H.-Q. Lin, Physica B **163**, 306 (1990); Phys. Rev. Lett. **64**, 475 (1990).
26. M. Marder, N. Papanicolaou, and G. C. Psaltakis, Phys. Rev. B **41** 6920 (1990).
27. S. Hellberg and E. Manousakis, Phys. Rev. Lett. **78**, 4609 (1997).
28. V. J. Emery and S. A. Kivelson, Physica C **209**, 597 (1993).
29. B. O. Wells *et al.*, *Science* **277**, 1067 (1997).
30. O. Zachar, S. A. Kivelson, and V. J. Emery Phys. Rev. B **57**, 1422 (1998).
31. J. C. Phillips, this conference.
32. V. J. Emery and S. A. Kivelson in *Recent developments in High Temperature superconductivity* Edited by J. Klamut *et al.*, (Springer-Verlag, Berlin, Heidelberg, New York, 1996), p. 265.
33. See also A. H. Castro Neto, Phys. Rev. B **51**, 3254 (1995).
34. J. M. Tranquada *et al.*, *Nature* **375**, 561 (1995).
35. S.-W. Cheong, *et al.*, Phys. Rev. Lett. **67**, 1791-1794 (1991); T.E. Mason, *et al.*, Phys. Rev. Lett. **68**, 1414-1417 (1992); T. R. Thurston, *et al.*, Phys. Rev. B **46**, 9128-9131 (1992); K. Yamada *et al.* Phys. Rev. Lett. **75**, 1626 (1995).
36. H. A. Mook *et al.*, *Nature* **395**, 580 (1998) and this conference.
37. Z.-X. Shen *et al.*, *Science*, **280**, 259 (1998).
38. M. Salkola, V. J. Emery, and S. A. Kivelson, Phys. Rev. Lett. **77**, 155 (1996).
39. D. S. Dessau *et al.*, Phys. Rev. Lett. **71**, 2781 (1993).
40. H. Ding *et al.*, Phys. Rev. Lett. **78**, 2628 (1997).
41. M.-H. Julien *et al.*, Phys. Rev. Lett. **76**, 4238 (1996).
42. A. G. Loeser *et al.*, *Science* **273**, 325 (1996). H. Ding *et al.*, *Nature* **382**, 51 (1996).
43. J. R. Cooper and J. Loram, J. Phys. I **6**, 2237 (1996).
44. C. C. Homes *et al.*, Phys. Rev. Lett. **71**, 1645 (1993).
45. K. H. Wagenblast *et al.*, Phys. Rev. Lett. **79**, 2730 (1997).
46. W. N. Hardy, *et al.* in *Proceedings of the 10th Anniversary HTS Workshop*, edited by B. Batlogg *et al.*, (World Scientific, Singapore (1996) p. 223.

Metallic stripes in doped Hubbard model

Marcus Fleck,^{*} Alexander I. Lichtenstein,[†] and Andrzej M. Oleś^{*,‡}

^{*}Max-Planck-Institut FKF, Heisenbergstrasse 1, D-70569 Stuttgart, Germany

[†]Forschungszentrum Jülich, D-52425 Jülich, Germany

[‡]Institute of Physics, Jagellonian University, Reymonta 4, PL-30059 Kraków, Poland

Abstract. We report new types of metallic stripes with ferromagnetic order along the domain walls for the two-dimensional Hubbard model using the dynamical mean-field theory. The (1,0) stripes have the observed filling close to one doped hole per two atoms, while the (1,1) stripes are more extended. The stripe structures are stable at low temperatures $T < 70\text{K}$, and change into spin spirals at higher temperatures.

Localized holes organize into one-dimensional structures called stripes, which form commensurate patterns, as discovered in $\text{La}_{1.48}\text{Nd}_{0.4}\text{Sr}_{0.12}\text{CuO}_4$ [1]. The stripe phase has been predicted theoretically in several numerical studies within: the Hartree-Fock (HF) approximation [2–4], the Gutzwiller ansatz (GA) [5], and the density matrix renormalization group (DMRG) [6]. The observed antiferromagnetic (AF) domains [1] separated by domain walls filled by *one hole per two* 4×1 domain wall unit cells, so called *half-filled stripes* [4], are only locally stable in the HF studies, but become global minima when electron correlations are included either in the DMRG [6], or within the GA [5]. We will show that, in contrast to the static approaches [4], the stripes are *metallic* using a *local selfenergy* [7], found self-consistently within the dynamical mean-field theory (DMFT) [8]. Thereby we generalize our previous study of spin spirals [9] to the stripe phase.

We consider the two-dimensional (2D) Hubbard model on a square lattice,

$$H = - \sum_{mi,nj,\sigma} t_{mi,nj} a_{mi\sigma}^\dagger a_{nj\sigma} + U \sum_{mi} n_{mi\uparrow} n_{mi\downarrow}, \quad (1)$$

where the pair of indices $\{mi\}$ labels the unit cell m and the position $\mathbf{R}_m + \mathbf{r}_i$ of atom $i = 1, \dots, L$ within the unit cell. Effective parameters for the single band model of the cuprates (1) include hopping integrals between first-, second- and third-nearest neighbors, $t_{mi,nj} = t$, t' , and t'' , respectively [10]. The one-particle Green function in the stripe phase is given by a $(L \times L)$ matrix $G_{ij\sigma}(\mathbf{k}, i\omega_\nu)$, where ω_ν are fermionic Matsubara frequencies. Using a *local cell selfenergy* [8,9] we write,

$$G_{ij\sigma}^{-1}(\mathbf{k}, i\omega_\nu) = (i\omega_\nu + \mu)\delta_{ij} - \varepsilon_{ij\sigma}^{\text{HF}}(\mathbf{k}) - \Sigma_{ii\sigma}^{\text{SF}}(i\omega_\nu)\delta_{ij}. \quad (2)$$

Here $\varepsilon_{ij\sigma}^{\text{HF}}(\mathbf{k})$ is a $(L \times L)$ matrix which describes the kinetic energy and the self-consistent local HF potential, $U\langle n_{0i\bar{\sigma}} \rangle$ ($\bar{\sigma} = -\sigma$). The local Green function for each nonequivalent atom i is therefore calculated from the diagonal elements of the Green function matrix as given in Eq. (2), $G_{ii\sigma}(i\omega_\nu) = N_k^{-1} \sum_{\mathbf{k}} G_{ii\sigma}(\mathbf{k}, i\omega_\nu)$, and the spin-fluctuation (SF) part of the cell selfenergy ($\beta = 1/k_B T$),

$$\Sigma_{ii\sigma}^{\text{SF}}(i\omega_\nu) = \bar{U}_{ii}^2 \beta^{-1} \sum_{\mu} \left[\chi_{ii\bar{\sigma}\sigma}(i\omega_\mu) \mathcal{G}_{ii\bar{\sigma}}^0(i\omega_\nu - i\omega_\mu) + \chi_{ii\bar{\sigma}\bar{\sigma}}(i\omega_\mu) \mathcal{G}_{ii\sigma}^0(i\omega_\nu - i\omega_\mu) \right], \quad (3)$$

where ω_μ are bosonic Matsubara frequencies. The transverse, $\chi_{ii\bar{\sigma}\sigma}(i\omega_\mu)$, and longitudinal, $\chi_{ii\sigma\sigma}^{(0)}(i\omega_\mu)$, susceptibility in Eq. (3) are found in random phase approximation with renormalized interaction, $\bar{U}_{ii} = U/[1 + U\chi_{ii}^{pp}(0)]$ [9], with $\chi_{ii}^{pp}(0)$ standing for the scattering kernel. Finally, using the *cavity method* we write [8],

$$\mathcal{G}_{ii\sigma}^0(i\omega_\nu)^{-1} = G_{ii\sigma}(i\omega_\nu)^{-1} + \Sigma_{ii\sigma}^{\text{SF}}(i\omega_\nu). \quad (4)$$

Eqs. (2), (3), and (4) represent a solution for the one-particle Green functions within the DMFT. By solving them self-consistently at fixed hole densities δ , stripe phases have been found in the physically interesting regime of $8 \leq U/t \leq 12$ at low temperature, $T = 0.015t$. One finds a competition between the vertical (1,0) and diagonal (1,1) stripes (Fig. 1), with a crossover value at $U/t \simeq 11$, about twice larger than the respective HF value [2,4].

We find patches of close to half-filled vertical (1,0) domain-walls, using the effective single band model for $\text{La}_{2-x}\text{Sr}_x\text{CuO}_4$ [10] [Fig. 1(a)]. One might expect that they condense at low temperature to a connected hole-rich string, consisting of doped 3-leg ladders [4,6] and isolated half-filled AF-chains, while at higher temperatures strong fluctuations between different structures with similar energies are expected. Unlike in the HF calculations [4], the atoms at the domain-walls form a ferromagnetic (FM) chain, showing that FM polarons might also contribute to the stability of *static domain-walls*.

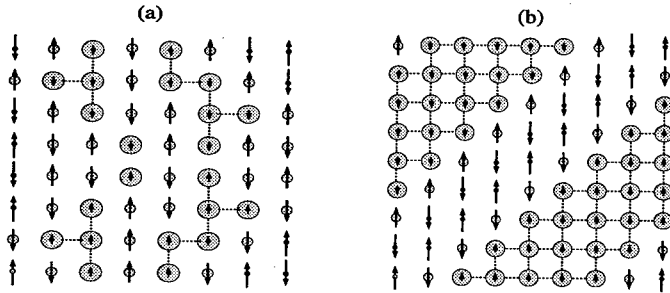


FIGURE 1. Stripe phases obtained for the Hubbard model at $T = 0.015t$ for: (a) $U = 10t$, $t' = -0.11t$, $t'' = 0.04t$, and $\delta = 1/8$; (b) $U = 12t$, $t' = -0.28t$, $t'' = 0.18t$, and $\delta = 1/10$. The diameter of the grey circles (length of arrows) is proportional to the doped hole density $1 - \langle n_{i\uparrow} + n_{i\downarrow} \rangle$ (magnetization $\langle n_{i\uparrow} - n_{i\downarrow} \rangle$). Dashed bonds indicate domain walls.

In contrast, extended (1,1) stripes were obtained for the parameters of $\text{YBa}_2\text{Cu}_3\text{O}_{6+x}$ [10] [Fig. 1(b)]. The FM walls extending over five neighboring atoms separate nearly undoped AF domains. The doped holes gain kinetic energy due to their delocalization along the FM (1,1) walls, while the magnetic energy is gained in the AF domains. Such a state is particularly favored at increased values of the extended hopping parameters, t' and t'' , which enhance FM correlations.

The charge and magnetic correlations in the stripe phases lead to characteristic maxima in the respective structure functions [4],

$$n_h(\mathbf{q}) = \frac{1}{N} \sum_{i_x, i_y} e^{-i(q_x i_x + q_y i_y)} \langle 1 - n_{(0,0)} \rangle \langle 1 - n_{(i_x, i_y)} \rangle, \quad (5)$$

$$S^z(\mathbf{q}) = \frac{1}{N} \sum_{i_x, i_y} e^{-i(q_x i_x + q_y i_y)} \langle S_{(0,0)}^z \rangle \langle S_{(i_x, i_y)}^z \rangle, \quad (6)$$

where $\langle 1 - n_i \rangle$ is doped hole density at site $i = (i_x, i_y)$, and $\langle S_i^z \rangle = \frac{1}{2} \langle n_{i\uparrow} - n_{i\downarrow} \rangle$. One finds that additional maxima develop in $S^z(\mathbf{q})$ around the (π, π) point, displaced either along the (1,0) and (0,1) directions in the (1,0) stripe phase [Fig. 2(a)], or along the (1,1) and $(\bar{1}, 1)$ directions in the (1,1) stripe phase [Fig. 2(b)], respectively. The AF maximum survives at the (π, π) point, but we expect it to loose intensity in the presence of a pinning potential, as realized in $\text{La}_{1.48}\text{Nd}_{0.4}\text{Sr}_{0.12}\text{CuO}_4$ [1]. We believe that the observed structures in neutron scattering experiments might correspond to strongly fluctuating stripes with nonmagnetic domain walls [4].

Finally we discuss the spectral properties using the total density of states, $N(\omega) = -\frac{1}{\pi} \langle \text{Im} G_{ii\sigma}(i\omega_\nu \rightarrow \omega + i0^+) \rangle$, obtained by averaging of local densities of states over the nonequivalent atoms within the unit cell. As for spin spirals [9], it is dominated by two maxima which correspond to the Hubbard subbands, separated by a large gap (Fig. 3). The Fermi energy falls within a *pseudogap* which

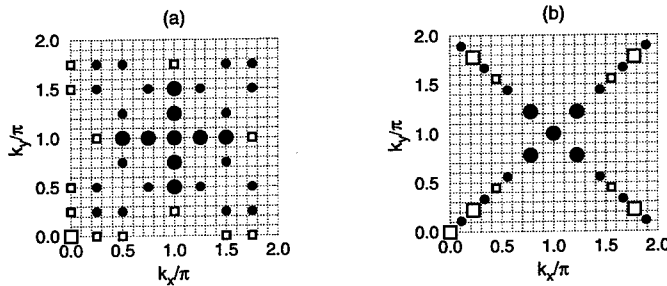


FIGURE 2. Hole-hole $n_h(\mathbf{q})$ (5) (open squares) and spin-spin $S^z(\mathbf{q})$ (6) (filled circles) correlation functions averaged over two equivalent directions, as obtained for the stripe phases of Fig. 1 for the same parameters. Relative intensities of $S^z(\mathbf{q})$ ($n_h(\mathbf{q})$) are proportional to the used symbol size, but the intensity of $n_h(\mathbf{q})$ is smaller by roughly one order of magnitude.

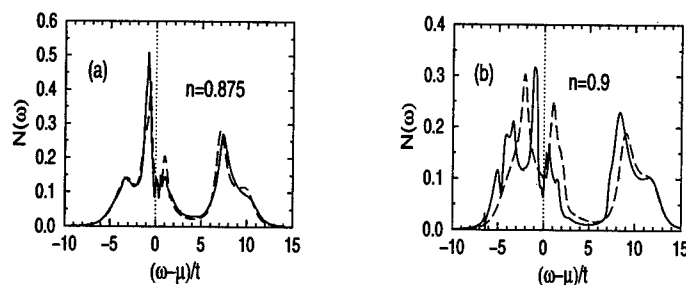


FIGURE 3. (a) Density of states $N(\omega)$ for the parameters of Fig. 1: (a) – (1,0) stripes, and (b) – (1,1) stripes. Solid and dashed lines refer to $T = 0.015t$ (stripes) and $T = 0.05t$ (spin spirals).

results from the magnetic order and demonstrates the *metallic* nature of the present stripes. We note that homogeneous spin spiral phase takes over at intermediate temperatures [9], $T \simeq 0.05t$, which explains why the stripe structures are so difficult to detect in the Monte-Carlo calculations. Such spin spirals are characterized by an increased pseudogap, and by coherent quasiparticles at larger binding energy.

In summary, we obtained new (1,0) and (1,1) metallic stripes which agree qualitatively with the experimental observations for La- and Y-based cuprates [1,11]. The large Mott-Hubbard gap accompanied by a pseudogap are found to be generic features of doped Mott-Hubbard insulators [9]. The present approach explains the stability of half-filled stripes in $\text{La}_{2-x}\text{Sr}_x\text{CuO}_4$ and makes a specific prediction of (1,1) extended stripes in the doped $\text{YBa}_2\text{Cu}_3\text{O}_{6+x}$ compounds [11]. Experimental verification is needed as we expect the latter structures to compete with the (1,0) stripes stabilized by the coupling to the lattice.

We thank J. Zaanen, O. K. Andersen, L. Hedin, and V. J. Emery for valuable discussions. AMO acknowledges the support by the Committee of Scientific Research (KBN) of Poland, Project No. 2 P03B 175 14.

REFERENCES

1. J. M. Tranquada *et al.*, Phys. Rev. Lett. **78**, 338 (1997).
2. J. Zaanen and O. Gunnarsson, Phys. Rev. B **40**, 7391 (1989).
3. D. Poilblanc and T. M. Rice, Phys. Rev. B **39**, 9749 (1989).
4. J. Zaanen and A. M. Oleś, Ann. Phys. (Leipzig) **6**, 224 (1996).
5. G. Seibold *et al.*, Phys. Rev. B **58**, 13 506 (1998).
6. S. R. White and D. J. Scalapino, Phys. Rev. Lett. **80**, 1272 (1998).
7. W. Metzner and D. Vollhardt, Phys. Rev. Lett. **62**, 324 (1989).
8. A. Georges *et al.*, Rev. Mod. Phys. **68**, 13 (1996).
9. M. Fleck *et al.*, Phys. Rev. Lett. **80**, 2393 (1998).
10. O. K. Andersen *et al.*, J. Phys. Chem. Solids **56**, 1573 (1995).
11. P. Dai, H. A. Mook, and F. Doğan, Phys. Rev. Lett. **80**, 1738 (1998).

Orbital Occupancy and Atom Charge States in $\text{RBa}_2\text{Cu}_3\text{O}_x$ High-temperature Superconductors

V. E. Gusakov

Institute of Solid State and Semiconductor Physics, P. Brovki 17, Minsk 220072, Belarus

Abstract. The distribution of charge states of all atoms in the unit cell of $\text{RBa}_2\text{Cu}_3\text{O}_x$; $x=6.7$ ($R = \text{Yb, Er, Ho, Y, Gd, Eu, Sm, Nd, Pr}$) is determined on the basis of comparison of the theoretical calculated electric field gradient tensor and existing experimental data. The variation of the charge states of the atoms as a function of the ionic radius is analyzed.

1. INTRODUCTION

The explanation of charge state attained by atoms in high-temperature (high- T_c) superconductors and the study of how the charge states change with variation of the composition are of fundamental value for analyzing the mechanism of high- T_c superconductivity. Detailed information on the distribution of the atomic charge states in the unit cell of a high- T_c superconductor can be obtained by analyzing the electric field gradient (EFG) tensor and the asymmetry parameter of the EFG tensor, both determined by experimental nuclear-quadrupole and magnetic resonance techniques.

In this article I analyze the orbital occupancy and distribution of charge states of all atoms in the unit cell of $\text{RBa}_2\text{Cu}_3\text{O}_x$ ($x=6.7$) on the basis of a calculation of the EFG tensor and a comparison of the calculated values with existing experimental results.

2. ANALYTICAL METHOD

I represent the EFG tensor at the nucleus of a given atom by sum of two terms: the tensors of the EFG generated by the effective charges (Z^*) of all atoms and the EFG generated by electrons localized in atomic orbitals of the given atom. I calculate the contribution from the effective charges Z^* by means of lattice sums [1]. For the EFG generated by electrons localized in atomic orbitals of the given atom the method [2] were used.

I analyze the distribution of charge states in $\text{RBa}_2\text{Cu}_3\text{O}_{7-d}$ as follows. I write the expression for the error function S :

$$S = \sum (\eta_k^{\text{exp}} - \eta_k^{\text{theor}})^2 + W_0 \sum (\Phi_{zz,k}^{\text{exp}} - \Phi_{zz,k}^{\text{theor}})^2,$$

where $\eta = |(F_{xx} - F_{yy})/F_{zz}|$ is the asymmetry parameter of the EFG tensor, $|F_{zz}| > |F_{yy}| > |F_{xx}|$, and W_0 is weighting factor. It follows from fomular that S is a function of the effective charges Z^* and the symmetry factors $N_{p(d)}$. Minimizing S with respect to all Z^* and $N_{p(d)}$, I can determine the distribution of charge states that most reliable describes the experimentally observed asymmetry parameters and principal components of the EFG tensor.

Table I shows the results of determining the effective charges Z^* and factors $N_{p(d)}$ for the system $\text{YBa}_2\text{Cu}_3\text{O}_x$ ($x=7$; $x=6$) after the minimization of S . The structural data and the experimental values of the asymmetry parameter and the principal components of the EFG tensor for $\text{YBa}_2\text{Cu}_3\text{O}_x$ ($x=6,7$) are taken from [3-6].

3. MAIN RESULTS AND DISCUSSION

Now I analyze the distribution of charge states in Table I.

TABLE I. Distribution of charge states in compounds $\text{RBa}_2\text{Cu}_3\text{O}_x$.

	$\text{YBa}_2\text{Cu}_3\text{O}_7$		$\text{YBa}_2\text{Cu}_3\text{O}_6$		$\text{RBa}_2\text{Cu}_3\text{O}_7$	
Atoms	Z^*	$N_{p(d)}$	Z^*	$N_{p(d)}$	dZ^*/dR_{ion}	dN/dR_{ion}
Cu(1)	+1.46	0.1	+0.81	0.06	1.74	3.15
Cu(2)	+2.0	-0.46	+2.0	-0.06	0.85	-3.08
O(2)	-2.01	-	-2.0	-	-0.17	-
O(3)	-2.16	-	-2.0	-	1.02	-
O(1)	-1.74	-1.0	-	-	-0.39	1.56
O(4)	-.067	+0.73	-2.07	0.39	1.0	0.8
Ba	+1.45	-	+2.08	-	-3.16	-
Y	+3.05	-	+3.18	-	-0.13	-

Notes: Z^* is given in unites of e, R_{ion} is in Å; O(4) is an apical atom; Z^* is determined within absolute error limits $\sim 10\%$

The charge state of a copper atom in the Cu(1) position corresponds to a partially filled d shell. Upon transition to the $x=6$ compound, the effective charge decreases, the d shell being completely filled ($3d^{10}$). Consequently, with a decrease in the oxygen index (increase in d) one should observed an increase in the concentration of monovalent copper. This behavior has been observed experimentally in an X-ray spectroscopic study of $\text{YBa}_2\text{Cu}_3\text{O}_{7-d}$ [7], where it has been shown that the concentration of monovalent copper increases upon transition to $\text{YBa}_2\text{Cu}_3\text{O}_6$. The electronic configuration of copper atom in the Cu(2) position is close to $3d^9$

(one hole in the $3d^{10}$ shell). The electronic configuration of Cu(2) remains practically unchanged in transition from $YBa_2Cu_3O_7$ to $YBa_2Cu_3O_6$. Experimental results of an analysis of electron density distribution in $YBa_2Cu_3O_7$ crystals [8] show that the equal-electron density (EED) levels are distributed symmetrically in the neighborhood of the atom Cu(1) and extend along the crystallographic c axis in the neighborhood of the atom Cu(2). The calculated filling of the $d_{x^2-y^2}$ and d_{z^2} orbitals is in perfect agreement with the experimental results [8]. Indeed, the orbital filling factor $N_d[Cu(1)]$ is close to zero, indicating symmetric filling of the $d_{x^2-y^2}$ and d_{z^2} orbitals. The factor $N_d[Cu(2)]$ is negative, hence the hole is localized predominantly in the d_{z^2} orbital. The hole is distributed as follows: $n(d_{x^2-y^2})=0.265$; $n(d_{z^2})=0.735$. The filling of these orbitals changes upon transition from $YBa_2Cu_3O_7$ to $YBa_2Cu_3O_6$, so that $n(d_{z^2})=n(d_{x^2-y^2})\simeq 0.5$. The charge states of oxygen atoms in the O(2), O(3), and O(1) position are close to their ordinary values O^{-2} and scarcely change in transition from $x=7$ to $x=6$. In the compound $YBa_2Cu_3O_7$ the magnitude and sign of the factor N_p for the atom O(1) suggest that it plays a significant role in the binding of the p_x and p_y orbitals. The charge state of an oxygen atom in the O(4) position undergoes the most pronounced change in transition from the superconducting to the nonsuperconducting state. The effective charge changes from -0.67 to -2. The magnitude and sign of the factor $N_p[O(4)]$ in the compound $YBa_2Cu_3O_7$ indicates that p_x and p_y orbitals, i.e., atomic orbitals situated in the plane of barium atoms, participate in the charge transfer. Here the EED levels must extend over the xy plane, consistent with the experimentally observed electron distribution [8]. The possibility of a partial covalent bond between oxygen atoms in the O(4) position and barium atoms can be assumed in the given situation. This possibility is further supported by the decrease in the effective charge of the Ba atom from +2.0 to +1.45. I call attention to the fact that the degree of oxidation of barium is lowered with an increase in the oxygen content, as has been observed experimentally [10] in an analysis of photoelectron spectra. I note that metals of this type tend to form peroxides [9]. In the nonsuperconducting compound $YBa_2Cu_3O_6$ the O(4), Ba atoms have respective charge states O^{-2} and Ba^{+2} .

Next I analyze the charge distribution in $RBa_2Cu_3O_7$. Table I shows the average rates of change and the filling factor $N_{p(d)}$ as a function of the ionic radius R_{ion} . First and foremost, I note that not only the effective charge, but also the nature of the distribution of electrons among the orbitals changes as the ionic radius is varied. When the ionic radius is increased, the effective charges of Cu(1) and Cu(2) are observed to grow, which should cause the x-ray spectra to shift toward lower energies. Such a shift has been observed in [11], and the rate of change ~ 2.4 agrees satisfactorily with the calculated charge rate of change ~ 2.6 . Two structural fragments are distinguishable in the $RBa_2Cu_3O_7$ unit cell: a fragment of Cu(1)-O(1) chains with nearest-neighbor Ba and 2O(4) atoms, and a fragment of $2[Cu(2)-O(2)-O(3)]$ planes. The calculated variation of the net charge of these fragments with variation of the ionic radius is close to zero, i.e., charge exchange between the fragments takes place as the structure changes. When this happens,

hole transfer from the fragment of chains to the fragment of planes is observed as the ionic radius increases. Electron transfer into the chain structure is accompanied by lowering of the charge of apical oxygen atom, indicating a possible increase in the covalence of the bonds of the given atom with the barium atom. An analysis of variation of the orbital filling factors shows that with an increase in the ionic radius the filling of the orbital decreases. Bearing in mind the experimental fact that the maximum T_c is attained at hole densities ~ 0.2 [per copper atom Cu(2)], I conclude that the superconducting transition temperature must become higher as the ionic radius increases. This behavior of T_c has indeed been observed [11]. I notice the weak dependence of the charge state of R on the ionic radius. The charge state R^{+3} is observed for practically the entire R series (Yb, Er, Ho, Y, Gd, Eu, Sm, Nd). Extrapolating the data into the range of the ionic radius of Pr, one could assume that the charge state of the Pr atom in the compound $\text{PrBa}_2\text{Cu}_3\text{O}_7$ is close to Pr^{+3} . To elucidate the charge state of the Pr atom, I have calculated the EFG tensor using experimental data [12] for the compound $\text{Y}_{1-x}\text{Pr}_x\text{Ba}_2\text{Cu}_3\text{O}_7$ ($x=0.2$). I find that the charge state of the Pr atom is in fact close to Pr^{+3} ($Z^* \sim 3.04$); the effective charge of Pr atom will necessary decrease slightly with an increase x .

REFERENCES

1. Gusakov, V. E., *Vesti Akad. Navuk Belarus. No. 5-6*, 83 (1992).
2. Gusakov, V. E., *Low Temp. Phys.* **21**, 621 (1995).
3. Cava, R. J., Hewat, A. W., Hewat, E. A., Batlog, B., Marezio, M., Rabe, K. M., Krajewski, J. J., Peck, W. F. and Rupp, L. W., *Physica C* **165**, 419 (1990).
4. Pennington, C. H., Durand, D. J., Zax, D. B., Slichter, C. P., Rice J. P. and Ginsberg, D. M., *Phys. Rev. B* **37**, 7944 (1988).
5. Takigawa, M., Hammel, P. C., Heffner, R. H., Fisk, Z., Ott, K. C., and Thompson, J. D., *Phys. Rev. Lett.* **63**, 1865 (1989).
6. Schwarz, K., Ambrosch-Draxl, C., and Blaha P., *Phys. Rev. B* **42**, 2051 (1990).
7. Tranquada, J. M., Heald, S. M., Moodendaugh, A. R., and Xu, Y., *Phys. Rev. B* **38**, 8893, (1988).
8. Sullivan, J. D., Bordet, P., Marezio, M., Takenaka, K., and Uchida, S., *Phys. Rev. B* **48**, 10638 (1993).
9. Fedorov, V. E., *Physica C* **185-189**, 705 (1991).
10. Dobrovolskii, V. D., Prisedskii, V. V., Rozenblat, E. M., Sinel'nichenko, A. K., Udosov, I. A., Gusakova, L. G., Molchakovskaya, G. M., and V. Maiboroda, P., *Metallofizika* **11**, 124 (1989).
11. Itoh, M., Karamishima, K., Keogoku, M. and Aoki E., *Physica C* **160**, 177 (1989).
12. Groen, W. A., de Leeuw, D. M. and Geelen G. P. J., *Physica C* **73**, 375 (1990).

Quasi-particle Spectrum around a Single Vortex in *s*-wave Superconductors

Masaru Kato ^{*†} and Kazumi Maki^{*}

^{*}*Department of Physics and Astronomy, University of Southern California
Los Angeles, CA 90089*

[†]*Department of Mathematical Sciences
Osaka Prefecture University, Sakai, Osaka 599-8531, Japan*

Abstract. Making use of the Bogoliubov-de Gennes equation, we study quasi-particle spectrum and the vortex core structure of a single vortex in quasi 2D *s*-wave superconductors for small $p_F \xi_0$, where p_F is the Fermi momentum and ξ_0 is the coherence length. During our numerical calculation the electron number is conserved for each $p_F \xi_0$. We find that the number of bound states decreases rapidly for decreasing $p_F \xi_0$. Also we find that the core structure, the current density distribution and the local density of states strongly depend on the value of $p_F \xi_0$ due to the number and the peak positions of bound states.

Since the discovery of high T_c cuprate superconductors, the vortex states have attracted much attention. Perhaps the superconductivity of High T_c cuprates is *d*-wave [1,2] and in the quantum limit [3,4]. Here we study the vortex structure of *s*-wave superconductor in the quantum limit [5]. In our earlier study we neglected the number conservation. However number conservation should be crucial in the quantum limit as pointed out by van der Marel [6]. Indeed number conservation gives a chemical potential which decreases with increasing T for $T > T_c$, while it decreases also as $\Delta(T)$ increases [6].

In the following we consider a single vortex within the quasi-two dimensional superconductors as in [5]. The corresponding Bogoliubov-de Gennes equation is written down in Gygi and Schlüter [7]. Also we use the same basis set for Fourier-Bessel expansion as in Eq. 7 in [7]. On the other hand, in [7] they considered the case $p_F \xi_0 = 2E_F/\Delta_0 \sim 40$. Here we limit ourselves to $p_F \xi_0 = 1, 2$ and 4. Also unlike in [5], we impose the electron number conservation. The total electron number is defined by

$$N_e = \int \sum_n \{ |u_n(\mathbf{r})|^2 f(E_n) + |v_n(\mathbf{r})|^2 [1 - f(E_n)] \} d^2\mathbf{r}, \quad (1)$$

which is then independent of T . Here $f(E)$ is the Fermi distribution function.

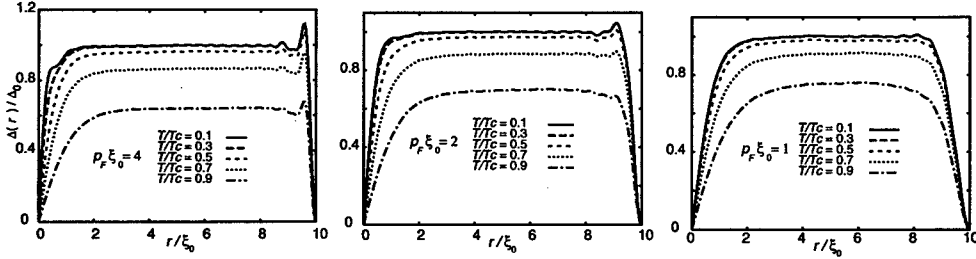


FIGURE 1. Structure of order parameter for a few temperatures.

First, in Fig. 1, we show $|\Delta(r)|$ for a few temperatures for $p_F\xi_0 = 4, 2$ and 1 . For $p_F\xi_0 = 4$, $|\Delta(r)|$ exhibits a shoulder in the vortex core for $T/T_c = 0.1$, which disappears for $p_F\xi_0 = 2$ and 1 .

In Fig. 2, we show the temperature dependence of the core size as defined by [8]

$$\frac{1}{\xi_1} = \frac{g}{\Delta_0} \sum_{E_{nm} \leq E_c} \sum_{j_1 j_2} u_{n0j_1} v_{n0j_2} [1 - 2f(E_{n0})] \phi_{j_1 0}(0) \frac{d\phi_{j_2 1}}{dr}(0). \quad (2)$$

For $p_F\xi_0 = 4$, ξ_1^{-1} increases with decreasing temperature exhibiting the Kramer-Pesch effect [8] which stops around $T/T_c = 0.1$. On the other hand, no Kramer-Pesch effect appears to be seen for $p_F\xi_0 = 2$ and 1 .

The quasi-particle spectrum is shown in Fig. 3. The number of bound states inside the energy gap decreases rapidly with decreasing $p_F\xi_0$. There are 20 for $p_F\xi_0 = 4$, 6 for $p_F\xi_0 = 2$ and 1 or 2 for $p_F\xi_0 = 1$.

The current density distribution is given by,

$$j(r, \theta) = \frac{e}{2m_e i} \sum_{nm} \{ f(E_{nm}) u_{nm}^*(r, \theta) \nabla u_{nm}(r, \theta) + [1 - f(E_{nm})] v_{nm}(r, \theta) \nabla v_{nm}^*(r, \theta) - \text{h.c.} \}, \quad (3)$$

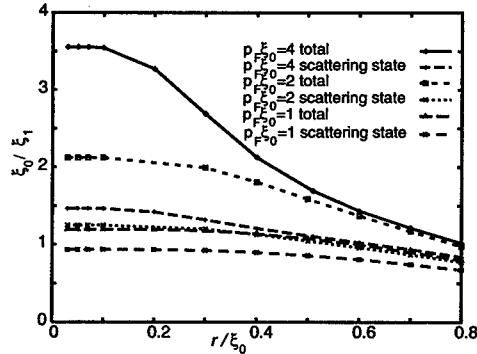


FIGURE 2. Temperature dependence of core radius.

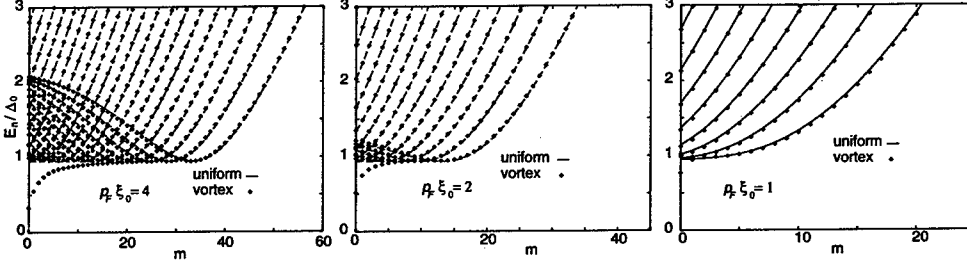


FIGURE 3. Quasi-particle spectrum.

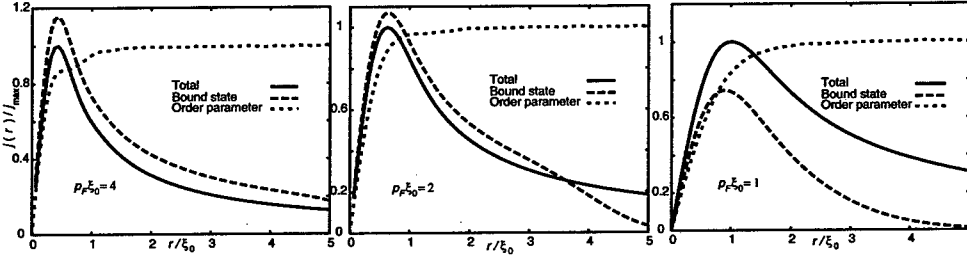


FIGURE 4. Current density distribution.

and it has only θ component, j_θ , and depends only on r because of a rotational symmetry around the vortex. In Fig. 4, we show $|j_\theta(r)|$ for $p_F \xi_0 = 4, 2$ and 1 . The peak position of $|j_\theta(r)|$ is mainly determined by the lowest bound state contribution as pointed out in [5]. However, for $p_F \xi_0 = 1$, the contribution of the scattering states is much larger than the one in [5].

Finally, the local density of states,

$$N(r, E) = \sum_{nm} \{ |u_{nm}(r)|^2 f'(E_{nm} - E) + |v_{nm}(r)|^2 f'(E_{nm} + E) \}, \quad (4)$$

is shown in Fig. 5 for $p_F \xi_0 = 4, 2$ and 1 .

The self-consistent solution of the Bogoliubov-de Gennes equation around a single vortex for $p_F \xi_0 = 4, 2$ and 1 has been obtained for the first time. Number conservation is crucial in the quantum limit. In particular it appears to play crucial role in limiting the number of the bound state around a single vortex. More details will be published elsewhere.

One of us (MK) thanks the support by the Japanese Ministry of Education, Science and Culture through the exchange researcher program. The present work is supported in part by NSF under grant number DMR9531720.

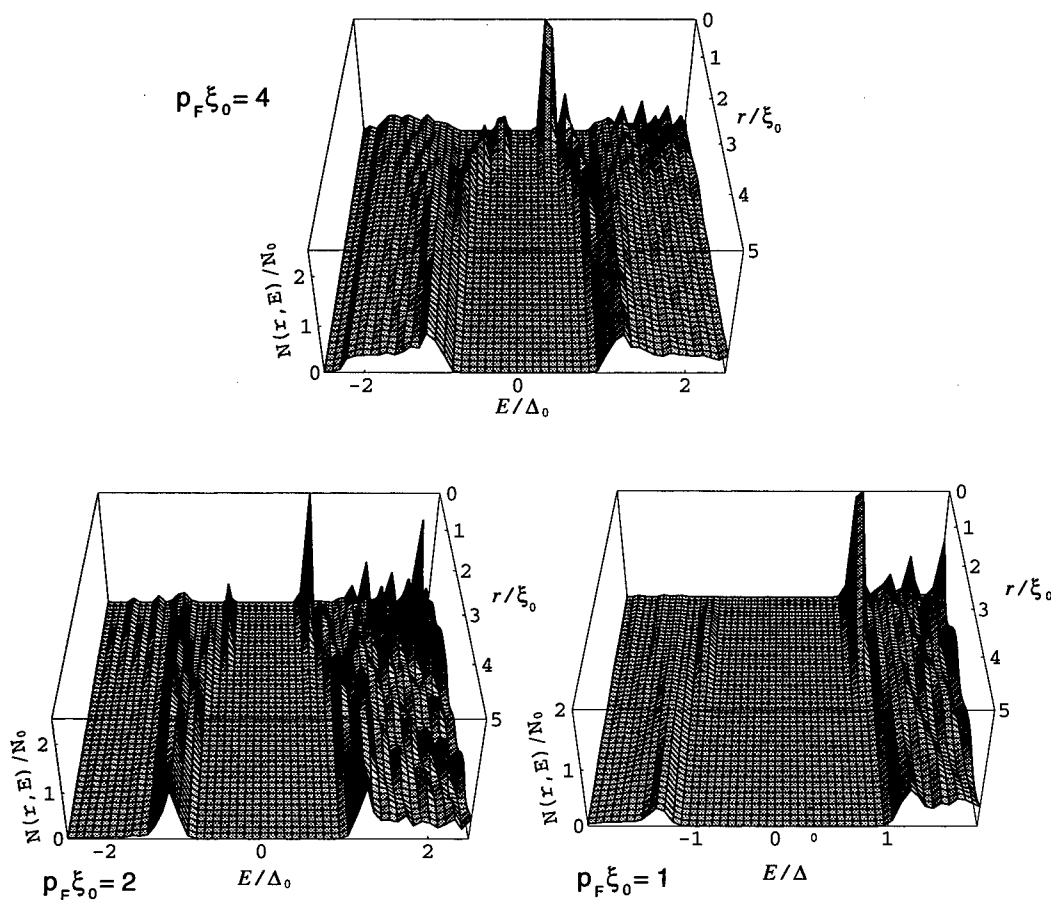


FIGURE 5. Local density of states

REFERENCES

1. C. C. Tsuei and J. R. Kirtley, *Physica C* **282-287**, 4 (1997)
2. D. J. Van Harlingen, *Physica C* **282-287**, 128 (1997)
3. K. Maki and H. Won, *J. Phys. I(Paris)* **6**, 2317 (1996)
4. S. G. Doettinger, R. P. Huebener and S. Kittelberg, *Phys. Rev. B* **55**, 6044 (1997)
5. M. Kato and K. Maki, submitted to *Phys. Rev. B and cond-mat/9810187*.
6. D. van der Marel, *Physica C* **165**, 35 (1990)
7. F. Gygi and M. Schlüter, *Phys. Rev. B* **41**, 822 (1990); F. Gygi and M. Schlüter, *Phys. Rev. B* **43**, 7609 (1991)
8. L. Kramer and W. Pesch, *Z. Physik* **269**, 59 (1974)

Pseudogap Phenomena in the Superconducting Phase of the Cuprates

Ioan Kosztin, Qijin Chen, Boldizsár Jankó, and K. Levin

James Franck Institute, University of Chicago, 5640 South Ellis Avenue, Chicago, IL 60637

Abstract. The presence of a normal state spectral (pseudo) gap at the superconducting transition temperature in the underdoped cuprates has important implications for the associated superconducting phase. We argue that this normal state pseudogap derives from pairing fluctuations, which necessarily persist below T_c and which have important implications on the superconducting state. Our Greens function approach, based on the equation of motion method, can be viewed as a natural extension of BCS theory for sufficiently strong pairing interaction, suggested by the short coherence length of the cuprates. In addition to the usual fermionic excitations, there are also incoherent (but not pre-formed) pairs of finite center of mass momentum which must be self consistently incorporated in computing T_c and other superconducting properties, such as the superfluid density and the Josephson critical current. Finally, we discuss some of the experimental implications of our theory for the cuprates.

INTRODUCTION

ARPES experiments [1] on the cuprates underline the important point that in these exotic materials, the excitation gap Δ and the order parameter Δ_{sc} must be distinct. The former is finite above T_c , where the latter is zero. This situation, which is to be distinguished from that of BCS theory, leads us to define a new parameter

$$\Delta_{pg}^2 = \Delta^2 - \Delta_{sc}^2 \quad (1)$$

which can be calculated quantitatively and plays a central role in this paper.

In what follows we show that Δ_{pg} (i) is most naturally incorporated into extensions of BCS theory which are based on the BCS-Bose Einstein (BEC) crossover scenario [2], (ii) corresponds to a new degree of freedom, with associated dynamics, which we call the “pairon”, (iii) is responsible for important corrections to the results of BCS theory in physical properties such as the penetration depth λ and in ratios such as $\Delta(0)/T_c$.

The BCS-BEC crossover theory was first formulated by Leggett [2] as a description of the ground state of a superconductor. As a function of variable coupling constant g it was demonstrated that the $T = 0$ state could be continuously deformed between the two limiting cases. For intermediate coupling (corresponding to the pseudogap phase of the cuprates), the excitations of this ground state are expected to be a

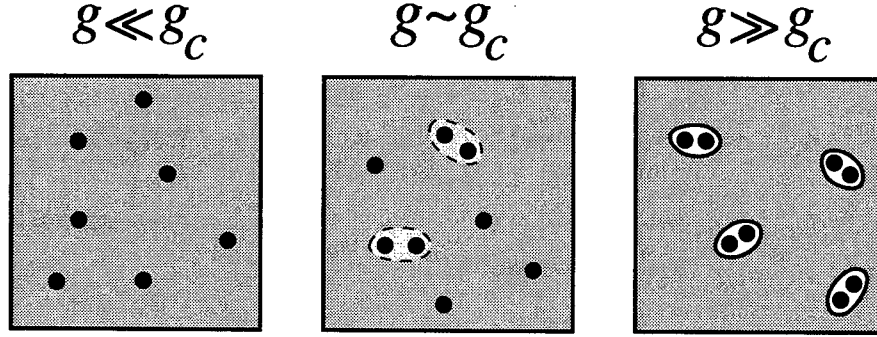


FIGURE 1. BCS-BEC crossover scenario below T_c . The gray background denotes the condensate of Cooper pairs. The pseudogap phase ($g \sim g_c$) is intermediate between the BCS ($g \ll g_c$) and BEC ($g \gg g_c$) limits.

combination of those of the BCS limit (which have fermionic character) and those of the BEC case (which correspond to bosons, or pairs of fermions). This situation is indicated schematically in Fig. 1. The finite center of mass momentum pair excitations are the pairons characterized by Δ_{pg} .

Before introducing the mathematical formalism, several important points should be stressed. Equation (1) is of interest only in the case of intermediate coupling: in the BCS case the right hand side is trivially zero, and in the BEC limit this equation is of little relevance, since fermionic excitations (and the related energy scale Δ) are not considered. Pairons are associated with the amplitude, not phase degrees of freedom. Their energy dispersion Ω_q will be seen to be *quadratic* and not linear in q as in the phase collective modes. (In this sense, the calculations are similar to those used to obtain the $q^2\xi^2$ contributions to the Landau-Ginzburg free energy). Pairons are gapless. This is in contrast to the normal state resonant pairs [3] which retain a gap. This gaplessness, shown from Eq. (3a) below, is associated with the continuity in the fluctuation spectrum of the excitation gap around its $q = 0$ value. A gap in the pairon spectrum would require that the system be rigid with respect to deviations of the excitation gap Δ from the order parameter Δ_{sc} . While different from collective modes (which relate to correlation functions involving Δ_{sc}), pairons play an important role in obtaining the correct collective mode spectrum of the superconducting state (discussed elsewhere), as well as through the generalized Ward identity, arriving at a consistent treatment of the superfluid density.

MATHEMATICAL FORMALISM

As a simple model for the cuprate band structure, we consider a tight-binding, anisotropic dispersion $\epsilon_k = 2t_{||}(2 - \cos k_x - \cos k_y) + 2t_{\perp}(1 - \cos k_{\perp}) - \mu$, where $t_{||}$ (t_{\perp}) is the hopping integral for the in-plane (out-of-plane) motion and $t_{\perp} \ll t_{||}$. We assume that the fermions interact via an effective pairing interaction with d -wave symmetry $V_{k,k'} = -|g|\varphi_k\varphi_{k'}$ so that $\varphi_k = \frac{1}{2}(\cos k_x - \cos k_y)$. The present approach is built

on previous work [3–6] based on the equation of motion method for Greens functions, first introduced by Kadanoff and Martin [7], and subsequently extended by Patton [8].

The “pairing approximation” of Refs. [7,8] leads to

$$\Sigma(K) = \sum_Q t(Q) G_o(Q - K) \varphi_{\mathbf{k}-\mathbf{q}/2}^2, \quad (2a)$$

$$g = [1 + g\chi(Q)]t(Q), \quad (2b)$$

where $\Sigma(K)$ is the self-energy, and $\chi(Q) = \sum_K G(K) G_o(Q - K) \varphi_{\mathbf{k}-\mathbf{q}/2}^2$ is the pair susceptibility. Equations (2), along with the number equation $n = 2 \sum_K G(K)$, self-consistently determine both the Green’s function $G(K)$ and the pair propagator, i.e., T-matrix $t(Q)$. We use a four-vector notation, e.g., $K \equiv (\mathbf{k}; i\omega)$, $\sum_K \equiv T \sum_{i\omega, \mathbf{k}}$ and $G_o(K) = (i\omega - \epsilon_{\mathbf{k}})^{-1}$.

We write the T-matrix and self-energy below T_c as $t(Q) = t_{sc}(Q) + t_{pg}(Q)$, and $\Sigma(K) = \Sigma_{sc}(K) + \Sigma_{pg}(K)$. The condensate contribution assumes the familiar BCS form $t_{sc}(Q) = -\delta(Q) \Delta_{sc}^2 / T$, where Δ_{sc} is the superconducting gap parameter (and can be chosen to be real) and $\Sigma_{sc}(K) = \Delta_{sc}^2 \varphi_{\mathbf{k}}^2 / (i\omega + \epsilon_{\mathbf{k}})$. Inserting the above forms for the T-matrix into Eq. (2b), one obtains the excitation gap equation $1 + g\chi(0) = 0$, as well as (for any non-zero Q), $t_{pg}(Q) = g / (1 + g\chi(Q))$. Note that because of the gap equation, $t_{pg}(Q)$ is highly peaked about the origin, with a divergence at $Q = 0$. As a consequence, in evaluating the associated contribution to the self-energy, the main contribution to the Q sum comes from this small Q divergent region so that $\Sigma_{pg}(K) \approx -G_o(-K) \Delta_{pg}^2 \varphi_{\mathbf{k}}^2$, where we have defined the pseudogap parameter

$$\Delta_{pg}^2 \equiv - \sum_Q t_{pg}(Q) = - \sum_Q \frac{g}{1 + g\chi(Q)}. \quad (3a)$$

Thus, both Σ_{pg} and the total self-energy Σ can be well approximated by a BCS-like form, i.e., $\Sigma(K) \approx \Delta^2 \varphi_{\mathbf{k}}^2 / (i\omega + \epsilon_{\mathbf{k}})$, where $\Delta \equiv \sqrt{\Delta_{sc}^2 + \Delta_{pg}^2}$ is the magnitude of the total excitation gap, with the \mathbf{k} dependence given by the d -wave function $\varphi_{\mathbf{k}}$. Within the above approximations, the gap and number equations reduce to

$$1 + g \sum_{\mathbf{k}} \frac{1 - 2f(E_{\mathbf{k}})}{2E_{\mathbf{k}}} \varphi_{\mathbf{k}}^2 = 0, \quad (3b)$$

$$\sum_{\mathbf{k}} \left[1 - \frac{\epsilon_{\mathbf{k}}}{E_{\mathbf{k}}} + \frac{2\epsilon_{\mathbf{k}}}{E_{\mathbf{k}}} f(E_{\mathbf{k}}) \right] = n, \quad (3c)$$

where the quasiparticle energy dispersion $E_{\mathbf{k}} = (\epsilon_{\mathbf{k}}^2 + \Delta^2 \varphi_{\mathbf{k}}^2)^{1/2}$ contains the full excitation gap Δ .

The set of equations (3) can be used to determine the superconducting transition temperature T_c (where $\Delta_{sc} = 0$), and the temperature dependence of the various gap parameters. Equation (3a) contains the physics of the pair excitations, or pseudogap. The remaining two Eqs. (3b) - (3c) are analogous to their BCS counterparts but with a finite (as a result of non-zero Δ_{pg}) excitation gap at T_c . In a similar fashion, this formalism can be used to deduce other measurable quantities [6], such as the penetration depth and critical current. Here the generalized Ward identity plays a profoundly important role.

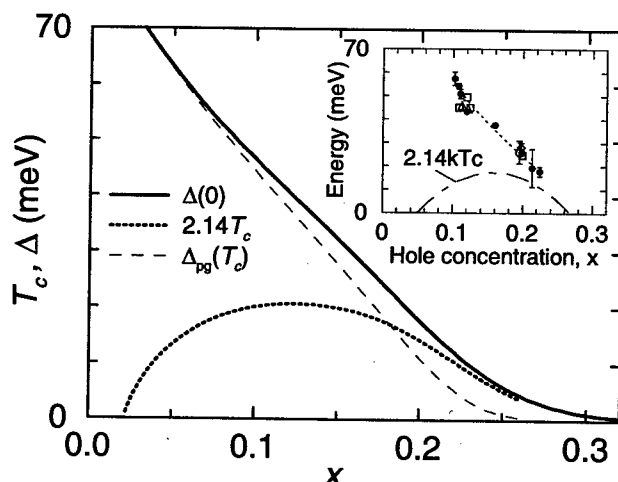


FIGURE 2. The cuprate phase diagram. Plotted are T_c , $\Delta(0)$, and $\Delta(T_c)$, as a function of hole doping x . Experimental data from ref. [11] are shown in the inset. The gaps plotted are the magnitude at $(\pi, 0)$.

APPLICATION TO THE CUPRATES

The remainder of this paper is directed towards understanding three experimental characteristics of the cuprates: the phase diagram, the superfluid density and the Josephson critical current.

In order to generate physically realistic values of the various energy scales, we make two assumptions: (1) We take g as doping-independent (which is not unreasonable in the absence of any more detailed information about the pairing mechanism) and (2) incorporate the effect of the Mott transition at half filling, by introducing an x -dependence into the in-plane hopping matrix elements $t_{||}$, as would be expected in the limit of strong on-site Coulomb interactions in a Hubbard model [9]. Thus the hopping matrix element is renormalized as $t_{||}(x) \approx t_0(1-n) = t_0x$, where t_0 is the matrix element in the absence of Coulomb effects. This x dependent energy scale is consistent with the requirement that the plasma frequency vanish at $x = 0$. These assumptions leave us with one free parameter $-g/4t_0$, for which we assign the value 0.15 to optimize the overall fit of the phase diagram to experiment. We take $t_{\perp}/t_{||} \approx 0.01$, and $t_0 \approx 0.6$ eV, which is reasonably consistent with experimentally based estimates [10].

The results for T_c , obtained from Eqs. (3), as a function of x are plotted in Fig. 2. Also indicated is the corresponding zero temperature excitation gap $\Delta(0)$ as well as the pseudogap Δ_{pg} at T_c . These three quantities provide us, for use in subsequent calculations, with energy scales which are in reasonable agreement with the data of Ref. [11], shown in the inset. The relative size of $\Delta_{pg}(T_c)$, compared to $\Delta(0)$, increases with decreasing x . In the highly overdoped limit this ratio approaches zero, and the BCS limit is recovered. Moreover, while not shown here, our calculations indicate that the excitation gap Δ is, generally, finite at T_c , the superconducting gap Δ_{sc} is established at and below T_c , while the pseudogap Δ_{pg} decreases to zero as T is reduced from T_c to 0. This last observation

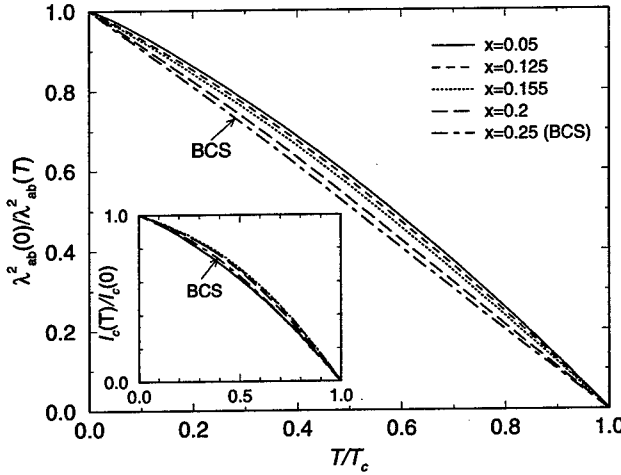


FIGURE 3. Normalized in-plane superfluid density (main figure) and the c-axis Josephson critical current (inset) as a function of T/T_c for various doping concentrations x .

is consistent with general expectations for $\Delta_{pg}^2 \approx \langle |\Delta|^2 \rangle - |\Delta_{sc}|^2$.

It is important to stress, that our subsequent results for the superfluid density and Josephson current, need not be viewed as contingent on the detailed x -dependence used to derive the phase diagram. One can approach the calculations of these quantities by taking $T_c(x)$ and the various gap parameters (shown in the inset) as phenomenological inputs, within the context of the present formalism.

The superfluid density (normalized to its $T = 0$ value) is plotted in Fig. 3 as a function of T/T_c for several representative values of x , ranging from the highly over- to highly underdoped regimes. These plots clearly indicate a “quasi-universal” behavior with respect to x : $\rho_s(T)/\rho_s(0)$ vs. T/T_c depends only slightly on x . Moreover, the shape of these curves follows closely that of the weak-coupling BCS theory. The, albeit, small variation with x is systematic, with the lowest value of x corresponding to the top curve. Recent experiments provide some preliminary evidence for this universal behavior [12,13]. However, a firm confirmation requires further experiments on a wider range of hole concentrations, from extreme under- to overdoped samples. This universal behavior, which has been discussed elsewhere [6], is associated with pairon effects.

Similar quasi-universal behavior is also predicted for the normalized c-axis Josephson critical current $I_c(T)/I_c(0)$, as shown in the inset of Fig. 3. This behavior is in contrast to the strongly x dependent quasiparticle tunneling characteristics which can be inferred from the temperature dependent excitation gap. At this time, there do not appear to be detailed studies of $I_c(T)$ as a function of x . In future experiments the quasiparticle tunneling characteristics should be simultaneously measured, along with $I_c(T)$, so that direct comparison can be made to the excitation gap, and the predictions can be tested.

Physically, this universality is associated with two compensating contributions, arising from the quasiparticle and pair excitations. In the overdoped regime the former dominate,

whereas in the underdoped regime the latter are more important. One can thus infer that the destruction of the superconducting state comes predominantly from pair excitations at low x , and quasiparticle excitations at high x .

CONCLUSIONS

In summary, in this paper we have proposed a scenario for the superconducting state of the cuprates. This state evolves continuously with hole doping x , exhibiting unusual features at low x (associated with a large excitation gap at T_c) and manifesting the more conventional features of BCS theory at high x . In this scenario the pseudogap state is associated with pair excitations, which act in concert with the usual quasiparticles. Despite the fact that the underdoped cuprates exhibit features inconsistent with BCS theory ($T_c/\Delta(0)$ is strongly x dependent and Δ is finite at and above T_c) we deduce an interesting quasi-universality of the normalized ρ_s and I_c as a function of T/T_c . In these plots the over- and under-doped systems essentially appear indistinguishable. Current experiments lend support to this universality in ρ_s , although a wider range of hole concentrations will need to be addressed, along with future systematic measurements of I_c .

ACKNOWLEDGMENTS

This work was supported by the NSF grants DMR 91-20000 (through STCS) and DMR 9808595 (through MRSEC).

REFERENCES

1. Ding, H. *et al.*, *Nature* **382**, 51-54 (1996); Loeser, A.G. *et al.*, *Science* **273**, 325-29 (1996).
2. Leggett, A.J., *J. Phys. (Paris)* **41**, C7/19-26 (1980); Nozières, P. and Schmitt-Rink, S., *J. Low Temp. Phys.* **59**, 195-211 (1985); Randeria, M., Duan, J.-M., and Shieh, L.-Y., *Phys. Rev. Lett.* **62**, 981-984 (1989).
3. Jankó, B., Maly, J., and Levin, K., *Phys. Rev. B* **56**, R11 407-10 (1997); Maly, J., Jankó, B., and Levin, K., *Phys. Rev. B* **59**, 1354-57 (1998); cond-mat/9805018.
4. Chen, Q., Kosztin, I., Jankó, B., and Levin, K., *Phys. Rev. B* **59**, in press.
5. Kosztin, I., Chen, Q., Jankó, B., and Levin, K., *Phys. Rev. B* **58**, R5936-39 (1998).
6. Chen, Q., Kosztin, I., Jankó, B., and Levin, K., *Phys. Rev. Lett.* **81**, 4708-11 (1998).
7. Kadanoff, L.P. and Martin, P.C., *Phys. Rev.* **124**, 670-97 (1961).
8. Patton, B. R., Ph.D thesis, Cornell University, 1971.
9. Baskaran, G., Zou, Z. and Anderson, P.W., *Solid State Commun.* **63**, 973-76 (1987).
10. Shen, Z.-X. *et al.*, *Science* **267**, 343-50 (1995).
11. Miyakawa, N., Guptasarma, P., Zasadzinski, J. F., Hinks, D. G. and Gray, K. E., *Phys. Rev. Lett.* **80**, 157-60 (1998); Miyakawa, N. *et al.*, cond-mat/9809398.
12. Bonn, D.A., Kamal *et al.*, *Czech J. Phys.* **46**, suppl. 6, 3195-202 (1996).
13. Panagopoulos, C., Cooper, J.R., and Xiang, T., *Phys. Rev. B* **13** 422-25 (1998).

Forward Electron-Phonon Scattering and HTS

Miodrag L. Kulić¹ and Oleg V. Dolgov²

¹Physikalisches Institut, Uni. Bayreuth, 95440 Bayreuth, Germany

²Institut für Theoretische Physik, Uni. Tübingen, Germany

Abstract. Tunneling and point contact spectroscopy show clear phonon features and together with optic measurements give strong support that the electron-phonon interaction (*EPI*) is large in *HTS* oxides. Strong correlations in *HTS* oxides renormalize the *EPI* (and interaction with impurities) so that the **forward scattering peak** (*FSP*) develops for small hole doping $\delta \ll 1$. The *FSP* mechanism explains important properties of the normal and superconducting state.

INTRODUCTION

The peculiar normal state properties and high T_c in *HTS* oxides can be explained by the *EPI* [1]. In that respect one can rise the following questions: (1) If in some *HTS* oxides d -wave pairing and the large *EPI* are realized, how they are compatible?; (2) Why is the pairing in some *HTS* oxides less anisotropic than in others?; (3) Why is the transport coupling constant $\lambda_{tr} (\approx 0.4 - 0.6)$ (sometimes much) smaller than the pairing coupling constant $\lambda (\sim 2)$? (1) - (3) are explained by strong correlations which renormalize the *EPI* giving rise to the forward scattering peak (*FSP*) (at small $|\mathbf{q}|$) in the pairing potential $V(\mathbf{q})$, while the backward scattering (large $|\mathbf{q}|$) is suppressed [1], [2] - see below.

EXPERIMENTAL EVIDENCES FOR THE *EPI*

A. Optic and transport measurements. (1) The dynamical conductivity $\sigma(\omega)$ and the resistivity $\rho(T)$ in *HTS* oxides are erroneously interpreted by the non-phonon (spin-fluctuation) scattering, where the analysis is based on the assumption that the quasiparticle scattering rate $\gamma(\omega, T) = 2 |\text{Im } \Sigma|$ and the transport scattering rate $\gamma_{tr}(\omega, T)$ (entering the dynamical conductivity $\sigma(\omega)$) are equal. If $\gamma(\omega, T) \approx \gamma_{tr}(\omega, T)$ were realized for the *EPI* in *HTS* oxides, then because $\gamma_{tr}^{\text{exp}}(\omega, T)$ is linear in ω up to high $\omega_s \sim 2000 \text{ cm}^{-1}$ (where it saturates with $\omega_s \gg \omega_{ph}^{\text{max}}$ - the maximal phonon frequency) this would make the *EPI* irrelevant.

However, this is not the case in *HTS* oxides, where the *EPI* spectral functions $\alpha^2 F(\omega)$, $\alpha_{tr}^2 F(\omega)$, are spread over the broad ω -range (up to 80 meV - see Fig.2 below). This gives that $\gamma^{EP}(\omega, T) \neq \gamma_{tr}^{EP}(\omega, T)$ [3], and that $\gamma^{EP}(\omega, T)$ saturates at $\omega \sim \omega_{ph}^{max}$, while $\gamma_{tr}^{EP}(\omega, T)$ saturates at $\omega \gg \omega_{ph}^{max}$ - see Fig.1. [3]. So, the right interpretation of physical quantities favors the *EPI* as the origin of the transport properties in the normal state, including the flatness of the electronic Raman scattering spectra [5]. The linear resistivity $\rho(T) \sim \lambda_{tr} T$ (for $T > T_c$) implies a rather small $\lambda_{tr} (\ll \lambda \sim 2) \leq 0.4 - 0.6$. This can be explained by the *FSP* mechanism for the *EPI* [2], [1] - see below. (2) The Fano shape in the phonon Raman scattering [6] of the normal state and the strongly superconductivity-induced phonon renormalization of the A_{1g} phonons at 240 and 390 cm^{-1} (by 6 and 18 % respectively) in $HgBa_2Ca_3Cu_4O_{10+x}$ ($T_c = 123$ K), as well as at 235 cm^{-1} and 360 cm^{-1} in $(Cu, C) - 1234$ with $T_c = 117$ K, give strong evidences for the strong *EPI* in *HTS* oxide.

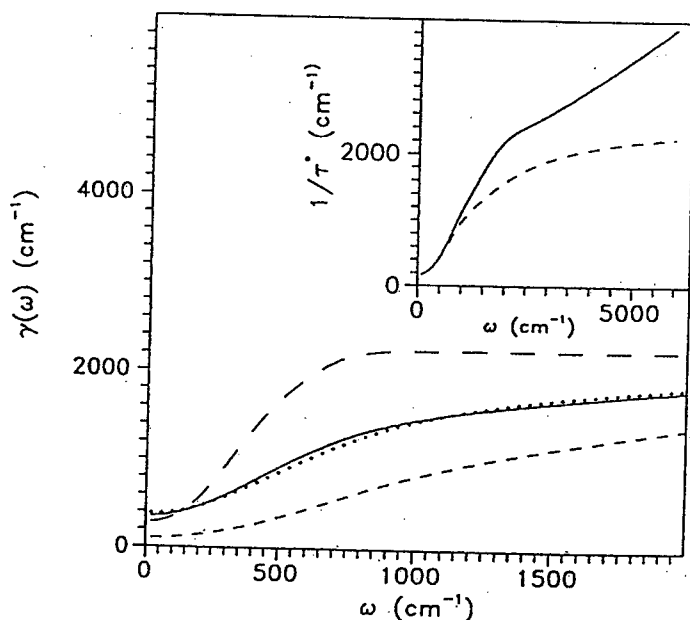


FIGURE 1. Theoretical $\gamma(\omega, T)$, $\gamma_{tr}(\omega, T)$ and $\gamma_{tr}^*(\omega, T)$ for $\alpha^2 F(\omega)$. Reprinted from Physica C 178, S. V. Shulga, O. V. Dolgov, E. G. Maksimov, 266-274, © 1991, with permission from Elsevier Science.

B. Tunneling measurements. The tunneling measurements on $Bi_2Sr_2CaCu_2O_8$ [4], [1] show pronounced phonon peaks in the extracted $\alpha^2 F(\omega)$ for ω up to 80 meV - see Fig.2, which coincide with the peaks in the phonon density of states $F(\omega)$. They show that almost all phonons contribute to the *EPI* giving

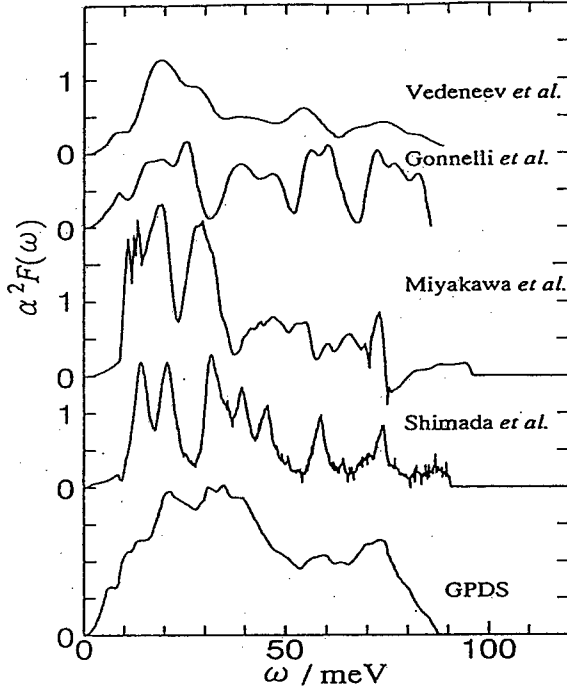


FIGURE 2. $\alpha^2 F(\omega)$ from various tunneling measurements. The GPDS curve is proportional to $F(\omega)$ - from [4].

rise to $\lambda \sim 2$ and $T_c \sim 100$ K. The pronounced isotope effect in the under(over)-doped oxides supports the *EPI* mechanism of pairing [1] too.

THEORY OF THE *EPI* WITH *FSP*

Several mechanisms produce (separately or combined) the *FSP* in the *EPI*: (1) strong electronic correlations [2]; (2) due to the ionic-metallic structure of *HTS* the Madelung energy contribution to the *EPI* is substantial [7] and (3) the nearness to the phase separation [8]. However, (1) in conjunction with (2) is the most probable mechanism for the *FSP* in the *EPI* of *HTS* oxides. The renormalization of the *EPI* and of the nonmagnetic impurity scattering by strong correlations is proportional to $\gamma_c^2(\mathbf{k}_F, \mathbf{q})$ (the charge vertex) [2]. At low doping (δ) γ_c is peaked at small \mathbf{q} and suppressed for large \mathbf{q} [2] - the *FSP* mechanism, which gives rise to [1]: (i) the suppression of the *EPI* in transport properties ($\lambda_{tr} \ll \lambda$) [2],

i.e. $\rho(T) \sim \lambda_{tr}T$ in the broad temperature region [9], and to the non-Drude behavior of $\sigma(\omega)$ - Fig.3; (ii) the pseudogap in the density of states $N(\omega)$ - Fig.4; (iii) the (normalized) s - wave EPI coupling $\Lambda_1(\equiv \Lambda_s)$ and the transport coupling constant Λ_{tr} decrease by decreasing δ , while the d - wave coupling $\Lambda_3(\equiv \Lambda_d)$ increases. By lowering δ (going from overdoped to optimally doped systems) the residual Coulomb repulsion triggers from (anisotropic) s - to d - wave pairing [2], [8], [1] - Fig.5; (iv) the robustness of d - wave pairing in the presence of nonmagnetic impurities. In the extreme FSP limit (with the cutoff $q_c \ll k_F$ in $V_{ep}(\mathbf{q})$) the equation for the critical temperature in the weak coupling limit has the form [9]

$$1 = V_{ep}T_c \sum_{\omega_n=-\Omega}^{\Omega} \frac{1}{\omega_n^2}.$$

If the phonon frequency Ω fulfills $\Omega \gg T_c$ one obtains $T_c = \lambda/4N(0)$, where $\lambda = N(0)V_{ep}$. Note, $T_c \sim \lambda$ and large T_c is reached even for small λ [9].

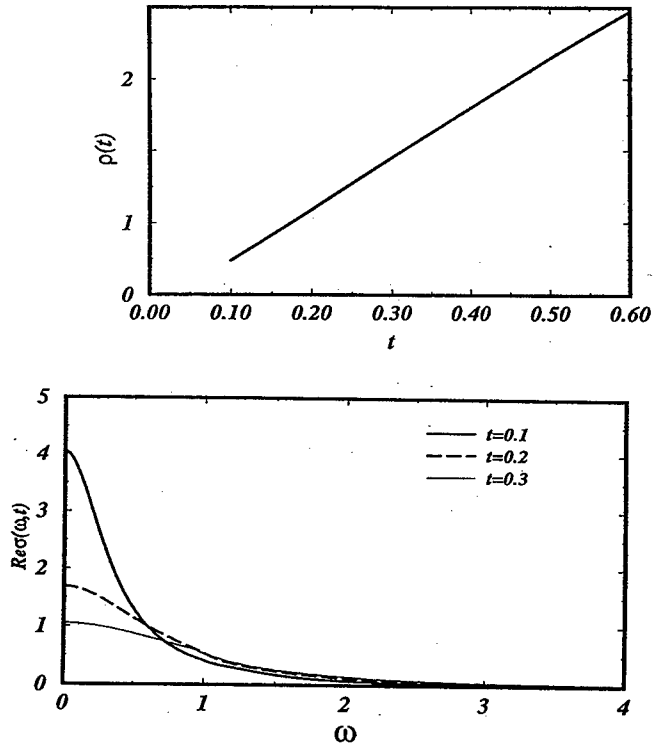


FIGURE 3. The prediction of the FSP theory for $\rho(T)$ and $\sigma(\omega, T)$ - in arbitrary units; $q_c = 0$, $t \equiv \pi T/\Omega$, Ω - the phonon frequency; the coupling constant $l(\equiv \lambda/\pi N(0)\Omega) = 0.1$.

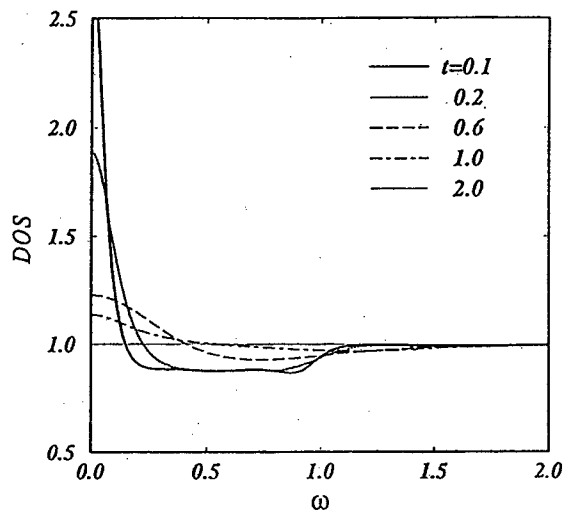


FIGURE 4. The prediction of the *FSP* theory for $N(\omega)$ for $q_c = 0$, $l = 0.1$ and various temperatures t - from O. V. Danylenko, O. V. Dolgov, M. L. Kulić, V. Oudovenko, *Int. Jour. of Mod. Phys. B* 12, Nos. 29-31, 3083-3086 (1998); *Euro. J. of Phys., B*, (1999) (in press).

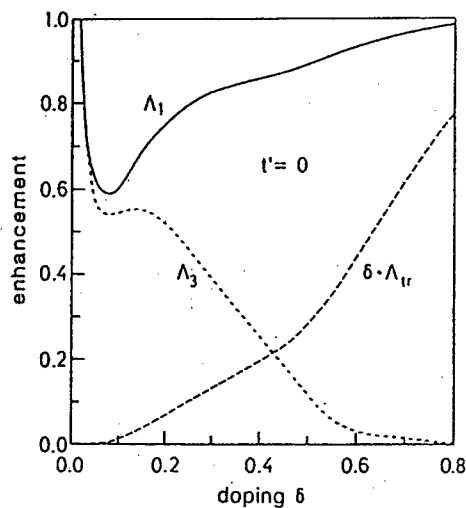


FIGURE 5. The normalized coupling constants $\Lambda_1(\equiv \Lambda_s)$, $\Lambda_3(\equiv \Lambda_d)$, Λ_{tr} as a function of doping δ in the $t-t'-J$ model ($t' = J = 0$) - from [2]

In summary the theory of the *EPI* with the forward scattering peak can explain the most relevant properties in the normal and superconducting state of *HTS* oxides.

ACKNOWLEDGMENTS

We are grateful to O.V. Danilenko and V. Oudovenko for collaboration on the *FSP* subject.

REFERENCES

1. M. L. Kulić, review, preprint Uni. Bayreuth, 1998
2. M. L. Kulić, R. Zeyher, Phys. Rev., **B 49**, 4395 (1994); R. Zeyher, M. L. Kulić, Phys. Rev., **B 53**, 2850 (1996); Phys. Rev., **B 54**, 8985 (1996)
3. O. V. Dolgov, E. G. Maksimov, S. V. Shulga, in **Electron-Phonon Interaction in Oxide Superconductors**, World Scien., p.30 (1991); S. V. Shulga, O. V. Dolgov, E. G. Maksimov, Physica, **C 178**, 266 (1991)
4. D. Shimada, Y. Shiina, A. Mottate, Y. Ohyagi and N. Tsuda, Phys. Rev., **B 51**, 16495 (1995); S. I. Vedenev, A. G. M. Jensen, P. Samuely, V. A. Stepanov, A. A. Tsvetkov and P. Wyder, Phys. Rev., **49**, 9823 (1994)
5. S. N. Rashkeev and G. Wendin, Phys. Rev., **B 47**, 11603 (1993)
6. V. G. Hadjiev, X. Zhou, T. Strohm, M. Cardona, Q. M. Lin, C. W. Chu, Phys. Rev., **B 58**, 1043 (1998); V. G. Hadjiev, T. Strohm, M. Cardona, Z. L. Du, Y. Y. Xue, C. W. Chu, preprint MPI, Stuttgart, 1998
7. A. A. Abrikosov, Physica, **C 244**, 243 (1995); M. Weger, B. Barbelini, M. Peter, Z. Phys., **B 94**, 387 (1994)
8. G. Varelogiannis, Phys. Rev., **B 57**, 13743 (1998); M. Grilli, C. Castellani, Phys. Rev., **B 50**, 16880 (1994); U. Trapper et al., Z. Phys., **B 93**, 465 (1994)
9. O. V. Danylenko, O. V. Dolgov, M. L. Kulić, V. Oudovenko, Int. Jour. of Mod. Phys., **B 12**, Nos. 29-31, 3083-3086 (1998); Euro. J. of Phys., **B 9**, 201, (1999)

SO(6)-Generalized Pseudogap Model of the Cuprates

R. S. Markiewicz^{a,b}, C. Kusko^{a,b,1}, and M. T. Vaughn^a

Physics Department (a) and Barnett Institute (b), Northeastern U., Boston MA 02115

Abstract. The smooth evolution of the tunneling gap of $\text{Bi}_2\text{Sr}_2\text{CaCu}_2\text{O}_8$ with doping from a pseudogap state in the underdoped cuprates to a superconducting state at optimal and overdoping reflects an underlying SO(6) instability structure of the $(\pi, 0)$ saddle points. The pseudogap is probably not associated with superconductivity, but is related to competing nesting instabilities, which are responsible for the stripe phases.

We earlier introduced a simple *Ansatz* of this competition in terms of a pinned Balseiro-Falicov (pBF) model of competing charge density wave and (s-wave) superconductivity. This model gives a good description of the phase diagram and the tunneling and photoemission spectra. Here, we briefly review these results, and discuss some recent developments: experimental evidence for a non-superconducting component to the pseudogap; and SO(6) generalizations of the pBF model, including flux phase and d-wave superconductivity.

Recent photoemission [1,2] and tunneling [3,4] studies in underdoped cuprates find a remarkably smooth evolution of the pseudogap into the superconducting gap as doping increases. This has led to the suggestion that the pseudogap is caused by superconducting fluctuations or precursor pairing [5]. We suggest alternatively that the pseudogap represents a *competing* ordered state closely related to the stripe phases, with the smooth evolution due to an underlying SO(6) symmetry of the instabilities of the Van Hove singularity (VHS).

In this picture, the stripe phases represent a nanoscale phase separation, between a magnetic (spin-density wave or flux phase) instability at half filling and a charge-density wave (CDW) near optimal doping [6]. We have introduced a simple *Ansatz*, the pinned Balseiro-Falicov (pBF) [7,8] model, which captures the essential features of the stripe-superconductivity competition.

Pseudogap Phase Diagram: By comparing simultaneous measurements [9] of the photoemission gap Δ with the pseudogap onset temperature T^* , we find an approximately constant ratio $2\Delta(0)/k_B T^* \simeq 8$, which allows us to plot the Bi-2212 pseudogap phase diagram as T^* vs x , providing a direct comparison with transport-derived pseudogaps in LSCO and YBCO [10], Fig. 1a. Remarkably, all

¹⁾ On leave of absence from Inst. of Atomic Physics, Bucharest, Romania

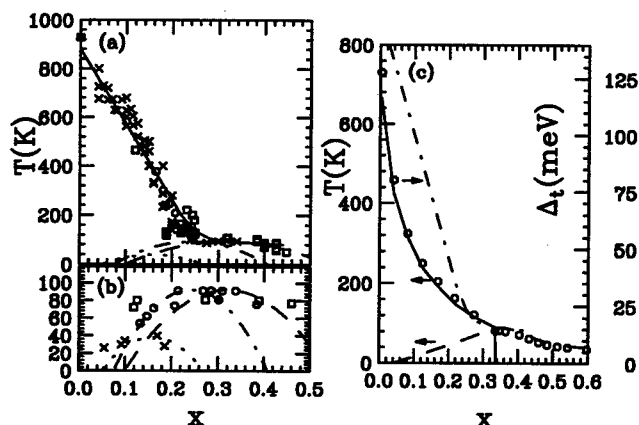


FIGURE 1. (a) Pseudogap phase diagram for Bi-2212 (squares) determined from photoemission [9], and LSCO (x's) and YBCO (circles) determined from transport [10]. (YBCO data shifted by 10% for better scaling.) Solid line = guide to the eyes; other lines = parabolic approximations to superconducting T_c for LSCO (dotted line), YBCO (dashed line) and Bi-2212 (dot-dashed line). (b) Uemura plot, with n/m scaled to x . Symbols and curves have same meanings as in (a). (c) Model pseudogap phase diagram for Bi-2212. Solid line = CDW transition T_p ; dashed line = superconducting transition T_c ; circles = total gap Δ_t at 1K; dotdashed line = solid line from Fig. 1a.

three materials scale onto a single, universal phase diagram, the scaling involving only a shift of the x-axes, relative to LSCO. Such a shift is, however, not consistent with a universal scaling of the superconducting T_c 's – optimal T_c falls at a different x for each material (parabolic curves in Fig. 1a,b). On the other hand, the Uemura plots [11] also find that optimal T_c falls at very different values of n/m for different cuprates. The simple assumption [12] that $n/m \propto x$ (with the constant of proportionality fixed by the LSCO data), *unifies the Uemura plot (symbols in Fig. 1b) with the pseudogap scaling of T_c (curves, Fig. 1b)*. This strongly suggests that the scaling for YBCO and Bi-2212 merely converts the data to the correct value of x . The resulting phase diagram can be well fit by the pBF model, Figure 1c, although the ratio $2\Delta/k_B T^*$ is 4.1, somewhat lower than experiment.

SO(6): The group structure of the model should be thought of not as a symmetry group, but more in a renormalization group sense, as in the one-dimensional metal g-ology. (The group structure of g-ology has been discussed by Solomon and Birman [13].) Due to the logarithmic divergence of the density of states near a VHS, the Fermi surface *almost* reduces to two points – the VHS's at $(\pi, 0)$ and $(0, \pi)$. The possible instabilities of the model have an underlying SO(6) symmetry [14], but which instabilities are observed depend sensitively on the form of the coupling constants – corresponding to the g's of g-ology. There are fundamentally two classes of instability – nesting instabilities which couple the two VHS's and pairing

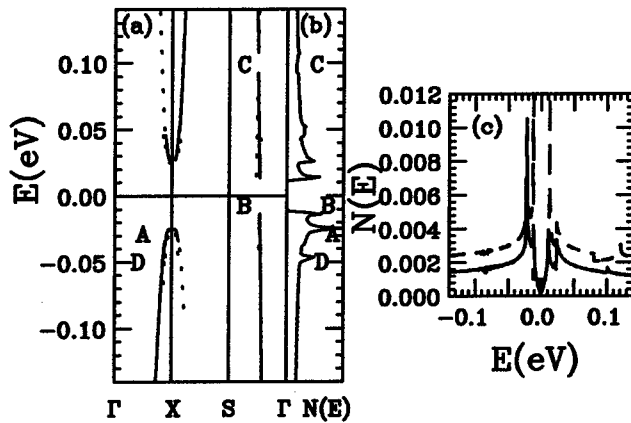


FIGURE 2. (a) Energy dispersion near Fermi level for underdoped cuprate [7], illustrating spectral weight. Coherence factor ≥ 0.6 : solid lines; between 0.1 and 0.6: dashed lines; between 0.001 and 0.1: dotted lines. (b) Tunneling dos. (c) Comparing tunneling dos for CDW-s-wave superconductivity (dashed line, shifted up by 0.001) and flux phase - d-wave superconductivity (solid line).

instabilities, which are intra-VHS.

The $SO(6)$ symmetry of the model is most clearly manifested in the equation for the total gap at $(\pi, 0)$:

$$\Delta_t = \sqrt{\sum_i \Delta_i^2}, \quad (1)$$

where the Δ_i are the individual gaps associated with each instability. (Note the g-ology flavor of this result: there is no underlying symmetry which says that all the Δ_i 's are equal.) In this case, the pBF model amounts to the replacement $\Delta_{SDW}^2 + \Delta_{CDW}^2 \rightarrow \Delta_p^2$, where Δ_p is the net pseudogap, which has similar form to a CDW gap. Equation 1 shows that the smooth evolution of the tunneling gap with doping is consistent with a crossover from magnetic behavior near half filling to superconducting behavior at optimal doping.

Photoemission and Tunneling Spectra: Fig. 2 compares the energy dispersion (a) and the tunneling spectra (b) near the Fermi level, in the underdoped regime. It can be seen that structure in the tunneling dos is directly related to features in the dispersion of the gapped bands. Thus, peak A is associated with the dispersion at $(\pi, 0)$ – the VHS peak split by the combined CDW-superconducting gap. Peak B is due to the superconducting gap away from $(\pi, 0)$ – particularly near $(\pi/2, \pi/2)$. Feature C is associated with the CDW gap G_k near $(\pi/2, \pi/2)$.

An equation similar to Eq. 1 arises in the theory of Bilbro and McMillan [15] – also a (three-dimensional) VHS theory – and was postulated to explain thermodynamic data on the pseudogap [16]. What is new here is that the vector addition is found

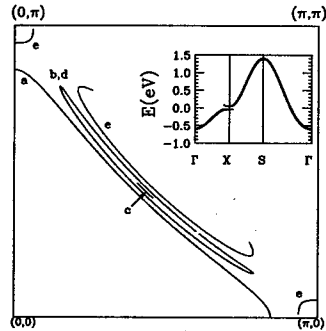


FIGURE 3. Constant energy surfaces for mixed flux phase - d-wave superconductivity: energy = -50 (a), -20 (b), -1 (c), 20 (d), and 50 meV (e). Inset: Corresponding dispersion, with thickness of line proportional to coherence factor.

to hold only near the saddle points, while the gaps split near $(\pi/2, \pi/2)$, and only the superconducting gap is near the Fermi surface there. This is consistent with Panagopoulos and Xiang [17], who found that, near the gap zero at $(\pi/2, \pi/2)$, the slope of the gap scales with T_c , and not with the gap near $(\pi, 0)$. Similarly, Mourachkine [18] has found evidence for two tunneling gaps, very similar to features A and B of Fig. 2b; as predicted, feature B scales with T_c , and not with the pseudogap, feature A. Feature B arises from the superconducting gap at the hole pockets, as can be seen from the energy dispersion at the B gap energy, curve b,d in Fig. 3.

The phase diagram is most naturally fit by assuming that the pseudogap represents a nesting instability, and superconductivity a pairing instability. A more precise determination will require careful experimentation. Thus, Fig. 2c compares the tunneling spectra for two models, the original pBF model in terms of a CDW and an s-wave superconductor, and a modified version involving flux phase - d-wave superconductivity competition. The resulting spectra are, as expected, nearly identical. Close inspection shows differences near (π, π) , where the gap is purely due to the pairing instability.

Van Hove Pinning: An essential ingredient of the model is that the gap remains centered at $(\pi, 0)$ over the full doping range from half filling to optimal doping - that is, that the VHS is pinned at the Fermi level. This remarkable consequence of strong correlation effects was first pointed out in 1989 [19], and has been rederived numerous times since then [20]. We have noted that this pinning should be measurable, both in tunneling and in photoemission, and a preliminary analysis of the data appears to confirm the prediction [7].

Evidence for a Nonsuperconducting Pseudogap: The photoemission and tunneling spectra near optimal doping have a very characteristic form below T_c . There is a sharp quasiparticle peak at an energy Δ above (or below) the Fermi level, with a pronounced dip near 2Δ , followed by a broad hump at higher energies.

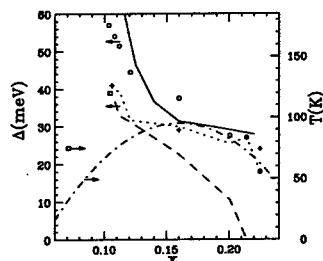


FIGURE 4. Tunneling gaps in BSCCO. Circles = net tunneling gap, Δ ; dotted (dashed) line = estimate for Δ_s (Δ_p); dot-dashed line = T_c ; +’s = $10I_cR$, where I_cR is the average I_cR product [22]; squares = estimate of T_{c0} from Ref. [24]; solid line: from Ref. [7].

The dip is most probably associated with reduced quasiparticle scattering within the superconducting state, which terminates when pairbreaking sets in at energies above twice the superconducting gap, $2\Delta_s$ [21]. Recently, Miyakawa, et al. [22] showed how the tunneling gap in Bi-2212 evolves with doping, scaling a series of tunneling curves to the respective Δ ’s. These curves show significant deviations from scaling of the dip feature with the tunneling gap, which suggest that in the underdoped regime, $\Delta_s < \Delta$. By assuming that the dip scales exactly with Δ_s , it is possible to extract the doping dependence of Δ_s , and correspondingly of Δ_p , the non-superconducting component of the gap [23], Fig. 4.

Shown also is recent Terahertz data from Corson, et al. [24], who extract a bare superconducting transition temperature $T_{c0} > T_c$ from a Berezinski-Kosterlitz-Thouless analysis of superconducting fluctuations. (The effective T_{c0} is found to be strongly frequency dependent; the squares in Fig. 4 are an estimate based on the highest frequency data, 600GHz.) Note that T_{c0} is considerably smaller than the pseudogap onset and has very different scaling, actually decreasing with increased underdoping. Indeed, this T_{c0} is consistent with the values of Δ_s estimated in Ref. [23], with the same ratio of Δ to T_c as found for the total gap in the overdoped regime (where the nonsuperconducting component is absent). The data suggest a rather modest pair-breaking effect of the stripes, reducing the optimal T_c from $\sim 125K$ to $95K$.

Conclusions: The simple pinned Van Hove *Ansatz* for the striped pseudogap phase in the cuprates provides a detailed explanation for the phase diagram and the experimental tunneling and photoemission spectra. In particular: (1) The fact that the tunneling peaks are experimentally found to coincide with the $(\pi, 0)$ photoemission dispersion [4] shows that the $(\pi, 0)$ dispersion has a gap – that is, that the pseudogap is associated with VHS nesting [6]. (2) The interpretation is self-consistent, in that the experiments seem to find that the Fermi level is pinned near the VHS in the underdoped regime [7]. (3) The tunneling gap has a characteristic asymmetry which vanishes at optimal doping; this is evidence that optimal doping is that point at which the Fermi level exactly coincides with the VHS [7]. (4)

While there are superconducting fluctuations in the underdoped regime, a large fraction of the pseudogap has a non-superconducting origin. (5) Portions of the tunneling spectra associated with the Fermi surface near $(\pi/2, \pi/2)$ show distinct scaling with T_c , not T^* . (6) The pseudogap phase diagrams for Bi-2212, LSCO, and YBCO appear to be universal and consistent with the Uemura plot, while optimal doping x_c varies from compound to compound.

Our interest in the tunneling studies was sparked by conversations with A.M. Gabovich. We would like to thank NATO for enabling him to visit us. MTV's work was supported by DOE Grant DE-FG02-85ER40233. Publication 757 of the Barnett Institute.

REFERENCES

1. D. S. Marshall, et al., Phys. Rev. Lett. **76**, 4841 (1996); A. G. Loeser, et al., Science **273**, 325 (1996).
2. H. Ding, et al., Nature **382**, 51 (1996).
3. Ch. Renner, et al., Phys. Rev. Lett. **80**, 149 (1998).
4. N. Miyakawa, et al., Phys. Rev. Lett. **80**, 157 (1998).
5. M. Randeria, unpublished (cond-mat/9710223).
6. R. S. Markiewicz, Phys. Rev. B **56**, 9091 (1997).
7. R. S. Markiewicz, C. Kusko and V. Kidambi, unpublished (cond-mat/9807068).
8. C. Balseiro and L. Falicov, Phys. Rev. B **20**, 4457 (1979).
9. H. Ding, et al., J. Phys. Chem. Sol. **59**, 1888 (1998).
10. B. Batlogg, et al., Physica C **235-240**, 130 (1994).
11. Y. J. Uemura, et al., Phys. Rev. Lett. **62**, 2317 (1989).
12. R. S. Markiewicz and B. C. Giessen, Physica C **160**, 497 (1989).
13. A. I. Solomon and J. L. Birman, J. Math. Phys. **28**, 1526 (1987).
14. R. S. Markiewicz and M. T. Vaughn, J. Phys. Chem. Sol. **59**, 1737 (1998), and Phys. Rev. B **57**, 14052 (1998).
15. G. Bilbro and W. L. McMillan, Phys. Rev. B **14**, 1887 (1976).
16. J. W. Loram, et al., J. Supercond. **7**, 243 (1994).
17. C. Panagopoulos and T. Xiang, Phys. Rev. Lett. **81**, 2336 (1998).
18. A. Mourachkine, unpublished (cond-mat/9810161).
19. R. S. Markiewicz, J. Phys. Cond. Matt. **2**, 665 (1990).
20. Earlier references summarized on p. 1223 of R. S. Markiewicz, J. Phys. Chem. Sol. **58**, 1179 (1997); more recent references include N. Furukawa and T. M. Rice, J. Phys. Cond. Matt. **10**, L381 (1998), and G. Hildebrand, E. Arrigoni, C. Gröber, and W. Hanke, unpublished (cond-mat/9801181).
21. D. Coffey and L. Coffey, Phys. Rev. Lett. **70**, 1529 (1993).
22. N. Miyakawa, et al., unpublished (cond-mat/9809398).
23. R. S. Markiewicz and C. Kusko, unpublished (cond-mat/9810214).
24. J. Corson, et al., unpublished (cond-mat/9810280).

Stripe Disordering Transition

R.S. Markiewicz^{1,2} and M.T. Vaughn¹

Physics Department (1) and Barnett Institute (2), Northeastern U., Boston MA 02115

Abstract. We have recently begun Monte Carlo simulations of the dynamics of stripe phases in the cuprates. A simple model of spinodal decomposition of the holes allows us to incorporate Coulomb repulsion and coherency strains. We find evidence for a possible stripe disordering transition, at a temperature below the pseudogap onset. Experimental searches for such a transition can provide constraints for models of stripe formation.

The relationship between stripe phases and the pseudogap in underdoped cuprates is not well understood. In our model [1-3] the pseudogap is primary. It represents an instability of the hole Fermi liquid driven by Van Hove nesting [4]. However, there is a competition of instabilities, with an antiferromagnet (or flux phase [5-7]) at half filling and a charge-density wave (CDW) at the bare Van Hove singularity (VHS) near optimal doping. This competition leads to a classical phase separation of the holes - two minima in the free energy [8,1]. This is restricted to a nanoscopic scale by long-range Coulomb effects, leading to phases similar to the experimentally observed stripe phases [9].

For such a nanoscale phase separation, the correct dispersion and pseudogap must be found by appropriate averaging over the heterogeneous, usually fluctuating stripes. Fortunately, tunneling and photoemission are sensitive mainly to the pseudogaps, and hence can be described by a simple *Ansatz* of the stripe phase [2,3]. For other purposes, a more detailed picture of the stripes is needed.

As a first step, we have begun Monte Carlo calculations of a classical picture of this restricted phase separation. Using the derived form of the free energy vs doping, we calculate the dynamic spinodal decomposition of the holes in the presence of Coulomb interactions. We find that there can be a stripe disordering transition, Fig. 1, at a temperature below the pseudogap onset. The disordering temperature is proportional to the free energy barrier between the two end-phases, inset, Fig. 2.

Technical details of the calculation are as follows: we work with a generic form of the free energy, $F = F_0 x(x - x_c)^2$, which approximates the calculated free energy of Ref. [1]. The calculations are done on 128×128 lattices, with periodic boundary conditions. The critical doping x_c is taken as $1/6$, which necessitates

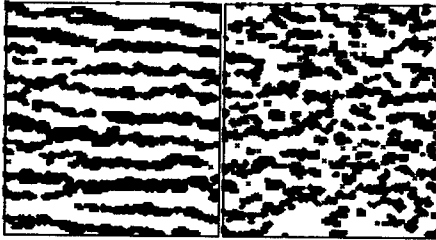


FIGURE 1. Monte Carlo calculated striped phases, with $x = 0.06$, at two temperatures: a low T (left), and near the melting point of the stripes (right). Orthorhombic axes, $\epsilon = 180$.

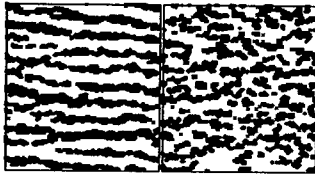


FIGURE 2. Striped phase melting transition at $x=0.04$, $\epsilon = 23$: hole distribution function at temperatures (from bottom to top, at $x = 2/30$) $k_B T = 10, 0.1, 30, 60, 100, 400, 200$ meV. Inset: Assumed free energy vs. doping.

a non-Markovian algorithm – a particular lattice site must retain memory of the average hole occupation over several cycles. We typically choose 30 cycles, which means that a single hole must spread out over 6 lattice sites – close to the size of a magnetic polaron [10]. The algorithm chosen is able to find the correct ground states in the low doping limit (which can be found analytically). The stripes are not topological, and the stripe-like domains are produced by coherency strains [11]. In the absence of such strains, the domains would be irregular shaped, approximately equiaxed, as found by Veillette, et al. [12] The coherency strains produce a mixture of stripes along both x and y axes; to get single-axis stripes, as in the figure, it is assumed that there are local martensitic domains.

The phase separation can be most clearly seen in a plot of the distribution of site occupancies by holes, Fig. 2. At low temperatures, this is a two-peaked structure, with one peak (off scale in the figure) at zero doping, and the other near x_c (it is actually at a doping below x_c , due to charging effects). As the temperature increases, the two-peak structure is gradually smeared out, and at high temperatures there is only a monotonic distribution. This finite system has a crossover rather than a sharp transition. For the parameters chosen, the transition is centered near $k_B T_m \sim 30 \text{ meV}$, which is approximately the barrier height of the free energy (inset). This result is not very sensitive to the value of dielectric constant, ϵ .

Thus, as the underdoped cuprate cools from high temperatures, there can be a

series of phase transitions. At high temperatures, there will be the pseudogap onset. In our simplified mean field *Ansatz* [3], this appears as a long-range ordered CDW phase, but the inclusion of two-dimensional fluctuations [13,14] leads to appropriate pseudogap behavior. The stripe phase ordering temperature found here could in principle fall at a lower temperature. The stripes in our simulations continue to fluctuate, and the long-range stripe order phase seen by Tranquada [9] may be yet another transition. The two-branched transition to a stripe phase bears some resemblance to the phase diagram of Emery, Kivelson, and Zakhar [15], but is in fact different. Their upper transition (T_1^*) corresponds to the onset of stripe order, their lower (T_2^*) to the onset of a spin gap on the hole doped stripes.

There is not much experimental evidence for the onset of short-range stripe order, although phase separation in $\text{La}_2\text{CuO}_{4+\delta}$ starts near 400K [16], much lower than the pseudogap onset temperature, $\sim 800\text{K}$ [17]. In most materials, the incommensurate magnetic modulations near (π, π) broaden out and disappear near the pseudogap T^* , which is a lower temperature ($\sim \leq 150\text{K}$ for the compositions studied) [18]. The best place to look would be in the extremely underdoped regime, where T^* is highest.

While the above calculations reproduce the general properties of the stripes, there are a number of features which are not well reproduced. First, for the elastic constants of LSCO [19], the stripes lie along the orthorhombic axes – i.e., they are diagonal stripes. Further, for the parameters assumed, the charged stripes tend to grow wider with increased doping, maintaining a constant interstripe spacing, whereas experiment [20] suggests that the stripe shape stays constant, but the stripes move closer, as doping increases, at least for $x \leq 0.12$. This suggests that some important feature has been omitted from the model, most probably the topological nature of the stripes as magnetic antiphase boundaries.

MTV's work was supported by DOE Grant DE-FG02-85ER40233. Publication 758 of the Barnett Institute.

REFERENCES

1. R.S. Markiewicz, Phys. Rev. B **56**, 9091 (1997).
2. R.S. Markiewicz, C. Kusko and V. Kidambi, unpublished (cond-mat/9807068).
3. R.S. Markiewicz, C. Kusko and M.T. Vaughn, this conference.
4. T.M. Rice and G.K. Scott, Phys. Rev. Lett. **35**, 120 (1975).
5. I. Affleck and J.B. Marston, Phys. Rev. B **37**, 3774 (1988).
6. R.B. Laughlin, J. Phys. Chem. Sol. **56**, 1627 (1995).
7. X.-G. Wen and P.A. Lee, Phys. Rev. Lett. **76**, 503 (1996).
8. R.S. Markiewicz, J. Phys. Cond. Matt. **2**, 665 (1990).
9. J.M. Tranquada, B.J. Sternlieb, J.D. Axe, Y. Nakamura, and S. Uchida, Nature **375**, 561 (1995); J.M. Tranquada, J.D. Axe, N. Ichikawa, A.R. Moodenbaugh, Y. Nakamura, and S. Uchida, Phys. Rev. Lett. **78**, 338 (1997).
10. A. Auerbach and B.E. Larson, Phys. Rev. Lett. **66**, 2262 (1991).

-
11. P. Fratzl and O. Penrose, *Acta Mater.* **44**, 3227 (1996).
 12. M. Veillette, Ya.B. Bazaliy, A.J. Berlinsky, and C. Kallin, unpublished (cond-mat/9812282).
 13. A. Kampf and J. Schrieffer, *Phys. Rev.* **B41**, 6399 (1990), **B42**, 7967 (1990).
 14. R.S. Markiewicz, *Physica C* **169**, 63 (1990).
 15. V.J. Emery, S.A. Kivelson, and O. Zakhar, *Phys. Rev.* **B56**, 6120 (1997).
 16. P.G. Radaelli, J.D. Jorgensen, R. Kleb, B.A. Hunter, F.C. Chou, and D.C. Johnston, *Phys. Rev.* **B49**, 6239 (1994).
 17. B. Batlogg, H.Y. Hwang, H. Takagi, R.J. Cava, H.L. Kao, and J.Kwo, *Physica C* **235-240**, 130 (1994).
 18. T.E. Mason, unpublished (cond-mat/9812287); H.A. Mook, personal communication.
 19. A. Migliori, J.L. Sarrao, W.M. Visscher, T.M. Bell, M. Lei, Z. Fisk, and R.G. Leisure, *Physica B* **183**, 1 (1993).
 20. K. Yamada, C.H. Lee, K. Kurahashi, J. Wada, S. Wakimoto, S. Ueki, H. Kimura, Y. Endoh, S. Hosoya, G. Shirane, R.J. Birgeneau, M. Greven, M.A. Kastner, and Y.J. Kim, *Phys. Rev.* **B57**, 6165 (1998).

Suppression and restoration of superconductivity in $\text{PrBa}_2\text{Cu}_3\text{O}_7$ (a mini-review).

I.I. Mazin

Code 6391, Naval Research Laboratory, 4555 Overlook Ave. N.W., Washington, DC 20375

Abstract. I discuss the physics of superconductivity and conductivity suppression in Pr-doped $\text{REBa}_2\text{Cu}_3\text{O}_7$ superconductors, and point out the experiments that indicate $\text{Pr}(f)\text{-O}(p)$ hybridization as the cause of such suppression. I also show on a qualitative level how the existing experimental facts about this system are described by the hybridization model.

One of the most exciting cases of superconductivity suppression in high- T_c cuprates is that of $\text{RE}_{1-x}\text{Pr}_x\text{Ba}_2\text{Cu}_3\text{O}_7$, where RE stands for a rare earth (see Refs. [1,2] for reviews). Even more exciting are indications that conductivity and superconductivity can be restored in stoichiometric $\text{PrBa}_2\text{Cu}_3\text{O}_7$ [3,4]. This is such an unexpected result [5] that it is still not generally accepted and further experimental confirmation is required. Nevertheless, this fact was reported by several independent groups, and it is time now to understand the theoretical consequences of this finding. The most important message, if this finding is true, is that at $x = 1$, and, presumably, at intermediate x 's, there are free carriers in $\text{RE}_{1-x}\text{Pr}_x\text{Ba}_2\text{Cu}_3\text{O}_7$, and the suppression of metallic conductivity at sufficiently large x must be due to localization of those carriers. In this paper I review the principal experimental findings about superconductivity, suppression thereof, and related properties of $\text{RE}_{1-x}\text{Pr}_x\text{Ba}_2\text{Cu}_3\text{O}_7$ (a comprehensive review of the data published before 1992 can be found in Ref. [1], and many of more recent references are discussed in Ref. [2]) in a decision-tree manner, eliminating the models substantially incompatible with established experimental facts, eventually focussing on the $pf\sigma$ hybridization models and listing on a verbal level the interpretations of the existing experiments as they emerge from such models.

The first three experimental facts that I want to emphasize are

1. Normal state conductivity drops sharply with the Pr concentration x , and the material becomes essentially insulating at concentrations comparable to the concentration at which superconductivity is fully suppressed.
2. The dependence of T_c on x does not follow the classical Abrikosov-Gor'kov law

for superconductivity suppression by pair-breaking impurities.

3. In samples where T_c is suppressed by alloying with Pr, it can be restored back by partial substitution of Y by Ca, which adds holes to the system.

These three observations essentially eliminate the 'pair breaking model' where suppression of T_c is ascribed to the pair-breaking effect of Pr, acting like an impurity. The rationale of this model is that Pr electrons are to some extent present at the Fermi level, as witnessed by the unusually large Neel temperature, and that for the d -wave superconductivity all impurities are pair-breaking. Let me now explain why the experimental facts above eliminate this possibility:

(i) Theory of the pair-breaking impurity scattering is known in details. Characteristic parameter is $\tau\Delta = 2\pi\xi/l$, where Δ is the superconducting order parameter, ξ is coherence length, $l = \tau v_F$ is the mean free path for the pair breaking impurity scattering. On the other hand, carrier localization due to impurities occurs when $l \sim a$ (lattice parameter), which is nearly two orders of magnitude stronger condition on l than the Abrikosov-Gor'kov condition $2\pi\xi/l \sim 1$. Thus one expects superconductivity to be suppressed well before the normal state conductivity becomes nonmetallic, as it happens in conventional superconductors with magnetic impurities.

(ii) The Abrikosov-Gor'kov law is very universal and particularly robust at small impurity concentration. In particular, the law states that T_c suppression is linear in impurity concentration. This is compatible with the measurements on some $RE_{1-x}Pr_xBa_2Cu_3O_7$ compounds (*e.g.*, $Nd_{1-x}Pr_xBa_2Cu_3O_7$), but not on the others (like $Y_{1-x}Pr_xBa_2Cu_3O_7$), where suppression starts essentially quadratically.

(iii) Substituting Y with Ca, with the remaining composition unchanged, drives the material into the so-called "overdoped regime" (hole concentration above the optimum), which is characterized by a lower T_c and a smaller order parameter Δ than the "optimally doped" material, $YBa_2Cu_3O_{6.92}$. If Pr suppresses the superconductivity via pair-breaking, and does not change in the number and/or character of the carriers, it should suppress T_c further, not less, in $(Y,Ca)_{1-x}Pr_xBa_2Cu_3O_7$ compared with $Y_{1-x}Pr_xBa_2Cu_3O_7$.

Having established that impurity pairbreaking is *not* the cause of the T_c suppression, we are left with two options: (a) the pairing interaction, whatever it may be, is weakened by the Pr doping, or (b) the number or the character of the charge carriers changes. While I am not aware of any experiment directly eliminating the first possibility, it is disfavored by the fact (iii) above. Moreover, we know that Pr does not donate electrons into the superconducting $pd\sigma^*$ Cu-O band ("four-valent Pr model"), because

4. in the oxygen reduced samples, $Y_{1-x}Pr_xBa_2Cu_3O_{7-\delta}$, T_c is suppressed with x slower than in fully oxygenated ($\delta = 7$) samples.

The next illuminating experimental fact is

5. unusually high Néel temperature of $PrBa_2Cu_3O_7$, $T_N \approx 14$ K (all other $REBa_2Cu_3O_7$ have T_N of a few K). This indicates that Pr f states are present at the Fermi level. This has direct connection with the T_c suppression because

6. this suppression is enhanced when external pressure is applied (of course, com-

pression reduces the Pr-Cu and Pr-O bond lengths and increases the corresponding hybridizations). This tells us that the relevant interactions are either Pr(*f*)-O(*p*) or Pr(*f*)-Cu(*d*).

7. Another fact which often overlooked is that while there is no T_c suppression in $RE_{1-x}Nd_xBa_2Cu_3O_7$ at normal conditions, it appears at a higher pressure in a way similar to $RE_{1-x}Pr_xBa_2Cu_3O_7$ [13].

There are two messages in this finding: (a) The relevant hybridization of the *f* states is with some states close to Fermi level, because the Nd(*f*) states are farther away from E_F than Pr(*f*), so that larger hopping is required for the same hybridization effect on the Cu-O states; however, (b) the Pr-CuO hybridization should be stronger than some threshold for the suppression to appear, thus the relevant hybridization is not with the superconducting CuO $pd\sigma^*$ band, but with some other states, initially not at the Fermi level. The main question now is to identify those states. It was done by Fehrenbacher and Rice [7], who noted that in the YBCO structure the nearest neighbors for a *RE* atom are 8 oxygens forming nearly an ideal cube, and that there is one particular *f* orbital, $(x^2 - y^2)z$, which has 8 lobes pointing exactly at those 8 oxygens, allowing for $pf\sigma$ interaction. It was verified by LDA+U calculations (which is a very good approximation for *f* electrons) that indeed

8. this orbital is the one (and the only one) occupied in $PrBa_2Cu_3O_7$ [6], and that the largest Pr-CuO hopping is in the $pf\sigma$ channel.

It was furthermore suggested [7] and checked by calculations [6] that the total number of Cu-O holes changes little upon Pr doping, but rather their character does; namely, that the $pd\sigma^*$ holes are being transferred to another state which we will call tentatively $pf\sigma^*$ (because the transfer is caused by the $pf\sigma$ hopping), keeping in mind however that admixture of other states, first of all of the $pd\pi^*$ states, is not excluded by symmetry.

This chain of arguments, based on experimental data and numerical calculations, essentially eliminates all other models except for the $p - f$ hybridization model. There are, however, open questions about the details of this model. In particular, a key question is whether without crystallographic disorder the "new" states are itinerant or localized? The facts seem to point in the opposite directions:

- Large indirect exchange suggest itinerancy. However, it might be that that the indirect exchange is not the only reason for high Neel temperature.
- LDA+U calculations render a highly itinerant state. However, LDA has a tendency to overestimate hoppings.
- $PrBa_2Cu_3O_7$ is stoichiometric, and it is disputed whether the Pr-Ba disorder is sufficient to localize the carriers in the $pf\sigma^*$ band. However, the observation of superconductivity in $PrBa_2Cu_3O_7$ suggests that it probably is a metal.

Fortunately, there is a nearly unambiguous clue in favor of the itinerant model. Namely, there is a stunning observation which was at first received as a total mystery, that the suppression rate of T_c in different members of the $RE_{1-x}Pr_xBa_2Cu_3O_7$

family is entirely different. For instance, T_c is suppressed by less than 40% in $\text{Y}_{0.7}\text{Pr}_{0.3}\text{Ba}_2\text{Cu}_3\text{O}_7$ or $\text{Yb}_{0.7}\text{Pr}_{0.3}\text{Ba}_2\text{Cu}_3\text{O}_7$, while in $\text{Nd}_{0.7}\text{Pr}_{0.3}\text{Ba}_2\text{Cu}_3\text{O}_7$ the suppression is nearly complete. Of course, without Pr doping all these compounds have nearly the same T_c . Of course, a state localized at a given Pr ion does not know about what RE is sitting in the other cells, so one concludes that the “hole-grabbing” state which appears due to the $pf\sigma$ hybridization should be itinerant. A question of secondary importance remains of whether this state exists in the undoped $RE\text{Ba}_2\text{Cu}_3\text{O}_7$, but is fully occupied, and the role of the $pf\sigma$ hybridization is merely to move this state closer to the Fermi level, or the $pf\sigma$ hybridization *creates* this state. The first case corresponds to the LDA+U calculations of Ref. [6], where the state in question is a $pd\pi^*$ band, with the width of about 1/2 of that of the $pd\sigma^*$ band, and lies entirely under the Fermi level in all $RE\text{Ba}_2\text{Cu}_3\text{O}_7$ except for $RE = \text{Pr}$. The neglect of the $pd\pi$ hopping leads to the second case, when the width of the “hole-grabbing” band is proportional to the $pf\sigma$ hopping [9]. The linear T_c suppression in $\text{Nd}_{1-x}\text{Pr}_x\text{Ba}_2\text{Cu}_3\text{O}_7$ is easier to explain in the first case, but the second gives better agreement [6] with the measured number of the $\text{O}(p_z)$ holes [10]. For most experiments the difference between the two cases is insignificant, and the conclusions can be formulated as follows:

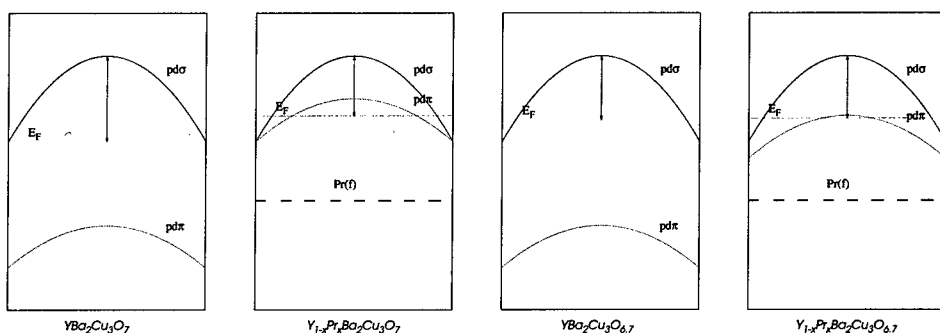
- With Pr doping, electrons are transferred from the usual superconducting $pd\sigma^*$ band to a new band, which includes $pd\pi^*$ and/or $pf\sigma^*$ states.
- The new band is (a) heavy and (b) likely to be strongly renormalized by magnetic interactions.
- Because of that, the carriers in this band are easily localized.
- As a consequence, we expect this band to show its metallic character only in well-ordered, stoichiometric samples, and probably only at a short length scale.

Regarding the newly observed superconductivity (Ref. [6] and other) in $\text{PrBa}_2\text{Cu}_3\text{O}_7$, it appears to be a more novel superconductor than all other cuprate high T_c materials known: it is the only one where superconducting carriers are not residing in the $\text{Cu}(x^2 - y^2) - \text{O}(p_\sigma)$ bands, but are of entirely different character. One can ask why are the critical temperatures in the two compounds, YBCO and PBCO, so similar? In the framework of the suggested model it is a sheer coincidence, which should be removed, for instance, by external pressure. Indeed, it was observed recently [13] that the pressure coefficient dT_c/dP in PBCO is an order of magnitude larger than in any other $RE\text{Ba}_2\text{Cu}_3\text{O}_7$. Interestingly, in the $df\sigma$ hybridization model one expects dT_c/dP to be negative in $RE_{1-x}\text{Pr}_x\text{Ba}_2\text{Cu}_3\text{O}_7$ at small x , because pressure increases hybridization and thus the charge transfer from the $pd\sigma^*$ to the $pf\sigma^* - pd\pi^*$ states, while the same argument predicts dT_c/dP to be positive in $\text{PrBa}_2\text{Cu}_3\text{O}_7$ (since in this system the superconductivity occurs in the $pf\sigma^* - pd\pi^*$ band itself). Both predictions are in agreement with the experiment. Finally, I would like to point out recent measurements [12] that yielded qualitatively

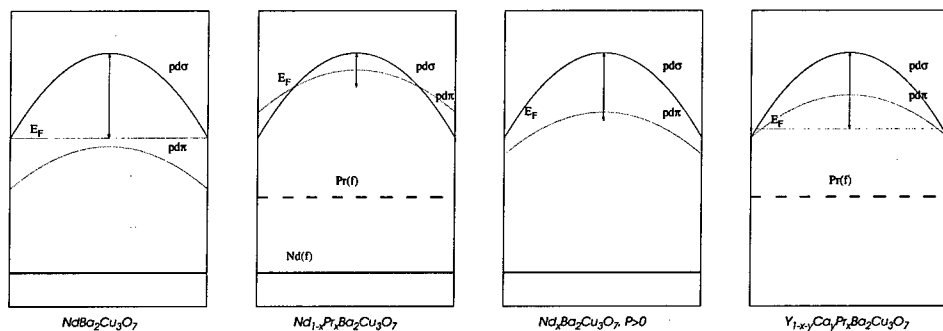
different Compton profiles in $\text{YBa}_2\text{Cu}_3\text{O}_7$ and $\text{PrBa}_2\text{Cu}_3\text{O}_7$. This usually indicates different topology of the Fermi surface and is in agreement with the concept of qualitatively different carriers in this two compounds.

This work was supported by the Office of Naval Research.

Appendix. The following cartoons illustrate how the $p\sigma - pd\pi$ hybridization model explains the main experimental facts.

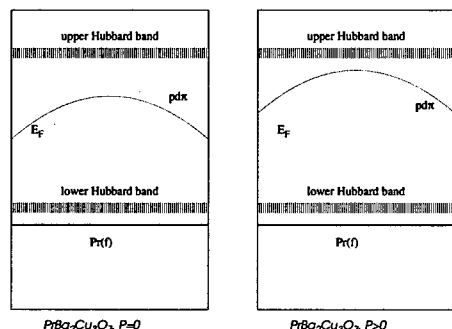


(a) In $\text{YBa}_2\text{Cu}_3\text{O}_7$ the $pd\pi^*$ band is fully occupied and does not influence transport properties or superconductivity. (b) In $\text{Y}_{0.8}\text{Pr}_{0.2}\text{Ba}_2\text{Cu}_3\text{O}_7$ this band is pushed up and grabs some holes from the superconducting $pd\sigma^*$ band. (c,d) Since in $\text{YBa}_2\text{Cu}_3\text{O}_{6.7}$ the Fermi level is higher than in $\text{YBa}_2\text{Cu}_3\text{O}_7$, the same shift of the $pd\pi^*$ band produces smaller changes in the hole concentration in the $pd\sigma^*$ band.



(e) In $\text{NdBa}_2\text{Cu}_3\text{O}_7$ the $pd\pi^*$ is pushed up by the $p\sigma$ interaction, but barely not enough to cross the Fermi level. (f) In $\text{Nd}_{0.8}\text{Pr}_{0.2}\text{Ba}_2\text{Cu}_3\text{O}_7$ this band lies higher than in $\text{Y}_{0.8}\text{Pr}_{0.2}\text{Ba}_2\text{Cu}_3\text{O}_7$, because it was substantially higher even without Pr; furthermore, (g) external pressure increases the $p\sigma$ hybridization so that even in the pure $\text{NdBa}_2\text{Cu}_3\text{O}_7$ the $pd\pi^*$ band crosses the Fermi level. (h) Doping with Ca introduces additional holes into the system which offset the depleting effect of the $pd\pi^*$ band on the $pd\sigma^*$ band.

These cartoons illustrate how external pressure increases the T_c in $\text{PrBa}_2\text{Cu}_3\text{O}_7$.



(i) When Y is fully substituted by Pr, the $pd\sigma^*$ band is so close to half-filling that it undergoes the Mott-Hubbard transition. The conductivity and superconductivity is carried instead by the holes in the new $pd\pi^*$ band. (j) At a higher pressure, due to increased $pf\sigma$ interaction, the position of this band is higher than at $P = 0$, and thus the number of holes in this band is larger.

REFERENCES

1. H. Radousky J. Mater. Res. **7**, 1917 (1992).
2. W.E. Pickett and I.I. Mazin, in: *Handbook on the Physics and Chemistry of rare earths: Rare earth high temperature superconductivity*, Eds. K.A. Gschneider, L. Eyring, and M.B. Maple, Elsevier, in press.
3. H.A. Blackstead and J.D. Dow, Phys. Rev. **B 51**, 11 830 (1995).
4. Z. Zou, K. Oka, T. Ito, and Y. Nishihara, Jap. J. Appl. Phys. Lett. **36**, L18 (1997); Z. Zou, J. Ye, K. Oka, and Y. Nishihara, Phys. Rev. Lett. **80**, 1074 (1998).
5. Note however that even in earlier works electrical properties of $RE_{1-x}\text{Pr}_x\text{Ba}_2\text{Cu}_3\text{O}_7$ were found to depend nonmonotonically on x , $\text{PrBa}_2\text{Cu}_3\text{O}_7$ being more metallic than intermediate compounds, see, e.g., M. Lee, M. L. Stutzman, Y. Suzuki, and T. H. Geballe, Phys. Rev. **B 54**, 3776 (1996).
6. A.I. Liechtenstein and I.I. Mazin, Phys. Rev. Lett., **74**, 1000 (1995).
7. R. Fehrenbacher and T.M. Rice, Phys. Rev. Lett. **70**, 3471 (1993).
8. K. Koyama *et al*, Physica C, **235-240**, 1469, 1994.
9. In the original paper [7] Fehrenbacher and Rice concluded that the $pf\sigma^*$ state is essentially dispersionless. This conclusion, however, was due to a mathematical mistake. See (I.I. Mazin, cond-mat/9806246) for the details.
10. M. Merz *et al*, Phys. Rev. **B 55**, 9160 (1997).
11. J. Ye, Z. Zou, A. Matsushita, K. Oka, Y. Nishihara, and T. Matsumoto, Phys. Rev. **B 58**, R619 (1998).
12. A. Shukla, B. Barbiellini, A. Erb, A. Manuel, T. Buslaps, V. Honkimäki, and P. Suortti, cond-mat/9805225.
13. V. Dyakonov, I. Fita, N. Doroshenko, M. Baran, S. Piechota, and H. Szymczak, Physica C **276**, 245 (1997).

Microscopic Theory for High- T_c Superconductivity

Itai Panas

*Department of Inorganic Environmental Chemistry
Chalmers University of Technology, S-41296 Goteborg, Sweden.*

Abstract. An understanding of superconductivity in the holes doped cuprates is formulated as resulting from (i) recovery of superexchange interactions at $T(\text{spin-gap})$, (ii) appearance of a holes clustering instability at the $T(\text{pseud-gap})$, and (iii) virtual spin excitations in the AF background mediating the phase coherence among holes cluster resonances producing Off-Diagonal Long-Range Order.

Basic considerations

Superconductivity is one property of a quantum mechanical (QM) state of matter which reflects macroscopic phase rigidity [1]. Any strategy to analyze a superconducting (SC) ground state in terms of elementary components must eventually produce this phase rigidity and involve the choice of microscopic independent particle basis. The efficiency a particular strategy depends on (a) the correctness of the physical understanding, (b) how well the employed non-interacting particles spectrum of a pre-selected model hamiltonian approximates the effective interactions of the physical understanding, and (c) the ability to systematically improve on the description. In formulating a non-trivial macroscopic QM ground state, the two crucial signatures of superconductivity comprise pairing and phase coherent randomness [2]. Because the resulting electrodynamical action is understood to require a microscopic phase coherent quantum dynamics, non-adiabatic coupling to a medium which communicates phase information must be introduced for such a ground state to be accessed.

The atom, the molecule (atomic cluster), and the electron gas are three model systems for which the single-particle spectra are in principle known. As superconductivity was originally discovered in metals, the extended independent particle states of the electron gas comprise the physical basis of choice for expanding the correlated many-body wave function at the Fermi surface of elemental metals, alloys and intermetallics. The plane wave basis succeeds in describing these systems because the relevant portion of the independent particle spectrum results from contributions from a large number of atoms. A scenario based on non-adiabatic coupling between electrons and lattice at low temperatures was proposed to enforce the rebuilding of the single-particle spectrum in general and to introduce a coupling between the near-degenerate momentum states in the vicinity of the Fermi surface in particular [2,3]. Phase transition to the SC state becomes associated with the access of an increased momentum space volume, when phase coherent pair states are formed at the expense of an increased Coulomb repulsion.

Ever since the discovery of superconductivity in the cuprates, i.e materials that exhibit extremely short coherence lengths, a major challenge has been to articulate the SC ground state in terms of a *Phase Coherent Holes Cluster Resonance* (PCHCR) scenario, which employs zero-dimensional atomic cluster states as building blocks. Extended objects, such as stripes [4,5] would comprise particular effective objects within such a scenario [6].

Heuristics

A working strategy to discover new SC materials in the electron-phonon scenario would be to make such alloys or intermetallics, which would display increased electron-lattice couplings as compared to the pure elements.

It is precisely here that an opposite approach can be formulated, as a poor metal is equivalent to a poor insulator. Because doped insulators can be understood to possess local sites, such as color centers or dangling bonds, where charge carriers can be easily trapped or released, a model composed from a cluster of atoms is expected to be efficient in describing one such sink. Taking the cluster approach one additional step ahead, we write down a macroscopic wave function ansatz in terms of a generalized Hartree product

$$\Psi_i = \prod_i \Phi_i \quad (1)$$

where Φ_i is a local embedded cluster wave function which contains e.g. a color center at sites i . Thus, we arrive at a cross road from where three routes emerge: either we envisage (a) one charge carrier in each cluster and inter-cluster pairing (e.g. the spin bag scenario [7]), or (b) each Φ_i accommodates one Cooper pair (e.g. the bipolaron scenario [8]), or finally (c) the PCHCR approach, where each Φ_i describes a number of charge carriers and the Cooper pairs become *non-local* pair-preserving resonances, which we span in a product of local correlated many-body wave functions [9,10]. Inter-cluster phase coherence implies communication as to what particular local cluster resonance is employed in each cluster. In [10] couplings of virtual excitations in the charge carrier channel and local AF background were demonstrated, and proposed to provide the necessary physics for Off-Diagonal Long-Range Order (ODLRO). Accordingly, the coherence length is reflected in the shortest distance between resonating clusters.

The Phase-Coherent-Holes-Cluster-Resonance Scenario

We formulate and apply the PCHCR scenario for the cuprate superconductors [9,10]. This scenario is physical for these materials because of (a) the well documented short coherence length (≈ 20 Å), (b) the extreme locality involved in the Cu-O-Cu super-exchange interaction which is known experimentally to couple to superconductivity [11,12], and (c) holes clusters are well defined QM objects for which detailed wave

function based quantum chemical techniques are applicable [9]. Below, the simplest scenario for the high- T_c SC cuprates is sketched. Following closely [10], we write a schematic projected wave function ansatz, which includes the charge carrier portion alone, as

$$\Psi = \Pi_i [u_i (\mu_i c_{i1s\uparrow}^\dagger c_{iD\uparrow}^\dagger + v_i c_{i1s\uparrow}^\dagger c_{i2s\uparrow}^\dagger + \zeta_i c_{i2s\uparrow}^\dagger c_{iD\uparrow}^\dagger) + e^{i\theta} v_i (\alpha_i c_{i1s\downarrow}^\dagger c_{i1s\uparrow}^\dagger + \beta_i c_{iD\downarrow}^\dagger c_{iD\uparrow}^\dagger + \kappa_i c_{i2s\downarrow}^\dagger c_{i2s\uparrow}^\dagger)] | 0 > \quad (2)$$

Comparing eqs. (1) and (2), we note that Φ_i has become a correlated two-particle wave function where the two holes are spanned in a mix of singlet and triplet states, each of which in turn are expressed in the single particle eigenstates of the cluster hamiltonian (1S has neither angular nor radial nodes, 2S has one radial node, and D has two angular nodes but no radial node). Such a mix of spin and space symmetry states cannot contribute to the ground state of a free molecule, but non-adiabatic coupling to an external perturbation is required (*vide infra*). As the symmetry of the order parameter becomes the symmetry of the pair breaking excitation, both S and D symmetry order parameters contribute in general to the ground state. A simplified description [9] focuses on the D-wave channel alone:

$$\Psi = \Pi_i [u_i c_{iS\uparrow}^\dagger c_{iD\uparrow}^\dagger + e^{i\theta} v_i (\alpha_i c_{iS\downarrow}^\dagger c_{iS\uparrow}^\dagger + \beta_i c_{iD\downarrow}^\dagger c_{iD\uparrow}^\dagger)] | 0 > \quad (3)$$

where $\alpha_i^2 + \beta_i^2 = 1$, $u_i^2 + v_i^2 = 1$, and for which the reduced hamiltonian becomes

$$H_{red} = \sum_{iL\sigma} \epsilon_{iL} c_{iL\sigma}^\dagger c_{iL\sigma} + 1/2 \sum_j (c_{jD\downarrow}^\dagger c_{jS\uparrow} - c_{jS\downarrow}^\dagger c_{jD\uparrow}) \sum_i V_{ij} (c_{iS\uparrow}^\dagger c_{iD\downarrow} - c_{iD\uparrow}^\dagger c_{iS\downarrow}) \quad (4)$$

Employing literally the configuration space analog of the BCS treatment [2] results in a local gap function in terms of local wave function properties and local excitation energies of the cluster [10], i.e.

$$\Delta^2 = (x/2)^2 (\alpha + \beta)^2 V^2 - \gamma^2 (\alpha - \beta)^2 \quad (5)$$

where α and β are the amplitudes of the local two-particle singlet states built from S×S and D×D single-particle states, γ is the $\epsilon_D - \epsilon_S$ orbital energy difference, and x is the number of neighboring clusters that contribute to Δ . It is noted that the gap function is maximized when the amplitudes are equal, i.e. when γ is zero. Hence, we have deduced the local analog to the Cooper instability. The interaction $-|V|$ ensures that the pair states are *shared* between holes clusters, meaning that energy is gained if the local pair amplitudes v_i are accessed coherently. A particular understanding was demonstrated in [9,10], as the non-adiabatic coupling to the local AF background was shown to allows for the local incommensurate spin and symmetry states in eqs. (2) and (3) to mix. A scenario which associates (i) the “spin gap” to AF fluctuations, (ii) holes clustering to the opening of the “pseudogap”, and (iii) virtual spin excitations in the range of the local pair-breaking excitation energy communicating the phase

information in general and producing ODLRO in particular. Thus, AF fluctuations become a necessary prerequisite for high- T_c SC in the cuprates.

Future directions - *Mesoscopics and new materials*

The acquired understanding of superconductivity in the cuprates will be employed to formulate Josephson tunneling across grain boundaries. We will discuss how microscopic phase coherence is maintained across a break junction. This is in order to illustrate the potential of the particular PCHCR formulation for nano-technology. The strategy is to look more closely into the holes clustering instabilities, as the radius of the de-clustering excitation should define the lengthscale of the width of the junction. We employ the wave function ansatz

$$\Psi = \Psi_{L(\text{eft})}(\theta_L) \times \Psi_{R(\text{ight})}(\theta_R) \quad (6)$$

where

$$\Psi_{\text{Side}} = \prod_{i \in \text{Side}} \Phi_i \quad (7)$$

and Φ_i is defined in eq. (1). The reduced phasing hamiltonian is extracted from the blocked reduced hamiltonian according to

$$H^{\text{red}} = H_L^{\text{red}} + H_R^{\text{red}} + H_{L-R}^{\text{red}} \quad (8)$$

where

$$H_{L-R}^{\text{red}} = \sum_{j \in R} (c_{jD\downarrow}^\dagger c_{j1S\uparrow} - c_{j1S\downarrow}^\dagger c_{jD\uparrow}) \sum_{i \in L} V_{ij}^{L-R} (c_{i1S\uparrow}^\dagger c_{iD\downarrow} - c_{iD\uparrow}^\dagger c_{i1S\downarrow}) + \\ \sum_{j \in R} (c_{j2S\downarrow}^\dagger c_{j1S\uparrow} - c_{j1S\downarrow}^\dagger c_{j2S\uparrow}) \sum_{i \in L} V_{ij}^{L-R} (c_{i1S\uparrow}^\dagger c_{i2S\downarrow} - c_{i2S\uparrow}^\dagger c_{i1S\downarrow}) + \\ \sum_{j \in R} (c_{jD\downarrow}^\dagger c_{j2S\uparrow} - c_{j2S\downarrow}^\dagger c_{jD\uparrow}) \sum_{i \in L} V_{ij}^{L-R} (c_{i2S\uparrow}^\dagger c_{iD\downarrow} - c_{iD\uparrow}^\dagger c_{i2S\downarrow}) \quad (9)$$

For nearest neighbor sites across a junction, the more extended cluster states involving $2S_i$ and $2S_j$ are non-orthogonal and must mix. The second and third term in eq.(9), of S and D symmetry, respectively, will contribute most to the tunneling current as these describe delocalized pairs at the grain boundary. The first term in eq. (9) is expected to contribute negligibly because the junction comprises a disconnecting medium, and thus the phase difference $|\theta_L - \theta_R|$ is maintained exclusively by the inter-grain orbitals overlap. *Note particularly the required continuous transition into a single superconductor upon fusion.* This again implies the existence of two overlap driven (Fermi liquid like) inter-cluster channels of both S and D symmetry, and one non-overlap driven (non-Fermi liquid like) channel of D-symmetry, which all contribute to the SC ground state.

The very purpose of projecting a SC ground state onto a cluster basis was originally to provide a strategy for making new high- T_c SC materials and improve on old ones. The mixing of paired and pair-broken states in eq. (2,3) assumes non-adiabatic coupling between the charge carrier channel and a second fermionic sub-system. Phase coherence is required though, in order to benefit from the possibility of mixing. This in turn implies that the fermionic bath should display some sort of long-range order, e.g.

AF, and the phase information be communicated e.g. by means of virtual excitations in an AF background. The challenge of eq. (5) becomes to condense compounds which possess local near-degenerate independent particle states e.g. due to lattice instabilities.

Acknowledgements

This on-going program is supported by the Swedish Consortium for Superconductivity and the Swedish Natural Sciences Research Council.

References

1. F. London, *Superfluids* Vol. 1 (London; Wiley 1950).
2. H. Frölich, Phys. Rev. **79** (1950) 845.
3. J. Bardeen, L. N. Cooper, and J. R. Schrieffer, Phys. Rev **108** (1957) 1175.
4. See Special Proceeding on Stripes, J. Superconductivity, **10** (1997)
5. O. Zachar, S.A. Kivelson, and V.J. Emery, Phys. Rev. **B57** (1998) 1422.
6. I. Panas, R. Gatt, Chem. Phys. Letters, **266** (1997) 410.
7. J.R. Schrieffer, X.G. Wen and S.-C. Zhang, Phys. Rev. Letters **10** (1988) 944.
8. See e.g. P.P. Edwards, N.F. Mott, and A.S. Alexandrov, J. Superconductivity, **11** (1998) 151.
9. I. Panas, J. Superconductivity, submitted.
10. I. Panas, Phys. Rev. **B** submitted.
11. H.F. Fong, B. Keimer, D.L. Milius, and I.A. Aksay, Phys. Rev. Letters **78** (1997) 713.
12. H.A. Mook, Pengcheng Dai, S.M. Hayden, G. Aeppli, T.G. Perring, and F. Dogan, Nature **395** (1998) 580.

Influence of Ionic Dielectricity on the Dynamic Superconducting Order Parameter.

M. Peter¹ and M. Weger²

¹*DPMC, Geneva University, Geneva, Switzerland.*

²*Racah Institute of Physics, Hebrew University, Jerusalem, Israel.*

Abstract. We investigate the effect of a ferroelectric transition that is close to a superconducting transition. The closeness of the ferroelectric transition manifests itself in a large ionic dielectric constant ϵ , which is not present in “normal” metals where the conduction electrons shield it out. This reduces the Debye screening parameter from q_D to $q_D/\sqrt{\epsilon}$ at frequencies below the dispersion frequency $\omega_t \approx 20$ meV of $\epsilon(\omega)$. The electron-phonon matrix element is renormalized as a result. We extend the Eliashberg equations for this renormalized interaction, and develop an algorithm to solve them along the real- ω axis. We find that various anomalous properties, such as the high value of T_c , the high value of $2\Delta_0/T_c$, the d-wave symmetry of the gap parameter, the extended Van-Hove singularity, the damping of the electronic states near the FS, the pseudogap, and various other properties of the cuprates, as well as organic metals, are accounted for.

INTRODUCTION

The problem of the origin of high-temperature superconductivity is still one of the most topical problems of condensed matter physics. The quest continues to find an interaction strong enough to produce a superconducting phase transition at temperatures much higher than what is observed in “normal” metals. There are serious reasons to believe that antiferromagnetic exchange can indeed serve as a stronger pairing mechanism than the conventional phonon-mediated interaction [1]. Moreover, if an interaction is found which is sufficiently strongly coupled to the electrons, then can strong coupling theory describe the superconducting state, or do fluctuations make this approach ineffective, so that some new method of calculation has to be used [2,3]? Can this method be handled with available computer power?

Because of the complexity of observable phenomena, and the diversity of properties of different substances, it is very difficult to build a scheme which takes into account all aspects of the phenomenon, and as a preliminary step, one can try to account for different factors separately, having in view to estimate their relative

importance. In the present work we take into account one such effect. We present a model based on a “nearly ferroelectric” scenario, which we believe fits the perovskites, and use the Lyddane-Sachs-Teller picture for the ionic dielectric constant $\epsilon(\omega)$. This model yields an interesting behavior for the functions $Z(\omega)$, $\Delta(\omega)$, etc. which characterize the superconducting state. The effect of a very large and highly-dispersive ionic dielectric constant was (to our knowledge) not considered before. The dielectric constant modifies the Eliashberg equations [4] in an *essential* way.

It was suggested a long time ago [5] that near-ferroelectricity is favorable for superconductivity, and indeed doped SrTiO_3 which is a semiconductor that is not expected to be superconducting *at all* (because $N(E_F)$, and consequently λ , are very small), is superconducting at about 1 K. Baratoff and Binnig [6] accounted for this by claiming that the electronic screening which reduces the electron-ion potential is no longer effective when the phonon frequency is higher than the electronic plasma frequency. In metallic cuprates, the plasma frequency (1.3 eV) is much higher than the phonon frequency (40 meV) and this argument doesn't hold. Nevertheless, Bednorz and Müller [7] discovered high- T_c superconductivity in the perovskite cuprates. We attempt to find out whether a more elaborate theory can account for this discovery, as due to the near-ferroelectric nature of the perovskites.

A different mechanism by which the large dielectric constant can enhance superconductivity was suggested by Babichenko and Kagan [8]. The large ϵ_0 reduces the Coulomb term μ^* that reduces T_c . However, there is also a second-order interaction due to the Coulomb term, which is attractive and enhances T_c , as pointed-out originally by Kondo [9]. This second-order term, being a high-frequency effect, is screened just by the small ϵ_∞ rather than by ϵ_0 . Therefore this second-order term may actually take-over and enhance T_c .

We explore the influence of an ionic dielectric constant due to ions whose electrons do not directly participate in the superconducting state (e.g. the apex oxygen, the alkaline earths, the rare earths, ions like Bi, Hg, etc.) on the strength of superconducting pairing [10]. The mechanism considered here is the diminution of the electronic shielding (by the conduction electrons) of the electron-phonon interaction caused by the ionic dielectric constant, which “preempts” the electronic screening. This effect is shown in a dramatic way by Kamimura and Sano [11]. They show that when the chain copper has 0.55 holes in its 3d shell, the splitting between the Zhang-Rice triplet and singlet states centered around the planar copper vanishes (Fig.1a). Denoting this splitting U_{eff} , and defining an effective dielectric constant by: $U_{\text{eff}} = U_{\text{bare}}/\epsilon$, we see that ϵ is extremely large. Note that this effective dielectric constant is a local property, on a scale of a lattice constant, and can by no means be regarded as homogeneous, i.e. here $\epsilon(r_1, r_2) \neq \epsilon(r_1 - r_2)$, in contrast with the background dielectric constant in semiconductors [12].

It is clear that the influence of dielectricity on superconductivity will be felt not only through the weakening of the electronic shielding, but also through other channels [46], but we have shown [13] that the diminution of electronic shielding may be the dominant effect, not automatically compensated through other contributions. We consider the possibility that the interaction between the planar oxygen (and

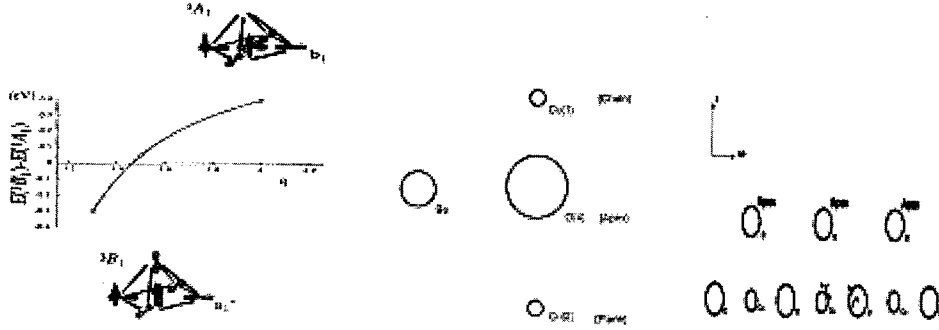


FIGURE 1. (a) right, (b) center and (c) left

copper) ions and the conduction electrons is modified by the Ba (or Sr, Ca) atoms, in conjunction with the neighboring (apex) oxygen which possesses a very high polarizability, as well as rare-earth atoms such as La and their neighboring oxygens. The ionic dielectric constant of the cuprates is very large, $\epsilon_0 \approx 30-50$ with a dispersion at a rather low frequency ($\omega_{\text{trans}} \approx 15-30$ meV) [14]. This is the frequency of low-lying transverse-optical (TO) modes, involving predominantly the motion of the barium (or other alkaline earth) atoms. The effect of the c-axis motion of the barium, reducing U_{eff} , was also suggested implicitly by Panas and Gatt [47].

We denote the dielectric constant that describes the shielding of the interaction between the planar oxygen ions and the conduction electrons by the "Ba" unit (Fig.1b), $\epsilon_{\text{O-Ba-el}}(\omega, q)$, whereas the interaction between *two conduction electrons* is shielded by the ionic dielectric constant $\epsilon_{\text{el-Ba-el}}(\omega, q)$. The large difference between $\epsilon_{\text{O-Ba-el}}$ and $\epsilon_{\text{el-Ba-el}}$ arises from the different location in space of the interacting charges in the extremely inhomogeneous material, in accord with the quantum-chemical calculation [11]. The first is in the vicinity of the planar oxygen, and the second is in the vicinity of the planar copper - apex oxygen. We illustrate this in Fig.1c.

In such a model we obtain a modified electron-ion interaction of the form:

$$V_{\text{O-el}}(\omega, q) = \left[\frac{4\pi Ze^2}{\epsilon_{\text{O-Ba-el}}(\omega, q)} \right] \frac{1}{q^2 + 4\pi e^2 N(E_F) / \epsilon_{\text{el-Ba-el}}(\omega, q)}$$

Whether the potential $V_{\text{O-el}}(\omega, q)$ will be diminished or strengthened by the dielectric contribution from the "Ba" depends on the relative strength of the two dielectric constants. When they are equal, the potential becomes weaker except at $q = 0$ where it retains the value $Z/N(E_F)$ [15], ϵ dropping out. When the two dielectric functions are no longer the same, as a result of the inhomogeneity of the system, this is no longer the case.

In Fig.2a we plot $1/\epsilon_{\text{O-Ba-el}}(0, q)$ and $1/\epsilon_{\text{el-Ba-el}}(0, q)$ (i.e. $\omega = 0$) as function of q (from ref.13). We see that at $q = 0$, both equal $1/\epsilon_0$, and at large q , both approach 1. However, at $q = q_D/\sqrt{\epsilon_0}$ which is small (i.e. about $k_F/3$), but not

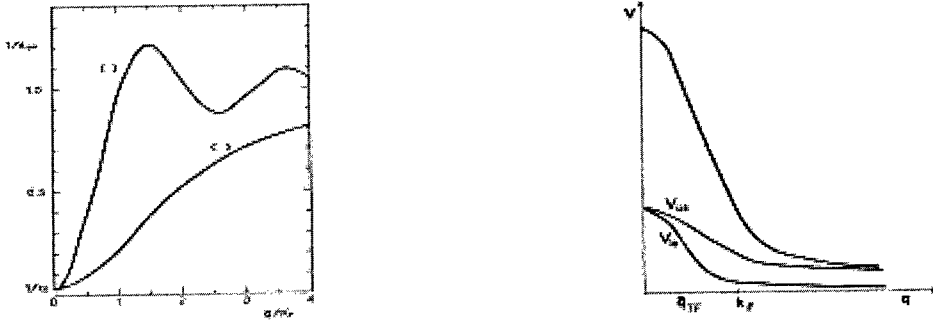


FIGURE 2. (a) right and (b) left

extremely small, $1/\epsilon_{\text{O-Ba-el}}(0, q_D/\sqrt{\epsilon_0}) \approx 1$ while $1/\epsilon_{\text{el-Ba-el}}(0, q_D/\sqrt{\epsilon_0}) \approx 1/\epsilon_0$, the difference between them being very large, causing $V_{\text{O-el}}(\omega, q)$ to be enhanced by a large factor. Since most of the contribution to the electron-phonon coupling comes from the region $q \sim q_D/\sqrt{\epsilon_0}$, we approximate the dielectric constants by their values at this q value. We illustrate $V_{\text{O-el}}$ and the electron-phonon matrix element I (at $\omega = 0$) in Fig. 2b,2c, as well as the unrenormalized values, i.e. the values when $\epsilon = 1$. The enormous enhancement of $I(q)$ at $q \sim q_D/\sqrt{\epsilon_0}$ is striking.

Some support for the very large value of $I(q)$ at $q \sim q_D/\sqrt{\epsilon_0}$ is provided by the stripes seen in many cuprates [16]. These are CDW's with a wavevector $q_{\text{stripe}} = 0.24 \text{ \AA}^{-1}$ which happens to be just equal to $q_D/\sqrt{\epsilon_0}$. The high-density region of the CDW is metallic, while the low-density region is insulating. We consider the stripes as an *indication* of the large value of $I(q)$ at $q = q_{\text{stripe}}$, rather than the *cause* of the high- T_c [17].

The treatment of the inhomogeneous medium is in the spirit of the central cell correction of the Kohn-Luttinger theory of shallow donors in semiconductors [12]. In that theory, space is divided into a region close to the donor ("central cell") where $\epsilon = 1$, and a more distant region, where the background dielectric constant ϵ is the average, measured dielectric constant of the insulating semiconductor. Our $\epsilon_{\text{O-Ba-el}}$ is analogous the ϵ of the central cell of the Kohn-Luttinger theory, and our $\epsilon_{\text{el-Ba-el}}$ is analogous to that of the distant region of that theory.

The dielectric function $\epsilon_{\text{el-Ba-el}}(\omega, q)$ determines the ionically-screened Thomas-Fermi cutoff: $\tilde{q}_D = [4\pi e^2 N(E_F)/\epsilon_{\text{el-Ba-el}}(\omega, q)]^{1/2}$.

We approximate $\epsilon_{\text{el-Ba-el}}(\omega, q)$ by the $q = 0$ value, taken in the form suggested by Lyddane, Sachs, and Teller [18]:

$$\epsilon = \frac{\omega^2 - \omega_{\text{long}}^2}{\omega^2 - \omega_{\text{trans}}^2} \epsilon_{\infty}$$

ω_{long} is the frequency of the longitudinal optic phonons (LO), which is about 80 meV in the cuprates.



FIGURE 3. (a) right and (b) left

We consider coupling with phonons of frequency Ω . For the cuprates, $\Omega \approx 40$ meV [19]. The mode Ω involves vibrations of the Cu-O bonds in the $(\text{CuO}_2)_n$ planes, perpendicular to the bond direction.

For $q = 0$, the potential $V_{\text{O-el}}$ is thus multiplied by $\epsilon(\omega)$. Since the coupling constant is proportional to $V_{\text{O-el}}^2$, we take a weighted phonon propagator (WPP) given by:

$$D_{\text{WPP}}(\omega) = \frac{\epsilon^2(\omega)\lambda\Omega}{\omega^2 - \Omega^2}$$

This renormalized phonon propagator is to be distinguished from the “bare” phonon propagator $D_0(\omega) = \lambda\Omega/(\omega^2 - \Omega^2)$. λ is a dimensionless coupling constant of order 1, which is calculated, for example, in band-structure calculations [20].

SOLUTION OF THE ELIASHBERG EQUATIONS GENERALIZED FOR THE FERROELECTRIC SCENARIO

2.1 Gap Functions for Imaginary Frequency

In Fig. 3a we show the WPP, as function of the imaginary frequency, plotted in units of $i\omega/\omega_{\text{long}}$ for two values of ϵ_0 , namely $\epsilon_0 = 1$ and $\epsilon_0 = 4$. Also we chose $\omega_{\text{long}} = \Omega$, $\epsilon_\infty = 1$, and $\lambda = 1$. The WPP for $\epsilon_0 = 4$ is much higher as $\omega \rightarrow 0$ than for $\epsilon_0 = 1$ ($\propto \epsilon_0^2$), but narrower, as seen by comparison with the scaled $\epsilon_0 = 1$ curve.

We solved the Eliashberg equations [4] for this WPP. We show the solutions, i.e. the gap Δ and renormalization function Z as function of the imaginary frequency in Fig. 3b. All calculations are carried out for low temperatures ($T \ll T_c$) (except for the determination of T_c , of course). The ratio $2\Delta(0)/T_c$ is found to be close to that found by Carbotte [21]. It reflects the fact that potentials which can differ strongly along the real axis, look remarkably similar for the Matsubara frequencies.

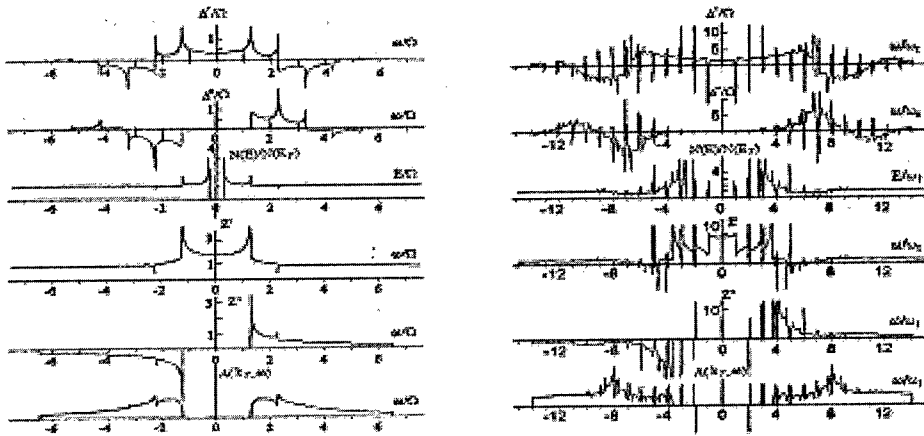


FIGURE 4. (a) right and (b) left

From this imaginary axis calculation, which is simple and well behaved, one sees that the ϵ -function creates an anomalously large Z at low frequencies, while the critical temperature T_c and gap Δ are not increased to the same degree. This result is expected, since $T_c \propto \sqrt{\lambda_{\text{eff}}}$ (for very strong coupling) while $Z(0) \approx 1 + \lambda_{\text{eff}}$; thus the increase in effective coupling brought about by ϵ increases $Z(0)$ more than T_c and $\Delta(0)$. We notice therefore that the enhanced kernel influences $\Delta(0)$ and $Z(0)$ in different ways. Note that when the cutoff is in the k -channel (rather than the ω -channel), Z is *decreased* and Δ *increased* significantly [10]. Observation of the ratios of $\Delta(0)$ to $Z(0)$ can therefore be of interest in estimating the nature of the interaction, and particularly the role of $\epsilon(\omega)$.

2.2 Gap Functions for Real Frequency

We have calculated the functions $\Delta(0)$ and $Z(0)$, the tunneling density of states, and the spectral function, for real frequencies, by analytic continuation of the above functions for imaginary frequencies. To do this, we have used the method due to Marsiglio, Schossmann, and Carbotte [21]. We show the results for one set of parameters in Fig.4. In Fig.4a we show the standard solution ($\epsilon_0 = 1$), and in Fig.4b, the solution for $\epsilon_0 = 4$. We see that $\Re[\Delta(\omega)]$ consists of a rather smooth background (in both cases), with spikes at the phonon frequencies (McMillan Rowell structure). Some of the main differences between the standard solution and the "nearly ferroelectric" solution are:

2.2.1 The large value of $\Delta(0)/T_c$.

It is well-known from strong-coupling theory that the value of $2\Delta(0)/T_c$ exceeds the BCS weak-coupling value of 3.53 and can reach values of about 4-5. In cuprates

higher values are found, in particular in underdoped materials [22], and in organic (BEDT-TTF)₂I₃ a value of 14 was measured [23]. For the conventional Eliashberg equations this ratio saturates at 11 for an infinite coupling constant. Here we find much larger values. There are two causes for the anomalously large value of the gap. One is the large value of λ_{eff} , which brings about a very-strong-coupling scenario even if λ is small. The second is more subtle. $\Delta(0)$ is the solution of the equation: $\Delta(\omega = \Delta_0) \approx \Delta_0$. The function $\Delta(\omega)$ is nearly constant for small values of ω , therefore $\Delta_0 \approx \Delta(0)$. Even for very large values of λ it is found numerically that this relationship holds for the “conventional” Eliashberg equations [21]. For the *extended* Eliashberg equations this is no longer the case, and Δ_0 is found in many cases to be significantly larger than $\Delta(0)$.

The increase in $2\Delta_0/T_c$ is due to the large value of ϵ ; therefore in underdoped materials where ϵ is larger than in optimally-doped ones (where the conduction electrons screen-out the ionic ϵ to some extent), $2\Delta_0/T_c$ is even larger. This is in accord with experiment [22].

2.2.2 Extended Van Hove singularity.

The renormalization Z' is very large up to $\omega \approx \omega_{\text{trans}} \approx 20\text{meV}$. For values of $\epsilon \approx 30\text{--}40$ characteristic of the cuprates, $Z' \approx 30$. Thus the renormalization energy $Z'\omega_{\text{trans}} \approx 0.5\text{ eV}$ is enormously large, and the E vs. k curve is flattened over a region where the unrenormalized band energy is within $\pm 0.5\text{ eV}$ of E_F , i.e. about half the Brillouin zone (in the region of k -space in the vicinity of the Van Hove singularity, which is at $\vec{k} = (0, \pi/a)$). This may account for the observed Extended Van-Hove singularity [24] in terms of an electron-phonon coupling.

Experimentally, the states in the EVHS have a small weight. This excludes a normal band interpretation, as in the A15's [25], and indicates a very large renormalization effect. This renormalization may be due to electron-electron interactions [26] as well as to an electron-phonon one. The IR measurements indicate a large mass-enhancement over a frequency region that coincides with the phonon spectrum (in contrast to the relaxation rate, which extends to 1 eV at least); the mass enhancement becoming particularly large at very low frequencies. This is in accord with the present calculation (Fig.4b).

2.2.3 Overdamping.

The large value of Z'' for $\omega \approx \omega_{\text{trans}}$ indicates a very strong damping of the electronic states, due to the electron-phonon coupling. Since ω_{trans} is so small, this occurs practically on the Fermi surface. Overdamping of electronic states is indeed observed by ARPES measurements [27]. This occurs in particular in underdoped samples, where ϵ is particularly large. This is in line with the results of the present work, which attributes these features to a very large ϵ .

Also, the maxima of Z' and Z'' are about the same (Fig. 4b). This is in line with the phenomenological picture of Chubukov [26], which describes the damping and points out a phase of $\pi/4$, i.e. nearly equal values of the real and imaginary

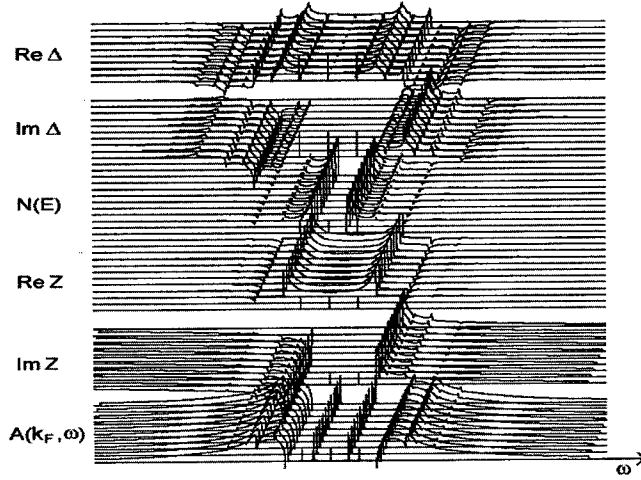


FIGURE 5. With q -dependent electron-phonon interaction

components of the self-energy. However, Chubukov attributes the self-energy to electron-electron interactions, while we attribute it to electron-phonon coupling.

2.2.4 Pseudogap.

Since $\epsilon(\omega)$ is cutoff at $\omega = \omega_{\text{trans}}$, the anomalies are cutoff at this energy causing a pseudogap at this energy. A pseudogap was explicitly calculated for this scenario, by calculating the electron-electron scattering rate $\frac{1}{\tau_{ee}(\omega)}$ [28]. Here also the pseudogap increases with ϵ , i.e. for underdoped materials, in accord with experiment. Again, this is only one way to account for the observed pseudogap, in addition to the several other possibilities that have been proposed.

Thus, the specific highly-anomalous spectroscopic features of the cuprates *can* follow directly from an electron-phonon scenario, in which a ferroelectric transition is nearby.

2.3 Gap Functions for Real Frequency

The calculation shown in Fig. 4 has been done for simplicity for an isotropic Fermi surface, assuming a q -independent electron-phonon matrix element. We have by now extended the algorithm to a q -dependent electron-phonon interaction. We show the result in Fig. 5. We divided a quadrant of the FS into 10 sections ("bands") with a matrix-element between sections as in Fig. 2c. The results for $\Re\Delta$, $\Im\Delta$, quasiparticle DOS, $\Re Z$, $\Im Z$, and spectral density, are essentially the same as before; however, some sharp peaks which are numerical artifacts no longer appear. Thus, we are confident that our algorithm is now applicable also to an anisotropic FS, and a strongly q -dependent interaction.

DISCUSSION

3.1 Low Frequency Scenario.

Normally it is believed that in order to obtain high- T_c superconductivity, it is necessary to mediate the interaction by *high* frequency bosons: $T_c = \omega_{\text{boson}} \exp[-(1 + \lambda)/\lambda]$ where ω_{boson} is the boson frequency, and λ the coupling constant. For an antiferromagnetic scenario, ω_{boson} may be the exchange frequency, which being of an electronic nature, may be higher than the phonon frequency. Excitons, plasmons, polarons with a high binding energy, charge transfer excitations, etc. being invoked frequently. Here we claim the contrary: Namely, that high-temperature superconductivity arises from a very *low* frequency cutoff, but with an enormous effective coupling constant $\lambda_{\text{eff}} \approx 10$. For very strong coupling, the formula for T_c is [29]: $T_c = 0.18\omega_{\text{boson}}\sqrt{\lambda/(1+2.6\mu^*)} = 0.18I\sqrt{N(E_F)/M(1+2.6\mu^*)}$ and the boson frequency is seen to cancel-out between the prefactor and $\lambda = \langle I^2 \rangle N(E_F)/M\omega_{\text{boson}}^2$. There remains the factor $\mu^* = \mu/[1 + \mu \ln(E_F/\omega_{\text{boson}})]$ which is small, leading to a somewhat higher T_c when ω_{boson} is small.

We claim here that the matrix element I is renormalized: $I_{\text{max}} = (2\pi Ze^2/q_D)\sqrt{\epsilon_0} = (2\pi Ze^2/q_D)\sqrt{\epsilon_\infty}(\omega_{\text{long}}/\omega_{\text{trans}}) = I(\omega_{\text{long}}/\omega_{\text{trans}})$ and the *small* value of ω_{trans} is responsible for the high- T_c . Pairing is attributed to the region $\omega < \omega_{\text{trans}} \approx 15\text{-}20$ meV. This assignment is novel and unusual.

In this very-low-frequency regime, spin-fluctuations are weak, as can be seen from the elaborate formulation of Chubukov [26] in which below $\omega_{\text{sf}} (\approx 14$ meV) spin fluctuations are suppressed, or from a more naïve Golden-Rule calculation [28], or from the IR measurements [30] that show a sharp fall in the Drude relaxation rate $1/\tau(\omega)$ for small ω . Therefore, there is no significant suppression of “conventional” pairing due to the spin fluctuations in this (and only in this) low-frequency region.

A problem with the very large λ_{eff} associated with this scenario, is the problem of instabilities. For a Holstein Hamiltonian, we may expect instabilities for $\lambda_{\text{eff}} \approx 10$, and a bipolaron scenario [3] is more suitable. However, here the renormalized coupling constant $\tilde{\lambda}(\omega) \approx \epsilon(\omega)^2 \lambda_\infty$ is a function of frequency, and therefore the “standard” solution of the Holstein Hamiltonian does not apply. We have to distinguish between *real* processes, where $\omega = \Omega$ and $\tilde{\lambda}(\Omega)$ is small (since $\Omega > \omega_{\text{trans}}$ and therefore $\epsilon(\Omega)$ is small), and *virtual* processes, where $\omega \leq \omega_{\text{trans}} < \Omega$ and $\tilde{\lambda}$ is very large. The pairing interaction is caused by exchange of *virtual* phonons, rather than real ones, and therefore the large value of $\tilde{\lambda}_{\text{eff}}$ contributes. We suggest here (without proof) that the value of $\tilde{\lambda}$ relevant to instabilities is $\tilde{\lambda}(\Omega)$ which is small, therefore instabilities are prevented in spite of the large value of $\tilde{\lambda}(0)$.

In Fermi liquid theory, the effective mass $m^*(\omega)$ is renormalized, and therefore different experiments yield different values of m^* . Here the proximity of the ferroelectric transition causes the coupling constant λ to be renormalized, therefore different experimental techniques *naturally* yield entirely different values of T_c . The value of T_c which depends on the virtual processes yields the very large value of

$\tilde{\lambda} \approx 10$, while the normal-state resistivity, which is due to real processes, yields a very small value of $\tilde{\lambda} < 0.1$. Forward scattering, nesting, and anisotropy of the Fermi surface obviously contribute to this difference as well; however, we believe that the discrepancy of more than two orders, as well as the stability, requires the large renormalization of $\tilde{\lambda}$.

In the “conventional” superconductor niobium, the effect of the anisotropy of the FS was studied very thoroughly and found to be extremely small [31]. In the cuprates we expect bigger effects due to the proximity of the VHS to some parts of the FS, and the forward scattering nature of the electron-phonon interaction. However, we doubt whether the variations of more than two orders between values of λ measured by different methods can be accounted for in this way. In this regard, organic superconductors serve a very useful purpose; namely, the FS there is much more isotropic. A similar behavior is seen there as well, and this serves as additional evidence for the interpretation proposed here.

A low-frequency scenario is also alluded-to by the work of Ashkenazi [32], who suggests electronic states of one type (“spinless polarons”), with a strong electron-phonon coupling very close to the FS, and states of a different nature (“semi-MFA carriers”) further away from the FS.

3.2 Two-dimensionality.

The use of the potential $V(q) = 4\pi Ze^2/(q_x^2 + q_y^2 + q_D^2)$ is far from obvious. An ordinary 3D potential includes a q_z^2 term in the denominator, and an ordinary 2D potential is given by: $V(q) = 4\pi Ze^2/(\sqrt{q_x^2 + q_y^2} + q_D)$. Here we use a 3D potential with a 2D FS, which is unconventional. The 3D potential is given by: $V(r) = Ze^2/r$. (We consider the oxygen ion as a point-charge, rather than a charge extended along the c -axis direction). $V(q)$ is given by the matrix element $\langle \psi_k | V(r) | \psi_{k+q} \rangle$ rather than by the Fourier transform (which is the ordinary 3D potential in q -space). The wavefunctions ψ_k and ψ_{k+q} are free-electron like in the $a - b$ plane, and extreme tight-binding like in the c -direction. Consequently the matrix element can be decomposed into intra-layer terms, where the contributions to ψ_k and ψ_{k+q} come from the *same* layer n (in the $a - b$ plane), and inter-layer terms, where the contributions come from different layers n, n' . In the intra-layer terms, q_z does not appear (the contributions from ψ_k and ψ_{k+q} cancel out). In the inter-layer terms, the factor $\exp[iq_z(n - n')]$ appears, but in the extreme tight-binding limit these terms are small and we ignore them. The extreme tight-binding limit in the c -direction reflects the 2D nature of the FS. In this way, the “unusual” form of $V(q)$ is obtained. Note that to obtain the plasmon dispersion relation in 2D, we do not use point-charges, but charge distributions extended in the c -direction, and consequently the anomalous dispersion relation $\bar{\omega}_p(q) \propto \sqrt{q}$ for small $q = \sqrt{q_x^2 + q_y^2}$ is obtained [33]. The unusual form of the potential causes $I_{\max} = (2\pi Ze^2/q_D)\sqrt{\epsilon_0}$ to diverge with ϵ_0 . The McMillan coupling constant λ_{eff} is given by integration of $I(q)^2$ over the FS, i.e. multiplication of I_{\max}^2 by the area on the FS where $I(q)$ is large, i.e. $(2q_D/\sqrt{\epsilon_0})(2\pi/c)$ (c is the lattice constant in the

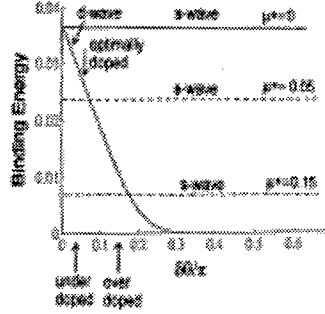


FIGURE 6. Condensation energies for *s*- and *d*-wave pairing

c-direction). Thus, (λ_{eff}) diverges like $\sqrt{\epsilon_0}$, and $T_c = 0.18\omega_{\text{trans}}\sqrt{\lambda_{\text{eff}}}$ diverges like $\epsilon_0^{1/4}$, which is a rather weak divergence. Therefore a very large value of ϵ_0 (≈ 30) is needed to obtain a significant increase in T_c (a factor of 2-3). An additional factor of 3 or so is obtained by the screening of the Coulomb interaction μ to: $\tilde{\mu} = \mu/\epsilon_0$. Thus we obtain an overall enhancement of T_c by a factor of 7-8 over the classical "McMillan" value of 30-40 K.

In 3D, the area over the FS where $I(q)$ is big and given by $\pi q_D^2/\epsilon_0$ therefore λ_{eff} does not diverge, and an enhancement of T_c comes only from the screening of the Coulomb interaction μ . A more detailed calculation is given in ref. [13].

3.3 d-wave Pairing.

The observation of d-wave pairing is one of the most seminal discoveries in the field of high- T_c superconductivity. It was motivated by the Pines theory, and therefore is used as an argument against the phonon mechanism. However, it was pointed out here in Miami at the Jan. 1995 conference, that the phonon mechanism can give rise to d-wave pairing for the case of forward scattering [34]. For exact forward scattering (δ -function, $\Delta\theta = 0$) and no Coulomb interaction, the condensation energies for *s*- and *d*-wave pairing are the same; a weak Coulomb interaction will favor the *d*-wave state (Fig.6). Due to the dielectric background, the scattering angle is given by $\Delta\theta = q_D/k_F\sqrt{\epsilon_0} \approx 0.3$ radians, and for this (small) scattering angle, *d*-wave pairing "wins" for a rather small value of the Coulomb interaction μ^* .

A degeneracy between *d*- and *s*-wave pairing was also proposed (phenomenologically) by Mueller [35]. Small-angle scattering was considered also by Abrikosov [36], arising from the Van Hove singularity (a band-structure effect). Kulic and Zeyher [37] considered small-angle scattering arising from correlations. Varelogianis considers small-angle scattering, and the effect of the near-degeneracy between *d*-wave and *s*-wave pairing, enhancing the effect of the orthorhombic distortion in $\text{YBa}_2\text{Cu}_3\text{O}_7$ [38].

Annett [39] describes this situation as an accidental degeneracy. Accidental degeneracy has the property to be removed by a small perturbation, just as the acci-

dental degeneracy between 2s and 2p states in hydrogen is removed by an electric field. In the present case, strong-coupling favors the s-wave state over the d-wave one [40]. The reason that the d-wave persists under conditions of strong coupling, is the large anisotropy of the FS, with regions near the Van-Hove singularity with a large λ ("hot spots"), and regions removed from it, with a small λ ("cold spots") [34].

The present theory, attributing the forward-scattering to the large ϵ , predicts that when ϵ is reduced, for example by overdoping (the conduction electrons screening-out the ionic polarizability), s-wave pairing should take over without a large change in T_c . This is perhaps observed [41]. In Fig.6 we illustrate the values of $\Delta\theta$ for underdoped, optimally doped, and overdoped materials.

Also, when no apex oxygen is present, ϵ is smaller and s-wave pairing is expected. This is the situation in the electron-doped NdCeCuO superconductors.

THE PHONON MECHANISM AFTER ALL ?

While most workers in the field attribute the superconducting pairing to magnetic interactions, this assignment is by no means certain. Mean-field theory is used in a regime where spin fluctuations are enormously strong [30]; there are serious doubts whether the large effect is not removed by a vertex correction [42], and a recent NMR experiment seems to show that the correlation length is far too small to account for the high- T_c [43].

Admittedly, the objections to a phonon-mediated interaction are more numerous. (i) T_c is expected to be below 30 K. (ii) There should be no d-wave symmetry. (iii) The electron scattering rate should saturate at frequencies above the phonon frequency. (iv) The McMillan coupling constant λ calculated from band theory is about 1, while high- T_c requires a value of about 10. (v) There is almost no pulling of phonon frequencies. (vi) There is almost no isotope effect in optimally-doped materials. (vii) Normal state properties are highly anomalous. (viii) A pseudogap is observed above T_c . (ix) An extended Van Hove singularity is observed. (x) High- T_c is restricted to 2D systems. (xi) High- T_c is greatly affected by atoms far-away from the $(\text{CuO}_2)_n$ planes [2]. (xii) The conventional Eliashberg equations do not work. (xiii) Stripes are frequently observed, which do not fit the "conventional" scenario, etc.

None of these objections is decisive, but the accumulated weight of a dozen or so objections seems to be overwhelming. However, close scrutiny shows that all these objections are not independent, yet depend on *one* factor only: Namely, the assumption that the screening length is given by $q_D \approx 0.7 \text{ \AA}$, which is the smallest length-scale in the problem. When we replace q_D^{-1} by the *true* screening length $\tilde{q}_D \approx 4 \text{ \AA}$, which is larger than the Bohr radius a_0 or k_F , the interatomic spacing, etc. all the objections disappear *simultaneously*. And this replacement is justified both from *ab initio* [12,13] and empirical [16,17] considerations, and substantiated by the group-theoretical SO(5) formulation [44]. In the present work we show this

for some, though not all, of these objections. A more detailed analysis is given in another publication [45]. We feel that the case made for the local dielectric medium scenario, which is so characteristic of the nearly-ferroelectric perovskites, merits a serious consideration.

ACKNOWLEDGEMENTS.

The work of M. W. was supported by a grant from the Max Planck Institute in Stuttgart, and benefitted from discussions with O. K. Andersen, O. Gunnarson, G. Zwicknagl, C. Bernhard, and close cooperation with D. Schweitzer. We benefitted from detailed constructive criticism of D. Pavuna. We also acknowledge fruitful discussions with J. Appel, D. Fay, A. Bille, K. H. Bennemann, and D. Manske.

REFERENCES

1. D. J. Scalapino, *Phys. Reports* **250** (1995) 329.
2. P. W. Anderson, *Theory of Superconductivity of the High T_c Cuprates*; Princeton University Press 1997.
3. N. F. Mott and A. S. Alexandrov, *High Temperature Superconductors and Other Superfluids*, Taylor and Francis 1994.
4. G. M. Eliashberg, *Sov. Phys. JETP* **11** (1960) 696; **12** (1961) 1000.
5. V. L. Gurevich et al, *Sov. Phys. Solid State* **4**(1962) 131. M. L. Cohen, *Phys. Rev. A* **134** (1964) 511. J. Appel, *Phys. Rev.* **180** (1969) 508.
6. A. Baratoff and G. Binnig, *Physica* **108B** (1981) 1335.
7. S.G. Bednorz and K.A. Mueller, *Rev. Mod. Phys.* **60** (1988) 685.
8. V.S. Babichenko and Yu. Kagan, *JETP Lett.* **56** (1992) 303.
9. J. Kondo *Prog. Theor. Phys.* **29** (1963) 1; M. Fibich et al, *Physica C* **197** (1992) 84.
10. M. Weger, B. Barbiellini, M. Peter, *Z. Phys. B* **94** (1994) 387; M. Weger, B. Barbiellini, T. Jarlborg, M. Peter, G. Santi, *Ann. Phys.* **4** (1995) 431.
11. H. Kamimura and A. Sano, *J. Superconductivity* **10** (1997) 279.
12. W. Kohn and J.L. Luttinger, *Phys. Rev.* **96** (1954) 802.
13. M. Weger, M. Peter, L. P. Pitaevskii, *Z. Phys. B* **101** (1996) 573.
14. C. Y. Chen et al, *Phys. Rev. B* **43** (1991) 392; J. Humlicek et al, *Physica C* **206** (1993) 345; R. Henn et al, *Phys. Rev. B* **56** (1997) 6295; J. Kircher et al, *J. Opt. Soc. Am. B* **14** (1997) 705.
15. V. Heine, P. Nozieres, J.W. Wilkins, *Phil. Mag.* **13** (1966) 741.
16. A. Bianconi et al, *Phys. Rev. Lett.* **76** (1996) 3412.
17. M. Weger, *J. Superconductivity* **10** (1997) 435.
18. R. H. Lyddane, R.G. Sachs, E. T. Teller, *Phys. Rev.* **59** (1941) 673. N. W. Ashcroft and N. B. Mermin, *Solid State Physics*, pp. 547-548, Holt Saunders, Philadelphia 1976.
19. S. I. Vedenev et al, *Physica C* **198** (1992) 47; D. Mandrus et al, *Europhysics Lett.* **22** (1993) 199; Ch. Renner and Ø. Fischer, *Phys. Rev. B* **51** (1995) 9208.

20. S. Massidda et al, *Physica C* **176** (1991) 159. C. O. Rodriguez et al, *Phys. Rev B* **42** (1990) 2692. B. Barbiellini and T. Jarlborg, *Phys. Rev. B* **50** (1994) 3239.
21. F. Marsiglio and J. P. Carbotte, *Phys. Rev. B* **43** (1991) 5355.
22. Ch. Renner et al, *Phys. Rev. Lett.* **80** (1998) 149.
23. M. Weger, A. Nowack, D. Schweitzer, *Synth. Metals* **42** (1991) 1885; G. Ernst et al, *Europhys. Lett.* **25** (1994) 303.
24. J. Ma et al, *Phys. Rev. Lett.* **51** (1995) 3832.
25. M. Weger, I. B. Goldberg, *Solid State Phys.* **28** (1973) 1; T. Jarlborg, A. Manuel, M. Peter, *Phys. Rev. B* **27** (1983) 4210.
26. A. V. Chubukov, *Phys. Rev. B* **52** (1995) R3840.
27. D. S. Marshall et al, *Phys. Rev. Lett.* **76** (1996) 4841; M. S. Norman et al, *Phys. Rev. Lett.* **52** (1995) 15107.
28. J.I. Gersten and M. Weger, *Physica B* **225** (1996) 33.
29. V. Z. Kresin, H. Gutfreund, W. A. Little, *Solid state Commun.* **51** (1984) 339.
30. A. V. Puchkov, D. N. Basov, T. Timusk, *J. Phys. Cond. Matt.* **8** (1996) 10049.
31. M. Peter, J. Ashkenazi, M. Dacorogna, *Helv. Physica Acta* **50** (1977) 267.
32. J. Ashkenazi, *J. Superconductivity* **8** (1995) 559.
33. T. Ando, A. B. Fowler, F. Stern, *Rev. Mod. Phys.* **54** (1982) 438.
34. G. Santi et al, *J. Supercon.* **8**(1995)215; *Physica C* **259** (1996) 253.
35. K. A. Müller, *Nature* **337** (1995) 133.
36. A. A. Abrikosov, *Physica C* **244** (1995) 243.
37. R. Zeyher and M.L. Kulić, *Phys. Rev. B* **53** (1996) 2850.
38. G. Varelogiannis, *Phys. Rev. B* **57** (1998) R732.
39. J. F. Annett, N. Goldenfeld, A. J. Leggett, *J. Low Temp. Phys.* **105** (1996) 473.
40. R. Combescot, *Phys. Rev. Lett.* **67** (1991) 148.
41. R. J. Kelley et al, *Science* **271** (1996) 1255.
42. J. R. Schrieffer, *J. Low Temp. Phys.* **99** (1995) 397.
43. K. R. Gorny et al, *Phys. Rev. Lett.* **81** (1998) 2340.
44. J. Birman and A.I. Solomon, *Phys. Rev. Lett.* **49** (1982) 230. S.C. Zhang, *Science* **285** (1997) 1089.
45. M. Peter, M. Weger, L. P. Pitaevskii, *Ann. Physik* **7** (1998) 174.
46. J. Röhler, *J. Superconductivity* **9** (1996) 457.
47. I. Panas and R. Gatt, *Chem. Phys. Lett.* **259** (1996) 241,247.

Filamentary Dopant Condensation in $\text{HgBa}_2\text{CuO}_{4+\delta}$

J. C. Phillips

Bell Laboratories, Lucent Technologies (Retired), Murray Hill, N. J. 07974-0636

Abstract. Diffraction experiments on the titled compound indicate that the O_δ dopants may partially occupy two sites, one of which is coplanar with Hg but does not produce superconductivity, while occupancy of the out-of-plane site does; occupancies of the two configurations cross abruptly near $\delta = \delta_2 = 0.19$. The phase diagram, with a plateau in $T_c(\delta)$, $\delta_1 < \delta < \delta_2$, rather than the usual parabola, is remarkably similar to that seen in the thermal properties of uncompensated semiconductor impurity bands near the metal-insulator transition, as the author suggested previously. Here the nature of the defects which play the compensating role is identified for other cuprates, in order to explain why the titled compound, alone among the cuprates, has been observed to display "ideal" behavior. Some intrinsic limitations of Rietveld analysis of powder diffraction data for identifying filamentary formation are also discussed, as is the possibility of explaining the data with antiferromagnetic stripe models. Predictions are made for the phase diagram of the superconductive filling factor.

LOCAL STRUCTURE AND CONNECTIVITY

Recent studies (1,2) of the distribution of the O_δ dopants in the titled Hg cuprate by Rietveld refinement of neutron powder diffraction data have shown that there exist two dopant sites, labeled O3 and O4. The occupation numbers of these sites change discontinuously near $\delta = \delta_2 = 0.19$, as do other structural parameters, such as the cell volume and the apical O z coordinate. This composition corresponds to the upper end of a novel plateau in $T_c(\delta)$, shown in Fig. 1, which is quite different from the usual parabola for

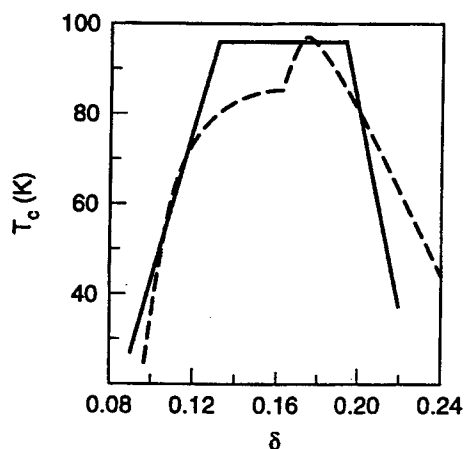


FIGURE 1. The plateau $T_c(\delta)$ in $\text{Ba}_2\text{HgCuO}_{4+\delta}$ (1) sintered at low T (solid line), compared with a double-sided parabola obtained for samples (18) sintered at high T (dashed line). The base line for the latter has been adjusted to match optimal doping and scaled to make the overall widths similar. Note the interesting kink at optimal doping in the (18) samples, which agrees with a first-order feature predicted theoretically (6); for the Argonne samples (1) the site occupancies (see Fig. 2) and the cell volume also show discontinuities near optimal doping ($\delta = 0.19$).

$T_c(x)$ which is found for LSCO and BSCCO, for example (3), and for $L^*B_2^*Cu_3O_{7 \pm \delta}$ (4), with $L^* = (La, Ca)$ and $B^* = (Ba, La)$.

The similarity of this plateau, $\delta_1 = 0.13 < \delta < \delta_2 = 0.19$, to the thermal properties of the intermediate phase associated with the metal-insulator transition in uncompensated semiconductor impurity bands, such as Si:P or Ge:Ga (5-9) led to the suggestion (10) that the Hg cuprates may be the materials where the filamentary character (11,12) of high-temperature superconductivity (HTSC) is most clearly expressed experimentally. Even in this "ideal material", however, the chemical cationic complexity of the unit cell, and the need to avoid contamination (for example, from CO_3) (13) is highly restrictive, and so far cationically ordered samples of the purity necessary to provide reliable values of δ have been made only in powder form at one laboratory.

Apart from the similarities of the phase diagrams, there are other aspects of the diffraction data which can be used to characterize the internal structure of the Hg cuprates, and which provide strong support for the filamentary model, as distinguished from other models, also based on nanoscale spatial inhomogeneities. The most popular of the latter are the "stripe" models (14) based on antiferromagnetic interactions which *suppress* HTSC when they are realized near commensurate doping compositions (such as $x = 0.125$ in $La_{2-x}Sr_xCuO_4$) which support spin density waves. A detailed critique of stripe models has been given elsewhere (15), and is available in full from the author upon request.

The most striking aspect of the Hg cuprates is that there is no evidence for antiferromagnetism in these materials in the limit $\delta = 0$, in contrast to the Ln-based cuprates in the limit $x = 0$. When we reflect that the average doping level for optimizing T_c in $Ba_2HgCuO_{4+\delta}$ is $\delta = 0.16$ (rather similar to $x = 0.16$ in $La_{2-x}Sr_xCuO_4$), and that the optimized T_c in $Ba_2HgCuO_{4+\delta}$ is more than twice that in $La_{2-x}Sr_xCuO_4$, it is already difficult to believe that localized magnetic interactions are anything other than harmful to HTSC. In fact, even in alloys where Hg has been partially replaced by Cr, such as $Hg_{0.6}Cr_{0.4}Sr_2CuO_{4+\delta}$ (16), where tetrahedral Cr and octahedral Hg stripes may alternate, the apparent *absence* of antiferromagnetism explains why T_c is reduced only to 60K.

More can be gleaned from the still-limited Hg cuprate data which are available so far (1,2). Already two possibilities have been proposed for the regimes with δ above or below 0.19, either the two O3 and O4 sites, or cationic disorder with Cu partially on the Hg sites, as in the Tl cuprate, which, however, does not exhibit the broad δ plateau for T_c that the Hg cuprate does (17). We note, however, that the Pauling ionic radii for Cu^+ , Tl^{3+} , and Hg^{2+} , respectively, are 0.96, 0.95 and 1.10Å, so that Cu fits well on the Tl site, but not on the much larger Hg site. Thus the two oxygen sites are much more likely to be the origin of the observed discontinuities.

CHAIN SEGMENTS

Within the framework of Rietveld analysis one considers partial site occupancies, and varies these occupancies and the site coordinates to optimize the fit to the powder data. However, isolated sites are unlikely to produce the abrupt changes in relative occupancies as a function of δ which have been reported and which are reproduced for the reader's convenience in Fig.

2. Such abrupt changes would be expected if the O4 sites were actually condensed into chain segments for smaller δ , with large stress fields surrounding each segment, and with each segment defining a certain strained volume from which other chain segments are excluded. As the dopant density increases and these volumes begin to overlap, and a liquid-gas-like (essentially a first-order finite-size) transition occurs, from connected, strained and lowered symmetry O4 sites to dispersed, symmetric and less strained O3 sites, as illustrated very schematically in Fig.3. This transition has a re-entrant character (the volume which was decreasing as δ increased ratchets up at $\delta = \delta_1$ and then continues its decrease) because the O4-based filaments are locally more metallic than the more weakly connected O3 gas, and therefore are more effective in contracting the volume.

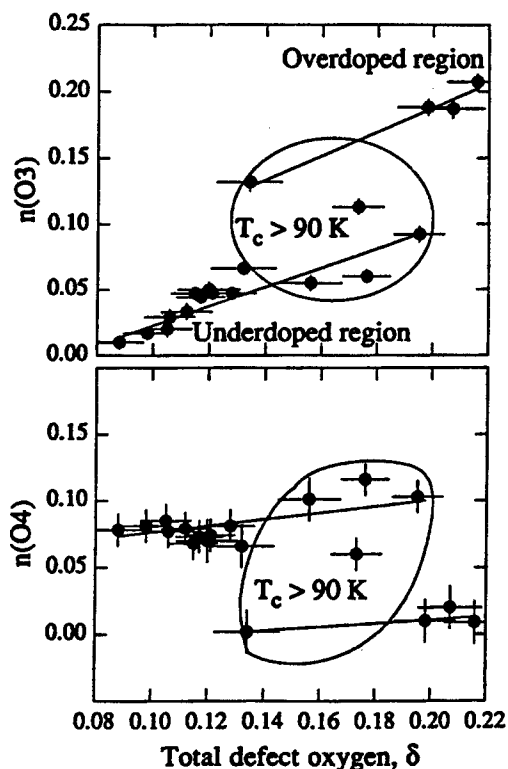


FIGURE 2. Partial site occupancies $n(\text{O3})$ and $n(\text{O4})$ as a function of doping $\delta = n(\text{O3}) + n(\text{O4})$ in $\text{Ba}_2\text{HgCuO}_4 + \delta$ (1).

In order to produce a diffraction pattern for such chain segments one would have to know many structural parameters and to go beyond one-cell Rietveld analysis to construct supercells containing the condensed chain segments, such as those observed by electron diffraction for $\text{Hg}_{0.6}\text{Cr}_{0.4}\text{Sr}_2\text{CuO}_{4+\delta}$ (16). For example, one would have to specify the local apical O and Hg coordinates relative to the O4 sites, which may be displaced from the plane $z = 0$ to connect better with the apical O (17). It is not easy to see how these multiple parameters could be determined from the limited amount of information available in neutron powder data. Nevertheless, the chain-segment condensation mechanism has many attractive features:

- (1) It explains the first-order character of the transition in Fig. 3, and the re-entrant behavior of the volume as a function of δ doping.

- (2) The chain segments are analogous to the CuO_{1-x} chain segments in YBCO. Such segments play a very important role in forming connected filaments which explain all the normal-state transport anomalies in the cuprates (12).
- (3) The filamentary model also helps us to understand why only the Hg cuprates show the "ideal" plateau in $T_c(\delta)$, which is not observed in the other cuprates.

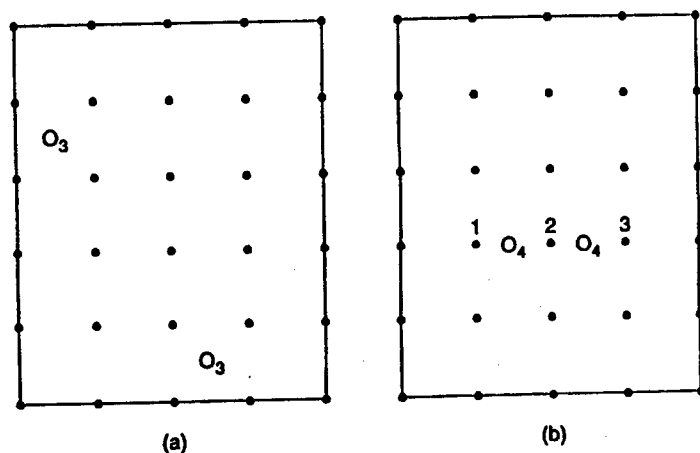


FIGURE 3. Sketch of the Hg O_s plane for $\delta \sim 0.1$. In (a) only the O_3 sites are occupied in a disconnected way. In (b) only the O_4 sites are occupied in a connected way. A filamentary segment can be imagined by the reader if he supposes that the central Hg1 (filled circle) - O_4 (open circle) - Hg2 - O_4 - Hg3 segment is vertically displaced upwards to connect better to downwardly displaced apical O's above the terminal Hg1,3 atoms, which connect in turn to two CuO_2 nanodomains, so that the Hg1...Hg3 chain segment enables the filament to bypass the nanodomain wall separating the two CuO_2 nanodomains.

CATION DISORDER

Previously (10) it was observed that a strong similarity exists between the phase diagram for the thermal properties of uncompensated semiconductors, such as Si:P, near their metal-insulator transition, and the Hg cuprate $T_c(\delta)$, while the dopant plateau structure is lost in partially (more than a few %) compensated semiconductors and all other cuprate HTSC. In the cuprates the role of the compensating impurities can be played by any secondary source of inhomogeneous strain fields. In LSCO this secondary source is the non-random doping or clustering of the Sr cation dopants, which have low mobilities at the growth temperature, in contrast to very high oxygen anion dopant mobilities. It is possible that the intermediate phase is not achieved in YBCO_{7-x} because the concentration x of dopant O chain vacancies is limited by internal strain for small x , and for larger x ideal behavior is masked by the pseudo-tetragonal mixing of orthorhombic nanodomains in the 60K phase. In Tl2201 one has Cu on the Tl sites; in BSCCO one has the native Sr, Ca disorder, and in $\text{L}^*\text{B}^*\text{CO}$ there is the L^* , B^* cation disorder. Only in $\text{Ba}_2\text{HgCuO}_{4+\delta}$ synthesized at low T are these secondary disorder sources, primarily cationic, which interfere with homogeneous nucleation of filamentary segments, absent. However, cationic disorder is easily added by synthesizing

at high T (18), where Cu probably partially occupies the Hg sites, when the plateau in $T_c(\delta)$ should cross over to a parabola. By analogy with semiconductor impurity bands, I estimate that the crossover should take place at around 8 % Cu_[Hg].

This situation presents a quite satisfying parallel with the uncompensated/compensated dichotomy in semiconductor impurity bands. There a small percentage of compensating impurities is sufficient to erase the kink in the electronic specific heat coefficient $\gamma(n)$ and the first-order discontinuity in the Debye $\theta(n)$ [which contains the electron-phonon ion-screening terms which determine the Cooper pair attraction in superconductors]. This kink occurs at the high-dopant-density edge of the intermediate phase, corresponding here to $\delta = 0.19$. The kink is erased because the compensating impurities pin energy levels and thereby prevent complete correlation-energy driven rearranging to form the band of filamentary states (Phillips 1998a) characteristic of the intermediate phase. Secondary strain fields can similarly suppress the anti-Jahn-Teller polarization effects which play the same role for all the HTSC except the Hg cuprates, which explains their uniquely ideal behavior.

The transition at the low-density edge of the intermediate phase is essentially a continuous percolative transition from an insulator to a filamentary metal. This means that the filling factor for filamentary states which become superconductive should have an essentially triangular form, increasing from zero with a power law $\propto (\delta - \delta_1)^\mu$ with a break in slope at $\delta = \delta_1 = 0.13$, and returning discontinuously to zero at $\delta = \delta_2 = 0.19$. The ideal value for μ is $1/2$, just as in the impurity band case (Phillips 1998a,b, 1999b; Itoh et al. 1996). In imperfect samples with residual cation disorder, the triangular corners would, of course, be rounded, and μ might increase to ~ 1 . It might be possible to measure this filling factor thermally.

OTHER PHASE DIAGRAMS

Some comments are added here concerning sample preparation and characterization methods. There have been more than 1000 papers published on Hg cuprates, but only a few of them actually contain phase diagrams similar to the Argonne data sketched with a solid line in Fig. 1. The one (18) which contains results most nearly comparable to those discussed here is shown by the dashed line in Fig. 1. It utilized sintering at 700K and achieved the highest T_c at 1 at. oxygen. The Argonne results discussed here utilized low-temperature (300-400K) sintering and achieved highest T_c at higher partial oxygen pressures. The nominal optimal value of δ measured iodometrically for the Tokyo samples is half that for the Argonne samples. The latter are preferred and discussed here for several reasons: (I) It is easy to see how Hg/Cu disproportionation could occur in the high T sintering process (II) This could obscure the plateau and replace it with nearly a parabola (but note in Fig. 1 the interesting kink on the low-doping side of the Tokyo T_c at optimal doping, reminiscent of the first-order effects expected theoretically (10) at the upper edge of the plateau), and (III) It is difficult to see how the plateau, with its sharp edges, could be an artifact.

I am grateful to Dr. J. Jorgensen for several helpful discussions.

REFERENCES

1. Jorgensen, J. D., Chmaissem, O., Wagner, J. L., Jensen, W. R., Dabrowski, B. Hinks, D. G., and Mitchell, J. F., *Phys. C*, **282-287**, 97-100 (1997).
2. Chmaissem, O., Jorgensen, J. D., Hinks, D. G., Wagner, W. R., Dabrowski, B. G., and Mitchell, J. F., *Phys. B*, **241-243**, 805-807 (1998).
3. Nakano, T., Monomo, N., Oda, M., and Ido, M., *J. Phys. Soc. Jap.*, **67**, 2622-2625 (1998).
4. Chmaissem, O., Jorgensen, J. D., Short, S., Knizhnik, A., Eckstein, Y., and Shaked, H. *Nature* (1998).
5. Phillips, J. C., *Proc. Nat. Acad. Sci.*, **95**, 7264-7269 (1998).
6. Phillips, J. C., *J. Phys. Soc. Japan* **67**, 3346-3348 (1998).
7. Phillips, J. C., *Sol. State Com.*, (in press). (1999).
8. Itoh, K.M., Haller, E. E., Beeman, J. W., Hansen, W. L., Emes, J., Reichertz, L.A., Kreysa, E., Shutt, T., Cummings, A., Stockwell, W., Sadoulet, B., Muto, J., Farmer, J. W., & Ozhogin, V. I. *Phys. Rev. Lett.* **77**, 4058-4061 (1996).
9. Watanabe, M., Ootuka, Y., Itoh, K. M., and Haller, E., *Phys. Rev. B*, **58**, 9851-9857 (1998).
10. Phillips, J. C., *Phil. Mag. B* (in press, 1999).
11. Phillips, J. C., *Phys. Rev. B*, **41**, 8968-8973 (1990).
12. Phillips, J. C. *Proc. Natl. Acad. Sci.*, **94**, 12771-12775 (1997).
13. Raveau, B., Huve, M., Maignan, A., Hervieu, M., Michel, C., Domenges, B., and Martin, C. *Physica C*, **209**, 163-166 (1993).
14. Emery, V. J. and Kivelson, S. A. *Phys. Rev. Lett.*, **64**, 475-478 (1990).
15. Phillips, J. C., 1998c *unpublished*.
16. Chmaissem, O., Argyriou, D. N., Hinks, D. G., Jorgensen, J. D., Storey, B. G., Zhang, H., Marks, L. D., Wang, Y. Y., David, V. P., and Dabrowski, B. G., *Phys. Rev. B*, **52**, 15636-15643 (1995).
17. Wagner, J. L., Chmaissem, O., Jorgensen, J. D., Hinks, D. G., Radaelli, P. G., Hunter, B. A., and Jensen, W. R. *Phys. C*, **277**, 170-182(1997).
18. Fukuoka, A., Tokiwa, Y., Yamamoto, A., Itoh, M., Usami, R., Adachi, S., Yamauchi, H., and Tanabe, K. *Phys. C*, **265**, 13-18 (1996).

Thermodynamics of the van Hove BCS model: Mixed gap symmetries.

D. Quesada, R. Peña and C. Trallero-Giner

*Department of Theoretical Physics, Faculty of Physics,
University of Havana, Havana 10 400, Cuba*

Abstract. An analysis of the electronic specific heat and the thermodynamic critical magnetic field as a function of the temperature is carried out in the cases of gap with isotropic-s, d and $s + id$ symmetries. While the isotropic-s gap shows an exponential attenuation in the electronic superconducting specific heat for low temperatures ($T \ll T_c$) the d-wave gap presents a quadratic dependence in a wide range of temperatures and goes through a maximum at $T < 1$ K. In the case of the $s + id$ mixing a double peak transition has been obtained from the numerical computations. In the $C_{en}(T)/T$ dependence a maximum at a certain temperature T^* is obtained which moves to the side of high temperatures when the Fermi level is far away from the van Hove singularity. The temperature dependence of the critical magnetic field presents a great departure from the parabolic law in the case of an isotropic-s gap while in the d-wave case, the mentioned dependence approaches the parabolic one.

I TOY MODEL CONTAINING A MIXTURE OF GAP SYMMETRIES.

The phenomenon of high temperature superconductivity (HTSc) has motivated the appearance of new views on the solid state theory as a whole. In this context, the study of the thermodynamics of the new layered perovskites constitutes a cornerstone in the understanding of many unusual behaviors observed up to date. The inclusion of the van Hove singularity (vHs) observed in ARPES measurements [1] into the BCS theory has been done by different authors [2,3]. These ideas have been extended in order to include gap symmetries different from the s-wave one [4]. Even though the existence of gap anisotropy has been confirmed experimentally, such real symmetry under rotations it is still a matter of debate [5]. On the other hand, in the normal state of underdoped materials an apparent pseudogap is observed whose nature is still awaiting explanation.

According to symmetry operations of the tetragonal group D_{4h} [5] the following gap has been considered.

$$\Delta_{\vec{k}}(T) = \Delta_s(T) + \exp(i\theta) \Delta_d(T) (\cos k_x p - \cos k_y p)$$

where, θ is the relative phase angle between s and d-wave components. While $\theta = 0$ corresponds to a $s+d$ mixing, $\theta = \pi/2$ yields to a $s+id$ mixing. The symmetry mixing yields in principle to an existence of two different critical temperatures T_{cs} and T_{cd} so that the T_c of the whole material is determined by $T_c = \max(T_{cs}, T_{cd})$. The temperature dependence of the gap may be modelled by the following expression:

$$\frac{\Delta(T)}{\Delta(0)} = \tanh \left[2 \sqrt{\frac{T_c^{s,d} - T}{T}} \right], \quad (1)$$

which differs slightly from the conventional BCS dependence. The evolution from the s- to a d-wave gap has been modelled by means of the following equations:

$$\frac{k_B T_c^s(c)}{2t} = \frac{1}{\exp[(c - 0.3)/0.04] + 1}, \quad \frac{k_B T_c^d(c)}{2t} = 1 - \frac{1}{\exp[(c - 0.5)/0.06] + 1},$$

where c is a parameter that drives the amount of d-wave component is presented. Even though the limits $c = 0$ and $c = 1$ correspond to the nearly s- and d-wave gaps respectively this model reproduces the fact of existence of three region in two of which a dominant gap symmetry is presented (s or d) and other, with a mixture of these two symmetries.

II SPECIFIC HEAT AND CRITICAL MAGNETIC FIELD.

The superconducting-state electronic specific heat can be obtained from the usual BCS expression [6], where the derivative of the square of the gap is given by:

$$\frac{d|\Delta_{\vec{k}}(T)|^2}{dT} = \frac{d\Delta_{\vec{k}}^s(T)^2}{dT} + \frac{d\Delta_{\vec{k}}^d(T)^2}{dT} + 2 \cos(\theta) \left[\frac{d\Delta_{\vec{k}}^s(T)}{dT} \Delta_{\vec{k}}^d(T) + \Delta_{\vec{k}}^s(T) \frac{d\Delta_{\vec{k}}^d(T)}{dT} \right] \quad (2)$$

The derivative of the gap and its square with respect to the temperature are computed from Eq.(1). In the case of the $s+d$ mixing a square root singularity in the specific heat should be presented when both T_c^s and T_c^d are different. However, up to date experimental reports on the presence of this kind of singularity are still absent, therefore, for the $s+d$ symmetry is presented the critical temperatures for both components ($\Delta_{s,d}$) need to be the same. It is important to remark that this result does not have anything to do with the concrete form of the DOS or any criteria of stability of this phase under certain crystalline symmetry. It is worth noticing too, that in the case of the $s+id$ mixing this problem does not appear, because the relative phase between the two components of the gap is $\pi/2$ and then the cosine in Eq.(2) is equal to zero.

In Fig.(1) the specific heat is shown for those values of c for which a mixture of gap symmetries occurs. The T_c of the material has been assumed equal to 100 K. In both panels (a and b) the peaks other than the s-wave (d-wave) one represent

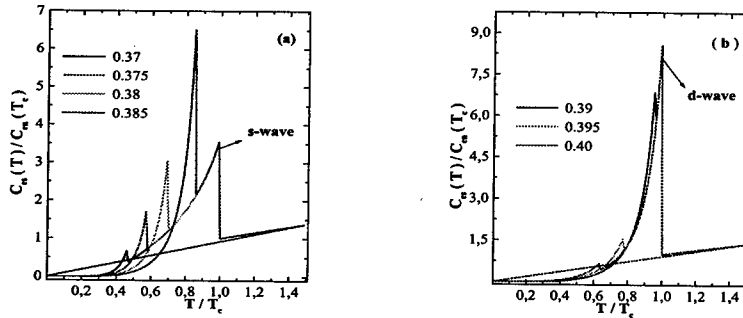


FIGURE 1. The electronic specific heat in the superconducting state as a function of temperature in the symmetry mixing region. In a panel (a) the T_c is ruled out by the s-wave component, while in (b) it is ruled out by the d-wave component of the gap.

the contribution coming from the second component of the gap. From this picture it is clear that the specific heat jump associated with the d-wave gap is larger than the respective one coming from the s-wave gap. This is due to the new layered superconductors are influenced by a gap anisotropy, which is reinforced by the presence of saddle point singularities in contrast to conventional superconductors, in which the DOS is a constant over the entire Fermi surface.

The specific heat in the superconducting state at very low temperatures presents a finite s-wave component which does not rule out the quadratic law observed for the d-wave gap in a wide range of low temperatures [8]. Even more, this quadratic dependence goes through a maximum near $T = 0.01T_c$. This anomaly appears only when the vHs and the d-wave symmetry are both present simultaneously, otherwise it does not occur. It seems to be associated with the complicated topology of the quasiparticle excitation energy surface.

In agreement with Ref. [6], the critical magnetic field is computed and shown in Fig.(2). In the case of s-wave gap, the $H_c(T)$ dependence departs from the old parabolic law irrespective of the values of the energy cut-off and the dimensionless interaction constant BCS parameters. In contrast, the d-wave symmetry yields to a dependence very close to the parabolic one. This fact could be understood by taking into account the power law dependence of the specific heat in the d-wave case.

III CONCLUSIONS

The phenomenon of mixture of gap symmetries containing s and d-wave components seems to be the most suitable for high temperature superconductors. The compelling evidence favoring the d-wave symmetry of the gap in CuO planes is not enough by itself. The inclusion of a small s-wave component does not rule

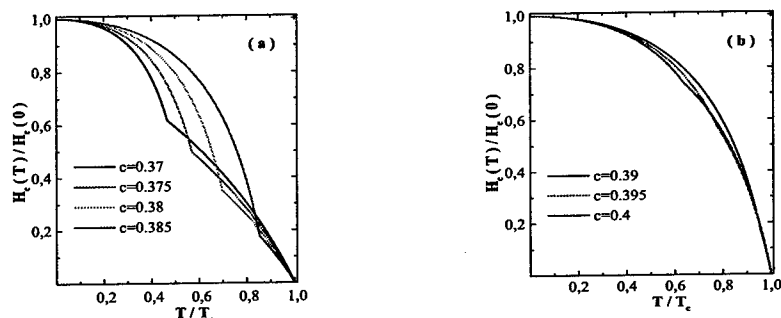


FIGURE 2. Thermodynamic critical magnetic field as a function of temperature for values of c where the s-wave (a) (d-wave (b)) gap rules out the superconducting transition.

out the expected for the d-wave gap a quadratic law of the specific heat at low temperatures.

The joined effect of the vHs and the gap anisotropy seems to fix a good starting point in understanding many unusual behaviors observed up to date in layered perovskites.

ACKNOWLEDGMENTS

One of the authors D.Q would like to thank the hospitality and the computer facilities of the Department of Physics of the University of Miami.

REFERENCES

1. Z.X. Shen and D.S. Dessau, Phys. Rep. **253**, 1 (1995).
2. J. Labbe and J. Bok, Europhys. Lett. **3**, 1225 (1987); R.S. Markiewicz, J. Phys. Cond. Matter **2**, 665 (1990); C.C. Tsuei, D.M. Newns, C.C. Chi and P.C. Pattnaik, Phys. Rev. Lett. **65**, 2724 (1990).
3. D. Quesada, C. Trallero-Giner and R. Baquero, Rev. Mex. Fis. **41**, 747 (1995); R. Baquero, D. Quesada and C. Trallero-Giner, Physica C **271**, 122 (1996).
4. M. Liu, D.Y. Xing and Z.D. Wang, Phys. Rev. B **55**, 3181 (1997); D.M. Newns, C.C. Tsuei and P.C. Pattnaik, Phys. Rev. B **52**, 13611 (1995); C. O'Donovan, J.P. Carbotte, Physica C **252**, 87 (1995).
5. R.A. Klemm, C.T. Rieck, K. Schamberg, cond-mat 9811303, Los Alamos (1998).
6. J.R. Schrieffer, Theory of Superconductivity, W.A. Benjamin Inc. (1964).
7. A. Junod in Physical Properties of High Temperature Superconductors II, edited by D.M. Ginsberg, p. 13, World Scientific, Singapore (1990).
8. M. Ido, M. Oda, N. Momono, C. Manabe and T. Nakano, Physica C **263**, 225 (1996); N. Momodo and M. Ido, Physica C **264**, 311 (1996).

Role of the long-range Coulomb interaction on the formation of striped phases in the two-dimensional Hubbard model

G. Seibold[†], C. Castellani*, C. Di Castro*, and M. Grilli*

[†] *Institut für Physik, BTU Cottbus, PBox 101344, 03013 Cottbus, Germany; * Istituto Nazionale di Fisica della Materia e Dipartimento di Fisica, Università di Roma "La Sapienza" Piazzale A. Moro 2, 00185 Roma, Italy*

Abstract. The formation of striped phases in the two-dimensional Hubbard model is investigated within an unrestricted slave-boson approach. We analyze in detail the stability of these structures as a function of doping. It turns out that the inclusion of a long-range Coulomb potential together with the strong local interaction favors the formation of half-filled vertical stripes for doping concentrations $x \leq 1/8$. Our results show that, besides the underlying lattice structure, also the electronic interactions can contribute to determine the different domain wall textures in Nd doped copper oxides and nickel oxides. An eventual spiral contribution to the striped spin textures in the copper oxide compounds is restricted to the low doping regime according to our calculations.

The observation of charged domain walls in the high- T_c superconductors presently attracts a lot of interest also with regard to possible pairing scenarios [1,2]. The pinning of incommensurate spin fluctuations together with the occurrence of incommensurate charge order has first been measured in Nd doped LSCO and nickel oxide compounds [3]. In the LSCO material the domain walls are oriented along the Cu-O bond direction with one hole per every second Cu site along the wall. Moreover neutron scattering experiments show that the doping dependent inverse domain wall spacing varies as $2x$ for $0.05 < x < 1/8$ whereas for $x > 1/8$ it stays relatively constant [3].

In the present paper we show that within a proper treatment of the strong local repulsion U and the inclusion of a sizable but still realistic long-range Coulomb repulsion, half-filled vertical stripes may become the ground-state configuration of the two dimensional Hubbard model. We will argue that the electronic interactions, besides the pinning by the tetragonal lattice potential, may also play an important role in establishing different domain wall structures. Another point we will be concerned with is a possible spiral contribution to the domain wall phases. Based

on a Landau free-energy analysis of coupled charge and spin-density-wave order parameters it has been shown in Ref. [4] that within some region of parameter domain walls may have a spiral component. Whereas this type of ordering is not observed in the Ni-oxides, some spiral contribution cannot be rigorously excluded to be present in the Nd-doped compounds [3]. According to our analysis presented below, elliptical stripes are not stable for concentrations around 1/8 but may be formed in the very low doping limit.

We consider the two-dimensional Hubbard model on a square lattice, with hopping restricted to nearest neighbors (indicated by the bracket $\langle i, j \rangle$) and an additional LR interaction:

$$H = -t \sum_{\langle ij \rangle, \sigma} c_{i, \sigma}^\dagger c_{j, \sigma} + U \sum_i n_{i, \uparrow} n_{i, \downarrow} + \sum_{i \neq j, \sigma \sigma'} V_{ij} n_{i, \sigma} n_{j, \sigma'} \quad (1)$$

where $c_{i, \sigma}$ destroys an electron with spin σ at site i , and $n_{i, \sigma} = c_{i, \sigma}^\dagger c_{i, \sigma}$. U is the on-site Hubbard repulsion and t the transfer parameter. For all calculations we take $t = 1$. For the Coulomb potential we assume an interaction of the form $V_{ij} = \frac{V_0 e^{-|\mathbf{R}_i - \mathbf{R}_j|/\lambda}}{\sqrt{(\mathbf{R}_i - \mathbf{R}_j)^2 + \alpha^2}}$ where the parameters V_0 and α are specified through the on-site repulsion U and the nearest-neighbor interaction $V_{n, n+1}$ via $\alpha = V_{n, n+1} / \sqrt{U^2 e^{-2/\lambda} - V_{n, n+1}^2}$ and $V_0 = \alpha U / 2$.

To proceed we treat the strong on-site correlation term in the slave-boson version of the Gutzwiller approximation proposed by Kotliar and Ruckenstein [5]. The long-range part is linearized via the HF decoupling. We do not restrict the solution to a specific functional form but allow for an unrestricted variation of the bosonic and fermionic fields (for further details of this approach see [6]).

Single stripe calculation. – From Fig. 1(a) we observe that the most stable domain wall filling x decreases with increasing on-site repulsion U . However, contrary to the tJ-model (uppermost curve in Fig. 1(a), from Ref. [7]) one obtains that within the one-band model half-filled walls are stabilized for very large values of U ($> 16t$) only. For stripe fillings $x < 1/2$ the binding energy rapidly increases since in this case the ‘antibonding bands’ in the Mott-Hubbard gap are occupied (see Ref. [8] for a detailed discussion of the mean-field band structure) leading to a rapid destabilization of the domain walls. This opens the way for the stabilization of half filled walls by including the repulsive effect of a long-range potential. To demonstrate the effect of repulsive forces for isolated stripes we show in Fig. 1(b) the corresponding binding energies for $U = 11.43t$ where the ‘long-range part’ of the Coulomb potential is restricted to next- and next-nearest neighbors. As a result one observes that for a reasonable nearest neighbor repulsion $V_{n, n+1} \approx 0.2$ the most stable stripe filling shifts to $x = 0.5$. It should be mentioned that diagonally oriented half-filled walls are much higher in energy than the vertical ones considered here [9].

Interstripe interaction and spin-polaron lattice. – Figs. 1(c) - 1(e) display the binding energy of vertically oriented stripes for three different doping concentrations and stripe fillings, which now has been calculated with respect to the polaronic

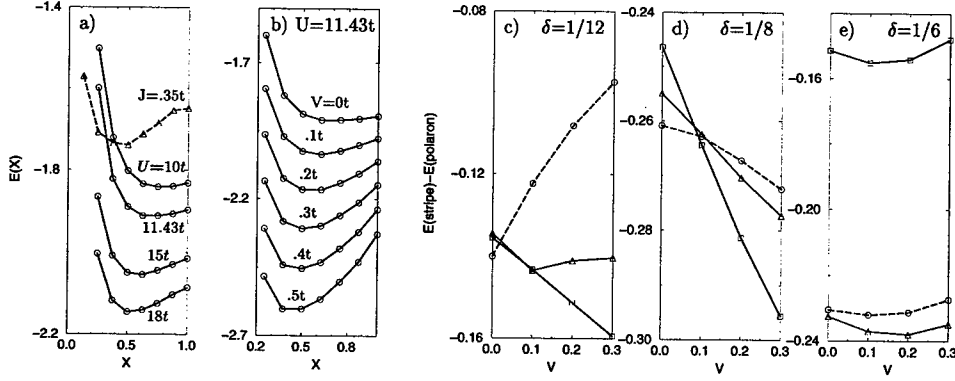


FIGURE 1. (a) Binding energy per hole for a single vertical domain wall as a function of 'stripe-doping' and various values of the on-site repulsion U . The uppermost curve has been obtained for the tJ-model (from Ref. [7]). (b) As in a) but now with inclusion of nearest and next nearest neighbor repulsions and a fixed value of $U = 11.43t$ ($\sim J \approx 0.35t$ in the strong coupling limit). The calculations have been performed for a 16×6 lattice with the stripes parallel to the x-direction and to draw comparison with similar considerations for the tJ-model, boundaries have been used according to Ref. [7]. (c) - (e): Energy differences between vertically striped phases and the 'interacting' spin-polaron Wigner lattice as a function of the nearest neighbor contribution $V_{n,n+1}$ to the long-range potential (in units of t). Solid line (\square): half filled vertical stripe; dashed line (\circ): completely filled vertical stripe; dotted line (\triangle): 3/4 filled stripe. System size $L_x \times 4$, $U=10t$.

Wigner lattice (the Wigner lattice corresponds to N_h spin polarons with maximum distance). For concentrations $x \leq 1/8$ we obtain a crossover to half-filled vertical domain walls for $V \approx 0.1t$. However, for $x = 1/6$ the energy of half-filled walls is shifted to higher energies for $V_{n,n+1} = 0$ already. Indeed for this concentration the spacing between half-filled stripes is 3 lattice constants only and the finite width of the walls causes them to repel rather strong. Instead the 3/4 filled walls now acquire the lowest energy and are also stable for finite values of $V_{n,n+1}$. Note that a stripe filling of 3/4 for $x = 1/6$ means an average stripe separation of 4.5 lattice constants. We find that the system minimizes its energy in this case by alternately choosing stripe separations of 4 and 5 lattice constants respectively.

Elliptical domain walls - To investigate the possibility of spiral stripes we have used a spin-rotational invariant generalization of our approach [10] by including additional bosons for the transversal spin degrees of freedom. Only vertical domain walls have been considered and open (periodic) boundary conditions were applied in the x- (y-) direction. In case of a completely filled domain wall (i.e. one hole per site along the wall) we only find collinear solutions whereas coplanar structures become stable for half-filled walls. Fig. 2 shows a possible vortex-antivortex domain wall structure together with the corresponding spin current. Spin fields and currents display a quadrupled structure along the wall which is a necessary

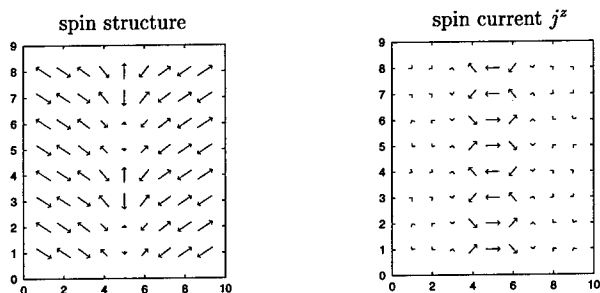


FIGURE 2. Possible spin structure for an elliptical domain wall together with the corresponding spin current. The on-site repulsion is $U = 6t$ and open (periodic) boundary conditions in x- (y-) direction have been used. Shown are the results for a 9×8 lattice doped with 4 holes.

condition for stability within any mean-field approach [8]. We find that elliptical half-filled stripes become favored with respect to collinear domain walls for not too large values of the on-site repulsion U ($< 9t$).

Since we have used open boundaries in x-direction the angle of spin rotation Θ across the domain wall is only $\approx 3/4$ of the expected value of π . This is due to the fact that the system now can acquire a state which has zero total spin current, whereas for periodic boundaries the spiral component always requires a net flow in x-direction. However, since for a regular array of stripes the charge periodicity and the spin modulation have to be related by $k^{charge} = 2k^{spin}$ [4] the domain wall induced kink type spin rotation has to be supplemented by an additional spiral field. The corresponding additional energy can become small enough in the low doping regime so that elliptical stripe configurations may be favored for small hole concentrations.

REFERENCES

1. C. Castellani et al., Phys. Rev. Lett. **75**, 4650 (1995); C. Castellani et al., Z. für Physik, **103**, 137 (1997).
2. V. J. Emery et al., Phys. Rev. **B56**, 6120 (1997).
3. J. M. Tranquada et al., Nature **375**, 561 (1995); J. M. Tranquada et al., Phys. Rev. **B54**, 7489 (1996). J. M. Tranquada et al., Phys. Rev. Lett. **78**, 338 (1997).
4. O. Zachar et al., Phys. Rev. **B57**, 1422 (1998).
5. G. Kotliar et al., Phys. Rev. Lett. **57**, 1362 (1986).
6. G. Seibold et al., Phys. Rev. **B57**, 6937 (1998).
7. Steven R. White et al., Phys. Rev. Lett. **80**, 1272 (1998).
8. J. Zaanen et al., Ann. Physik **5**, 224 (1996).
9. G. Seibold et al., Phys. Rev. **B58**, 13506 (1998).
10. T. Li et al., Phys. Rev. **B40**, 6817 (1989); R. Frésard et al., Int. J. Mod. Phys. **B6**, 237 (1992); G. Seibold, Phys. Rev. **B58**, 15520 (1998).

Spontaneous ferroelectric state induced by external fields in a high T_c superconductor

S.E. Shafranjuk

RIEC, Tohoku University, 2-1-1, Katahira, Aoba-ku, Sendai 980-77, Japan

Abstract. The Josephson plasma mode (JPM) in layered cuprate superconductors is strongly affected by the external tunneling injection and/or by the ac field applied. In the model of the c axis tunneling transport, the dielectric function $\epsilon(\omega)$ is calculated. For the cases of the tunneling injection and of the microwave, we obtain the conditions when the JPR is shifted and vanishes. It causes the arising of a non-equilibrium instability in respect to the transition into a ferroelectric state characterized by a genuine bias voltage along the c axis of a cuprate superconductor sample that can be observed experimentally.

The unique electromagnetic properties of cuprate superconductors suggest new capabilities that can be used in new devices. Consequently, a great deal of attention is paid to the intrinsic Josephson effect [1] that occurs due to the weak coupling of adjacent superconducting atomic CuO_2 layers through the interstitial block regions. Therefore, the coherence is well established across the crystal that is constituted as an array of microscopic Josephson junctions. In such the natural atomic multilayer, the Josephson plasma mode (JPM) is composed by the c axis tunneling electric currents and by the polarized electromagnetic field. Due to the low damping at the typical plasma frequencies $\Omega_{pl} \ll \Delta$ (Δ is the magnitude of the energy gap), the observed JPM is very sharp [2]. The screening properties of the cuprate superconductors in respect to c axis polarized fields are described by the dielectric function $\epsilon(\omega)$ that itself depends on the distribution of quasiparticle excitations in the atomic CuO_2 layers. In this Report we would like to show that when the quasiparticles are excited by an intensive external field, the screening properties of S are strongly modified, resulting also in the shift of the JPM frequency. At such the non-equilibrium conditions, the JPM may vanish causing the arising of an instability. The system experiences transition to an electronic ferroelectric (FE) state characterized by a finite spontaneous bias voltage established along the c axis of S electrode. To determine the non-equilibrium shift of JPM

and the FE instability, we implement the kinetic equation that describes how the external fields (e.g., quasiparticle tunneling injection, see Fig. 1, electromagnetic irradiation, or ultrasound) cause the deviation of their distribution function n_e from the equilibrium.

Taking then into account the Josephson coupling between the CuO_2 layers, we compute the transverse dielectric function $\epsilon(\omega)$ in the non-equilibrium state. The JPM frequency is determined as the solution Ω_{pl} of equation $\text{Re}\{\epsilon(\omega)|_{\omega=\Omega_{pl}}\} = 0$. When n_e changes its shape, the $\epsilon(\omega)$ may also be strongly modified in the way that Ω_{pl} is shifted and even vanish. Then $\text{Re}\{\epsilon(\omega)\}$ inverses its sign and may diverge signifying a transition to the electronic FE state.

The transverse dielectric function is expressed as $\epsilon(\omega) = \epsilon_\infty - 4\pi i\sigma_\perp(\omega)/\omega$, ϵ_∞ being the high-frequency dielectric constant, and $\sigma_\perp(\omega) = \sigma_{N\perp}\mathcal{I}(\omega)/\omega$ being the c axis ac conductivity that is calculated from the microscopic tunneling approach [3], $\sigma_{N\perp}$ is the average normal state interlayer tunneling conductivity. Here we also used the tunneling function $\mathcal{I}(\omega) = \int d\varepsilon [u_{\varepsilon-\omega}u_\varepsilon + v_\varepsilon v_{\varepsilon-\omega}](n_{\varepsilon-\omega} - n_\varepsilon)$, $u_\varepsilon = \varepsilon/\xi_\varepsilon$, $v_\varepsilon = \Delta/\xi_\varepsilon$, $\xi_\varepsilon = \sqrt{\varepsilon^2 - \Delta^2}$.

The non-equilibrium effect in the above formulas is accounted for the electron distribution function n_e . This function can significantly change its shape under the external influence. The average electron energy is also increased, and then it dissipates due to inelastic elementary collision processes. In the cuprate S sample,

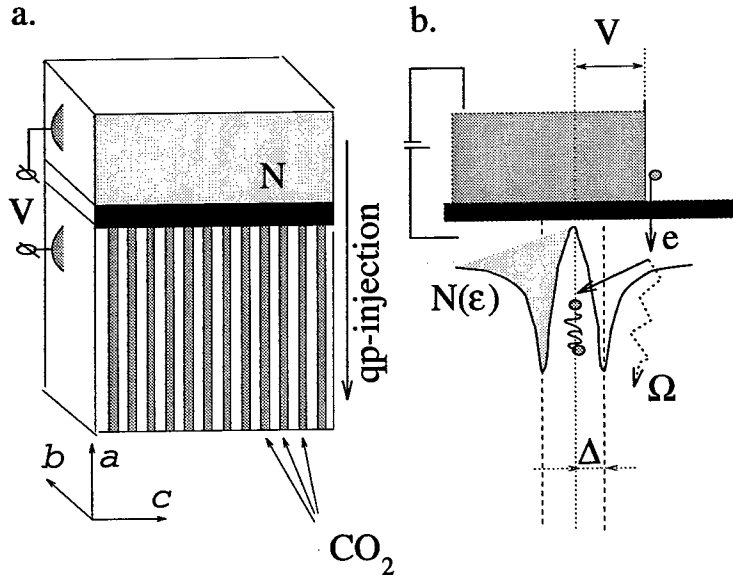


FIGURE 1. The tunneling injection to a cuprate SC single crystal (N is the normal electrode, I is the tunneling barrier while S is the cuprate single crystal S).

due to the sharp plasma resonance [2], that is positioned presumably below all the peaks in the phonon density of states, the probability of the electron-plasma collisions is expected to dominate. Then in S, the electron distribution function is determined from the kinetic equation

$$\tilde{u}_\epsilon \dot{n}_\epsilon = \alpha_{e-pl} \mathcal{J}^{e-pl} + \alpha_{e-ph} \mathcal{J}^{e-ph} + \tilde{u}_\epsilon \cdot (\dot{n}_\epsilon)_{ext} \quad (1)$$

where \mathcal{J}^{e-pl} is the collision integral of electrons with plasmons, $\tilde{u}_\epsilon = \text{Re} u_\epsilon$, $\alpha_{e-pl} = (2/3)(l_\perp^2/\tau_\perp)(eE_{pl}/\Omega_{pl})^2$ is the electron-plasmon collision rate that must be determined self-consistently, l_\perp is the c axis electron mean free path, τ_\perp is the c axis scattering time, α_{e-ph} is the electron-phonon collision rate, and E_{pl} is the c axis polarized electric field amplitude of the elementary Josephson plasma oscillations in S. Formally E_{pl} is related to the interlayer phase difference $\varphi_{n,n-1}$ by the Josephson relationship $E_{pl} = (\hbar/2e)(\dot{\varphi}_{n,n-1}/c_\perp)$. The last term in the formula (1) describes the pumping by external fields.

The non-equilibrium shift of the JPM and the conditions of arising the FE instability is considered in this report for the non-equilibrium pumping by quasiparticle injection, by the electromagnetic field, and by ultrasound. In the tunneling N-I-S-setup (see Fig. 1a), the quasiparticles are injected from the normal electrode N into the S electrode creating there a non-equilibrium state. The diagram in Fig.

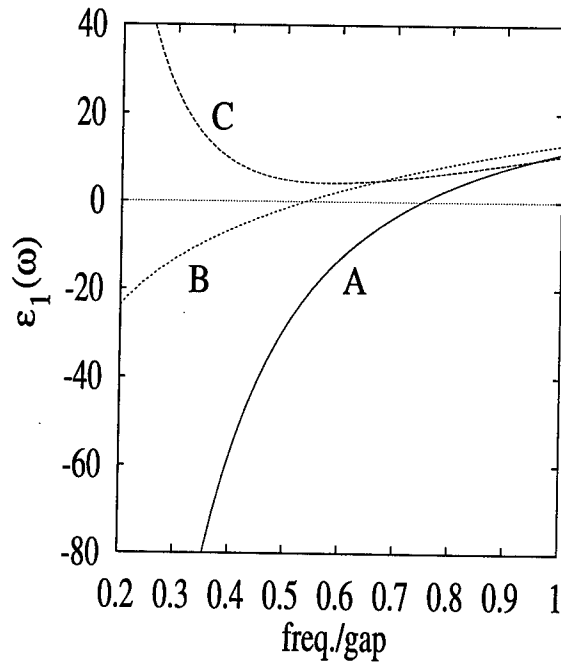


FIGURE 2. The $\text{Re}\epsilon(\omega)$ at different level of external pumping.

1b shows that the electron energy relaxation presumes an emission of Josephson plasmons Ω_{pl} . We compute the dielectric function $\epsilon(\omega)$ that itself depends on the distribution function of electrons n_e using the normal state parameters being typical for a cuprate: $\epsilon_\infty = 23$, $\sigma_{N1} = 1.6 \Omega^{-1} cm^{-1}$. The calculated results for the real part $\epsilon_1(\omega)$ in conditions of tunneling injection from an adjacent normal electrode N to the cuprate S are presented in Fig. 2. The curve A in Fig. 2 belongs to the equilibrium case at the temperature $T = 0$ with no bias voltage applied across the junction, $V = 0$. One can see that $\epsilon_1(\omega)$ vanishes at $\omega = 0.74$ (the frequency variable ω , the electron energy ϵ and the temperature all are expressed in the units of energy gap magnitude Δ at $T = 0$). At $\omega = 0.74$, one obtains $\epsilon_2 = \text{Im}\{\epsilon(\omega = 0.74)\} \approx 0.5$ that is small enough to provide a sharp resonance (JPM) with $\Omega_{pl}^{(0)} = 0.74$. The electron distribution in the non-equilibrium but stationary case $\dot{n}_e = 0$ is found numerically from Eq. (1). Implementing the condition of the plasma resonance $\epsilon_1(\omega) = \text{Re}\{\epsilon(\omega)\} |_{\omega=\Omega_{pl}} = 0$, one obtains the non-equilibrium value of the plasma frequency Ω_{pl} . The alternation of Ω_{pl} is well illustrated by Fig. 2 where we plot $\epsilon_1(\omega)$ for different intensity of the quasiparticle injection. At finite bias voltage, the quasiparticle tunneling injection from the N-electrode changes the shape of n_e in S, causing the shift of JPM down. This tendency is observed already at a relatively small intensity of the quasiparticle injection. From curve B of Fig. 2 related to $V = 4.95$ one finds the new value $\Omega_{pl} = 0.53$ that is significantly smaller compared to $\Omega_{pl}^{(0)}$. If the external influence is increased, the JPM is washed out. Such kind of behavior corresponds to a non-equilibrium instability of S in respect to its screening properties causing a static homogeneous electronic FE state.

The FE state can be also excited by other types of the external pumping, i.e., by the laser irradiation, or by ultrasound in a similar way.

In conclusion, the calculation of the JPM frequency in non-equilibrium condition of tunneling injection show that Ω_{pl} is shifted down and may vanish manifesting the transition to a homogeneous stationary ferroelectric state characterized by the formal divergence of $\epsilon_1(\omega)$ at $\omega \rightarrow 0$. The FE state is accompanied by a finite bias voltage on the length l_D across the S electrode.

I would like to thank Tohoku University for its hospitality.

REFERENCES

1. R. Kleiner and P. Müller, Phys. Rev. B **49**, 1327 (1994); P. Müller, in *Festkörperprobleme*, Advances in Solid State Physics Vol 34, edited by R. Helbig (Vieweg, Braunschweig, 1994).
2. Y. Matsuda, M.B. Gaifullin, K. Kumagai, K. Kadowaki, and T. Mochiku, Phys. Rev. Lett. **75**, 4512 (1995); O.K.C. Tsui, N.P. Ong, Y. Matsuda, Y.F. Yan, and J.B. Peterson, Phys. Rev. Lett. **73**, 724 (1994); O.K.C. Tsui, N.P. Ong, and J.B. Peterson, Phys. Rev. Lett. **76**, 819 (1996).
3. S.E. Shafranuk, M. Tachiki, and T. Yamashita, Phys. Rev. B **53**, 15136 (1996-II); S.E. Shafranuk, M. Tachiki, and T. Yamashita, Phys. Rev. B **55**, 8425 (1997-I).

THE FERMION-LOCHON MODEL AND THE PSEUDOGAP IN CUPRATE SUPERCONDUCTORS

K. P. Sinha *

Department of Physics and Jawaharlal Nehru Center for Advanced Scientific
Research
Indian Institute of Science Campus, Bangalore 560012, India

*present address: 9805 Juniper Hill Road
Rockville, MD 20850; e-mail: sinha@sinha.net

The interaction mechanism involving fermions and lochons (local charged bosons) located at polarizable dielectric regions in the layered cuprate systems is discussed in the context of the pairing symmetry, the appearance of the resonance peak and the pseudogap which is seen above T_c . It is found that the mechanism allows both s and d waves and the dominance of one or the other depends on the relative values of the Fermi energy and the nearest neighbor hopping integral. The model accounts for the pseudogap and the resonance peak is identified with the local pair fluctuation state. The mechanism, along with a weak phonon contribution, emerges as an acceptable model for HTSC.

INTRODUCTION

The pairing interaction mediated by lochons (local charged bosons, local singlet pairs, bipolarons or negative U centers) has a long history. It was first suggested, over thirty years ago, for the pairing of fermions in conventional superconductors to achieve the enhancement of its superconducting transition temperature T_c [1,2]. The model envisages the existence of centers or complexes which can harbour lochons and undergo double charge fluctuation in interaction with fermions of the metallic matrix of the system. The interaction mechanism involves the splitting of a lochon into a pair of fermions (belonging to a wide band) and the inverse process in which a fermion pair get localized at such centers. The discovery of high temperature cuprate superconductors led to the revival of this mechanism by several groups from 1987 onwards [3-7]. This mechanism, along with a weak phonon contribution, has been found to explain many of the properties of cuprate superconductors [7]. In what follows, its role is discussed in the context of pairing symmetry, the appearance of the resonance peak and the pseudogap in these systems [8,9].

LOCHON (BOSON) - FERMION MODEL

For this model the Hamiltonian for layered cuprates is given by [3,7]

$$H = \sum_k \epsilon_k (n_{k\sigma}) + \sum_L E_L b_L^\dagger b_L + \sum_{\mathbf{k}} g_L(\mathbf{k}) (C_{i\mathbf{k}\uparrow}^\dagger C_{i-\mathbf{k}\downarrow}^\dagger b_L + \text{h.c.}), \quad (1)$$

CP483, *High Temperature Superconductivity*, edited by S. E. Barnes et al.

© 1999 American Institute of Physics 1-56396-880-0/99/\$15.00

where $n_{ik\sigma} = C_{ik\sigma}^\dagger C_{ik\sigma}$ with $C_{ik\sigma}^\dagger$ ($C_{ik\sigma}$) denoting the fermion creation (annihilation) operators in the state $|ik\sigma\rangle$; k is the wave vector, σ the spin index, i denotes the layer and ϵ_k is the single particle energy taken independent of the layer index i . The lochon creation and annihilation operators are

$$b_L^\dagger = C_{L\uparrow}^\dagger C_{L\downarrow}^\dagger; \quad b_L = C_{L\downarrow} C_{L\uparrow} \quad (2)$$

and they are composites of fermions in the singlet spin state and localized in the orbital state $|L\rangle$ at site L , E_L being its energy. The third term of (1) is the interaction between the lochons (L) and the fermions of the i^{th} conduction layer, where $g_{Li}(\mathbf{k})$ is the coupling constant. It has been shown that for a two dimensional plane with two-dimensional configuration of atoms in CuO_2 planes the coupling constant has the general form [6,7]

$$g_{Li}(\mathbf{k}) = \Phi_{ik} g, \quad (3)$$

where
$$\Phi_{ik} = m_s \Phi_{sik} + m_d \Phi_{dik} \quad (4)$$

with
$$\Phi_{sik} = [\cos(k_x a) + \cos(k_y a)]_i, \quad \Phi_{dik} = [\cos(k_x a) - \cos(k_y a)]_i \quad (5)$$

and belong to different irreducible representations of the square symmetry. Here a is the lattice constant.

The important point to note is that the lochon-fermion interaction allows both s-wave and d-wave pairing symmetry. Further the mixing coefficients satisfy

$$|m_s|^2 + |m_d|^2 = 1 \quad (6)$$

This would be in conformity with the suggestion that in cuprates both s and d-wave pairing coexist [10].

The relative values of the critical temperature T_{cs} and T_{cd} depend on the ratio $|\epsilon_F|/2t$, where ϵ_F is the Fermi energy and t the nearest neighbour hopping integral. It is found that for

$$(i) \quad |\epsilon_F| \ll 2t, \quad T_{cs} \ll T_{cd},$$

$$(ii) \quad |\epsilon_F| \gg 2t, \quad T_{cs} \gg T_{cd},$$

$$(iii) \quad |\epsilon_F| \sim 2t, \quad T_{cs} \sim T_{cd}.$$

Thus lochon mediated pairing interaction predicts under what condition d-wave or s-wave will dominate and when both components will be present with appreciable

strength. A precise knowledge of the values of the parameters involved is needed to avoid the danger of over estimating one symmetry relative to the other.

The intralayer and interlayer pairing interaction is obtained by the standard canonical transformation. The transformed and reduced Hamiltonian is

$$H = \sum \epsilon_k n_{ik\sigma} + \sum E_L b_L^\dagger b_L - \sum V_{ii}(\mathbf{k}\mathbf{k}') C_{ik'\uparrow}^\dagger C_{i,-k'\downarrow}^\dagger C_{i,-k\downarrow} C_{i,k\uparrow} - \sum V_{ij}(\mathbf{k}\mathbf{k}') C_{ik'\uparrow}^\dagger C_{i,-k'\downarrow}^\dagger C_{j,-k\downarrow} C_{j,k\uparrow}, \quad (7)$$

$$\text{where } V_{ii} = [g_L(\mathbf{k}) g_L(\mathbf{k}')]/E_L, \quad V_{ij} = [g_L(\mathbf{k}) g_L(\mathbf{k}')]/E_L \quad (8)$$

Both intralayer and interlayer pairing is possible in the model as lochon centers are also located in the intervening polarizable dielectric layers. The gap equation at $T=0$ and on the Fermi surface will have the form

$$\Delta(k_F) = \Phi_{kF} (\Delta_0 + \sum \Phi_{kF} \Delta_1/2), \quad (9)$$

where Δ_0 is a positive quantity involving the intralayer contribution and $\Delta_1 = g^2/E_L$. The second term in (9) comes from the interlayer contribution.

Some recent work suggests that the lochon (negative U) model will have singularity like feature and the density of states peaks near the Fermi level [7,11]. This arises from two particle resonance states. There is a strong local pair correlations in the normal state which amplify as one goes to the superconducting state as indeed seen by experiments[8]. This peak at $M(\pi, 0)$ point in the Brillouin Zone (BZ) visible at about 40 meV in the normal state sharpens in the superconducting state[12]. These modes are identified with lochon (local pair fluctuation) states and the effect is enhanced below T_c owing to fermion-lochon interaction when more Cooper pairs are formed. The calculation of susceptibility parallels that of ref [15]. By solving the gap equation for various values of Δ_1 and the fermion-lochon coupling constant λ_L [7,8], the peak is obtained by using the density of states

$$N(\epsilon_F) = (2/\pi W) \ln |W/\epsilon_F|, \quad (10)$$

where W is the width of the singularity like feature near the Fermi energy (~ 72 meV). The evolution of the electronic density of states as a function of temperature is such that it shows a peak around 40 meV, which sharpens on going to the superconducting state. The lochons (local charged bosons) configuration can be extended to comprise both charge and lattice degrees of freedom existing together in a coherent quantum state [13].

The calculated intensity of photoemission spectrum within this model shows a broad feature in the high temperature region and a pseudogap when the temperature is

lowered. This is accompanied with a broad incoherent region. The temperature dependence of the pseudogap is connected with the incoherent part of the quasiparticle spectrum. The appearance of the pseudogap happens because of the resonant exchanges between otherwise free unpaired fermions and lochons (localized fermions in the singlet state). As this is driven by the insulator-metal cross over the pseudogap can open above the superconducting phase transition at T_c .

CONCLUDING REMARKS

The experimental observations of the pseudogap and the appearance of a resonance peak around 40 meV in cuprate superconductors in underdoped and optimally doped systems are among the most important signatures, along with pairing symmetry, of high T_c superconductors. There are various theoretical models suggested by different research groups to explain these results [8,13-16]. Of these the fermion-lochon (local charged boson) model appears capable of explaining all these features and other properties of cuprates discussed elsewhere [7]. Thus this model, combined with a weak phonon contribution, is emerging as a strong contender for an acceptable mechanism for those oxide HTSC materials.

ACKNOWLEDGEMENT

The author would like to thank the University Grants Commission, New Delhi, India for a contingency grant to support this research work.

REFERENCES

1. B. N. Ganguly, U. N. Upadhyaya and K. P. Sinha, Phys. Rev. 146, 317(1966).
2. U. N. Upadhyaya and K. P. Sinha, Phys. Rev. 169, 395(1968).
3. K. P. Sinha and M. Singh, J. Phys. C21, L231 (1988).
4. K. P. Sinha and S. L. Kakani, High Temperature Superconductivity: Current Results and Novel Mechanisms (Nova Science Publishers, New York, 1994) for other references.
5. J. Ranninger and J. M. Robin, Physica C23, 279 (1995) and references there in.
6. C. P. Enz, Phys. Rev. B54, 3589 (1996) and references there in.
7. K. P. Sinha, Mod. Phys. Lett. B12, 805 (1998) and references.
8. K. P. Sinha, Some theoretical models for the pseudogap in HTSC, to appear in the series "Studies of High Temperature Superconductors" ed. A.V. Narlikar (Nova Science Pub. Inc., New York). Also contains a brief account and references to experimental results.
9. C. C. Tsuei and J.R. Kirtley, J. Low Temp. Phys, 107, 445(1997).
10. K. A. Muller, Nature 377, 133 (1995).
11. J. A. Wilson, J. Phys. Condens. Matter 9 6061 (1997)..
12. M. R. Norman et al., Phys. Rev. Lett 79, 3506 (1997).
13. J. Ranninger and A. Romano, Phys. Rev. Lett. 80, 5643 (1998).
14. Z. X. Shen and J. R. Schrieffer, Phys. Rev. Lett. 788, 1771 (1997).
15. L. Yin, S. Chakravarty and P. W. Anderson, Phys. Rev. Lett. 78 3559 (1997).
16. D. K. Morr and D. Pines, Phys. Rev. Lett. 81, 1086 (1998).

Canonical BCS Approximation for the Attractive Hubbard Model

K. Tanaka and F. Marsiglio

Department of Physics, University of Alberta, Edmonton, Alberta, Canada T6G 2J1

Abstract. We test the canonical BCS wave functions for fixed number of electrons for the attractive Hubbard model. We present results in one dimension for various chain lengths, electron densities, and coupling strengths. The ground-state energy and energy gap to the first excited state are compared with the exact solutions obtained by the Bethe ansatz as well as with the results from the conventional grand-canonical BCS approximations. While the canonical and grand-canonical BCS results are both in very good agreement with the exact results for the ground state energies, improvements due to conserving the electron number in finite systems are manifest in the energy gap. As the system size is increased, the canonical results converge to the grand-canonical ones. The “parity” effect that arises from the number parity (even or odd) of electrons are studied with our canonical scheme.

In recent experiments on nanoscale superconducting Al particles (e.g., Ref. [1]), the number of electrons in a particle was fixed by charging effects and the excitation spectrum has been measured by tunneling of a single electron. They have observed the number “parity” effect, the difference in the excitation spectra that arises due to the number of electrons in a particle being even or odd. For these systems, the validity of the BCS theory that utilizes the grand canonical ensemble is questionable. We address this issue by using the attractive Hubbard model, which serves as the minimal model to describe s-wave superconductivity. We test the canonical BCS wave function that has a fixed number of electrons for this system. While our formulation can be applied for larger systems up to three dimensions, we present results for one dimension, for various system sizes, electron densities and coupling strengths. Exact solutions are available in one dimension via Bethe Ansatz techniques [2], and the grand canonical BCS solutions have recently been evaluated for large system sizes [3].

The attractive Hubbard Hamiltonian is given by

$$H = - \sum_{i,\delta} t_{\delta} (a_{i+\delta,\sigma}^{\dagger} a_{i\sigma} + \text{h.c.}) - |U| \sum_i n_{i\uparrow} n_{i\downarrow} \quad (1a)$$

$$= \sum_{\mathbf{k}\sigma} \epsilon_{\mathbf{k}} a_{\mathbf{k}\sigma}^{\dagger} a_{\mathbf{k}\sigma} - \frac{|U|}{N} \sum_{\mathbf{k}\mathbf{k}'} a_{\mathbf{k}\uparrow}^{\dagger} a_{-\mathbf{k}+\mathbf{k}'}^{\dagger} a_{-\mathbf{k}'+\mathbf{k}} a_{\mathbf{k}\uparrow}, \quad (1b)$$

where $a_{i\sigma}^\dagger$ ($a_{i\sigma}$) creates (annihilates) an electron with spin σ at site i and $n_{i\sigma}$ is the number operator, $n_{i\sigma} = a_{i\sigma}^\dagger a_{i\sigma}$ (i is the index for the primitive vector \mathbf{R}_i). The t_δ is the hopping rate of electrons from one site to a neighbouring site \mathbf{R}_δ away. In this work, we include the nearest neighbours only, and $t \equiv t_\delta$. The $|U|$ is the coupling strength between electrons on the same site, and we have explicitly included the fact that the interaction is attractive. In Eq.(1b), we have Fourier transformed the Hamiltonian with periodic boundary conditions for N sites in each dimension. The kinetic energy is given by

$$\epsilon_{\mathbf{k}} = -2 \sum_{\delta} t_{\delta} \cos \mathbf{k} \cdot \mathbf{R}_{\delta}, \quad (2)$$

where \mathbf{R}_{δ} is the coordinate vector connecting sites i to $i + \delta$.

We perform variational calculations using the component of the BCS wave function that has a given number of pairs ν and thus conserves the number of electrons $N_e = 2\nu$. The BCS wave function is a superposition of pair states with all the possible numbers of pairs $\{\nu\}$:

$$|\text{BCS}\rangle_{\text{GC}} = \prod_{\mathbf{k}} (u_{\mathbf{k}} + v_{\mathbf{k}} a_{\mathbf{k}\uparrow}^\dagger a_{-\mathbf{k}\downarrow}^\dagger) |0\rangle \equiv \sum_{\nu=0}^{\infty} |\Psi_{\nu}\rangle, \quad (3)$$

where $|0\rangle$ denotes the vacuum state, and $|\Psi_0\rangle \equiv |0\rangle$. The ν -pair component $|\Psi_{\nu}\rangle$ can be obtained by rearranging $|\text{BCS}\rangle_{\text{GC}}$ into a power series of the pair creation operator $a_{\mathbf{k}\uparrow}^\dagger a_{-\mathbf{k}\downarrow}^\dagger$ and can be written as

$$|\Psi_{2\nu}\rangle = \frac{1}{\nu!} \prod_{i=1}^{\nu} \left(\sum_{\mathbf{k}_i} g_{\mathbf{k}_i} a_{\mathbf{k}_i\uparrow}^\dagger a_{-\mathbf{k}_i\downarrow}^\dagger \right) |0\rangle, \quad (4)$$

where $\mathbf{k}_i \neq \mathbf{k}_j$ for all $i \neq j$, and we have defined $g_{\mathbf{k}_i} = \left(\prod_{\mathbf{k}} u_{\mathbf{k}} \right)^{1/\nu} v_{\mathbf{k}_i} / u_{\mathbf{k}_i}$. An alternative way of formulating the problem is to express the above wave function as a particle-number projection of $|\text{BCS}\rangle_{\text{GC}}$ [4-6]. The wave function with an odd number of electrons $N_e = 2\nu + 1$ is defined by

$$|\Psi_{2\nu+1}\rangle = a_{\mathbf{q}\sigma}^\dagger \frac{1}{\nu!} \prod_{i=1}^{\nu} \left(\sum_{\mathbf{k}_i} g_{\mathbf{k}_i} a_{\mathbf{k}_i\uparrow}^\dagger a_{-\mathbf{k}_i\downarrow}^\dagger \right) |0\rangle, \quad (5)$$

with $\mathbf{k}_i \neq \mathbf{k}_j$ for all $i \neq j$. We construct the energy gap by the definition

$$\Delta_{N_e} = \frac{1}{2} (E_{N_e-1} - 2E_{N_e} + E_{N_e+1}). \quad (6)$$

In Fig. 1 we show the ground state energy as a function of the electron density $n = N_e/N$ for $N = 16$, for $|U|/t = 10$ and 4. The improvements of the canonical over the grand canonical energies can be seen, while the former with even N_e 's converge to the latter for smaller n and larger $|U|$, and both results are in very good

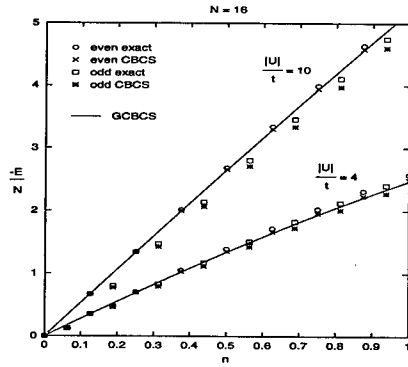


FIGURE 1. Ground state energy as a function of the electron density for $N = 16$.

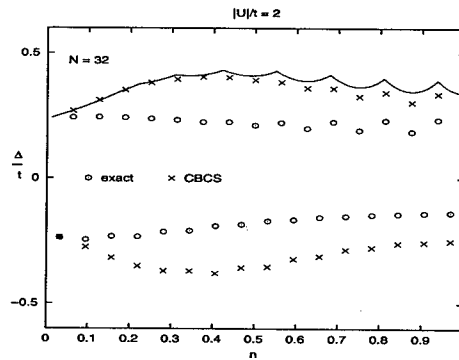


FIGURE 2. Energy gap as a function of the electron density for $N = 32$ and $|U|/t = 2$.

agreement with the exact ones for small n . The difference between the energies with even and odd N_e 's is apparent for large $|U|$.

The energy gap (scaled by the kinetic energy parameter t) is shown in Fig. 2 as a function of the electron density, for $N = 32$ and $|U|/t = 2$. The canonical method improves the grand canonical one significantly for small system size and weak coupling. As the system size or the coupling strength is increased, the canonical results converge towards the grand canonical ones. For $|U|/t = 2$, $N = 32$ is large enough that the canonical gaps are closer to the grand canonical ones than to the exact solutions, and the canonical and grand canonical gaps are more or less converged for small n . The gap for odd N_e is negative. Its magnitude is different from the even N_e gap for larger density and weak coupling. Also in this limit, the even gap oscillates as a function of the density. Both of these effects result from the quantized (unperturbed) energy levels due to finite size, and become negligible for strong coupling and for large system size (small density).

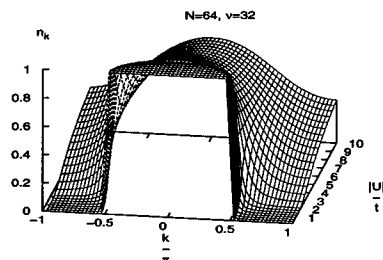


FIGURE 3. Occupation probability for different k states as a function of the coupling strength for $N = 64$ and $\nu = 32$.

Finally, in Fig. 3, we show the occupation probability of different k states as a function of the coupling strength. In the strong coupling limit, all the unperturbed states are more or less equally occupied (in Fig. 3, this limit is not reached yet). As the coupling strength goes to zero, the distribution function for free electrons is recovered. Though the figure shown has been produced by the canonical scheme, the grand canonical approximation also yields the same probability distribution for such a large system size.

In conclusion, the canonical method yields improvements in the energy gap for small system size and weak coupling. Further study is being made for comparison with the grand canonical scheme that conserves the number parity [7].

Acknowledgments

F. M. acknowledges support from NSERC of Canada, and the Canadian Institute for Advanced Research. K. T. acknowledges generous support from the Avadh Bhatia Fellowship. We thank Bob Teshima for suggestions to improve the numerical efficiency for evaluating required integrals. Calculations were performed on the 42 node SGI parallel processor at the University of Alberta.

REFERENCES

1. Black, C.T., Ralph, D.C., and Tinkham, M., *Phys. Rev. Lett.* **76**, 688 (1996).
2. Lieb, E.H., and Wu, F.Y., *Phys. Rev. Lett.* **20**, 1445 (1968).
3. Marsiglio, F., *Phys. Rev. B* **55**, 575 (1997).
4. Dietrich, K., Mang, H.J., and Pradal, J.H., *Phys. Rev.* **135**, B22 (1964).
5. Braun, F., and von Delft, J., *Phys. Rev. Lett.* **81**, 4712 (1998).
6. Tanaka, K., and Marsiglio, F., in preparation.
7. Jankó, B., Smith, A., and Ambegaokar, V., *Phys. Rev. B* **50**, 1152 (1994).

Theory of the Photoemission Spectral Function in High T_c Cuprates

Takami TOHYAMA, Susumu NAGAI, Yasumasa SHIBATA,
and Sadamichi MAEKAWA

Institute for Materials Research, Tohoku University, Sendai 980-8577, JAPAN

Abstract. We present our theoretical study of the single-particle spectral function in two-dimensional cuprates by using numerically exact diagonalization method on small clusters of the extended t - J model containing long-range hopping matrix elements. For a set of the parameter values, the calculated spectral function systematically explains the angle-resolved photoemission spectroscopy (ARPES) data for $\text{Bi}_2\text{Sr}_2\text{CaCu}_2\text{O}_{8+\delta}$. For $\text{La}_{2-x}\text{Sr}_x\text{CuO}_4$ (LSCO), it is found that slightly smaller values of long-range hoppings are necessary for understanding an observed change of the Fermi surface topology with x . In addition, the dramatic suppression of spectral weight along $(0,0)$ - (π,π) direction observed in under-doped LSCO is found to be explained by introducing an additional potential for holes which stabilizes vertical charge stripes.

Knowledge of the electronic structure is a critical first step toward a microscopic understanding of high T_c superconductors. The angle-resolved photoemission spectroscopy (ARPES) experiments provide unique information for this problem. Not only the dispersion but also the line shape of the ARPES spectrum shows the characteristic features. In $\text{Bi}_2\text{Sr}_2\text{CaCu}_2\text{O}_{8+\delta}$ (Bi2212), the spectral shape at $(\pi,0)$ rapidly changes from a broad edge-like feature for underdoped samples to a sharp peak for overdoped ones, while the spectrum near $(\pi/2,\pi/2)$ consists of a single relatively sharp peak [1]. Recently, Ino *et al.* [2] have performed ARPES experiment on $\text{La}_{2-x}\text{Sr}_x\text{CuO}_4$ (LSCO) and have reported different behaviors from Bi2212: (i) The Fermi surface (FS) undergoes a dramatic change from a hole-like shape centered at $\mathbf{k}=(\pi,\pi)$ in underdoped and optimally doped samples to an electron-like one centered at $(0,0)$ in overdoped ones, and (ii) the spectral weight along $(0,0)$ - (π,π) direction is very broad and weak in underdoped samples. The differences between the two typical families may provide a clue of high T_c superconductivity.

In this paper, we examine the single-particle spectral function in high T_c cuprates by using numerically exact diagonalization method on small clusters of the extended t - J model containing long-range hopping matrix elements. For a set of the parameter values, the calculated spectral function systematically explains the ARPES data for Bi2212 from under- to over-doped samples [1]. The result indicates that the

carrier density is a unique variable to control the physical properties. For LSCO, it is found that slightly smaller values of long-range hoppings are necessary for understanding the change of the FS topology. In addition, the dramatic suppression of spectral weight along $(0,0)$ - (π,π) direction is found to be explained by introducing a "stripe" potential that stabilizes the vertical charge stripes [3]. This suggests a crucial role of the stripe in underdoped LSCO.

The t - J Hamiltonian with long-range hoppings, termed the t - t' - t'' - J model, is

$$H = J \sum_{\langle i,j \rangle_{1st}} \mathbf{S}_i \cdot \mathbf{S}_j - t \sum_{\langle i,j \rangle_{1st}\sigma} c_{i\sigma}^\dagger c_{j\sigma} - t' \sum_{\langle i,j \rangle_{2nd}\sigma} c_{i\sigma}^\dagger c_{j\sigma} - t'' \sum_{\langle i,j \rangle_{3rd}\sigma} c_{i\sigma}^\dagger c_{j\sigma} + \text{H.c.}, \quad (1)$$

where the summations $\langle i,j \rangle_{1st}$, $\langle i,j \rangle_{2nd}$ and $\langle i,j \rangle_{3rd}$ run over first, second and third nearest-neighbor (NN) pairs, respectively. No double occupancy is allowed, and the rest of the notation is standard.

Recent analysis of ARPES data in Bi2212 has shown that t' and t'' are necessary for understanding not only the dispersion but also the line shape of the spectral function [1]. By using a set of the parameter values ($t=0.35$, $t'=-0.12$, $t''=0.08$ and $J=0.14$ in units of eV), the doping dependence of the line shape was systematically explained (see Fig. 1(a)). In LSCO, we estimated the ratio t'/t and t''/t to be -0.12 and 0.08 , respectively, by fitting the tight-binding (TB) FS to the experimental one in overdoped sample [2] on the assumption that in the overdoped region the FS shape of the TB band is the same as that of the t - t' - t'' - J model. These numbers are slightly smaller than those for Bi2212, $t'/t=-0.34$ and $t''/t=0.23$. The contribution of apex oxygen to the band dispersion may be the origin of the difference.

The single-particle spectral function, $A(\mathbf{k}, \omega)$, is expressed as

$$A(\mathbf{k}, \omega) = A_-(\mathbf{k}, \omega) + A_+(\mathbf{k}, \omega), \quad (2)$$

$$A_{\pm}(\mathbf{k}, \omega) = \sum_{\nu\sigma} |\langle \nu | a_{\mathbf{k}\sigma} | 0 \rangle|^2 \delta(\omega \pm E_{\nu} \mp E_0), \quad (3)$$

where $a_{\mathbf{k}\sigma} = c_{\mathbf{k}\sigma}^\dagger$ and $c_{\mathbf{k}\sigma}$ for A_+ and A_- respectively. $|\nu\rangle$ is the ν -th eigenvector with eigenvalue E_{ν} . $|0\rangle$ denotes the ground state.

Figures 1 shows the doping dependence of the electron-removal spectral function $A_-(\mathbf{k}, \omega)$ for a $\sqrt{20} \times \sqrt{20}$ -site cluster in the t - t' - t'' - J model, using the parameter values for Bi2212 (Fig. 1(a)) and LSCO (Fig. 1(b)). In Bi2212, the $(\pi,0)$ spectrum is broad at $\delta=0.1$, where δ is carrier concentration. The spectrum becomes sharp at $\delta=0.3$. On the other hand, the $(\pi,0)$ spectrum in LSCO broad at $\delta=0.3$, because the position of the quasi-particle peak shifts above the Fermi level. This means that the $(\pi,0)$ point is outside of the FS, being consistent with the experiments [2]. In the underdoped region, however, the results for LSCO show sharp peaks at $\mathbf{k}=(2\pi/5, \pi/5)$ and $(\pi/5, 3\pi/5)$, both of which are near the $(0,0)$ - (π,π) direction. This seems to be inconsistent with the ARPES data [2] that show the broad spectrum, implying the presence of an additional effect that is not included in the t - t' - t'' - J model.

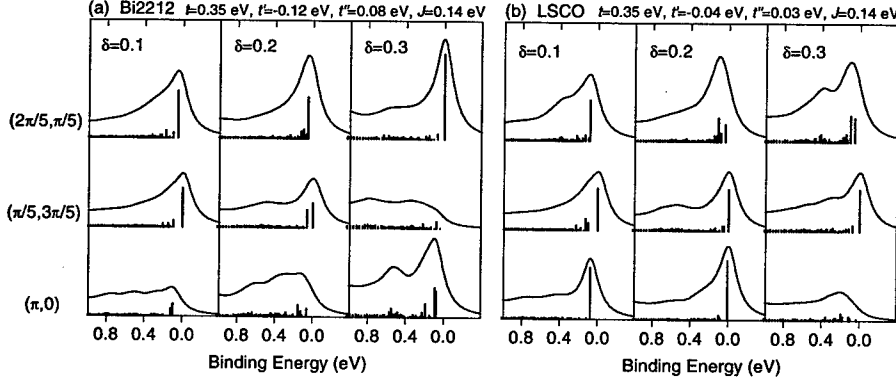


FIGURE 1. Electron-removal spectral functions for various dopings ($\delta=0.1, 0.2$ and 0.3) in the t - t' - t'' - J model. (a) Bi2212 and (b) LSCO. The calculation was performed on a 20-site cluster, and a Lorentzian broadening of 0.10eV was used. The binding energy is measured from the energy of the first ionization state.

Several experimental data in LSCO have revealed anomalous behaviors of structural [4,5], electronic [6,7] and magnetic properties [8]. In particular, at $x=0.12$, an incomplete phase transition from the low temperature orthorhombic (LTO) phase to the low temperature tetragonal (LTT) phase (approximately 10% in volume) has been observed [9]. At the same hole density, the incommensurate antiferromagnetic (AF) long-range order has been reported [10]. It is interesting that the LTT phase of Nd-doped LSCO with $x=0.12$, $\text{La}_{1.48}\text{Nd}_{0.4}\text{Sr}_{0.12}\text{CuO}_4$, has shown similar long-range order accompanied by charge order, which is interpreted as charge/spin stripe order that consists of vertical charge stripes and antiphase spin domains [11]. Therefore, such stripes are expected to play an important role in the family of LSCO.

It is controversial whether the t - J model itself has the stripe-type ground state [15–17]. For small-size clusters, the stripe state is not stable in the ground state (GS) [16]. Furthermore, the long-range hopping matrix elements with proper sign weaken the stripe stability [18]. A possible origin of the appearance of stable stripe phase is due to the presence of the long-range part of the Coulomb interaction [19,20] and/or the coupling to lattice distortions. In LSCO, the LTT fluctuation seems to help the latter mechanism [4,5]. As shown below, we introduce a stripe potential into the t - J model, which makes the vertical stripes stable.

In the following, we use a $\sqrt{18} \times \sqrt{18}$ cluster with two holes as an underdoped system. The number of holes in the final state of $A(\mathbf{k}, \omega)$ is, therefore, one and three for electron-addition and removal processes, respectively. Since, in such a small cluster, the stripe state is not the ground state [16], we introduce a “stripe” potential V_s to make the state stable. Noting that the 18-site cluster forms three columns under the periodic boundary condition (BC), the magnitude of V_s is assumed to depend on the number of holes n_h in each column, that is, $V_s(n_h)$ with $V_s(0) = V_s(1) = 0$, $V_s(2) = -2V$, and $V_s(3) = -3V$, being $V > 0$. Examples for

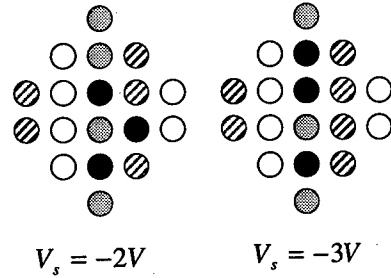


FIGURE 2. Illustration of the stripe potential V_s for the 18-site cluster with periodic BC. The cluster is divided into three columns represented by the empty, shaded and slash circles. When two (three) holes represented by full circles are on single column, $V_s = -2V$ ($-3V$).

two configurations are shown in Fig. 2. $V_s(n_h)$ behaves like an attractive potential for holes independent of distance between holes. We treat the three columns as equivalent, so that the translational symmetry is preserved [21] but the symmetry with respect to 90 degree rotation is broken. In the following, we assign the x and y directions to be perpendicular and parallel to the stripes, respectively.

Let us start on the GS properties of the 18-site cluster with two holes as functions of the potential parameter V . The total momentum of the GS is always $(0,0)$, and a level crossing occurs at $V/t=0.6$. For $0 \leq V/t < 0.6$ the two holes dominantly form a diagonally bounded pair, while for $V/t > 0.6$ both holes are mainly on single column with two-lattice spacing. The latter, which becomes stable under the stripe potential, corresponds to the charge stripes expected in LSCO.

Figure 3 shows $A(\mathbf{k}, \omega)$ of the t - t' - t'' - J model with the stripe potential. When there is no potential (Fig. 3(a)), the QP peaks with large weight are clearly seen below and above the Fermi level at $(\pi/3, \pi/3)$ and $(2\pi/3, 2\pi/3)$, respectively. For $V/t=1$ (Fig. 3(b)), however, there is no distinct QP peak and the spectra become more incoherent. At $(\pi/3, \pi/3)$, a peak is seen above the Fermi level. This may be due to the fact that the stripe potential behaves like an attractive force between holes. Here, we note that the reduction of QP weight originating from the charge stripes is more or less seen at all momenta, although its magnitude depends on their direction. In the presence of the potential, the coupling between charge-carriers in the stripes and neighboring spin domains becomes weak [3]. The spin correlation across the stripes is also small. The implication of the results is an increase of the number of configurations that participate in the GS. According to the configuration interaction picture, such an increase results in the suppression of the QP weight and the increase of incoherent structures. Therefore, the stripe has a general tendency to make the spectrum broad. For $V/t=2$ (Fig. 3(c)), split-off states from incoherent structures are clearly seen at $\omega/t=0.7$ for $(\pi/3, \pi/3)$ and $(2\pi/3, 0)$. This is due to the localization of carriers along the direction perpendicular to the stripes [22]. For $V/t=1$, the tendency to the localization may be involved in the low-energy peaks at $(2\pi/3, 0)$, but can not be recognized at $(\pi/3, \pi/3)$. The broadness of the spectrum

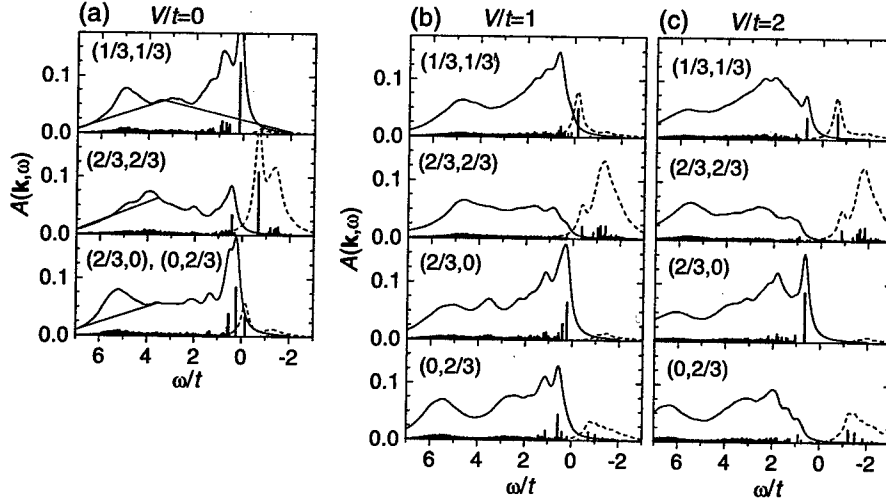


FIGURE 3. Single-particle spectral function $A(\mathbf{k}, \omega)$ of the t - t' - t'' - J model with the stripe potential on a 18-site 2-hole cluster. $J/t=0.4$, $t'/t=-0.12$ and $t''/t=0.08$, corresponding to a set of the parameter values for LSCO. (a), (b) and (c) are results for $V/t=0$, 1, and 2, respectively. The delta functions (vertical bars) are broadened by a Lorentzian with a width of $0.2t$ (solid and dashed curves for the electron-removal and addition spectra, respectively). The momentum is measured in units of π .

at $(\pi/3, \pi/3)$, i.e. along $(0,0)$ - (π, π) direction, is thus emphasized in contrast to the spectra for other momenta. As a consequence, our results for $V/t=1$ explain the ARPES data [2]. We also found that the broadness can not be explained by a diagonal stripe potential.

In summary, we have investigated the photoemission spectral function in Bi2212 and LSCO by using the t - t' - t'' - J model. For Bi2212 and overdoped LSCO, the model can explain the spectral line shape as well as the FS topology. For underdoped LSCO, however, the model is insufficient to describe the ARPES data. We have introduced a microscopic model containing the vertical stripes, and have found that the model explains the ARPES data with suppressed weight along $(0,0)$ - (π, π) direction. This suggests that the vertical stripe is an essential ingredient for the explanation of the physical properties of LSCO, although the d -wave superconductivity is suppressed by the stripes [3].

Part of this work has been done in collaboration with C. Kim, P. J. White, Z.-X. Shen at Stanford University and B. O. Wells, Y. J. Kim, R. J. Birgeneau and M. K. Kastner at MIT. We would like to thank them for fruitful collaboration. We also would like to thank A. Ino, A. Fujimori and S. Uchida for enlightening discussions. This work was supported by a Grant-in-Aid for Scientific Research from the Ministry of Education, Science, Sports and Culture of Japan, NEDO, and CREST. The computation was performed on the supercomputers at ISSP,

University of Tokyo and IMR at Tohoku University.

REFERENCES

1. Kim C., White P.J., Shen Z.-X., Tohyama T., Shibata Y., Maekawa S., Wells B.O., Kim Y.J., Birgeneau R.J., and Kastner M.A., *Phys. Rev. Lett.* **80**, 4245 (1998).
2. Ino A., Kim C., Mizokawa T., Shen Z.-X., Fujimori A., Takaba M., Tamasaku K., Eisaki H., and Uchida S., *cond-mat/9809311*.
3. Tohyama T., Nagai S., Shibata Y., and Maekawa S., *cond-mat/9901011*.
4. Saini N.L., Lanzara A., Oyanagi H., Yamaguchi H., Oka K., Ito T., and Bianconi A., *Phys. Rev. B* **55**, 12759 (1997).
5. Božin E.S., Billinge S.J.L., Kwei G.H., and Takagi H., *Phys. Rev. B* **59**, Number 5 (1999).
6. Ino A., Mizokawa T., Fujimori A., Tamasaku K., Eisaki H., Uchida S., Kimura T., Sasagawa T., and Kishio K., *Phys. Rev. Lett.* **79**, 2101 (1997).
7. Uchida S., Ido T., Takagi H., Arima T., Tokura Y., and Tajima S., *Phys. Rev. B* **43**, 7942 (1991).
8. Yamada K., Lee C.H., Kurahashi K., Wada J., Wakimoto S., Ueki S., Kimura H., Endoh Y., Hosoya S., Shirane G., Birgeneau R.J., Greven M., Kastner M.A., and Kim Y.J., *Phys. Rev. B* **57**, 6165 (1998).
9. Moodenbaugh A.R., Wu Lijun, Zhu Yimei, Lewis L.H., and Cox D.E., *Phys. Rev. B* **58**, 9549 (1998).
10. Suzuki T., Goto T., Chiba K., Shinoda T., Fukase T., Kimura H., Yamada K., Ohashi M., and Yamaguchi Y., *Phys. Rev. B* **57**, R3229 (1998).
11. Tranquada J.M., Sternlieb B.J., Axe J.D., Nakamura Y., and Uchida S., *Nature (London)* **375**, 561 (1995).
12. Emery V.J., Kivelson S.A., and Zachar O., *Phys. Rev. B* **56**, 6120 (1997).
13. Zaanen J., *J. Phys. Chem. Solids* **59**, 1769 (1998) and references therein.
14. Castellani C., Castro C.Di, and Grilli M., *Phys. Rev. Lett.* **75**, 4650 (1995); *Physica C* **282-87**, 260 (1997).
15. White S.R. and Scalapino D.J., *Phys. Rev. Lett.* **80**, 1272 (1998); *ibid.* **81**, 3227 (1998).
16. Hellberg C.S. and Monousakis E., *cond-mat/9812022*.
17. Kobayashi K. and Yokoyama H., *Physica B* to be published (1998).
18. Tohyama T., Gazza C., Shih C.T., Chen Y.C., Lee T.K., Maekawa S., and Dagotto E., *cond-mat/9809411*.
19. Emery V.J. and Kivelson S.A., *Physica C* **209**, 597 (1993).
20. Seibold G., Castellani C., Castro C.Di, and Grilli M., *Phys. Rev. B* **58**, 13506 (1998).
21. This treatment enables the enlargement of the cluster size. The conclusions in our study do not depend on whether the translational symmetry is preserved or not.
22. Salkola M.I., Emery V.J., and Kivelson S.A., *Phys. Rev. Lett.* **77**, 155 (1996).

Surface Roughness, NIS tunneling, and the Zero Bias Conductance Peak

M.B. Walker and P. Pairor

*Department of Physics
University of Toronto Toronto, Ont. M5S 1A7 Canada*

Abstract. We note that the zero bias conductance peak observed in tunneling into the [110] surface of a $d_{x^2-y^2}$ superconductor has a width that is independent of disorder either in the bulk or at the surface. This remarkable property is accounted for qualitatively in terms of the tunneling into surface bound states in the superconductor which have widths that depend strongly on the momentum of the surface bound state.

INTRODUCTION

One of the new phenomena that is made possible by the sign changes of the gap function that occur in the $d_{x^2-y^2}$ state of the high temperature superconductors is the existence, at a [110] surface, of quasiparticle surface bound states [1]. These states have zero energy, i.e. an energy equal to the chemical potential for electrons in the superconductor.

It is known that the tunneling conductance measured in tunneling into a superconductor via an NIS (normal to insulating to superconducting) junction is approximately proportional to the quasiparticle density of states in the superconductor at the junction surface (see [2] for a demonstration of this for d -wave superconductors). Thus the surface bound states which occur at zero energy should be observed as a peak at zero voltage in a conductance versus voltage graph. This peak, called the zero bias conductance peak (ZBCP), has now been observed in many experiments (for recent examples of its observation in $\text{YBa}_2\text{Cu}_3\text{O}_{6+x}$, see [3-5]). In so far as we are able to determine from the data on conductance versus voltage presented in these three references, the width of the ZBCP is the same in all cases (i.e. a half intensity half width of about 2 to 2.5 mV). The width of the ZBCP measured on samples that vary widely in defect concentration and surface roughness thus appears to be a universal width, independent of disorder in the bulk or at the surface. This width is also independent of the junction resistance provided one is in the weak transmission limit. This is unexpected in view of existing theories which attribute the width of the zero bias conductance peak either to impurity scattering or surface roughness and which thus predict that the width increases with the amount

of the disorder [6-10]; it is also in disagreement with models where the width is due to the decay of the superconducting surface bound state quasiparticles due to its tunneling across the insulating barrier into the normal metal [2,11,12]. This independence of the width of the ZBCP on disorder contrasts sharply with the behavior of its height, which decreases strongly with increasing defect concentration [4]. A principle objective of this article is to present a qualitative argument showing how this behavior can be understood if one takes account of surface roughness, and also assumes that the width of the surface bound states has a strong momentum dependence.

The idea that the tunneling conductance is proportional to the density of quasiparticle excitations at the junction surface of the superconductor is embodied in the intuitively apparent formula

$$G = \frac{2e^2}{\hbar} \langle T(k_{\parallel}) \rho(k_{\parallel}, eV) \rangle, \quad \rho = \frac{\pi^{-1} \delta(k_{\parallel})}{(eV)^2 + \hbar^2 k_{\parallel}^2} \quad (1)$$

derived elsewhere [12,13] by solving the Bogoliubov-de Gennes equations in an appropriate manner. Here ρ is the density of states at energy $E = eV$ for a surface bound state of wave vector k_{\parallel} parallel to the surface, nominal energy zero, and relaxation rate γ . T is related to the transmission coefficient of the barrier and the angular brackets indicate an average over k_{\parallel} . It should be emphasized that Eq. 1 gives only that contribution to the conductance due to tunneling into the surface bound states, and neglects tunneling into the continuum states. Its usefulness is thus limited to a description of the ZBCP, which occurs near zero voltage. Finally, we note an interesting study of surface roughness in a discrete lattice model which describes the spatial dependence of the local density of states [14], and also remark that we make no attempt here to take into account the splitting of the zero bias conductance peak at low temperatures in a magnetic field observed in [15] and explained in [8].

Note that the idea of the "tunneling cone," which is taken into account for example in [5,8], is not included in Eq. 1. This is because the insulator to superconducting interface is rough on the scale of the quasiparticle wavelength in all experiments of interest. Thus a random component of momentum parallel to the average surface will be added to the quasiparticle when it crosses the interface.

If the surface bound states have a width \hbar , which is independent of the momentum k_{\parallel} , then the ZBCP will also have a width which is proportional to \hbar , and will have a height inversely proportional to \hbar . Increasing γ (e.g. by increasing the impurity scattering rate) will increase the width while decreasing the height. This is in disagreement with the experimental facts cited above. Thus the hypothesis that the surface bound states have a width that is independent of momentum is not tenable.

A reason that surface bound states must have a width that depends on momentum is that the scattering of quasiparticles from a rough surface is strongly momentum dependent. The probability that a quasiparticle is scattered specularly

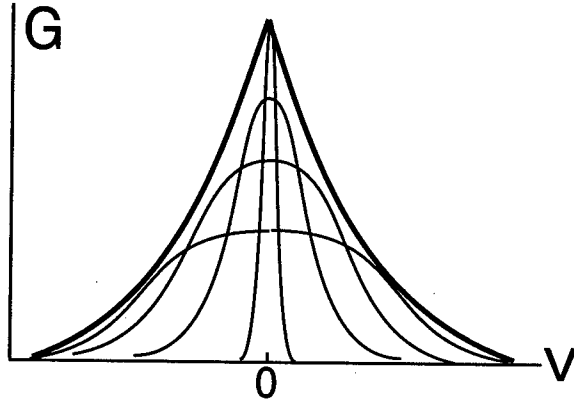


FIGURE 1. The zero bias conductance peak (bold line) can be viewed as a continuous superposition of Lorentzian components of different widths. Four representative components are shown (lighter lines).

at a rough surface is given approximately, in the tangent plane approximation, by $P = \exp[-(k_{\perp}\eta)^2]$ where η is the root mean square value of the height fluctuations of the surface [16]. Since the surfaces of interest are never atomically flat, and since the wavelength of a quasiparticle is of the order of a lattice constant, it is easily seen that only grazing incidence quasiparticles scatter specularly. *Hence only grazing incidence quasiparticles form surface bound states.* Furthermore, the surface bound states formed from these grazing incidence quasiparticles will have a width due to surface roughness scattering that increases with increasing k_{\perp} (and is zero when k_{\perp} is zero). A second mechanism limiting the lifetime of surface bound states, which has a similar momentum dependence, is surface Umklapp scattering [12,13].

Fig. 1 shows schematically a ZBCP which is a superposition of Lorentzian peaks of different widths as described by Eq. 1. The width, $\gamma(k_{\parallel})$ is written $\gamma(k_{\parallel}) = \gamma_{imp} + \delta(k_{\parallel})$ where γ_{imp} is a momentum independent impurity scattering rate, and $\delta(k_{\parallel})$ is the momentum dependent part which goes to zero at grazing angles. The result of summing the various contributions for the case $\gamma_{imp} = 0$ is the cusp-shaped peak shown in Fig. 1. It is the very narrow states of quasiparticles with k_{\perp} close to zero which contribute all of their weight near $V = 0$ and give the ZBCP a rather high cusp at $V = 0$. Now consider adding a small momentum independent γ_{imp} to the widths of all of the component parts of the ZBCP. This added width will have a strong effect on those surface bound states with original widths less than or the order of γ_{imp} , reducing their contributions to the height of the ZBCP, and hence reducing the overall maximum height of the ZBCP, which is mainly due to the narrow surface bound states. The overall width of the ZBCP is however largely unaffected by this added impurity scattering since this overall width is largely due

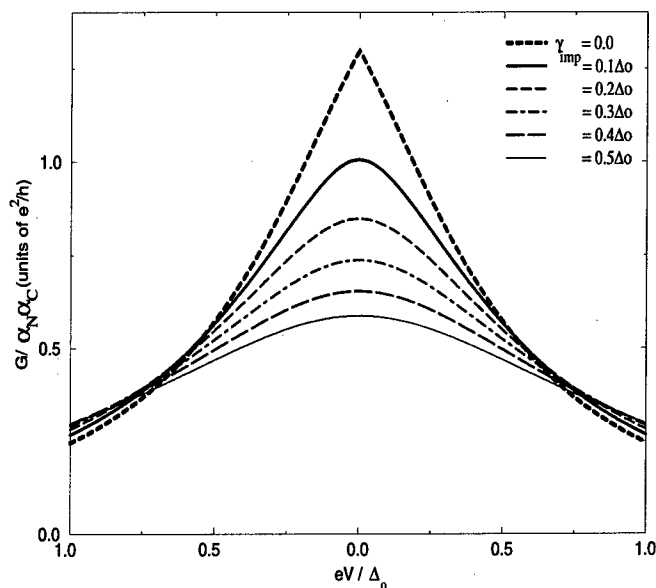


FIGURE 2. The zero bias conductance peak as calculated using Eq. 1 for several different values of γ_{imp} .

to the very broad surface bound states which will be little affected by a small additional contribution γ_{imp} to their width.

The above considerations are further illustrated by a detailed calculation of the shape of the ZBCP for different impurity scattering rates using Eq. 1, and this is shown in Fig. 2. In this case we have used a momentum-dependent width for the surface bound states which is due to the surface Umklapp scattering of the quasiparticles making up the surface bound state and which has been calculated [12] by a detailed solution of the Bogoliubov-de Gennes equations. This momentum-dependent width turns out to have a scale determined by the maximum d -wave gap, Δ_0 . The overall width of the ZBCP is thus determined by Δ_0 in this model, and is universal [i.e. independent of either surface or bulk disorder, or of the junction resistance (except that the Giaever limit is assumed)].

In the initial suggestion [13] of a momentum-dependent width for the surface bound states, the width due to the tunneling of the surface bound state quasiparticles from the superconductor through a flat insulating barrier into the normal metal was evaluated. This could account for the lack of sensitivity of the ZBCP width to defect concentration. However, it also gives a width of the ZBCP which depends on the transmission coefficient of the barrier, which this is not in agreement with the observation that all experiments carried out in the Giaever limit on $\text{YBa}_2\text{Cu}_3\text{O}_{6+x}$ appear to give the same width for the ZBCP. This is why the expression for the tunneling conductance given in [2] can not account for the universal width of the

ZBCP.

This research was supported by the Natural Sciences and Engineering Research Council of Canada.

REFERENCES

1. C. R. Hu, *Phys. Rev. Lett.* **72**, 1526 (1994).
2. S. Kashiwaya, Y. Tanaka, M. Koyanagi, H. Takashima, and K. Kajimura, *Phys. Rev. B* **51**, 1350 (1995).
3. L. Alff, H. Takashima, S. Kashiwaya, N. Terada, and H. Ihara, *Phys. Rev. B* **55**, 14757 (1997).
4. M. Aprili, M. Covington, E. Paraoanu, B. Niedermeier, and L. H. Greene, *Phys. Rev. B* **57**, R8139 (1998).
5. J. Y. T. Wei, N.-C. Yeh, D. F. Garrigus, and M. Strasik, *Phys. Rev. Lett.* **81**, 2542 (1998).
6. M. Matsumoto and H. Shiba, *J. Phys. Soc. Jpn.* **64**, 1903 (1995).
7. K. Yamada, Y. Nagato, S. Higashitani, and K. Nagai, *J. Phys. Soc. Jpn.* **65**, 1540 (1996).
8. M. Fogelström, D. Rainer, and J. A. Sauls, *Phys. Rev. Lett.* **79**, 281 (1997); Rainer *et al.*, cond-mat/9712234.
9. Yu. S. Barash, A. A. Svidzinsky, and H. Burkhardt, *Phys. Rev. B* **55**, 15282 (1997).
10. A. Poenicke, Yu. S. Barash, C. Bruder, and V. Istyukov, cond-mat/9807052.
11. J. H. Xu, J. H. Miller, Jr., and C.S. Ting, *Phys. Rev. B* **53**, 3604 (1996).
12. M. B. Walker and P. Pairor, cond-mat/9809070.
13. M. B. Walker and P. Pairor, *Phys. Rev. B* **59**, 1421 (1999).
14. Y. Tanuma, Y. Tanaka, M. Yamashiro, and S. Kashiwaya, *Phys. Rev. B* **57**, 7997 (1998).
15. M. Covington, M. Aprili, E. Paraoanu, L. H. Greene, F. Xu, J. Zhu, and C. A. Mirkin, *Phys. Rev. Lett.* **79** 277 (1997).
16. A. G. Voronovich, *Wave Scattering from Rough Surfaces*, Berlin, Springer-Verlag (1994).

On the Coexistence in $\text{RuSr}_2\text{GdCu}_2\text{O}_8$ of Superconductivity and Ferromagnetism

R. Weht, A. B. Shick, and W. E. Pickett

Department of Physics, University of California, Davis CA 95616

Abstract. We review the reasons that make superconductivity unlikely to arise in a ferromagnet. Then, in light of the report by Tallon and collaborators that $\text{RuSr}_2\text{GdCu}_2\text{O}_8$ becomes superconducting at ~ 35 K which is well below the Curie temperature of 132 K, we consider whether the objections really apply to this compound. Our considerations are supported by local spin density calculations for this compound, which indeed indicate a ferromagnetic RuO_2 layer. The Ru moment resides in t_{2g} orbitals but is characteristic of itinerant magnetism (and is sensitive to choice of exchange-correlation potential and to the atomic positions). Based on the small exchange splitting that is induced in the Cu-O layers, the system seems capable of supporting singlet superconductivity an FFLO-type order parameter and possibly a π -phase alternation between layers. If instead the pairing is triplet in the RuO_2 layers, it can be distinguished by a spin-polarized supercurrent. Either type of superconductivity seems to imply a spontaneous vortex phase if the magnetization is rotated out of the plane.

INTRODUCTION

Tallon and collaborators ([1,3] report the remarkable observation of superconductivity arising up to at least $T_s = 35$ K in $\text{RuSr}_2\text{GdCu}_2\text{O}_{8-\delta}$ (Ru1212), a compound reported originally by Bauerfeind *et al.*, [2] in spite of its having become ferromagnetic (FM) already at $T_m = 132$ K. The ferromagnetism is evident from the magnetization vs. field curve and also from zero-field muon spin rotation data that indicate a uniform field in the sample below T_m . Superconductivity (SC) is evident from the loss of resistivity, reversal of the susceptibility, and from specific heat measurements that reflect a bulk transition at T_s . Although Felner *et al.* have reported related results in $\text{R}_{1.4}\text{Ce}_{0.6}\text{Sr}_2\text{GdCu}_2\text{O}_{10}$, $R = \text{Eu}$ or Gd , [4], they indicate that their system is a canted antiferromagnet, with a saturation field an order of magnitude smaller than Ru1212. Thus Ru1212 appears to be unique as a FM that becomes superconducting well within the FM phase.

Ru1212 presents scientific questions on several levels (not to mention the novel applications that a superconducting FM might have). There are questions on the phenomenological level: how can SC and FM coexist? does the magnetic field

arising from the frozen magnetization lead to supercurrent flow? is the SC pairing singlet or triplet? There are also questions on the microscopic level: what is the FM like – is it Ru, as interpreted so far? how much does FM affect the carriers in the CuO_2 planes? how does c -axis dispersion compare with other cuprates? In this paper we begin to address both the phenomenological and the microscopic questions.

QUESTIONS OF COEXISTENCE OF SUPERCONDUCTIVITY WITH FERROMAGNETISM

The first question, and easiest to deal with, is the possibility of paramagnetic limiting. The observed saturation magnetization is about $1 \mu_B$ per unit cell, which translates into an internal field $B_{int} = 4\pi M = 700$ G. Spin splitting $2g\mu_B B_{int}$ of the two electrons of the pair is negligible compared to the superconducting gap $2\Delta \sim 4k_B T_c$, so paramagnetic limiting is no problem.

Since there is a strong tendency for singlet pairing in materials with CuO_2 layers such as Ru1212 has, and substitution of Zn for Cu strongly reduces T_s as in cuprates, we examine the possibility of a singlet SC (sSC) state in FM Ru1212 by considering two fundamental problems: (1) how does the SC order parameter accommodate itself to the vector potential arising from the intrinsic magnetization, and (2) what type of pairing occurs when the exchange field splits majority and minority Fermi surfaces? We find that it is primarily the latter item (exchange splitting) that presents difficulty for singlet SC in this system, and we consider briefly whether the problem can be alleviated by development of a FFLO phase [9] or by “ π phase” formation. [10] We note further that triplet pairing in the RuO_2 layer, which appears to occur in Sr_2RuO_4 , should not be forgotten. If Ru1212 is instead a triplet superconductor (in the Ru plane), it would have several exciting characteristics, such as a polarized supercurrent.

ISSUES OF COEXISTENCE

Early on, Ginzburg [6] observed that, although constant bulk magnetization M does not induce supercurrent flow, the vanishing of M at the boundaries induces surface currents that try to shield the exterior from the internal magnetic field $B_{int} = 4\pi M$ (inverse Meissner effect). This increase in energy would suppress the SC state unless the sample cross section is not much larger than the penetration depth. In type II superconductors, however, it was observed by Krey [7] that a spontaneous vortex phase (SVP) can be formed that avoids Ginzburg’s difficulty. Since that time there have been studies of the competition between FM and SC, [8] including suggestions that a SVP may have been observed, but almost always for the case where T_m is less than but comparable to T_s .

One exception to this regime is the recent work of Felner and collaborators, [4,5] who suggest that a SVP may occur in the canted antiferromagnet $R_{1.4}\text{Ce}_{0.6}\text{Sr}_2\text{GdCu}_2\text{O}_{10}$, $R = \text{Eu}$ and Gd . Ru1212 is different in two ways: (1) the saturation field is itself a factor of ten larger; however, this is of limited importance because Pauli limiting is not a factor in either type of material, and (2) Ru1212, being FM, has an exchange splitting of the order of 1 eV (we show below) that will induce an exchange splitting of the paired electrons in the CuO_2 planes and thereby cause additional difficulty for SC pairing.

Tallon *et al.* expect the magnetization M to lie in the plane, based on the magnitude of the field at the muon site observed in zero field μSR studies. [1] If this is the case, it reduces some of the coexistence questions, because orbital kinetic energy change of the electrons (or pairs) would require the (very small) c axis hopping, and thus is expected to be negligible compared to the gap energy. Then the remaining effect of the internal field is to lift the degeneracy of the up and down spin electrons (Zeeman splitting). This effect makes the up and down Fermi surfaces inequivalent and causes singlet pairs to have a net momentum $Q \equiv k_{F\uparrow} - k_{F\downarrow} \neq 0$. The result can be a state of the type first discussed by Fulde and Farrel and by Larkin and Ovchinnikov [9] (FFLO), in which the SC order parameter becomes inhomogeneous to accommodate the non-zero momentum pairs. Another way to decrease the competition between SC and FM is to form a π phase in which the SC order parameter vanishes in the FM Ru layer. [10]

Burkhardt and Rainer [11] have made an extensive study of the two dimensional superconductor in a magnetic field, and they find that an FFLO phase is preferred over a homogeneous SC state above a lower critical field B_{c1} , but only well below T_s and at relatively high field. To some extent their analysis may be applicable to Ru1212, with the change that the "magnetic field" is frozen in and arises from electronic exchange. The exchange splitting, even if small on an electronic energy scale, may correspond to a very large field, and its magnitude is one feature we address below.

MICROSCOPIC ELECTRONIC AND MAGNETIC STRUCTURE

Electronic Structure Methods

To address the question of magnetism in Ru1212 we have applied both the local density approximation (LDA) [15] and the 'semilocal' generalized gradient approximation (GGA) [16] to describe the effects of exchange and correlation. The predictions actually differ considerably, and we report only the GGA results here. Calculations were done using the linearized augmented plane wave (LAPW) method [12-14] to find the electronic and magnetic ground state, the band structure and projected densities of states (PDOS).

Crystal Structure

The structure of Ru1212, of the triple-perovskite type, is comprised of double CuO_2 (O_{Cu} site) layers separated by a Gd layer, sandwiched in turn by SrO (O_{apical} site) layers. The unit cell is completed by a RuO_2 (O_{Ru} site) layer, making it structurally related to $\text{YBa}_2\text{Cu}_3\text{O}_7$. The difference is that the CuO chain layer is replaced by a RuO_2 square planar layer, with resulting tetragonal symmetry. The oxygen variability that occurs lies primarily in the Sr layers, and there are displacements from the ideal positions [1] for all O ions, with the displacements being largest for O_{Ru} .

Discussion of Results

Gd behaves as a magnetic trivalent ion as expected, with moment very close to $7 \mu_B$. In expectation that the Gd moment has little effect on the electronic and magnetic behavior in the rest of the cell, we have treated only a FM alignment of Gd ions. (They actually order antiferromagnetically around 2.6 K, but antiferromagnetic order would require doubling of the unit cell with no gain of information or insight.) We have found that the electronic and magnetic structure in the cuprate and ruthenate layers does not depend on whether the Gd moment is parallel or antiparallel to the Ru moment.

We obtain a FM Ru layer, with the band structure shown in Fig. 1 and the relevant projected densities of states presented in Fig. 2. The moment (besides that on Gd) is $\sim 2.5 \mu_B$ per cell, about $1.5 \mu_B$ of which is directly assignable to the Ru ion. The remainder is spread among the six neighboring O ions, all of which are strongly polarized (for a nominally O^{2-} ion). Our total moment is substantially more than the $1 \mu_B$ reported by Tallon *et al.* As mentioned above, they have

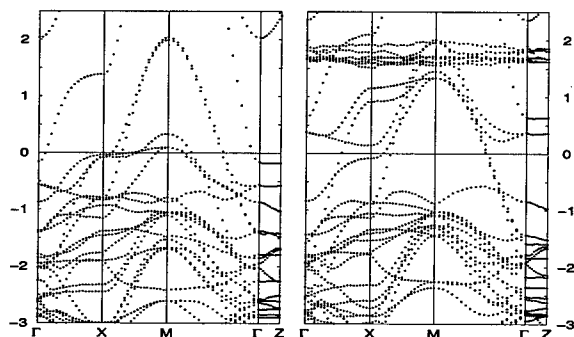


FIGURE 1. Majority (left) and minority (right) bands near E_F in tetragonal $\text{RuSr}_2\text{GdCu}_2\text{O}_8$ along high symmetry directions. Note that the distinctive Cu-O bands that reach their maximum at M lie at the same position for both spins, whereas the Ru bands are split by ~ 1 eV. The flat bands near 2 eV are the minority Gd 4f states.

evidence of displacements of the O ions in the Ru layer from their ideal positions by as much as 0.4 Å. We have observed in our calculations strong sensitivity of the moment to the position of the apical O and to the distance between the Ru and Cu atoms, so it is quite possible that a more realistic structure will give a moment much closer to the observed value. Stoichiometry will be important as well.

The Ru moment arises within the Ru t_{2g} subshell. The charge state is difficult to specify due to the metallic character of the Ru-O layer, but it is *not* close to Ru^{5+} and may be closer to Ru^{4+} . The exchange splitting of the Ru t_{2g} bands is 1 eV, but the induced splitting in the CuO_2 layers is close to two orders of magnitude smaller. The very small coupling is due to the fact that the Ru t_{2g} states couple only to the O_{apical} p_x, p_y orbitals, and these do not couple either to the Cu $d_{x^2-y^2}$ or s orbitals, so the coupling path is more indirect (perhaps $\text{O}_{\text{Ru}}-\text{O}_{\text{apical}}-\text{O}_{\text{Cu}}$). The induced moment is roughly $0.01 \mu_B$ per CuO_2 layer, which leads to a displacement of spin up and spin down barrel Fermi surfaces of only $\delta k_F \approx 0.01 k_F$. The work of Burkhardt and Rainer [11] suggest that a model independent feature of FFLO-like solutions is that the wavelength of modulation of the superconducting order parameter $\lambda_Q = 2\pi/\delta k_F$ must be greater than (not necessarily comparable to) the coherence length ξ . Our estimate is $\lambda_Q \sim 140a$, which is much greater than representative cuprate values $\xi \sim 5 - 15a$. Hence the exchange splitting we obtain is small enough to allow the possibility of an FFLO-like phase in Ru1212 .

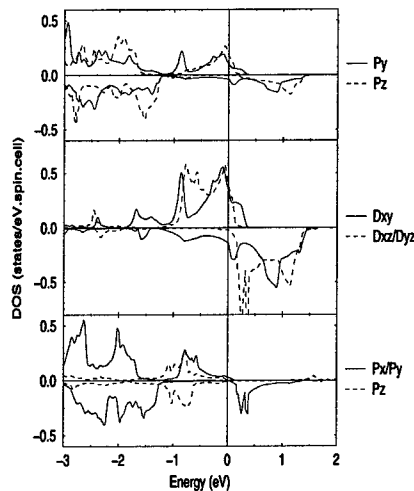


FIGURE 2. Atom projected densities of states for O_{Ru} (top), Ru (middle), and O_{apical} (bottom), clearly indicating spin splitting in all Ru t_{2g} states and all p orbitals of O_{Ru} , but in only the p_x, p_y orbitals of O_{apical} .

SUMMARY AND ACKNOWLEDGMENTS

With this paper we have begun the study of the superconducting ferromagnet Ru1212. Although magnetism in the Ru layer is strong, the exchange coupling to the Cu layers is quite small. The most likely scenario seems to be an FFLO-like inhomogeneous SC order parameter in the cuprate layers.

We acknowledge important close communication with J. Tallon and a preprint of [3] from C. Bernhard. This research was supported by Office of Naval Research Grant No. N00014-97-1-0956 and National Science foundation Grant DMR-9802076. Computation was supported by the National Partnership for Advanced Computational Infrastructure (NPACI).

REFERENCES

1. J. Tallon *et al.*, unpublished, and elsewhere in this volume.
2. L. Bauernfeind, W. Widder, and H.F. Braun, *J. Low Temp. Phys.* **105**, 1605 (1996).
3. C. Bernhard *et al.*, cond-mat/9901084.
4. I. Felner, U. Asaf, Y. Levi, and O. Millo, *Phys. Rev. B* **55**, R3374 (1997).
5. E. B. Sonin and I. Felner, *Phys. Rev. B* **57**, R14000 (1998).
6. V. L. Ginsburg, *Sov. Phys. JETP* **4**, 153 (1957).
7. U. Krey, *Int. J. Magnetism* **4**, 153 (1973).
8. C. G. Kuper, R. Revzen, and A. Ron, *Phys. Rev. Lett.* **44**, 1545 (1980); O. Fischer *et al.*, *Phys. Rev. Lett.* **55**, 2972 (1985); T. K. Ng and C. M. Varma, *Phys. Rev. Lett.* **78**, 330 (1997); A. Knigavko and B. Rosenstein, *Phys. Rev. B* **58**, 9354 (1998).
9. P. Fulde and R. A. Ferrell, *Phys. Rev.* **135**, A550 (1964); A. I. Larkin and Yu. N. Ovchinnikov, *Zh. Eksp. Teor. Fiz* **47**, 1136 (1964) [*Sov. Phys. JETP* **20**, 762 (1965)].
10. V. Prokić, A. I. Budzin, and L. Dobrosavljevic-Grujic, *Phys. Rev. B* **59**, 587 (1999).
11. H. Burkhardt and D. Rainer, *Ann. Physik* **3**, 181 (1994).
12. D. J. Singh, *Planewaves, Pseudopotentials, and the LAPW Method* (Kluwer, Boston, 1994).
13. P. Blaha, K. Schwarz, and J. Luitz, WIEN97, Vienna University of Technology, 1997. Improved and updated version of the original copyrighted WIEN code, which was published by P. Blaha, K. Schwarz, P. Sorantin, and S. B. Trickey, *Comput. Phys. Commun.* **59**, 399 (1990).
14. The sphere radii used in fixing the LAPW basis were chosen to be 2.00 a.u for Sr and Gd, 1.9 for Ru and Cu, and 1.60 for N. Local orbitals for semicore states and for Gd 4f were added to the basis set for extra flexibility and to allow semicore states to be treated within the same energy window as the band states. The LAPW plane wave cutoff corresponded to energy of 14 Ryd, making the matrix dimension approximately 1400.
15. D. M. Ceperley and B. J. Alder, *Phys. Rev. Lett.* **45**, 566 (1980), as parametrized by J. P. Perdew and Y. Wang, *Phys. Rev. B* **45**, 13244 (1992) or by Vosko, Wilk and Nusair, *Can. J. Phys.* **58**, 1200 (1980).
16. J. P. Perdew, S. Burke, and M. Ernzerhof, *Phys. Rev. Lett.* **77**, 3865 (1996).

Why T_c is too high when antiferromagnetism is underestimated? — An understanding based on the phase-string effect

Z. Y. Weng

*Texas Center for Superconductivity, University of Houston
Houston, TX 77204-5932
E-mail: zyweng@uh.edu*

Abstract. It is natural for a Mott antiferromagnetism in RVB description to become a superconductor in doped metallic regime. But the issue of superconducting transition temperature is highly nontrivial, as the AF fluctuations in the form of RVB pair-breaking are crucial in determining the phase coherence of the superconductivity. Underestimated AF fluctuations in a fermionic RVB state are the essential reason causing an overestimate of T_c in the same system. We point out that by starting with a *bosonic* RVB description where both the long-range and short-range AF correlations can be accurately described, the AF fluctuations can effectively reduce T_c to a reasonable value through the phase string effect, by controlling the phase coherence of the superconducting order parameter.

It was first conjectured by Anderson [1] that the ground state of the two-dimensional (2D) $t-J$ model may be described by some kind of resonating-valence-bond (RVB) state. Perhaps the most natural consequence of a RVB description is the superconductivity once holes are introduced into the system, which otherwise is a Mott insulator, as preformed spin pairs become mobile, i.e., carrying charge like Cooper pairs.

Even though the RVB state was proposed [1] to explain the then-newly-discovered high- T_c superconductor in cuprates, the mean-field estimate of T_c turned out to be way too high ($\sim 1000K$ at doping concentration $\delta \sim 0.1$ [2]) as compared to the experimental ones ($\sim 100K$). Another drawback for the earlier fermionic RVB theory (where spins are in fermionic representation) is that the antiferromagnetic (AF) correlations are always underestimated, which becomes obvious in low-doping limit where long-range AF ordering (LRAFO) cannot be naturally recovered. Even at finite-temperature where the LRAFO is absent, the spin-lattice relaxation rate calculated based on those RVB theories shows a wrong temperature-dependence as compared to that well-known for the Heisenberg model, indicating an absence of

AF fluctuations.

Intuitively, a fermionic RVB state should become superconducting of BCS type at finite doping where the RVB pairs are able to move around carrying charge. But since the RVB pair-breaking process corresponds to AF fluctuations at insulating phase while it also represents Cooper pair-breaking in superconducting state, it is not difficult to see why the underestimate of AF fluctuations in the fermionic RVB theory would be generally related to an overestimated T_c .

Of course, the above-mentioned drawback in describing antiferromagnetism does not include all RVB theories. There actually exists a RVB state which can describe the AF correlations extremely well. As shown by Liang, Douct, and Anderson [3], the trial wavefunction of RVB spins in *bosonic* representation can reproduce almost exact ground-state energy at half-filling (which implies a very accurate description of short range spin-spin correlations). A simple mean-field theory of bosonic RVB studied by Arovas and Auerbach [4] (usually known as the Schwinger-boson theory) can easily recover the LRAFO at zero-temperature and reasonable behavior of magnetic properties at finite temperature.

Thus, one may classify two kinds of RVB states based on whether the spins are described in fermionic or bosonic representation. In principle, both representations should be equivalent mathematically due to the constraint that at each site there can be only one spin. But once one tries to do a mean-field calculation by relaxing such a constraint, two representations will result in qualitatively different consequences: in fermionic representation, even an exchange of two spins with the same quantum number will lead to a sign change of the wavefunction as required by the fermionic statistics. At half-filling, this is apparently redundant as the true ground-state wavefunction only changes sign when two opposite spins at different sublattice sites exchange with each other, known as the Marshall sign [5] which can be easily incorporated into the bosonic RVB description. That explains the great success of the bosonic RVB mean-field theory over the fermionic ones at half-filling.

Since the bosonic RVB description of antiferromagnetism is proven strikingly accurate at half-filling, one may wonder why we cannot extend such a formalism to the doped case by literally doping the Mott-insulating antiferromagnetism into a metal (superconductor). In fact, people have tried this kind of approach based on the so-called slave-fermion representation but the mean-field theories always lead to the so-called spiral phase [6] which is inherently unstable against the charge fluctuations [7]. In other words, an instability boundary seems to prevent a continuous evolution of the mean-field bosonic RVB description into a short-ranged spin liquid state at finite doping.

It implies that some singular effect must have been introduced by doping which was overlooked in those theories. Indeed, it was recently revealed [8] that a hole hopping on the antiferromagnetic background always leaves a string of phase mismatch (disordered Marshall signs) on the path which is non-repairable at low-energy (because the spin-flip term respects the Marshall sign rule). The implication of the existence of phase string is straightforward: a hole going through a closed loop will acquire a nontrivial Berry phase and a quasiparticle picture no longer holds here.

This explains why the mean-field theory in the slave-fermion representation, where the topological effect of the phase string is smeared out by mean-field approximation, always results in an unphysical spiral-phase instability.

This barrier can be immediately removed once the nonlocal phase string effect is explicitly incorporated into the Schwinger-boson, slave-fermion representation through a unitary transformation – resulting in the so-called phase string formulation [9] where the mean-field treatment generalized from the Schwinger-boson mean-field state at half-filling [4] becomes workable at finite doping. A metallic phase [10] with short-range spin correlations can be then obtained in which the ground state is, not surprisingly, always superconducting.

What becomes special here is that the phase string effect introduces a phase-coherence factor to the superconducting order parameter [10]:

$$\Delta_{ij}^{SC} \propto \rho_s^0 \Delta^s e^{\frac{i}{2}(\Phi_i^s + \Phi_j^s)} \quad (1)$$

where Δ^s denotes the mean-field RVB order parameter for bosonic spinons and $\rho_s^0 \sim \delta$ is the bare superfluid density determined by holons (both spinon and holon are bosonic in this representation), i and j refer to two nearest-neighbor sites. The phase-coherence factor $e^{\frac{i}{2}\Phi_i^s}$ is related to the spin degrees of freedom as follows

$$\Phi_i^s = \sum_{l \neq i} \text{Im} \ln (z_i - z_l) \sum_{\alpha} \alpha n_{l\alpha}^b \quad (2)$$

with $n_{l\alpha}^b$ being defined as the spinon number operator at site l . The physical interpretation of the phase-coherence factor (2) is that each spinon contributes to a phase-vortex (anti-vortex).

At zero temperature, when all spinons are paired, so are those vortices and anti-vortices, such that superconducting order parameter Δ^{SC} achieves phase-coherence [11]. At finite temperature, free excited spinons or dissolved vortices (anti-vortices) tend to induce a Kosterlitz-Thouless type transition once the “rigidity” of the condensed holons breaks down which may be estimated as the excited spinon number becomes comparable to the holon number [10].

The superconducting transition temperature obtained this way is shown in Fig. 1 versus a spinon characteristic energy scale E_g . The definition of E_g is shown in Fig. 2 where the local (\mathbf{q} -integrated) dynamic spin susceptibility as a function of energy is given at $\delta = 0.143$ (solid curve) at zero temperature. As compared to the undoped case (\diamond curve), a resonance-like peak emerges at low-energy E_g due to the phase string effect. The doping-dependence of E_g is illustrated in the insert of Fig. 2.

Therefore, in the bosonic RVB state where the AF correlations are well described, the superconducting transition temperature is essentially decided by the low-lying spin characteristic energy. According to Fig. 2, $J \sim 100 \text{ meV}$ gives rise to $E_g = 41 \text{ meV}$ at $\delta = 0.15$ which are consistent with the neutron-scattering data for such a compound [12]. Then at the same E_g , one finds $T_c \sim 100 \text{ K}$ according to Fig.

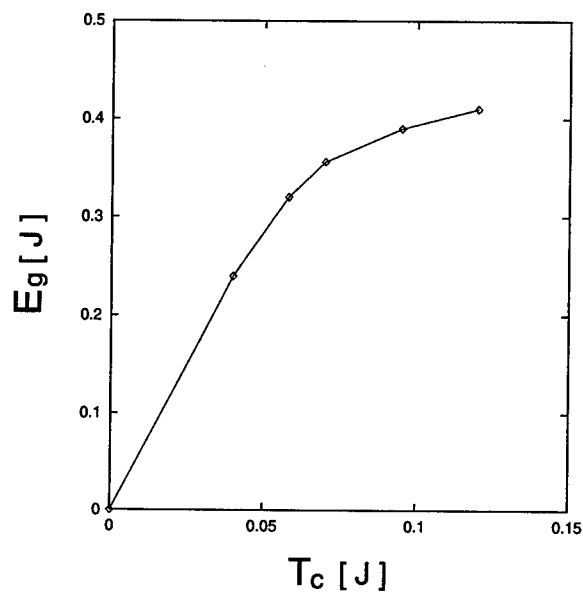


FIGURE 1. The relation of T_c with the spin characteristic energy E_g defined in Fig. 2

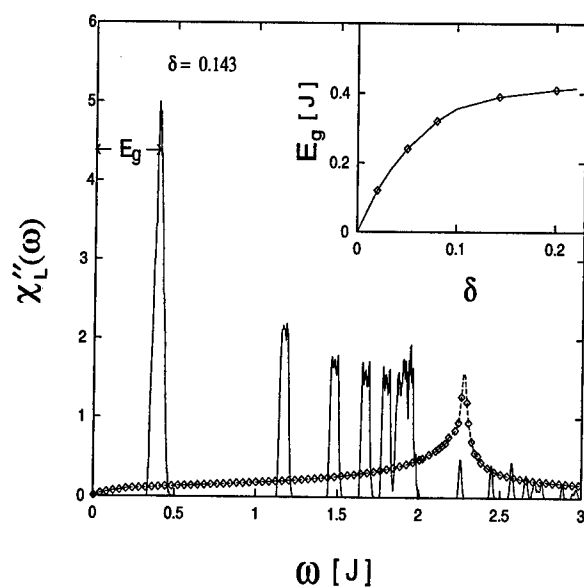


FIGURE 2. The local dynamic spin susceptibility function versus energy at $\delta = 0$ (\diamond curve) and $\delta = 0.143$ (solid curve). The insert: E_g versus the doping concentration.

1 which is very close to the experimental number in the optimal-doped *YBCO* compound.

The overall picture goes as follows. The bosonic RVB order parameter Δ^s controls the short-range spin correlations which reflects the "rigidity" of the whole phase covering both undoped and doped regimes, superconducting and normal (strange) metallic states. On the other hand, T_c is basically determined by the phase coherence: for those preformed RVB pairs to become true superconducting condensate, the extra phase frustration introduced by doping has to be suppressed. Here we see how the AF fluctuations and superconductivity interplay: the former in a form of RVB pair-breaking fluctuations causes strong frustration on the charge part through the phase string effect and its energy scale thus imposes an upper limit for the transition temperature of the latter. It is interesting to see that AF fluctuations and superconducting condensation do compete with each other, although the driving force of superconductivity already exists in the Mott antiferromagnet in a form of RVB pairing.

To summarize, even though it is very natural for a RVB pairing description of the Mott-insulating antiferromagnetism to develop a superconducting condensation in the neighboring metallic regime, the issue of superconducting transition temperature is highly nontrivial as the AF fluctuations in a form of RVB pair-breaking process are the *key* effect to scramble the phase coherence of the superconductivity. The underestimated AF fluctuations in a fermionic RVB state are the essential reason causing an overestimate of T_c in the same system. We pointed out that by starting with a *bosonic* RVB description where both the long-range and short-range AF correlations can be accurately described, the AF fluctuations can effectively reduce T_c to a reasonable value through the phase string effect controlling the phase coherence of the superconducting order parameter.

ACKNOWLEDGMENTS

This talk is based on a series of work done in collaboration with D. N. Sheng and C. S. Ting. I would like to acknowledge the support by the Texas ARP program No. 3652707 and the State of Texas through the Texas Center for Superconductivity at University of Houston.

REFERENCES

1. P.W. Anderson, *Science* **235**, 1196 (1987); G. Baskaran *et al.*, *Solid State Comm.* **63**, 973 (1987); Z. Zou and P. W. Anderson, *Phys. Rev.* **B37**, 627 (1988).
2. N. Nagaosa and P. A. Lee, *Phys. Rev. Lett.* **64**, 2450 (1990); P. A. Lee and N. Nagaosa, *Phys. Rev.* **B46**, 5621 (1992).
3. S. Liang, B. Doucot, and P. W. Anderson, *Phys. Rev. Lett.* **61**, 365 (1988).
4. D.P. Arovas and A. Auerbach, *Phys. Rev.* **B38**, 316 (1988).
5. W. Marshall, *Proc. Roy. Soc. (London)* **A232**, 48 (1955).

-
6. B. I. Shraiman and E. D. Siggia, Phys. Rev. Lett. **62**, 1564 (1989); **61**, 467 (1988).
 7. Z. Y. Weng, Phys. Rev. Lett. **66**, 2156 (1991).
 8. D. N. Sheng, *et al.*, Phys. Rev. Lett. **77**, 5102 (1996).
 9. Z. Y. Weng, *et al.*, Phys. Rev. B **55**, 3894 (1997).
 10. Z. Y. Weng, *et al.*, Phys. Rev. Lett. **80**, 5401 (1998); preprint, cond-mat/9809362.
 11. V. J. Emery and S. A. Kivelson, Nature, **374**, 434 (1995).
 12. M. A. Mook, Yethiraj, G. Aeppli, T. E. Mason, and T. Armstrong, Phys. Rev. Lett. **70**, 3490 (1993); H. F. Fong, B. Keimer, P. W. Anderson, D. Renzik, F. Doğan, and I. A. Aksay, Phys. Rev. Lett. **75**, 316 (1995).

Magnetic Scattering; Pair-Breaking Effect and Anomalous Diamagnetism Above H_{c2} And T_c

S. Wolf⁽¹⁾, Yu.Ovchinnikov^(2,3), V.Kresin⁽³⁾

⁽¹⁾ Naval Research Laboratory, Washington, DC 20375

⁽²⁾ Lawrence Berkeley Laboratory, Berkeley, CA 94720

⁽³⁾ Landau Institute for Theoretical Physics, Moscow, Russia

Abstract. An anomalous diamagnetic moment can be observed above T_c and H_{c2} in inhomogeneous superconductors. Such inhomogeneity can be caused by a non-uniform distribution of magnetic impurities. The model describes recent experimental data on overdoped cuprates.

INTRODUCTION.

Magnetic scattering is a key ingredient of high T_c superconductivity. A number of phenomena (unconventional isotope effect, drastic decrease in T_c upon overdoping, a sharp upturn in the temperature dependence of the upper critical field, etc.) can be explained by the presence of localized magnetic moments. A study of these phenomena allows us to evaluate an important parameter, namely an upper limit of T_c for this class of materials. The interaction between localized magnetic moments and Cooper pairs which are in the singlet state, destroys the pair correlation and is accompanied by spin-flip scattering (such scattering provides the conservation of the total spin).

The influence of magnetic impurities (pair-breaking, appearance of gaplessness at some value of the concentration of magnetic impurities, depression in T_c , etc.) was described in [1]. We studied this phenomenon for the cuprates in [2,3]. Here we describe a main concept and present some new results.

RECOVERY EFFECT. CRITICAL FIELD.

The dependence of H_{c2} on T which is drastically different from the conventional picture, has been observed in the overdoped high- T_c oxides [4]. As we know, conventional bulk superconductors are characterized by linear temperature dependence of H_{c2} near T_c , a quadratic behavior as $T \rightarrow 0$, and by negative curvature over the entire temperature region. Contrary to this picture, the layered cuprates are described by linear dependence near $T=0K$ and by positive curvature at all temperatures. In

addition, the value of $H_{c2}(0)$ greatly exceeds the value that follows from the conventional theory [5]. Similar effect has been observed in the Sm-Ce-Cu-O and in Y-Ba-Zn-Cu-O [6] systems.

Let us describe here a qualitative picture (a more detailed description see in [3]). The superconducting state of the Cu-O plane is greatly affected by magnetic impurities. Spin-flip scattering leads to a depression of the superconducting state, and this is reflected in relatively small values of T_c and H_{c2} . The magnetic impurities can be treated as independent [1], and the spin-flip scattering by the impurities provides the conservation of the total spin. However, at low temperatures (in the region $T=1K$), because of the correlation of the magnetic moments, the trend to ordering of the moments becomes important, and this trend frustrates the spin-flip scattering. Pairing becomes less depressed ("recovery effect"), and this leads to a large increase in the value of H_{c2} and, correspondingly, to a positive curvature in H_{c2} vs T .

The ordering of the impurities was observed for the Sm-Ce-Cu-O compound by direct measurements of the magnetic susceptibility [6a].

The general equation describing a layered superconductor in the presence of magnetic impurities and an external field (at $H=H_{c2}$) has the form (see [3]):

$$\ln(2\gamma\Gamma_{cr}/\pi T) - [\psi(0.5 + (\Gamma/2\pi T)) - \psi(0.5)] = f(H_{c2}, T); \quad (1)$$

$$f(H_{c2}, T) = (H_{c2} v^2 / \Gamma) \{ \Gamma^{-1} [\psi(0.5 + (\Gamma/2\pi T)) - \psi(0.5 + (\Gamma/4\pi T))] - (4\pi T)^{-1} \psi(0.5 + (\Gamma/2\pi T)) \}$$

Here ψ is the psi-function, $\ln\gamma=C=0.58$ is the Euler constant, $\Gamma=t_s^{-1}$ is the amplitude of the spin-flip scattering, t_s is the relaxation time; Γ_{cr} corresponds to the complete suppression of superconductivity ($T_c=0$).

Pair-breaking leads to a depression in T_c and, eventually, at some value of the concentration of magnetic impurities $n_M = n_{M_{cr}}$, to the total suppression of superconductivity. This suppression is preceded by the appearance of the gapless state.

There is an interesting question about the nature and location of magnetic impurities. First of all, one should note that the oxygen depletion leads to formation of the Cu^{++} ions on the chains. In addition, one can observe the formation of magnetic clusters in the Cu-O planes. Moreover, the additional magnetic moments are localized on the Ba-O layer, which is adjacent the Cu-O layer for overdoped Tl- and Bi-based compounds. Localized magnetic moments can be formed on the apical oxygen site. Probably, we are dealing with the formation of the paramagnetic radical O_2^- , and this also involves the apical oxygen, as well as an additional oxygen in the Tl-O (Bi-O) layers.

DIAMAGNETISM ABOVE T_c .

The inhomogeneity of a superconducting system gives rise to an interesting situation when at $T > T_c^{\text{res}}$ (T_c^{res} is characterized by a relatively sharp resistive transition) one can observe an anomalously large magnetic moment. Inhomogeneity leads to the situation when T_c becomes spatially dependent. Let us focus on the case when the sample contains regions with local T_c higher than the average value \bar{T}_c . In other words, at $T > \bar{T}_c$, the superconducting grains are embedded in a normal matrix. For example, one can consider the case when the sample contains a non-uniform distribution of magnetic impurities. Such case is perfectly realistic, particularly for non-stoichiometric compounds such as overdoped cuprates.

The inhomogeneous superconductor containing magnetic impurities is described in detail by the equations introduced by Larkin and one of the authors [7]:

$$\alpha\Delta - \beta\omega + \frac{D}{2} \left(\alpha\partial_-^2 \beta - \beta \frac{\partial^2 \alpha}{\partial \mathbf{r}^2} \right) = \alpha\beta\Gamma \quad (2a)$$

$$\alpha^2 + |\beta|^2 = 1 \quad (2b)$$

$$\Delta = 2\pi T |\lambda| \sum_{\omega > 0} \beta \quad (2c)$$

Here α and β are the usual and pairing Green's functions averaged over energy, Δ is the order parameter, $\partial_- = (\partial/\partial \vec{r}) - 2ie\vec{A}$, \vec{A} is the vector potential. Because of the inhomogeneity, all of these quantities are spatially dependent. We consider the "dirty" case, so that D is the diffusion coefficient.

Assume that the sample contains a sufficient amount of magnetic impurities so that $\tau, T_c^0 < 1$; as a result $T_c \ll T_c^0$, where T_c is the average value of the critical temperature, and T_c^0 corresponds to the transition temperature with no magnetic impurities. We obtain the following equation for the order parameter:

$$\Delta = 2\pi T |\lambda| \sum_{\omega > 0} \left(\Gamma + \omega - \frac{D}{2} \partial_-^2 \right)^{-1} \left\{ \Delta - \frac{\omega}{2} \beta_0 |\beta_0|^2 + \frac{D}{4} \beta_0 \frac{\partial^2}{\partial Z^2} |\beta_0|^2 \right\} \quad (3)$$

Let us focus on the temperature region $T > T_c(H)$. Then the order parameter is localized near some clusters. In such a region ($\vec{r} \equiv \vec{r}^0$) the operator $(\Gamma + \omega - (D/2)\partial_-^2)$ has discrete eigenvalues.

One can evaluate the order parameter (at $T > T_c(H)$) for the inhomogeneous structure and then the current and the corresponding magnetic moment. The order

parameter can be found in the form $\Delta = C\Delta_0$, where C is the solution of the equation:

$$\ln(T_c^0/T_c) = \psi\left[\frac{1}{2} + \frac{\Gamma_\infty + \lambda_1}{2\pi\Gamma_c}\right] - \psi(1/2) + \frac{C^2}{12\Gamma_\infty^2} \frac{(\Delta_0^{*2}\Delta_0^2)}{(\Delta_0^*\Delta_0)} \quad (4)$$

Eq. (4) is the generalization of the equation obtained in [1] for inhomogeneous case that was studied.

For the most interesting case when the variation of the amplitude $\delta\Gamma(\vec{r}) = \Gamma - \Gamma_\infty$ has the form

$$\delta\Gamma(\vec{r}) = \begin{cases} \delta\Gamma(\rho) & ; \rho < \rho_0 \\ 0 & ; \rho > \rho_0 \end{cases} \quad (5)$$

We obtain the following expression for the magnetic moment

$$M_z = -A(B - T^2 + T_c^2)H \quad (6)$$

Here

$$A = (8\pi^3 e^2 v_{DL} / \Gamma_\infty)(\rho_0 / z_0)^4 (\tilde{x}_2^3 \tilde{x}_2 / \tilde{x}_4)$$

If $\delta\Gamma \ll \Gamma_\infty \equiv \pi T_c^0$, the value of the local critical temperature $T_{c,L}$ greatly exceeds its average value. In this case the magnetic moment for $T > T_c$ has a simple temperature dependence

$$M_z = -A(B - T^2)H \quad (7)$$

As a result, one can observe a noticeable diamagnetic moment. One can consider a more general case when the magnetic scattering amplitude Γ depends on temperature [3].

Let us focus on the overdoped cuprates. The authors [8] describe torque measurements performed on a $Tl_2Ba_2CuO_6$ overdoped sample ($T_c \approx 14K$; this value of T_c has been determined by resistive measurements). A diamagnetic moment, proportional to an external magnetic field, has been observed at $T > T_c$. This observation can be explained by our theory. Indeed, the overdoping is provided by an additional oxidation. Since the oxygen distribution is non-uniform, the sample becomes inhomogeneous with a non-uniform distribution of magnetic impurities. As a result, one can expect (see above) the appearance of a diamagnetic moment at $T > T_c^{res} \approx 15K$. The analysis is in good agreement with the data [8]

Let us note also, that the paper [8] was aimed at the investigation of the problem whether the $H_{c2}(T)$ curves obtained in [4] represents the critical field (then the curve separates superconducting and normal regions) or the irreversibility line (in this case the line separates vortex lattice and vortex liquid regions). Torque magnetometry

is an ideal tool for such a study. The measurements [8] demonstrated the absence of vortices above the curve, but, nevertheless, a puzzling diamagnetic response was observed in the region $H > H_{c2}$. Moreover, a similar response has been observed above $T_c \approx 15\text{K}$, and this observation makes the problem go beyond the nature of the $H_{c2}(T)$ dependence.

We think that the observed phenomenon is due to an inhomogeneity of the sample. The curve $H_{c2}(T)$ as well as the value $T_c^{\text{res}} \approx 15\text{K}$ separates superconducting and "normal" regions, and the "normal" region displays normal transport properties. As for the magnetic response, it is determined by the presence of small superconducting regions with $T_{c,L} > T_c^{\text{trans}}$, and this leads to the phenomenon observed in [8].

Therefore, inhomogeneous superconductivity allows, in principle, to separate the resistive and magnetic transitions to the superconducting state.

The research of YNO was supported by the CRDF under Contract No. RP1-194. The research of VZK was supported by the US Office of Naval Research under the Contract No. N00014-98-F0006.

REFERENCES.

1. A. Abrikosov and L. Gor'kov, *Sov. Phys.-JETP* **12**, 1243 (1961).
2. P. de Gennes, *Superconductivity in Metals and Alloys*, Benjamin, NY (1966).
3. V. Kresin and S. Wolf, *Phys. Rev. B* **46**, 6458 (1992)
4. Yu. Ovchinnikov, V. Kresin, *Phys. Rev. B* **54**, 1251 (1996)
4. a) A. P. Mackenzie et al., *Phys. Rev. Lett.* **71**, 1938 (1993);
b) M. Osofsky et al., *Phys. Rev. Lett.* **71**, 2315 (1993).
5. L. Gor'kov, *Sov. Phys. JETP* **10**, 593 (1960);
E. Helfand, and N. R. Werthamer, *Phys. Rev. Lett.* **13**, 686 (1964);
Phys. Rev. **147**, 288 (1966).
6. a) Y. Dalichaouch et al., *Phys. Rev. Lett.* **64**, 599 (1990).
b) D. Warner et al., *Phys. Rev. B* **51**, 9375 (1995)
7. A. Larkin and Yu. Ovchinnikov, *Sov. Phys.-JETP* **28**, 1200 (1969).
Yu. N. Ovchinnikov, *JETP* **39**, 538 (1974)
8. C. Bergemann et al., *Phys. Rev. B* **57**, 14387 (1998)

EXPERIMENT HIGH T_c CUPRATES

NMR studies of the original magnetic properties of the cuprates: effect of impurities and defects

H. Alloul, J. Bobroff, A. Mahajan, P. Mendels and Y. Yoshinari.

*Laboratoire de Physique des Solides, UMR 8502 CNRS,
Université Paris-Sud 91405, Orsay, France.*

Abstract. Substitutional impurities in the CuO_2 planes of the cuprates allow us to probe the electronic properties of the host material. The pseudo-gap in the underdoped regime is unmodified far from the impurities even though T_c is greatly reduced. The spin polarisation induced by magnetic impurities has an oscillatory behaviour reflecting the existing AF correlations between the Cu spins. Its influence on the NMR spectra opens a way to determine the \mathbf{q} dependence of the static spin susceptibility and the T dependence of the AF correlation length. NMR measurements demonstrate that non-magnetic impurities such as Zn induce a local moment behaviour on the neighbouring Cu sites. This magnetism revealed by spin-less sites can be understood on theoretical grounds in the case of undoped quantum spin systems, while here the carriers greatly complicate the situation. Susceptibility data show that the magnitude of the local moment decreases with increasing hole doping. This experimental evidence directly reflects the influence of AF correlations and the interference between the carriers and the Cu hole spins in the cuprates. The anomalously large scattering of the carriers on spinless defects is another indication of the originality of the electronic properties of the cuprates, which apparently extends even to the overdoped regime.

I INTRODUCTION: MAGNETIC PROPERTIES OF PURE MATERIALS

It is now experimentally well established that the CuO_2 planes display anomalous magnetic properties in the metallic normal state of the cuprates, at least in the underdoped and optimally doped states. The occurrence of magnetic correlations was first shown by the existence of an enhanced non-Korringa nuclear spin relaxation rate $1/T_1$ on ^{63}Cu and not on ^{17}O and ^{89}Y [1,2]. In the recent past, considerable interest has been focused on the pseudo-gap in the excitation spectrum of the cuprates. It was detected first in microscopic NMR measurements of the susceptibility χ_p of the CuO_2 planes [2], which exhibit a large reduction in the homogeneous $\mathbf{q} = 0$ excitations at low T in underdoped materials, as shown in Fig.1. Similar low T reductions of the imaginary part of the susceptibility at

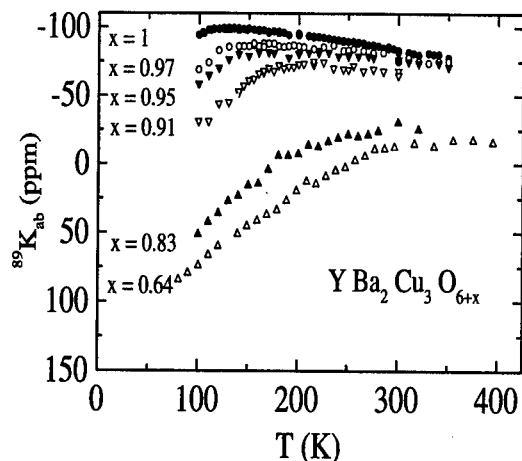


FIGURE 1. The ^{89}Y NMR shift data evidence the occurrence of pseudo-gaps from a large decrease of the susceptibility χ_p of the CuO_2 planes, in YBCO_{6+x} . The temperature at which the pseudo-gap begins to open, which corresponds to the χ_p maximum, increases markedly with decreasing x , that is decreasing hole doping (the original data [2] are less accurate than those displayed here).

the AF wave vector $\mathbf{q} = (\pi, \pi)$ were observed in ^{63}Cu $1/T_1T$ data and inelastic neutron scattering experiments [3]. Presently, the pseudo-gap of the underdoped high- T_c superconductors is also studied by many techniques such as transport and angle resolved photoemission, which yields its \mathbf{k} dependence. Various explanations are proposed for the pseudo-gaps which are believed to be essential features of the physics of the normal state (and perhaps the superconducting state) of the cuprates.

Atomic substitutions in the planar Cu site have naturally been found the most detrimental to superconductivity. This has in parallel triggered a large effort, particularly in our research group, to use such impurities to reveal the original normal-state magnetic properties of the cuprates. We shall see that NMR, as a local magnetic probe, is an essential tool which lends weight to this approach. In section II we present the effect of impurities on the phase diagram and the pseudo-gaps. We will distinguish the average effect of impurities on the physical properties far from the impurity site from the local magnetic perturbations. The study of the distribution of the spin polarisation induced by magnetic impurities is shown in sec. III to be a direct probe of the non-local magnetic response $\chi'(\mathbf{r})$ of the pure system, a quantity which is hard to access by other experimental approaches. In section IV we consider the case of non-magnetic impurities like Zn ($3d^{10}$) which, upon substitution on the Cu site of the CuO_2 plane, strongly decreases the superconducting transition temperature T_c . It has been anticipated [4], and subsequently shown experimentally

[5], that, although Zn itself is non-magnetic, it induces a modification of the magnetic properties of the correlated spin system of the CuO_2 planes. We shall recall how ^{89}Y NMR demonstrated [6] that local magnetic moments are induced on the Cu near neighbour (*n.n.*) of the Zn substituent in the CuO_2 plane. Experiments on $\text{La}_{2-x}\text{Sr}_x\text{CuO}_4$ have confirmed [7] that the occurrence of local moments induced by non-magnetic impurities on the Cu sites is a general property of cuprates. Recent measurements of the variation with hole doping of the effective magnetic moment associated with non magnetic impurities will be reviewed. Finally, we shall discuss briefly in sec.V the influence of impurities on transport properties.

II IMPURITIES AND PHASE DIAGRAMS

The main effect of impurities is to depress superconductivity, usually much faster in the underdoped regime than in the optimally doped case. Similarly the increase of resistivity is larger for underdoped materials. This results in a shift of the Insulator-Metal transition towards higher hole concentration in presence of impurities. So what happens then to the crossover pseudo-gap lines? There is a controversy which has arisen because of the differences between macroscopic and microscopic measurements of the pseudo-gap. NMR has the advantage that the sites in the vicinity of the impurity usually display well shifted resonance lines. Therefore, the main NMR line corresponds to sites far from the impurity. Its broadening, to be studied in section III, is associated with the oscillatory induced polarisation of the host. Its position measures then the average χ_p far from the impurities which reflects their influence on the homogeneous magnetic properties. The T dependence of the shifts $\Delta K(T)$ of the ^{89}Y or ^{17}O NMR mainlines [5,6,8] are found to be unmodified by impurity substitutions, as can be seen in Fig. 2.

This demonstrates that, contrary to the Metal-Insulator transition, the *pseudo-gap* is *unaffected* by impurity substitutions at large distance from the impurities. Incidentally these data also ensure that the hole doping is not significantly modified. Conversely if hole doping is changed, i.e. by Pr substitution on the Y site [9], NMR shift data can be used to estimate its variation by comparison with calibrated curves for χ_p in the pure material (Fig 1).

Other experiments, which very often probe the macroscopic behaviour of the sample, have sometimes been interpreted differently, as they do not directly distinguish local from large distance properties. For instance, it was initially suggested [10] on the basis of neutron scattering experiments, that the pseudo-gap vanishes at $\mathbf{q} = (\pi, \pi)$ upon Zn substitution. However, the careful neutron data of Sidis *et al.* [11] indicate that the opening of the pseudo-gap still occurs at the same T^* although new states appear in the pseudo-gap. Such states may be associated with local magnetic modifications induced around the Zn, which will be described in section IV. In any case, far from the impurities the pseudo-gap is quite robust upon impurity substitution. These results are quite natural if the pseudo-gaps are only

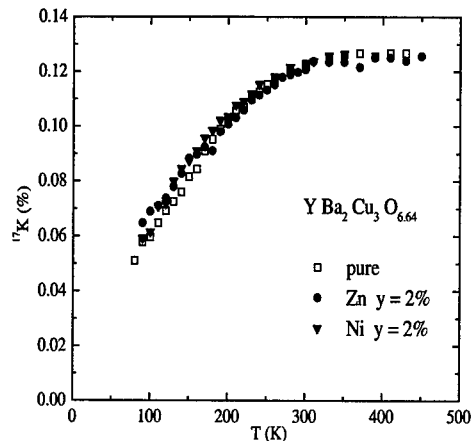


FIGURE 2. The spin susceptibility χ_p and therefore the temperature T^* of the ^{17}O NMR shift maximum, characteristic of the opening of the pseudo-gap, are not modified upon Zn or Ni substitution, while T_c is significantly reduced (from 60K to $\approx 20\text{K}$ for 2% Zn) (similar data were taken first [5] on ^{89}Y).

associated with the occurrence of AF correlation effects. However, in the scenario in which the pseudo-gaps are associated with the formation of local pairs below T^* , they indicate that impurities do not prevent the formation of local pairs except possibly in their vicinity.

III EXTENDED RESPONSE TO A LOCAL MAGNETIC EXCITATION

In noble metals hosts, any local charge perturbation is known to induce long distance charge density oscillations (also called Friedel oscillations). Similarly a local magnetic moment induces a long distance oscillatory spin polarisation (RKKY) which has an amplitude which scales with the magnetization of the local moment and with its coupling J_{ex} with the conduction electrons. This oscillatory spin polarisation gives a contribution to the NMR shift of the nuclei which decreases with increasing distance from the impurity. In very dilute samples, if the experimental sensitivity is sufficient, the resonances of the different shells of neighbours of the impurity can be resolved [12]. These resonances merge together if the impurity concentration is too large, resulting in a net broadening $\Delta\nu_{imp}$ of the host nuclear resonance. For some impurities, like rare earths substituted on the Y site, the hybridisation and therefore the exchange coupling J_{ex} are extremely weak. The plane nuclear spins only sense the moment through its dipolar field. But for moments

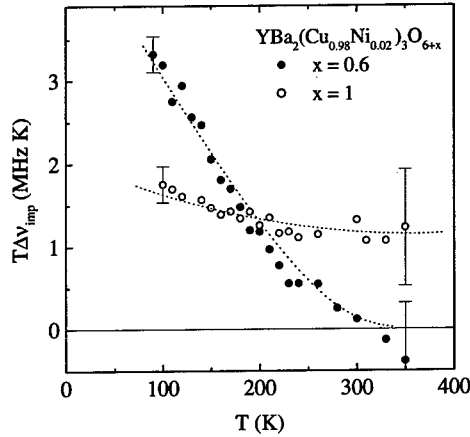


FIGURE 3. The ^{17}O NMR broadening $\Delta\nu_{\text{imp}}$ multiplied by T is plotted versus T for Ni substituted YBCO samples [8]. The variation of this quantity is related to that of the susceptibility $\chi'(\mathbf{q})$, which is peaked near the AF wave vector. The dotted lines are guides to the eye.

located in the planes such as Ni, the induced spin polarisation dominates, especially for the ^{17}O and ^{63}Cu nuclei. The large ^{17}O NMR broadening induced by Ni has been therefore studied in great detail by Bobroff *et al* [8]. It has been found that in underdoped YBCO, the linewidth increases much faster than $1/T$ at low temperature, contrary to what one might expect in a non-correlated metallic host (Fig.3). This fast increase is a signature of the anomalous magnetic response of the host which displays a peak in $\chi'(\mathbf{q})$ near the AF wavevector (π, π) , which can be characterized by a correlation length ξ . Therefore the T variation of the NMR spectra yields a method to study the T dependence of $\chi'(\mathbf{q})$ and ξ . The analysis of such data depends on the phenomenological shape given to the \mathbf{q} dependence of $\chi'(\mathbf{q})$, especially as the O site probes $\chi'(\mathbf{r})$ on its two neighbours, and therefore is governed somewhat by the gradient of $|\chi'(\mathbf{r})|$. Assuming a Gaussian shape for $\chi'(\mathbf{q})$, it is found that the linewidth is nearly insensitive to the T dependence of ξ , in contrast to the case of a Lorentzian shape [13]. The experiment on a single nuclear site does not by itself allow deduction of $\xi(T)$. However comparison with spin-spin relaxation data, which also measures an integral quantity involving $\chi'(\mathbf{q})$ yields some complementary information. With a Gaussian shape we find that ξ increases with T while for a Lorentzian, it would decrease with increasing T . Similarly a comparison of the respective broadenings of the ^{17}O , ^{89}Y and ^{63}Cu spectra, which probe differently $\chi'(\mathbf{r})$, lead us to conclude that the Lorentzian model is somewhat better, implying that ξ increases at low T as one might expect [14]. More accurate studies of the shape of the spectra as well as their concentration dependence are required to arrive at quantitative conclusions on the variation of $\xi(T)$. We should

point out here that, for YBCO₇, the ¹⁷O width varies roughly like 1/*T*, while the Ni moment still displays a Curie law. This indicates that the *T* dependence of $\chi'(\mathbf{q})$ is not as large in optimally doped systems. In such cases the detailed shape of $\chi'(\mathbf{q})$ could not be analysed up to now.

IV LOCAL MAGNETISM INDUCED BY NON-MAGNETIC ZN

Surprisingly it has been found that, as for Ni substitution, a 1/*T* broadening of the ⁸⁹Y line occurs [5] in YBCO₇:Zn, even though Zn is expected to be in a non-magnetic 3d¹⁰ state. This was the first experimental evidence *for the occurrence of "local moment like" behaviour induced by Zn*. A more refined picture of the response of the host to a non-magnetic substituent has been obtained in the case of underdoped YBCO_{6.64}, as distinct resonances of ⁸⁹Y were observed and could be attributed to Y *n.n.* sites of the substituted Zn [6]. The measured Curie-like contribution to the NMR shift of the first *n.n.* line (Fig.4), and the shortening of its *T*₁ at low-*T* are striking evidence which justify the denomination "local moment", that we have been using throughout ¹.

The Zn induced local moments are quite clearly located in the vicinity of the Zn. As is shown by analysis of the *n.n.* ⁸⁹Y NMR intensity data, the Zn substitutes essentially on the plane copper site. Therefore, the Zn contribution χ_c to the macroscopic susceptibility could be inferred from SQUID data taken on samples free of parasitic impurity phases [18,19]. The hyperfine couplings deduced from the comparison of the ⁸⁹Y NMR shift data to χ_c have the correct order of magnitude to demonstrate that the local moment resides mainly on the Cu *n.n.* to the Zn. Assuming that they are not modified with respect to pure YBCO, the data can be analysed consistently with *a locally AF state extending over a few lattice sites*. This might also explain the existence of a line corresponding to Y second *n.n.* to the Zn [16].

In the superconducting state, ⁶³Cu NQR relaxation [20] and Mössbauer experiments [21] indicate the existence of states in the gap. In neutron scattering experiments [11], the local states induced by the Zn, both in the pseudo-gap and in the spin-gap detected below *T*_c, are found at the (π , π) scattering vector, and correspond to a real state extension of about 7Å. These thus constitute direct evidence for the persistence of AF correlations in the vicinity of the impurities [22].

¹) The validity of these observations has been periodically put into question, for instance as similar *n.n.* resonances were not detected [15] in ESR experiments on Gd (substituted on Y). From the *T*₁ data for ⁸⁹Y NMR, we have shown that the large expected relaxation rate for Gd corresponds to a significant line broadening of the Gd ESR *n.n.* lines which prohibits their detection [16]. It has also been conjectured that substitution of Zn on Cu and Ca on Y yield similar disorder effects on the NMR [17]. This is not true as the line broadening does not exhibit a Curie like *T* variation for Ca substituted samples.

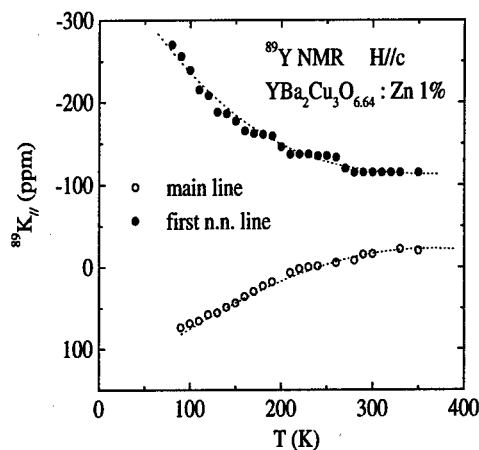


FIGURE 4. The *n.n.* ^{89}Y NMR shift obtained in $\text{YBCO}_{6.64}:\text{Zn}$ displays a paramagnetic Curie like component in contrast to the decreasing (pseudo-gap) susceptibility of the host material [6].

It is clear that the observed local moment behaviour is original inasmuch as it is the *magnetic response of the correlated electron system to the presence of a spinless site*, as has been proposed from various theoretical arguments [4,23–26]. As complete understanding of the magnetic properties of pure cuprates is far from being achieved, it is no surprise that present theoretical descriptions of impurity induced magnetism are rather crude, and for example, do not address its microscopic extent. Our results also fit well in the context of recent theoretical work on undoped quantum spin systems. For instance Martins [27] predicts static local moments induced by doping $S = 1/2$ Heisenberg AF chains or ladders with non-magnetic impurities. NMR experiments on the $S = 1/2$ Heisenberg chain system Sr_2CuO_3 are consistent with the prediction of an induced local moment with a large spatial extent along the chain [28]. In this undoped insulating quantum liquid, the response is purely magnetic. Since AF correlations persist in the metallic cuprates, the appearance of a local moment near the Zn might be anticipated, but its properties could depend strongly on the density of charge carriers. Magnetisation data by Mendels *et al.* [18,19], shown in Fig. 5, demonstrate that the Curie constant decreases steadily from $\text{YBCO}_{6.64}:\text{Zn}$ to $\text{YBCO}_7:\text{Zn}$. However existing experiments do not, at present, distinguish the respective roles of the AF correlation length and screening by the conduction holes in defining the local moment magnitude and spatial extent.

In the slightly overdoped YBCO_7 , the occurrence of a local moment was confirmed from ^{17}O NMR linewidth data [29]. The fact that we could not resolve the ^{89}Y *n.n.* signal in YBCO_7 is consistent with the weak magnitude found for the Curie-like contribution to the local susceptibility. Furthermore, Ishida *et al* [7] showed that our observation extends to another cuprate family, as non-magnetic

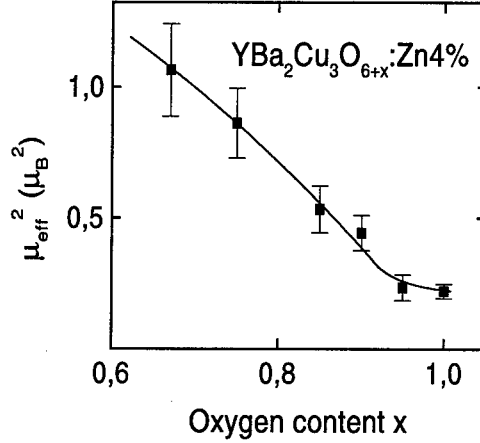


FIGURE 5. The Curie constant for the local moment induced by Zn in YBCO_{6+x} , as measured by macroscopic magnetic susceptibility measurements is found to decrease markedly with hole doping [19]

Al exhibits a local moment behaviour in optimally doped $\text{La}_{2-x}\text{Sr}_x\text{CuO}_4$. A local signature of this fact was found in the shift of the ^{27}Al NMR which exhibits a Curie-Weiss T dependence of χ_c , with a sizable Weiss temperature ($\theta \approx 50\text{K}$). It is not very clear from these data whether such a high value of θ corresponds to a genuine single impurity effect or if it varies with Al content, thereby revealing a strong coupling between the local moments. By analogy with our results this observation is supposed to result from a local moment residing on the *n.n.* copper orbitals, which are coupled to the ^{27}Al nuclear spin via transferred hyperfine couplings.

V MAGNETISM AND TRANSPORT PROPERTIES

Let us now consider briefly the influence of impurities on *transport properties*. Most analyses of the resistivity data [30,31] suggest a large magnitude for the Zn scattering, not far from the unitary limit. Such results are generally observed for most local defects induced in the CuO_2 planes, such as irradiation defects [32]. It has occasionally been assumed [33] that strong scattering is due to potential scattering. In the present case, for which no charge difference occurs between Zn^{2+} and Cu^{2+} , the scattering cannot be associated with charge difference, but rather is due indirectly to the fact that Zn is a spin-less defect. So, as for Kondo impurities in normal metal hosts, unitary scattering is associated with a magnetic effect. These remarks are of course included in most analyses of impurity scattering done in the strong correlation approaches [4,23–26]. Different behaviour of spinons and holons

is at the root of the anomalous impurity scattering in such theories. However none is at present sufficiently advanced to provide quantitative results which could be compared to experimental data.

As for the reduction of T_c induced by "non-magnetic" impurities, the situation has evolved since our first report [6], since the d wave symmetry of the order parameter is now well established in most cuprates. In this case, any type of impurity scattering depresses T_c . This is exemplified by recent resistivity measurements performed on electron irradiated samples [34]. It is found that a universal law applies between the respective variations ΔT_c and $\Delta \rho$ of the superconducting temperature and of the resistivity induced by defects. The most remarkable feature detected in these experiments is that the universal relation extends to the overdoped regime, suggesting that the d wave symmetry of the order parameter is valid for the entire phase diagram, even in the doping range for which Fermi liquid behaviour seems to apply.

VI CONCLUSIONS

The studies presented above have allowed us to demonstrate that valuable information on the magnetic properties of the cuprates are obtained from the local study of their response to substitutional impurities in the CuO_2 planes. It could be anticipated, by analogy with RKKY effects in simple metals, that the large distance modifications of the host properties would directly reflect the non-local magnetic response of the host. This is indeed apparent in the NMR studies of the modifications of the central ^{89}Y or ^{17}O NMR lines, which give us some insight on the q and T dependence of the static susceptibility, i.e. of the AF correlation length. These studies also show that the pseudo-gap is unaffected by impurities and is therefore either a purely magnetic effect associated with AF fluctuations, or due to a local pairing which is not disrupted by impurities in contrast with the macroscopic superconducting condensate.

More surprising are the actual properties associated with spin-less impurities. The existence of magnetic correlations are responsible for the occurrence of local moment behaviour induced by non-magnetic impurities on the neighbouring Cu sites. While one might expect that the spin 1/2 moment which is released by such a defect in a magnetic quantum spin system should extend on a distance comparable to the AF correlation length, the measured decrease of the effective moment with increasing hole content is more likely to be associated with an interaction with charge carriers. As transport properties indicate that isovalent impurities produce a large scattering of the carriers, one can anticipate that this is due to the occurrence of a resonant state. But the actual Curie dependence of the susceptibility would not be expected then to extend to low T . However, the occurrence of superconductivity limits somewhat our experimental capability to investigate the magnetic properties of the metallic ground state. From SQUID data [19] it was concluded that in underdoped $\text{YBCO}_{6.6}:\text{Zn}4\%$, for which T_c is reduced to zero, the susceptibility follows

a Curie-Weiss law down to 10K, with $\theta \approx 4K$. Does this correspond to a Kondo like energy scale characteristic of the width of the impurity resonant state? Such a Kondo-like effect is a candidate mechanism [26] for the reduction of the magnitude of the local moment in YBCO₇:Zn. However in these systems, one does not a priori expect the physical properties to mimic those obtained for Kondo effect in noble metals in a classical sd exchange model. Such difficulties have already been pointed out by Hirschfeld [35] in view of our preliminary data [6]. Obviously further efforts are required to complete this approach both experimentally and theoretically in the context of a correlated electron system.

We should like to acknowledge A. MacFarlane for helpful discussions and careful reading of the manuscript.

REFERENCES

1. M. Takigawa *et al*, Phys. Rev. Lett. **63**, 1865 (1989); Phys. Rev. **B 43**, 247 (1991).
2. H. Alloul, T. Ohno, and P. Mendels, Phys. Rev. Lett. **63**, 1700 (1989).
3. C. Berthier, M. H. Julien, M. Horvatic and Y. Berthier, Appl. Magn. Reson. **3**, 449 (1992).
4. A. M. Finkelstein, V. E. Kataev, E. F. Kukovitskii, and G. B. Teitelbaum, Physica C **168**, 370 (1990).
5. H. Alloul *et al*, Phys. Rev. Lett. **67**, 3140 (1991).
6. A. V. Mahajan, H. Alloul, G. Collin, J. F. Marucco, Phys. Rev. Lett. **72**, 3100 (1994).
7. K. Ishida *et al*, Phys. Rev. Lett. **76**, 531 (1996).
8. J. Bobroff *et al*, Phys. Rev. Lett. **79**, 2117 (1997).
9. A. MacFarlane *et al*, to be published.
10. K. Kakurai *et al*, Phys. Rev. **B 48**, 3485 (1993).
11. P. Bourges *et al*, Journal of Physics **46**, 1155 (1996); P. Bourges, *et al*, J. Phys. Chem. Solids **56**, 1937 (1995); Y. Sidis *et al*, Int. J. of Modern Phys. B, to be published.
12. J. B. Boyce and C. P. Slichter, Phys. Rev. Lett. **32**, 61 (1974); H. Alloul, F. Hippert, and H. Ishii, J. Phys. F **4**, 725 (1979) and references therein.
13. D. K. Morr, J. Schmalian, R. Stern and C. P. Slichter, Phys. Rev. Lett. **80**, 3662 (1998); J. Bobroff *et al*, Phys. Rev. Lett. **80**, 3663 (1998).
14. J. Bobroff, thesis (unpublished).
15. A. Janossy, J. R. Cooper, L. C. Brunel, and A. Carrington, Phys. Rev. **B 50**, 3442 (1994).
16. A. V. Mahajan, H. Alloul, G. Collin, J. F. Marucco, to be published.
17. G. V. M. Williams and J. L. Tallon, Phys. Rev. **B 57**, 10984 (1998).
18. P. Mendels *et al*, Phys. Rev. **B 49**, 10035 (1994).
19. P. Mendels *et al*, to be published in Europhysics Letters.
20. K. Ishida *et al*, J. Phys. Soc. Japan **62**, 2803 (1993).
21. J. A. Hodges, P. Bonville, P. Imbert, and A. Pinatel-Philippot, Physica C **323**, 246 (1995).

22. H. Alloul, J. Bobroff, and P. Mendels, Phys. Rev. Lett. **78**, 2494 (1997).
23. N. Nagaosa and T. K. Ng, Phys. Rev. **B 51**, 15588 (1995).
24. D. Poilblanc, D. J. Scalapino, and Hanke, Phys. Rev. Lett. **72**, 884 (1994); see also Phys. Rev. **B 50**, 13020 (1994).
25. G. Khaliullin, R. Killian, S. Krivenko, and P. Fulde, Physica C **282-287**, 1749 (1997).
26. A. Nagaosa and P. Lee, Phys. Rev. Lett. **79**, 3755 (1997).
27. G. B. Martins, M. Laukamp, J. Riera, and E. Dagotto, Phys. Rev. Lett. **78**, 3563 (1997).
28. M. Takigawa, N. Motoyama, H. Eisaki, and S. Uchida, Phys. Rev. **B 55**, 14129 (1997).
29. Y. Yoshinari, J. Bobroff *et al* (unpublished).
30. T. R. Chien, Z. Z. Wang, and N. P. Ong, Phys. Rev. Lett. **67**, 2088 (1991).
31. K. Mizuhashi, K. Takenaka, Y. Fukuzumi, and S. Uchida, Phys. Rev. **B 52**, R3884 (1995).
32. A. Legris, F. Rullier-Albenque, E. Radeva and P. Lejay, J. de Physique (France) I **3**, 1605 (1993).
33. C. Bernhardt *et al*, Phys. Rev. Lett. **77**, 2304 (1996).
34. F. Rullier-Albenque *et al* (to be published).
35. L. S. Borkowski and P. J. Hirschfeld, Phys. Rev. **B 49**, 15404 (1994).

Incommensurate Spin Dynamics of Superconductor $\text{YBa}_2\text{Cu}_3\text{O}_{6+x}$

M.Arai¹, T.Nishijima¹, Y.Endoh², S.Tajima⁴, K.Tomimoto⁴, Y.Shiohara⁴,
M.Takahashi⁵, A.Garrett¹, S.M.Bennington⁵

¹ *Institute of Materials Structure Science, KEK, Oho, Tsukuba, 305, Japan*

² *Department of Physics, Tohoku Univ., Aoba, Sendai, 980, Japan*

³ *Department of Physics, Tsukuba Univ., Tsukuba, 305, Japan*

⁴ *Superconductivity Research Laboratory, ISTEC, Koutou-ku, Tokyo, 135, Japan*

⁵ *Rutherford Appleton Laboratory, Chilton, Didcot, Oxon, UK*

Abstract According to the recent neutron scattering data on $\text{YBa}_2\text{Cu}_3\text{O}_{6+x}$, it has been concluded that the incommensurability of the spin dynamics is a common feature among oxide high-Tc superconductors, which cannot be explainable by Fermi surface anomaly. In this paper, we summarize neutron data on the incommensurability and show a strong correlation between it and superconductivity, for which spin singlet formation in the spin stripe could play an important role.

INTRODUCTION

The spin dynamics plays an important role for the pairing mechanism in oxide high-Tc superconductivity. Hence, many studies have been devoted to clarifying the magnetic correlation between spins at a microscopic level by means of neutron scattering. Since the stripe domain structure model was proposed by Tranquada on $\text{La}_{2-x-y}\text{Nd}_y\text{Sr}_x\text{CuO}_4$ [1], it has become a very important task to prove the existence of stripe spin dynamics as a common feature among various high-Tc system. Therefore we have studied a typical oxide high-Tc material $\text{YBa}_2\text{Cu}_3\text{O}_{6+x}$, in which incommensurability has not been found so far. Recently we have performed inelastic neutron scattering experiments on underdoped $\text{YBa}_2\text{Cu}_3\text{O}_{6.7}$ (YBCO6, $T_c \sim 67\text{K}$, $n_h \sim 0.12$) [2] and $\text{YBa}_2\text{Cu}_3\text{O}_7$ (YBCO7, $T_c \sim 90\text{K}$, $n_h \sim 0.25$) [3]. Both of the sample showed incommensurate spin correlation with the same symmetry as that of LSCO, which could not be explained by Fermi surface

anomaly, hence the results prompted possibility of existence of a stripe domain structure as a common feature in high-Tc materials.

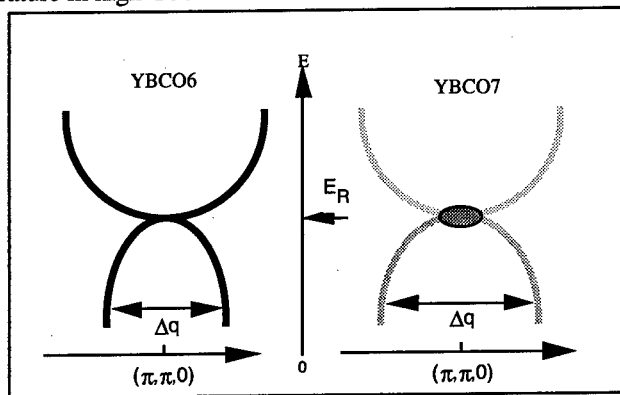


Figure 1 Illustration of $S(Q,E)$ along $(h,h,0)$, for the underdoped YBCO6 and the optimally doped YBCO7. There is two legs below the resonance energy E_R . There is a broad dispersive feature observed only in YBCO6 [2,3] but prominent resonance peak for YBCO7.

SUMMARY OF NEUTRON DATA

In Fig.1 we illustrate observed spin dynamical structure factor $S(Q,E)$ of YBCO6 and YBCO7, which is projected onto the $(h,-h,0)$ direction. $S(Q,E)$ of YBCO6 has two legs as a function of energy and momentum transfer which characterize the incommensurate spin dynamics. Those merge to form an intense single peak, referred to as the resonance peak, at the resonance energy E_R and split again with broad and dispersive feature above E_R . On the other hand, YBCO7 has a prominent spot only at E_R below T_c . However, there appears very weak two legs above T_c below E_R with a wider separation in the incommensurability than that of YBCO6. In Table 1 the extracted parameters from $S(Q,E)$ are summarized. First of all we note that the incommensurability is very close to 1/8 and 1/6 for YBCO6 and YBCO7 respectively.

TABLE 1 Parameters extracted from $S(Q,E)$ [2,3]. n_h is approximate hole concentration, δ is incommensurability, ξ_{INC} and ξ_{RES} are magnetic correlation length estimated from incommensurate peak and resonance peak respectively.

	n_h	δ [r.l.u]	2δ	ξ_{INC} [Å]	ξ_{RES} [Å]
YBCO6	0.12	~ 0.12 (1/8)	1/4	11~13Å	6
YBCO7	0.25	~ 0.17 (1/6)	1/3	10Å	6

In Fig.2 the transition temperature T_c normalized by the maximum of it $T_c(\max)$ is plotted as a function of incommensurability δ , together with the results of LSCO [4]. It seems that there is a universal line in this relation, though T_c of LSCO starts dropping above hole concentration of 0.18, and there is a gap between $\delta \sim 0.12$ ($\sim 1/8$) and $\delta \sim 0.17$ ($1/6$), the latter was observed only in YBCO7. The peak width as a function of hole concentration observed by Regnault *et al.* [5] is reproduced in Fig. 3. Regnault *et al.* could not resolve the two-peak structure of the incommensurability, however, the width in Fig. 3 reasonably agrees to the peak separation of two incommensurate peaks along the $[h,h,0]$ direction observed in the present work. Here we can recognize that there is a step at hole concentration of about $0.17 \sim 1/6$. Hence, the step in the width could be understood as a step from the incommensurability of $1/8$ r.l.u in the 60K-system to that of $1/6$ r.l.u. of the 90K-system. This step may come from the existence of the oxygen chain site for YBCO, which adjust the hole concentration in the CuO_2 plane.

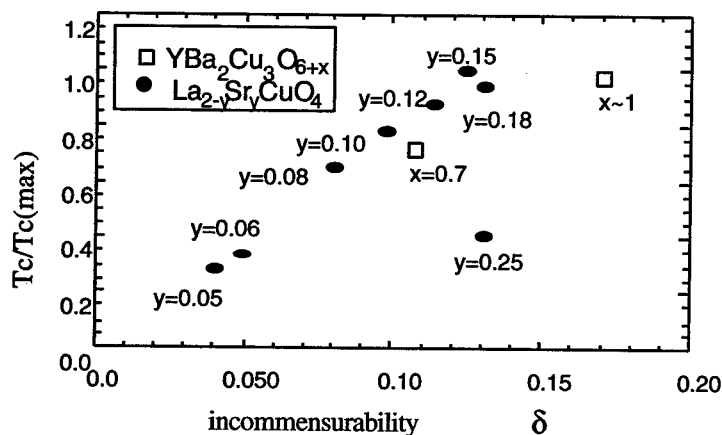


Figure 2 A plot of the transition temperature T_c normalized by the maximum $T_c(\max)$ is shown as a function of the incommensurability δ together with the results for LSCO[4]

DISCUSSION

If the observed incommensurability can be explained by a stripe domain structure, the incommensurate magnetic intensity comes from the double periodicity of stripe structure[1]. Hence, we can understand that the possible stripe structure for YBCO6 and YBCO7 has the periodicity of $1/4$ r.l.u. and $1/3$ r.l.u. (hereafter we refer to these as the $1/4$ -stripe and the $1/3$ -stripe). For the $1/3$ -stripe, two spins are sandwiched by two charge stripe. Probably this is a very preferable situation for forming singlet pairs, i.e.

RVB states, in the spin stripe. A coherent behaviour of charges in the separated charge stripes may create superconductivity.

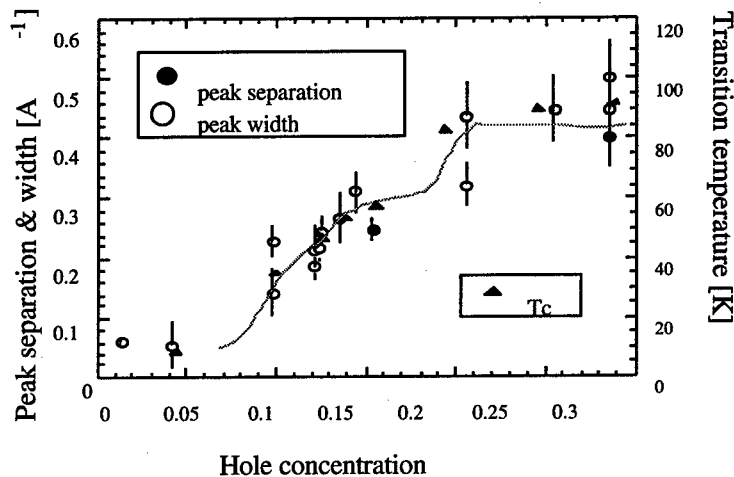


Figure 3 Peak width of magnetic intensity at the commensurate position as a function of oxygen concentration reproduced from [5] and peak separation, see in the text.

For underdoped sample, the 1/4-stripe is dominant, where fluctuating spins exist in addition to the RVB states. This may reduce T_c and enhance antiferromagnetic fluctuation as observed in the dynamical structure factor in the underdoped sample. However, for conclusion we need further intensive experiments.

ACKNOWLEDGMENT

The authors acknowledge Drs. J.W.Jang, A.I.Rykov, M.Kusao, S.Koyama for preparing the sample. This work was supported by a Grant-in-Aid on Scientific Research on Priority Areas "Anomalous Metallic State near the Mott Transition" (07237102) of Ministry of Education, Science, Sports and Culture, Japan, and done under the collaboration with NEDO.

REFERENCES

- [1] J.M.Tranquada et al., Nature 375 (1995) 561
- [2] M.Arai et al., unpublished
- [3] T.Nishijima et al., unpublished
- [4] K. Yamada, et al., Phys. Rev. B57, (1998) 6165
- [5] L.P.Regnauld et al., Physica B 213&214 (1995) 48

Decreasing superconductivity suppression of Pr in RE:123 compounds by isolating the same from Cu-O conduction band

V.P.S. Awana*, O.F. de Lima*, S.K. Malik[#], W.B. Yelon[‡], and A.V. Narlikar[@]

^{*}Instituto de Fisica "Gleb Wataghin" UNICAMP, 13083-970, CAMPINAS, SP, Brazil.

[#]Tata Institute of Fundamental Research, Bombay 400005, India.

[‡]Research Reactor Facility, University of Missouri, Columbia, MO 65211, USA.

[@]National Physical Laboratory, K.S. Krishnan Marg, New Delhi 110012, India.

Abstract. We present the results on structure, superconducting T_c , and magnetic ordering temperature of Pr moments of several Pr substituted rare earth (RE) oxide systems such as $Y_{1-x}Pr_xBaSrCu_3O_7$ (Y/PrBaSr:123), $La_{1-x}Pr_xBaCaCu_3O_7$ (La/PrBaCa:123) and $Nd_{1-x}Pr_xBaCaCu_3O_7$ (Nd/PrBaCa:123). We observe that the suppression of superconductivity due to Pr in all these systems is less in comparison to that in their RE:123 counterparts, i.e. in Pr substituted Y:123, La:123 and Nd:123, respectively. Interestingly with full Pr substitution in RE:123 compounds, the Pr moments order antiferromagnetically at 17K, while in the presently studied three systems, the same happens at around 10K only. Antiferromagnetic ordering temperature of the Pr moments of the end member of the series, which may be taken to be a measure of the strength of the hybridization of Pr-4f orbitals with Cu-O conduction band, appears to have a direct correlation with suppression of superconductivity in the corresponding series. Our results suggest that by various on-site substitutions or by modifying the parent unit cell of Pr:123 compound, one may be able to isolate the Pr-4f magnetic moments or decrease their interaction with the Cu-O conduction band, and achieve superconductivity in the presence of Pr.

INTRODUCTION

Since the discovery of high temperature superconductivity in rare earth (RE) based cuprate perovskite materials, the unique behavior of Pr has attracted a lot of activity in this field [1-5]. Unlike other $REBa_2Cu_3O_7$ (RE:123) materials, which show superconductivity with T_c of nearly 90K, Pr:123 is not superconducting down to very low temperatures. In fact, it is an antiferromagnetic insulator with Cu moments ordering above room temperature and the Pr moments ordering at an unusually high temperature of about 17K [3,4]. Several possible models have been put forward to explain the mysterious physical properties of Pr:123 [see ref. 3, and references cited there in]. The most widely accepted model is the one which invokes the hybridization and the consequent magnetic interaction of the Pr-4f electrons with Cu-O conduction band [6,7,8]. While ref. [6] provided one of the early experimental evidence suggesting the above mentioned hybridization and the magnetic interaction of Pr moments with Cu-O conduction band based on the studies of $RE_{1-x}Pr_xBa_2Cu_3O_7$ compounds with various RE, ref. 7, and 8 provided the successful theoretical

models, based on band structure calculations, which clearly invoke the hybridization of Pr-4f with Cu-O conduction band. It is shown [8] that the Pr-4f band touches the fermi surface in Pr:123, unlike in other similar compounds such as Nd:123. This makes Pr:123 different from all other RE:123 which are superconducting with T_c of about 90K. In the present paper, we provide evidence which suggests that the suppression of superconductivity due to Pr in $RE_{1-x}Pr_x$:123 compounds and its unusually high T_N of 17K are inter-linked. Our present results on $Nd_{1-x}Pr_xBaCaCu_3O_7$ along with those on $La_{1-x}Pr_xBaCaCu_3O_7$ [9], and $Y_{1-x}Pr_xBaSrCu_3O_7$ [10], compounds suggest that both dT_c/dx (T_c suppression due to Pr in a given $RE_{1-x}Pr_x$:123 system) and the T_N of the Pr in the same system follow a systematic trend. Lower T_N of Pr gives rise to a lower dT_c/dx in that system

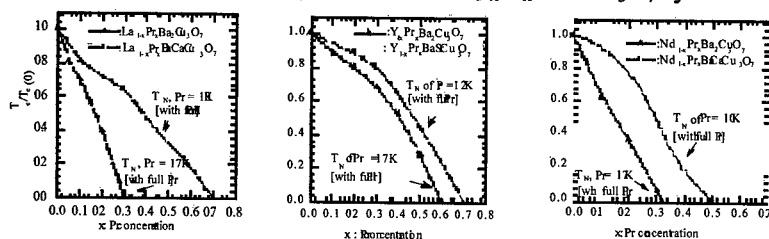
EXPERIMENTAL

All the samples in the series $Nd_{1-x}Pr_xBaCaCu_3O_7$, $La_{1-x}Pr_xBaCaCu_3O_7$, and $Y_{1-x}Pr_xBaSrCu_3O_7$ were synthesized through a solid state reaction route [9,10]. Lattice parameters of all the samples were obtained from X-ray diffraction studies. Magnetic ordering temperatures were determined using a SQUID magnetometer. The superconducting transition temperatures (T_c) were determined from AC susceptibility measurements carried out with an applied rms field of 0.01Oe at a frequency of 117Hz.

RESULTS AND DISCUSSION

Figure 1 depicts the reduced T_c [$T_c(x)/T_c(0)$] versus Pr concentration (x) behavior for $La_{1-x}Pr_xBaCaCu_3O_7$ and $La_{1-x}Pr_xBa_2Cu_3O_7$ systems. Results for $La_{1-x}Pr_xBa_2Cu_3O_7$ are taken from ref. [11]. All the samples of $La_{1-x}Pr_xBaCaCu_3O_7$ series crystallize in tetragonal RE:123 structure (space group P4/mmm) and show sharp superconducting transitions until $x = 0.60$. The samples with $x = 0.75$ and $x = 1.0$ are found to be non superconducting [9]. It is clear from this figure that Pr destroys superconductivity more effectively in the case of $La_{1-x}Pr_xBa_2Cu_3O_7$ system compared to that in $La_{1-x}Pr_xBaCaCu_3O_7$ system. With full Pr substitution, i.e., in $PrBaCaCu_3O_7$, the Pr moments order antiferromagnetically at around 10K, while the same happens at 17K in $PrBa_2Cu_3O_7$. Lower T_N of around 10K for $PrBaCaCu_3O_7$ is confirmed both from magnetic susceptibility and heat capacity measurements, (for details, see ref. 9). The T_N of 17K for $PrBa_2Cu_3O_7$ is well known from neutron diffraction, heat capacity, and magnetic susceptibility measurements [3,12]. It may be mentioned that neutron diffraction studies on $LaBaCaCu_3O_7$ suggest that there is intermixing of La and Ca at the nominal RE site and the Ba site in this compound [13]. The same is expected in $La_{1-x}Pr_xBaCaCu_3O_7$ system with some Pr going to the Ba site.

Reduced T_c versus x plots for $Y_{1-x}Pr_xBaSrCu_3O_7$ and $Y_{1-x}Pr_xBa_2Cu_3O_7$ systems are given in figure 2. Results for $Y_{1-x}Pr_xBa_2Cu_3O_7$ are taken from ref.14. Again it is clear from this figure that Pr destroy superconductivity more effectively in the case of $Y_{1-x}Pr_xBa_2Cu_3O_7$ system than in $Y_{1-x}Pr_xBaSrCu_3O_7$ system.



FIGURES 1,2&3. Reduced T_c [$T_c(x)/T_c(0)$] versus Pr concentration (x) for $La_{1-x}Pr_xBaCaCu_3O_7$ and $La_{1-x}Pr_xBa_2Cu_3O_7$, $Y_{1-x}Pr_xBaSrCu_3O_7$ and $Y_{1-x}Pr_xBa_2Cu_3O_7$ and for $Nd_{1-x}Pr_xBaCaCu_3O_7$ and $Nd_{1-x}Pr_xBa_2Cu_3O_7$ systems

In PrBaSrCu₃O₇, the Pr moments appear to order antiferromagnetically at around 12K, which needs to be confirmed by heat capacity measurements. Reduced T_c versus x plots for presently studied Nd_{1-x}Pr_xBaCaCu₃O₇ and Nd_{1-x}Pr_xBa₂Cu₃O₇ systems are given in figure 3. Detailed structural and superconductivity measurements on Nd_{1-x}Pr_xBaCaCu₃O₇ samples showed them to be single phase. Data for Nd_{1-x}Pr_xBa₂Cu₃O₇ are taken from ref. [14]. It is evident from this figure that Pr destroys superconductivity more effectively in the case of Nd_{1-x}Pr_xBa₂Cu₃O₇ system than in Nd_{1-x}Pr_xBaCaCu₃O₇. In PrBaCaCu₃O₇, the Pr moments order antiferromagnetically at around 10K compared to the T_N of 17K for PrBa₂Cu₃O₇.

It is worth mentioning here that the T_c suppression power of Pr in RE_{1-x}Pr_x:123 systems, depends on host rare earth also. This was proposed by some of us long back [6]. This is the reason that we compare in figures 1, 2 and 3 the results for same host RE, i.e. for La in figure 1, Y in figure 2, and Nd in figure 3. This makes it clear, that the results of a particular system in any of figures can not be compared with the results in other figures. What seems more interesting is that as the T_c suppression power of Pr decreases from La_{1-x}Pr_xBa₂Cu₃O₇ to La_{1-x}Pr_xBaCaCu₃O₇, from Y_{1-x}Pr_xBa₂Cu₃O₇ to Y_{1-x}Pr_xBaSrCu₃O₇ and from Nd_{1-x}Pr_xBa₂Cu₃O₇ to Nd_{1-x}Pr_xBaCaCu₃O₇ systems, the T_N of Pr also decreases. This indicates that if one could get a RE:123 system, where Pr does not order magnetically with unusually high T_N ($> 0.5K$), one may observe superconductivity with full Pr substitution. One example could be PrSr₂MCu₂O₈ (M= Nb, Ga, etc) [Pr:1212] type materials. In these compounds Pr does not show high T_N , despite sitting between Cu-O₂ planes, as in RE:123 [15]. In our opinion the high temperature high pressure synthesized PrSr₂Cu₃O₇ and

$\text{PrSr}_2\text{Cu}_2\text{NbO}_8$ could be the best candidates to become superconducting with RE:123 structure. Finally, we note that there is a recent report on the observation of superconductivity in Pr:123 single crystal with $T_c = 80\text{K}$ [16]. This single crystal has an unusually large c-parameter of about 11.8Å.

ACKNOWLEDGEMENT

One of us (VPSA) acknowledges the financial support from FAPESP. Part of this work at MURR was supported by the US Department of Energy Grant No. DE-FE0290ER45427 through the Mid-west Superconductivity Consortium.

REFERENCES

1. H. Oesterreider, M. Smith, *Mater. Res. Bull.* **22**, 1709 (1987).
2. L. Soderholm, K. Zhang, D.G. Hinks, M.A. Beno, J.D. Jorgensen, C.U. Segre, I.K. Schuller, *Nature* **328**, 604 (1987).
3. H.B. Radousky, *J. Mater. Res.* **7**, 1917 (1992).
4. S.K. Malik, C.V. Tomy, in "Physical and Material Properties of High Temperature Superconductors", Eds. S.K. Malik and S.S. Shah, Nova Science, New York, 1994, p. 283.
5. I. Felner, G. Hilscher, H. Michor, G. Wortmann, J. Dumschat, V.P.S. Awana, S.K. Malik, *Phys. Rev. B* **54**, 11999 (1996).
6. S.K. Malik, C.V. Tomy, P. Bhargava, *Phys. Rev. B* **42**, 4823 (1990).
7. R. Feherenbacher, T.M. Rice, *Phys. Rev. Lett.* **70**, 3471 (1993).
8. A.I. Liechtenstein and I.I. Mazin, *Phys. Rev. Lett.* **74**, 1000 (1995).
9. V.P.S. Awana, S.X. Dou, S.K. Malik, Rajvir Singh, A.V. Narlikar, D.A. Landinez Tellez, J.M. Ferreira, J. Albino Aguiar, S.Uma, E. Gmelin, W.B. Yelon, *J. Magn. and Magn. Materials*, **187**, 192 (1998).
10. V.P.S. Awana, J. Horvat, S.X. Dou, A. Sedky, A.V. Narlikar, *J. of Magn. and Magn. Materials*, **182**, L280 (1998).
11. K. Sekizawa, Y. Takano, K. Kanno, H. Ikuta, H. Ozaki, H. Enomoto, *Physica B* **194-196**, 1937 (1994).
12. S. Skanthakumar, J.W. Lynn, N. Rosov, G. Cao, J.E. Crow, *Phys. Rev. B* **55**, 3406 (1997).
13. V.P.S. Awana, O.F. de Lima, S.K. Malik, W.B. Yelon and A.V. Narlikar, to Appear in *Physica C* (1999).
14. Yunhui Xu, Weiyuan Guan, *Phys. Rev. B* **45**, 3176 (1992).
15. V.P.S. Awana, Latika Menon and S.K. Malik, *Physica C* **262**, 266 (1996).
16. Z. Zou, K. Oka, T. Ito, Y. Nishihara, *Jpn. J. Appl. Phys.* **36**, L18 (1997).

Lattice-Charge Stripes and Spectral Weight Near the Fermi Surface

A. Bianconi, N.L. Saini and A. Lanzara

*Unità INFN and Dipartimento di Fisica, Università di Roma "La Sapienza"
P. A. Moro 2, 00185 Roma, Italy*

Abstract. Investigations of short range lattice fluctuations and anharmonic lattice modulation of the CuO_2 plane, in the $\text{Bi}_2\text{Sr}_2\text{CaCu}_2\text{O}_{8+\delta}$ superconductors, with high momentum resolution extended x-ray fine structure (EXAFS) and x-ray diffraction (XRD), show the coexistence of the polaronic and itinerant charges ordered in lattice-charge stripes with the wavevector q_{lattice} and a strong second harmonic content with $2q_{\text{lattice}}$. The study of momentum distribution of spectral weight around the Fermi level, measured by angle resolved photoemission (ARPES), reveals a large suppression of spectral weight due to coupling of charge carriers with joint incommensurate charge density wave at $q(-0.4\pi, 0.4\pi) \sim 2q_{\text{lattice}}$ in the diagonal direction and the spin density wave at $G(\pi, \pi)$ in the direction of the stripes. The lattice-charge stripes and their implication on the electronic spectral weight are briefly discussed.

INTRODUCTION

New theoretical ideas are emerging on the basis of recent experiments and it seems that the normal state properties of the high T_c superconductors are difficult to be accounted by a homogeneous electronic structure. The key matter is to deal with a physical system where the electrons are strongly interacting with collective excitations related with lattice, charge and spin degrees of freedom. There are several reports on the key role of lattice fluctuations and polarons in the cuprates (1-13). Direct evidences for the presence of polarons were given by several isotope effect experiments (6-8), however, the key role of polarons is still under scientific debate because of small lattice deformations, coexisting itinerant charge carriers (9-13) and their segregation in striped domains (1-3). Furthermore the stripes coexist with slow dynamic 1D spin fluctuations (14) making the normal phase more complex. However, a large isotope effect on the lattice fluctuations (15) have suggested that the polaronic carriers are indeed important.

$\text{Bi}_2\text{Sr}_2\text{CaCu}_2\text{O}_{8+\delta}$ (Bi2212) is one of the most suitable system to investigate the lattice-charge stripes and explore their implication to the electronic structure. The lattice distortions due to i) the mismatch between the CuO_2 layers and the intercalated rocksalt layers and; ii) the chemical dopants, that are usually difficult to resolve in other superconducting families, they give a one dimensional long range superstructure. In this heterogeneous structure, two components of doped charges, namely pseudo Jahn-Teller polarons and itinerant electron gas, have been observed in the CuO_2 planes using a fast

and local (short range) probe as EXAFS and x-ray diffuse scattering experiments (16-19). This charge segregation arises from the instability of a polaron gas near the critical density for a polaronic generalized Wigner CDW, at doping 0.125 (20).

The ordering of polarons gives a particular segregation of the two components in alternated parallel stripes. This phase appears to be quite stable in the Bi2212 system near the optimum doping since the "short range" lattice-charge modulation, due to ordering of polarons in the CuO_2 plane, and the crystalline "long range" superstructure due to the dopants and the mismatch have the same incommensurate in plane wave vector $q \sim 0.21b^*$. In this striped phase, the dimensionality of the electronic structure lies between 1D (Luttinger liquid) and a 2D (Fermi liquid) electron gas, due to reduced hopping between the stripes and the physics of these materials approaches towards that of 1D conductor where collective excitations play important role and the dispersing quasiparticles are strongly interpolated by lattice, spin and charge excitations.

This communication is addressed to the lattice-charge stripes and their implication to the electronic states near the Fermi level. High k-resolution polarized EXAFS measurements were performed to measure instantaneous distortions of the CuO_2 lattice that was followed by x-ray diffraction to measure the superstructure due to lattice and charge modulation. To explore the implication of the stripe structure on the electronic structure we have performed ARPES measurements to study the k-distribution of the electronic states near the Fermi level (21).

THE EXPERIMENTS

The experimental results reported here were obtained on high quality single crystals, grown by travelling solvent floating zone (TSFZ) method (16, 19, 21). The crystals were well characterized for their transport and structural properties. The samples were optimally doped. The polarized Cu K-edge absorption measurements were mainly performed on the beam-lines BL-13B of Photon Factory, Tsukuba and BM29 of ESRF, Grenoble. The spectra were recorded by detecting the fluorescence yield (FY) using solid state x-ray detectors to extract partial cross-section only due to transition from Cu 1s levels. The details about the absorption measurements are provided in our earlier publications (17-19). The x-ray diffraction measurements were performed on the beam-line ID-11 of ESRF, Grenoble and 5.2R of Elettra, Trieste. The diffraction patterns were collected by image plate detectors providing global information of diffracted photons making us to identify and quantify the weaker intensity satellite diffraction peaks. Advantage of anomalous diffraction was taken to get selective information on the Cu-sublattice due to strong variation of the scattering factor near the Cu K threshold. A part of the experimental results are published with the experimental details (16). The photoemission experiments were performed on the beamline SU6 of Laboratoire pour l'Utilisation du Rayonnement Electromagnetique (LURE), Orsay. The map of spectral weight were obtained by centering the electron energy window at the E_F and collecting the electrons within an energy window of the order of spectrometer resolution (~ 50 meV) using a photon energy of 32 eV. The technical details about the experiment are given elsewhere (21).

For the photoemission measurements, the polarization vector of the synchrotron light, the direction of the photon beam and the surface normal were kept in the same horizontal plane, called "scattering plane". The "mirror plane", defined by the sample normal and

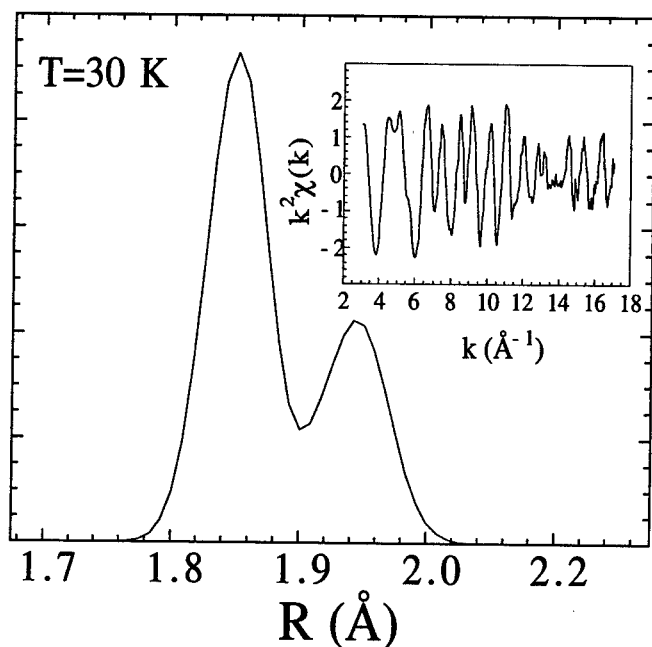


FIGURE 1. Cu-O bond distribution derived from in-plane polarized EXAFS. The inset shows a high k -resolution polarized Cu K-edge EXAFS spectrum.

the direction of the emitted photoelectron selected by the detector position. The spectral weight was measured in the "even" geometry in which the scattering plane and mirror plane were coplanar. In this geometry the transition from the initial state of b_1 symmetry (formed by a mixing of Cu $3d_{x^2-y^2}$ and O $2p_{x,y}$ orbitals) states, forming the conduction band, is fully allowed for k_i in the Γ -M $(0,\pi)$ and equivalent directions (22, 23) and hence the spectral weight could be well studied in this direction. The detector was moved in the fixed "mirror" plane to select different values of the wave vector in the superconducting CuO_2 plane (k_{\parallel}). The direction of the initial state k_{\parallel} is selected by rotating the sample around its normal, that is collinear with the crystallographic c -axis.

RESULTS AND DISCUSSION

EXAFS is a powerful tool to measure local distortions, however, care should be taken to exploit the technique; for example, to study lattice distortions in the CuO_2 plane of cuprates, the main limitation is a drastic damping of the Cu-O backscattering at the high k -values and the small Cu-O signal could be easily masked by experimental noise. In addition, the solution of the lattice displacements is limited by the k -resolution and there

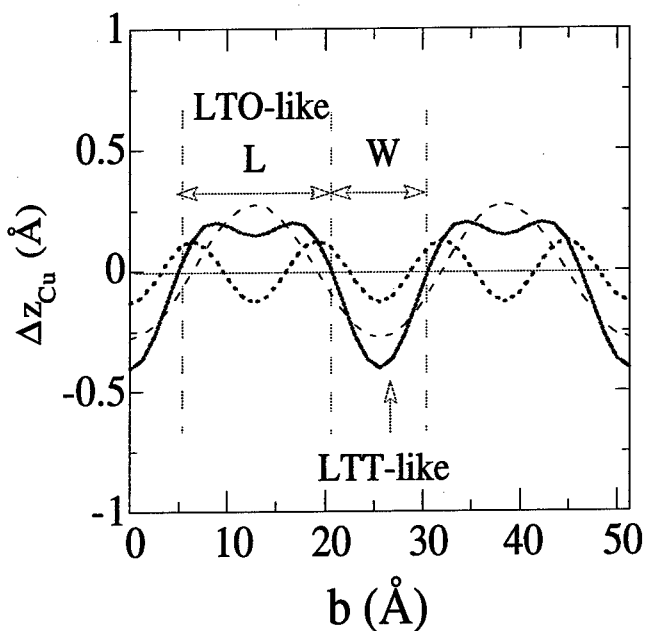


FIGURE 2. Anharmonic modulation of the Cu atom along the z-axis (solid line). Strong contribution of second harmonic is shown (dotted line) alongwith the first harmonic (dashed line).

could be further damping of signal because of distribution of distance ($\Delta R_{\min} = \pi/2k_{\max}$). Considering the limitations we have made the EXAFS measurements with high signal to noise ratio and high k-resolution to study the local lattice displacements with high precision. The Cu-O bond distribution obtained by the analysis of the EXAFS signal due to the Cu-O backscattering shows large distribution, in the range of 1.8-2.05 Å with two peak appearing at ~1.88Å and ~1.98Å (Fig. 1). The large distribution shows distorted nature of the CuO₂ square plane (16-19).

While Cu K-edge EXAFS have provided directly the pair distribution function (PDF), the x-ray anomalous diffraction was exploited for selective information on the Cu-sublattice. Fig. 2 shows modulation of the z coordinate of the Cu atoms in the Bi2212 indicating that the Cu position is anharmonically modulated in the out-of-plane direction with strong contribution from the second harmonic. The 1D anharmonic modulation results in stripes of flat Cu lattice (U-stripes or LTO-like) separated by stripes of distorted Cu lattice (D stripes or LTT-like) with a period of about 25 Å in the diagonal direction. The U stripes are separated by the D stripes of width W~10Å.

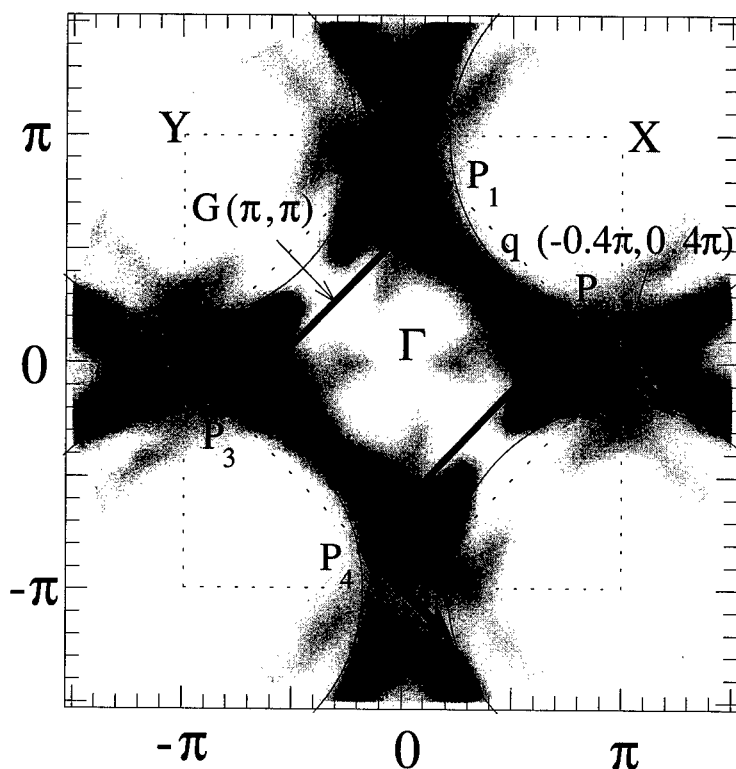


FIGURE 3. Map of the spectral weight near the Fermi surface of the Bi2212 system. The photointensity increases from light to dark colors and the maximum corresponds to the black colour. The spectral weight suppression occurs at P_n due to lattice charge stripes in the system.

The results shown in Fig. 2 represent to the long range superstructure of the type $q=p\mathbf{b}^* + (1/n)\mathbf{c}^*$ ($p=0.21$; $n=2$). Around the optimum doping, the long range and short range superstructure (given by diffuse scattering and wavevector $q=d\mathbf{b}^*$) appear with a similar wavevector along the \mathbf{b}^* direction, i.e., $p=d$ (present case). The long range modulation shows small change with doping while the short range modulation is strongly doping dependent and related with the asymmetric pair distribution of Cu-O bonds and found to show similar temperature dependence as the PDF.

At this point we turn to the implication of the lattice-charge stripes on the electronic structure near the Fermi level. The electronic spectral weight near the Fermi surface of the Bi2212 superconductor is shown in Fig. 3. The dark regions indicate higher intensity of emitted photoelectrons excited from the specified energy window near the E_F and with in-plane wavevector $(k_{||})$ spanned over reciprocal space of the two dimensional

CuO₂ plane. The photointensity is absent along the Γ -Y direction in the first Brillouin zone due to matrix element effects (22, 23).

Looking at the photointensity map we could see a strong suppression of spectral weight around the $(\pi, 0)$ and equivalent locations. We find a large suppression (about 70%) of spectral weight near the Fermi surface in the first Brillouin zone. After a careful analysis we have identified two well defined wave-vectors on the map connecting the points where a suppression of the spectral weight occurs. These points in the first Brillouin zone are $P_1(0.2\pi, 0.8\pi)$, $P_2(0.8\pi, 0.2\pi)$, $P_3(-0.8\pi, -0.2\pi)$ and $P_4(-0.2\pi, -0.8\pi)$. They are connected by the vectors $q(-0.4\pi, 0.4\pi)$ and $G(\pi, \pi)$. These vectors are the wavevectors of collective excitations that suppress the spectral weight of the quasiparticles at P_n . We have found that the wavevector $q(-0.4\pi, 0.4\pi)$ is the second harmonic of the incommensurate and anharmonic lattice fluctuation and is associated with diagonal charge density waves. Therefore the lattice-charge stripes give rise to a large suppression of spectral weight on the Fermi surface. It is found that the points P_n are located at the lines connecting the M-M₁ points. In addition, the joint interaction of electrons with a spin density wave (SDW) of wavevector $G(\pi, \pi)$ is clearly indicated by the fact that the points P_n are connected also by the G vector.

In summary, we have presented experimental results showing lattice-charge stripes in the Bi2212 superconductor at the optimum doping. The investigation of the short range lattice fluctuations shows coexisting polarons and an anharmonic lattice modulation revealing lattice charge stripes. A complete k -distribution of spectral weight near the Fermi surface shows a non Fermi liquid behavior of an electron gas in the reduced dimensionality due to stripes. We have shown that lattice induced charge segregation in stripes is responsible for disappearance of electronic states near the M points. The spectral weight suppression occurs at specific points connected by a wavevector $q(-0.4\pi, 0.4\pi) \sim 2q_{\text{lattice}}$ (i.e., the second harmonic of the structural polaronic modulation) due to incommensurate charge density wave with the wavevector $G(\pi, \pi)$ due to spin density wave providing direct evidence for strong interaction of electrons with lattice and spin fluctuations. In conclusion, the present work suggests that electrons moving in a superlattice of quantum stripes are strongly interacting with spin and charge collective excitations and the lattice needs to be considered properly in the models for the electronic structure of CuO₂ plane alongwith the spin and charge fluctuations.

ACKNOWLEDGEMENTS

This work was partially funded by Istituto Nazionale di Fisica della Materia (INFM) and Consiglio Nazionale delle Ricerche (CNR) of Italy. The authors would like to thank the fruitful collaboration with groups of H. Oyanagi, P.G. Radaelli, P. Bordet, M. C. Asensio and S. Tajima.

REFERENCES

1. Goodenough, J.B. and Zhou, J.S., *Nature* **386**, 229 (1997) and references therein.
2. Müller, K. A., Zhao, Guo-meng, Conder, K., Keller, H., *J. Phys. Condens. Matter* **10** L291 (1998) and references therein.
3. Bianconi, A., Saini, N.L., Lanzara, A., Missori, M., Rossetti, T., Oyanagi, H., Yamaguchi, H., Oka, K., and Ito, *Phys. Rev. Lett.* **76** 3412 (1996) and references therein.
4. Calvani, P., Dore, P., Lupi, S., Paolone, A., Maselli, P., Giura, P., Ruzicka, B., Cheong S.-W., Sadowski, W., *J. Superconductivity* **10**, 293 (1997).
5. Xiang-Xin Bi and Eklund, P. C., *Phys. Rev. Lett.* **70** 2625 (1993).
6. Crawford, M. K., Kunchur, M. N., Farneth, W. E., McCarron III, E. M., Poon, S. J., *Phys. Rev. B* **41**, 282 (1990).
7. Zhao, G.-m., Hunt, M. B., Keller, H., Müller, K. A., *Nature* (London) **385**, 236 (1997); Zhao, G.-m., Conder, K., Keller, H. and Müller, K. A., *J. Phys.: Condens. Matter* **10** 9055 (1998).
8. Franck, J. P., Harker, S., Brewer, J. H. *Phys. Rev. Lett.* **71**, 283 (1993).
9. Stevens, C.J., Smith, D., Chen, C., Ryan, J.F., Podobnik, B., Mihailovic, D., Wagner, G.A., and Evetts, J.E., *Phys. Rev. Lett.* **78**, 2212 (1997).
10. Alexandrov, A.S., Bratkovsky, A.M., Mott, N.F., Salje, E.H., *Physica C* **215**, 359 (1993).
11. Ranninger, J., *J. Superconductivity* **10**, 285 (1997).
12. Sinha, K.P., *Mod. Phys. Lett. B* **12** 805 (1998).
13. Ashkenazi, J., *J. Superconductivity* **10**, 379 (1997).
14. Mook, H. A., Dai, P. C., Hayden, S. M., Aeppli, G., Perring, T. G., Dogan, F., *Nature* (London) **395**, 580 (1998); Tranquada, J. M., Sternlieb, B. J., Axe, J. D., Nakamura, Y. and Uchida S., *Nature* (London) **375** 561 (1995).
15. Lanzara, A., Saini, N.L., Bianconi, A., Zhao, G.-m., Conder, K., Keller, H. and Müller, K. A., (unpublished).
16. Bianconi, A., Lusignoli, M., Saini, N.L., Bordet, P., Kvik, Å., Radaelli, P.G., *Phys. Rev. B* **54**, 4310 (1996); Bianconi, A., Saini, N.L., Rossetti, T., Lanzara, A., Perali, A., Missori, M., Oyanagi, H., Yamaguchi, H., Nishihara, Y., Ha, D.H., *Phys. Rev. B* **54**, 12018 (1996).
17. Lanzara, A., Saini, N.L., Bianconi, A., Hazemann, J.L., Soldo, Y., Chou F.C., Johnston, D.C., *Phys. Rev. B* **55**, 9120 (1997).
18. Saini, N.L., Lanzara, A., Oyanagi, H., Yamaguchi H., Oka, K., and Ito, T., Bianconi, A. *Phys. Rev. B* **55** 12759 (1997).
19. Saini, N.L., Lanzara, A., Bianconi, A., and Oyanagi, H., *Phys. Rev. B* **58**, 11768 (1998).
20. A. Bianconi *Sol. State Commun.* **91**, 1 (1994); *ibidem* **91**, 287 (1994); *Physica C* **235-240**, 269 (1994).
21. Saini, N.L., Avila, J., Bianconi, A., Lanzara, A., Asensio, M.C., Tajima, S., Gu, G.D., and Koshizuka, N., *Phys. Rev. Lett.* **79**, 3464 (1997); *Phys. Rev. B* **57**, R11101 (1998).
22. Randeria, M., Ding, H., Campuzano, J. C., Bellman, A., Jennings, G., Yokoyama, T., Takahashi, T., Katayama-Yoshida, H., Mochiku, T., and Kadowaki, K., *Phys. Rev. Lett.* **74**, 4951 (1995).
23. Shen, Z.-X., and Dessau, D. S., *Physics Reports* **253**, 1 (1995) and references therein.

High-temperature Superconductivity is Charge-reservoir Superconductivity

Howard A. Blackstead* and John D. Dow†

*Physics Department, University of Notre Dame, Notre Dame, Indiana 46556 USA

†Department of Physics, Arizona State University, Tempe, Arizona 85287-1504 USA

Abstract. An overview is presented of some evidence that the charge-reservoirs, not the cuprate-planes, are the loci of the primary superconductivity in high-temperature superconductors.

INTRODUCTION

One of the most widely believed tenets in the history of science is that the superconductivity in high-temperature superconductors invariably originates in the cuprate-planes thought to be common to all such superconductors. However, the primary experimental foundation for this tenet is that the onset of superconductivity in $YBa_2Cu_3O_x$ as a function of x coincides with a jump in the charge on the cuprate-plane Cu ions [1], and has since been repudiated experimentally [2] — although most researchers still endorse cuprate-plane models nevertheless [3], despite a great deal of contrary evidence [4].

One especially interesting fact is that $Ba_{1-x}K_xBiO_3$ superconducts with T_c as high as 32 K [5] and has many properties shared by the cuprate superconductors, yet this material is *not* classified as a high-temperature superconductor by most theorists who favor cuprate-plane models, presumably because it has no Cu and no cuprate-planes. (YSr_2RuO_6 doped with $\approx 10\%$ Cu is a (not confirmed) superconductor with $T_c > 60$ K, and lacks cuprate-planes [6].)

In this paper, we discuss a few of the many experiments which (independently) show that the cuprate-plane picture of high-temperature superconductivity is inadequate, and find that the locus of the primary superconductivity is in the charge-reservoir layers of high-temperature superconductors.

PREDICTED SUPERCONDUCTORS

Using a model that assigns the primary superconductivity to the charge-reservoir layers (vicinity of the $Cu-O$ chains of $YBa_2Cu_3O_7$, interstitial re-

gions of $Nd_{2-z}Ce_zCuO_4$, SrO layers of $Nd_{2-z}Ce_zSr_2Cu_2NbO_{10}$), we have *successfully predicted* [7–9] that three materials which were consensus non-superconductors, must superconduct, which they subsequently did: $PrBa_2Cu_3O_7$ [10–12], $Gd_{2-z}Ce_zSr_2Cu_2TiO_{10}$ [13], and $Pr_{2-z}Ce_zSr_2Cu_2NbO_{10}$ [14] ($Pr_{222}Nb-10$). In the cases of $PrBa_2Cu_3O_7$ and $Pr_{2-z}Ce_zSr_2Cu_2NbO_{10}$ the critical temperatures (≈ 90 K and ≈ 28 K) were also predicted — as were the facts that both of the Pr compounds must experience shortened c -axis lattice constants, increased Néel temperatures, and high concentrations of Pr on alkaline-earth sites [12]. (Pr on an alkaline-earth site breaks Cooper pairs.)

PAIR-BREAKING

With data favoring a charge-reservoir model for the superconductivity, we examined the observed chemical trends found for pair-breaking by Zn and Ni impurities on Cu sites [15]. In the simplest model, the exchange scattering by non-magnetic Zn is absent (except for the contribution associated with Cu being replaced), and the direct non-magnetic impact of Zn and Ni should have about the same magnitude — by virtue of the locations of Zn and Ni in the Periodic Table adjacent to Cu . For all high-temperature superconductors, the effects on T_c by Zn and Ni should have two parts: the short-ranged scattering by Ni should be stronger than by Zn for direct magnetic scattering (the opposite for spin-fluctuation pairing), and the long-ranged scattering should be of approximately the same magnitude for Zn and Ni .

On the one hand, if the main superconducting condensate is in the cuprate-planes (which are virtually the same geometrically for all high-temperature superconductors), then the amount of dopant u (of either Zn or Ni) required to drive T_c to zero, u_c , should be nearly independent of the superconductor. The charge-reservoir supplies the charges that form into Cooper pairs. Only when this reservoir becomes too distant from the cuprate-planes to efficiently dope them, should u_c decline.

On the other hand, if the main condensate occupies the charge-reservoir layers, then the Zn or Ni sites in the cuprate-planes become distant from the charge-reservoirs as d , the distance between the cuprate-plane Cu and the nearest charge-reservoir oxygen, increases. This implies that, as d increases, the *difference* between scattering by Zn and by Ni will eventually vanish, after which u_c will be the same for Zn and Ni .

The data show that the predictions of the charge-reservoir model are obeyed, although the predictions of a cuprate-plane model are very different: Zn and Ni break pairs the same in all high-temperature superconductors except $Nd_{2-z}Ce_zCuO_4$ (Nd_{21-4}) — which is the sole such superconductor whose charge-reservoirs are adjacent to its cuprate-planes [15]. The data are consistent with the primary superconducting condensate being in the charge-reservoir layers, not in the cuprate-planes.

CHEMICAL TRENDS IN T_c

The chemical trends in T_c as d changes should reflect the fact that all cuprate-planes have almost the same geometry: In a cuprate-plane model T_c should be independent of d , until d becomes so large that efficient doping of the cuprate-planes becomes impossible; and in a charge-reservoir model, T_c should increase with d . The observed trends are $T_c \approx (15 \text{ K}/\text{\AA})d$, in accord with a charge-reservoir model [16].

DIFFERENT LAYERS SUPERCONDUCT

Most workers in the field would assume that the layers that superconduct in $R_{2-z}Ce_zCuO_4$ ($R21-4$) and in $R_{2-z}Ce_zSr_2Cu_2NbO_{10}$ ($R222Nb-10$) are the same. If they are, then the assumed fact that for $R = Nd$, both the $R21-4$ and the $R222Nb-10$ compounds superconduct in their cuprate-planes, implies that for all other rare-earth ions R (and for $R = Gd$, in particular) that the $R21-4$ and the $R222Nb-10$ compounds must both superconduct or must both not superconduct [17]. The fact is that $Gd21-4$ does not superconduct and $Gd222Nb-10$ does. This implies that the superconducting layers are different in the two classes of compounds.

We have proposed that the superconducting condensate involves interstitial oxygen in $R21-4$, and occupies the SrO layers in $R222Nb-10$ compounds [17]. The facts that $Gd21-4$ exhibits pair-breaking, but $Gd222Nb-10$ does not, and that interstitials are found in the $R21-4$ compounds, but not in $R222Nb-10$, indicate that the primary superconducting layers are different in the two classes of compound.

SUMMARY

There are many different independent experiments, all showing that the primary superconductivity in the high-temperature superconductors resides in the charge-reservoir layers, not in the cuprate-planes. Space limitations prevent us from discussing some of the most powerful proofs that the superconductivity resides primarily in the charge-reservoirs. Many of these involve magnetic and Mössbauer studies, and will be reported elsewhere.

ACKNOWLEDGMENTS

We thank the Army Research Office and Department of Energy (MISCON) for their support (Contracts DAAG55-97-1-0387 and DE-FG02-90ER45427).

REFERENCES

1. Cava, R. J., Hewat, A. W., Hewat, E. A., Batlogg, B., Marezio, M., Rabe, K. M., Krajewski, J. J., Peck, Jr., W. F., and L. W. Rupp, Jr., L. W., *Physica C* **165**, 419 (1990).
2. Jorgensen, J. D., Veal, B. W., Paulikas, A. P., Nowicki, L. J., Crabtree, G. W., Claus, H., and Kwok, W. K., *Phys. Rev. B* **41**, 1863 (1990).
3. Blackstead, H. A., and Dow, J. D., *J. Superconduct.* **9**, 563 (1996).
4. Blackstead, H. A., and Dow, J. D., *J. Appl. Phys.* **81**, 6285 (1997).
5. Goodrich, R. G., Grienier, C., Hall, D., Lacerda, A., Haanappel, E. G., Rickel, D., Northington, T., Schwarz, R., Mueller, F. M., Koelling, D. D., Vuillemin, J., Van Bockstal, L., Norton, M. L., and Lowndes, D. H., *J. Phys. Chem. Solids*
6. Wu, M. K., Chen, D. Y., Chien, F. Z., Sheen, S. R., Ling, D. C., Tai, C. Y., Tseng, G. Y., Chen, D. H., and Zhang, F. C., *Z. f. Physik B* **102**, 37 (1997).
7. Blackstead, H. A., and Dow, J. D., *Phys. Rev. B* **51**, 11830 (1995).
8. Blackstead, H. A., Dow, J. D., Heilman, A. K., and Pulling, D. B., *Solid State Commun.* **103**, 581 (1997).
9. Blackstead, H. A., Dow, J. D., Felner, I., Luo, H.-h., and Yelon, W. B., "Evidence of granular superconductivity in $Pr_{2-z}Ce_zSr_2Cu_2NbO_{10}$," *Intl. J. Mod. Phys. B*, in press.
10. Blackstead, H. A., Chrisey, D. B., Dow, J. D., Horwitz, J. S., Klunzinger, A. E., and Pulling, D. B., *Phys. Lett. A* **207**, 109 (1995); *Physica C* **235-240**, 1539 (1994).
11. Zou, Z., Oka, K., Ito, T., and Nishihara, Y., *Jpn. J. Appl. Phys. Lett.* **36**, L18 (1997).
12. Blackstead, H. A., and Dow, J. D., these proceedings.
13. Blackstead, H. A., Dow, J. D., Goldschmidt, D., and Pulling, D. B., *Phys. Lett. A* **245**, 158 (1998).
14. Blackstead, H. A., Dow, J. D., Felner, I., Luo, H.-h., and Yelon, W. B., "Evidence of granular superconductivity in $Pr_{2-z}Ce_zSr_2Cu_2NbO_{10}$," *Intl. J. Mod. Phys. B*, in press.
15. Blackstead, H. A., and Dow, J. D., *Europhys. Lett.* **41**, 659 (1998).
16. Blackstead, H. A., and Dow, J. D., *Philos. Mag. B* **74**, 681 (1996).
17. Blackstead, H. A., and Dow, J. D., "Comparison of bulk $R_{2-z}Ce_zCuO_4$ with superlattice $R_{2-z}Ce_zCuO_4/SrO/NbO_2/SrO/CuO_2$," unpublished.

Superconductivity in $\text{Pr}_{2-z}\text{Ce}_z\text{Sr}_2\text{Cu}_2\text{NbO}_{10}$ and in $\text{Gd}_{2-z}\text{Ce}_z\text{Sr}_2\text{Cu}_2\text{RuO}_{10}$

Howard A. Blackstead*, John D. Dow†, Israel Felner‡,
Damon D. Jackson‡, and David B. Pulling*

*Physics Department, University of Notre Dame, Notre Dame, Indiana 46556 USA

†Department of Physics, Arizona State University, Tempe, Arizona 85287-1504 USA

‡Racah Institute of Physics, The Hebrew University, Jerusalem 91904, Israel

‡National High Magnetic Field Laboratory, Tallahassee, Florida 32306 USA

Abstract. The detection of granular superconductivity in $\text{Pr}_{222}\text{Nb-10}$ leads to the conclusion that $R_{2-z}\text{Ce}_z\text{CuO}_4$ (R21-4) compounds and $R_{2-z}\text{Ce}_z\text{Sr}_2\text{Cu}_2\text{NbO}_{10}$ ($\text{R}_{222}\text{Nb-10}$) compounds both superconduct for $R=\text{Pr}$. The fact that Gd_{21-4} does not superconduct, but $\text{Gd}_{222}\text{Nb-10}$ does, indicates that the superconducting layers are different in the two classes of compounds. Magnetic resonance studies of $\text{Gd}_{222}\text{Ru-10}$ and Gd_{21-4} indicate either that ordered magnetism and superconductivity co-exist in the cuprate-planes or else that the cuprate-planes are not the primary superconducting layers in $\text{Gd}_{222}\text{Ru-10}$.

$\text{Pr}_{222}\text{Nb-10}$ MUST SUPERCONDUCT, AND DOES

$\text{Pr}_{2-z}\text{Ce}_z\text{Sr}_2\text{Cu}_2\text{NbO}_{10}$ ($\text{Pr}_{222}\text{Nb-10}$) was predicted to superconduct at ≈ 28 K [1], despite the fact that most authors who had grown the material had reported that it had failed to superconduct at all. But recent microwave measurements revealed that $\text{Pr}_{222}\text{Nb-10}$ is indeed a (granular) superconductor with $T_c \approx 28$ K [2].

The granular superconductivity in $\text{Pr}_{222}\text{Nb-10}$ partially resolves an important dilemma: (Rare-earth) $_{222}\text{Nb-10}$ is $(\text{Rare-earth})_{2-z}\text{Ce}_z\text{CuO}_4$ (R21-4) combined with the additional $/\text{SrO}/\text{NbO}_2/$ layers in each super-cell to form a superlattice (with the doping adjusted to $z \approx 0.5$, rather than 0.15). Since R21-4 and $\text{R}_{222}\text{Nb-10}$ both superconduct for $R=\text{Nd}$, then both compounds must simultaneously either superconduct or not superconduct, for any choice of the rare-earth ion R (in the usual picture of high-temperature superconductivity). If the geometrical element that superconducts in both compounds is the same, then changing both compounds the same way can only result in the same behavior for both compounds: superconducting or non-superconducting properties for both. Therefore

the failure of Pr222Nb-10 to superconduct when Pr21-4 does superconduct is incompatible with the origin of superconductivity being in the same regions of both materials, *e.g.*, in the cuprate-planes. Clearly Pr222Nb-10 (and Gd21-4) must superconduct, or else the superconducting layers in the R21-4 and R222Nb-10 superconductors are *not* the same layers in general, *viz.*, not in the cuprate-planes. Therefore the failure of Pr222Nb-10 (or Gd21-4) to superconduct, when Pr21-4 (and Gd222Nb-10) do superconduct, would contradict one of the most widely held ideas of high-temperature superconductivity: that the cuprate-planes are the loci of the primary superconductivity.

R222Nb-10 is a superlattice of R21-4 and the layers $/SrO/NbO_2/SrO/CuO_2/$, with only a somewhat different optimum doping: $z=0.5$ instead of 0.15. (The doping, in the conventional viewpoint, affects the optimum value of T_c and how well the material superconducts, not *whether* the material superconducts.) Since R21-4 and R222Nb-10 materials superconduct for $R=Nd, Sm, \text{ and } Eu$, with roughly the same critical temperatures [3,4], and, if (as assumed) the superconductivity originates in the cuprate-planes for $R=Nd, Sm, \text{ and } Eu$, then for $R=Pr$ (and also for $R=Gd$) either both the R21-4 and the R222Nb-10 materials must superconduct or neither must superconduct — which is definitely not the case experimentally. The facts that Pr222Nb-10 and Gd21-4 do not superconduct while Pr21-4 and Gd222Nb-10 do superconduct must be explained.

Our explanation of the Pr anomaly was to show that Pr222Nb-10 superconducts, much as its homologues do [2]. The observed superconductivity was granular, rather than bulk, superconductivity — and so we await fabrication of cleaner Pr222Nb-10 material which exhibits *bulk* superconductivity.

We rather doubt that Gd21-4 will superconduct, because it has been so thoroughly studied (and because our attempts to measure granular superconductivity have revealed none). Hence, we believe that the primary superconducting regions in the R21-4 and R222Nb-10 compounds *are not the same* — and hence are not both in the cuprate-planes. (We think that the superconducting regions of superconducting R21-4 compounds involve interstitial oxygen, and the corresponding regions of R222Nb-10 involve the *SrO* layers.)

THE CUPRATE-PLANES ARE WEAKLY FERROMAGNETIC IN SUPERCONDUCTING Gd222Ru-10

In an electron spin resonance (ESR) experiment on Gd222Ru-10, when the applied magnetic field \mathbf{H} is parallel to the *rf* field \mathbf{H}_{rf} , the ESR absorption is forbidden unless the paramagnetic (Gd) spin system experiences a local field which is not precisely parallel to the applied field \mathbf{H} . Under such circumstances, a Gd spin experiences an *rf* torque and resonates, because the magnetization vector \mathbf{M} has a component *perpendicular* to the *rf* field. This transverse magnetization

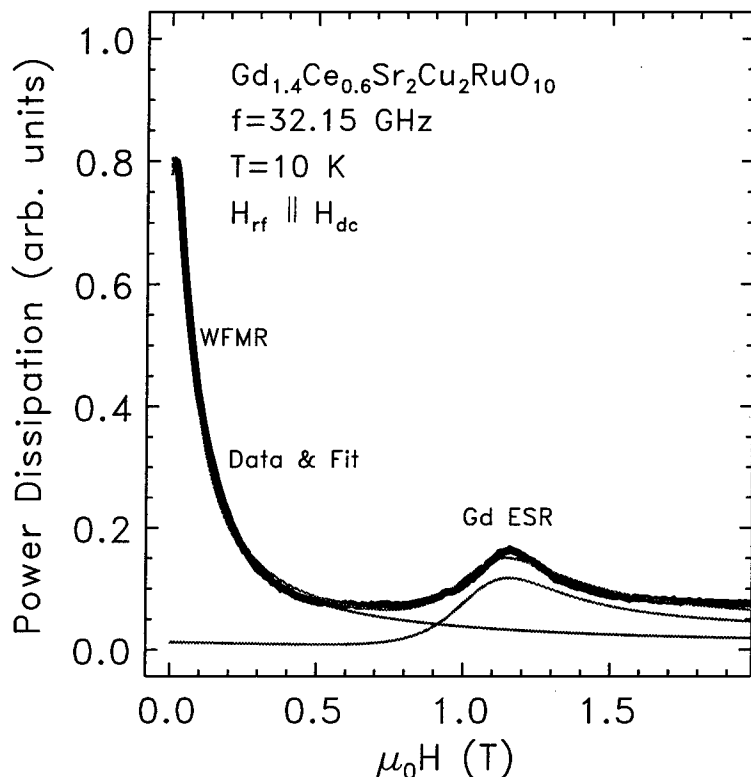


FIGURE 1. “Forbidden” power dissipation *vs.* applied field (parallel to the *rf* field) for $Gd_{1.4}Ce_{0.6}Sr_2Cu_2RuO_{10}$ with *rf* frequency of 21.15 GHz, at a temperature of 10 K. The line-shape is decomposed into a weak ferromagnetic resonance and a Gd ESR line.

is associated with short-ranged exchange or super-exchange coupling to the adjacent cuprate-planes (the RuO_2 layers are too distant), and the cuprate-planes are necessarily magnetically ordered (*e.g.*, weakly ferromagnetic or antiferromagnetic). Therefore the transverse magnetization observed at a temperature of 10 K in Gd222Ru-10 implies that the cuprate-planes are magnetically ordered [5], as they clearly are in non-superconducting Gd21-4 [6]. In the case of Gd222Ru-10, we find from the predicted position of the $g=2$ resonance an internal field of ≈ 0.04 T, and we conclude that the cuprate-plane magnetic order co-exists with the primary superconducting condensate, which is either not in the cuprate-planes (our viewpoint) or else inhabits the very layers that are magnetically ordered (the cuprate-planes) — difficult for many theorists to accept. (See Figure 1.)

Furthermore, the Gd lineshape of Figure 1 is asymmetric in superconducting Gd222Ru-10, indicating that a Gd spin is coupled to carriers and to the Fermi surface — and showing that the assumption that the Gd spins are isolated from

the Fermi surface is invalid. The corresponding lineshape of non-superconducting Gd21-4 is symmetric. This, of course, means that the Gd, which is a magnetic trivalent rare-earth ion with $L=0$, should break Cooper pairs in the cuprate-planes of Gd222Ru-10, and implies again that the primary superconducting condensate is not in the cuprate-planes of that material.

SUMMARY

Pr222Nb-10 now superconducts (in grains) and probably will soon exhibit bulk superconductivity. The one remaining anomaly is that Gd21-4 does not superconduct, but Gd222Nb-10 does — indicating that the superconducting regions in the R21-4 and R222Nb-10 compounds are different, probably involving interstitial oxygen in the R21-4 compounds, and involving SrO layers in R222Nb-10.

The ordered magnetism of the Gd222Ru-10 compounds inhabits the cuprate-planes and the RuO₂ layers (which may be ferromagnetic), and leaves open the question of where the superconductivity that coexists with it is — perhaps not in the cuprate-planes.

ACKNOWLEDGMENTS

H. A. B., J. D. D., D. B. P., and D. D. J. thank the Department of Energy (MISCON), the Army Research Office, the Office of Naval Research, and the National Science Foundation (the National High Magnetic Field Laboratory) for their support (Contracts DE-FG02-90ER45427, DAAG55-97-1-0387, N00014-98-10137, and DMR-9527035). We also thank the Israel Academy of Science and Technology and the Klachky Foundation for Superconductivity for their financial support of the work of I. F.

REFERENCES

1. Blackstead, H. A., and Dow, J. D., J. Appl. Phys., **83**, 1536 (1998); Phys. Rev. **B** **57**, 10798 (1998).
2. Blackstead, H. A., Dow, J. D., Felner, I., Luo, H.-h., and Yelon, W. B., "Evidence of granular superconductivity in $Pr_{2-z}Ce_zSr_2Cu_2NbO_{10}$," Intl. J. Mod. Phys. **B**, in press.
3. Goodwin, T. J., Radousky, H. B., and Shelton, R. N., Physica **C** **204**, 212 (1992).
4. Bauerinfeld, L., Widder, W., and Braun, H. F., Physica **C** **253**, 151 (1995), give the values of T_c for compounds with *Ru* replacing *Nd*.
5. Felner, I., Asaf, U., Levi, Y., and Millo, O., Phys. Rev. **B** **55**, R3374 (1997); Felner, I., and Nowick, I., Supercond. Sci. Technol. **8**, 121 (1995).
6. Thompson, J. D., Cheong, S.-W., Brown, S. E., Fisk, Z., Oseroff, S. B., Tovar, M., Vier, D. C., and Schultz, S., Phys. Rev. **B** **39**, 6660 (1989).

Superconductivity in $\text{PrBa}_2\text{Cu}_3\text{O}_7$

Howard A. Blackstead* and John D. Dow†

*Physics Department, University of Notre Dame, Notre Dame, Indiana 46556 USA

†Department of Physics, Arizona State University, Tempe, Arizona 85287-1504 USA

Abstract. The evidence that $\text{PrBa}_2\text{Cu}_3\text{O}_7$ is a bulk superconductor is reviewed, together with evidence that the primary superconducting layer involves the charge-reservoir CuO layer and its neighboring BaO layers.

INTRODUCTION

One of the surprises of the early days of high-temperature superconductivity was the realization that $\text{PrBa}_2\text{Cu}_3\text{O}_7$ (Pr123-7) did not superconduct. Apparently Pr was the only rare-earth R (recognized at the time) that failed to superconduct in an $R123-7$ compound [1]. Since then there have been literally more than a thousand claims that Pr123-7 does not superconduct, with a variety of explanations for *why*; many of these were reviewed by Radousky [2]. Now two other rare-earth or actinide ions lead to non-superconductivity, namely $R = \text{Ce}$ and $R = \text{Cm}$ — although Ce is not 100% soluble on the rare-earth site, and so has been measured only in $\text{Nd}_{1-x}\text{Ce}_x\text{Ba}_2\text{Cu}_3\text{O}_{7+\delta}$ (for $x < 0.35$) [3] and in $\text{Y}_{1-x}\text{Ce}_x\text{Ba}_2\text{Cu}_3\text{O}_{7+\delta}$ (for $x < 0.3$) [4]. These observations suggested that *large* magnetic rare-earth ions cause the breakdown of superconductivity, and led to the prediction that these large ions are sufficiently soluble on Ba sites to break Cooper pairs and destroy superconductivity [5–7]. Hence T_c for the non-superconducting compounds $R123-7$ can be raised to ≈ 90 K by keeping Pr , Cm , and Ce off the Ba -sites.

Early studies of Pr123-7 capable of detecting granular superconductivity, either in surface resistance or in electron spin resonance (ESR), showed at first that the material is indeed a *granular* superconductor with $T_c \approx 90$ K [8,9]. Then Zou *et al.* produced bulk superconducting material to the astonishment of the various theorists [2] who by then had “proven” that the material could not superconduct [10]. There are now eight groups [8–20] which have detected superconductivity in Pr123-7 , all with T_c approaching 90 K. The highest T_c in a non-granular material was 89.9 K, produced by Usagawa *et al.* in thin films [16,21,22]. Now with some of the best crystal-growers in the world having produced superconducting Pr123-7 , there can be little doubt that Pr123-7 superconducts when grown properly — and even less doubt that superconducting material is difficult to grow.

The main remaining problem with high-temperature superconductivity in Pr_{123-7} is that many workers in the field now *believe* that the seat of superconductivity is in the cuprate-planes of all high-temperature superconductors — although (i) some such superconductors have no cuprate-planes (*e.g.*, $Ba_{1-a}K_aBiO_3$ with T_c as high as 32 K [23] or YSr_2RuO_6 with $T_c \approx 80$ K [24]); (ii) the data purportedly providing the evidence of a jump in cuprate-plane charge at the onset of superconductivity have been shown to be incorrect [25], casting doubt on the original arguments locating the superconducting condensate in the cuprate-planes [26]; and (iii) the facts in Pr_{123-7} are that Pr on a Pr -site has no significant effect on the superconductivity, while Ba -site Pr (Pr_{Ba}) destroys superconductivity — although the cuprate-plane is essentially mid-way between the Pr and the Pr_{Ba} . (Our original prediction that clean Pr_{123-7} would superconduct was based on the idea that the superconducting condensate is *not* in the cuprate-planes of R_{123-7} compounds, but in the charge-reservoirs — namely in the vicinity of the chain-layers [6].) Now, quite incredibly, there is an effort to explain the observation of ≈ 90 K superconductivity in “clean” Pr_{123-7} in terms of defects such as Ba_{Pr} [27]! (It would be truly remarkable if a defect restored the superconductivity of Pr_{123-7} to *exactly* the T_c of 90 K found for all other perfect R_{123-7} compounds.)

In this paper we argue (i) that Pr_{123-7} superconducts, (ii) that the layers most responsible for the superconductivity are the charge-reservoir layers (not the cuprate-planes), and (iii) that defects such as Pr_{Ba} are responsible for destroying the superconductivity.

HOLE-FILLING, HYBRIDIZATION, AND Ba_{Pr}

The three most popular mechanisms for explaining the *failure* of intrinsic Pr_{123-7} to superconduct have all been shown to be invalid: (i) Soderholm *et al.* [28] have ruled out hole-filling, namely that Pr is Pr^{+4} and the extra electron from the reaction $Pr^{+3} \rightarrow e^- + Pr^{+4}$ annihilates a hole, making Pr_{123-7} an insulator, rather than a superconductor. (ii) Hybridization of the Pr on the rare-earth site with cuprate-plane oxygen has been disproven as a mechanism for reducing T_c to zero, by experiments showing that increasing the hybridization *increases* T_c and does not suppress it [12,29,30]. (iii) And the possibility of Ba_{Pr} defects playing an important role [10] is ruled out by common sense: the volume of Ba^{+2} is approximately *twice* the volume of Pr^{+3} , so the Ba^{+3} cannot fit without rendering the crystal unstable, according to Linde’s Rule that $>10\%$ changes of radii are impermissible [31].

Pr_{Ba} DEFECTS.

Our proposal has been that “clean” Pr_{123-7} is a ≈ 90 K superconductor, and that Pr_{123-7} does not superconduct because it contains too many pair-breaking Pr -on-the- Ba -site defects (Pr_{Ba}). The reason that these defects were not noticed before is that Pr and Ba have nearly the same neutron scattering lengths. There

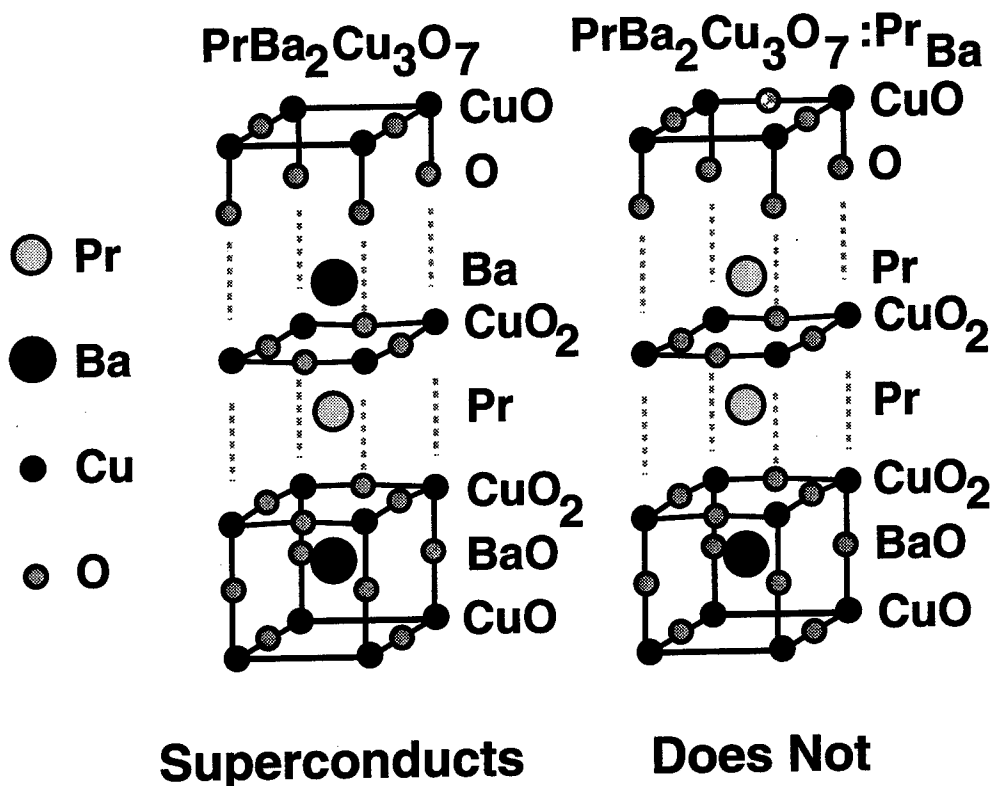


FIGURE 1. Crystal structures of *Pr*123-7 (left) in the pristine, superconducting form and (right) with *Pr*_{Ba} defects which cause the *Pr*123-7 to not superconduct.

are, however, many *indirect* indications of the presence of *Pr*_{Ba} defects. These include: (i) the production of excess *BaCuO₂* (observable in wet chemistry or with ESR) to compensate for the extra *Ba*-site *Pr* [32], (ii) the formation of oxygen ions on the *O*(5) or antichain sites between the *Cu* and adjacent chains [5,6] (one fully charged such oxygen is needed to balance charge with two nearby *Pr*_{Ba}⁺³ defects); (iii) the occurrence of an anomalously large Néel temperature (≈ 17 K in *Pr*123-7 [3] and ≈ 22 K in *Cm*123-7 [33], compared with ≈ 2 K in most superconducting *R*123-7 compounds), because the effective lattice constant of the Néel magnets is shortened by the *Pr*_{Ba} magnetic defects; (iv) the direct observation of *Pr*_{Ba} in spin-dependent neutron scattering [34], and (v) the presence of *Pr*_{Ba} lines in magic-angle spinning nuclear magnetic resonance spectra of *Pr*123-7 [35]. All have been observed. (See Figure 1.)

SHORTENED *c*-AXIS

One of the noteworthy features of the data is that the *c*-axis lengths obtained from most of the (*Rare-earth*)123-7 compounds define a straight line (as a function of rare-earth size) and this length, for $R = Pr$, is shorter for flux-grown *Pr*123-7 than that found for the *Pr*123-7 compounds grown by Zou *et al.* [10] using the traveling solvent floating zone method. (A similar short *c*-axis is found for non-superconducting *Cm*123-7.) An obvious interpretation of these data is that *Pr*123-7 grown by the traveling solvent floating zone method produces material lacking Pr_{Ba} defects which bridge between regular *Pr* sites, and consequently has neither the high Néel temperature of order ≈ 20 K observed in both *Pr*123-7 and *Cm*123-7, nor the short *c*-axis. In this regard, it is noteworthy that the data for *Pr*123-7 crystals grown by the traveling solvent floating zone method reveal neither a Néel temperature above 2.2 K [36], nor a short *c*-axis.

SUMMARY

In conclusion, we find that *Pr*123-7 superconducts when grown carefully by the traveling solvent floating zone method. Neither the hybridization models, the claims of Pr^{+4} , nor the hole-filling models are valid for this compound. It is rather easy to form Pr_{Ba} however, and that defect is responsible for many of the noteworthy properties of *Pr*123-7. Removal of the defect makes *Pr*123-7 very similar to other (*Rare - earth*)123-7 compounds.

Perhaps the most disturbing feature of this entire story is that it requires that the primary superconductivity be located, not in the cuprate-planes (as widely assumed), but in or near the charge-reservoir layers. No doubt, it will take time for this new view of the high-temperature superconductors to be accepted.

ACKNOWLEDGMENTS

We are grateful to the U.S. Army Research Office, the U.S. Office of Naval Research, the National Science Foundation, for their financial support of this work (Contract Nos. DAAG55-97-1-0387, N00014-94-10147, and DE-FG02-90ER45427).

REFERENCES

1. Kebede, A., Jee, C. S., Schwegler, J., Crow, J. E., Mihalisin, T., Myer, G. H., Salomon, R. E., Schlottmann, P., Kuric, M. V., Bloom, S. H., and Guertin, R. P., *Phys. Rev. B* **40**, 4453 (1989)
2. For a review of the old ideas which assumed the failure of *Pr*123-7 to superconduct to be intrinsic, see Radousky, H. B., *J. Mater. Res.* **7**, 1917 (1992).

3. Cao, G., Bolivar, J., O'Reilly, J. W., Crow, J. E., Kennedy, R. J., and Pernambuco-Wise, P., *Physica B* **186-188**, 1004 (1993) also find a Néel temperature of 17 K. *Tb* doping, unlike *Ce* doping, does not depress T_c : Blackstead, H. A. and Dow, J. D., *Superlatt. Microstruct.* **14**, 231 (1993).
4. Fincher, Jr., C. R., and Blanchet, G. B., *Phys. Rev. Lett.* **67**, 2902 (1991).
5. Blackstead, H. A. and Dow, J. D., *Solid State Commun.* **96**, 313 (1995).
6. Blackstead, H. A. and Dow, J. D., *Phys. Rev. B* **51**, 11830 (1995).
7. Blackstead, H. A. and Dow, J. D., *Superlatt. Microstruct.* **14**, 231 (1993); *J. Supercond.* **8**, 653 (1995).
8. Blackstead, H. A., Chrisey, D. B., Dow, J. D., Horwitz, J. S., Klunzinger, A. E., and Pulling, D. B., *Physica C* **235-240**, 1539 (1994); *Phys. Lett. A* **207**, 109 (1995).
9. Blackstead, H. A., Dow, J. D., Chrisey, D. B., Horwitz, J. S., McGinn, P. J., Black, M. A., Klunzinger, A. E., and Pulling, D. B., *Phys. Rev. B* **54**, 6122 (1996).
10. Zou, Z., Oka, K., Ito, T., and Nishihara, Y., *Jpn. J. Appl. Phys., Part 2*, **36**, L18 (1997).
11. Romanenko, A. I., and Kozeeva, L. P., *Phys. Lett. A* **223**, 132 (1996).
12. Ye, J., Zou, Z., Matsushita, A., Oka, K., Nishihara, Y., and Matsumoto, T., *Phys. Rev. B* **58**, R619 (1998).
13. Zou, Z., Ye, J., Oka, K., and Nishihara, Y., *Phys. Rev. Lett.* **80**, 1074 (1998); Oka, K., Zou, Z., and Ito, T., *Physica C* **282-287**, 479 (1997); Oka, K., Zou, Z., Ito, T., and Nishihara, Y., *Physica C* **282-287**, 481 (1997).
14. Kadowaki, K., public statement at the 1996 Fall Meeting of the Materials Research Society.
15. Luszczek, M., Sadowski, W., and Olchowik, J., Abstract Book, 5th International Conf. Materials and Mechanisms of Superconductivity High-Temperature Superconductors, Feb. 28-Mar. 4, 1997, Beijing, China, p. 143: "Growth of single crystals and induced superconductivity in $PrBa_2Cu_3O_{7-\delta}$ "; Sadowski, W., Luszczek, M., Olchowik, J., Susla, B., and Czajka, R., *Molec. Phys. Rpts.* **20**, 213 (1997).
16. Usagawa, T., Ishimaru, Y., Wen, J., Utagawa, T., Koyama, S., and Enomoto, Y., *Jpn. J. Appl. Phys.* **36**, L1583 (1997) find that [1,1,0] films superconduct. Note that Usagawa, T., Ishimaru, Y., Wen, J., Utagawa, T., Koyama, S., and Enomoto, Y. [*Appl. Phys. Lett.* **72**, 1772 (1998)] find that, unlike [1,1,0] films, [0,0,1] films do not superconduct. This is consistent with the pair-breaking defect being Pr_{Ba} in Pr_{123} -7.
17. Cooley, J. C., Hulst, W. E., Peterson, E. J., Robinson, R. A., and Smith, J. L., " $PrBa_2Cu_3O_x$ superconducting and magnetic properties," *Intl. J. Mod. Phys. B*, in press.
18. Cooley, J. C., Hulst, W. L., Peterson, E. J., Dow, J. D., Blackstead, H. A., and Smith, J. L., *Bull. Amer. Phys. Soc.* **Q35.07** (March, 1998); Hulst, W. L., Cooley, J. C., Peterson, E. J., Blackstead, H. A., Dow, J. D., and Smith, J. L., " $PrBa_2Cu_3O_7$ polycrystalline superconductor preparation," *Intl. J. Mod. Phys. B*, in press.
19. A. Shukla, A., B. Barbiellini, B., A. Erb, A., Manuel, A., Buslaps, T., Honkimäki, V., and Suortti, P., "Insulating Pr_{123} and superconducting Y_{123} : charge-transfer modified by disorder," to be published. Preprint cond-mat/9805225 19 May 1998. These authors claim that they have Pr^{+4} on the *Ba*-site, which is forbidden by the

Madelung potential and ruled out by inelastic neutron diffraction experiments of Ref. 28.

20. Blackstead, H. A., Cooley, J. C., Dow, J. D., Hults, W. L., Malik, S. K., Pulling, D. B., Smith, J. L., and Yelon, W. B., *J. Phys. Chem. Solids*, **59**, 1798 (1998).
21. Earlier studies by Norton *et al.* [22] on $Pr_{1-x}Ca_x$ 123-7 thin films for $x=0.5$ had observed superconductivity with a rather low T_c of 43 K, but these results were considered as not symptomatic of pure Pr123-7 being superconductive by some of the authors (private communication).
22. Norton, D. P., Lowndes, D. H., Sales, B. C., Budai, J. D., Jones, E. C., and Chakoumakos, B. C., *Phys. Rev. B* **49**, 4182 (1994). See also Liu, H. B., Morris, D. E., Sinha, A. P. B., Kwei, G. H., *Physica C* **223**, 51 (1994).
23. Goodrich, R. G., Grienier, C., Hall, D., Lacerda, A., Haanappel, E. G., Rickel, D., Northington, T., Schwarz, R., Mueller, F. M., Koelling, D. D., Vuillemin, J., Van Bockstal, L., Norton, M. L., and Lowndes, D. H., *J. Phys. Chem. Solids*, **54**, 1251 (1993).
24. Chen, D. Y., Chien, F. Z., Ling, D. C., Tseng, J. L., Sheen, S. R., Wang, M. J., and Wu, M.K., *Physica C* **282-287**, 73 (1997).
25. Jorgensen, J. D., Veal, B. W., Paulikas, A. P., Nowicki, L. J., Crabtree, G. W., Claus, H., and Kwok, W. K., *Phys. Rev. B* **41**, 1863 (1990).
26. Cava, R. J., Hewat, A. W., Hewat, E. A., Batlogg, B., Marezio, M., Rabe, K. M., Krajewski, J. J., Peck, Jr., W. F., and Rupp, Jr., L. W., *Physica C*, **165**, 419 (1990).
27. Pieper, M. W., Wiekhorst, F., and Wolf, T., "Carrier doping in $Pr_{1+x}Ba_{2-x}Cu_3O_7$ studied by NMR," preprint cond-mat.9803336, 27 Mar 1998.
28. Soderholm, L., Loong, C.-K., Goodman, G. L., and Dabrowski, B. D., *Phys. Rev. B* **43**, 7923 (1991).
29. Kim, C. C., Skelton, E. F., Osofsky, M. S., and Liebenberg, D. H., *Phys. Rev. B* **48**, 6431 (1993).
30. Blackstead, H. A. and Dow, J. D., *Phys. Rev. B* **57**, 5048 (1998).
31. Lindemann, F., *Phys. Z.* **11**, 609 (1910).
32. Karen, P., Fjellvag, H., Braaten, O., Kjekshus, A., and Bratsberg, H., *Acta Chem. Scand.* **44**, 994 (1990).
33. Soderholm, L., Goodman, G. L., Welp, U., Williams, C. W., and Bolender, J., *Physica C* **161**, 252 (1989) find a Néel temperature of 22 K.
34. Nutley, M. P., Boothroyd, A. T., and McIntyre, G. J., *J. Magnetism Magnetic Mater.* **104-107**, 623 (1992); Nutley, M. P., Warwick University thesis, Fig. 5.3.
35. Han, Z. P., Dupree, R., Paul, D. McK., Howes, A. P., and Caves, L. W. J., *Physica* **181**, 355 (1991).
36. Z. Zou, private communication.

Investigations of the Vortex Matter in $\text{Bi}_2\text{Sr}_2\text{Ca}_1\text{Cu}_2\text{O}_{8+\delta}$ Single Crystals

T. Blasius¹, Ch. Niedermayer¹, J. Schiessling¹, U. Bolz¹,
J. Eisenmenger¹, B.-U. Runge¹, P. Leiderer¹, J.L. Tallon²,
D.M. Pooke², A. Golnik³, C.T. Lin³ and C. Bernhard³

¹*Fakultät für Physik, Universität Konstanz, D-78457 Konstanz, Germany*

²*The New Zealand Institute for Industrial Research, Lower Hutt, New Zealand*

³*Max-Planck-Institut für Festkörperforschung, D-70569 Stuttgart, Germany*

Abstract. We report transverse-field muon spin rotation studies of the magnetic field distribution $n(\mathbf{B})$ in the vortex state of the high temperature superconductor $\text{Bi}_2\text{Sr}_2\text{Ca}_1\text{Cu}_2\text{O}_{8+\delta}$ (Bi-2212) and present data on three sets of overdoped, nearly optimized and underdoped single crystals which to our best knowledge provide the first evidence that a two-stage melting transition of the vortex matter occurs under equilibrium conditions. In addition, we compare the TF- μ SR results with those from DC-magnetization measurements and magneto-optic experiments on the same crystals.

INTRODUCTION

The vortex matter in the cuprate high- T_c superconductors exhibits a complex (H, T) -phase diagram where thermal fluctuations dominate the vortex state well below the upper critical field $H_{c2}(T)$ [1]. Early on, a melting transition of the flux-line lattice (FLL) was proposed [2] and confirmed experimentally [3]. However, the details of this melting transition are not yet fully understood. When a magnetic field is applied perpendicular to the CuO_2 planes the flux-lines can be viewed as stacks of pancake vortices [4]. Both the intra-planar vortex order and the inter-planar coupling between the pancake vortices can be overcome by thermal fluctuations. In principle, these processes may occur independently and at different temperatures. Based on these considerations a two-stage melting transition has been proposed [5]. Recently, experimental evidence for this two-stage melting scenario has been obtained from non-equilibrium experiments [6]. The equilibrium vortex structure, however, can be studied with the technique of transverse-field muon spin rotation (TF- μ SR) which has already provided valuable information on the vortex state, in particular, on the vortex matter transition at the irreversibility line (IL) and the so called 'dimensional crossover' from a 3D to a 2D vortex structure [7,8].

TF- μ SR EXPERIMENTS

In TF- μ SR experiments positive muons come to rest in the bulk of the crystal at interstitial locations, r , which are randomly distributed on the length scale of the magnetic penetration depth λ [9]. An external magnetic field H_{ext} is applied perpendicular to the initial muon spins which start to precess in the local magnetic field $B_{int}(r)$ with the Larmor frequency $\omega_\mu = \gamma_\mu B_{int}(r)$ where $\gamma_\mu = 851.4 \text{ MHz/T}$ is the gyromagnetic ratio of the muon. The time evolution of the muon spin polarization function $P(t)$ is then measured by monitoring the decay positrons which are preferentially emitted along the muon spin direction at the instant of decay (for details see [10]). The probability distribution of the local magnetic field $n(B)$, the so called ' μ SR-lineshape', is extracted from $P(t)$ either via Fast Fourier Transform or Maximum Entropy techniques and contains detailed information on the vortex structure. For a 3D flux line lattice, $n(B)$ is strongly asymmetric [11] with a pronounced tail towards high fields due to muons that stop near the vortex cores, a cusp which corresponds to the field at the saddle point between adjacent vortices and a cutoff on the low field side corresponding to the field minimum at the point which is most remote from the vortex cores. The asymmetry or 'skewness' of the ' μ SR-lineshape' can be characterized by the dimensionsless parameter [7] $\alpha = \langle \Delta B^3 \rangle^{1/3} / \langle \Delta B^2 \rangle^{1/2}$, where $\langle \Delta B^n \rangle$ is the n^{th} central moment of $n(B)$. A value of $\alpha \approx 1$ is typical for the ' μ SR-lineshape' due to a static 3D FLL [7,8]. A reduced value of $1 > \alpha > 0$ either indicates a disorder of the static vortex structure or else vortex dynamics in excess of the typical μ SR time scale of $\tau < 10^{-6} \text{ s}$ [7,8].

With increasing temperature a FLL will be subject to thermal fluctuations and α will be continuously reduced towards rather small but still positive α -values. In contrast, α has been shown to undergo a sudden and discontinuous change from positive to negative values at the IL. This behavior has been attributed to an one-stage transition where the intra-planar melting and inter-planar decoupling occur simultaneously at T_m [7]. In the following we present TF- μ SR data which indicate that a second transition occurs in the irreversible regime well below the IL [12]. Figure 1a summarizes the results for α and the shift of the cusp-field with respect to the external field (cusp-shift, B_{sh}). The data have been obtained by field cooling in an applied field well below the dimensional crossover field H^* [8,12] and the signature of a 3D vortex lattice, i.e. $\alpha \approx 1$, is observed at low temperature. The ' μ SR-lineshape' exhibits the most pronounced changes in the vicinity of the IL, where α exhibits a sudden drop and changes sign at T_{dc} . In addition, the T-dependence of the ' μ SR-lineshape' exhibits a second anomaly at a temperature T_{ab} well below the IL. We argue that the observed transition may be related to the intra-planar melting of the flux-line lattice to a flux-line liquid phase. This phase persists over a sizable temperature interval for $T_{ab} < T < T_{dc}$ before the individual flux-lines are decoupled at a significantly higher temperature T_{dc} at the IL [12].

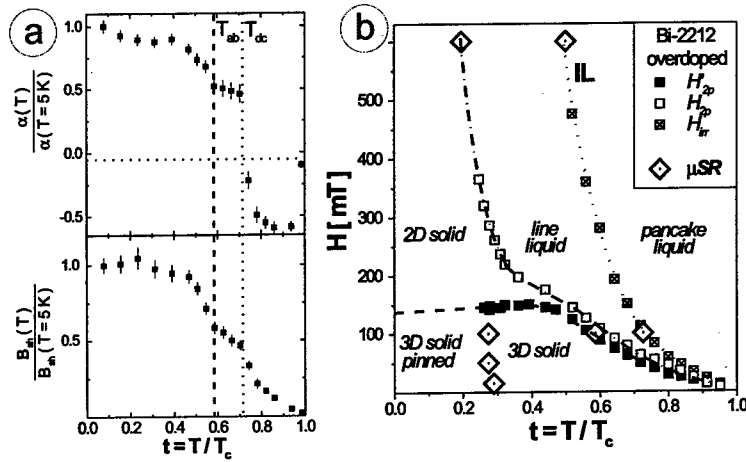


FIGURE 1. (a) Data from field-cooled TF- μ SR experiments on overdoped Bi-2212 single crystals ($T_c = 64$ K) in an applied field of $\mu_0 H_{ext} = 100$ mT. T-dependence of α (top) and the cusp-shift (bottom) of $n(B)$. T_{ab} and T_{dc} denote the temperature for the intra-planar melting and the inter-planar decoupling, respectively. (b) (H, T) -phase diagram constructed from μ SR and VSM data. Shown are the irreversibility field H_{irr} , the field for the second peak in $M(H)$, H_{2p} , and for the peak in the corresponding derivative dM/dH , H'_{2p} . The lines are guide to the eye.

For fields $H > H^*$ the low-temperature vortex-state is quasi-2D [7,8]. In this regime the ' μ SR-lineshape' becomes almost symmetric giving rise to strongly reduced values of α and B_{sh} . Figure 2a shows the T-dependence for α and B_{sh} which has been obtained for the underdoped set for $H_{ext} = 100$ mT $> H^* \sim 7.5$ mT. The most pronounced changes occur again in the vicinity of the IL. Once more a second anomaly is apparent in the T-dependence of the ' μ SR-lineshape' which occurs at a temperature well below the IL. In contrast to the behavior in the FLL state at $H < H^*$ (where α and B_{sh} decrease with increasing T) the 'skewness' now exhibits a small but significant increase and the cusp-shift also becomes somewhat larger. Both effects are indicative of a restoration of the flux-lines as the intra-planar order of the quasi-2D pancake vortex lattice diminishes at T_{ab} . Especially the increase of α signals the formation of vortex-line segments on a length scale along the c-axis direction exceeding the in-plane magnetic penetration depth [8]. At low T the adjustment to the pinning sites was achieved by suppressing the inter-planar coupling of the individual flux-lines in favor of the persistence of quasi-2D intra-planar order of the pancake vortices. At the in-plane melting transition, however, the intra-planar order is lost and there is no further need for the decoupling of the individual vortex lines in order to obtain a favorable adjustment to the pinning sites. The vortex lines therefore become at least partially restored. We note that the same trend has been observed at a higher field of $H_{ext} = 600$ mT and $H_{ext} = 1$ T for the underdoped and the overdoped Bi-2212 single crystals.

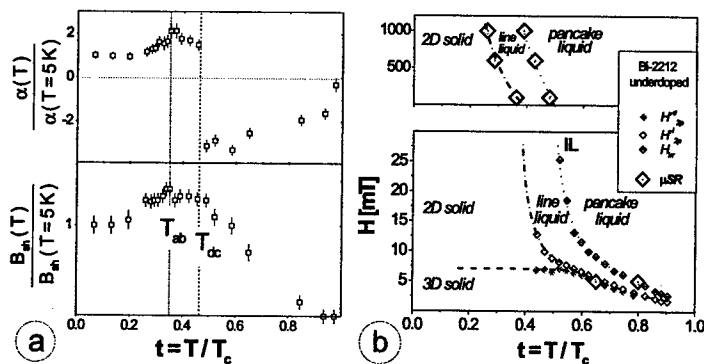


FIGURE 2. (a) Data from field-cooled TF- μ SR experiments on a set of underdoped Bi-2212 single crystals ($T_c = 77$ K) in an applied field of $\mu_0 H_{ext} = 100$ mT. (b) (H, T) -phase diagram constructed from μ SR and VSM data. Panels are as described in Figure 1.

DC-MAGNETIZATION MEASUREMENTS

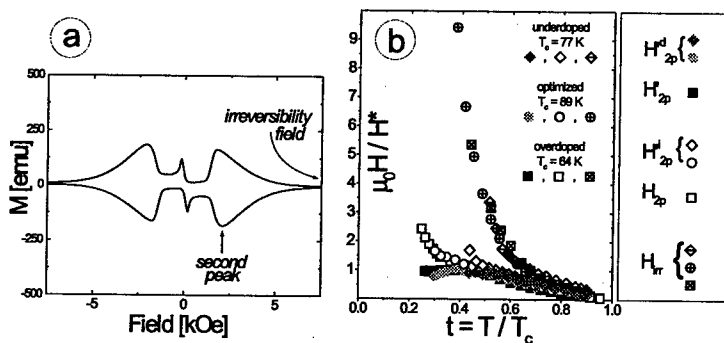


FIGURE 3. (a) representative $M - H$ loop at $T = 24$ K. (b) Rescaled VSM data (scaling factor H^*) for different doping states of Bi-2212 single crystals.

The μ SR results support our assumption that the second-peak effect in the DC-magnetization (Figure 3a) is related to the dimensional crossover [8]. The decoupling of the vortex lines and the concomitant enhancement of the pinning of the quasi-2D pancake lattice increase progressively as the magnetic field is increased above H^* until it goes through a maximum right at the in-plane melting point. At even higher magnetic fields in the line-liquid phase the pinning properties decline due to enhanced thermal fluctuations before the magnetic behavior becomes

reversible beyond the irreversibility field. A rather interesting question is how our observation of a two-stage melting transition fits in with the reports of a one-stage melting transition. It seems likely that the key to the answer lies in the *c*-axis coupling strength. In fact, we obtain a rather unique (*H*, *T*) phase diagram from μ SR (Figure 1b and 2b) and DC-magnetization (Figure 3b, scaling factor H^*) data for a wider series of Bi-2212 single crystals. This would imply that a two-stage melting process is experimentally observable if $H \geq H^*$ while a seemingly one-stage melting process occurs when T_{ab} and T_{dc} do collapse for $H \ll H^*$. Such a trend is even visible from our data on the Bi-2212 crystals for which the $T_{ab}(H)$ - and $T_{dc}(H)$ -lines seem to merge for $H \ll H^*$. For the much less anisotropic Y-123 compound H^* should be in excess of 10 T and accordingly most of the experiments have been done for $H < H^*$ where in fact a single-stage transition is observed.

MAGNETO-OPTIC EXPERIMENTS

The magneto optical method is based on the Faraday effect, i.e. the rotation of the polarization plane of linearly polarized light which passes a magneto-optically active layer exposed to the magnetic field of the underlying superconductor. Since the rotation angle depends on the magnetic field one can visualize the flux distribution in a polarization microscope. This technique has already been shown to be a powerful tool to investigate e.g. artificial defects in thin films [13]. In Figure 4 are displayed pictures of the magnetic field distribution received from underdoped Bi-2212 single crystals in an applied field of 10 mT for different temperatures. The experiment has been performed in 10 mT after zero field cooling. Shown are the pictures taken at (a) 10 K in the strong pinning regime, no flux penetrates the sample (sample dark, edges white due to pile up of flux), (b) 34 K in the vicinity of the depinning temperature (different gray scales due to inhomogeneous flux distribution), (c) 36 K in the line-liquid regime above T_{ab} (almost homogeneous contrast due to nearly randomly distributed flux) and (d) 60 K, above T_{ab} (no more contrast due to reversible vortex state and high thermal fluctuations). Details will be presented in forthcoming publications (spatial resolved [14] and time resolved [15]).

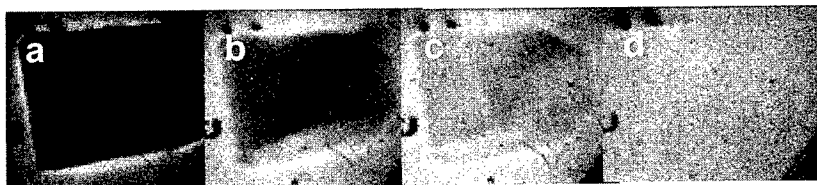


FIGURE 4. Magneto-optical picturing of the magnetic field distribution on a underdoped Bi-2212 single crystal in an applied field of 10 mT after zero field cooling ($T = 10$ K, 34 K, 36 K and 60 K, from left to right)

SUMMARY

From muon spin rotation measurements on three sets of overdoped ($T_c = 64$ K), nearly optimized ($T_c = 90$ K) and underdoped ($T_c = 77$ K) $\text{Bi}_2\text{Sr}_2\text{CaCu}_2\text{O}_{8+\delta}$ single crystals, we have obtained evidence for a two-stage melting transition of the vortex matter under equilibrium conditions. Two marked changes in the ' μSR -lineshape' have been observed and related to transitions in the vortex state. The well-known transition at the higher temperature T_{dc} coincides with the IL, as determined from DC-magnetization measurements, and is related to the decoupling of the individual flux-lines which results in a pancake liquid state with reversible magnetic behavior. The second transition of the vortex state occurs at a temperature T_{ab} well below the IL. For all sets of Bi-2212 single crystals this transition is found to coincide with the second-peak effect as seen in the DC-magnetization measurements. We interpret this second transition as the intra-planar melting of the vortex structure which leads to a line-liquid state with irreversible magnetic behavior.

The experiments described herein have been performed at the Paul-Scherrer-Institute, Villigen, CH and TRIUMF, Vancouver, Canada. We thank these institutions and their support staff for continuing assistance. The financial support of the German BMFB and the DFG is gratefully acknowledged.

REFERENCES

1. G. Blatter *et al.*, *Rev. Mod. Phys.* **66**, 1125 (1994).
2. D.R. Nelson and H.S. Seung, *Phys. Rev. B* **39**, 9153 (1989); E.H. Brandt, *Phys. Rev. Lett.* **63**, 1106 (1989); A. Houghton *et al.*, *Phys. Rev. B* **40**, 6763 (1989).
3. P.L. Gammel *et al.*, *Phys. Rev. Lett.* **61**, 1666 (1988).
4. J.R. Clem, and M.W. Coffey, *Phys. Rev. B* **42**, 6209 (1990).
5. L.I. Glazman, and A.E. Koshelev, *Phys. Rev. B* **43**, 2835 (1991); L.L. Daemen *et al.*, *Phys. Rev. Lett.* **70**, 1167 (1993); Y.H. Li and S. Teitel, *Phys. Rev. B* **49**, 4136 (1994); S. Ryu *et al.*, *Phys. Rev. Lett.* **77**, 2300 (1996).
6. M.C. Hellerqvist *et al.*, *Physica C* **230**, 170 (1994); K. Kadowaki, *Physica C* **263**, 164 (1996); C.D. Keener *et al.*, *Phys. Rev. Lett.* **78**, 1118 (1997); D.T. Fuchs *et al.*, *Phys. Rev. Lett.* **80**, 4971 (1998).
7. S.L. Lee *et al.*, *Phys. Rev. Lett.* **71**, 3862 (1993); *ibid.*, **75**, 922 (1995); and *Phys. Rev. B* **55**, 5666 (1997); J.W. Schneider *et al.*, *Phys. Rev. B* **52**, 3790 (1995);
8. C. Bernhard *et al.*, *Phys. Rev. B* **52**, R7050 (1995).
9. W.K. Dawson *et al.*, *J. Appl. Phys.* **64**, 5803 (1988).
10. A. Schenck: *Muon Spin Rotation Spectroscopy*, Bristol, Adam Hilger, 1985.
11. E.H. Brandt, *Phys. Rev. B* **37**, 2349 (1988); E.H. Brandt, *J. Low Temp. Phys.* **73**, 355 (1988); E.H. Brandt, *Rep. Prog. Phys.* **58**, 1465 (1995).
12. T. Blasius *et al.*, to be published.
13. J. Eisenmenger *et al.*, *IEEE Trans. Appl. Supercond.* (to be published)
14. J. Schiessling *et al.*, to be published.
15. B.-U. Runge *et al.*, to be published.

Spin dynamics in high- T_C superconductors

Ph. Bourges¹, Y. Sidis¹, H.F. Fong², B. Keimer^{2,3}, L.P. Regnault⁴,
J. Bossy⁵, A.S. Ivanov⁶, D.L. Milius⁷, and I.A. Aksay⁷,

¹ *Laboratoire Léon Brillouin, CEA-CNRS, CE Saclay, 91191 Gif sur Yvette, France*

² *Department of Physics, Princeton University, Princeton, NJ 08544, USA*

³ *Max-Planck-Institut für Festkörperforschung, 70569 Stuttgart, Germany*

⁴ *CEA Grenoble, Département de Recherche Fondamentale sur la matière Condensée, 38054 Grenoble cedex 9, France*

⁵ *CNRS-CRTBT, BP 156, 38042 Grenoble Cedex 9, France*

⁶ *Institut Laue-Langevin, 156X, 38042 Grenoble Cedex 9, France*

⁷ *Department of Chemical Engineering, Princeton University, Princeton, NJ 08544 USA*

Abstract. Key features of antiferromagnetic dynamical correlations in high- T_C superconductors cuprates are discussed. In underdoped regime, the sharp resonance peak, occurring exclusively in the SC state, is accompanied by a broader contribution located around ~ 30 meV which remains above T_C . Their interplay may induce incommensurate structure in the superconducting state.

INTRODUCTION

Over the last decade, a great deal of effort has been devoted to show the importance of antiferromagnetic (AF) dynamical correlations for the physical properties of high- T_C cuprates and consequently for the microscopic mechanism responsible for superconductivity [1,2]. To elucidate how these electronic correlations are relevant, it is then necessary to put the spectral weight of AF fluctuations on a more quantitative scale. Inelastic neutron scattering (INS) provides essential information

on this matter as it directly probes the full energy and momentum dependences of the spin-spin correlation function. Recently, efforts have been made to determine them in absolute units by comparison with phonon scattering. The following definition, corresponding to $\frac{1}{3}$ of the total spin susceptibility, is used [3],

$$\chi^{\alpha\beta}(Q, \omega) = -(g\mu_B)^2 \frac{i}{\hbar} \int_0^\infty dt \exp^{-i\omega t} \langle [S_Q^\alpha(t), S_{-Q}^\beta] \rangle \quad (1)$$

Our results are then directly comparable with both Nuclear Magnetic Resonance (NMR) results and theoretical calculations. Here, some aspects of the spin dynamics obtained in a bilayer system will be presented in relation with recent results reported by other groups [4,5]. However, it is before useful to recall the main features of magnetic correlations in the $\text{YBa}_2\text{Cu}_3\text{O}_{6+x}$ (YBCO) system over doping and temperature [6–12].

ENERGY-DEPENDENCES

We first emphasize the energy dependence of the spin susceptibility at the AF wave vector, $Q_{AF} = (\pi, \pi)$, for $x \geq 0.6$ $Im\chi$ in the normal state is basically well described in the underdoped regime by a broad peak centered around $\simeq 30$ meV (see Fig. 1) [11]. Upon heating, the AF spin susceptibility spectral weight is reduced without noticeable renormalization in energy. Going into the superconducting state, a more complex line shape is observed essentially because a strong enhancement of the peak susceptibility occurs at some energy. This new feature is referred to as the resonance peak, as it is basically resolution-limited in energy (see e.g. [6,9,15]). With increasing doping, the resonant peak becomes the major part of the spectrum [11,12]. At each doping, the peak intensity at the resonance energy is characterized by a striking temperature dependence displaying a pronounced kink at T_C [13–15]. Therefore, this mode is a novel signature of the unconventional superconducting state of cuprates which has spawned a considerable theoretical activity. Most likely, the magnetic resonance peak is due to electron-hole pair excitation across the superconducting energy gap [9,11].

The resonance peak may or may not be located at the same energy as the normal state peak. Fig. 1 displays a case where both occurs at different energies. However, at lower doping, these two features are located around similar energies, $\hbar\omega \sim 30$ –35 meV for $x \sim 0.6$ –0.8 [11,12,14]. Indeed, the resonance energy more or less scales with the superconducting temperature transition [11–14] whereas the normal state maximum does not shift much over the phase diagram for $x \geq 0.6$ [11,12].

In Fig. 1, the broad contribution, maximum around ~ 30 meV at $T=100$ K, is still discernible in the superconducting state in addition to the sharp resonance peak as a shoulder around ~ 35 meV. Below T_C , the energy shape of $Im\chi$ looks indeed more complex as the low energy spin excitations are removed below a threshold, so-called spin gap [6,7,11,12], likely related to the superconducting gap itself. The non-resonant contribution has not received much attention so far. However, its

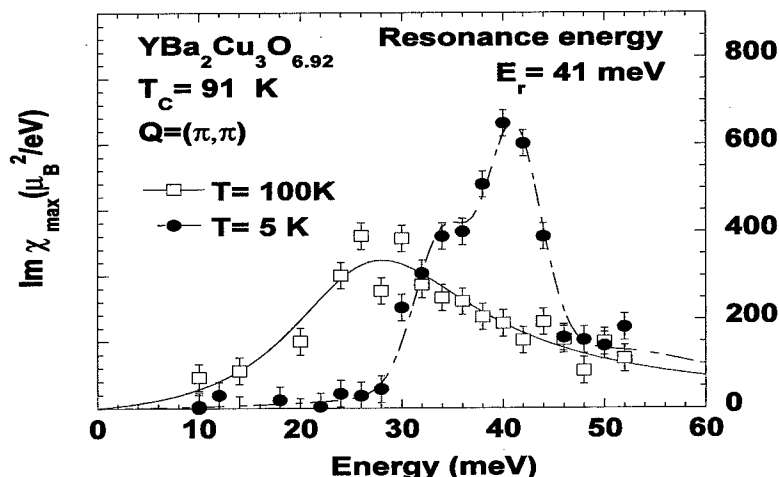


FIGURE 1. Low temperature (closed circles) and $T=100$ K (open squares) spin susceptibility at $Q = (\pi, \pi)$ in absolute units in $\text{YBCO}_{6.92}$ (2T-Saclay).

spectral weight in the normal state is important and may be crucial for a mechanism for the high- T_C superconductivity based on antiferromagnetism [2].

With increasing doping, the non-resonant contribution is continuously reduced, and becomes too weak to be measured in INS experiments in the overdoped regime YBCO_7 [7,9–11]. Using the same experimental setup and the same sample [7,11], no antiferromagnetic fluctuations are discernible in the normal state above the nuclear background. Consistently, in the SC state, an isolated excitation around 40 meV is observed corresponding to the resonance peak. Above T_C , an upper limit for the spectral weight can be given [10] which is about 4 times smaller than in $\text{YBCO}_{6.92}$ [11]. Assuming the same momentum dependence as in $\text{YBCO}_{6.92}$, it would give a maximum of the spin susceptibility less than $80 \mu_B^2/\text{eV}$ at (π, π) in our units. Therefore, even though YBCO_7 may be close to a Fermi liquid picture [11] with weak magnetic correlations, the spin susceptibility at $Q = (\pi, \pi)$ can still be ~ 20 times larger than the uniform susceptibility reported by macroscopic susceptibility or deduced from NMR knight shift measurements [2].

Therefore, $\text{Im}\chi$ is then naturally characterized in the superconducting state by two contributions having opposite doping dependences, the resonance peak becoming the major part of the spectrum with increasing doping. The discussion of $\text{Im}\chi$ in terms of two contributions has not been emphasized by all groups [15]. However, we would like to point out that this offers a comprehensive description consistent with all neutron data in YBCO published so far. In particular, it provides an helpful description of the puzzling modification of the spin susceptibility induced by zinc substitution [16,17] by noticing that, on the one hand, zinc reduces the resonant part of the spectrum and, on the other hand, it restores AF non-resonant correlations in the normal state [11]. Interestingly, the incommensurate peaks recently

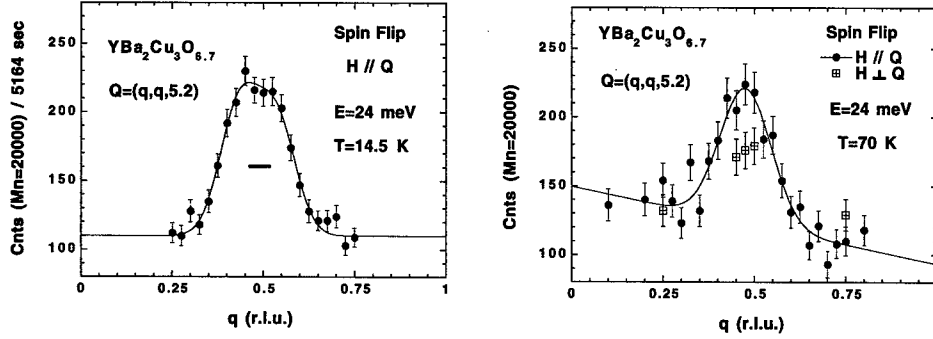


FIGURE 2. Spin-flip Q-scans at 24 meV along the (11) direction in $\text{YBCO}_{6.7}$ ($T_C = 67$ K): $T = 14.5$ K (right) and 70 K (left) (IN20-Grenoble). Polarized beam field was applied either parallel to Q (closed circles) or perpendicular to Q (dashed squares). The bar represents the q -resolution.

observed below the resonance peak in $\text{YBCO}_{6.6}$ [4,5,18] support the idea of two distinct contributions as the low energy incommensurate excitations cannot belong to the same excitation as the commensurate sharp resonance peak. However, these two contributions do not have to be considered as independent and superimposed excitations: the occurrence of the sharp resonance peak clearly affects the full energy shape of the spin susceptibility [6,11–15]. We shall see below that the q -shape of the spin susceptibility is actually also modified below T_C .

MOMENTUM-DEPENDENCES

In momentum-space, although both contributions are most generally peaked around the commensurate in-plane wavevector (π, π) , they exhibit different q -widths. The resonance peak is systematically related to a doping independent q -width, $\Delta q^{\text{reso}} = 0.11 \pm 0.02 \text{ \AA}^{-1}$ [8] (HWHM), and hence to a larger real space distance, $\xi = 1/\Delta q^{\text{reso}} \simeq 9 \text{ \AA}$ in real space. Recent data [15,14,18] agree with that conclusion. In contrast, the non-resonant contribution exhibits a larger and doping dependent q -width, so that, the momentum width displays a minimum versus energy at the resonance peak energy [8,14,18]. Interestingly, the non-resonant q -width scales with the superconducting temperature for a wide doping range [19].

Recently, in the underdoped regime $x = 0.6$, Dai et al [4] reported low temperature q -scans at $\hbar\omega = 24$ meV which were peaked at an incommensurate wavevector. Later, Mook et al [5] have detailed the precise position of these features, displaying a complex structure of the incommensurability with a squared-like shape with more intense four corners at $Q = (\pi, \pi(1 \pm \delta))$ and $Q = (\pi(1 \pm \delta), \pi)$ with $\delta = 0.21$. Interestingly, the energy at which this structure is reported is systematically located in a small energy range below the resonance energy, $E_r = 34$ meV [15,18]. Further, this structure is only clearly observed at temperatures below T_C . In the

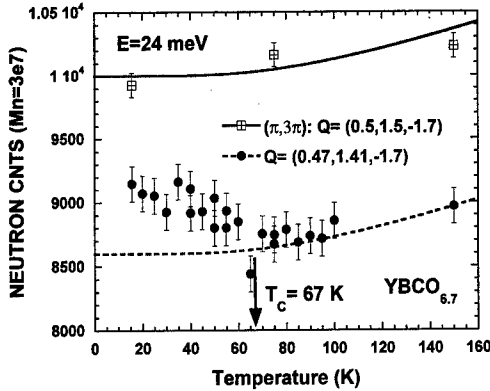


FIGURE 3. Temperature dependence of unpolarized neutron intensity at $\hbar\omega = 24$ meV in $\text{YBCO}_{6.7}$ at commensurate position (dashed squares) and at the incommensurate wavevector (closed circles) ($k_F = 3.85 \text{ \AA}^{-1}$, 2T-Saclay). Lines are guide to the eye to sketch for the temperature evolution of the nuclear background.

normal state, its existence remains questionable owing to background subtraction difficulties in such unpolarized neutron experiments [5,18]. A broad commensurate peak is unambiguously recovered above 75 K in polarized beam measurements [15].

To clarify the situation, we have performed a polarized neutron triple-axis experiment on an underdoped sample $\text{YBCO}_{6.7}$ with $T_C = 67$ K [13]. The experiment was carried out on IN20 at the Institut Laue Langevin (Grenoble) with a final wavevector $k_F = 2.662 \text{ \AA}^{-1}$ (experimental details will be reported elsewhere). Fig. 2 displays q-scans at $\hbar\omega = 24$ meV in the spin-flip channel at two temperatures: $T = 14.5$ K and $T = T_C + 3$ K. The polarization analysis, and especially the comparison of the two guide field configurations ($H \parallel Q$ and $H \perp Q$), allows unambiguously to remove the phonon contributions [10]. Surprisingly, the magnetic intensity is basically found commensurate at both temperatures. Tilted goniometer scans have been performed to pass through the locus of the reported incommensurate peaks [5]: less magnetic intensity is measured there meaning that there is no clear sign of incommensurability in that sample. However, Fig. 2 shows different momentum shapes at both temperatures: a flatter top shape is found at low temperature indicating that the momentum dependence of the spin susceptibility evolves with temperature. Fig. 3 underlines this point as it displays the temperature dependence of the intensity at both the commensurate wavevector and at the incommensurate positions (along the (130) direction as reported in Ref. [4]). Two complementary behaviors are found: at the commensurate position, the peak intensity is reduced at T_C [15] whereas at the incommensurate position the intensity increases at a temperature which likely corresponds to T_C . As quoted by Dai *et al* [4], on cooling below T_C , the spectrum rearranges itself with a suppression at the commensurate point accompanied by an increase in intensity at the incommensurate positions.

Therefore, even though our $\text{YBCO}_{6.7}$ sample does not exhibit well-defined incommensurate peaks, quite similar temperature dependences are observed in both samples. Superconductivity likely triggers a redistribution of the magnetic response in momentum space, that may marginally result in an incommensurate structure

in a narrow energy range. Interestingly, the sharp resonance peak simultaneously occurs. Thus, superconductivity affects the spin susceptibility shape in **both** the momentum and the energy spaces. Then, the interplay between the resonant and the non-resonant contributions may induce the incommensurate structure. In this respect, the magnetic incommensurability found in $\text{La}_{2-x}\text{Sr}_x\text{CuO}_4$ would have a different origin as the wavevector dependence of $\text{Im}\chi$ in LSCO remains essentially the same across the superconducting transition [20].

CONCLUDING REMARKS

Energy and momentum dependences of the antiferromagnetic fluctuations in high T_C cuprates YBCO have been discussed. The sharp resonance peak occurs exclusively below T_C . It is likely an intrinsic feature of the copper oxides as it has been, recently, discovered in $\text{Bi}_2\text{Sr}_2\text{CaCu}_2\text{O}_{8+\delta}$ [21]. This resonance peak is accompanied in underdoped samples by a broader contribution remaining above T_C .

REFERENCES

1. N. Nagaosa, *Science*, **275**, 1078, (1997); B. Batlogg *et al.*, *Nature*, **382**, 20.
2. D. Pines, *Z. Phys. B*, **103**, 129 (1997).
3. P. Bourges, *et al.*, *Phys. Rev. B*, **56**, R11439, (1997) (cond-mat/9704073).
4. P. Dai, *et al.*, *Phys. Rev. Lett.* **80**, 1738, (1998) (cond-mat/9707112).
5. H.A. Mook, *et al.*, *Nature*, **395**, 580, (1998).
6. J. Rossat-Mignod, *et al.*, *Physica C*, **185-189**, 86, (1991).
7. L.P. Regnault, *et al.*, *Physica C*, **235-240**, 59, (1994); *Physica B*, **213&214**, 48, (1995).
8. P. Bourges, *et al.*, *Physica B*, **215**, 30, (1995); *Phys. Rev. B*, **53**, 876, (1996).
9. H. F. Fong, *et al.*, *Phys. Rev. Lett.*, **75**, 316 (1995).
10. H.F. Fong, *et al.*, *Phys. Rev. B*, **54**, 6708 (1996).
11. P. Bourges in *The gap Symmetry and Fluctuations in High Temperature Superconductors* Edited by J. Bok, G. Deutscher, D. Pavuna and S.A. Wolf. 357-379 (Plenum Press, 1998) (cond-mat/9901333).
12. L.P. Regnault *et al.*, in *Neutron Scattering in Layered Copper-Oxide Superconductors*, Edited by A. Furrer, 85 (Kluwer, Amsterdam, 1998).
13. H.F. Fong, *et al.*, *Phys. Rev. Lett.* **78**, 713 (1997).
14. P. Bourges *et al.*, *Europhys. Lett.* **38**, 313 (1997).
15. P. Dai, *et al.*, *Phys. Rev. Lett.* **77**, 5425, (1996).
16. Y. Sidis *et al.*, *Phys. Rev. B* **53**, 6811 (1996).
17. H.F. Fong, *et al.*, *Phys. Rev. Lett.*, **82**, 1939 (1999) (cond-mat/9812047).
18. M. Arai, T. Nishijima, Y. Endoh, T. Egami, K. Tomimoto, *et al.*, preprint (1999).
19. A.V. Balatsky and P. Bourges (cond-mat/9901294) to appear in *Phys. Rev. Lett.*
20. T.E. Mason, *et al.*, *Phys. Rev. Lett.*, **71**, 919, (1993).
21. H.F. Fong, *et al.*, *Nature*, **398**, 588, (1999).

1/8 Doping Anomalies and Oxygen Vacancies in Underdoped Superconducting Cuprates

Joshua L. Cohn

Department of Physics, University of Miami, Coral Gables, FL 33124

Abstract. Measurements of thermal conductivity (κ) versus temperature and doping for several cuprate superconductors are discussed. Suppressed values of the normal-state κ and the slope change in κ at T_c , observed near 1/8 doping in both $\text{YBa}_2\text{Cu}_3\text{O}_{6+x}$ and Hg cuprates, are attributed to local lattice distortions and the suppression of the superconducting condensate, respectively. Both phenomena are proposed to arise from small domains of localized planar holes, presumably a manifestation of phase separation. It is suggested that the phase behavior of κ reflects stripe dynamics and the 1/8 doping anomalies stripe pinning by oxygen-vacancy clusters.

INTRODUCTION

There is mounting experimental evidence that novel charge- and spin-ordered phases are generic to underdoped cuprates [1]. The doped holes in Nd-doped $\text{La}_{1-x}\text{Sr}_x\text{CuO}_4$ segregate into periodic stripes that separate antiferromagnetically ordered, hole-poor domains. Lattice distortions pin these stripes, and this pinning is most effective for planar hole concentrations near $p=1/8$ where the stripe modulation wavelength is commensurate with the lattice. In the absence of pinning, stripe modulations are presumed to be fluctuating and/or disordered, and this is the emerging picture for $\text{La}_{1-x}\text{Sr}_x\text{CuO}_4$ (La-214) and $\text{YBa}_2\text{Cu}_3\text{O}_{6+x}$ (Y-123) [2]. We have recently demonstrated, through measurements of thermal conductivity (κ) [3], that both Y-123 and $\text{HgBa}_2\text{Ca}_{m-1}\text{Cu}_m\text{O}_{2m+2+\delta}$ [Hg-12($m-1$) m , $m=1, 2, 3$] exhibit doping anomalies near $p=1/8$ that can be attributed to the presence of localized charge and associated lattice distortions. Here we discuss the oxygen doping behavior of the anomalies in Hg cuprates and present new results on vacancy-free Ca-doped $\text{YBa}_2\text{Cu}_4\text{O}_8$ (Y-124) that suggest elastic properties may reflect stripe dynamics and stripe fragments may pin near oxygen-vacancy clusters.

The $p=1/8$ features (Fig. 1) are evident in the doping behavior of the normal-state thermal resistivity, $W = 1/\kappa$, and the normalized change in temperature derivative of κ that occurs at T_c , $\Gamma \equiv -d(\kappa^s/\kappa^n)/dt|_{t=1}$ [$t = T/T_c$ and $\kappa^s(\kappa^n)$ is the thermal conductivity in the superconducting (normal) state]. For Y-123, there is

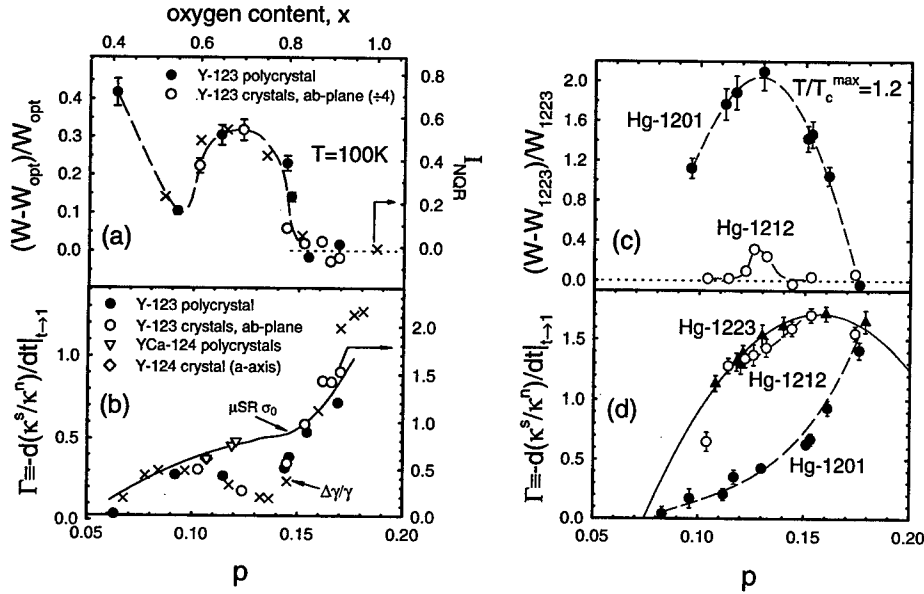


FIGURE 1. (a) Thermal resistivity at $T=100\text{K}$ relative to that at $p_{opt} = 0.16$ for Y-123 polycrystals and the ab-plane of single crystals [4] [$W_{opt} = 0.21 \text{ mK/W}$ (0.08 mK/W) for the polycrystal (crystals)]. The hole concentration per planar Cu atom, p , was determined from thermopower measurements and the empirical relations with bond valence sums 59 established by Tallon *et al.* [5]. Also plotted (\times 's) is the relative intensity of anomalous ^{63}Cu NQR signals [6]. The dashed curve is a guide to the eye. (b) The normalized slope change in $\kappa(T)$ at T_c vs doping for each of the Y-123 specimens in (a), for the a-axis of single-crystal Y-124 [7], and for polycrystal $\text{Y}_{1-x}\text{Ca}_x\text{-124}$ [8]. The $\text{Y}_{1-x}\text{Ca}_x\text{-124}$ data are multiplied by 2.3 so that they coincide with the Y-124 crystal data at $x=0$. Solid (open) symbols are referred to the left (right) ordinate. Also shown (\times 's) are the normalized electronic specific heat jump [9], $\Delta\gamma/\gamma$, and (solid curve) the μSR depolarization rate [10] (in μs^{-1}), divided by 1.4 and 2.7, respectively, and referred to the right ordinate. (c) Thermal resistivity for Hg-1201 and Hg-1212 polycrystals relative to that of Hg-1223 [3]. Dashed curves are guides. (d) The normalized slope change in $\kappa(T)$ at T_c vs doping for Hg cuprates. The solid line is $1.71 - 250(p - 0.157)^2$. Dashed curves are guides.

a compelling correlation of $W(p)$ and $\Gamma(p)$ with the doping behavior of anomalous ^{63}Cu NQR spectral weight [6], attributed to localized holes, and the electronic specific heat jump [9], $\Delta\gamma/\gamma$, respectively [crosses in Fig.'s 1 (a) and (b)]. Thus W probes lattice distortions associated with localized holes, and Γ the change in low-energy spectral weight induced by superconductivity.

Since both Γ and $\Delta\gamma/\gamma$ provide bulk measures of the superfluid volume, it is significant that the muon spin rotation (μSR) depolarization rate [σ_0 in Fig. 1

(b)], proportional to the superfluid density, exhibits no anomalous behavior near $1/8$ doping. The μ SR signal originates in regions of the specimen where there is a flux lattice. The apparent discrepancy between σ_0 and Γ or $\Delta\gamma/\gamma$ is resolved if the material is inhomogeneous, composed of non-superconducting clusters embedded in a superconducting network. The suppression of Γ and $\Delta\gamma/\gamma$ below the scaled σ_0 curve in Fig. 1 (a) are then measures of the non-superconducting volume fraction. Taken together, the W and Γ data imply that the non-superconducting regions are comprised of localized holes and associated lattice distortions, i.e. polarons. It is plausible that these hole-localized regions are stripe domains akin to those inferred from neutron scattering [1]. That they produce lattice thermal resistance implies they are static on the timescale of the average phonon lifetime, estimated as a few ps in the ab-plane of Y-123 [3]. Given that T_c is not substantially suppressed near $p=1/8$ implies that these regions do not percolate, and thus the picture is one of small clusters of localized holes and their associated lattice distortions, perhaps no larger than the stripe unit cell ($2a \times 8a$ where a is the lattice constant [1]), separated by a distance comparable to the phonon mean free path (about $100\text{\AA} \sim 25a$ at 100K).

For the Hg materials the $p=1/8$ enhancement of W and suppression of Γ is most prominent in single-layer Hg-1201, less so in double-layer Hg-1212, and absent or negligible in three-layer Hg-1223. This trend follows that of the oxygen vacancy concentration: a single HgO_δ layer per unit cell contributes charge to m planes in $\text{Hg-12}(m-1)m$ so that the oxygen vacancy concentration, $1 - \delta$, increases with decreasing m [11]. The absence of suppression in Γ near $1/8$ doping for Hg-1223 [Fig. 1 (d)] suggests that this material has sufficiently few localized-hole domains that their effects in W and Γ are unobservable. Thus we employ the Hg-1223 $W(p)$ data as a reference and plot the differences for the other two compounds in Fig. 1 (c). Comparing Fig.'s 1 (c) and (d) we see that for both Hg-1201 and Hg-1212 W is enhanced and Γ is suppressed relative to values for Hg-1223 in common ranges of p , with maximal differences near $p=1/8$.

STRIPES ALTER THE PHONON DISPERSION?

That $1/8$ doping anomalies are observed in both Y-123 and Hg cuprates suggests they are a generic feature of underdoped CuO_2 planes. In this context the doping behavior of κ for Hg-1223 [Fig. 2 (a)] is of interest since it presumably approximates the phase behavior in the absence of localized holes. We expect the electronic contribution, κ_e , to increase smoothly with increasing p . The upturn in κ above optimal doping ($p=0.16$) is presumably attributable to this rising κ_e . The most reliable estimate of κ_e in the cuprates comes from thermal Hall conductivity measurements [12] on Y-123 which imply $\kappa_e/\kappa \simeq 0.1$ for in-plane heat conduction near optimal doping. The data in Fig. 1 (a), (b) suggest that this ratio is roughly the same in polycrystals, thus motivating the dotted and dashed curves in Fig. 2 (a) as an educated guess for the electronic and lattice terms, respectively, in Hg-1223.

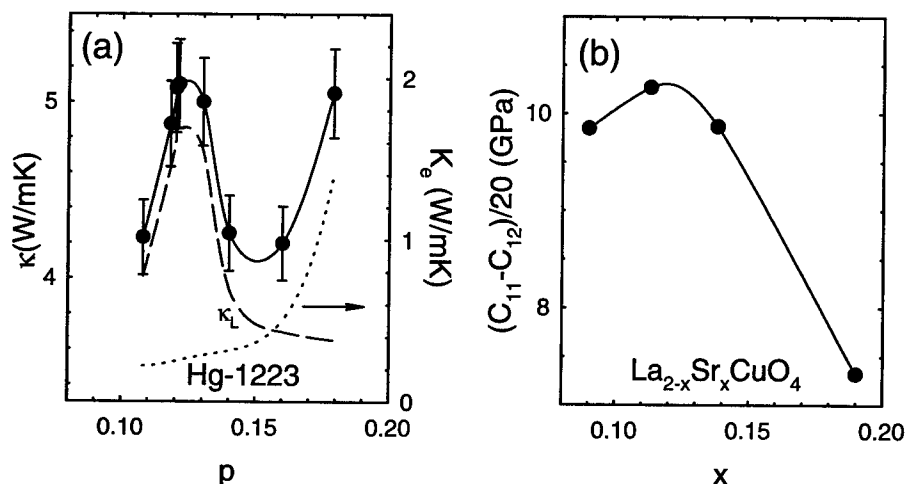


FIGURE 2. (a) Thermal conductivity of Hg-1223 polycrystal versus doping. The dotted and dashed curves are proposed electronic (right ordinate) and lattice thermal conductivities, respectively. The solid line is a guide to the eye. (b) sound velocity data for single-crystal La-214 from Ref. [13].

The lattice conductivity, $\kappa_L = \kappa - \kappa_e$, predominates in the underdoped regime and is peaked near $p=1/8$.

There is experimental support for the proposal that this peak in κ is associated with doping-dependent changes in the phonon dispersion which are generic to underdoped cuprates. Figure 2 (b) shows the behavior of the normal-state, transverse shear elastic constant (proportional to the square of the sound velocity) for single-crystal La-214 [13], the only material for which doping-dependent measurements for all the main symmetry directions have been reported to our knowledge. A substantial hardening of the lattice in the underdoped regime, with a maximum near $p = x \simeq 1/8$, was observed for all symmetries, indicating that the changes with doping are systemic.

It is possible that the phase behavior of the elastic constants for La-214 and κ_L for Hg-1223 reflect a renormalization of the lattice dispersion due to changes in stripe dynamics with doping. At $p=1/8$ the stripes are maximally commensurate with the lattice, and their fluctuations should be minimal. Enhanced fluctuations are to be expected at higher doping, due to the destabilizing role of repulsive interactions in stripes that neutron scattering results (Yamada *et al.* [2]) suggest, are charge compressed. For $p < 1/8$, the cluster spin-glass state observed by μ SR studies [14] is characterized by increasing magnetic disorder with decreasing p in the range

$0.08 < p < 0.12$, possibly associated with increasing disorder [15] in the stripe period. It is plausible that disorder in the stripe system at both higher and lower doping about $p=1/8$ induces a softening of the lattice that is reflected in Fig. 2. Theoretical investigations of elastic coupling to the stripe system would certainly be of interest.

OXYGEN VACANCIES AND $1/8$ ANOMALIES

Returning now to the enhancement of W and suppression of Γ near $p=1/8$, our measurements suggest these phenomena reflect stripe pinning (or reduced stripe fluctuations) associated with oxygen vacancy clusters. Raman studies of defect modes in the Hg materials [16] provide a measure of the density of vacancy clusters. The 590 cm^{-1} Raman mode in Hg cuprates is attributed to c-axis vibrations of apical oxygen in the presence of oxygen vacancies on each of the four nearest-neighbor sites in the HgO_8 layers. The amount by which the thermal resistivity and Γ values of Hg-1201 and Hg-1212 differ from those of Hg-1223 at $p=1/8$ both correlate well with the integrated oscillator strength of this vibrational mode normalized by that of the 570 cm^{-1} mode (Fig. 3), the latter attributed to apical vibrations in the presence of fewer than four vacancies, and common in the spectra [16] of all three Hg materials. We infer that oxygen-vacancy clusters, of size four or more in the Hg cuprates, can pin a stripe fragment.

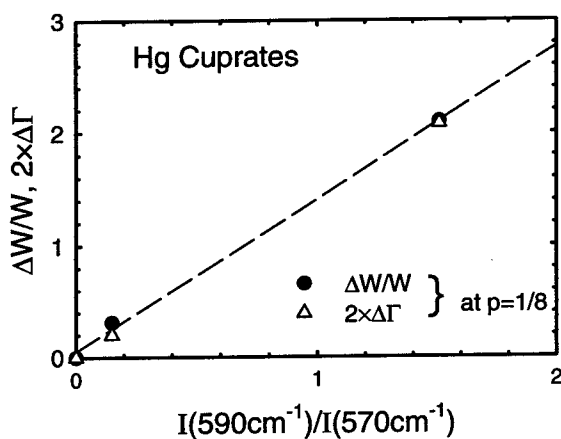


FIGURE 3. (a) The enhancement in thermal resistivity and suppression in Γ for the Hg compounds at $p=1/8$, relative to values for Hg-1223, plotted versus the oscillator strength ratio of Raman-scattering defect modes (Ref. [16]).

Supporting the role of oxygen vacancies in the observed $1/8$ features for Y-123 are our recent measurements on oxygen-stoichiometric $Y_{1-x}Ca_x$ -124 [8]. The Γ values for $x=0, 0.10, 0.15$ are plotted in Fig. 1 (b). There is no evidence for suppression of Γ near $1/8$ doping, and the data follow the scaled μ SR curve quite well. Within the context of the interpretation we have outlined, we conclude that Ca substitution for Y (at the level of $\leq 15\%$) is not as effective in stripe pinning as are oxygen vacancy clusters. It remains to be determined by what mechanism these clusters induce pinning.

ACKNOWLEDGEMENTS

This work was supported by NSF Grant No. DMR-9631236.

REFERENCES

1. J. M. Tranquada *et al.*, Nature **375**, 561 (1995); Phys. Rev. Lett. **78**, 338 (1997); T. Suzuki *et al.*, Phys. Rev. B **57**, R3229 (1998).
2. J. M. Tranquada, J. Phys. Chem. Solids **59**, 2150 (1998); H. Mook *et al.*, Nature **395**, 580 (1998); P. Dai *et al.*, Phys. Rev. Lett. **80**, 1738 (1998); K. Yamada *et al.*, Phys. Rev. B **57**, 6165 (1998).
3. J. L. Cohn *et al.*, Phys. Rev. B **59**, 3823 (1999).
4. C. P. Popoviciu and J. L. Cohn, Phys. Rev. B **55**, 3155 (1997); J. L. Cohn, *ibid.* **53**, R2963 (1996).
5. J. L. Tallon *et al.*, Phys. Rev. B **51**, 12911 (1995).
6. P. C. Hammel and D. J. Scalapino, Phil. Mag. **74**, 523 (1996); H. Yasuoka *et al.*, Phase Trans. **15**, 183 (1989).
7. J. L. Cohn and J. Karpinski, Phys. Rev. B **58**, 14617 (1998).
8. J. L. Cohn *et al.*, unpublished.
9. J. W. Loram *et al.*, Phys. Rev. Lett. **73**, 1721 (1993).
10. Y. J. Uemura *et al.*, Phys. Rev. Lett. **66**, 2665 (1991); J. L. Tallon *et al.*, *ibid.* **74**, 1008 (1995).
11. O. Chmaissem *et al.*, Physica C **217**, 265 (1993); E. V. Antipov *et al.*, *ibid.* **218**, 348 (1993); Q. Huang *et al.*, Phys. Rev. B **52**, 462 (1995).
12. K. Krishana *et al.*, Phys. Rev. Lett. **75**, 3529 (1995).
13. S. Sakita *et al.*, Physica B **219-220**, 216 (1996); M. Nohara *et al.*, Phys. Rev. B **52**, 570 (1995).
14. Ch. Niedermayer *et al.*, Phys. Rev. Lett. **80**, 3843 (1998).
15. S. A. Kivelson and V. J. Emery, cond-mat/9809082.
16. X. Zhou *et al.*, Phys. Rev. B **54**, 6137 (1996).

Low-energy electronic structure in $\text{Y}_{1-x}\text{Ca}_x\text{Ba}_2\text{Cu}_3\text{O}_{7-\delta}$: comparison of time-resolved optical spectroscopy, NMR, neutron and tunneling data.

J.Demsar, K.Zagar, V.V.Kabanov and D.Mihailovic
"J.Stefan Institute", Jamova 39, 1001 Ljubljana, Slovenia;
contact:dragan.mihailovic@ijs.si

Abstract. Time-resolved optical measurements give information on the quasiparticle relaxation dynamics in YBCO, from which the evolution of the gap with doping and temperature can be systematically deduced. In this paper these optical charge-channel "pseudogap" data are compared with the "pseudogap" obtained from the NMR Knight shift K_s , spin polarized neutron scattering (SPNS) and single particle tunneling measurements. A simple energy level diagram is proposed to explain the different "gap" magnitudes observed by different spectroscopies in $\text{YBa}_2\text{Cu}_3\text{O}_{7-\delta}$, whereby the spin gap Δ_s in NMR and SPNS corresponds to a triplet local pair state, while Δ_p in the charge excitation spectrum corresponds to the pair dissociation energy. At optimum doping and in the overdoped state, an additional T -dependent gap becomes evident, which closes at T_c , suggesting a cross-over to a more conventional BCS-like superconductivity scenario.

I INTRODUCTION

Spectroscopic studies of cuprates over the years have shown that at low energies these materials exhibit quite a complex spectral structure, which changes with temperature and doping in a complicated way. Often there appears to be reasonable agreement regarding some of the main features between various experimental techniques. For example, optical femtosecond quasiparticle relaxation measurements and single-particle (Gievers) tunneling show a similar size pseudogap in the spectrum over a large portion of the phase diagram, and the latter is remarkably similar to the spectral features measured by angle-resolved photoemission. However, the pseudogap Δ_s as observed by spectroscopies like NMR and spin-polarized neutron scattering appears to be smaller than the optical and tunneling pseudogap Δ_p by approximately a factor of 2, for which there is as yet no accepted theoretical explanation. Thus in spite of the availability of spectral data over a large range of doping in many materials, the interpretation of the low-energy excitation spectrum is still highly controversial. In this paper we summarize some of the results of

time-resolved quasiparticle recombination spectroscopy as a function of doping and temperature in $\text{YBa}_2\text{Cu}_3\text{O}_{7-\delta}$, which appear to give qualitative new insight into the origin of the low-energy spectral features of this material and its phase diagram. We compare the doping-evolution of the pseudogap Δ_p obtained from time-resolved spectroscopy with a quantitative analysis of the "spin-gap" from the NMR knight shift K_s in the underdoped state using the same type of T -independent gap as deduced from the quasiparticle relaxation data. We find that the time-resolved QP relaxation data are quite consistent with Giever tunneling and ARPES data and suggest that all the observations together can be explained by the existence of a pair-breaking pseudogap Δ_p and a triplet-state local pair excitation Δ_s at $E \approx \Delta_p/2$.

II TIME-RESOLVED SPECTROSCOPY RESULTS

The time-resolved optical spectroscopy applied to superconductors and other materials with a gap has been given in detail elsewhere [1,2], so here we shall discuss only the results. The equations describing the temperature dependence of photoexcited QP density and their lifetime as a function of temperature are given by Kabanov et al [1]. Using these equations, the properties of the gap can be investigated as a function of doping and temperature. Systematic experiments on

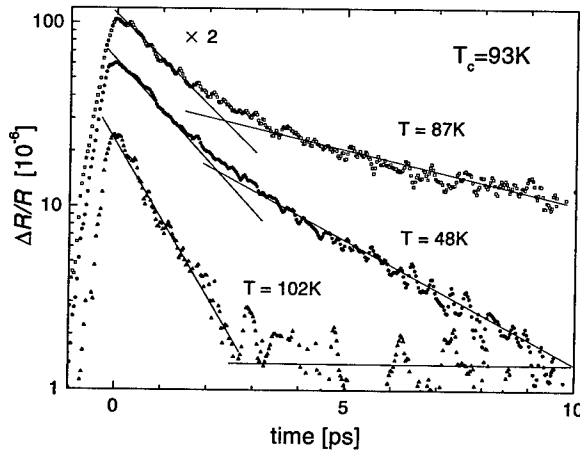


FIGURE 1. The photoinduced reflectivity in $\text{YBa}_2\text{Cu}_3\text{O}_{6.95}$ showing the two-component relaxation below T_c attributed to the two gaps Δ_p and Δ_{BCS} .

YBaCuO as a function of O concentration over a wide range of δ have shown very clear and systematic behavior of the QP dynamics [1]. Particularly important is that the results are quite insensitive to surface quality and have been repeated after a period of a year with the same results. Single crystals were also studied and no

significant differences were found in comparison with the thin film data. These measurements have recently been extended to the overdoped state using calcium-doped $(Y,Ca)Ba_2Cu_3O_{7-\delta}$ crystals by Demsar et al [2], giving data on the whole phase diagram from insulating and underdoped to overdoped YBCO. A typical time-resolved signal in the optimally doped phase is shown in Figure 1. Above T_c , one exponential short-lived decay is observed whose amplitude is decreasing as T is increased (Figure 2), while below T_c , two exponentials are clearly seen, one of which has a longer lifetime which is temperature-dependent and diverges as $T \rightarrow T_c$. Such behaviour is typical also for overdoped samples, but not for underdoped samples, where only a single exponential decay is observed, with a T -independent time constant $\tau_p \sim 0.4$ ps showing no anomaly at T_c . From these experiments we can deduce that in underdoped state the evolution of the QP dynamics with temperature and doping is dominated by a temperature-independent pseudogap Δ_p . Near optimum doping an *additional* BCS-like temperature-dependent gap Δ_{BCS} appears below T_c , which is present also in all the overdoped samples [2] and gives rise to the additional temperature-dependent relaxation process below T_c .

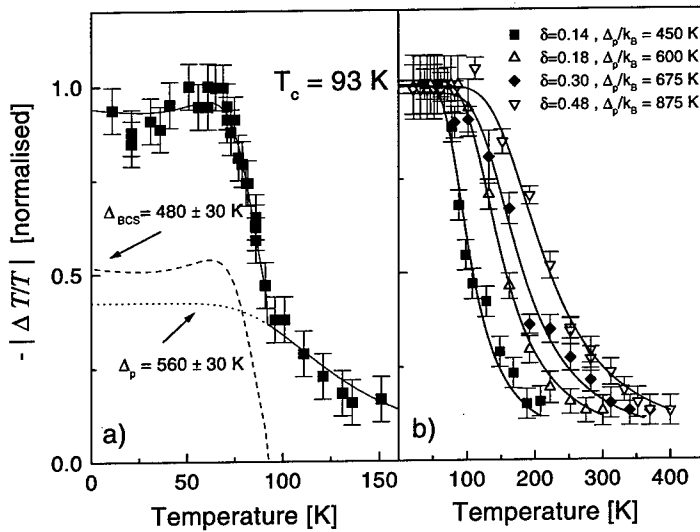


FIGURE 2. The amplitude of the photoinduced absorption (PIA) as a function of temperature for optimally doped $YBa_2Cu_3O_{7-\delta}$ ($\delta \sim 0.05$). Overdoped samples with substituted Ca for Y show similar 2-component T -dependence for all Ca concentrations. b) The temperature dependence of the PIA for underdoped $YBa_2Cu_3O_{7-\delta}$ ($\delta > 0.15$). The lines are the theoretical fits to the data [Ref. 1] with Δ_p or $\Delta_{BCS}(T = 0K)$ as the only fitting parameter.

The fact the τ diverges near T_c unambiguously signifies that $\Delta_{BCS} \rightarrow 0$ at T_c . Thus close to optimum doping and in the overdoped state two gaps appear to be present simultaneously, a feature consistent with the spatially inhomogeneous

ground state [3] in which the pair-breaking excitation is represented by Δ_p , while the Δ_{BCS} is a gap associated with the collective behaviour of high-carrier density stripes or clusters which start to form near optimum doping. The values of the gaps Δ_p and Δ_{BCS} as a function of doping obtained by fitting the temperature dependence of the photoinduced signal amplitude as shown in Fig. 2 with the model calculation of Kabanov et al [1] are plotted in Figure 4.

III COMPARISON WITH OTHER SPECTROSCOPIES

From the time-resolved data on the underdoped YBCO we have deduced that the low-energy spectrum can be described by a single *temperature-independent gap* Δ_p . Starting from this observation we decided to analyse the temperature dependence of the NMR Knight shift K_s available from the literature using the same T -independent Δ_p . The aim is a) to see if the simple model can describe the T -dependence of K_s and b) to see if the values of the pseudogap obtained for the NMR K_s agree with the optical values. The NMR knight shift for such a case can be written as [4] $K_s = K_0 + AT^{-\beta} \exp[-\Delta_s/k_B T]$, where K_0 is the value of K_s at zero temperature, β is an exponent which depends on the shape of the singularity of the DOS at the gap and A is a constant depending on the NMR nucleus.

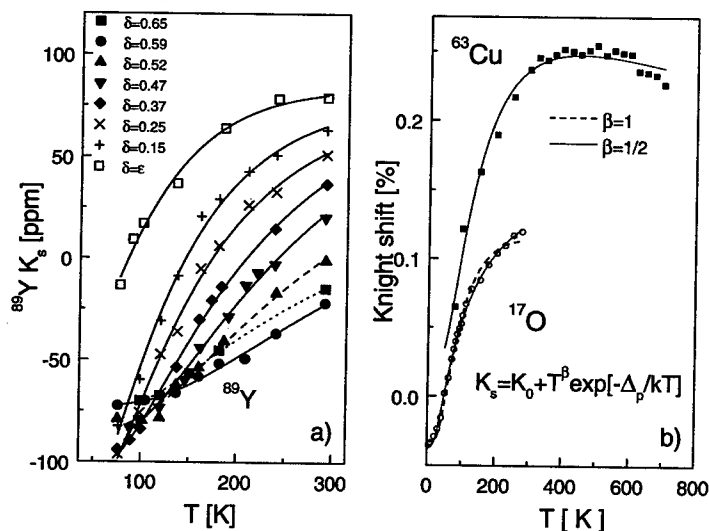


FIGURE 3. The ^{89}Y NMR Knight shift K_s as a function of temperature in YBa₂Cu₃O_{7- δ} for different δ [5]. b) K_s as a function of temperature in YBa₂Cu₄O₈ ($T_c=81$ K). The solid squares data are for ^{63}Cu from Curro et al [6] and the open circles for ^{17}O from Williams et al [7].

The results of fits to published data in YBCO 123 and 124 on ^{89}Y [5], ^{63}Cu [6] and ^{17}O [7] are shown in Figure 3 using $\beta = 1/2$. In spite of its simplicity, the

model appears to describe the data very well. The gap values Δ_s with $\beta = 1/2$ obtained for $\text{YBa}_2\text{Cu}_3\text{O}_{7-\delta}$ are shown in Figure 4. Δ_s appears consistently lower than the Δ_p by approximately a factor of 2.

Apart from NMR K_s , spin-polarized neutron scattering (SPNS) also shows a spin-excitation peak at 34 meV (~ 390 K) in underdoped $\text{YBa}_2\text{Cu}_3\text{O}_{6.6}$, which is smaller than Δ_p by approximately a factor of 2. However, the anomalies in the phonons signifying the presence of *charge* excitations occur near 70 meV (~ 810 K), also approximately twice the spin excitation energy and very close to the Δ_p in Fig. 4. (see Mook et al, this volume).

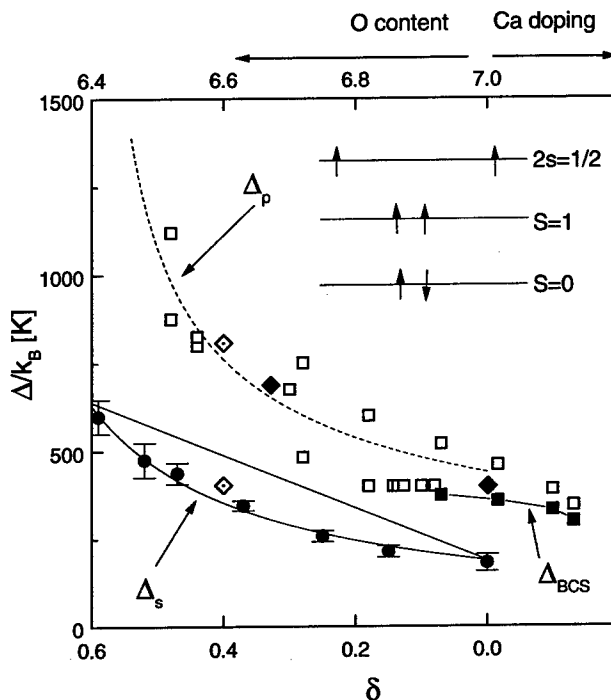


FIGURE 4. The energy gap(s) Δ_p and Δ_s and Δ_{BCS} as a function of doping. The open squares are from time-resolved QP relaxation [1,2]. The full circles are from NMR [5]. The open diamonds are the neutron data (H.Mook this volume), while the full diamonds are the tunneling data (G.Deutscher, this volume). The solid squares represent Δ_{BCS} from time-resolved data.

To explain the two different gaps Δ_p and Δ_s , we propose a rather straightforward electronic structure in YBCO. A schematic diagram is shown in the insert to Fig. 4. The ground state is composed of *local* $S=0$ singlet Cooper pairs. Since Δ_p is a QP charge excitation it is clearly associated with pair breaking. However, if $J < \Delta_p$, the triplet local pair state also exists and lies within the gap. It should be visible by spin-flip spectroscopies like NMR and SPNS, but not by optical spectroscopy

or SP tunneling which are charge excitations. We therefore propose that the Δ_s observed by NMR and SPNS is the $S=1$ *local pair* triplet excited state. From the experimental data in Fig. 4, both Δ_p and Δ_s decrease with increasing doping, more or less as $1/x$, where x is the hole density. For low doping, at $\delta \sim 0.6$, $J \approx 800\text{K}$, consistent with Raman and neutron measurements. We note that possibly the situation might be different in $\text{La}_{2-x}\text{Sr}_x\text{CuO}_4$, where the optical gap and the NMR gap appear to have the same energy scale [8], suggesting that either $J \gtrsim \Delta_p$ in this material or that the triplet pair state is not a bound state in this material.

In underdoped YBCO, at T_c there is no anomaly in either the QP relaxation [1] or the NMR K_s [5, 6]. Similarly the SPNS intensity at 34 meV shows no anomaly at T_c itself, but only a gradual drop with increasing T . From this we can deduce that there is no change in the DOS at T_c in the underdoped state, and that all changes of the DOS are gradual with T . This is equivalent to there being no condensation energy associated with the superconducting transition itself which is consistent with the Bose condensation of local pairs scenario, where at T_c macroscopic phase coherence is established with no change in pairing amplitude. A 3D superconducting state forms when phase coherence percolates through the entire sample resulting in a transition to a coherent macroscopic state at T_c . In contrast, in optimally doped and overdoped YBCO as the carrier density increases, the pairs begin to overlap, collective effects become important and a transition to a more conventional BCS-like scenario takes place [1]. QP relaxation, NMR K_s , SPNS and tunneling data all show an abrupt anomaly at T_c signifying that pairing and phase coherence occur at the same (or nearly the same) temperature.

The most important feature of the QP relaxation data not available from other spectroscopies is the simultaneous unambiguous observation of 2 gaps in optimally doped and overdoped samples, one T -independent Δ_p and the other T -dependent Δ_{BCS} , with a BCS-like T dependence.

REFERENCES

1. V.V.Kabanov, et al Phys.Rev.B **59**, 1497 (1999), J.Demsar et al, Europhys. Lett. **45**, 381 (1999)
2. J.Demsar, B. Podobnik, V.V. Kabanov, D. Mihailovic and T.Wolf, subm. to Phys. Rev. Lett (1998)
3. D.Mihailovic and K.A.Müller, p 243 "High- T_c Superconductivity 1996: Ten years after the Discovery" Ed. E.Kaldis, E.Liarokapis, K.A.Muller NATO Series E: Applied Sciences vol. **343** (Kluwer Academic Publishers 1997)
4. A.S.Alexandrov, V.V.Kabanov and N.F.Mott, Phys. Rev.Lett. **77**, 4796 (1996)
5. H.Alloul, T.Ohno, P.Mendels, Physica **162-164**, 193 (1989)
6. Curro et al, Phys.Rev. B **56**, 877 (1997)
7. Williams et al, Phys.Rev.Lett. **78**, 721 (1998)
8. K.A.Müller, Guo-meng Zhao, K.Conder and H.Keller, J.Phys.:Condens.Matter **10**, L291 (1998)

Study of Superfluid Condensation in the Cuprates by Andreev Reflections

Guy Deutscher

*School of Physics and Astronomy, Raymond and Beverly Sackler Faculty of Exact Sciences
Tel Aviv University, Ramat Aviv, Tel Aviv 69978, Israel*

Abstract. A brief review is given of the advantages of Andreev scattering in the study of unconventional superconductors such as the cuprates. The use of clean interfaces is made possible by the Point Contact method. Andreev scattering is sensitive to the presence of nodes in the order parameter, which has allowed for an easy check of its symmetry in a large number of cuprates. NdCeCuO and LaSrCuO near optimum doping are two interesting exceptions to a d-wave symmetry. Andreev scattering probes the coherence energy scale in the superconducting state, which has been found to be smaller than the single particle excitation energy gap in the underdoped regime. The implications of this result for current models of the pseudogap are discussed.

INTRODUCTION

The properties of Superconducting/Normal metal (S/N) contacts include two rather different phenomena: the proximity effect for clean and transparent interfaces, and tunneling for interfaces comprising strong dielectric barriers. The proximity effect may be conceived as the leakage of Cooper pairs from S to N, while tunneling describes the transfer of single particles from N into S. For an arbitrary interface, both phenomena coexist, the first one dominating below the gap, and the second one above the gap.

Excitations from N having an energy (measured from the Fermi level) smaller than Δ cannot propagate in S. Such a particle, upon hitting the interface, is reflected along the incoming trajectory as a particle of opposite charge, while a Cooper pair flows in the S side. This is known as the Andreev reflection, described in detail by Saint James (1). If N is in the form of a thin film of thickness d_n , these reflections lead to the formation of bound states having a finite energy above the Fermi level, roughly proportional to $(1/d_n)$. For ideally clean interfaces, Andreev reflections lead to an enhancement of the conductance of Point Contacts (PC) by a factor of two: for each incoming electron, a hole is reflected. This enhancement may also be understood as a reduction of the normal state resistance of the contact when one side is superconducting. Although somewhat naive, this explanation of the Andreev effect underlines that it is a macroscopic coherent quantum phenomenon. In the presence of an interface barrier, Andreev reflections produce a small subgap conductance.

Above the gap, the current returns for all interfaces to a single particle current. Hence, for a clean interface, the conductance at $E > \Delta$ is smaller than at $E < \Delta$. In the presence of a barrier, it is smaller. The character of the S/N interface is then easily established by a measurement of its $I(V)$ characteristic. Blonder, Tinkham and Klapwijk (BTK, 2) have calculated this characteristic for an arbitrary interface, characterized by a parameter Z ,

which includes the effect of a dielectric barrier as well as that of a mismatch of the Fermi velocities in N and S. When $Z < 1$, the characteristic is Andreev like, for $Z > 1$, it is Giaever like. The gap edge is identified in the first case by a decrease of the conductance, and in the second case by an increase.

Before presenting and discussing our results, we briefly review the respective properties of Andreev and tunneling contacts.

EXPERIMENTAL CONSIDERATIONS

Experimentally, each type of contact presents its own difficulties and advantages. At biases of the order of the gap, a large current density flows through an Andreev contact. It is in fact of the order of the depairing current. In order to avoid heating effects, the contact must be ballistic, namely its area must be smaller than the mean free path. It should therefore be in the submicron range. This can be achieved by the Point Contact method, as first shown by Sharvin (3). This method consists in driving carefully, with a micrometer screw, a sharpened point (Au for instance) into the superconductor, until a metallic contact is achieved. The practical advantage of the PC method is that it can be applied to all superconducting materials. Its main disadvantage is that the contacts are not very reproducible, and that they are not stable upon changing the temperature.

Tunneling, on the other hand, requires a pinhole free dielectric barrier, to avoid large subgap leakage currents. At the same time, the barrier must be thin enough to allow a significant tunneling current. In practice, very few materials are suitable to make such barriers. One of them is aluminium oxide. In the specific case of the HTS, oxide barriers are formed in fact by oxidizing the normal metal electrode through oxygen diffusion from the HTS material itself (4), whose probed surface is then necessarily underdoped. Because of the high sensitivity of the HTS properties to the oxygen content, and because of the fact that the superconductor is being probed over the depth of the coherence length, which is very short, this method is not suitable for the study of optimally doped (or *a fortiori* overdoped) samples. The use of PC is then the only one that can be used.

This is in contrast with the LTS metal superconductors, for which the tunneling method was the preferred one. In their case, the oxide barrier does not affect the properties of the metal, and furthermore the coherence length is so large that any surface deterioration does not affect the tunneling measurement.

ANDREEV REFLECTIONS IN THE HTS: INITIAL MOTIVATION AND RESULTS

Our initial motivation to use the PC spectroscopic method was twofold. The first one was to determine the gap value, as explained above, without modifying the oxygen content by the formation of a barrier. Secondly, the normal state conductance of the contact is by itself an excellent indication of one of the fundamental properties of the normal state of the HTS, namely the existence of a large Fermi surface. As already mentioned, a mismatch of the Fermi velocities between N and S is equivalent to an interface barrier. Furthermore, as shown by Deutscher and Nozieres (5), the effective velocities that determine this mismatch are not affected by the mass enhancement effects due to many body interactions. If the

HTS had no Fermi surface, or only a small one, the effective interface barrier would be so large as to put it in the large Z limit, even for a metallurgically clean interface. In other terms, the observation of an Andreev like characteristic is by itself sufficient proof of the existence of a large Fermi surface in the HTS (or other exotic superconductor) under investigation.

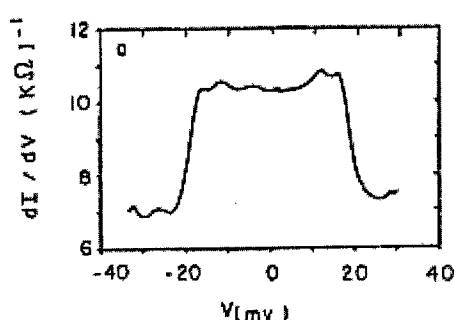


Fig.1. Andreev conductance for an in-plane Point Contact with optimally doped YBCO. The surface of the sample is perpendicular to the $[100]$ direction. The data is in good agreement with a d-wave order parameter and a gap value of about 20 meV (ref.6)

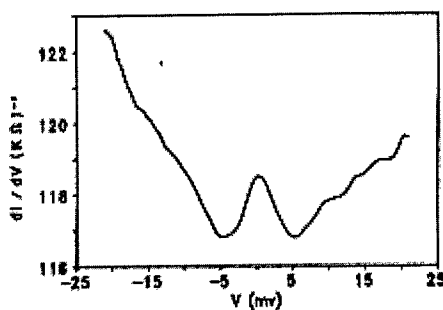


Fig.2. Conductance of a Point Contact with same sample as in Fig.1, but the surface being perpendicular to the $[001]$ direction. There are basically no Andreev reflections, due to the mismatch of the Fermi velocities.

Our first PC results, obtained on single crystal quality, optimally doped YBCO, showed that for interfaces perpendicular to the CuO planes, contacts were definitely in the Andreev limit (6). The ratio of the small to large bias conductances was repeatedly found to be close to 1.5. For a clean interface, this corresponds to a ratio of the Fermi velocities between the YBCO sample and the Au point of about 2, a modest mismatch. It must be outlined that this conclusion is reached based on a conductance *ratio*, and is independent of the effective contact area, generally not known. A rather sharp decrease of the conductance was observed at a bias value close to 20 meV, which was interpreted as the gap value (Fig.1). For interfaces parallel to the CuO planes, no Andreev like characteristic was observed, confirming the quasi two-dimensional character of the cuprate (Fig.2).

Yet, the interpretation of the detailed shape of the conductance characteristic presented two problems. BTK predict that for any finite barrier, the conductance should show a peak at the gap edge. Instead, the measured conductance is practically flat up to the gap edge. Also unexplained was a small conductance peak at small bias. We understand to day that these two features are due to the unconventional symmetry of the order parameter in YBCO which is predominantly d-wave, while the calculations of BTK applied to an s-wave order parameter.

ANDREEV REFLECTIONS AND ORDER PARAMETER SYMMETRY

It turns out that one of the main advantages of Andreev spectroscopy is that it gives us information on the anisotropy of the order parameter, including on its symmetry. The data shown Fig.1 was taken at a surface perpendicular to the [100] direction. For a clean contact ($Z < 1$) with a d-wave superconductor, the conductance peak at the gap edge is then suppressed (7). An even more spectacular effect of the d-wave symmetry occurs for the [110] orientation. As first shown by Hu (8), changes of sign of the order parameter around the Fermi surface give rise in that case to a sharp conductance maximum at zero bias.

Let us follow Hu (8) and consider the case of an order parameter having the $d_{x^2-y^2}$ symmetry, with the surface of the sample perpendicular to the [110] direction, covered by a normal layer of thickness d_n . An electron coming in from N at a 45° angle will be Andreev reflected as a hole by, say, a positive order parameter. This hole, after undergoing a normal reflection at the outer surface of N, will be Andreev reflected as an electron by a negative order parameter, and after a second normal reflection, the cycle will start again. During each cycle, the incoming normal excitation has seen opposite signs of the order parameter. They add up algebraically to a null value: the cycle can take place for an incoming particle having an energy arbitrarily close to the Fermi surface, irrespective of the value of d_n , which can be arbitrarily small. For a vanishing value of d_n , we have a surface bound state of zero energy.

When probed through a tunnel junction at the surface of the sample, surface bound states give rise to a zero bias conductance peak (ZBCP). This peak should not be observed for a surface perpendicular to the [100] direction, because in that case there is no sign reversal of the order parameter upon successive Andreev reflections. This is the geometry used in the measurement shown Fig.1. In practice, surface roughness effects cannot be ignored (9), and often gives rise to a small ZBCP for orientations where it should not occur, as seen Fig.1 and Fig.2. Large ZBCPs have indeed been reported in YBCO for the [110] orientation (10).

The study of Andreev reflections is a useful and practical way to test the universality of the d-wave symmetry in the cuprates. Besides YBCO, a ZBCP has also been reported in the Bi (11) and Hg (12) compounds. One notable exception is NdCeCuO (10). Another one is LaSrCuO (13) near optimum doping and at low temperatures, though underdoped ($T_c = 24\text{K}$). Grain boundary Junctions of this cuprate do show a ZBCP (14). No tri-junction interference experiment has been reported so far for these two cuprates.

ANDREEV AND GIAEVER ENERGY SCALES

The pseudo gap observed above T_c has been considered by some authors as a precursor of the superconducting gap below T_c . It is indeed a striking feature of photoemission (15) and tunneling (16) spectra that in the underdoped regime they do not show any significant change at T_c . If one accepts that experiments at $T \ll T_c$ do measure the superconducting gap, it follows that the pseudogap seen at $T \gg T_c$ must be a precursor effect. The pseudogap would then be the energy required to break local, uncondensed pairs (per particle), or more generally to destroy a pairing amplitude without phase coherence.

The assumption that the tunneling (or photoemission) gap seen below T_c is the superconducting gap can be tested by performing Andreev scattering experiments. If this

assumption is correct, the Andreev gap should be equal to the tunneling gap. We have found that this is in fact not the case in the underdoped regime (17). The Andreev gap then follows the doping dependence of T_c , not that of the pseudogap. In YBCO, BSCCO and LaSrCuO, for an underdoping such that T_c is reduced by about one third, the tunneling gap is about three to four times larger than the energy scale up to which Andreev scattering is observed. We have called this energy scale Δ_c (the "Andreev gap"). Whatever the doping level is, the strong coupling ratio ($2\Delta_c/kT_c$) remains in the range of 4 to 6 for all cuprates investigated so far (Table 1). Hence the tunneling gap is not the BCS, coherent, superconducting gap. Rather, it is the Andreev gap that behaves like the BCS gap, with a reasonable strong coupling ratio (the strong coupling ratio calculated for the tunneling gap reaches values in excess of 20 in the underdoped range, see ref.17).

Table 1. The Andreev strong coupling ratio ($2\Delta_c/kT_c$) for different cuprates.

LSCO 30K (ref.13)	LSCO 24K (ref.14)	LSCO 16K (ref.17)	YBCO 90K (ref.6)
6	6	4.5	5.3
YBCO 70K (ref.17)	YBCO 60K (ref.14)	BSCCO 90K(ref.14)	BSCCO70K(ref.11)
4.5	6	6.6	4.5

What is then the nature of the pseudogap? The Andreev experiments tell us that in the underdoped regime there exists an energy scale, characteristic of the condensed state, that is smaller than the single particle excitation energy gap (measured by tunneling and photoemission experiments). The question is whether this last gap measures a pairing amplitude, already finite above T_c , or whether it is unrelated to superconductivity (it could be some form of insulating gap).

Kostyn et al. (18) have calculated an order parameter for the case of a BCS to Bose Einstein condensation crossover. They have found that, in the underdoped regime, it is substantially smaller than the excitation gap at temperatures slightly below T_c . However it converges to it at low temperatures. The predictions of this theory thus seem to be in contradiction with the Andreev scattering experiments, although the authors have not made any specific prediction regarding Andreev scattering. The stripe model is another case where a pairing amplitude subsists well above T_c (19), but theoretical predictions for the Andreev effect in the framework of this model have not yet been worked out either.

The possibility that the pseudogap is basically an insulating gap has also been suggested. In fact, the expression pseudogap was first coined by Mott to describe a case where an insulating gap is "smeared" by disorder effects (20). If, for instance, the AF phase was a band insulator, as has been proposed by Friedel (21), the pseudogap would be an energy scale related to the properties of the AF phase, and not to those of the superconducting one. Instead of being a precursor of superconductivity, as has often been claimed (16), the pseudogap would be at the origin of the depression of superconductivity in the underdoped regime, through the decrease of the density of states in the pseudogap range. It is the Andreev gap that would be the true superconducting energy scale, characteristic of the condensate, and varying of course as T_c as a function of doping, as observed. But here also, a more specific comparison with experiments requires a theory of Andreev scattering in the superconducting state of a "pseudo-insulator".

ACKNOWLEDGEMENTS

I am particularly indebted to Jacques Friedel for discussions on the pseudogap issue. This work was supported in part by the Heinrich Hertz Minerva Center for High Temperature Superconductivity, by a grant of Darpa and the US Navy, and by the Oren Family Chair of Experimental Solid State Physics.

REFERENCES

- 1) D.Saint James, Journal de Physique **15**, 899 (1964).
- 2) G.E.Blonder, M.Tinkham and T.M.Klapwijk, Phys.Rev.B **25**, 4515 (1982).
- 3) Y.V.Sharvin, JETP **21**, 655 (1965).
- 4) D.Racah and G.Deutscher, Physica C **263**, 218 (1996).
- 5) G.Deutscher and P.Nozieres, Phys.Rev.B **50**, 13557 (1994).
- 6) N.Hass, D.Ilzycer, G.Deutscher et al., Journal of Superconductivity **5**, 191 (1992)
- 7) Y.Tanaka, in "Coherence in High Temperature Superconductors",
Eds. G.Deutscher and A.Revcolevschi, World Scientific (Singapore) 1996, pp.393.
- 8) C.R.Hu, Phys.Rev.Lett.**72**, 1526 (1994).
- 9) M.B.Walker and P.Pairor, Cond-mat/9809070
- 10) L.Alff et al., in "Advances in Superconductivity IX", S.Nakajima
and M.Murakami eds., Springer Verlag Tokyo (1997), p.49..
- 11) Saion Sinha and K.W.Ng, Phys.Rev.Lett.**80**, 1296 (1998).
- 12) A.Kohen, private communication
- 13) N.S.Achsaf, D.Goldschmidt, G.Deutscher et al., Journal of Low Temperature
Physics **105**, 329 (1996).
- 14) L.Alff, A.Beck, R.Gross et al., Phys.Rev.B **58**, 11197 (1998).
- 15) H.Ding, T.Yokoya, J.C.Campuzzano et al., Nature **382**, 51 (1996).
- 16) C.Renner, B.Revaz, J.Y.Genoud et al., Phys.Rev.Lett.**80**, 149 (1998).
- 17) G.Deutscher, Nature **397**, 410 (1999).
- 18) Q.Chen, I.Kosztin, B.Janko and K.Levine, Phys.Rev.Lett.**81**, 4708 (1998).
- 19) V.Emery, S.Kivelson and O.Zachar, Phys.Rev.B **56**, 6120 (1997).
- 20) J.Friedel, private communication.
- 21) J.Friedel and M.Kohmoto, to be published

Low Temperature Anomaly of LO Phonons in $\text{La}_{1.85}\text{Sr}_{0.15}\text{CuO}_4$ and $\text{YBa}_2\text{Cu}_3\text{O}_7$

T. Egami¹, R. J. McQueeney², Y. Petrov³, M. Yethiraj⁴, G.
Shirane⁵, and Y. Endoh⁶

¹Department of Materials Science and Engineering, University of Pennsylvania, Philadelphia, PA 19104, ²Los Alamos National Laboratory, Los Alamos, NM 87545, ³Department of Physics and Astronomy, University of Pennsylvania, Philadelphia, PA 19104, ⁴Oak Ridge National Laboratory, Oak Ridge, TN 37831, ⁵Brookhaven National Laboratory, Upton, NY 11973, ⁶Department of Physics, Tohoku University, Sendai 980, Japan

Abstract. Inelastic neutron scattering measurements of $\text{La}_{1.85}\text{Sr}_{0.15}\text{CuO}_4$ and $\text{YBa}_2\text{Cu}_3\text{O}_7$ show that the dispersion of the high energy LO phonon mode along the (1,0,0) direction is strongly temperature dependent, and at low temperatures develops an anomalous feature indicative of dynamic cell-doubling. The anomaly does not change through superconducting transition and gradually disappears between 50 and 250 K in LSCO. Possible implications are discussed.

INTRODUCTION

It has long been assumed that the phonons play little or no role in the high temperature superconductivity of cuprates, since the isotope effect is small and the normal state properties show no evidence of strong electron-phonon coupling [1,2]. However, a large number of experimental observations suggest significant lattice involvement [3], including our recent inelastic neutron scattering measurements of the LO phonons in LSCO [4]. We found that the normal continuous dispersion observed at room temperature was replaced, at low temperatures, with a dispersion that was discontinuous at the half-way point of the Brillouin zone in the [1,0,0] direction. More recently we observed basically the same behavior in the optimally doped YBCO. In this paper we review these results and discuss their implications.

EXPERIMENTAL RESULTS

Inelastic neutron scattering measurements were carried out with the triple-axis spectrometer at the High Flux Isotope Reactor at Oak Ridge National Laboratory

on single crystals of $\text{La}_{1.85}\text{Sr}_{0.15}\text{CuO}_4$ ($T_C = 37$ K) and $\text{YBa}_2\text{Cu}_3\text{O}_{6.93}$ ($T_C = 95$ K). We used a beryllium crystal (002) as the monochromator and pyrolytic graphite (002) as the analyzer which was set to give a final energy of 14.87 meV. In order to achieve the energy transfer up to 90 meV we had to use the incident neutron spectrum far in the epithermal region. Thus the flux was low, resulting in low counting rates of only 1 - 5 counts/minute. Also we had to identify and stay away from numerous spurious peaks, for instance those involving Bragg scattering from the sample and inelastic scattering from the analyzer.

Figure 1 describes the phonon dispersion for the highest energy LO mode in the $[Q_x, 0, 0]$ direction in the tetragonal index (parallel to the Cu-O bond in the CuO_2 plane) for LSCO at $T = 10$ K and room temperature [4]. These LO modes involve almost exclusively the displacements of in-plane oxygen ions within the CuO_2 plane. The dispersion at 300 K is largely in agreement with the previous room temperature measurements on $\text{La}_{1.9}\text{Sr}_{0.1}\text{CuO}_4$ [5]. The dispersion is strongly dependent upon temperature, and at 10 K it splits into two parts. The low-energy branch is well defined and nearly dispersionless down to $(3.25, 0, 0)$, but then becomes very wide and diffuse. The high-energy portion is close to the dispersion in the undoped sample. Thus in the range from $Q_x = 3.1 - 3.4$, two peaks are observed in the constant Q energy scan, one strong and the other weak. The temperature dependence apparently is not related to superconducting transition at T_C : No appreciable change was observed between 10 K and 50 K. Similar results were obtained for YBCO as shown in Fig. 2 as intensity contour plots. The temperature dependence in YBCO appears to be weaker than in LSCO, but is much stronger than anticipated for the normal thermal effect due to anharmonicity.

DISCUSSION

The dispersion of the oxygen LO mode presented here shows two remarkable features. One is the apparent large discontinuity of dispersion around $(0.25, 0, 0)$ at 10 K, and the other is the strong temperature dependence. The apparent discontinuity in dispersion was observed also for $\text{Ba}_{0.6}\text{K}_{0.4}\text{BiO}_3$ [6], nickelate [7] and more recently in doped CMR manganite [8]. Since the softening of the oxygen LO phonons at the zone edge is clearly related to the presence of the doped holes [5,9,10], it may be argued that the discontinuity at $(0.25, 0, 0)$ must also be intimately connected with the presence of charges. Note that this mode, through the change in the Cu-O bond distance, induces charge transfer between Cu and O. We will first consider the possibility that this discontinuity is related to the spin/charge stripes, and discuss other possibilities.

A. Relation with the spin/charge stripes

While initially the behavior of cuprates has been discussed assuming perfect periodicity in the lattice, a large number of observations point to the possibility

of spatially inhomogeneous lattice and electronic structure including some sort of spin/charge phase separation [3,11-15]. More recently the observation of the spin/lattice stripes in the non-superconducting cuprates with the charge density of $x = 1/8$ [16] strengthened this view. While static stripes were observed for non-superconducting cuprates, it has been assumed that similar stripes exist even in the superconducting phase but they are dynamic, since similar incommensurate magnetic scattering has been observed only by inelastic neutron scattering [17].

The magnetic periodicity of our LSCO sample as determined by inelastic magnetic scattering is approximately $8a$ [18]. This would result in the charge periodicity of $4a$ in the stripe model, with the corresponding superlattice periodicity of $(0.25, 0, 0)$. However, such a charge density modulation would create a new Brillouin zone boundary and a gap in the phonon dispersion at $(0.125, 0, 0)$, and indeed a simple spring model suggests that should be the outcome, which does not agree with the observation.

A more plausible scenario is that the Kohn anomaly is responsible to the observed anomaly. For instance if the stripe periodicity of $4a$ is related to the Fermi momentum [19,20] by $2k_F = 0.25$, the screening function will have a singularity at $q = 0.25$. This could result in sharp decline in the dispersion. However, it does not explain why two modes are seen at the same Q at low temperatures.

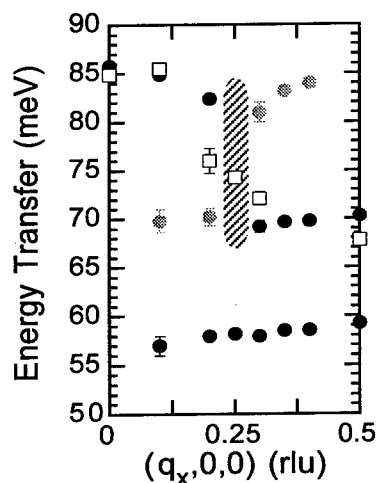


FIGURE 1. The dispersion relation of the high energy longitudinal optic branches of $\text{La}_{1.85}\text{Sr}_{0.15}\text{CuO}_4$ along $(Q_x, 0, 0)$ at $T = 10$ K (circles) and room temperature (squares). The shadowed circles indicate the energy of the weak extra branches. The shade at $(3.25, 0, 0)$ indicates a broad peak in the intensity [4]. The low energy branch (57 - 60 meV) is shown just as a reference, and is not related to the discussion in this paper.

B. 2nd CDW scenario

The discontinuity of dispersion at $(0.25, 0, 0)$ is indicative of cell-doubling that creates a new Brillouin zone boundary at $(0.25, 0, 0)$. Indeed a simple spring model with the periodicity of $2a$ reproduces the observed dispersion remarkably well [4]. Such cell-doubling can result from charge ordering (CDW) on oxygen in the CuO_2 plane with the periodicity of $2a$ [4]. A similar model with the charges on Cu does not reproduce the observed dispersion at all. It should be noted, however, that this charge ordering, if it exists, is most likely dynamic, since a superlattice diffraction at $(0.5, 0, 0)$ corresponding to such ordering has never been reported, including our own search, in the elastic or quasi-elastic scattering. The charge ordering also is most probably short range, since the absence of dispersion of the 70 meV mode suggest localization. The flat dispersion extends over the range, $0.25 < q_x < 0.75$ and $-0.1 < q_y < 0.1$, suggesting that the coherence lengths of the localized phonon to be $5a \times 2a$, or 20×8 in the a - b plane. It is interesting to note that the same coherence lengths were detected in $\text{YBa}_2\text{Cu}_4\text{O}_8$ by the pulsed neutron pair-density function (PDF) study [21]. The possibility of a charge density wave (CDW) being involved in high-temperature superconductivity has been suggested by several authors [22–24]. The conflict between this CDW and the stripe state

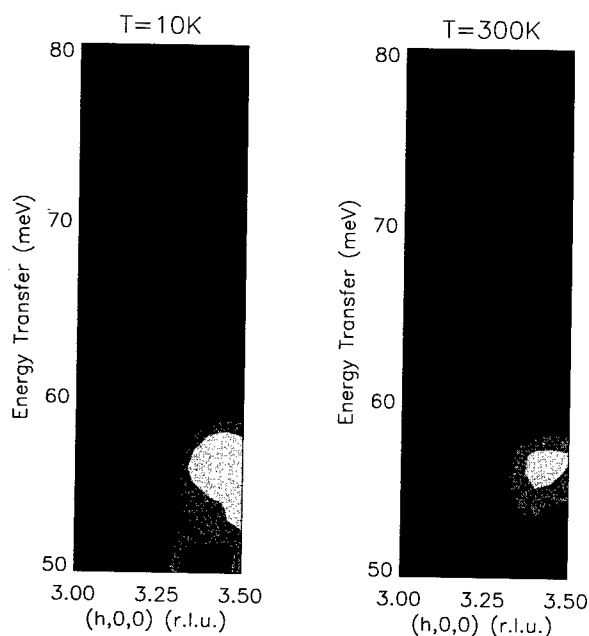


FIGURE 2. Intensity contour plot for the LO phonon branches of $\text{YBa}_2\text{Cu}_3\text{O}_{6.93}$ at $T = 10$ K (left) and at room temperature (right).

may be preventing either from developing into static long range order. It is possible that the LO phonons are resonantly coupling the two CDW states, producing the vibronic ground state [23].

A possible origin of the dynamic charge density modulation the Hubbard-Peierls instability [10,25]. Since the Cu band is nearly half-full, the Peierls instability can soften the zone-edge mode. Note that the $q = 0$ (zone-center) LO mode results in modulation of charges (CDW) on Cu, while the $q = 0.5$ (zone-edge) LO mode produces ferroelectric polarization. Charge transfer in the former case (Cu to Cu) is easier than in the latter (Cu to O), since the latter involves a large charge transfer gap (~ 2 eV). In this scenario the wavevector of the phonon anomaly remains nearly 0.5 regardless of the amount of doping, however, there are indications that it may change with doping [26]. It is important to study the composition dependence of the phonon anomaly. Within a few months we plan to study the phonon dispersion of an underdoped YBCO with T_C of 60 K. It is equally important to confirm dynamic charge ordering more directly. In addition to the inelastic neutron scattering study at low energy transfer range, we are planning to carry out high-resolution electron-energy-loss-spectroscopy (EELS) measurements to study the charge dynamics in the system.

C. Pair-scattering scenario

Another possibility is that the anomaly is caused by the phonon scattering involving electron pairs. While the backscattering of phonons by a single electron (hole) in the stripe state will result in momentum transfer of 0.25, the backscattering by a pair of electrons can create momentum transfer of 0.5 and a pseudo-Brillouin zone boundary at 0.25. In the BCS theory a Cooper pair is made of carriers with the opposite momenta, k and $-k$, resulting in zero total momentum. However, the electrons that form the stripe state with the momentum of 0.125 are heavy carriers in the extended saddle point (M point) [19,20], and their ground state is the standing wave. Thus the pair can have 0 or $2k$ total momentum. Such a pair-scattering is obtained from the Frölich Hamiltonian through the usual canonical transformation by preserving the pair creation and annihilation terms, for instance, in the Hartree-Fock approximation. If this is the case our observation will provide a direct evidence of the strong phonon involvement in pairing.

The observation of similar discontinuity in nickelates and manganites may appear to weaken the argument on direct connection to superconductivity, but their cases involve samples with twice the charge density and half the stripe periodicity [7,8], and thus may be due to single carrier scattering. It should be noted that the energy of the carriers in the extended saddle point is of the order of 100 meV or less. Thus electrons and phonons are likely to be resonantly coupled also to form vibronic states [23,27]. For such a system the adiabatic approximation would not be valid, making the theoretical treatment difficult [28]. It may be argued that such a strong electron-phonon coupling is incompatible with the high normal

state conductivity, but the conductivity is dominated by the light carriers in the vicinity of the X ([0.25, 0.25]) point, and the contribution from the M point may be totally masked. Regardless of the exact origin of the anomaly, the observed phonon dispersion strongly suggests that LO phonons may be intimately involved in the high-temperature superconductivity.

REFERENCES

1. Kresin, V. Z., Moravitz, H., and Wolf, S. A., *Mechanisms of Conventional and High T_C Superconductivity* (Oxford University Press, Oxford, 1993).
2. Anderson, P. W., *Theory of Superconductivity in the High- T_C Cuprates* (Princeton University Press, Princeton, 1997).
3. Egami, T., and Billinge, S. J. L., in *Physical Properties of High Temperature Superconductors V*, edited by D. Ginsberg (World Scientific, Singapore, 1996), p. 265.
4. McQueeney, R. J., Petrov, Y., Egami, T., Shirane, G., and Endoh, Y., *Phys. Rev. Lett.*, in press.
5. Reichardt, W., Pyka, N., Pintschovius, L., *et al.*, *Physica C* **162-164**, 464 (1989).
6. Braden, M. *et al.*, *J. Supercond.* **8**, 1 (1995).
7. Pintschovius, L., *et al.*, *Phys. Rev.* **B40**, 2229 (1989).
8. Reichardt, W., and Braden, M., unpublished.
9. Pintschovius, L., and Reichardt, W., in *Physical Properties of High Temperature Superconductors IV*, edited by D. Ginsberg (World Scientific, Singapore, 1994), p. 295.
10. Ishihara, S., Egami, T., and Tachiki, M., *Phys. Rev. B* **55**, 3163 (1997).
11. Gor'kov, L. P., and Sokol, A. V., *JETP Lett.*, **46**, 420 (1987).
12. *Phase Segregation in Cuprate Superconductors*, eds. Sigmund, E., and Müller, K. A., (Springer Verlag, Berlin, 1994).
13. Poilblanc, D. and Rice, T. M., *Phys. Rev. B* **39**, 9749 (1989).
14. Zaanen, J., and Gunnarson, O., *Phys. Rev. B* **40**, 7391 (1989).
15. Emery, V. J., Kivelson, S. A., and Lin, H. Q., *Phys. Rev. Lett.* **64**, 475 (1990).
16. Tranquada, J. M., *et al.*, *Nature* **375**, 561 (1995).
17. Cheong, S. W., *et al.*, *Phys. Rev. Lett.* **67**, 1791 (1991).
18. Yamada, K., *et al.*, *Phys. Rev. Lett.* **75**, 1626 (1995).
19. Salkola, M. I., Emery, V. J., and Kivelson, S. A., *Phys. Rev. Lett.*, **77**, 155 (1996).
20. Norman, M. R., *et al.*, *Phys. Rev. Lett.* **79**, 3506 (1997).
21. Sendyka, T. R., *et al.*, *Phys. Rev. B* **51**, 6747 (1995).
22. Tanaka, S., *Physica C*, **182**, 137 (1991).
23. Tachiki, M., and Takahashi, S., *Phys. Rev. B* **38**, 218 (1988).
24. Perali, A., *et al.*, *Phys. Rev. B* **54**, 16216 (1996); Castellani, C., Di Castro, C., and Grilli, M., *Los Alamos archive depository, cond-mat* 9702112.
25. Petrov, Y., and Egami, T., *Phys. Rev. B* **58**, 9485 (1998).
26. Mook, H., *private communication*.
27. Green, B., *private communication*.
28. Thornber, K. K., and Feynman, R. P., *Phys. Rev. B* **1**, 4099 (1970).

Direct and continuous measurements of the irreversibility line of high- T_c superconductors using an automatic PID controller.

L.E. Flores, C. Noda, C. Abascal, E. Altshuler, and J.L. Gonzales

Superconductivity Laboratory, IMRE, University of Havana, Zapata y G, S/N, Ciudad de la Habana 10400, Cuba.

Abstract. In this work we present the results of the application, in a novel way, of an automatic proportional-integral-derivative controller to the measurements of the irreversibility line in high temperature superconductors. The system operates by applying to the sample a controlled dc field that maximizes the imaginary (out-of-phase) component of the ac susceptibility, commonly used as a criterion for the determination of such dependencies. Through this technique, for the first time, direct and continuous determination of irreversibility lines are possible, allowing the measurement of a whole curve in only one temperature sweep, such as in a typical resistivity versus temperature curve.

I INTRODUCTION

From a practical point of view one important parameter in superconductors is the critical current density (J_c), the highest current that can be applied to the sample without dissipation. Depending on the temperature and the magnetic field applied on a superconductor, this parameter can be zero or have a finite value. In the $H-T$ plane, two regions are separated by a line called "irreversibility line" [1,2] below which J_c has a finite value and it turns to zero by crossing this boundary.

In order to measure the irreversibility line in superconductors several techniques have been used [2-7], which are based in the magnetic response of the material under study to an external excitation of a magnetic field either constant or periodic in time. Although these methods differ in several ways, they all have one thing in common it takes a long time and several thermal and magnetic cycles to obtain an irreversibility line curve with few points. In this work we present a technique that allows, using a proportional-integral-derivative (PID) controller [8], the determination of the irreversibility line continuously and fast. Our method needs only one thermal cycle, with an automatic control of the dc field to adjust it to the value that provokes a maximum in the out of phase component of the ac susceptibility.

This is done by superimposing a low frequency field to the ac field commonly used in the ac susceptibility measurements. This field modulates the ac susceptibility signal and allows, using a double lock-in detection scheme, the measurement of the magnetic field derivative of the out of phase component of the susceptibility as a dc voltage. This voltage is used as an error signal fed into the PID controller, whose output drives a programmable current source used to apply the dc magnetic field. As the controller tends to null the error signal at its input, the loop will lock in a state where the applied field matches the irreversibility one. This system allows the measurement of the irreversibility line by sweeping only the temperature in the range of interest, while the controller adjust continuously the irreversibility field.

II SYSTEM DESCRIPTION

Figure 1 shows a general block diagram of the system described in this work; it is based on a standard three coils ac susceptometer setup [9], where a fourth coil is added. The pick-up coils are wound in opposite directions to null the signal induced when no sample is placed inside them. One of the outer coils is used to generate the ac excitation field, from which the ac susceptibility is obtained. The other one is used to generate a low frequency field (about 0.2 mT at 10Hz) for modulation purposes, as explained below. Another coil placed outside the cryostat is used to generate dc fields up to 100 mT (1000 Oe). The signal of the pick-up coils is differentially measured by the first lock-in amplifier with the phase adjusted for the measurement of the out of phase component of the susceptibility.

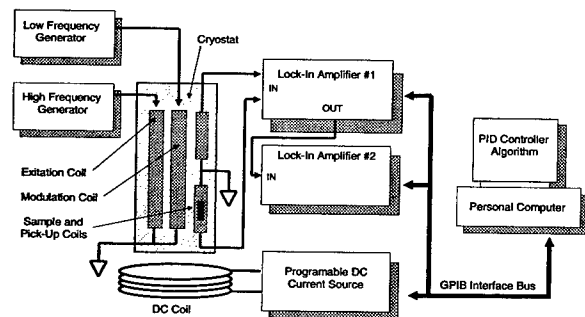


FIGURE 1. Schematic diagram of the experimental setup. The excitation, modulation, and pick-up coils are wound coaxially inside the cryostat. The dc coil is immersed in liquid nitrogen surrounding the cryostat.

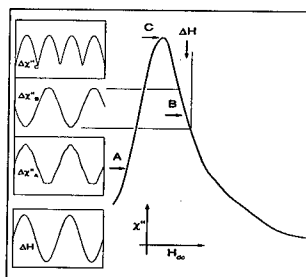


FIGURE 2. Illustration of the working principle for the determination of the peak position (H_{peak}).

Although the low frequency field applied to the sample generates an ac susceptibility signal at its frequency (effect that we will ignore in this work), it also can be understood in terms of a small modulation (ΔH) of the dc applied field (H_{dc}).

Figure 2 shows the effect of such modulation in a χ'' versus H_{dc} curve; where three regions are observed. In each case the ac low frequency field provokes some modulation of the χ'' signal. For $H_{dc} < H_{peak}$ (case A) the χ'' modulation is in phase with the field oscillation, for $H_{dc} > H_{peak}$ (case B) it is dephased 180 degrees, and when $H_{dc} = H_{peak}$ (case C) the signal at the modulation frequency disappear, and a signal at twice this frequency is obtained.

It is obvious that if we synchronously rectify this signal with the second lock-in amplifier, (using as a reference a voltage proportional to the low frequency ac field) at this lock-in output will exist a dc voltage: positive for $H_{dc} < H_{peak}$, negative for $H_{dc} > H_{peak}$, and zero in the peak position, and, in general proportional to the magnetic field derivative of χ'' . If we use this voltage as an error signal in a PID controller that adjust the current applied to the dc solenoid, and with the proper settings of the PID and circuit parameters, we obtain a control loop that will try to adjust the dc field to guarantee that this error signal equals zero.

In our system, a C++ program running in a personal computer (PC) performs the PID control action. The computer handles all the measurement process: it adjusts the phase settings of both lock-in amplifiers, sweeps the temperature in the range of interest, and controls the dc magnetic field through the PID controller program. The algorithm implemented dynamically adjusts the PID coefficients to improve the controller response [8].

The whole system works as follows: the temperature is stabilized for a while at the highest value desired, then the PID controller starts to adjust the dc field until the peak position, at that temperature, is reached. At this point the temperature is swept down, at a fixed rate, while the controller follows the variations of the peak position. This process ensures that the magnetic field will be continuously increasing, avoiding hysteretic phenomena in the measurement.

III RESULTS

In order to test our system intergranular irreversibility lines of several BSCCO ceramic samples were measured. The result, for one sample, (Fig. 3, line) shows excellent agreement with the curve measured point-by-point (circles), i.e., the one obtained by measuring several $\chi''(H_{dc})$ curves at different temperatures. In the inset of the figure we can see the voltage at the second lock-in output, i.e., the error signal at the PID input. This voltage gives a criterion of the controller performance. Its value must be as close to zero as possible, and, more importantly, it must remain as constant as possible, during the measurement. Its deviation from zero is small and constant enough to ensure that the peak position was maintained during the whole measurement.

Finally figure 4 shows size dependencies of the irreversibility line for one of the samples under study, and the inset shows the irreversibility field at several temperatures versus sample width.

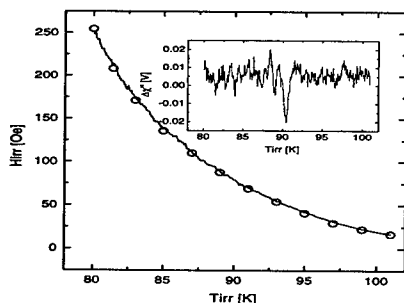


FIGURE 3. Intergranular irreversibility line for a BSCCO ceramic sample measured by our system (continuous line) and by the standard point-by-point method.

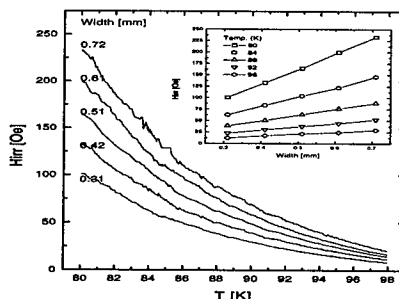


FIGURE 4. Size dependencies of the irreversibility line for a BSCCO ceramic sample, the inset shows the irreversibility field, at several temperatures, versus sample width

IV CONCLUSIONS

In this work a novel technique for fast and reliable measurement of the irreversibility line is presented. Its main advantage relies in the celerity of the measurement. A whole irreversibility line can be measured in the same time used to obtain a resistivity versus temperature curve, which is several times faster than the time required by other methods.

The results presented above belong to high- T_c superconductor intergranular irreversibility lines. This method could be useful not only for these polycrystalline materials, but for the determination of irreversibility lines of samples that exhibit loss peaks in the out of phase component of the susceptibility, such as single-crystals or thin-films.

REFERENCES

1. K.A. Müller, M. Takashige, and J.G. Bednorz, Phys. Rev. Lett., 58, 1143 (1987).
2. M.C. Frischherz, F.M. Sauerzopf, H.W. Weber, M. Murakami, and G.A. Emel'chenko, Superconductor Science and Technology, 8, 485 (1995).
3. J. Vanacken, E. Osquiguil, and Y. Bruynseraede, Physica C, 183, 163 (1991).
4. A.Neminsky, J.Dumas, B.P. Thrane, and C. Schlenker, Phys. Rev. B, 50, 3307, (1994).
5. J.L González, P. Muné, L.E. Flores, and E. Altshuler, Physica C, 255, 76 (1995).
6. E.R. Yacoby, A. Shaulov, Y. Yeshurun, M.Konczykowski, and F. Rullier-Albenque, Physica C, 199, 15 (1992).
7. A. Shaulov, and D. Dorman, Appl. Phys. Lett., 53, 2680 (1988).
8. A. Marsik, Problems of control and Information theory, 12, 267 (1983).
9. M. Nikolo, American Journal of Physics, 63, 57, (1995).

Where do the doped holes go in $\text{La}_{2-x}\text{Sr}_x\text{CuO}_4$? A close look by XAFS

Daniel Haskel, Victor Polinger and Edward A. Stern

Physics Department Box 351560, University of Washington, Seattle WA 98195, USA

Abstract.

Polarized x-ray absorption fine structure (XAFS) measurements at the La and Sr sites in $\text{La}_{2-x}\text{Sr}_x\text{CuO}_4$ ($0.075 \lesssim x \lesssim 0.35$) indicate that doped holes introduced with Sr are not uniformly distributed in the CuO_2 planes but reside in impurity states with the majority of charge located on CuO_6 octahedra coupled to the Sr dopants by an apical oxygen (denoted as Sr octahedra). A model based on doped hole-induced Jahn Teller (JT) distortions of these Sr octahedra indicates the impurity states are overlapping singlet and triplet ones resulting from pairings of intrinsic and extrinsic holes. The more mobile singlet pairs reside in the CuO_2 planes, are bound by more than 0.1 eV and could Bose-condense into a superconducting state. The predominant appearance of (mostly) out-of plane triplet states at high x is intimately related to the 2D-3D crossover in transport properties and could relate to the observed loss of high T_c in the overdoped regime, as confinement of carriers to the CuO_2 planes is reduced.

INTRODUCTION

La_2CuO_4 is a strongly correlated electron system with one *intrinsic* hole per molecular unit. The Coulombic repulsion between neighboring holes (U_d) being larger than the overlap bandwidth at half filling results in a Mott-Hubbard (M-H) insulator with full (empty) lower (upper) Hubbard bands. Substituting Sr^{+2} for La^{+3} adds *extrinsic* (or doped) holes which are localized at low x but become itinerant for $x \gtrsim 0.06$ where a 2D insulator-metal (I-M) transition is observed together with high T_c superconductivity. The lack of a complete understanding of the anomalous normal state properties [1] is partly due to the lack of information on the character of the *doped* holes: Are they periodic in the CuO_2 planes as in a Zhang Rice singlet band? Do all the doped holes contribute to metallic transport above the I-M transition? Is there doped charge density outside the CuO_2 layers?

Polarized x-ray absorption near-edge structure (XANES) [2] measurements have been instrumental in providing insight into the orbital character of intrinsic and extrinsic holes. These measurements, however, cannot distinguish between the in-

equivalent oxygen sites (O(1) in the CuO_2 planes and O(2) in the rock-salt La-O layers) or those nearby Sr or La atoms, as they average over all O atoms. XAFS measures the local environment about the La and Sr atoms separately despite their residing in the same crystallographic site with a majority of La atoms. This is of advantage over other techniques for average and local structure determination which measure a weighted average of La and Sr sites, dominated by the La sites. Diffraction techniques assume periodicity, while the randomly doped system is inherently non-periodic and local structural distortions around the dopants will therefore go undetected by diffraction.

How can XAFS give information on the electronic states of the doped holes? Only if the electronic and structural degrees of freedom are coupled which is the case here as evident in the *Jahn-Teller* (JT) [9] deformation of CuO_6 octahedra in La_2CuO_4 .

EXPERIMENTAL

Quite complete information on the local structures about both La and Sr atoms was obtained from our data and, together with experimental details and analysis methods, can be found in refs. 4,5. Here we present results of new measurements at the Sr *K*-edge extending the x -range far beyond the values previously reported [5]. We concentrate on the results for the apical oxygens.

The apical oxygens about La atoms have a similar distribution as in the pure material, i.e., a single site located at a distance of 2.36(1) Å from the La atom (2.41(1) Å from the almost collinear Cu atom). We denote the CuO_6 octahedra with only La atoms bonded to its two apical oxygens as La-octahedra. The apical oxygens about the Sr impurity atoms, however, have a double-site distribution peaked at distances of 2.55(2) Å and 2.25(3) Å from Sr (2.22(2) Å and 2.52(3) Å from the Cu atom, respectively), with the sum of occupation of the two sites being one oxygen [5]. No significant change in both the occupation and disorder of each site is found up to room temperature (RT). The improvement of the two site model over the one site model decreases with x (Fig. 1) due to changes in the relative occupation of the two sites, the long Sr-O(2) distance becoming more occupied at the expense of the short distance (Fig. 2a). No measurable variation of the Sr-O(2) apical distances occurs with x (Fig. 2b).

DISCUSSION

Whereas a different local environment around Sr could be expected due to a different charge/ionic radius of Sr^{+2} compared to La^{+3} , a *double* site distribution is inconsistent with charge/size effects. It is, however, an indication of both strong lattice-hole interaction occurring around the Sr atoms and the dopant-induced holes being peaked on the CuO_6 octahedra bonded to a Sr atom, i.e., the Sr-octahedra. This result is different from the splitting in the apical oxygen reported in other

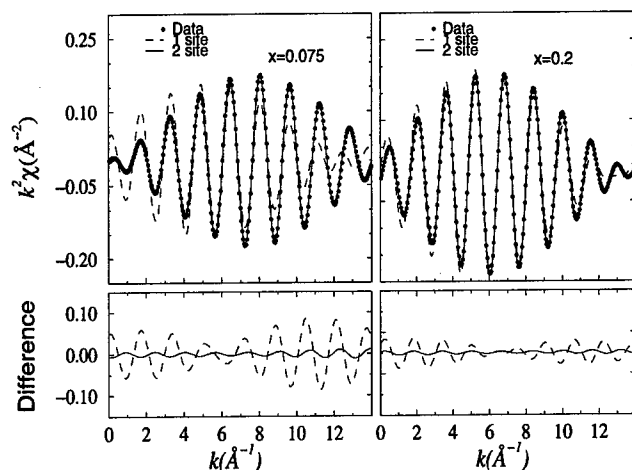


FIGURE 1. Fits to isolated Sr-O(2) XAFS for $x = 0.075, 0.2$ at $T=10\text{K}$ using both single and double site models. Difference spectra (Fit - Data) shown in the lower panel for both models. Statistical noise (1σ) is about 0.003.

investigations of high T_c superconductors [6], where the splitting occurs periodically throughout the solid. Here, the double site occurs *only* near the dopant Sr atoms.

In this scenario, the La-octahedra have only an intrinsic hole while the Sr-octahedra have two holes, one intrinsic and one extrinsic. Contrary to the periodic distribution of intrinsic holes, the extrinsic holes produce an impurity wave func-

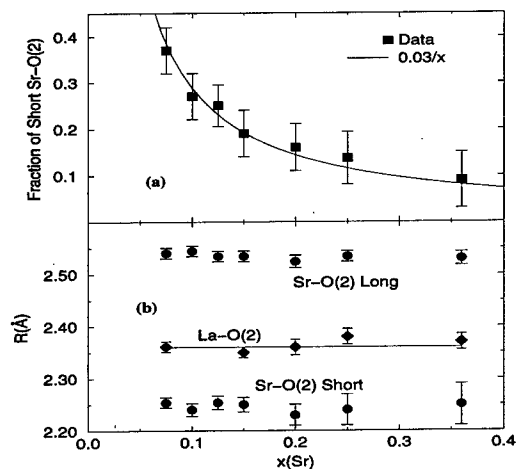


FIGURE 2. (a) Fractional occupation of Short Sr-O(2) distance and (b) Sr-O(2), La-O(2) distances versus x .

tion distribution. Since $\text{La}_{2-x}\text{Sr}_x\text{CuO}_4$ remains insulating up to a critical value of $x_c \sim 0.06$, it follows that in the dilute limit the doped holes are localized in the Sr-octahedra until the impurity band broadening is sufficient to overcome the localization energy. Since overlap is small a tight-binding approximation can describe the impurity states of doped holes residing in Sr-octahedra.

The La-octahedra, also in the undoped material, have the electron energy levels shown in Fig. 3a. The $x^2 - y^2$ and z^2 orbitals are non-degenerate due to both the tetragonal crystal field and the JT nature of the Cu $3d^9$ ions, resulting in an elongated CuO_6 octahedra with distances $\text{Cu-O}(2) \approx 2.41 \text{ \AA}$ and $\text{Cu-O}(1) \approx 1.90 \text{ \AA}$.

Figures 3(b,c) show the impurity energy levels for Sr-octahedra with intrinsic and extrinsic holes. Even though these states have the symmetry of Cu $3d$ -orbitals, the extrinsic holes reside not only on the Cu atoms but on the octahedron with a majority of the hole charge on the oxygen atoms [7,8]. The singlet $^1A_{1g}$ state (3b) has both holes in the $x^2 - y^2$ state and is analogous to the Zhang-Rice singlet [7] (two important differences are discussed below). The triplet $^3B_{1g}$ state (3c) has holes in each of $x^2 - y^2$ and z^2 orbitals with parallel spins. Here the exchange interaction lowers the triplet state energy to near that of the singlet state. In the triplet state no JT force is present since equal populations of $x^2 - y^2$ and z^2 orbitals result in no energy gain induced by a tetragonal distortion. This results in hole-induced contraction of the Sr-octahedra, the *anti-JT* effect [10,11]. In the singlet state, however, the JT energy gain is twice that of the La-octahedra resulting in an *enhanced JT* elongation of the Sr-octahedra.

The JT distortions of Sr-octahedra explain the double site observed by XAFS for the apical oxygen bridging Cu and Sr atoms. In the *enhanced JT* case (singlet)

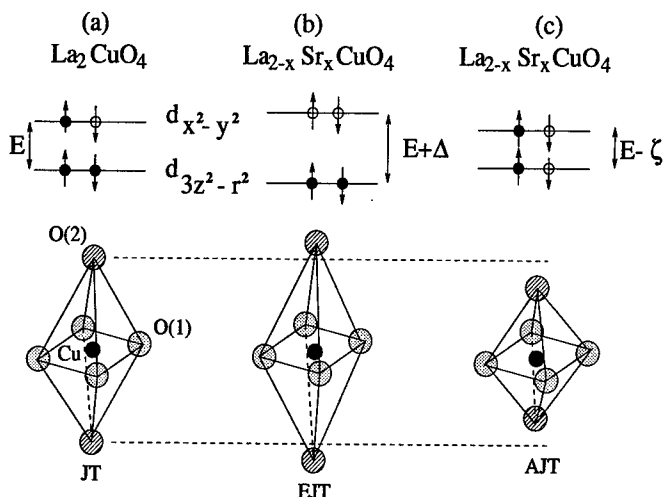


FIGURE 3. Energy levels and resultant octahedral distortions due to intrinsic and extrinsic holes: (a) Intrinsic hole; La-octahedra (b) Spin-singlet, enhanced JT case (c) Spin-triplet, anti-JT case.

the apical oxygens are shifted away from Cu towards the Sr, producing the short Sr-O(2) distance. In the *anti-JT* case (triplet) the apical oxygen shifts towards Cu away from the Sr atom, producing the long Sr-O(2) distance. The two sites detected by XAFS thus give evidence for two kinds of spin-differentiated JT distortions induced by the donated holes. It is interesting to note that the contraction of the Sr-octahedra in the anti-JT case (0.2 Å) results in a Cu-O(2) distance nearly the same as Ni-O(2) in La_2NiO_4 , where Ni^{+2} is in its high spin, non-JT state.

No temperature dependence in the occupation of singlet and triplet states is found by XAFS, up to RT, indicating their binding energies are larger than 300 $K_B \approx 25$ meV and that there is significant overlap between these states. This is in agreement with LDA + U first principles calculations [11] which find that doped holes occupy impurity states with $x^2 - y^2$ symmetry located inside the M-H gap with an ionization energy of ~ 0.1 eV. The same paper calculates, neglecting the impurity potential, the triplet state to lie only ≈ 54 meV above the ground state. Including the Sr impurity potential could reasonably lower the triplet to overlap the singlet band, resulting in both being populated by doped holes. Fractional hole occupancy of both states is essential for impurity band conduction, as full occupancy of either would result in a full $x^2 - y^2$ insulating singlet band (Fig. 3b) or half filled $x^2 - y^2$ and z^2 triplet bands with an insulating Hubbard gap.

The binding interaction between the Sr-impurity and its extrinsic hole is essential for producing the impurity states. At a concentration $x_c \approx 0.06$ the impurity local energy levels transform into impurity bands and metallic conduction occurs. The singlet state, having a greater overlap integral (at least by a factor of three) than the triplet [13] at any given x , dominates the conductivity above x_c and probably does so throughout the range where high T_c exists.

The 2D nature of conductivity observed at the I-M transition [1] is expected since singlet states have mostly in-plane orbital character. At higher x triplet states with mostly out-of-plane character increase their fraction of the doped holes (Fig. 2a). This increased occupation, together with increased overlap, explain the reduction in resistivity anisotropy ratio ρ_c/ρ_{ab} with x that brings about the 2D-3D crossover in transport properties at $x \sim 0.25 - 0.3$ [1]. We note that the anisotropy ratio predicted by band theory (~ 30 , an order of magnitude smaller than observed) is not very dependent on x , in contrast with experiment.

We note that the doped charge distribution in the singlet impurity band differs from that of the Zhang-Rice singlet band [7], where doped holes are periodic over all of the CuO_6 octahedra. Also both singlet and triplet impurity states are accompanied by a distortion of the Sr-octahedra from the undoped configuration.

The self-binding of singlet JT pairs together with the small overlap between pairs resulting from their wavefunctions being peaked about the Sr sites suggest that they may be treated as an entity and could Bose-Einstein condense at low temperature. Therefore, high T_c of $\text{La}_{2-x}\text{Sr}_x\text{CuO}_4$ would be explained as superfluidity of charged bosons [14] where disappearance of superconductivity above T_c is not due to a dissociation of pairs but to loss of coherence between pairs.

Two inequivalent copper sites are found in NMR and NQR measurements [15,16],

one of them appearing and increasing with doping. These sites can be explained by the presence of La- and Sr-octahedra. Coupling of singlet and triplet states via perturbations such as spin-orbit and electron-electron interactions mixes these states at a rate much faster than the inverse linewidth of the NMR/NQR lines ($\sim 1\mu\text{sec}$), giving an average signal for the Sr-octahedra. Recent improved NMR measurements [17] found that both inequivalent Cu sites sit in axially symmetric environments, consistent with the enhanced JT and anti-JT distortions preserving the axial symmetry of the Sr-octahedra.

The large binding energy ($\gtrsim 0.1\text{ eV}$) of the impurity states pairs is consistent with RT polarized XANES measurements at the O K -edge of $\text{La}_{2-x}\text{Sr}_x\text{CuO}_4$ [2]. These show a large spectral weight transfer of the oxygen $2p$ hole states, with doping, from those in the upper Hubbard band (intrinsic holes) to the doped impurity hole states. This spectral weight transfer shows the impurity states are an intimate mixture of intrinsic and extrinsic holes due to the strong interaction between them, consistent with their strong pairing in our model.

We thank I. Bersuker and Y. Yacoby for stimulating discussions and D. G. Hinks, A. W. Mitchell and J. D. Jorgensen for providing samples. The support of DOE Grant No. DE-FG03-98ER45681 is greatly appreciated.

REFERENCES

1. Y. Nakamura and S. Uchida, *Phys. Rev. B* **47**, 8369 (1993).
2. C. T. Chen *et al.*, *Phys. Rev. Lett.* **68**, 2543 (1992); E. Pellegrin *et al.*, *Phys. Rev. B* **47**, 3354 (1993).
3. P. G. Radaelli *et al.*, *Phys. Rev. B* **49**, 4163 (1994).
4. D. Haskel *et al.*, *Phys. Rev. Lett.* **76**, 439 (1996).
5. D. Haskel *et al.*, *Phys. Rev. B* **56**, R521 (1997).
6. J. Mustre-de Leon *et al.*, *Lattice Effects in High T_c Superconductors*, Singapore: World Scientific press, 1992, p. 39; E. A. Stern *et al.*, *ibid* p. 51; A. Bianconi *et al.*, *ibid* p. 65; T. Egami *et al.*, *Electronic Structure and Mechanisms of High Temperature Superconductivity*, New York: Plenum Press, 1991.
7. F. C. Zhang and T. M. Rice, *Phys. Rev. B* **37**, 3759 (1988).
8. J. B. Grant and A. K. McMahan, *Phys. Rev. Lett.* **66**, 488 (1991).
9. H. Jahn and E. Teller, *Proc. R. Soc. London A* **161**, 220 (1936).
10. J. G. Bednorz and K. A. Müller, *Z. Physik B-Condensed Matter* **64**, 189 (1986).
11. V. I. Anisimov *et al.*, *Phys. Rev. Lett.* **68**, 345 (1992).
12. V. Polinger, D. Haskel and E. A. Stern, preprint cond-mat/9811425.
13. D. I. Khomskii and E. I. Neimark, *Physica C* **173**, 342 (1991).
14. R. Micnas *et al.*, *Rev. Mod. Phys.* **62**, 113 (1990).
15. K. Yoshimura *et al.*, *J. Phys. Soc. Jpn.* **58**, 3057 (1989); K. Kumagai and Y. Nakamura, *Physica C* **157**, 307 (1989).
16. J. Haase *et al.*, *Phys. Rev. Lett.* **81**, 1489 (1998); P. C. Hammel *et al.*, *Phys. Rev. B* **57**, R712 (1998).
17. J. Haase *et al.*, to appear in *J. Superconductivity*.

c -axis penetration depth in single crystal $\text{La}_{2-x}\text{Sr}_x\text{CuO}_4$

J. R. Kirtley

IBM T.J. Watson Research Center, P.O. Box 218, Yorktown Heights, NY 10598, USA

K. A. Moler

Dept. of Applied Physics, Stanford University, Stanford, CA 94305, USA

M. Nohara and H. Takagi

Inst. Solid State Physics, University of Tokyo, Roppongi, Minato-ku, Tokyo 106, Japan

Abstract. We have used a scanning SQUID microscope to image vortices emerging parallel to the planes in the high- T_c cuprate superconductor $\text{La}_{2-x}\text{Sr}_x\text{CuO}_4$. These images provide a value for the c -axis penetration depth, $\lambda_c \sim 5\mu\text{m}$, which is in reasonable agreement with previous measurements using optical techniques.

INTRODUCTION

Recently, scanning SQUID microscope magnetic imaging of interlayer vortices trapped between the planes of layered superconductors has been used to make direct measurements of the interlayer penetration depth in several layered superconductors [1-4]. These experiments provide local measurements of the interlayer supercurrent density, which have implications for the validity of the interlayer tunneling model [5] as a candidate mechanism for superconductivity in the high critical temperature cuprate superconductors. Quantitative values for the in-plane penetration depth are derived by fitting these images to an exact solution of London's equations for a straight vortex approaching a superconductor-vacuum interface normal to the interface, in an anisotropic superconductor [6]. This treatment takes into account the spreading of the vortex magnetic fields at the superconductor surface [7].

Although SQUID imaging is a direct method for measuring the penetration depth, there are uncertainties that must be considered. For example, the SQUID

microscope images the magnetic fields at the superconducting surface. It is possible that the penetration depth at the surface is different from that in the bulk, or that vortex spreading at the surface is not well modelled by an anisotropic London model. In addition, the vortex trapping is often spatially inhomogeneous. It is possible that the vortices trap where the interplane screening is locally reduced, so that our measurements overestimate the in-plane penetration depth. It is therefore of interest to compare our measurements with results from other techniques. Some comparisons have already been made. For example, the results from optical measurements are in good agreement with those obtained from SQUID microscope measurements in the single-layer cuprate superconductor $\text{Ti}_2\text{Ba}_2\text{CuO}_{6+\delta}$ (Ti-2201) [2]. However, it is still of interest to measure LSCO, which is the material for which the c -axis supercurrent properties have been studied most extensively using other techniques [8–10]. Measurement of the c -axis penetration depth in LSCO using the scanning SQUID microscope is a particularly stringent test of the technique, because this length is relatively short, of the same size as the smallest SQUID pickup loops currently available.

The sample for this study was a large, high quality single crystal of $\text{La}_{2-x}\text{Sr}_x\text{CuO}_4$ with a nominal Sr concentration $x=0.17$, a T_c (center of the magnetic susceptibility transition) of 36K, and a spread in the magnetic susceptibility transition (10% to 90%) of 1.6K. The crystal was cut into a disk with the c -axis parallel to the disk faces, and then polished to a mirror finish for scanning.

The sample magnetic fields were imaged with a scanning SQUID microscope [11] with an octagonal pickup loop $4\mu\text{m}$ in diameter. The LSCO crystal was cooled in a small field (typically about 1mG) through the superconducting critical temperature, and imaged at 4.2K, with both sample and SQUID directly immersed in liquid helium.

Some results of the SQUID imaging are shown in Figure 1. The total variation of magnetic flux through the pickup loop represented by the grey-scaling in these images, in units of $\phi_0 = hc/2e$, are labelled in Figures 1(a) and 1(c). Note that in these images there are vortices with z - component of the field going into the superconductor (black), as well as emerging from the superconductor (white). This often happens when we image interlayer vortices. Note also that the vortex images are elongated: the vortices are resolution limited perpendicular to the planes (since λ_{ab} is much smaller than the size of the pickup loop), but their length parallel to the planes (set by λ_c) is longer than the instrumental broadening. The interlayer vortices are relatively uniform in shape in this sample: A survey of 29 well separated vortices gave a full width at half maximum (FWHM) for cross-sections through the center of the vortex image, parallel to the planes, of $11.9 \pm 0.9\mu\text{m}$. In the ideal case the FWHM should be $1.87\lambda_c$ [6], giving the estimate $\lambda_c = 6.3 \pm 0.5\mu\text{m}$. This is an overestimate, because the $4\mu\text{m}$ diameter pickup loop introduces finite broadening, and because we are measuring the fields slightly above, rather than at, the superconductor surface. Detailed modelling is required to get a quantitative estimate of λ_c from scanning SQUID images.

Fig. 1a was taken with the sample oriented so that the ab planes were aligned

approximately vertical in the image, while Fig. 1b was taken with the sample rotated about its polished face so that the ab planes were approximately horizontal. The effective pickup area of the loop, shown schematically as white overlays in Figures 1(a) and 1(c), is slightly asymmetric, since it includes some contribution from the leads, as well as the loop itself. We model the loop as an octagon 3.9 microns in diameter. We add to the calculated flux through this octagon one third of the flux through a square 4 microns on a side, with one side of the square congruent to a side of the octagon. This additional square pickup area accounts for flux focussing effects from the shielded superconducting leads to the pickup loop. Repeating our measurements for two different orientations of the cuprate planes relative to the pickup loop leads is a good test of how well we account for these effects. Figures 1(b) and 1(d) show modelling to determine the c -axis penetration depth from the images of Figures 1(a) and 1(c) as follows:

We model the interlayer vortex as an anisotropic Ginzburg-Landau vortex, matching the boundary value conditions for the solution of London's equation inside the superconductor to the solution of Laplace's equation outside the superconductor. The z -component of the magnetic field of an interlayer vortex above the superconducting surface is given by [6]:

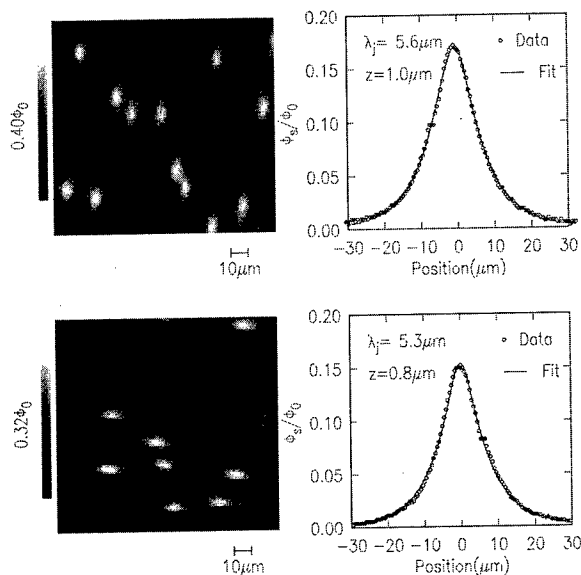


FIGURE 1. Scanning SQUID images of the edge of a $\text{La}_{2-x}\text{Sr}_x\text{CuO}_4$ single crystal with the ab planes oriented approximately vertical (a), or horizontal (c), in the image. A scaled schematic of the SQUID pickup loop is superimposed on the images, as well as a dashed line showing the track along which a cross-section through a particular vortex was taken for modelling. The open circles in Figs (b) and (d) are the data; the lines are fits as described in the text.

$$h_z(\mathbf{r}, z) = - \int \frac{d^2\mathbf{k}}{(2\pi)^2} k \phi(\mathbf{k}) e^{i\mathbf{k}\cdot\mathbf{r} - kz}, \quad (1)$$

where

$$\phi(\mathbf{k}) = - \frac{\phi_0(1 + m_1 k_x^2)}{m_3 \alpha_3 [m_1 k_x^2 \alpha_3 (k + \alpha_1) + k \alpha_3 + k_y^2]}, \quad (2)$$

$\alpha_1 = ((1 + m_1 k^2)/m_1)^{1/2}$, $\alpha_3 = ((1 + m_1 k_x^2 + m_3 k_y^2)/m_3)^{1/2}$, $k = (k_x^2 + k_y^2)^{1/2}$, $m_1 = \lambda_{ab}^2/\lambda^2$, $m_3 = \lambda_c^2/\lambda^2$, $\lambda = (\lambda_{ab}^2 \lambda_c)^{1/3}$, λ_{ab} is the in-plane penetration depth, $\phi_0 = hc/2e$ is the superconducting flux quantum, h is Planck's constant, c is the speed of light in vacuum, e is the charge on the electron, x is the distance perpendicular to the planes, and y is the distance parallel to the planes. The fields are summed over the geometry of the pickup loop. Assuming $\lambda_{ab} = 0.25 \mu m$ [12], this model has two free parameters: λ_c , which determines the length of the vortex, and z_0 , the distance between the sample surface and the pickup loop, which determines the magnetic amplitude of the vortex image. Fits to the two cross-sections in Figure 1 yield values for the interlayer penetration depth $\lambda_c = 5.6$ and $5.3 \mu m$. The difference between these two values is consistent with the $\sim 10\%$ differences in shape we observed from vortex to vortex. Combining the results from our detailed fitting of several vortices, as well as measuring the FWHM of many others, we estimate $\lambda_c = 5 \pm 1 \mu m$. The values obtained for z_0 are consistent with what we know of the tip geometry in contact with the surface.

The vortices imaged in Figure 1 are resolution limited in the c -axis direction. To get a better idea of the real vortex shape, the instrumental broadening can be convoluted out. For this paper we use the simplest possible deconvolution scheme:

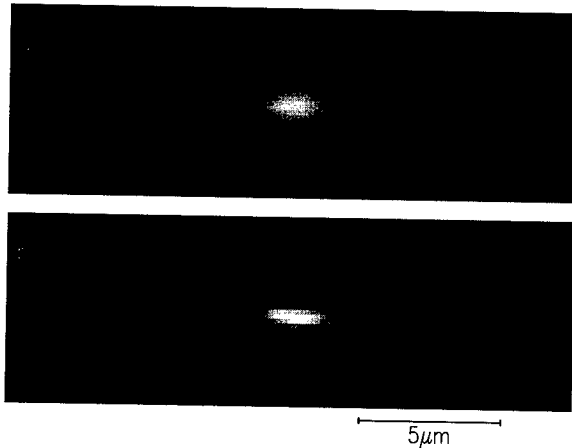


FIGURE 2. Magnified view of one vortex. (a) Raw data. (b) Image deconvoluted as described in the text to minimize the effects of instrumental broadening

If we denote the i, j th element of the finite 2-d Fourier transform of the image as I_{ij} , and that of the pickup loop flux acceptance function as L_{ij} , then the 2-d transform of the deconvoluted image is given by $I_{ij}L_{ij}^*/(L_{ij}L_{ij}^* + c)$, where $*$ denotes the complex conjugate, and c is a constant that reduces the effects of noise at high spatial frequencies. In practice we use the smallest c that produces images with acceptable spurious noise. Figure 2 shows the results from such a deconvolution for the vortex of Figure 1(d). The deconvolution significantly decreases the apparent width of the vortex, but has little effect on its length: The FWHM of the vortex image in the c -direction in Figure 2(a) is $6\mu\text{m}$, that of the deconvoluted image Figure 2(b) is $2.7\mu\text{m}$. Our modelling [6] predicts that this width should be $1.6\mu\text{m}$. (This is larger than $\lambda_{ab} \sim 0.25\mu\text{m}$ because of vortex spreading both below and above the superconducting surface.) We have found that it is difficult in practice to deconvolute instrumental broadening to reveal features smaller than a factor of two less than the size of the SQUID pickup loop.

On the other hand, the length of the vortex along the planes, which is the quantity of interest in determining λ_c , is relatively unaffected by instrumental broadening: The FWHM of Figure 2(a) along the planes (horizontally) is $13.3\mu\text{m}$; that of the deconvoluted image, Figure 2(b), is $13.2\mu\text{m}$. Figure 3 shows a comparison of a cross-section through the deconvoluted image, integrated over the c -axis direction, with the predictions of our modelling. The agreement is good.

We are aware of two reports of measurements of the c -axis penetration depth in LSCO as a function of Sr concentration x . In neither case was a sample with $x=0.17$ measured. However, in both cases an interpolation of data with x values above and below this value can be made. From the work of Uchida *et al.* [8], the interpolated value is about $4.1\mu\text{m}$. From the work of Shibauchi *et al.* [9], we obtain

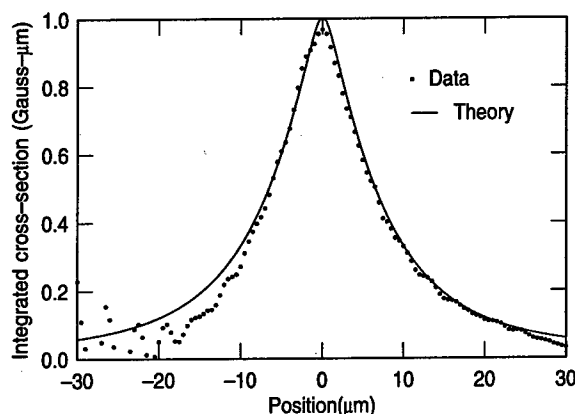


FIGURE 3. The dots are a cross-section through the center of the deconvoluted vortex image of Fig. 2b parallel to the planes, numerically integrated along the c -axis direction. The solid line is theory as described in the text.

a value between 2.9 and 4.6 μm , depending on how our interpolation of their data is made. This is to be compared with our value of $5 \pm 1 \mu\text{m}$. It appears that our values are slightly longer than those obtained using optical techniques, but this discrepancy could be due to the fact that we are not studying exactly the same samples: λ_c is strongly dependent on the Sr concentration x .

In conclusion, values for λ_c for LSCO obtained from scanning SQUID microscope measurements are in reasonable agreement with those obtained using optical techniques. This increases our confidence in measurements of λ_c in Hg-1201 [3] and Tl-2201 [1], in which disagreement with the predictions of the interlayer tunneling theory were found.

We would like to thank M. B. Ketchen for the design, and M. Bhushan for the fabrication, of the SQUIDs used in our microscope. K.A. Moler would like to acknowledge the support of an R H. Dicke post-doctoral fellowship, and NSF funding through the MRSEC award to Princeton University (DMR97-000362).

REFERENCES

1. Moler K. A., Kirtley J. R., Hinks D. G., Li T W., and Xu Ming, *Science* **279**, 1193 (1998).
2. Tsvetkov A. A. *et al.* *Nature* **395**, 360 (1998).
3. Kirtley J. R., Moler K. A., Villard G. and Maignan A., *Phys. Rev. Lett.* **81**, 2140 (1998).
4. Kirtley J. R., Moler K. A., Williams J. M. and Schlueter J. A., accepted for publication in *J. Phys. Cond. Matt.*
5. Wheatley J. Hsu T., and Anderson P. W., *Nature* **333**, 121 (1988); Anderson P. W., *Physica C* **185**, 11 (1991); *Phys. Rev. Lett.* **67**, 660 (1991); *Science* **256**, 1526 (1992); Chakravarty S., Sudbø A., Anderson P. W., and Strong S., *ibid* **261**, 331 (1993).
6. Kirtley J. R., Kogan V., Clem J.R., and Moler K. A., *Phys. Rev. B* 1 Feb. 1999 in press.
7. Pearl J., *J. Appl. Phys.* **37**, 4139 (1966).
8. Uchida S., Tamasaku K., Tajima S., *Phys. Rev. B* **53**, 14588 (1996).
9. Shibauchi T. *et al.*, *Phys. Rev. Lett.* **72**, 2263 (1994).
10. Schuetzmann J. *et al.*, *Phys. Rev. B* **55**, 11118 (1997).
11. Kirtley J. R. *et al.*, *Appl. Phys. Lett.* **66**, 1138 (1995).
12. Luke G. M. *et al.*, *Physica C* **282-287**, 1465 (1997).

Pinning strength of cuprate superconductors and pseudo-gap in the normal state

Koichi Kitazawa*, Jun-ichi Shimoyama*, Tetsuo Hanaguri*,
Takao Sasagawa and Kohji Kishio*

*Department of Superconductivity, Department of Applied Chemistry, The University of Tokyo,
Hongo, Bunkyo, Tokyo 113-8656, Japan*

**CREST, Japan Science and Technology Corporation,
Honcho, Kawaguchi, Saitama, 332-0012 Japan*

Abstract. This paper discusses the electronic structure in the vortex core in relation to the pinning potential under the influence of the pseudo-gap which opens in the normal state in the high-temperature superconductor (HTS). It is argued that the condensation energy may be significantly reduced in the under-doped regime where the pseudo-gap becomes pronounced and hence it should be deeply related with the small pinning force in this regime. The empirical scaling laws observed for the vortex behaviors in the mixed state phase diagram are also discussed in terms of the condensation energy and the anisotropy factor.

CONDENSATION ENERGY AS THE ORIGIN OF PINNING FORCE

When one considers the energy of the vortex, the penalty energy it pays in order to destroy the superconductivity becomes important, i.e.; the condensation energy as frequently expressed by

$$E_C = \frac{1}{2}N(0)\Delta_{SC}^2 \quad (1)$$

per volume in the conventional superconducting phenomenology where $N(0)$ is the density of states at the Fermi level and Δ_{SC} is the energy gap of superconductivity. Hence the minimum energy associated with the excitation of vortex from a point-like pinning center ΔE_{min} is taken as the product of E_C and the minimum possible volume of change ξ_{SC}^3 as

$$\Delta E_{min} = E_C \xi_{SC}^3 = \frac{1}{2}N(0)\Delta_{SC}^2 \xi_{SC}^3. \quad (2)$$

where ξ_{SC} is the coherence length of superconductivity. The energy ΔE_{min} is of the order of 1 eV in a typical metallic superconductor, adopting for example $\xi_{SC} = 40$ nm in Nb, which is much larger than the thermal energy in the temperature range of interest, hence minimizing the thermal fluctuation. However, in the cuprate HTS, ξ_{SC} is known to be much shorter, a few nm in the layer and only a fraction of a nm perpendicular to it. Although E_C is comparable in the conventional and HTS superconductors, ΔE_{min} in the HTS becomes much smaller, of the order of 10 meV which is comparable with the thermal energy; e.g., $k_B T = 7$ meV at 77 K. Therefore a serious thermal fluctuation may give rise to various different properties in the HTS.

PSEUDO-GAP AND CONDENSATION ENERGY

As shown in Fig. 1, a pseudo-gap develops in the HTS even above T_c , differing from the conventional superconductors.

The gap appears to continuously grow across T_c into the superconducting state. Because the distribution of the density of states is no more flat near the Fermi level, it seems that one has to equate E_C more rigorously as

$$E_C = \int (N_{NS}(E) - N_{SC}(E)) E dE \quad (3)$$

where $N_{SC}(E)$ and $N_{NS}(E)$ are the density of states in the superconducting and normal states, respectively. It has been known that the "pseudo-gap" becomes more pronounced as the carrier density reduces from over- to under-doped regimes. Consequently, one should expect E_C to decrease towards the under-doping.

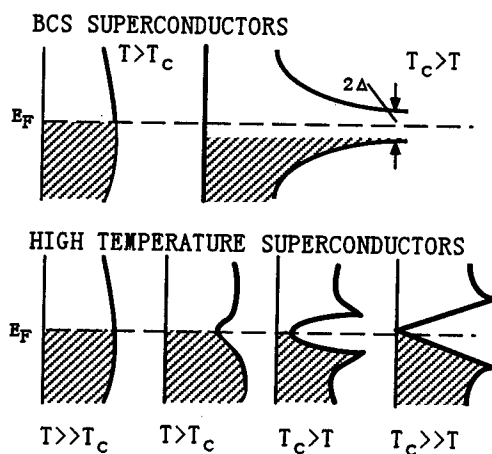


FIGURE 1. Difference in the density of states in a BCS superconductor and a HTS.

On the other hand, the superconducting gap does not decrease towards under-doping in spite of the fact that T_c goes down, violating the simple BCS relationship $2\Delta_{SC}/k_B T_c = 3.53$. This seems to be very unique to the HTS, implying that the condensation energy E_C could be the more fundamental parameter that scales T_c rather than the superconducting gap Δ_{SC} .

ANISOTROPY FACTOR, CONDENSATION ENERGY AND PSEUDO-GAP

The anisotropy factor γ defined from the resistivity anisotropy just above T_c is another parameter that changes with carrier density, increasing significantly towards under-doping. To our surprise, it is the anisotropy factor that solely determines the vortex phase diagram. In considering the vortex phase diagram, there are three important energy scales i.e. the thermal energy, the elastic energy of vortices and the pinning energy. Firstly, the competition between the thermal energy and the elastic energy determines the first order phase transition boundary, so-called vortex lattice melting or sublimation. The phase transition field B_{pt} can be universally scaled by the anisotropy factor γ as

$$B_{pt}(\text{Gauss}) = \frac{3}{\gamma^2 d} \left(\frac{T_c}{T} - 1 \right) \quad (4)$$

among the typical HTS [1], where d (in cm) is the distance between the superconducting layers.

Secondly, the competition between the thermal energy and the pinning energy determines the irreversibility field B_{irr} , a good indication of the pinning strength. In single crystals which contain rather dense pinning centers, B_{pt} is almost vanishes and B_{irr} is the only characteristic field at high temperatures. Although B_{irr} depends on the nature of the pinning centers, it is also empirically scaled [2] essentially by the anisotropy factor in a universal manner among many HTS single crystals as shown in Fig. 2.

$$B_{irr}(\text{Gauss}) = \frac{4 \times 10^7}{\gamma^2} \left(1 - \frac{T}{T_c} \right)^{1.5}. \quad (5)$$

In the lower temperature region, it is also scaled by γ as

$$B_{irr}(\text{Gauss}) \propto \left(1 - \frac{T}{T_c} \right)^{\gamma^{0.5}}. \quad (6)$$

Lastly, the peak field B_p in the magnetization curve interpreted as the disordering of the vortex lattice, namely the competition between the elastic energy of vortices and the pinning energy, is also scaled roughly by the anisotropy factor as

$$B_p(\text{Gauss}) = \frac{2 \times 10^{-7}}{\gamma^2 s^2} \quad (7)$$

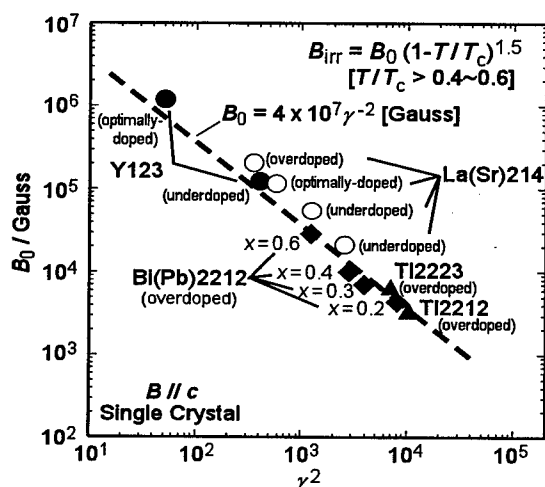


FIGURE 2. Scaling of the irreversibility field B_{irr} by the anisotropy factor γ for various HTS systems at high temperatures.

where s is the inter-layer spacing of CuO_2 . Therefore once the crystal structure of a cuprate superconductor is known, the whole magnetic phase diagram can be roughly predicted as shown in Fig. 3 as far as the anisotropy factor γ is given [3]. Small deviations are observed for the systems in which strong pinning centers are introduced by heavy particle irradiation, second phase precipitation, etc. or for the system in which pinning centers are deficient such as in the over-doped YBCO. But in the other cases, the empirical scaling laws proposed above universally hold in spite of the great difference in the anisotropy factor γ from ca. 5 of YBCO to 10^4 of Bi2212. The fact that vortex behaviors are essentially determined solely by the anisotropy factor indicates that the decrease in E_C should be understood as included in the increase in the anisotropy factor or vice versa. This leads one to think that the anisotropy must be related with the pseudo-gap. The mutual dependence among the pseudo-gap, condensation energy and anisotropy is hence a very interesting problem.

VORTEX CORE STATE: NORMAL CORE VS. LOCALIZED STATE

The eq. (3) would hold to the bulk condensation energy. Then the question is whether one can consider the vortex core state to be the same as the bulk normal state. If it is so, the vortex core must exhibit the "pseudo-gap". Renner *et al.* has observed a pseudo-gap like structure by STM/STS in a vortex core on Bi2212 [4]. Because E_C in eq. (3) decreases towards under-doping, the pinning potential would decrease accordingly. This is at least qualitatively in accord with the experimental

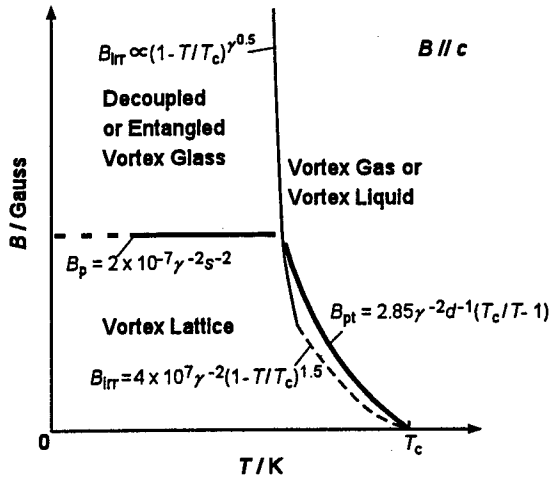


FIGURE 3. A schematic phase diagram of the HTS: the first order phase transition line B_{pt} , the irreversibility field B_{irr} , and the magnetization peak field B_p .

observations. On the other hand, when the vortex core is small enough, one expects a formation of the quantized state of the quasi-particle. Maggio-Aprile *et al.* observed a double peak tunneling structure in a vortex core on Y123 and claimed that this is the quantized state [5]. Since there have not been any further confirmation experiments made of this kind it is not yet clear why the two materials show such remarkable differences. In the latter case, eq. (3) should not directly give the condensation energy. In this regard, another question has been raised whether the quasi-particles can be confined in a vortex core in a d -wave superconductor. Although we do not go into details here, whether a localized state is formed would give influence when to consider the vortex pinning potential.

PSEUDO-GAP AT THE LOW TEMPERATURE

In order to evaluate the pinning potential by eq. (3) the two quantities $N_{NS}(E)$ and $N_{SC}(E)$ must be compared at the same temperature. It has been claimed that the pseudo-gap has the same symmetry $d_{x^2-y^2}$ as the superconducting gap. It suggests that the pseudo-gap would develop as temperature is lowered in a similar manner as the superconducting gap. It is not yet well discriminated experimentally how the pseudo-gap differs from superconducting gap in the low temperature region. In the tunneling experiments, at lowering the temperature, the pseudo-gap seems to grow gradually and continuously switches to the superconducting gap at T_c , growing further continuously. During this process it is quite strange that the gap size does not seem to change significantly but the gap only becomes more pronounced with the growth of the edge peaks below T_c . If the two gaps are exactly the same, the

E_C value estimated from eq. (3) would be zero. Of course this is not likely but it is possible that the condensation energy and hence the pinning potential may be greatly reduced because of this reason especially in the under-doped regime.

CORE STATE DIFFERING FROM THE NORMAL STATE

In the HTS there have been many possible electronic states proposed that might occur under some conditions of the doping state: anti-ferromagnetically (AF) ordered state, charge ordered state, CDW, SDW, spin singlet state, stripes, etc. Because of the extremely small core size, charging of this length scale would not cost much energy. For example, formation of an AF ordered state in a vortex core would prefer an expulsion of holes from the core to make the core negatively charged surrounded by the positive charge cloud. There has been some indication by Hall coefficient measurements in the mixed state to suggest the charged vortex core [6]. If this is the case, eq. (3) would under-estimate the condensation energy in relation with the pinning potential. The vortex state in the HTS still seems to be quite mysterious.

CONCLUSIONS

It has been discussed that the superconductivity phenomenology in the HTS is much complex and a due consideration must be paid to the presence of the pseudo-gap in the normal state. This can explain why the pinning strength becomes very small in the under-doped regime. But it is argued further that the core state may not be necessarily the same as the pseudo-gapped normal state in the bulk due to the extremely short coherence length.

The third phase may appear in the vortex core.

REFERENCES

1. T. Sasagawa, K. Kishio, Y. Togawa, J. Shimoyama, and K. Kitazawa, Phys. Rev. Lett., **80**, 4297 (1998).
2. J. Shimoyama, Supercond. Sci. and Technol. to be published as a review article.
3. K. Kitazawa, J. Shimoyama, H. Ikuta, T. Sasagawa, and K. Kishio, Physica C **282-287**, 335 (1997).
4. Ch. Renner, B. Revaz, J.-Y. Genoud, K. Kadowaki, and O. Fischer, Phys. Rev. Lett., **80**, 149 (1998).
5. I. Maggio-Aprile, Ch. Renner, A. Erb, E. Walker, and O. Fischer, Phys. Rev. Lett. **75**, 2754 (1995).
6. T. Nagaoka, Y. Matsuda, H. Obara, T. Terashima, I. Chong, M. and M. Suzuki, Phys. Rev. Lett., **80**, 3594 (1998).

c-Axis Twist $\text{Bi}_2\text{Sr}_2\text{CaCu}_2\text{O}_{8+\delta}$ Josephson Junctions: A New Phase-Sensitive Test of Order Parameter Symmetry¹

R. A. Klemm*, C. T. Rieck[†] and K. Scharnberg[†]

**Materials Science Division, Argonne National Laboratory
9700 South Cass Ave., Argonne, IL 60439 USA*

*[†]Fachbereich Physik, Universität Hamburg
Jungiusstraße 11, D-20355 Hamburg, Germany.*

Abstract. Li *et al.* found that the critical current density J_c^J across atomically clean c-axis twist junctions of $\text{Bi}_2\text{Sr}_2\text{CaCu}_2\text{O}_{8+\delta}$ is the same as that of the constituent single crystal, J_c^S , independent of the twist angle ϕ_0 , even at T_c . We investigated theoretically if a $d_{x^2-y^2}$ -wave order parameter might twist by mixing in d_{xy} components, but find that such twisting cannot possibly explain the data near to T_c . Hence, the order parameter contains an s-wave component, but *not* any $d_{x^2-y^2}$ -wave component. In addition, the c-axis Josephson tunneling is completely incoherent. We also propose a c-axis junction tricrystal experiment which does not rely upon expensive substrates.

EXPERIMENTAL INTRODUCTION

It has recently become possible to prepare extraordinarily perfect bicrystal Josephson junctions with $\text{Bi}_2\text{Sr}_2\text{CaCu}_2\text{O}_{8+\delta}$ (Bi2212). [1,2] These junctions are prepared by cleaving a very high quality single crystal of Bi2212 in the *ab*-plane, quickly examining the cleaved parts under a microscope, rotating one part an arbitrary angle ϕ_0 about the *c*-axis with respect to the other, placing them back together, and fusing them by heating just below the melting point for 30 h. [1,2] A schematic view of the resulting *c*-axis bicrystal is shown in Fig. 1. By examining these bicrystals with high resolution transmission electron microscopy (HRTEM), electron energy-loss spectroscopy, and energy dispersive x-ray spectroscopy, they were found to be atomically clean over the entire areas studied ($\approx 10^2 \mu\text{m}^2$), and the periodic lattice distortion was atomically intact on each side of the twist junction. [1]

¹) Supported by USDOE-BES through Contract No. W-31-109-ENG-38, by NATO through Collaborative Research Grant No. 960102, and by the DFG through the Graduiertenkolleg "Physik nanostrukturierter Festkörper." Send correspondence to klemm@anl.gov.

To each of the 12 bicrystals measured, six electrical leads were attached using Ag epoxy, two on opposite sides of each of the two constituent single crystals, and two across the bicrystal. By applying the current I across the central leads straddling the bicrystal, and a voltage V across two of the other leads, it was possible to measure the I/V characteristics of the c -axis transport across each constituent single crystal, and across the twisted bicrystal junction in the same run. The critical current I_c was easily identified, as V dropped by 5-8 orders of magnitude at a well-defined I value, provided that the temperature T was less than the transition temperature T_c . [1,2] For each bicrystal junction, they measured the critical current $I_c^J(T)$ and the junction area A^J . Similarly, for each constituent single crystal, they measured the critical current $I_c^S(T)$ and the area A^S . I_c was often unmeasurable at low T , so comparisons of all 12 samples were made at $0.9T_c$. [2]

Of the 12 bicrystal junctions, 7 were prepared with $40^\circ \leq \phi_0 \leq 50^\circ$, and one each at 0° and 90° . Although I_c^S and I_c^J at $T = 0.9T_c$ varied from sample to sample, and the critical current densities $J_c^S = I_c^S/A^S$ and J_c^J/A^J also varied from sample to sample, with only one exception (probably due to a sample that had weakly attached leads), *the ratio J_c^J/J_c^S of critical current densities was the same (1.00 ± 0.06) for each sample!* In a sample with $\phi_0 = 50^\circ$, $J_c^J(T)/J_c^S(T) = 1.0$ over the entire range $10 \text{ K} \leq T < T_c$, and $I_c(T)/I_c(0)$ fit the Ambegaokar-Baratoff curve. [2,3] As discussed in the following, these results comprise very strong evidence for an s -wave component of the superconducting order parameter (OP) at and below T_c , and *cannot* be explained within a dominant $d_{x^2-y^2}$ -wave scenario.

GROUP THEORY

Although the crystal structure of Bi2212 is orthorhombic, the orthorhombic distortion is *different* from that of $\text{YBa}_2\text{Cu}_3\text{O}_{7-\delta}$, with different unit cell lengths a and b along the *diagonals* between the Cu-O bond directions in the CuO_2 planes. In addition, there is an incommensurate lattice distortion $\mathbf{Q} = (0, 0.212, 1)$ along one of these diagonals, the b -axis, which is clearly seen in the HRTEM pictures of

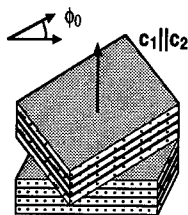


FIGURE 1. Illustration of a c -axis twist junction with twist angle ϕ_0 .

TABLE 1. Singlet superconducting OP eigenfunctions in the angular momentum (ℓ) and lattice (n, m) representations, their group theoretic (GT) notations, and character table for the orthorhombic point group C_{2v} in the form appropriate for Bi2212. σ_b represents the strict bc -mirror plane reflection.

GT	OP Eigenfunction	E	σ_a	σ_b	C_2
A_1	$ s + d_{xy}\rangle$ $\xrightarrow{\ell} \tilde{a}_0 + \sqrt{2} \sum_{n=1}^{\infty} \tilde{a}_n \cos[2n(\phi_k - \pi/4)]$ $\xrightarrow{n,m} \sum_{n,m=0}^{\infty} \{ \cos(nk_x a) \cos(mk_y a) [\tilde{a}_{nm} + \tilde{a}_{mn}]$ $+ \sin(nk_x a) \sin(mk_y a) [\tilde{c}_{nm} + \tilde{c}_{mn}] \}$	+1	+1	+1	+1
A_2	$ d_{x^2-y^2} + g_{xy}(x^2-y^2)\rangle$ $\xrightarrow{\ell} \sqrt{2} \sum_{n=1}^{\infty} \tilde{b}_n \sin[2n(\phi_k - \pi/4)]$ $\xrightarrow{n,m} \sum_{n,m=0}^{\infty} \{ \cos(nk_x a) \cos(mk_y a) [\tilde{a}_{nm} - \tilde{a}_{mn}]$ $+ \sin(nk_x a) \sin(mk_y a) [\tilde{c}_{nm} - \tilde{c}_{mn}] \}$	+1	-1	-1	+1

the twist junctions. [1] Since \mathbf{Q} contains a c -axis component, only the bc -plane is a strict crystallographic mirror plane. [1] Group theory and Bloch's theorem dictate that the superconducting OP must reflect the crystal symmetry. In Table 1, we have presented the allowable forms of the OP eigenfunctions for Bi2212. [4] We presented both the angular momentum (fixed k_F , variable ϕ_k , with quantum numbers ℓ) and the nearly tetragonal lattice (variable k_x, k_y , with quantum numbers n, m) representations of the OP eigenfunction forms. As indicated, the two OP eigenfunction forms are respectively even and odd with respect to reflections about the bc -plane (the σ_b operation). [5] Thus, in Bi2212, s -wave and $d_{x^2-y^2}$ -wave OP components are completely *incompatible*, and do not mix except possibly below a second (as yet unobserved) thermodynamic phase transition. [4]

LAWRENCE-DONIACH MODEL

Previously, we investigated whether it might be possible to explain the lack of any ϕ_0 -dependence of the c -axis critical current from a purely d -wave scenario. [6] We assumed that in the n th layer, the dominant OP component was $d_{x^2-y^2}$, the amplitude A_n of which became non-vanishing below $T_c = T_{cA}$. By choosing the sub-dominant OP component to be d_{xy} with amplitude B_n and bare transition temperature $T_{cB} < T_{cA}$, we considered whether the overall OP could "twist" by mixing $d_{x^2-y^2}$ - and d_{xy} -wave components, to accommodate for the physical twist in the Josephson junction between the adjacent layers $n = 1$ and $n = -1$.

There are basically two distinct, relevant energy scales in this problem. One is the relative amount of the two *incompatible* d -wave components. This is determined mainly by the different bare T_c values, T_{cA} and T_{cB} , arising from the pairing inter-

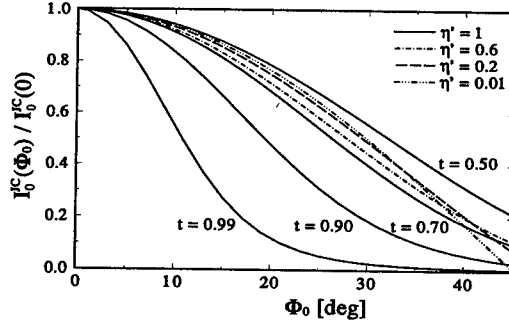


FIGURE 2. Plot of $I_c(\phi_0)/I_c(0)$ for the case of a dominant $d_{x^2-y^2}$ -wave and subdominant d_{xy} -wave OP, the relative amounts varying with layer index away from the twist junction. [6] In these curves, $T_{cB}/T_{cA} = 0.2$, $T_{cB}^</math>/ $T_{cA} = 0.1304$, $\epsilon/6\beta_A = 0.5$, $\delta/6\beta_A = 0.1$, and the $\eta = \eta' = 1$ curves are solid. At $t = T/T_{cA} = 0.7$, curves for $\eta = 1$ and various η' values are shown.$

actions. Assuming there is only one observable zero-field superconducting phase transition at $T_c = T_{cA}$, then $T_{cB} \ll T_{cA}$, the correspondingly suppressed bulk $T_{cB}^< < T_{cB}$, below which the OP is nodeless, and $|B_n| \ll |A_n|$ for $n \rightarrow \pm\infty$. This results in a strong locking of an anisotropic OP onto the lattice, with the anti-nodes of the purported $d_{x^2-y^2}$ -wave OP component locking onto the Cu-O bond directions on each side of the twist junction. For $\phi_0 = 45^\circ$, these OP eigenfunctions are thus orthogonal, and $I_c(45^\circ) = 0$.

The second energy scale is the strength of the Josephson coupling η (and η' across the twist junction) of the OP components between adjacent layers. This gives rise to a finite c -axis coherence length, which diverges as $T \rightarrow T_c$, allowing some *real* OP mixing (or twisting), suppressing $I_c(\phi_0)$ for $\phi_0 \neq 0$, as shown in Figs. 2 and 3. For strong interlayer coupling, $\eta \approx 1$, it is possible that $I_c(45^\circ) \neq 0$ for $T \approx 0.5T_c$, as pictured in Figs. 2 and 3. However, Bi2212 is extremely anisotropic, and we thus expect $\eta \approx \eta' \lll 1$. In Fig. 3, we recalculated $I_c(\phi_0, T)$ for this case. Clearly, for $\eta = \eta' = 0.001$, $I_c(45^\circ) \approx 0$ for $T \geq 0.5T_c$. Thus, it is *extremely difficult, if not impossible* to explain the data of Li *et al.* by assuming a dominant $d_{x^2-y^2}$ -wave OP component with nodes at low T . [2,4,6]

CONCLUSIONS

We thus conclude that the superconducting OP in Bi2212 is the the group A_1 , which contains the s -wave component, but does *not* contain any purported $d_{x^2-y^2}$ -wave component near to T_c . However, these experiments also provide information about the nature of the interlayer tunneling processes. If there were a substantial

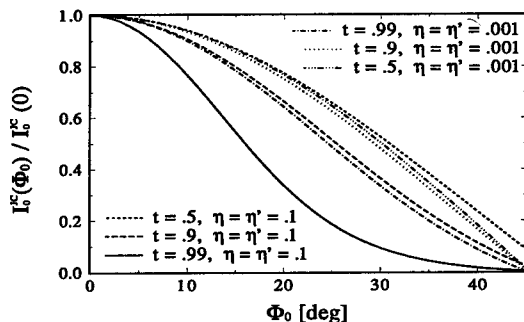


FIGURE 3. Plot of $I_c(\phi_0)/I_c(0)$ for the case considered in [6] of a dominant $d_{x^2-y^2}$ -wave and subdominant d_{xy} -wave OP, the relative amounts varying with layer index away from the twist junction. Curves for $\eta = \eta' = 0.1$ and $\eta = \eta' = 0.001$ with $t = T/T_{cA} = 0.99, 0.9, 0.5$ are presented. The other parameters are the same as in Fig. 2.

amount of coherent interlayer tunneling, then the OP would be entirely isotropic s -wave in form. For free-particle Fermi surfaces, this scenario is possible, as rotated Fermi surfaces on opposite sides of the twist are degenerate. However, Bi2212 is generally thought to have a tight-binding Fermi surface. In this case, intertwist coherent tunneling is only possible for $\phi_0 \approx 0, 90^\circ$, for which a finite fraction of the rotated Fermi surfaces are degenerate. Thus coherent tunneling would result in a larger $I_c(\phi_0)$ for $\phi_0 = 0^\circ, 90^\circ$ than for any other ϕ_0 value, contrary to experiment. [2] Hence, we conclude that the interlayer tunneling is entirely incoherent, without any discernible interlayer forward scattering, even between adjacent layers on the same side of the twist junction. [6]

Thus, the OP eigenfunction is $|s + d_{xy}\rangle$ with GT notation A_1 (Table 1), which contains the s -wave component. This OP eigenfunction could exhibit nodes, but it is *even* about reflections in the bc -mirror plane, and thus does not contain any amount of the odd $d_{x^2-y^2}$ -wave OP component. This conclusion is further supported by new c -axis Josephson junction experiments between Bi2212 and Pb, which showed strong evidence for an s -wave component at low T . [7]

NEW TRICRYSTAL EXPERIMENT PROPOSAL

Since the c -axis junctions are qualitatively superior to the ab -plane thin film junctions, we propose a new tricrystal (or tetracrystal) experiment using c -axis junctions, as pictured in Fig. 4. This experiment does not require any expensive substrates, and the grain boundaries are intrinsically far superior to those of the planar junctions. [1,8] In addition, since I_c for the c -axis junctions is ordinarily

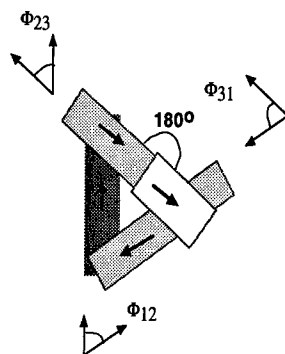


FIGURE 4. Proposed configuration of a c -axis version of the tricrystal ring experiment. Dark crystal: bottom. Light crystal: top. Intermediate shading: equal thickness crystals. Arrows indicate the direction of a given single crystal axis.

much larger than for the ab -plane due to larger junction areas, it is much easier to satisfy the experimental requirement $I_c L / \Phi_0 \gg 1$, where L is the induction of the ring and Φ_0 is the flux quantum. [4]

REFERENCES

1. Y. Zhu, Q. Li, Y. N. Tsay, M. Suenaga, G. D. Gu, and N. Koshizuka, *Phys. Rev. B* **57**, 8601 (1998); Y. N. Tsay, Q. Li, Y. Zhu, M. Suenaga, G. D. Gu, and N. Koshizuka, in *Superconducting Superlattices II: Native and Artificial*, I. Bozovic and D. Pavuna, editors, *Proceedings of SPIE* **3480**, 21 (1998); Y. Zhu, private communication.
2. Q. Li, Y. N. Tsay, M. Suenaga, R. A. Klemm, G. D. Gu, and N. Koshizuka, submitted to *Nature*.
3. V. Ambegaokar and A. Baratoff, *Phys. Rev. Lett.* **10**, 486 (1963); **11**, 104 (1963).
4. R. A. Klemm, C. T. Rieck, and K. Scharnberg, unpublished (cond-mat/9811303).
5. M. Tinkham, *Group Theory in Quantum Mechanics* (McGraw-Hill, New York, 1964).
6. R. A. Klemm, C. T. Rieck, and K. Scharnberg, *Phys. Rev. B* **58**, 1051 (1998).
7. M. Mößle and R. Kleiner, *Phys. Rev. B* **59**, xxxx (1999) (in press).
8. C. C. Tsuei, J. R. Kirtley, C. C. Chi, L. S. Yu-Jahnes, A. Gupta, T. Shaw, J. Z. Sun, and M. B. Ketchen, *Phys. Rev. Lett.* **73**, 593 (1994).

High pressure X ray diffraction studies of rare earth doped Bi 2212 system

Ravhi S Kumar, A. Sekar, N. Victor Jaya and S. Natarajan

Department of Physics, Anna University, Chennai 600 025, India

Abstract. High pressure X ray diffraction studies up to 15GPa were performed on the Y doped Bi2212 compound with the rare earth concentration $x = 0.1$ at the calcium site. From the studies it has been found that the system remains in the orthorhombic structure up to 15GPa. The relative volume is found to decrease around 15GPa. This may be a positive indication for a pressure induced structural transition in the system beyond 15GPa.

I INTRODUCTION

The bismuth cuprate Bi2212 has drawn much attention in recent years as it provides several important information about the metal - insulator transition (MIT) when a rare earth ion is doped at the calcium site [1,2]. Earlier it was believed that the change in the carrier concentration induces a MIT. The change in the carrier concentration was either achieved by doping or by changing the oxygen stoichiometry[3,4]. To reveal the pressure effect on the structure of the system high pressure X ray diffraction studies were performed up to 15GPa. The results show the structural stability of the system up to 15GP.

II EXPERIMENT

The $\text{Bi}_2\text{Sr}_2\text{Ca}_{0.9}\text{Y}_{0.1}\text{Cu}_2\text{O}_{8+y}$ crystals were grown by spontaneous nucleation technique as described elsewhere [5]. The crystals were crushed in to powder and loaded in to the 200 micron hole of a stainless steel gasket. The gasket is fixed in the Mao - Bell diamond anvil cell with 4:1 pressure transmitting medium. The powder X-ray diffraction experiments were performed employing a rotating anode X-ray generator operating at 50kV and 100mA. A high purity Ge detector has been used for the data collection. The pressure calibration is made by using the Ag sample. The experiments were performed up to 15GPa.

III RESULTS AND DISCUSSION

The cell parameters calculated at ambient conditions for the compound are $a=5.33(3)\text{\AA}$, $b=5.46(2)\text{\AA}$ and $c=30.50\text{\AA}$. The volume has been calculated to be $V=890.565\text{\AA}^3$. The experimental data on the pressure dependence of the relative volume were fitted using the Birch equation [6] as given below,

$$P = \frac{3}{2}B_0\left(\left(\frac{V_0}{V}\right)^{2.333} - \left(\frac{V_0}{V}\right)^{1.666}\right) \quad (1)$$

where P is pressure at the sample site and V_0 is the original volume V is the reduced volume and B_0 is the bulk modulus.

The bulk modulus value was calculated to be $164(5)\text{GPa}$. The cell parameters calculated at 12.5GPa are $a=5.43(1)\text{\AA}$, $b=5.31(1)\text{\AA}$ and $c=28.94\text{\AA}$. and the volume is obtained to be $V=835.227\text{\AA}^3$. When compared with the equation of state of other high T_c compounds the $\text{Bi}_2\text{Sr}_2\text{Ca}_{0.9}\text{Y}_{0.1}\text{Cu}_2\text{O}_{8+y}$ system is found to be more compressible. There exist no discontinuities in the reduced volume calculated for the compound. There is a large volume reduction observed in this system near 15GPa which may be a positive indication for a pressure induced structural transition beyond 15GPa , as there exist reports for the pressure induced structural transitions observed in the Y based high T_c compounds [7].

The orthorhombic structure of the compound is found to be stable up to 15GPa and this result is similar to the high pressure reports for the undoped $\text{Bi}2212$ compound where a tetragonal structure has been found stable up to 50GPa [8].

IV CONCLUSION

High pressure energy dispersive X ray diffraction experiments were performed for the $\text{Bi}_2\text{Sr}_2\text{Ca}_{0.9}\text{Y}_{0.1}\text{Cu}_2\text{O}_{8+y}$ system up to 15GPa . From the experiments, the compound is found to be in the orthorhombic structure up to 15GPa . A considerable reduction in the relative volume has been observed for the compound near 15GPa which may be an strong indication of a pressure induced structural transition beyond 15GPa .

V ACKNOWLEDGEMENT

The author Ravhi S Kumar wishes to thank CSIR, India for financial assistance

REFERENCES

1. A. Q. Pham, N. Merrian, A. Maignan, F. Studer, C. Michel and B. Raveau, *Physica C* **210**,350 (1993)
2. Noburu Fukushima and Masahiko Yoshiki, *Phys.Rev.B* **50**,2696, (1994)
3. W. A. Groen, D. M. de Leeuw and L. F. Fainer, *Physica C* **165**, 55, (1990)

4. N. Sanada, T. Nakadaira, M. Shimomura, Y. Suzuki, Y. Fukuda, M. Nagoshi, Y. Syono and M. Tachiki, *Physica C* **263**, 286, (1996)
5. R. Jayavel, A. Thamizhavel, P. Murugakoothan, C. Subramanian and P. Ramasamy, *Physica C* **215**, 429, (1993)
6. F. Birch, *Phys.Rev.B* **71**, 809, (1947)
7. J. S. Olsen, S. Streenstrup, I. Johannsen and L. Gerward, *Z.Phys.B* **72**, 165, (1988)
8. J. Staun Olsen and S. Streenstrup, *Physica Scripta* **44**, 211, (1991)

Violation of the Ambegaokar-Baratoff relation in the c -axis transport in Bi-2212 high quality stacks

Yu.I.Latyshev*[†] and T.Yamashita*

*Research Institute of Electrical Communication, Tohoku University, 2-1-1, Katahira, Aoba-ku, Sendai 980-8577, Japan

[†]Institute of Radio-Engineering and Electronics, Russian Acad. of Sciences, 11 Mokhovaya str., Moscow 103907, Russia

Abstract. We studied the c -axis transport in the high quality Bi-2212 stacked junctions fabricated by the double-sided focused ion beam (FIB) processing of the single crystal whiskers. We found the value of the critical current to be considerably (by factor 30) below the value given by the Ambegaokar-Baratoff (AB) relation in the BCS model at low temperatures. The results are discussed as a possibility of the d -wave partially coherent interlayer tunneling.

INTRODUCTION

The symmetry of the order parameter in the layered high- T_c cuprates has been the subject of the numerous experimental and theoretical studies of the last time. Some evidence of the d -wave type symmetry has been obtained from the photoemission experiments with the high angular resolution (APRES) [1] and from the in-plane tunneling experiments along different crystallographic directions [2]. The valuable information about the order parameter symmetry can also be found from the c -axis transport studies, in particular analyzing intrinsic Josephson effect (IJE) [3] originating from the Josephson tunneling between elementary $Cu-O$ layers. One of the problem in studies of the IJE is related with the selfheating and the quasiparticle injection effects [4] masking tunneling characteristics at the high bias voltage. Here we report on the fabrication of high quality stacked junctions in which both parasitic effects are substantially eliminated. By direct measurements of the gap voltage V_g and the normal state resistance R_N at $V > V_g$ we found that the value of the Josephson tunneling current is about 30 times smaller the value expected from the conventional AB relation [5].

TABLE 1. Parameters of the stacked Bi-2212 junctions.

No	S (μm^2)	R _N (k Ω)	I _c (μA)	J _c (A/cm ²)	T _c (K)	V _g (V)	N	V _g /N (mV)
#1	6.0	2.1	36	600	76	1.1	69	16
#2	2.0	6.5	12	600	76	1.3	65	20
#3	1.5	4.6	6	400	78	1.1	38	29
#4	0.6	10	0.24	40	76	1.7	34	50
#5	<1	13	0.30	30-60	-	-	-	-
#6	0.3	30	0.07	23	78	2.2	50	44

RESULTS AND DISCUSSION

We used the $\text{Bi}_2\text{Sr}_2\text{CaCu}_2\text{O}_{8+d}$ (Bi-2212) whiskers as the base material for the stacks fabrication. Whiskers have been grown by the Pb-free method [6] and have been characterized by TEM as a very perfect crystalline object [6]. We developed the FIB and the ion milling techniques for a fabrication of the Bi-2212 stacked junctions with in-plane size from several microns down to the submicron scale without degradation of T_c (see Table). The stages of the fabrication are shown at Fig. 1. We used for fabrication a conventional FIB machine of Seiko Instruments Corp., SMI-900 (SP) operating with the Ga^+ -ion beam with the energy ranging from 15 to 30 keV and the beam current from 8 pA to 50 nA. For the smallest current the beam diameter can be focused down to 10 nm. The overlap geometry of the stack let us to avoid the effect of the quasiparticle injection usually occurs in the junctions of the "mesa" type with the normal metal top electrode [3,4].

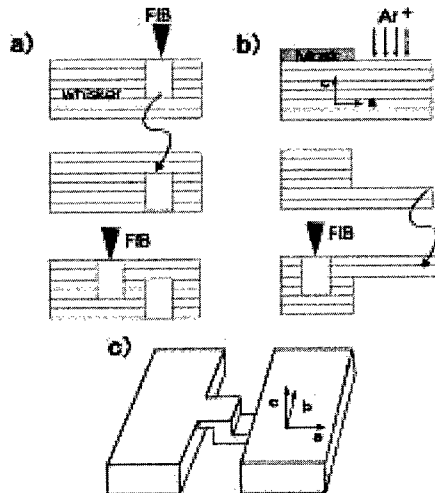


FIGURE 1. Stages of the stack fabrication with FIB (a), FIB combined with the ion milling (b), a schematic view (c) of the submicron Bi-2212 stacked junction.

The $\rho_c(T)$ dependences of the stacks were typical to the slightly overdoped *Bi-2212* case, with $T_c \approx 77$ K and $\rho_c(300) \approx 10\text{--}12$ Ω cm. The critical current density along the *c*-axis for the junctions with in-plane area $S > 2$ μm^2 was typically $J_c \approx 6 \cdot 10^2$ A/cm² at 4.2 K. The dependences of J_c on the parallel magnetic field for bigger stacks demonstrate quite good Fraunhofer patterns [7] which proved the presence of the DC intrinsic Josephson effect in our stacks.

Fig. 2 shows the large current and voltage scale *IV* characteristics of two stacks with a decrease of S down to 0.6 μm^2 . The gap voltage at $V = V_g$ and the normal state resistance R_N at $V > V_g$ are well defined. The R_N was practically temperature independent and corresponds to the resistivity value ρ_c ($V > V_g$) ≈ 12 Ωcm . It gives a possibility to estimate the number of the elementary junctions, N , using a simple formula: $N = R_N S / \rho_c(V > V_g) t$ with t the spacing between elementary superconducting layers. For the submicron junctions (Fig. 2b) we have not observed the *S*-shaped *IV* characteristics. It implies that the self-heating and the non-equilibrium injection effects [4] are essentially eliminated. As a result we found that the superconducting gap of the elementary junction $2 \Delta_0 = e V_g / N$ reaches in submicron junctions a value $2 \Delta_0 \approx 50$ meV (see Table), which is consistent with the value found recently from the surface tunneling measurements [8]. The extended scale *IV* characteristic for a bigger junction # 2 is shown in the Fig. 2c. The multibranch structure [3] is clearly seen. A variation of the critical current along the stack is not big, indicating a good uniformity of our structures.

One of the main purpose of the work was to check up the AB relation directly from the tunneling measurements at the possibly reliable conditions. For the elementary junction at low temperatures the AB relation at low temperatures can be

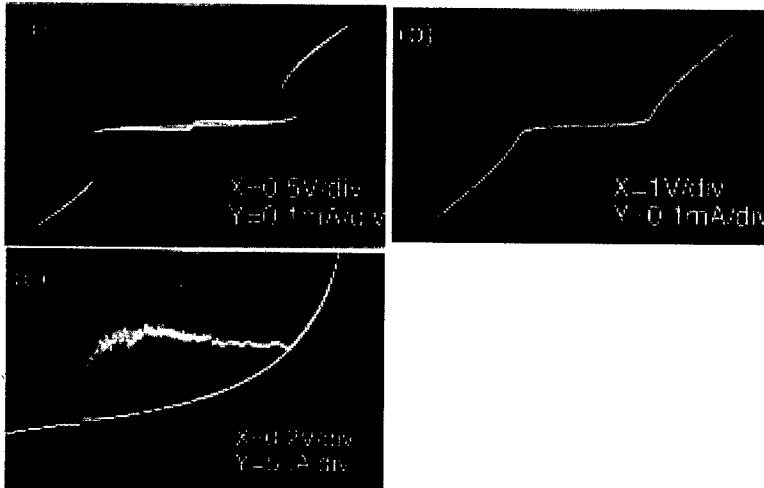


FIGURE 2. The large current and voltage scale (a,b) and the extended scale (c) *I-V* characteristics of the *Bi-2212* stacks: (a,c) #2, $S = 2$ μm^2 ; (b) #4, $S = 0.6$ μm^2 . $T = 4.2$ K.

expressed as follows $J_c \rho_c (V > V_g) t = (\pi/4)(2\Delta/e)$. We use for J_c the value $6 \cdot 10^2$ A/cm², found for bigger junctions, since for the submicron junctions the value of J_c is suppressed (see Table) as we consider [9] due to the Coulomb blockade effect. Using for ρ_c the value 12 Ω cm, and $s=1.5$ nm, we find for the left hand of expression the value 1.1 mV which is by factor 30 less than $(\pi/4)(2\Delta/e)$. It indicates that the observed critical current density is much less than the value predicted by the BCS model for the s -wave Josephson tunneling. The AB relation has been derived for the incoherent pair tunneling between the s -wave superconductors, i.e. in assumption that the momentum of the pair is not conserved in the process of tunneling. For the case of the d -wave symmetry the incoherent tunneling leads to the zero critical current [10]. Hence to explain the violation of the A-B relation in terms of the d -wave tunneling we should admit the d -wave tunneling to be partially coherent. Unfortunately the lack of the relevant theory do not let us do more certain conclusions concerning the degree of coherency in our case.

Another possibility to explain our result is to admit the mixed $d + s$ symmetry with a small contribution of the s -wave part, providing the critical current even in the case of the incoherent tunneling. That possibility appears to be less probable. Our preliminary studies of the c -axis transport on $\pi/2$ -twisted $S/N/S$ junctions, formed by the crossed *Bi-2212* whiskers, show very sharp zero bias conductance peak [11]. The result can be adequately explained by the zero energy Andreev bound state appearing in the N -layer due to the d -wave type of symmetry in the superconducting electrodes [11].

ACKNOWLEDGEMENT

The authors are acknowledged to L. Boulaevskii and S. Shafranuk for valuable discussions and to S.-J. Kim for an assistance in experiment. The work has been supported by the Russian HTS State Program, grant No. 95028.

REFERENCES

1. Z.-X. Shen, D.S. Dessau, B.O. Wells et al. Phys. Rev. Lett. 70, 1553 (1993).
2. See e.g. J.Y.T. Wei et al. Phys. Rev. Lett. 81, 2542 (1996).
3. R. Kleiner et al. Phys. Rev. Lett. 68, 239 (1992).
4. J. Takeya et al. Physica C, 293, 220 (1997); A. Yurgens et al. Phys. Rev. B53, R 887 (1996).
5. V. Ambegaokar and A. Baratoff, Phys. Rev. Lett. 10, 486 (1963); 11, 104 (1963).
6. Yu.I. Latyshev et al. Physica C, 216, 471 (1993).
7. Yu.I. Latyshev, J.E. Navelskaya, and P. Monceau, Phys. Rev. Lett. 77, 932 (1996).
8. N. Myakawa et al. Phys. Rev. Lett. 80, 157 (1998).
9. Yu.I. Latyshev, S.-J. Kim, and T. Yamashita, Pis'ma Zh. Eksp. Teor. Fiz. 69, 75 (1999).
10. R. A. Klemm et al. Phys. Rev. B 58, 14203 (1998).
11. Yu.I. Latyshev, S. Shafranuk, and T. Yamashita, unpublished.

Superconductivity-induced effect on c -axis electronic Raman scattering in $\text{Bi}_2\text{Sr}_2\text{CaCu}_2\text{O}_{8+\delta}$ single crystals

H.L. Liu,¹ G. Blumberg,¹ M.V. Klein,¹ P. Guptasarma,² and D.G. Hinks²

¹ *Department of Physics and Science and Technology Center for Superconductivity, University of Illinois at Urbana-Champaign, Urbana, Illinois 61801-3080*

² *Materials Science Division and Science and Technology Center for Superconductivity, Argonne National Laboratory, Argonne, Illinois 60439*

Abstract. We report on the c -axis-polarized electronic Raman scattering of $\text{Bi}_2\text{Sr}_2\text{CaCu}_2\text{O}_{8+\delta}$ single crystals with various oxygen concentrations. Below T_c , there is a low-energy redistribution of the electronic continuum and the presence of a 2Δ peak-like feature for all doping levels studied. The superconductivity-induced effect is also accumulated from frequencies as high as 40Δ .

INTRODUCTION

The unusual aspects of the c -axis charge dynamics in the high- T_c cuprates continue to attract much attention. A.J. Leggett and P.W. Anderson discussed this subject in their articles in "Science" [1]. Recent experiments have provided new insights about the c -axis electrodynamics of cuprates. Analysis of the interlayer infrared conductivity of $\text{Tl}_2\text{Ba}_2\text{CuO}_{6+\delta}$, $\text{La}_{2-x}\text{Sr}_x\text{CuO}_4$ and $\text{YBa}_2\text{Cu}_3\text{O}_{6.6}$ reveals an anomalously large energy scale extending up to mid-infrared frequencies that contributes to the spectral weight in the superconducting condensate [2]. New measurements of surface impedance in $\text{YBa}_2\text{Cu}_3\text{O}_{7-\delta}$ show that the c -axis penetration depth never has the linear temperature dependence seen in the ab plane [3]. Images of interlayer vortices in $\text{Tl}_2\text{Ba}_2\text{CuO}_{6+\delta}$ and $\text{HgBa}_2\text{CuO}_{4+\delta}$ give a value of c -axis penetration depth of a factor 10-20 longer than that predicted by the interlayer tunneling model, indicating the condensation energy available through this mechanism is much smaller than is required for superconductivity [4].

In this paper, we study the c -axis-polarized electronic Raman scattering in the $\text{Bi}_2\text{Sr}_2\text{CaCu}_2\text{O}_{8+\delta}$ (Bi-2212) cuprates. Raman scattering has been proved to be a valuable technique for understanding the quasiparticle dynamics on different regions of the Fermi surface in the cuprate systems by orienting incoming and outgoing

photon polarizations [5]. The electronic Raman spectra polarized in the *ab*-plane of Bi-2212 have been extensively studied [6]. In contrast, Raman data on the electronic scattering of Bi-2212 for photons polarized along the *c*-axis are rare [7]. This is primarily due to the fact that Bi-2212 grows easily as thin sheets along the *ab*-plane – it is very difficult to grow “thick” single crystals of this material.

EXPERIMENTAL

Single crystals of Bi-2212 were grown near-stoichiometric using a solvent-free floating zone process in a double-mirror image furnace modified for very slow growth. We have repeatedly studied the same single crystal of dimensions $5 \times 1 \times 0.5$ mm³ after successive annealing steps under controlled oxygen partial pressure. The superconducting transition determined by a dc magnetization measurement showed the sample to be successively overdoped (onset $T_c = 84$ K, $\Delta T_c = 4$ K), slightly overdoped ($T_c = 92$ K, $\Delta T_c = 2$ K), optimally doped ($T_c = 95$ K, $\Delta T_c = 1$ K), and underdoped ($T_c = 87$ K, $\Delta T_c = 4$ K).

The low-frequency Raman spectra were taken in pseudobackscattering geometry with $\hbar\omega_i = 1.92$ eV photons from a Kr⁺ laser. The laser excitation of less than 10 W/cm² was focused into a 50 μ m diameter spot on the sample surface. The temperatures referred to in this paper are the nominal temperatures inside the cryostat. The spectra were analyzed by a triple grating spectrometer with a liquid-nitrogen cooled charge-coupled device detector. We have also measured the high-energy Raman spectra excited with $\hbar\omega_i = 3.05$ eV. All spectra were corrected for the spectral response of the spectrometer and detector, the optical absorption of the sample as well as the refraction at the sample-gas interface [8].

RESULTS AND DISCUSSION

The imaginary parts of the *c*-axis-polarized Raman response functions, obtained by dividing the original spectrum by the Bose-Einstein thermal factor, are shown in Fig. 1 as a function of doping and for two different temperatures, 100 K ($T > T_c$) and 5 K ($T \ll T_c$). In the normal state, the most prominent features of the spectra are the electronic continuum and several $q \approx 0$ Raman allowed phonon modes, whose overall character is in good agreement with that reported previously [9]. We focus on the temperature behavior of the electronic Raman scattering response. Well below T_c , it can be seen in Fig. 1 that for the *zz* continuum there is a loss of scattering strength at low frequencies which redistributes into the weak and broad peak at higher frequencies for all doping levels studied, similar to the data (so-called coherent “ 2Δ peak”) observed in the *ab*-plane. We notice that the frequency scale associated with the characteristic loss of the *c*-axis electronic scattering intensity in the superconducting state does change with doping. For the overdoped Bi-2212 with $T_c = 84$ K, the suppression of the electronic continuum occurs at $\omega < 300$

cm^{-1} . As the doping level is decreased towards the underdoped with $T_c = 87$ K, the onset frequency related to the changes of zz continuum is about 600 cm^{-1} .

We have estimated the c -axis 2Δ peak energy in a different manner, where the 5 K spectrum is normalized by (1) dividing by the 100 K spectrum, (2) subtracting the 100 K spectrum, and (3) the difference of Raman spectra, as in (2), after first subtracting the phonon contributions. The 2Δ peak position for the overdoped Bi-2212 crystal ($T_c = 84$ K) occurs near 400 cm^{-1} (50 meV). With decreasing doping, the peak shifts monotonically upward in energy despite a decrease in T_c . $2\Delta/k_B T_c$ changes from a value ~ 7 for overdoped Bi-2212 to value approaching ~ 10 in the underdoped region. It is interesting to notice that this c -axis 2Δ feature, which has A_{1g} symmetry, is found at a higher frequency than that seen in the planar symmetries, but it has a smaller intensity than its in-plane counterparts [10].

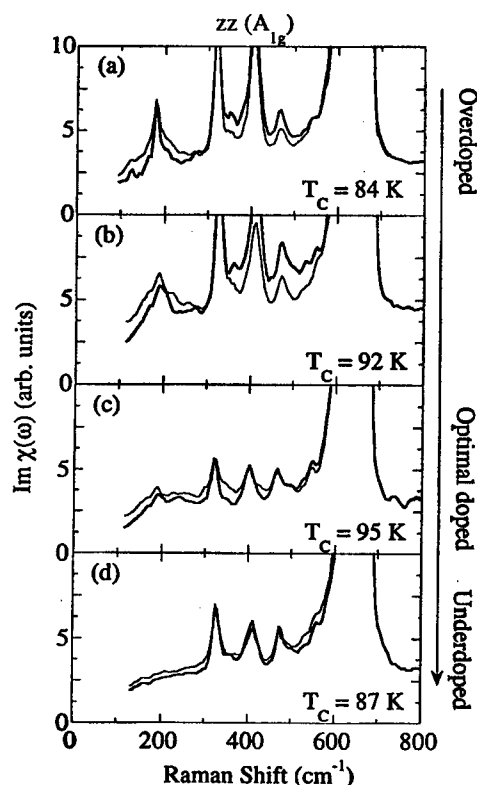


FIGURE 1. The low-energy portion of the c -axis Raman scattering spectra taken with red (1.92 eV) excitation as a function of doping (a) for overdoped sample with $T_c = 84$ K, (b) for slightly overdoped sample with $T_c = 92$ K, (c) for optimal doped sample with $T_c = 95$ K, and (d) for underdoped sample with $T_c = 87$ K. Thick line denotes the spectra taken at 5 K, and thin line at 100 K.

Why is the energy scale of the 2Δ peak associated with the out-of-plane and the in-plane response different? We can say with some certainty that the low-energy Raman scattering process in both cases creates two quasiparticles. With in-plane polarization they are most likely on the same CuO_2 plane, whereas with zz polarization they are most likely on adjacent planes. The two kinds of pairs could be expected to undergo different final state interactions and screening corrections. The c -axis Raman measurements on single-layer $\text{Bi}_2\text{Sr}_2\text{CuO}_x$ would augment this study nicely.

The effect of superconductivity on the high-energy parts of the c -axis electronic Raman scattering is shown in Fig. 2. Note that the room-temperature c -axis electronic continuum extends past 1.5 eV. Its intensity dramatically increases using near ultraviolet (UV) photon excitation, suggesting that the scattering process in zz geometry is dominated by a resonance Raman vertex. As the temperature is

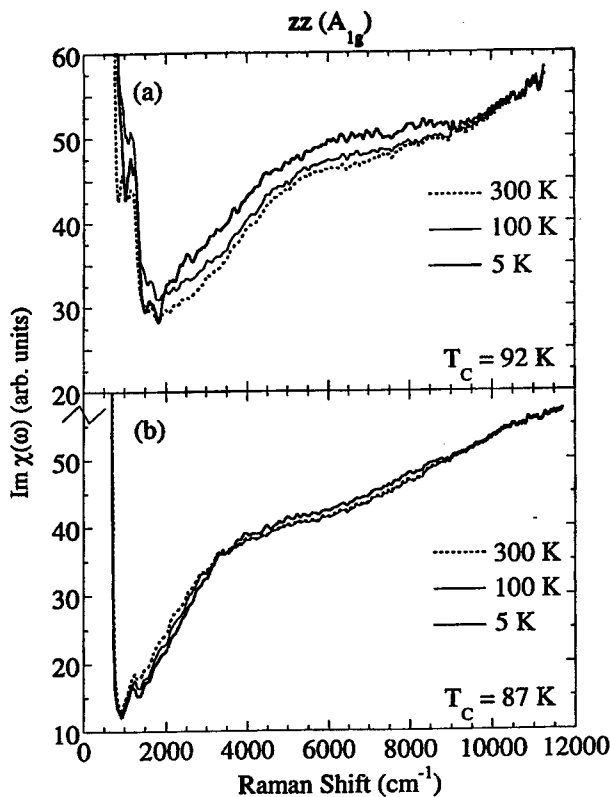


FIGURE 2. The high-energy portion of the c -axis Raman scattering spectra taken with UV (3.05 eV) excitation at three different temperatures (a) for slightly overdoped sample with $T_c = 92$ K, and (b) for underdoped sample with $T_c = 87$ K. The low-frequency rise is part of a phonon contribution.

lowered from 300 K to 100 K, we observe only small changes in the electronic Raman response. Below T_c , the rearrangement of the high-energy electronic Raman response occurs over an energy range between 1500 and 9000 cm^{-1} , in a manner reminiscent of its low-frequency redistribution of the electronic continuum. Furthermore, the fractional change in the integrated electronic scattering intensity, $[I(5\text{K}) - I(100\text{K})]/I(100\text{K})$ between 1500 and 12000 cm^{-1} , is about 3% for slightly overdoped Bi-2212 and less than 1 % in the underdoped sample. It is worth mentioning that a similar superconductivity-induced effect on the ab -plane high-energy electronic continuum was observed in optimally doped Bi-2212 and in the $\text{YBa}_2\text{Cu}_3\text{O}_{7-\delta}$ family of the high- T_c superconductors [11], but that effect is much stronger than the effect shown here.

In summary, c -axis electronic Raman scattering spectra have been investigated for Bi-2212 single crystals. Below T_c , there is a low-frequency redistribution of the electronic continuum and the formation of a 2Δ peak in the superconducting state. The monotonic increase of 2Δ and $2\Delta/k_B T_c$ with decreasing doping is unusual. In particular, this 2Δ feature, which has A_{1g} symmetry, is found at higher frequencies than those seen in the planar symmetries for all doping levels studied. We also find that the superconductivity-induced effect extends to the frequencies as high as 40Δ . The data presented in this study pose a new challenge to those attempting to understand the important mechanisms contributing to c -axis excitations in high- T_c superconductors.

ACKNOWLEDGEMENTS

We thank S.L. Cooper, T.P. Devereaux, K.E. Gray, and A.J. Leggett for helpful discussions. This work was supported by NSF Grant No. DMR-9705131 (H.L.L. and M.V.K.), and DMR-9120000 through the STCS (G.B., M.V.K., and P.G.), and DOE-BES W-31-109-ENG-38 (D.G.H.).

REFERENCES

1. A.J. Leggett, *Science* **279**, 1157 (1998); P.W. Anderson, *ibid.* **279**, 1196 (1998).
2. D.N. Basov *et al.*, (preprint) (1999).
3. A. Hosseini *et al.*, *Phys. Rev. Lett.* **81**, 1298 (1998).
4. K.A. Moler *et al.*, *Science* **279**, 1193 (1998); J.R. Kirtley *et al.*, *Phys. Rev. Lett.* **81**, 2140 (1998).
5. T.P. Devereaux and A.P. Kampf, *Int. J. Mod. Phys. B* **11**, 2093 (1997).
6. T. Stauffer, R. Hackl, and P. Müller, *Solid State Commun.* **79**, 409 (1991); T. Stauffer *et al.*, *Phys. Rev. Lett.* **68**, 1069 (1992); C. Kendziora and A. Rosenberg, *Phys. Rev. B* **52**, R9867 (1995); D. Einzel and R. Hackl, *J. of Raman Spectroscopy* **27**, 307 (1996); C. Kendziora, R.J. Kelley, and M. Onellion, *Phys. Rev. Lett.* **77**, 727 (1996); G. Blumberg *et al.*, *Science* **278**, 1427 (1997), and references therein.

7. M. Boekholt, M. Hoffman, and G. Guentherodt, *Physica C* **175**, 127 (1991); O.V. Misochko and Gu Genda, *ibid.* **288**, 115 (1997).
8. D. Reznik *et al.*, *Phys. Rev. B* **46**, 11725 (1992); D. Reznik *et al.*, *ibid.* **48**, 7624 (1993); G. Blumberg *et al.*, *ibid.* **49**, 13295 (1994).
9. V.N. Denisov *et al.*, *Solid State Commun.* **70**, 885 (1989); M. Boekholt *et al.*, *ibid.* **74**, 1107 (1990); Ran Liu *et al.*, *Phys. Rev. B* **45**, 7392 (1992); M. Kakihana *et al.*, *Phys. Rev. B* **53**, 11796 (1996).
10. H.L. Liu *et al.*, (unpublished).
11. M. Rübhausen *et al.*, *Phys. Rev. B* **56**, 14797 (1997); *ibid.* **58**, 3462 (1998).

Evidence for strong electron-lattice coupling in $\text{La}_{2-x}\text{Sr}_x\text{NiO}_4$

R. J. McQueeney* and J. S. Sarrao†

*Lujan Center and †Condensed Matter and Thermal Physics,
Los Alamos National Laboratory, Los Alamos, NM 87545

Abstract. The inelastic neutron scattering spectra were measured for several Sr concentrations of polycrystalline $\text{La}_{2-x}\text{Sr}_x\text{NiO}_4$. We find that the generalized phonon density-of-states is identical for $x = 0$ and $x = 1/8$. For $x = 1/3$ and $x = 1/2$, the band of phonons corresponding to the in-plane oxygen vibrations (> 65 meV) splits into two subbands centered at 75 meV and 85 meV. The lower frequency band increases in amplitude for the $x = 1/2$ sample, indicating that it is directly related to the hole concentration. These changes are associated with the coupling of oxygen vibrations to doped holes which reside in the NiO_2 planes and are a signature of strong electron-lattice coupling. Comparison of $\text{La}_{1.9}\text{Sr}_{0.1}\text{CuO}_4$ and $\text{La}_{1.875}\text{Sr}_{0.125}\text{NiO}_4$ demonstrates that much stronger electron-lattice coupling occurs for particular modes in the cuprate for modest doping and is likely related to the metallic nature of the cuprate.

INTRODUCTION

It has been known for some time that strong phonon anomalies occur in the superconducting cuprates as a function of hole concentration. These anomalies were originally observed by inelastic neutron measurements of the phonon density-of-states of several superconducting cuprates and manifested themselves as strong softening of in-plane polarized oxygen modes within the CuO_2 plane [1]. This softening behavior was confirmed by neutron scattering measurements of the phonon dispersion and was found to occur only for the longitudinal oxygen bond-stretching branch along the (1,0,0) direction (along the Cu-O bond) and near the Brillouin zone boundary [2]. This effect appears to be universal, and has been observed in all cuprate systems for which the measurement has been made. More recently, careful phonon peakshape measurements in $\text{La}_{1.85}\text{Sr}_{0.15}\text{CuO}_4$ have revealed anomalous splittings of this branch midway to the zone boundary at low temperatures [3]. This manifestation of strong and unique electron-lattice coupling for specific phonon polarizations and wavevectors in the cuprates brings several questions to mind: Are the phonon anomalies related to the inhomogeneous, or topological, distribution of doped holes, such as stripes? What is the origin of the temperature

effect? And finally, is the dynamic (or metallic) nature of the hole states important in the electron-lattice coupling?

To address these questions, we have undertaken measurements of the phonon density-of-states in the nickelate system, $\text{La}_{2-x}\text{Sr}_x\text{NiO}_4$, as a function of Sr (hole) concentration. The nickelates are isostructural to the 214-cuprates and are known to have similar phonon spectra in the undoped parent compounds [1]. For rather large Sr concentrations ($x > \sim 0.1$) [4,5], the nickelates form charge/spin ordered states similar to those proposed for the cuprates. However, in the nickelates the stripes are static and the system remains in insulator up to very large hole concentrations. Consequently, we can address several of the questions posed above. Additionally, the relevance of the electron-lattice coupling in the nickelate stripe ordering is an interesting question, and these measurements can help to address how the electron-lattice coupling enters in the stripe formation.

EXPERIMENTAL

In the present experiment, the inelastic neutron scattering spectra are measured for polycrystalline $\text{La}_{2-x}\text{Sr}_x\text{NiO}_4$ ($x = 0, 1/8, 1/4, 1/3, 1/2$) and also for $\text{La}_{1.9}\text{Sr}_{0.1}\text{CuO}_4$. The purpose is to obtain the dependence of the generalized phonon density of states (GDOS) on hole concentration, and also to determine the variation of the GDOS with temperature. This is the first systematic study of the doping and temperature dependence of the lattice dynamics of $\text{La}_{2-x}\text{Sr}_x\text{NiO}_4$ by neutron scattering. We pay particular attention to the contribution from in-plane polarized oxygen vibrations. This is made simple because the in-plane oxygen modes are well-separated in frequency from the other kinds of vibrations, as determined from model fits to phonon dispersion measurements. The features above 65 meV are associated entirely with planar oxygen vibrations.

$\text{La}_{2-x}\text{Sr}_x\text{NiO}_{4+\delta}$ powder samples were prepared by solid state reaction of stoichiometric ratios of La_2O_3 , SrCO_3 and NiO [6]. The $x = 0$ and $x = 1/8$ samples were subsequently annealed in flowing argon at 1100 °C for 20 hours to ensure that $\delta = 0$ [5]. X-ray powder diffraction measurements at room temperature yielded lattice constant values consistent with previous reports [7] and indicated predominantly single phase material, with only a small x -independent La_2O_3 impurity phase. Magnetic susceptibility measurements yielded data essentially equivalent to that of Cheong et al. [6], including the reported signal of stripe order for $x = 1/3$. The samples weighed about 40 grams each.

Time-of-flight inelastic neutron scattering measurements were performed on the Low Resolution Medium Energy Chopper Spectrometer at Argonne National Laboratory's Intense Pulsed Neutron Source. For all measurements, an incident neutron energy of 120 meV was chosen. Data were taken at $T = 10\text{K}$ and 300K for many different samples, some with the same Sr concentration but differing mass. Data were summed over all scattering angles from $2-120^\circ$ and corrected for background, absorption, sample mass, multiple scattering, and multiphonon processes. Excel-

lent agreement was achieved for different masses of the same stoichiometry. The data were then converted into the GDOS by accounting for the phonon amplitude factor.

RESULTS AND DISCUSSION

The GDOS of $\text{La}_{2-x}\text{Sr}_x\text{NiO}_4$ are shown for several Sr concentrations at $T = 10\text{K}$ in Figure 1. The GDOS for the $x = 0$ and $x = 1/8$ samples are identical, thus hole doping has little effect on the phonon spectrum at this level. This is in strong contrast to the cuprates. Figure 2 shows the GDOS obtained for $\text{La}_{1.875}\text{Sr}_{0.125}\text{NiO}_4$ and $\text{La}_{1.9}\text{Sr}_{0.1}\text{CuO}_4$ at $T = 10\text{K}$. While the GDOS of the undoped parent compounds are virtually identical, at $\sim 10\%$ doping the spectra differ greatly above 65 meV. In particular, the subband forming near 70 meV in the cuprate, which is associated with the anomalous bond-stretching modes, has not formed in the nickelate. Thus, simple mechanisms related to substitutional disorder or Madelung terms in the interatomic potential cannot possibly be responsible for the softening. Rather, the phonon softening in the cuprate must require hole mobility in addition to strong electron-lattice coupling. The formation of this subband may be related to the metal-insulator transition near the 5% doping level, although this has not been measured to date.

However, this does not preclude the presence of electron-lattice coupling in the

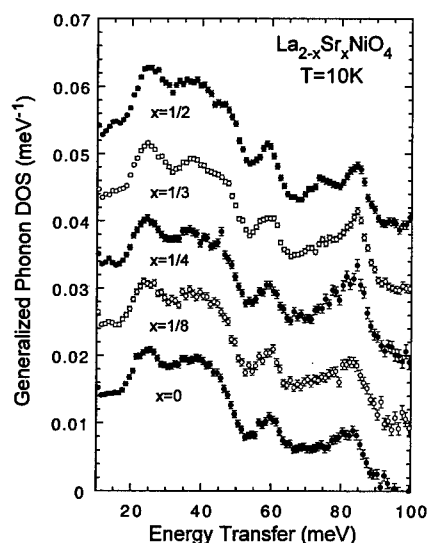


FIGURE 1. The generalized phonon density-of-states of $\text{La}_{2-x}\text{Sr}_x\text{NiO}_4$ for $x = 0, 1/8, 1/4, 1/3$ and $1/2$ at $T = 10\text{K}$. Data for each concentration is separated by 0.01 units for clarity.

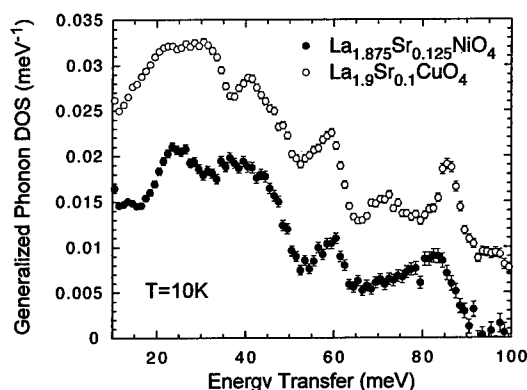


FIGURE 2. The generalized phonon density-of-states $\text{La}_{1.875}\text{Sr}_{0.125}\text{NiO}_4$ and $\text{La}_{1.9}\text{Sr}_{0.1}\text{CuO}_4$ at $T = 10\text{K}$. The cuprate GDOS is offset by 0.01 for clarity.

nickelates themselves. For the higher doping compounds, strong deviations are seen in the in-plane polarized oxygen modes above 65 meV. This is especially apparent in the $x = 1/2$ compound. Here, a subband of phonon modes is formed near 75 meV, quite similar to the cuprates although at a much higher doping level. This subband can also be seen very weakly in the $x = 1/3$ compound. Other changes, such as the narrowing and slight hardening of the band near 85 meV can be observed for the $x = 1/4$, $1/3$ and $1/2$ systems. Additionally, smaller changes are observed at the higher Sr concentrations, such as the changes near 45 meV. Unfortunately, many kinds of phonon modes involving different atomic species are involved below 50 meV, and it is not possible to discuss these changes with the present data alone.

It is tempting to associate the renormalization of the oxygen phonon modes in the nickelates with stripe formation. With the localization of holes and their real-space ordered arrangement, one might expect the interatomic potentials for the strongly covalent Ni-O bonds to be affected. For $\text{La}_{3/2}\text{Sr}_{1/2}\text{NiO}_4$ below 350K, the holes form a checkerboard pattern on the NiO_2 plane. Thus, the 75 meV and 85 meV bands could be related to vibrations of NiO_4 squares with or without a hole, respectively. An extension [8] of the recent theoretical work by Yi, et al. [9] has calculated the expected phonon spectrum of the NiO_2 plane in the presence of strong electron-lattice coupling in addition to the strong 2-orbital electron-electron interactions and in the background of stripe order using an inhomogeneous Hartree-Fock numerical method. The results show a quantitative agreement with the measured doping dependence shown here and relate the 75 meV subband to local lattice vibrations in the vicinity of the stripes (or phonon modes localized on the stripe). The level of electron-lattice coupling required for agreement with the GDOS within Yi's model is $\alpha \approx 3$. According to Yi's results, the strength of the electron-lattice coupling can

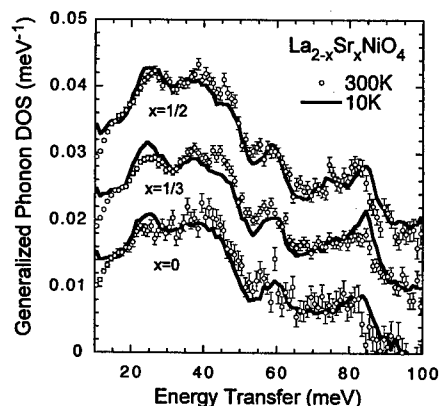


FIGURE 3. Comparison of the generalized phonon density-of-states of $\text{La}_{2-x}\text{Sr}_x\text{NiO}_4$ ($x = 0, 1/3, 1/2$) at $T = 10\text{K}$ and 300K . Each GDOS is offset by 0.01 for clarity.

dictate stripe position and this value is close to the transition from Ni-centered to O-centered stripes for $x = 1/3$. It has been shown experimentally that the stability of Ni-centered or O-centered stripes is quite sensitive to temperature.

Further connection of the stripe order and phonon subband formation in the nickelates can be obtained from the temperature dependence. For $\text{La}_{5/3}\text{Sr}_{1/3}\text{NiO}_4$, the stripe order is lost above $\sim 240\text{K}$. Figure 3 shows a comparison of the GDOS for the nickelate compounds with $x = 0, 1/3$, and $1/2$ at $T = 10\text{K}$ and 300K . The $x = 0$ and $1/2$ GDOS are very similar for the two temperatures, including the 75 meV subband for $x = 1/2$ which still retains hole order. For $x = 1/3$, the GDOS appears more like $x = 0$ and may be related to the loss of hole order. For such complicated crystal structures, it is difficult to compare different temperatures since the contributions of each chemical species vary with the Debye-Waller factor and multiphonon corrections are more significant. While these data do give the inference of the phonon renormalizations being sensitive to hole order, it is only suggestive.

Other observations such as mode splitting through the stripe ordering transition by Raman [10,11] and Infra-red [12] absorption; and the fact that charge order occurs before spin order in these systems [13] point to the importance of the lattice degrees of freedom in the nickelates. Considering our results in conjunction with these others, electron-lattice coupling may be crucial in the stabilization of charge-ordered states. Additionally, in the cuprates, phonon induced charge transfer excitations and the large and anomalous electron-lattice coupling may be relevant to the electronic transport properties. In short, both the nickelates and cuprates show strong electron-lattice coupling effects for oxygen modes in the transition metal-oxide plane.

ACKNOWLEDGMENTS

RJM would like to thank Ya-Sha Yi, A. R. Bishop and T. Egami for engaging discussions. RJM was supported by the U.S. Department of Energy under contract No. W-7405-ENG-36 with the University of California.

REFERENCES

1. Renker, B., Gompf, F., Adelman, P., et al. *Physica B* **180&181**, 450, (1992).
2. Pintschovius, L., et al. *Physica* **185C-189C**, 156, (1991).
3. McQueeney, R. J., Petrov Y., Egami T., et al. to appear in *Phys. Rev. Lett.*
4. Chen, C. H., Cheong, S.-W., and Cooper, A. S., *Phys. Rev. Lett.* **71**, 2461, (1993).
5. Sachan, V., Buttrey, D. J., Tranquada, J. M., et al. *Phys. Rev. B* **51**, 12742, (1995).
6. Cheong, S.-W., Hwang, H. Y., Chen, C. H., et al. *Phys. Rev. B* **49**, 7088, (1994).
7. Cava, R., Batlogg, B., Palestra, T. T., et al. *Phys. Rev. B* **43**, 1229, (1991).
8. Yi, Ya-Sha, McQueeney, R. J., et al., to be published.
9. Yi, Ya-Sha, Yu, Z. -G., Bishop, A. R., et al. *Phys. Rev. B* **58**, 503, (1998).
10. Blumberg, G., Klein, M. V., and Cheong, S. -W., *Phys. Rev. Lett.* **80**, 564, (1998).
11. Yamamoto, K., Katsufuji, T., Tanabe, T., et al. *Phys. Rev. Lett.* **80**, 1493, (1998).
12. Katsufuji, T., Tanabe, T., Ishikawa, T., et al. *Phys. Rev. B* **54**, R14320, (1996).
13. Tranquada, J. M., Buttrey, D. J., and Sachan, V., *Phys. Rev. B* **54**, 12318, (1996).

Photoinduced infrared absorption in $(\text{La}_{1-x}\text{Sr}_x\text{Mn})_{1-\delta}\text{O}_3$: observation of anti-Jahn-Teller polarons

T. Mertelj^{*†}, D. Kuščer[†], D. Mihailovic[†]

^{*} *University of Ljubljana, Faculty of Mathematics and Physics, Jadranska 19, 1000 Ljubljana, Slovenia*

[†] *Jozef Stefan Institute, P.O. Box 3000, 1001 Ljubljana, Slovenia*

Abstract. A photoinduced IR absorption peak centered at $\sim 5000 \text{ cm}^{-1}$ was observed in $(\text{La}_{1-x}\text{Sr}_x\text{Mn})_{1-\delta}\text{O}_3$ at low hole doping. The peak diminishes and softens as hole doping is increased. The peak is attributed to absorption due to the anti-Jahn-Teller polaron.

I INTRODUCTION

It has been shown in high T_c cuprates that measurements of the photoinduced (PI) absorption are extremely useful tool to understand a nature of electronic states [1], especially in the range of weak hole doping. We expect that similar holds for giant-magnetoresistance (GMR) manganites [2] since as in cuprates interplay between lattice and electronic degrees of freedom is essential for their low energy physics. [3] In this paper we present PI absorption measurements in $(\text{La}_{1-x}\text{Sr}_x\text{Mn})_{1-\delta}\text{O}_3$ at various hole doping levels concentrating mostly on weak hole-doping levels.

II EXPERIMENTAL

The method of preparation and characterization of ceramic samples with nominal composition $(\text{La}_{1-x}\text{Sr}_x\text{Mn})_{1-\delta}\text{O}_3$ ($x = 0, 0.1, 0.2$) is published elsewhere [4]. Their Curie temperatures were determined from AC susceptibility measurements. The Sr doped samples had $T_C \approx 210\text{K}$ and $T_C \approx 340\text{K}$ for $x = 0.1$ and 0.2 respectively. A part of the ferromagnetic (FM) $x = 0$ sample with $T_C \approx 170\text{K}$ was consequently treated at 900°C in Ar flow to obtain another $x = 0$ sample with smaller δ which is an antiferromagnetic (AFM) insulator below $T_N = 140\text{K}$.

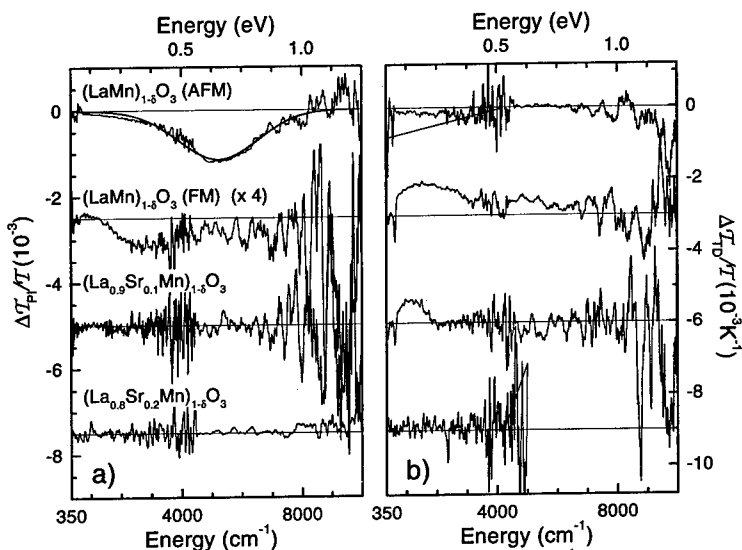


FIGURE 1. Low temperature ($T = 25\text{K}$) PI transmittance a) and TD transmittance b) spectra as a function of doping. The spectra are vertically shifted for clarity and thin lines represent zero for each spectrum. The thick line is the small polaron absorption [9] fit to the data.

Photoinduced IR transmittance measurements were performed with Bomem MB series Fourier transform spectrometers using standard KBr powder technique. A special care was taken that the KBr pallets were in a good thermal contact with the sample holder. The maximum excitation Ar^+ laser ($\lambda = 514.5\text{ nm}$) light fluence Φ was $\sim 500\text{ mW/cm}^2$.

At each temperature the thermal-difference (TD) transmittance change was also measured in absence of the laser light excitation by first measuring the reference spectrum and then increasing the sample holder temperature by 2K and measuring the sample spectrum.

In the $x = 0$ AFM sample a strong broad PI midinfrared (MIR) absorption (negative PI transmittance) centered at $\sim 5000\text{ cm}^{-1}$ ($\sim 0.62\text{ eV}$) is observed (Fig. 1a). Comparison with the virtually flat TD spectrum in Fig. 1b confirms that the PI absorption is not due to laser heating effects. In the frequency range of the phonon bands we observe PI phonon bleaching in the range of the 585-cm^{-1} phonon band and a slight PI absorption below 580 cm^{-1} . The PI phonon bleaching consists of two peaks at 600 and 660 cm^{-1} respectively with a dip in-between at 630 cm^{-1} . These two PI transmission peaks are reproducible among different runs, while the structure of the PI absorption below 580 cm^{-1} is not.

In the $x = 0$ FM sample there is much weaker PI absorption centered around $\sim 3000\text{ cm}^{-1}$ ($\sim 0.37\text{ eV}$) and comparison with the TD spectrum, which shows a relatively strong TD transmission below 4000 cm^{-1} , indicates that the signal is not

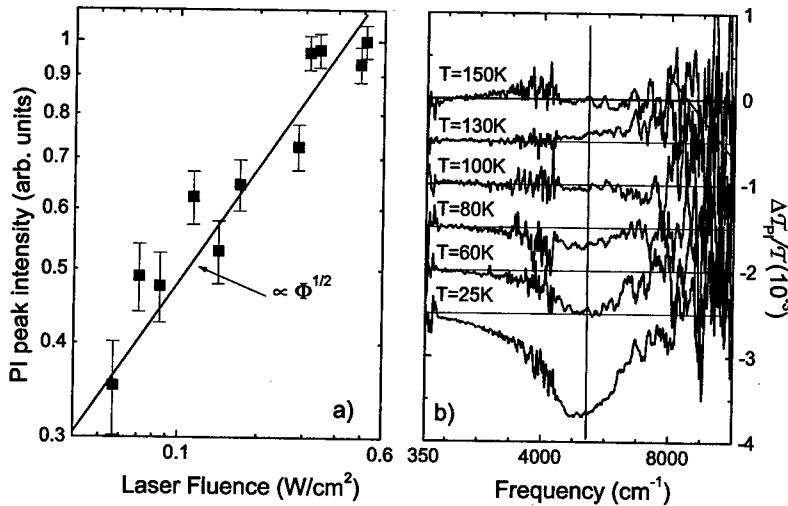


FIGURE 2. The PI-absorption peak intensity in the $x = 0$ AFM sample as a function of the laser fluence Φ panel a) and its temperature dependence panel b). The solid line in panel a) is $\sqrt{\Phi}$ fit to the data.

thermally induced. There is no PI signal in the spectra of the $x = 0.1$ and $x = 0.2$ samples.

In the $x = 0$ AFM sample the intensity of the PI absorption peak was measured as a function of the laser fluence and is shown in Fig. 2a. It can clearly be seen that the intensity of the peak is not proportional to the laser fluence Φ , but it is better fit with a square root of the laser fluence $\sqrt{\Phi}$, suggesting a bimolecular recombination process. This is also additional proof that the observed PI signal is not thermal in origin.

Temperature dependence of the PI-absorption-peak in the $x = 0$ AFM sample is shown in Fig. 2b. The intensity of the peak quickly diminishes with increasing temperature disappearing between 80 and 100K. There is no significant shift of the PI-absorption peak observed with increasing temperature and no changes in the PI-spectra are observed around T_N .

III DISCUSSION

Similar to high T_c cuprates, in $(\text{La}_{1-x}\text{Sr}_x\text{Mn})_{1-\delta}\text{O}_3$ a PI absorption of significant magnitude is observed at weak hole doping only. We attribute absence of the PI signal at higher doping levels to a much shorter photoexcitation lifetimes which

prevent their detection in a pseudo CW experiment. We therefore mainly focus to the $x = 0$ AFM sample in the rest of discussion.

It is instructive to compare the PI absorption spectrum peaked at 0.6 eV with IR conductivity spectra of chemically doped compounds to see whether the PI carriers show any similarity to the carriers introduced by chemical means. Indeed, Okimoto *et al.* [7] observe in the $x = 0.1$ $\text{La}_{1-x}\text{Sr}_x\text{MnO}_3$ a broad absorption peaked around 0.5 eV which is absent at room temperature and increases in intensity with decreasing temperature. They attribute it to localization of Jahn-Teller (JT) polarons at low temperatures. They also relate the peak energy of 0.5 eV to a JT polaron binding energy [5] E_{pJT} . The absorption shifts to lower energies as doping is increased [7]. Similar value of the polaron binding energy of 0.4 eV has also been inferred from transport measurements by De Teresa *et al.* [8]. They also find that the binding energy decreases with the increasing hole doping.

In our experiment the PI absorption peak energy of 0.6 eV is very similar to the above mentioned polaron binding energies. The peak energy decreases with increased doping as seen from the position of the PI absorption peak in the cation deficient $x = 0$ FM sample. We are therefore tempted to assign the PI absorption peak to an anti-JT-polaron absorption. In Fig. 1a a fit of absorption due to a small polaron given by Emin [9] for $x = 0$ (AFM) sample is shown. The theory fits well to the data with the small polaron binding energy $E_b = 350 \pm 8$ meV and the phonon frequency $\omega_{ph} = 300 \pm 40$ cm^{-1} . The small polaron binding energy obtained from the fit is very similar to the one determined by De Teresa *et al.* [8] and the frequency of the phonon is in the region of the oxygen related modes, as expected.

REFERENCES

1. Y. H. Kim, A. J. Heeger, L. Acedo, G. Stucky, F. Wudl, *Phys. Rev.* **B36** (1987) 7252., C. Taliani, R. Zamboni, G. Ruani, F. C. Matocotta, K. I. Pokhodnya, *Sol. Stat. Comm.* **66** (1988) 487.
2. R. M. Kusters, J. Singelton, D. A. Ken, R. McGreevy, W. Hayes, *Physica* **B155** (1989) 362.
3. See for example Ref. [6] for cuprates and Ref. [5] for manganites.
4. J. Holc, D. Kuščer, M. Horvat, S. Bernik, D. Kolar, *Solid State Ionics* **95** (1997) 259.
5. A. J. Millis, B. I. Sharaiman, R. Mueller, *Phys. Rev. Lett.* **77** (1996) 175., G-M. Zhao, H. Keller, R. L. Greene, K. A. Müller, to appear in *Physics of Manganites*, Editors: T. A. Kaplan and S. D. Mahanti, (Plenum publishing corporation, 1998).
6. *Proceedings of the International Workshop on Anharmonic Properties of High Tc Cuprates*, Editors: D. Mihailovic, G. Ruani, E. Kaldis, K. A. Müller, (World Scientific, Singapore, 1995).
7. Y. Okimoto, T. Katsufuji, T. Ishikawa, T. Arima, Y. Tokura, *Phys. Rev.* **B55** (1997) 4206.
8. J. M. De Teresa, K. Dorr, K. H. Müller, L. Shultz, *Phys. Rev.* **B58** (1998) R5928.
9. D. Emin, *Phys. Rev.* **B48** (1993) 13691.

Fermi Surface Geometry and the Ultrasonic Attenuation of a Clean d-wave Superconductor

E.J. Nicol*, I. Vekhter*, and J.P. Carbotte†

*Dept. of Physics, University of Guelph¹
Guelph, ON N1G 2W1 Canada

†Dept. of Physics, McMaster University
Hamilton, ON L8S 4M1 Canada

Abstract. The longitudinal ultrasonic attenuation coefficient for a clean d-wave superconductor has been calculated for the case of a $d_{x^2-y^2}$ order parameter and a simple two-dimensional tight-binding Fermi surface. We find that the attenuation coefficient exhibits a linear temperature dependence at low temperatures for all directions of the ultrasound wavevector and, in the nodal direction, a peak in the coefficient as a function of temperature occurs away from half filling.

INTRODUCTION

With the advent of crystals of the high temperature superconductors with mean free path of the order of 4–5 microns [1], the possibility arises of performing measurements of the ultrasonic attenuation coefficient in the clean, rather than the hydrodynamic limit. Such measurements with the ultrasound wave vector varied through several angles in the a-b plane could be used to confirm and examine in detail the nature of the superconducting state and determine important parameters in the existing theories [2]. Recently several calculations have been presented in the literature [3,4] for a d-wave energy gap, which implicitly assume that the gap amplitude, Δ_0 , is small relative to the Fermi energy E_f . In the high T_c cuprates Δ/E_f can be of order 0.1 or more, and we have recently found for a cylindrical Fermi surface that there are important effects due to Δ/E_f being relatively large and that the curvature of the Fermi surface plays an important role [2]. In this paper, we examine these effects for a tight-binding Fermi surface. Kostur et al. [4] have looked at the case of a d-wave order parameter with a tight-binding Fermi

¹⁾ We acknowledge support from NSERC of Canada and the Cottrell Scholar Program of Research Corporation.

surface, however, due to their approximation of $\Delta/E_f \ll 1$, their results are qualitatively different from what we present here.

FORMALISM

We examine a d-wave order parameter of the form $\Delta_{\vec{k}} = \Delta(T)[\cos(k_x a) - \cos(k_y a)]$, which has nodes along the diagonal of the Brillouin zone, $k_x = \pm k_y$ in a two-dimensional tight-binding band structure given by

$$\epsilon_{\vec{k}} = -2t[\cos(k_x a) + \cos(k_y a)] - \mu, \quad (1)$$

where t is the hopping parameter and μ is the chemical potential. For our calculations, a sum over the Brillouin zone is performed on a 2D lattice indexed by k_x and k_y and with lattice spacing a [5]. The results of a tight-binding band structure are shown in Figure 1 for reference. The left frame relates the dimensionless parameter $\mu/(2t)$ to the filling and the right frame illustrates the shape of the Fermi surface for various values of $\mu/(2t)$.

For a particular direction of the ultrasound wave vector \vec{q} , the ultrasonic attenuation coefficient in the superconducting state is given by the phase space where \vec{q} is perpendicular to the group velocity of the quasiparticles, $\nabla_{\vec{k}} E_{\vec{k}}$:

$$\alpha(T) \propto \frac{1}{T} \frac{1}{N} \sum_{\vec{k}} \frac{1}{\cosh^2 \frac{E_{\vec{k}}}{2T}} \frac{\epsilon_{\vec{k}}^2}{E_{\vec{k}}} \delta(\epsilon_{\vec{k}} \vec{v}_{\vec{k}} \cdot \vec{q} + \Delta_{\vec{k}} \frac{\partial \Delta_{\vec{k}}}{\partial \vec{k}} \cdot \vec{q}), \quad (2)$$

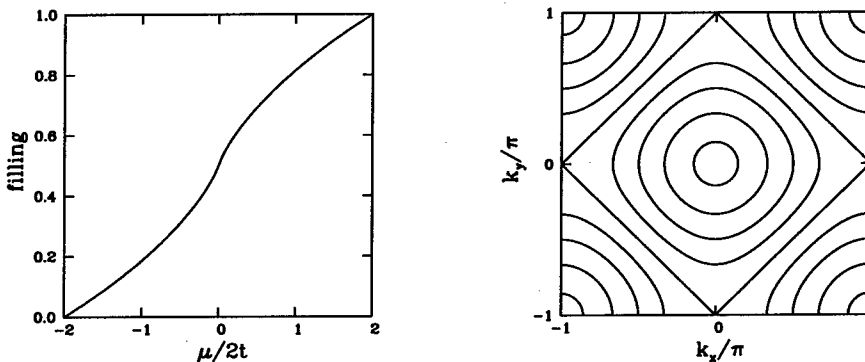


FIGURE 1. Left: Band filling as a function of $\mu/2t$. Right: Several Fermi surfaces corresponding to different $\mu/2t$. The half-filled case of $\mu/2t = 0$ is the square surface. The surfaces moving from the half-filled case inwards are for $\mu/2t = -0.5, -1.0, -1.5, -1.9$ and for the surfaces moving outwards from half-filling $\mu/2t = 0.5, 1.0, 1.5, 1.9$.

where $E_{\vec{k}} = \sqrt{\epsilon_{\vec{k}}^2 + \Delta_{\vec{k}}^2}$ and we have used a BCS-like temperature dependence for the gap given by [6] $\Delta(T) = \Delta_0(0.9963 + 0.7733T/T_c)\sqrt{1 - T/T_c}$.

RESULTS

In agreement with our previous discussion [2] (see also [7]) there are two major changes brought about by accounting for the terms of order Δ_0/E_f in unconventional superconductors. First, as a consequence of the lines $E_{\vec{k}} = \text{const}$ crossing the Fermi surface, in contrast to an s -wave material, the attenuation coefficient is linear in T at low temperatures for all orientations of the polarization \vec{q} in the ab plane. The slope of the linear T term and, consequently, the attenuation coefficient at a fixed temperature, exhibits a fourfold pattern as a function of the angle between \vec{q} and the crystalline axes, with a maximal attenuation for the ultrasound propagating along the nodal direction, as shown in Fig.2. This linear dependence was not found by Kostur et al. [4].

Second, we found that for a cylindrical Fermi surface and for \vec{q} in a near-nodal direction, the competition between the anisotropic gap and the curvature of the underlying Fermi surface gives rise to a maximum in the attenuation coefficient, $\alpha(T)$, below the transition temperature T_c . This increase, first predicted in Ref. [7], occurs as additional phase space becomes available for scattering near the nodal points of the order parameter. As the curvature of the Fermi surface depends strongly on the ratio $\mu/2t$ as seen in Fig.2, in the following we concentrate on

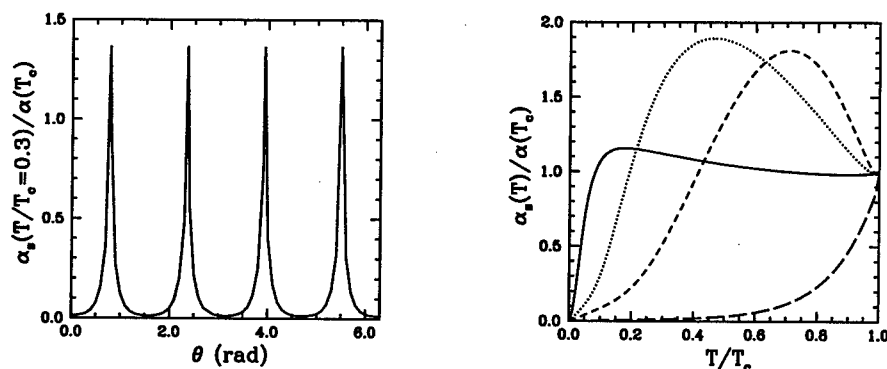


FIGURE 2. Left: The angular dependence of the ultrasonic attenuation for $T/T_c = 0.3$, $\Delta_0 = 3.5T_c$, $t = 15T_c$, and $\mu/2t = -1.1$. Right: The ultrasonic attenuation coefficient, with \vec{q} in the nodal direction, normalized to that at T_c for several values of the filling. Here, $t = 10T_c$, $\Delta_0 = 4T_c$ and $\mu/2t = -1.75$ (solid curve), -1 (dotted), -0.5 (short-dashed) and -0.05 (long-dashed).

the effect of the tight-binding Fermi surface on the attenuation in the near-nodal directions, the directions along the diagonals of the Brillouin zone in Fig.1.

As is clear from that figure for large values of the parameter $\mu/2t$ the Fermi surface is nearly circular, and the regions contributing to the attenuation in the normal state, where \vec{q} is perpendicular to the Fermi surface are also on a diagonal of the Brillouin zone. The additional phase space for scattering below T_c opens up in this region, resulting in a maximum in α , as for a circular Fermi surface. For cases near half-filling there are large regions of the Fermi surface parallel to the diagonals of the Brillouin zone which contribute to the attenuation in the normal state. Below the superconducting transition additional scattering processes become important near the gap nodes. However, they cannot compensate for the loss of scattering phase space over the entire "side" of the Fermi surface where a full energy gap opens up. As seen in Fig.2, for the situation where the nodal directions coincide with the flat regions on the Fermi surface the peak below T_c disappears completely.

We also note that the antinodal directions largely sample the effect of the local gap in that direction and hence the attenuation drops rapidly below T_c but retains the linear T dependence with a small slope at low T as discussed previously [2].

There is a dependence on Δ/t similar to the dependence of Δ/E_f from our cylindrical Fermi surface calculations [2]. Hence for large Δ/t , the peak appears in the nodal direction and moves to higher temperature and for smaller Δ/t , the peak reduces in size, shifts to lower T and eventually disappears in the limit of $\Delta/t \ll 1$.

CONCLUSIONS

We have calculated the ultrasonic attenuation coefficient for a clean d-wave superconductor in a model with a tight-binding Fermi surface. While we recover many of the results from our previous work with a cylindrical Fermi surface, we note here that having large flat pieces of Fermi surface reduces and eventually eliminates the attenuation peak below T_c . Finally, our results are quite different from those presented by Kostur et al. [4] whose approximation of $\Delta/E_f \ll 1$ neglected some of the important physics associated with the order parameter and the Fermi surface.

REFERENCES

1. A. Hosseini et al., cond-mat/9811041
2. I. Vekhter, E.J. Nicol, and J.P. Carbotte, *Phys. Rev. B* **59** March 1, in press
3. T. Wolenski and J. C. Swihart, *Physica C* **253**, 266 (1995).
4. V. N. Kostur, J. K. Bhattacharjee, and R. A. Ferrell, *JETP Lett.* **61**, 560 (1995).
5. E.J. Nicol, C. Jiang, and J.P. Carbotte, *Phys. Rev. B* **47**, 8131 (1993).
6. W. Zimmermann, E.H. Brandt, M. Bauer, E. Seider, and L. Genzel, *Physica C* **183**, 99 (1991).
7. S. N. Coppersmith and R. A. Klemm, *Phys. Rev. Lett.* **56**, 1870 (1986).

Hole Doping Dependence of the Antiferromagnetic Correlations in $\text{La}_{2-x}\text{Sr}_x\text{CuO}_4$ and $\text{Y}_{1-x}\text{Ca}_x\text{Ba}_2\text{Cu}_3\text{O}_6$

Ch. Niedermayer¹, T. Blasius¹, C. Bernhard²,
A. Golnik², A. Moodenbaugh³ and J. I. Budnick⁴

¹Fakultät für Physik, Universität Konstanz, D-78457 Konstanz, Germany

²Max-Planck-Institut für Festkörperforschung, D-70569 Stuttgart, Germany

³Department of Applied Science, Brookhaven National Laboratory, Upton, NY 11977

⁴Department of Physics and Institute for Materials Science, University of Connecticut, Storrs, CT 06269

Abstract. By zero field muon spin rotation we studied the antiferromagnetic correlations in the single layer system $\text{La}_{2-x}\text{Sr}_x\text{CuO}_4$ and the bilayer compound $\text{Y}_{1-x}\text{Ca}_x\text{Ba}_2\text{Cu}_3\text{O}_6$. We observe a common phase diagram as a function of hole doping per plane with two distinct transitions of the magnetic ground state. The first transition marks the border between the 3D antiferromagnetic state and a disordered state with short ranged correlations. The second transition coincides with the onset of superconductivity and marks a distinct change in the magnetic correlations that coexist with superconductivity. The data are discussed on the basis of a microscopic phase segregation of the doped holes into hole-rich and hole-poor regions.

Whenever the insulating composition of a given class of high T_c superconductors is chemically stable, it generally exhibits long-range antiferromagnetic (AF) order that is rapidly destroyed by small amounts of doped carriers. Short-range 2D AF correlations, however, persist into the superconducting regime. It is therefore of great importance to study the evolution of magnetism as more holes are doped into the CuO_2 planes and to explore the interplay between short-range magnetic order and superconductivity. The zero-field (ZF) μSR technique is especially suited for such studies since the positive muon is an extremely sensitive local probe able to detect internal magnetic fields as small as 0.1 mT and covering a time window from 10^{-6} s to about 10^{-10} s. Another advantage is the sensitivity of the muon probe to extremely short ranged magnetic correlations. For details on the μSR technique see e.g. [1].

Systematic μSR studies so far focused on the La-214 [2,3] and Y-123 [4,5] systems. In Y-123 the phase diagram has to be drawn versus oxygen content and a reliable determination of p , the fraction of doped holes per Cu atom in the CuO_2 plane,

is difficult due to the rather complicated charge transfer from the CuO chains to the CuO₂ planes. The Y_{1-x}Ca_xBa₂Cu₃O₆ system, i.e. with $\delta=1.0$, avoids this complication, because hole doping is achieved by the substitution of Y³⁺ by Ca²⁺. This allows one to directly control the hole concentration in the CuO₂ planes in a quantitative manner and $p = x/2$.

Representative ZF- μ SR time spectra are shown in Fig. 1. The damped oscillations in the time spectrum of the Y_{1-x}Ca_xBa₂Cu₃O₆ sample with $x = 0.06$ together with the high transition temperature of $T_N \sim 180$ K implies that this sample exhibits 3D long range antiferromagnetic order. A strongly overdamped frequency is observed at low temperatures for $x = 0.15$ ($p=0.075$), a superconducting sample with $T_c = 13$ K. Even for Y_{0.8}Ca_{0.2}Ba₂Cu₃O₆ ($T_c = 37$ K) a fast relaxing signal is observed, indicating the presence of strong magnetic correlations coexisting with superconductivity. The dotted curves in Fig. 1 are the fit to the data using the following Ansatz for the time evolution of the muon spin polarization:

$$G_z(t) = \frac{2}{3} \cos(\gamma_\mu B_\mu t) \exp(-\frac{1}{2}(\gamma_\mu \Delta B_\mu t)^2) + \frac{1}{3} \exp(-\lambda t) \quad (1)$$

where $\gamma_\mu = 851.4$ MHz/T is the gyromagnetic ratio of the muon, B_μ the average internal magnetic field at the muon site and ΔB its rms deviation. The two terms arise from the random orientation of the local magnetic field in a polycrystalline

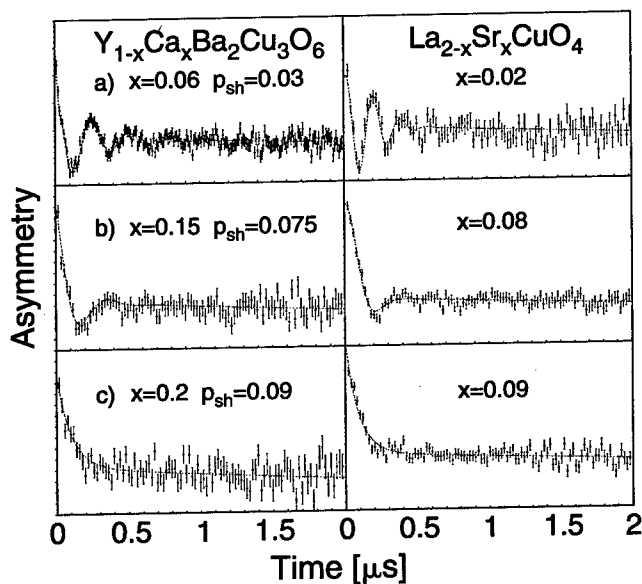


FIGURE 1. ZF- μ SR spectra obtained at low temperatures ($T < 1$ K) for various degrees of hole doping in Y_{1-x}Ca_xBa₂Cu₃O₆ and La_{2-x}Sr_xCuO₄. Dotted curves are the fit to the data using equation 1.

sample, which on average points parallel (perpendicular) to the muon spin direction with probability 1/3 (2/3) [1].

In analogy to NMR a slowing down of magnetic fluctuations typically causes a maximum of $1/T_1$ at $\omega_\mu \tau_c \approx 1$, where ω_μ is the μ^+ Zeeman frequency, and τ_c the average correlation time of the fluctuating transverse field components. A precessing 2/3 component indicates static magnetic order on the time scale of the μ SR technique ($\tau_c < 10^{-6}$ s). For $p > 0.08$ no oscillations were observed and the 2/3 part of $G_z(t)$ was better represented by an exponential relaxation $\exp(-\lambda t)$, which may indicate either a very strongly disordered static field distribution or rapid fluctuations.

As an example for the behaviour of an only lightly doped system we discuss the data on $Y_{0.95}Ca_{0.05}Ba_2Cu_3O_6$ which are displayed in Fig. 2. Well below the 3D Neel temperature of $T_N \sim 225$ K a second magnetic transition occurs at a temperature $T_f \sim 20$ K. This is evident from the peak in the longitudinal relaxation rate $1/T_1$ and the upturn of the muon spin precession frequency. A corresponding transition within the AF state has been reported recently from La-NQR [6] and μ SR studies [7] on La,Sr-214 where $T_f = (815 \text{ K}) p$ has been obtained for $p < 0.02$. This transition was ascribed to a freezing of the spins of the doped holes into a spin glass state which is superimposed on the preexisting 3D AF long-range order of the Cu^{2+} spins. Interestingly, we find that the spin freezing temperature T_f exhibits the same linear dependence on the planar hole content for Y,Ca-123 and La,Sr-214 (see Fig. 3). According to the model of Gooding et al. [8], in which $J_{eff} p \approx K_B T_f$, this implies that the effective in plane exchange coupling constant, J_{eff} , is identical for both systems and that the freezing of the spin degrees of freedom is a property of the hole dynamics within a single plane. The Neel-state, however, persists to higher hole content in Y,Ca-123 as compared to La,Sr-214. This suggests that the bilayer coupling makes the 3D AF-state more robust to the presence of doped holes. A similar result was reported from a ^{89}Y NMR study of T_N in Y,Ca-123 [9].

Only a single magnetic transition into a short range AF correlated spin-glass like state is observed for $p > 0.02$ in La,Sr-214 and $p > 0.035$ in Y,Ca-123. This transition is characterized by a slowing down of the AF fluctuations towards a glass transition which is defined by the maximum in $1/T_1$ (corresponding to a correlation time of the spin fluctuations of about 10^{-7} s). The spin-glass character of this magnetic state has been demonstrated recently for $La_{1.96}Sr_{0.04}CuO_4$ where the susceptibility exhibits irreversible and remanent behavior and obeys scaling laws [10]. T_g is significantly higher due to bilayer interactions in Y,Ca-123 than in La,Sr-214.

It is remarkable that the average internal field at the muon site is only modestly reduced while the transition temperature is lowered by about one order of magnitude. This is illustrated in Fig. 3b, where we display the zero temperature limit of the internal field at the muon site normalized to its value at zero doping. The width of the field distribution, ΔB , which is a measure of the degree of disorder of the magnetic state, increases linearly with hole doping in this regime as can be seen in Fig. 3c. The modest reduction of the average internal field and the strong

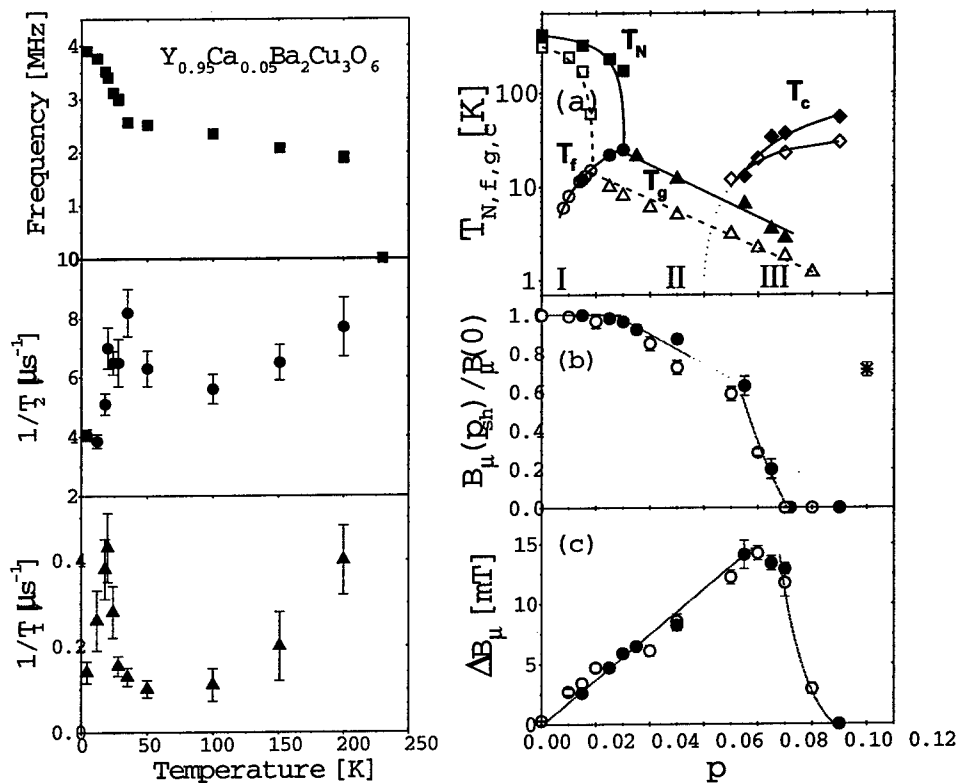


FIGURE 2. ZF- μ SR results on $\text{Y}_{0.95}\text{Ca}_{0.05}\text{Ba}_2\text{Cu}_3\text{O}_6$ plotted as a function of temperature. From top to bottom: Muon spin precession frequency and transverse relaxation rate $1/T_2$ and the longitudinal relaxation rate $1/T_1$.

FIGURE 3. Magnetic phase diagram as a function of the hole concentration per CuO_2 sheet for $\text{La}_{2-x}\text{Sr}_x\text{CuO}_4$ (open symbols) and $\text{Y}_{1-x}\text{Ca}_x\text{Ba}_2\text{Cu}_3\text{O}_6$ (full symbols). a) In regime I two transitions are observed. The Neel temperatures T_N (squares), at which the Cu^{2+} spins order into a 3D AF state and a freezing transition of the spins of the doped holes at $T_f = 815\text{K } p$ (circles, including data from Borsa et al.). T_g indicates a transition into a spin-glass like state (up triangles, regime II) with strong magnetic correlations which coexist with superconductivity in regime III. Diamonds represent the superconducting transition temperatures. b) Doping dependence of the normalized average internal magnetic field at the muon site. The star at $p = 0.12$ represents the data for $\text{La}_{1.58}\text{Nd}_{0.3}\text{Sr}_{0.12}\text{CuO}_4$. c) rms deviation ΔB . Data in b) and c) are for $T < 1\text{K}$.

increase of ρ_B with hole doping can be understood in terms of a phase separated electronic state where the holes segregate into metallic domains leaving mesoscopic hole poor regions with AF strongly correlated Cu^{2+} spins [11].

The spin glass regime extends far into the superconducting state. For strongly underdoped superconducting samples with $0.06 < p < 0.10$ we still observe a freezing of the spin degrees of freedom. Except for the somewhat smaller ordering temperature the signature of the transition is the same as for the non-superconducting samples. From the amplitude of the rapidly damped muon spin polarization in Fig.1 we can obtain information about the volume fraction of the magnetically correlated regions. We find that all the muons stopped inside the sample experience a non zero local magnetic field, which implies that the magnetic order persists throughout the entire volume of the sample. The magnetic ground state may still be inhomogeneous but the size of the non magnetic hole rich regions must be smaller than the typical length scale (about 2 nm) of the μSR experiment. By decoupling experiments in a longitudinal field we have confirmed the static nature of the magnetic ground state. From transverse field measurements we find that the flux line lattice which is formed below $T_c > T_g$ extends throughout the entire volume of the sample [12].

The consistency of our results suggests that the coexistence of SC and AF order is an intrinsic property of the CuO_2 planes and not an artifact of chemical or structural impurities. Our data show that the strength of the AF correlation is determined solely by the hole content of the CuO_2 planes and does not depend on the concentration of dopant atoms. For a given hole content the number of dopant atoms (Ca^{2+} or Sr^{2+}) is twice the number in Y,Ca-123 compared to La,Sr-214 .

In contrast to T_g which evolves rather smoothly, the internal magnetic field at the muon site exhibits a strong change for $p \approx 0.06-0.08$ as one enters the SC regime. The change in slope is rather significant and indicates a distinct change in the ground state properties of the CuO_2 planes. From the μSR experiment alone we can not decide whether it is the competition between the AF and the SC order parameter or an underlying change of the electronic properties of the CuO_2 planes which causes the suppression of the internal field. Further experiments will be required in order to clarify if the SC order parameter is affected by the static AF correlation.

Notably, the AF correlation is fully restored at $p \approx 1/8$. A depression of T_c at this hole concentration at first appeared to be uniquely present in $\text{La}_{2-x}\text{Ba}_x\text{CuO}_4$ [13], but recent studies on $\text{La}_{2-x}\text{Sr}_x\text{CuO}_4$ [14] have shown the presence of a shallow cusp at the same doping level and this behavior may also be related to the 60K plateau in Y-123 [15]. Detailed μSR studies [16] by Luke et al. and Kumagai et al. show that at this doping level static magnetic order is restored at temperatures below 35 K. Tranquada et al. [17] showed that the static order in $\text{La}_{1.6-0.125}\text{Nd}_{0.4}\text{Ba}_{0.125}\text{CuO}_4$ comprised a spatial separation of the spin and charge into AF stripes three lattice spacings wide (hole poor) separated by antiphase domain boundaries of one lattice dimension where the doped holes reside on every second site. If we consider a picture in which a stripe phase were to be established through connectivity of the

hole doped regions already existing in region II, the averaged internal magnetic field is expected to be 3/4 of the value of the undoped compound. Interestingly, this value is observed for both the SC compound $\text{La}_{1.93}\text{Sr}_{0.07}\text{CuO}_4$ and the non-SC static stripe phase compound $\text{La}_{1.58}\text{Nd}_{0.3}\text{Sr}_{0.12}\text{CuO}_4$.

In summary we have presented a magnetic phase diagram for the single layer system $\text{La}_{2-x}\text{Sr}_x\text{CuO}_4$ and the bilayer compound $\text{Y}_{1-x}\text{Ca}_x\text{Ba}_2\text{Cu}_3\text{O}_6$. We observe a common phase diagram which is characterized by two distinct transitions of the magnetic ground state. In the 3D AF regime we observe a freezing of the spin degrees of freedom of the doped holes at a temperature T_f , which increases linearly with the number of doped holes in both systems suggesting that the hole dynamics in a single plane is responsible for the observed behavior. For higher doping levels we observe a single magnetic transition into a spin glass like state which extends well into the superconducting regime. The evolution of the internal magnetic field with doping is understood on the basis of a microscopic phase segregation of the doped holes into hole rich and hole poor regions. We observe a microscopic coexistence of superconductivity and frozen antiferromagnetic correlations at low temperatures for underdoped samples.

REFERENCES

1. For a review of the μSR technique and application prior to HTSC see A. Schenck, *Muon Spin rotation Spectroscopy*, (Adam Hilger, Bristol, 1985).
2. J.I. Budnick et al., *Europhys. Lett.* **5**, 65 (1988).
3. A. Weidinger et al., *Phys. Rev. Lett.* **62**, 102 (1989).
4. N. Nishida et al., *J. Phys. Soc. Jpn* **57**, 597 (1988).
5. A. Weidinger et al., *Hyp. Int.* **63**, 147 (1990).
6. F.C. Chou et al., *Phys. Rev. Lett.* **71** 2323 (1993).
7. F. Borsa et al., *Phys. Rev. B* **52**, 7334 (1995).
8. R. J. Gooding et al., *Phys. Rev. B* **49**, 6067 (1994).
9. H. Casalta, H. Alloul and J.-F. Marucco, *Physica C* **204**, 331 (1993).
10. F. C. Chou et al., *Phys. Rev. Lett.* **75**, 2204 (1995).
11. V. J. Emery and S. A. Kivelson, *Physica C* **209**, (1993) 597
12. C. Bernhard et al., *Phys. Rev. B* **52**, 10488 (1995).
13. A.R. Moodenbaugh et al., *Phys. Rev. B* **38**, 4596 (1988).
14. P.G. Radaelli et al., *Phys. Rev. B* **49**, 4163 (1994).
15. J.L. Tallon et. al, *Physica C* **282-287**, 236 (1997)
16. G.M. Luke et al., *Physica C* **185-189**, 1175 (1991); K. Kumagai et al., *Physica C* **185-189**, 913 (1991)
17. J.M. Tranquada et al., *Nature* **375**, 561 (1995); J. M. Tranquada et al., *Phys. Rev. Lett.* **78**, 338 (1997)

Fermi Surfaces, Fermi Patches, and Fermi Arcs in High T_c Superconductors

M. R. Norman

Materials Science Division, Argonne National Laboratory, Argonne, IL 60439

Abstract. A defining property of metals is the existence of a Fermi surface: for two dimensions, a continuous contour in momentum space which separates occupied from unoccupied states. In this paper, I discuss angle resolved photoemission data on the cuprate superconductor BSCCO and argue that it is not best thought of in this conventional picture. Rather, the data are consistent with "patches" of finite area connected by more conventional "arcs". Novel physics is associated with the patches, in that the states contained in a patch are dispersionless and thus interaction dominated. In the pseudogap phase, the patches are gapped out, leaving the Fermi arcs disconnected. This unusual situation may be the key to understanding the microscopic physics of the high temperature superconductors, in that the pairing correlations are strongest in the patches, yet the superfluid density lives only on the arcs.

Perhaps no problem in recent history has captured the attention of the condensed matter physics community as much as that of the high temperature cuprate superconductors. After over a decade of work, it has become clear that conventional metal physics alone is not capable in describing all of their properties. In fact, it is strongly felt in a section of the community that new physics needs to be developed to fully solve the problem [1]. One difficulty has been to properly define what the problem to be solved exactly is. For instance, it is now generally accepted by the community that conventional metal physics should not break down for a two dimensional metal which exhibits a free electron dispersion [2]. This can be contrasted with the unusual excitations associated with the fractional quantum hall effect, including that of the still debated half integral case, which arise due to the degeneracy of states in an applied magnetic field (Landau levels). This points to the reasonable hypothesis that the novel physics associated with the high temperature cuprate superconductors has something to do with a dramatic departure of their dispersion from that of free electron metals.

The experimental tool to employ in this regard is angle resolved photoemission spectroscopy (ARPES). For two dimensional materials, if the impulse approximation is valid, then the ARPES intensity should be proportional to the product of the single particle spectral function and the Fermi function [3]. The 2D condition is almost certainly satisfied in the cuprates, in that there is no evidence, particularly

in BSCCO, for any c-axis dispersion in the data. For the photon energies typically employed, there is also evidence that the impulse approximation is satisfied. This is a result of the large number of available final states (due to the complexity of the crystal structure) coupled with the short escape depth of the photoelectrons (which limits the time for the photoelectron to interact with the photohole). As a consequence, the probe is surface sensitive, which has limited much of the most useful data to BSCCO, given its strongly two dimensional nature, with resulting cleaved surfaces characteristic of the bulk.

The importance of the single particle spectral function is self evident. It is the most fundamental quantity predicted by a many-body theory. Being proportional to the imaginary part of the Greens function, it can in principle be Kramers-Kronig transformed to yield the entire Greens function, which in turn defines the electron self-energy, the function that encapsulates the many-body physics of the material. The self-energy implicitly contains the energy dispersion, which as argued above, has strong relevance to the nature of the ground and excited states of the system.

Although ARPES only reveals the occupied part of the spectral function, we are fortunate in the cuprates in that scanning tunneling microscope (STM) measurements in BSCCO yield spectra which strongly resemble that from ARPES for the appropriate bias sign despite the fact that STM is a momentum averaged probe. This indicates that the tunneling matrix elements weight the spectra to certain regions of the Brillouin zone (to be identified later as the patches). Thus, not only do these data provide a useful complement to ARPES data, with the additional advantage of spatial resolution and much higher energy resolution, they can be additionally exploited to obtain crucial information concerning the unoccupied part of the spectral function.

With this introduction, we now turn to some general observations concerning ARPES data in Bi2212. The identification of what the actual Fermi surface is in this material is still of some controversy. This is easy to understand from early measurements of the Stanford group [4]. In a very illuminating figure of a paper by that group (Fig. 2), they show those regions of the Brillouin zone where spectral weight is seen within 50 meV of the Fermi energy, which was comparable to their energy resolution. They then interpreted this in terms of two conventional Fermi surfaces, an electron-like surface centered at the $(0,0)$ point of the zone, and a hole-like surface centered at the (π,π) point of the zone. This was conjectured to be due to the predicted bilayer splitting of the electronic structure due to the two CuO planes per bilayer unit. Subsequent measurements by the UIC-Argonne group [5] were able to attribute the Fermi crossing of the presumed electron-like sheet along $(0,0) - (\pi,0)$ to actually be that of a ghost image of the Fermi surface due to diffraction of the outgoing photoelectrons by the superstructure associated with the BiO surface layer. This led to what is now the mostly accepted picture of just a single hole-like surface centered around (π,π) , with the surprising result that somehow, the c-axis kinetic energy associated with bilayer splitting is missing in the dispersion of the spectral function.

I will now argue that this more or less conventional picture has been accepted

a bit too readily. As stated above, what the authors of Ref. [4] actually show is a plot of the near Fermi energy spectral weight in the zone. This plot is highly instructive. What is seen is a mass of states in the vicinity of the $(\pi, 0)$ points of the zone connected by more typical Fermi surface segments. That is, the most natural interpretation of the data is not that one has a Fermi surface that represents a continuous contour in momentum space. Rather, it appears that one has "Fermi patches" which occupy a finite *area* in momentum space, connected by "Fermi arcs" which resemble more typical behavior. This observation is reinforced by directly looking at the raw spectra. There, one sees that states in the "patch" region in the normal state are characterized by very broad linewidths which exhibit little dispersion. In fact, the often quoted "Fermi crossing" along the $(\pi, 0) - (\pi, \pi)$ direction is based not on dispersion, but rather on the drop in intensity of the spectra along this direction as would be expected from such a crossing.

This behavior becomes even more unusual in the superconducting state. Along the traditionally accepted hole-like Fermi contour, one sees a dispersion consistent with a superconducting order parameter of the $d_{x^2-y^2}$ form [6,7]. But in the "patch" region, one finds a narrow quasiparticle peak with little if any observable dispersion at an energy location given by the maximum of the d-wave gap [8]. This is separated by a spectral dip from a higher binding energy feature, the "hump", which does in fact have strong dispersion in the "patch". This dispersion becomes quite obvious in underdoped materials [9] where it begins to take on qualities reminiscent of the undoped magnetic insulator [10].

It is of interest to note that the quasiparticle peak only forms below T_c ; that is, the Fermi liquid superconducting state appears to arise from a non Fermi liquid normal state. This is most dramatic in the underdoped case, where a spectral gap already exists in the normal state in the patches [11-13]. In this case, one finds a strongly incoherent spectrum above T_c , which loses any resemblance to even a very broad peak as the doping is reduced. Yet, despite this, one finds the rather surprising presence of a sharp leading edge gap. This is a non-trivial finding which has yet to be reproduced by any theory which purports to explain the pseudogap. Below T_c , a quasiparticle peak forms at this gap edge. This is somewhat reminiscent of the formation of a bound state inside of a gap, which has suggested a composite nature for the incoherent weight beyond the gap edge [14]. Above T_c , the spectral gap "fills in", leading to a more or less flat spectrum at a characteristic temperature T^* [15]. This filling in effect is also inferred from specific heat data [16], and directly observed as well by STM [17] and c-axis optical conductivity [18].

The filling in seen in the patch region can be modeled by a very simple self-energy of the form $\Sigma = -i\Gamma_1 + \Delta^2/(\omega + i\Gamma_0)$ [19]. Γ_1 is a crude (i.e., frequency independent) approximation to the single particle scattering rate, which is extremely large in the normal state, and collapses precipitously in the superconducting state, strongly suggesting that electron-electron interactions determine the spectral lineshape. Γ_0 describes the filling in effect, and is found to be proportional to $T - T_c$, as would be expected if it represented an inverse pair lifetime. Δ , the gap parameter, is found to be essentially temperature independent for underdoped samples, as was

inferred earlier from specific heat data [16] and also observed in STM [17]. T^* is then simply the temperature at which Γ_0 becomes comparable to Δ , and thus does not represent a mean field transition temperature, despite its correlation with Δ [20]. Similar modeling has been found to describe STM [21] and c-axis optical conductivity [22] data. This indicates that these probes are weighted towards the patch regions of the Brillouin zone.

The above behavior can be contrasted with what occurs on the Fermi "arcs", which are the Fermi contour segments which connect the patches. On the arcs, Δ closes in a more or less BCS like fashion [19], and this occurs somewhat above T_c for underdoped samples. This behavior is found in the patch region only for overdoped samples. It is still an unresolved question experimentally whether Δ collapses at the same temperature along the entire arc, though this is a distinct possibility. It is interesting to note that the temperature at which this collapse occurs is similar to the temperature at which the high frequency superfluid response vanishes for an underdoped sample with a similar T_c [23]. This is consistent with the fact that the low energy states in the patch region are dispersionless; that is, the patches probably do not contribute to the superfluid density. Therefore, once Δ collapses on the arcs, the system no longer exhibits a superfluid response, even at high frequencies. The available ARPES data also point to an increase of the size of the patch region as the doping is reduced, with a consequent decrease in the length of the arcs. Once the patches "grab up" the entire zone, the metal collapses into the Mott insulating phase.

The novelty of these findings cannot be overemphasized. If one looks at the anisotropy of the gap at low temperatures, it traces out a d-wave form. This occurs even for underdoped samples [24]. That is, it appears as if there is only a single gap in the problem. Above T_c , though, there appears as if there are two gaps in underdoped samples, a more or less conventional superconducting gap along the Fermi arcs, and a temperature independent one in the patch regions. Yet, at any given \mathbf{k} point, the gap smoothly evolves with temperature, even through T_c . This behavior is impossible to understand from a mean field viewpoint, and simply cannot be fixed up by attributing the gap in the patch region to some other effect (SDW, CDW, etc.). This is reinforced by the fact that once the gap collapses on the arcs, the resulting Fermi surface is just a set of disconnected segments, and therefore not derivable from a mean field description which would have implied a continuous Fermi contour in momentum space.

This brings up the important question of what theoretical implications these findings have. A phenomenological model based on the arc-patch picture has been developed by Geshkenbein, Ioffe, and Larkin [25]. The results differ significantly in the pseudogap phase above T_c from standard models of superconducting fluctuations, since the patch regions, because of their dispersionless nature, do not support classical fluctuations. Their model provides a good framework for addressing various data in the underdoped regime. Another phenomenological approach has been advocated by Lee and Wen [26]. They observe that the superfluid density can be written in the form $\rho_s(T) = \rho_s(0) - \alpha T$, with the second term due to quasiparti-

cle excitations about the d-wave nodes. As α is proportional to the inverse of Δ , and $\rho_s(0)$ is proportional to x (the number of doped holes), then assuming that Δ is roughly independent of doping, one gets the result that T_c is equal to $x\Delta$ in the underdoped regime. As a consequence, \mathbf{k} points where $\Delta_{\mathbf{k}}$ is larger than T_c have spectral gaps which survive above T_c . That is, one has gapless Fermi arcs with gapped patch regions. It is interesting that this argument, though completely consistent with ARPES data, is made independent of such data.

On a microscopic level, the Lee-Wen picture can be motivated by a gauge theory approach to the t-J model [27]. This picture implies a d-wave gap at low T, but a collapse of the gap along the arc above T_c , very similar to what is seen by ARPES. The disconnected Fermi arcs are a consequence of strong fluctuations given the near degeneracy such a model predicts between the d-wave and flux phase states. The doping dependence of the arcs has been calculated in a related gauge theory approach [28] and are consistent with the ARPES doping trend discussed above. A different approach for describing the arc-patch behavior based on the t-J model has been offered by Furukawa, Rice, and Salmhofer [29]. Their results, utilizing a renormalization group treatment of interactions in the patches, suggest a phase separation in momentum space, with an insulating spin liquid phase in the patch regions connected by Fermi arcs, and is motivated by studies of three leg ladders. Finally, there has been a recent study by Putikka, Luchini, and Singh [30] where the momentum distribution, $n_{\mathbf{k}}$, for the t-J model has been obtained by high temperature expansion. The resulting contour plots show that the sharp drop in $n_{\mathbf{k}}$, which defines Fermi crossings, is only well defined on the arcs, very reminiscent of the ARPES data.

In this connection, the work of Khodel and Shaginyan deserves mention [31]. These authors discovered another solution besides the classic Landau Fermi liquid one. This solution is characterized by a flat band which is pinned to the chemical potential, either along a line, or in an entire region of the zone. This Fermion condensate tends to be realized by interactions which are long range in real space and attractive [32], and as a consequence is unstable to superconductivity at low temperatures. In the resulting superconducting state, dispersionless quasiparticle peaks are found, much like what is seen by ARPES in the region of the zone surrounding $(\pi, 0)$ [8]. Above T_c , one expects very broad spectral lineshapes [32], again consistent with ARPES results. In addition, $n_{\mathbf{k}}$ is predicted to have a ramp-like behavior for states inside of the Fermion condensate (patch). This behavior is descriptive of that observed for the frequency integrated ARPES weight along the $(\pi, 0) - (\pi, \pi)$ direction. Therefore, the Khodel state may indeed be the appropriate non Fermi liquid reference state for the patch regions of the zone.

The author thanks his collaborators, Juan Carlos Campuzano, Hong Ding, and Mohit Randeria, for the many discussions which led to the ideas presented here. Also, the author thanks Victor Khodel and Grisha Volovik for discussions concerning the Khodel state. This work was supported by the U. S. Dept. of Energy, Basic Energy Sciences, under contract W-31-109-ENG-38.

REFERENCES

1. P. W. Anderson, *The Theory of Superconductivity in the High T_c Cuprates* (Princeton Univ. Pr., Princeton, 1997).
2. J. R. Engelbrecht and M. Randeria, Phys. Rev. Lett. **65**, 1032 (1990).
3. M. Randeria *et al.*, Phys. Rev. Lett. **74**, 4951 (1995).
4. D. S. Dessau *et al.*, Phys. Rev. Lett. **71**, 2781 (1993).
5. H. Ding *et al.*, Phys. Rev. Lett. **76**, 1533 (1996).
6. Z.-X. Shen *et al.*, Phys. Rev. Lett. **70**, 1553 (1993).
7. H. Ding *et al.*, Phys. Rev. B **54**, R9678 (1996).
8. M. R. Norman *et al.*, Phys. Rev. Lett. **79**, 3506 (1997).
9. J. C. Campuzano *et al.*, unpublished.
10. F. Ronning *et al.*, Science **282**, 2067 (1998).
11. D.S. Marshall *et al.*, Phys. Rev. Lett. **76**, 4841 (1996).
12. H. Ding *et al.*, Nature **382**, 51 (1996).
13. A. G. Loeser *et al.*, Science **273**, 325 (1996).
14. R. B. Laughlin, Phys. Rev. Lett. **79**, 1726 (1997).
15. M. R. Norman *et al.*, Nature **392**, 157 (1998).
16. J. W. Loram *et al.*, J. Supercond. **7**, 243 (1994).
17. Ch. Renner *et al.*, Phys. Rev. Lett. **80**, 149 (1998).
18. C. C. Homes *et al.*, Physica C **254**, 265 (1995).
19. M. R. Norman, M. Randeria, H. Ding, and J. C. Campuzano, Phys. Rev. B **57**, R11093 (1998).
20. H. Ding *et al.*, J. Phys. Chem. Solids **59**, 1888 (1998).
21. M. Franz and A. J. Millis, Phys. Rev. B **58**, 14572 (1998).
22. C. Bernhard *et al.*, Phys. Rev. B **59**, R6631 (1999).
23. J. Corson *et al.*, Nature **398**, 221 (1999).
24. J. Mesot *et al.*, unpublished.
25. V. B. Geshkenbein, L. B. Ioffe, and A. I. Larkin, Phys. Rev. B **55**, 3173 (1997).
26. P. A. Lee and X.-G. Wen, Phys. Rev. Lett. **78**, 4111 (1997).
27. X.-G. Wen and P. A. Lee, Phys. Rev. Lett. **80**, 2193 (1998).
28. X. Dai and Z.-B. Su, Phys. Rev. Lett. **81**, 2136 (1998).
29. N. Furukawa, T. M. Rice, and M. Salmhofer, Phys. Rev. Lett. **81**, 3195 (1998).
30. W. O. Putikka, M. U. Luchini, and R. R. P. Singh, Phys. Rev. Lett. **81**, 2966 (1998).
31. V. A. Khodel and V. R. Shaginyan, JETP Lett. **51**, 553 (1990).
32. P. Nozieres, J. Phys. I France **2**, 443 (1992).

Doping dependence of electronic structure in $\text{Bi}_2\text{Sr}_2\text{CaCu}_2\text{O}_{8+x}$

M. Onellion^a, S. Christensen^a, B. Frazer^a, R. Gatt^a, R.J. Kelley^a, S. Misra^a,
T. Schmauder^a, H. Berger^b, M. Grioni^b, G. Margaritondo^b, I. Vobornik^b,
F. Zwick^b, M. Mölle^c, R. Kleiner^c and P. Müller^c

(a) *Physics Department, University of Wisconsin, Madison, WI 53706, USA*

(b) *Institut de Physique Appliquée, École Polytechnique Fédérale Lausanne, Lausanne, Switzerland*

(c) *Physikalisches Institut III, Universität Erlangen-Nürnberg, D-91058 Erlangen, Germany*

Abstract

We report on angle-resolved photoemission and superconductor-insulator-superconductor tunneling measurements of the normal and superconducting states of $\text{Bi}_2\text{Sr}_2\text{CaCu}_2\text{O}_{8+x}$ single crystal samples and $\text{Bi}_2\text{Sr}_2\text{CaCu}_2\text{O}_{8+x}$ - native oxide- lead (S-I-S) tunnel junctions.(1-7)

I. Introduction

The nature of the cuprate normal state, and how the cuprate electronic structure changes with carrier concentration, remains an important and complicated question.(1-11) The purpose of this report is to present experimental evidence on three points. Due to space limitations, we refer the reader to our previously published reports (6,12,13) for the details of equipment facilities, sample preparation, measurement methods and data analysis.

II. Results

A. Is the normal state a Fermi liquid?

In studying a Fermi liquid system with photoemission, there are two analytical results arising from the Green's function and independent of the strength of interactions in the system.(14) One is that the single-particle spectral function is cut off by the Fermi-Dirac distribution function. The other is that on the Fermi surface, the high binding energy side of any quasiparticle peak exhibits a Lorentzian lineshape. Some of us have studied both of these issues. As shown below and in Refs. 1-2, for samples where there is a sufficiently strong quasiparticle state to analyze, we find a systematic change with doping. For the part of the Fermi surface around the $(0,\pi)$ point, the lineshape changes from Lorentzian (Fermi-liquid) for overdoped samples to a non-Lorentzian shape for underdoped samples, the latter consistent with a particular non-Fermi liquid state reported by A. Chubukov.(1,15) We have also investigated the cutoff in the spectral function; these results are reported elsewhere.(16)

Figure One illustrates angle-resolved photoemission spectra for (a) overdoped and (b) underdoped $\text{Bi}_2\text{Sr}_2\text{CaCu}_2\text{O}_{8+x}$ single crystal samples. The overdoped samples exhibit a Fermi-liquid (Lorentzian) lineshape, while the underdoped samples do not exhibit such a lineshape. In addition to the Fermi liquid Green's function, Chubukov has recently (15) calculated a Green's

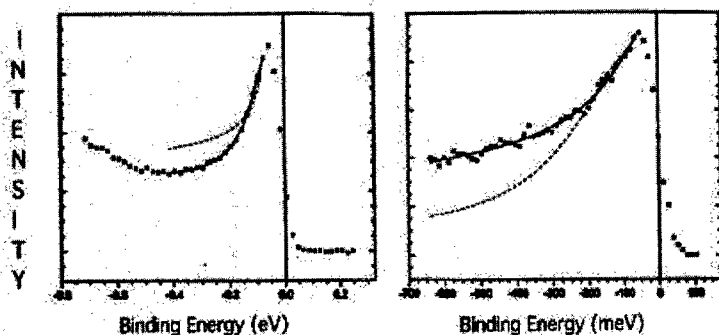


Figure 1. Angle-resolved photoemission spectra, including overdoped (left) and underdoped (right). The solid line shows a fit using a Fermi-liquid spectral function, while the dotted line shows a fit using the non-Fermi liquid spectral function of equation (1).

function based on the interaction between electrons and overdamped spin fluctuations. For the part of the Fermi surface near the $(0,\pi)$ point, this interaction leads to a qualitatively different Green's function, viz:

$$(1) \quad G^{-1}(\omega) = \frac{1}{Z} \frac{2\omega}{1 + \sqrt{1 - i|\omega|/\omega_{sf}}}$$

The samples were also compared to the Green's function of equation (1). The results indicate that underdoped samples are fit much better by this non-Fermi liquid Green's function, while the overdoped samples are fit much better by a Fermi-liquid Green's function. Altogether, we used seven different methods to analyze the photoemission data.(2) The qualitative results of these various methods is the same: near the $(0,\pi)$ point, overdoped samples exhibit spectra consistent with a Fermi-liquid state, while underdoped samples exhibit spectra consistent with the non-Fermi liquid state of equation (1).(1,2)

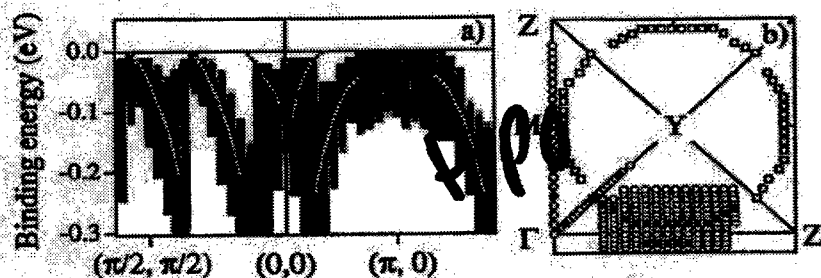


Figure 2. Dispersion relation (left) and Fermi surface (right) of overdoped BSCCO-2212 samples with $T_c \sim 60K$. Open and closed circles on right are data points, closed circles are measured Fermi surface crossings, and open squares are Fermi surface locations obtained by assuming symmetric surface.

B. Fermi surface topology

The $\text{Bi}_2\text{Sr}_2\text{CaCu}_2\text{O}_{8+x}$ system exhibits an extended, saddle-point van Hove singularity.(12,17-20) The significance of this band structure feature remains in some dispute.(21,22) Does the binding energy of the van Hove singularity affect, let alone control, the value of T_c ? One way to understand how T_c and the van Hove singularity are related is to measure the normal state Fermi surface for overdoped samples. Figure Two illustrates (a) the dispersion relation along the high-symmetry directions, and (b) the measured Fermi surface for overdoped samples with $T_c \sim 50$ -60K. These results indicate that the Fermi surface of the overdoped samples is $\sim 6\%$ larger than for optimally doped samples, but that the topology is qualitatively the same. Specifically, the van Hove singularity remains below the chemical potential, and both main and shadow Fermi surface features are clearly visible and can be distinguished from each other along the Γ -Y direction.(3)

C. C-axis S-I-S Tunneling

The phase sensitive measurements provide very strong evidence that there is a sign change in the superconducting order parameter- the gap.(23-26) Such measurements include a limit in how small a s-wave component can be measured. Earlier reports (27,28) indicate a small s-wave component in $\text{YBa}_2\text{Cu}_3\text{O}_{7-x}$ that have been attributed to the presence of chains- an orthorhombic rather than a tetragonal system in which planes containing neither $\langle\pi,\pi\rangle$ nor $\langle\pi,-\pi\rangle$ are planes of reflection symmetry.

Recently, M. Mölle, R. Kleiner, P. Müller and colleagues have reported measuring a supercurrent in c-axis S-I-S tunnel junction structures fabricated with $\text{Bi}_2\text{Sr}_2\text{CaCu}_2\text{O}_{8+x}$ - native oxide-lead.(6,7) The data in Refs. 6-7 were obtained from their own $\text{Bi}_2\text{Sr}_2\text{CaCu}_2\text{O}_{8+x}$ single crystal samples.

Quite recently, some of us established a collaboration to further investigate this system. Single crystal $\text{Bi}_2\text{Sr}_2\text{CaCu}_2\text{O}_{8+x}$ samples were grown and characterized at the University of Wisconsin. Angle-resolved photoemission measurements of these samples were performed at UW and at EPFL in Switzerland. S-I-S tunnel junction structures were fabricated in Erlangen, Germany and measured, using the same methodologies reported in Refs. 6-7. In Refs. 6-7, between 40-50 samples were measured with consistent results. In the more recent collaboration, 17 samples have been measured to date with consistent results.

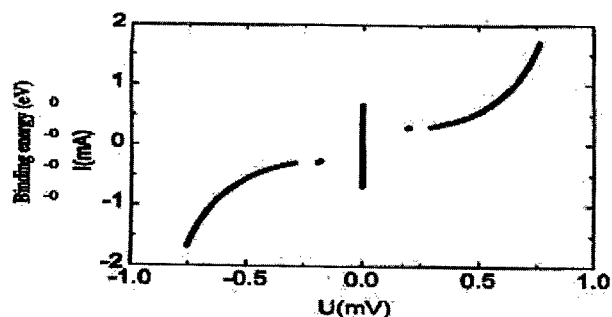


Figure 3. Current (I) versus voltage (U) for Pb-native oxide- BSCCO2212 (S-I-S) structure at a temperature of 4.2K. Note supercurrent (vertical line).

Figure Three illustrates the supercurrent observed (a) in Refs. 6-7 and (b) in our more recent collaboration. Note particularly the presence of a supercurrent below the T_c of lead.

Figure Four illustrates a Fraunhofer pattern obtained (a) in our more recent collaboration, and (b) in Ref. 7. In Fig. 4(b), the sample was repeatedly heated and slowly cooled to remove as much trapped flux as possible. In Fig. 4(a), there was more trapped flux in the sample, which distorted the Fraunhofer pattern compared to the better results obtained in Fig. 4(b). In both cases, however, there is a Fraunhofer pattern present.

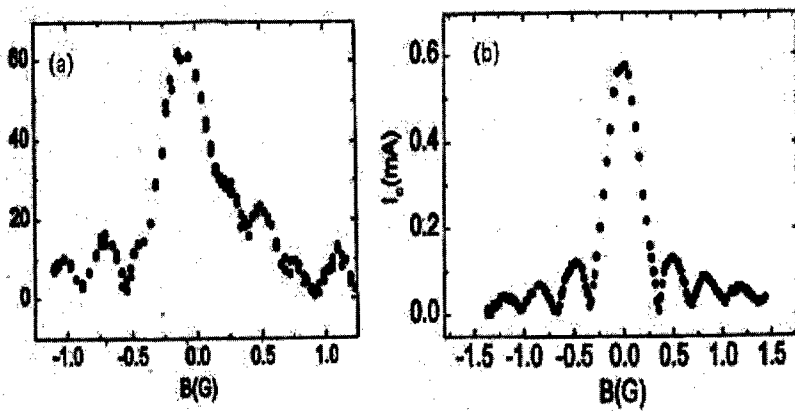


Figure 4. Critical current (I_c) versus applied magnetic field (B) in gauss for S-I-S structures at 4.2K. (a) present work, (b) Ref. 7. Note Fraunhofer pattern.

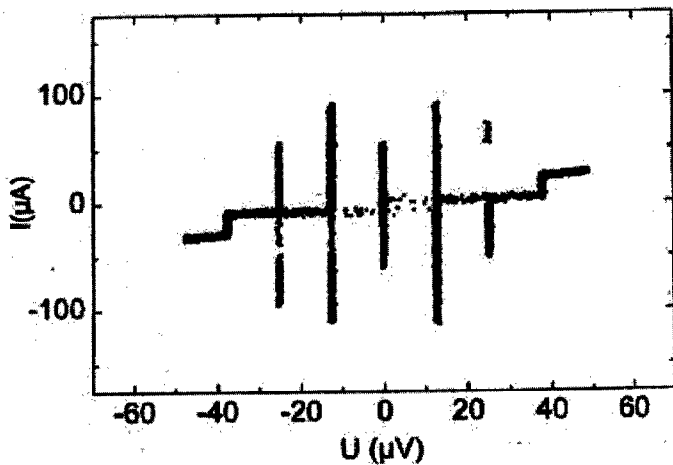


Figure 5. Current (I) versus voltage (U) for S-I-S structure at 4.2K, using 6.1 GHz microwaves.(7)

Figure Five illustrates current versus voltage measurements, using 6.1 GHz microwaves. Fig. 5 indicates that the tunneling is first-order tunneling ($e/2h$), not second order tunneling.(6,7)

The data in Refs. (6,7) and Figs. 3-5 are surprising. We investigated why the data are so consistently reproducible. Ref. 7 reports on the result of atomic force microscopy study of the Erlangen samples. The result indicates that the step density- which would lead to ab-plane tunneling- is very low, below 10^{-5} unit cells. The same study has not been performed on the Wisconsin samples; however, since the tunneling data is of comparable quality, it seems that having flat surfaces is essential for obtaining the results of Refs. (6,7) and Figs. 3-5.

The data in Refs. (6,7) and in Figs. 3-5 indicate that the $\text{Bi}_2\text{Sr}_2\text{CaCu}_2\text{O}_{8+x}$ samples possess a s-wave component to the order parameter even when underdoped. Such a conclusion is further supported by existing reports (29) that overdoped $\text{Bi}_2\text{Sr}_2\text{CaCu}_2\text{O}_{8+x}$ samples do not exhibit a gap node.

Our results indicate that there is a chemical reaction between the cuprate and the lead at the interface. The chemical reaction removes enough oxygen to alter the T_c of the last CuO_2 bilayer, and it is this bilayer that leads to the supercurrent and other data we obtained. Thus, for both the earlier work, Refs. 6-7 and the present work, the measurements are taken on underdoped $\text{Bi}_2\text{Sr}_2\text{CaCu}_2\text{O}_{8+x}$. At this time, we do not have a way to suppress this interface chemistry; work is in progress on this point.

III. Discussion and Conclusions

The normal state changes qualitatively, from a Fermi liquid metal toward some type of non-Fermi liquid ground state, as the carrier concentration decreases. The exact nature of this non-Fermi liquid ground state remains to be determined. The reduction in T_c value for overdoped samples does not seem due to any qualitative change in the Fermi surface topology. Our data do not establish what changes to the normal state electronic structure- if any- account for the reduction in T_c value.

The S-I-S tunneling results indicate a supercurrent, which means that the cuprate, although underdoped at the interface, exhibits a non-zero s-wave order parameter component. The $I_c R_n$ product is always lower than 15 microvolt, so the s-wave component is $\sim 10^{-3}$ of the d-wave order parameter component. At this time, we have no data for which the interface is overdoped. This is a small component, but the important point is that it is not zero, as expected for a pure d-wave order parameter. The extrapolated value of this s-wave component T_c is 12-20K, above the T_c of lead.(6,7) Thus, the supercurrent is not due to proximity effect coupling from the lead. There is no zero bias anomaly, which indicates that the supercurrent is not due to ab-plane tunneling. The Fraunhofer diffraction pattern indicates a homogeneous interface, no ab-plane tunneling, and the minima and maxima fit to the dimensions of the junction. The microwave data indicate first order tunneling, while tunneling from a purely d-wave cuprate would be second order tunneling or higher order. Said another way, the microwave data indicate a second order tunneling component below what can be detected, which if present would be too small to explain the tunneling data.

In the superconducting state, our data, both published (6,7) and in progress, (4,29) are in direct disagreement with the idea that the order parameter is purely d-wave. Instead, both photoemission and tunneling data indicate that there is a s-wave component to the order parameter. The results of Refs. 5-7 and Figs. 3-5 indicate that for underdoped samples with $T_c = 30\text{-}60\text{K}$, the s-wave component is $\sim 10^{-3}$ smaller than the d-wave component. The photoemission data indicate that for overdoped samples with $T_c \sim 60\text{K}$, the s-wave component is smaller than, but of the same order of magnitude as, the d-wave component.(4,29) We suggest the possibility that the size of the s-wave component grows rapidly as the carrier concentration increases.

ACKNOWLEDGEMENTS

We benefited from conversations with Robert Joynt and Andrey Chubukov. Financial support was provided by Fonds National and EPFL (Switzerland), by Bayerische Forschungsförderung and the Deutsche Forschungsgemeinschaft (Erlangen), and by the U.S. NSF and DOE (Wisconsin).

IV. References

1. Shashank Misra et.al., Phys. Rev. B 58, R8905 (1998).
2. Shashank Misra et.al., in preparation.
3. I. Vobornik et.al., submitted.
4. R. Gatt, I. Vobornik et.al., in preparation.
5. R. Gatt et.al., in preparation.
6. R. Kleiner et.al., Physica C 282, 2435 (1997).
7. M. Mölle and R. Kleiner, Phys. Rev. B, in press (1999).
8. P.W. Anderson, "The theory of superconductivity in the high- T_c cuprates," Princeton University Press, Princeton, NJ, 1997.
9. G.S. Boebinger et.al., Phys. Rev. Lett. 77, 5417 (1996).
10. J.W. Loram et.al., Physica C 235-240, 134 (1994).
11. A. Trokiner, NATO ASI 371, 331 (1997), and references therein.
12. Jian Ma et.al., Phys. Rev. B 51, 3832 (1995).
13. C. Kendziora et.al., Physica C 257, 74 (1996).
14. "A Guide to Feynman Diagrams in the Many-Body Problem," R.D. Mattuck, 2nd Ed., McGraw-Hill Co., New York, 1976, and references therein.
15. A. Chubukov, Phys. Rev. B 52, R3840 (1995).
16. I. Vobornik et.al., in preparation.
17. H. Ding et.al., Phys. Rev. B 50, 1333 (1994).
18. Z.-X. Shen et.al., Science 267, 343 (1995).
19. D.M. Newns et.al., Comm. Cond. Matt. Phys. 15, 273 (1992).
20. J. Labbé and J. Bok, Europhys. Lett. 3, 1225 (1987).
21. J. Bok and L. Force, Physica C 185-189, 1449 (1991).
22. A.A. Abrikosov et.al., Physica C 214, 73 (1993).
23. D. A. Wollman et.al., Phys. Rev. Lett. 71, 2134 (1993).
24. C. C. Tsuei et.al., Phys. Rev. Lett. 73, 593 (1994).
25. K.A. Kouznetsov et.al., Phys. Rev. Lett. 79, 3050 (1997).
26. P. Chaudhari and Y. Lin, Phys. Rev. Lett. 72, 1084 (1994).
27. Jian Ma et.al., Science 267, 862 (1995).
28. R.J. Kelley et.al., Science 271, 1255 (1996).
29. M. Mölle et.al., in progress.

The Specific Heat of $(\text{La}_{1.85}\text{Sr}_{0.15})\text{CuO}_4$: Evidence for d-Wave Pairing

N. E. Phillips¹, R. A. Fisher¹, A. Schilling¹,
B. Buffeteau², T. E. Hargreaves², C. Marcenat², R. Calemczuk²,
A. S. O'Connor³, K. W. Dennis³, R. W. McCallum³

¹MSD, Lawrence Berkeley National Laboratory, Berkeley, CA 94720, USA

²CENG/CEA, Grenoble, France

³Ames Laboratory, Iowa State University, Ames IA 50011, USA

Measurements of the specific heat of two samples of $(\text{La}_{1.85}\text{Sr}_{0.15})\text{CuO}_4$ in the superconducting and vortex states show evidence of the line nodes in the energy gap associated with d-wave pairing.

For $\text{YBa}_2\text{Cu}_3\text{O}_{7-\delta}$ (YBCO), measurements of the specific heat (C) as a function of magnetic field (H) have shown the presence of an $\propto T^2$ term for $H = 0$ and a $\beta H^{1/2}T$ term for $H \neq 0$ (1 - 3). The $H^{1/2}T$ term was predicted (4, 5), and the T^2 term is expected on quite general grounds (6, 7), for the line nodes in the energy gap associated with a d-wave order parameter. The analyses of the data for YBCO that identified these terms required substantial corrections to $C(H)$ for the contribution of the paramagnetic centers (PC's). (An approach based on the anisotropy of the H dependence of $C(H)$ avoided that complication, but gave no information on the T^2 term and a different H dependence (8).) It remains of interest to look for these effects in other cuprate superconductors, for which, unlike YBCO, there is relatively little evidence bearing on the symmetry of the order parameter. The obvious candidate is $(\text{La}_{2-x}\text{Sr}_x)\text{CuO}_4$ (LSCO) for which samples can be prepared with low concentrations of PC's. We report here measurements on two samples of $(\text{La}_{1.85}\text{Sr}_{0.15})\text{CuO}_4$ for which evidence of these effects can be recognized in the raw data.

The analysis of the data was limited to $T > 2.5\text{K}$ for one sample and $T > 3.0\text{K}$ for the other, where the small, but not negligible, contribution of PC's can be represented by a spin-1/2 Schottky anomaly. $C(H)$ is the sum of five terms: $C_{\text{DOS}}(H)$, the electron-density-of-states contribution; $C_{\text{mag}}(H)$, the contribution of PC's; $C_{\text{hyp}} = D(H)/T^2$, the hyperfine contribution, which is small in this region; C_{lat} , the phonon contribution; $\gamma^*(0)T$, the ubiquitous zero-field "linear term".

Figure 1 shows C/T^2 vs $H^{1/2}T$ for representative temperatures. One set of points (+'s) represents the raw data; a second (o's) represents the data corrected for C_{mag} and C_{hyp} . For each temperature there are eight points in each set corresponding to $H = 0, 0.5, 1, 2, 3, 5, 7$, and 9T . For $H > 0.5\text{T}$ the corrected data points for each temperature, which include

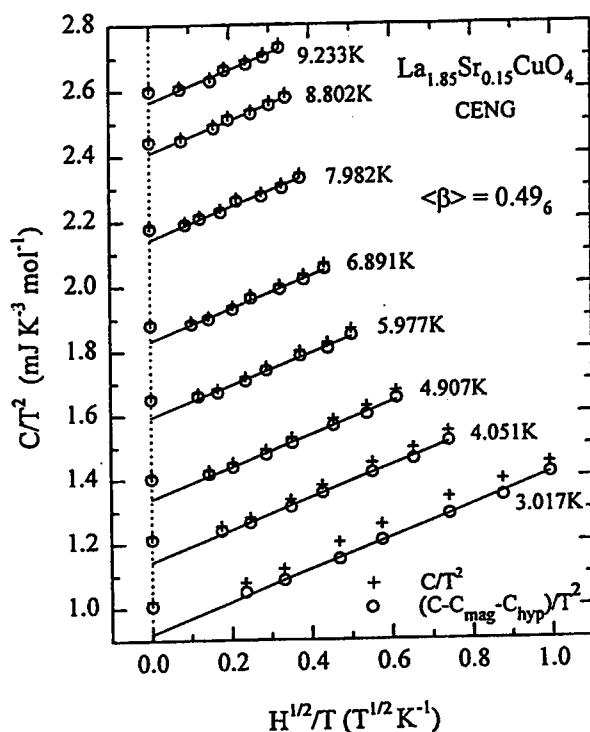


Fig. 1. Specific-heat data for representative temperatures. See text for discussion.

no other H -dependent contribution, have been fitted with a straight line that corresponds to $C_{\text{DOS}}(H) = \beta H^{1/2}T$. In the figure, the lines all have the same slope, the average value of β , but lines with the individual values of β (see Fig. 2) would not be perceptibly different. The conformity of the fitted points to the lines and the negligibly small deviations of the $0.5-T$ points, which were not included in the fit, show the $H^{1/2}T$ dependence of C_{DOS} predicted for $H \neq 0$. With that interpretation, the intercepts of the lines at $H^{1/2}T = 0$ are $[C_{\text{lat}} + \gamma^*(0)T]/T^2$, and the deviations of the points on that axis from the intercepts are $C_{\text{DOS}}(0)/T^2$. Those deviations would be the same for all temperatures if $C_{\text{DOS}}(0)$ were proportional to T^2 . It is apparent in Fig. 1 that they are not the same, and this is demonstrated more clearly in Fig. 3, where they are plotted as $\alpha = C_{\text{DOS}}(0)/T^2$ vs T . A test of the scaling relation (9), $C_{\text{DOS}}(H)/H^{1/2}T = F(H^{1/2}T)$, is shown in Fig. 4. The data in Figs. 1-4 are for a sample for which $\gamma^*(0) = 0.44 \text{ mJ K}^{-2} \text{ mol}^{-1}$ and the concentration of PC's is $0.96 \times 10^{-4} \text{ mol (mol LSCO)}^{-1}$; for the second sample those quantities are, respectively, $1.23 \text{ mJ K}^{-2} \text{ mol}^{-1}$ and $1.67 \times 10^{-4} \text{ mol (mol LSCO)}^{-1}$. In all other respects, the results for the second sample are essentially identical to those for the first.

With respect to the $H^{1/2}T$ term, the results reported here are very similar to those for YBCO. However, the T -dependence of α is different. This difference may arise,

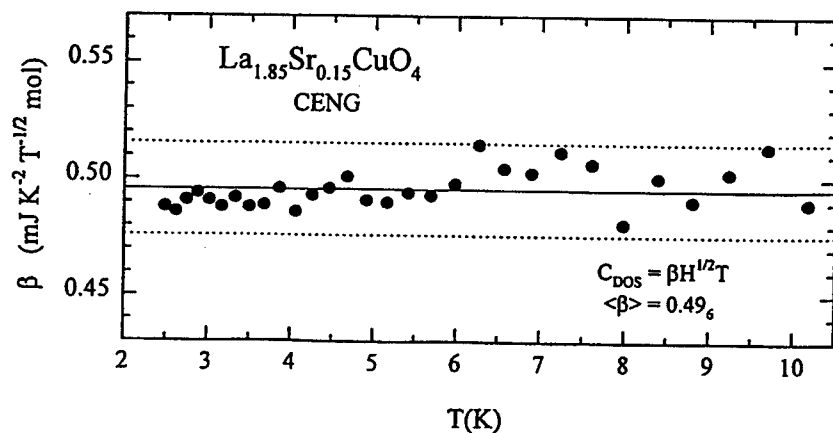


Fig. 2. Values of β determined for different temperatures.

in part, because the T^2 term is a low- T approximation and T_c is lower for LSCO than YBCO, and, in part, because the data at the lower limit of the temperature interval of the analysis are affected by uncertainty in C_{mag} .

Recent measurements on LSCO, $x = 0.16$, gave $\beta = 0.39 \text{ mJ K}^{-2} \text{T}^{-1/2} \text{mol}^{-1}$ and no detectable T^2 term (10). Other measurements (11) gave a substantially higher value of α than that reported here. They are also inconsistent with earlier data (3).

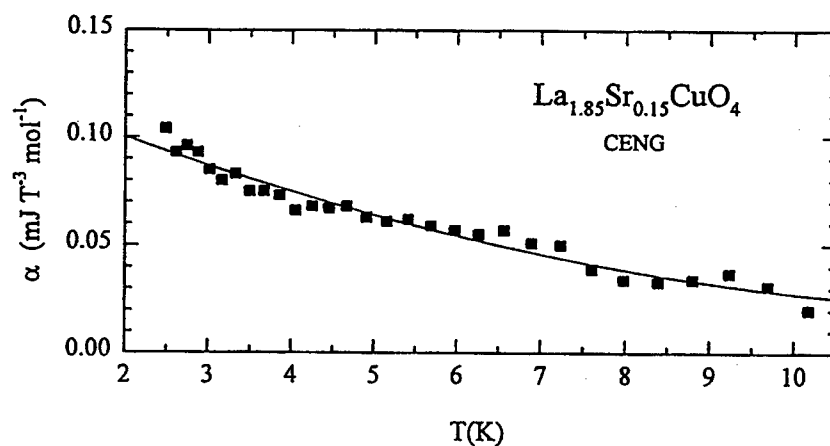


Fig. 3. Values of α determined for different temperatures.

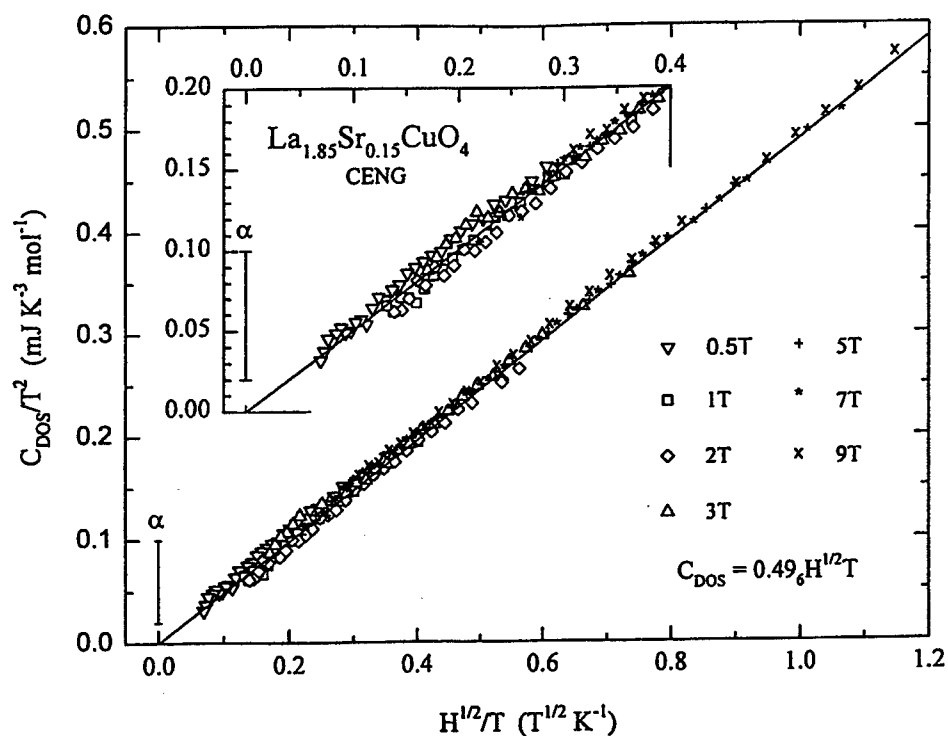


Fig. 4. Test of the scaling relation. The vertical bar represents the spread of values of α .

The work at Berkeley was supported by the Director, Office of Basic Energy Sciences, Materials Sciences Division of the U. S. Department of Energy under Contract No. DE-AC03-76SF00098.

REFERENCES

1. Moler, K. A. et al., Phys. Rev. Lett. 73, 2744 (1994).
2. Wright, D. A. et al., to be published.
3. Fisher, R. A. et al., Physica C 252, 237 (1995).
4. Volovik, G. E. JETP Lett. 58, 469 (1993).
5. Won, H. and Maki, K., Europhys. Lett. 30, 421 (1995).
6. Scalapino, D. J., private communication.
7. Kopnin, N. B. and Volovik, G. E., JETP Lett. 64, 690 (1996); Volovik, G. E., JETP Lett. 65, 491 (1997).
8. Revaz, B. et al., Phys. Rev. Lett. 80, 3364 (1998).
9. Simon, S. H. and Lee, P. A., Phys. Rev. Lett. 78, 1548 (1997).
10. Chen, S. J. et al., Phys. Rev B 58, 14753 (1998).
11. Momono, N. et al., Physica C 233, 395 (1994); Momono, N. and Ido, M., Physica C 264, 1 (1996).

Pressure Dependence of Flux Dynamics in High Temperature Superconductors¹

M. P. Raphael*, M. E. Reeves^{†,‡}, E. F. Skelton[‡], C. Kendziora[‡]

**Catholic University of America
Washington, DC 20032*

*†The George Washington University
Washington, DC 20052*

*‡Naval Research Laboratory
Washington, DC 20375*

Abstract.

One of the important problems of high-temperature superconductivity is to understand and ultimately to control fluxoid motion. We will describe a new technique for measuring the pressure dependence of T_c in a diamond anvil cell by the third harmonic of the ac susceptibility. It requires no background subtraction and allows the use of gasket materials made from hardened steels. More significantly, the third harmonic indicates the onset of irreversible (with respect to changes in applied magnetic field) flux motion. Thus we are able to simultaneously apply high (up to 10 GPa) pressures and high (up to 10 T) magnetic fields to study the effect of changes in interplanar coupling on the motion of flux. In other reported studies, the interplanar coupling has been adjusted by chemical doping which introduces defects (or pinning sites). By contrast, we can directly change the interplanar spacing without introducing defects. Thus, the effects of coupling can be separated from those of pinning. We will present results which show significant pressure induced shifts in the irreversibility line in $\text{YBa}_2\text{Cu}_3\text{O}_{7-\delta}$ and $\text{Bi}_2\text{Sr}_2\text{CaCu}_2\text{O}_8$.

INTRODUCTION

Since the discovery of high temperature superconductivity, the dynamics of flux motion has posed a major challenge to the application of these materials for use in high magnetic fields. [1] Early on, Nelson realized the important role played by reduced dimensionality in the crystal structure. [2] Further theoretical work by Fisher has revealed the possibility of a rich structure of phases in the H-T plane, encompassing the phenomena of flux lattice melting from a lattice or glass to a gas or liquid. [3] These developments have shifted the focus of research to

¹⁾ This work is sponsored by the Office of Naval Research and DARPA. We acknowledge helpful discussions with T. P. Devereaux, J. H. Claassen, M. S. Osofsky, and R. J. Soulen, Jr.

the physics of the properties of the fluxoids as a model system for a 2-d gas of bosons. [4-6] In this view, the weaker the coupling of fluxoids between planes, the more 2-d and Bose-gas-like will be the observed properties. Thus, of all the HTS materials studied, the most interesting is $\text{Bi}_2\text{Sr}_2\text{CaCu}_2\text{O}_{8+\delta}$ with its extraordinarily high anisotropy. [7] Recent experimental work on $\text{Bi}_2\text{Sr}_2\text{CaCu}_2\text{O}_8$ has revealed the distinction between surface and bulk effects, indicating the ranges of field and temperature over which 2-d rather than 3-d dynamics dominates. [8] This has been essential for illuminating the complex nature of the mixed-state phase diagram in this material. The importance of anisotropy underscores the need to quantify the effect of changes in the crystal structure (e.g. c -axis lattice spacing) with the observed properties of the flux motion. Several studies have shown shifts of the irreversibility and melting lines in $\text{Bi}_2\text{Sr}_2\text{CaCu}_2\text{O}_{8+\delta}$ by oxygen-reduction-induced changes in the c -axis lattice spacing. [9,10] In these and similar experiments, it has been shown that increasing the interplanar spacing strongly affects the flux motion by reducing the dimensionality of the system of fluxoids from 3-d to 2-d. However, in all experiments where atoms are added to or removed from the crystal structure, the defect density and hence the number of pinning sites must necessarily change. This effect cannot be discounted when analyzing the results of these experiments. Also, doping experiments change the anisotropy ratio by modifying properties of the superconducting condensate. A more direct means of determining the effect of lattice spacing on the anisotropy is desired, which, at the same time, maintains the underlying pinning structure in the superconductor. This would allow the separation of the effects of pinning on defect sites from those of anisotropy, and hence provide needed input to theoretical models for predicting the melting temperature of the flux matter. [11]

The experiment which we will describe addresses this question by the application of quasi-hydrostatic pressure to change the lattice spacing. We simultaneously monitor the flux motion by measurements of the third harmonic of the ac susceptibility. In the case of $\text{YBa}_2\text{Cu}_3\text{O}_{7-\delta}$ and even more so in $\text{Bi}_2\text{Sr}_2\text{CaCu}_2\text{O}_8$, the c -axis shows the largest compression. The results show that the irreversibility line in both materials shifts to higher temperatures as the lattice is compressed. In the case of $\text{Bi}_2\text{Sr}_2\text{CaCu}_2\text{O}_8$, this corresponds to an elevation in the temperature at which the interplanar coupling between the fluxoids ceases to be significant. Thus, the thermal energy required to effect flux motion is shown to depend very sensitively on the interplanar spacing.

EXPERIMENT

In our technique, quasi-hydrostatic pressure is applied to the sample using a diamond anvil cell. Primary and secondary coils, wound around the diamond facets, are used for the ac-susceptibility measurement with both the ac- and dc-magnetic fields applied parallel to the c -axis. Typical ac-field amplitudes of 0.5-1.0 mT are used at a frequency between 3 and 5 kHz. The pressure is applied and measured

at room temperature and a calibration is used to determine the pressure at low temperatures to within an uncertainty of ± 0.3 GPa. Details of this technique and of the diamond anvil cell are given in references [12] and [13]. The $\text{Bi}_2\text{Sr}_2\text{CaCu}_2\text{O}_8$ single crystal used in this study was grown by a self flux technique using a stoichiometric ratio ($[\text{Bi}]:[\text{Sr}]:[\text{Ca}]:[\text{Cu}]=2:2:1:2$) of cations. [14] The $\text{YBa}_2\text{Cu}_3\text{O}_{7-\delta}$ sample was grown using the a self-decanted flux method as described in reference [15]. The $\text{YBa}_2\text{Cu}_3\text{O}_{7-\delta}$ sample has a T_c of 92.0 K and the $\text{Bi}_2\text{Sr}_2\text{CaCu}_2\text{O}_8$ sample has a T_c of 86.3 K. Figure 1 shows a V_{3f} vs T scan for a $\text{YBa}_2\text{Cu}_3\text{O}_{7-\delta}$ sample of a typical size, $200 \times 200 \times 50 \mu\text{m}^3$. Despite the small sample size, the signal to noise ratio is excellent and there is no background subtraction necessary. [12] Upon cooling, irreversible flux motion gives rise to a nonlinear response in the superconductor at an onset temperature, T_1 (see Figure 1). The irreversibility line is defined to be the locus of points determined by H and T_1 . As the temperature is lowered further, the energies associated with pinning and the formation of a flux lattice begin to dominate the dynamics and the nonlinear response diminishes. In $\text{Bi}_2\text{Sr}_2\text{CaCu}_2\text{O}_8$, it has been shown that over a large portion of the phase diagram the vortex dynamics is dominated by surface barriers. The surface barrier energy increases abruptly as the sample is cooled and the 2-d vortices begin to couple between the planes. This gives rise to the sharp onset of the V_{3f} signal that we observe. In addition, surface barriers also give rise to a peak in the second harmonic of the ac susceptibility, which we observe for dc fields less the 500 mT. [8]

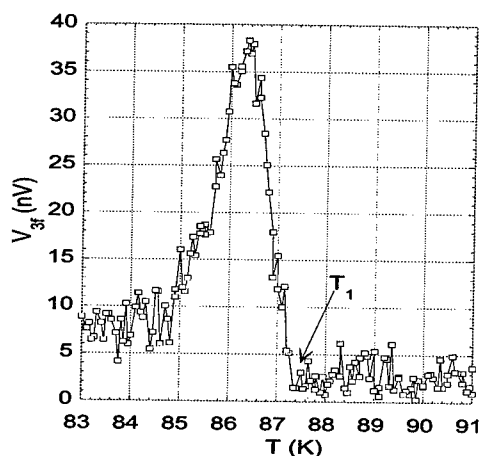


FIGURE 1. Third harmonic peak of a $\text{YBa}_2\text{Cu}_3\text{O}_{7-\delta}$ sample at 4 GPa and with an applied field of 2.5 Tesla.

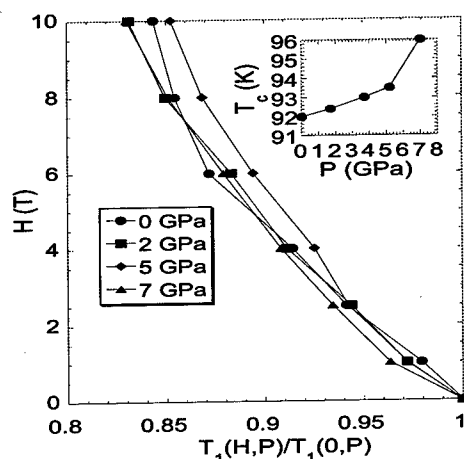


FIGURE 2. $\text{YBa}_2\text{Cu}_3\text{O}_{7-\delta}$ irreversibility lines at various pressures scaled by $T_c(P)$.

RESULTS AND DISCUSSION

Figure 2 shows the scaled irreversibility lines of the $\text{YBa}_2\text{Cu}_3\text{O}_{7-\delta}$ sample at various pressures. Each line is scaled by $T_c(P)$ (see inset) so that the relative changes are more easily identified. The largest change in the irreversibility line occurs at 5 GPa where it moves up significantly in field. At 7 GPa it moves back down, even below the 0 GPa data for most fields. Surface barriers in $\text{YBa}_2\text{Cu}_3\text{O}_{7-\delta}$ appear to be strongly influenced by twinning and oxygen content. [16,17] However, the observation of these effects is at fields well below 1 Tesla, so that pinning is expected to be the dominant cause of the nonlinear response for the field ranges shown in Figure 2.

The situation is quite different in $\text{Bi}_2\text{Sr}_2\text{CaCu}_2\text{O}_8$, for which Burlachkov *et al.* have considered the case in which the irreversibility line is governed by surface barriers. [18] For fields much greater than the penetration field, H_p , they derive an exponential form for the irreversibility field,

$$H_{irr} \approx \frac{H_{c2}}{\ln(\eta H_{c2}/H_{irr})} \exp(-2T/T_o) \quad (1)$$

$$T_o = \frac{\phi_o^2 d}{(4\pi\lambda)^2 \ln(t/t_o)} \quad (2)$$

where η is on the order of one, ϕ_o is the fluxon, λ is the penetration depth, d is the interlayer spacing, and t and t_o are time scales related to the rate of flux creep through the surface barrier. [19] In the high field regime ($H > 1T$)

we are able to determine T_o by fitting our data to equation (1) using reasonable values for H_{c2} ($50T < H_{c2} < 250T$) or equally well by the approximation $H_{irr} \approx H_{c2}(T_o/2T)\exp(-2T/T_o)$, valid for $T > T_o$. Fits using the latter equation are shown in Figure 3. For 0 GPa, 1.5 GPa, and 2.5 GPa we obtain for T_o values of 20.6 K, 23.5 K, and 22.9 K, respectively (± 2 K). The 0 GPa and the 1.5 GPa data merge while H_{irr} at 2.5 GPa is shifted to slightly higher fields.

At about 1 Tesla there is a crossover to a low field regime where the irreversibility line becomes strongly pressure dependent. While this crossover has been previously observed [20], these measurements are the first to show that the two regimes have very different dependencies on the interlayer coupling. We note that our low field data resemble the T_x line measured in reference [8] which separates more ordered vortex phases from that of the pancake gas. The correspondence between the two lines indicates that the increased coupling caused by pressure serves to aid in the transition to a 3-d phase. We note that our results at low fields are consistent with the observed shift in the irreversibility and melting lines caused by changes in oxygen content. [9,10,21] However, the changes in the c -axis parameter that we achieve with pressure are much greater than those caused by oxygen doping. In addition, oxygen doping significantly alters the superconducting condensate, changing T_c from 60K to 90K. On the other hand, by applying a pressure of 2.5 GPa to $\text{Bi}_2\text{Sr}_2\text{CaCu}_2\text{O}_8$, the c -axis parameter is changed by 0.05 nm (versus 0.01 nm in a typical doping experiment) with only a 4 K increase in T_c . [10,22,23]

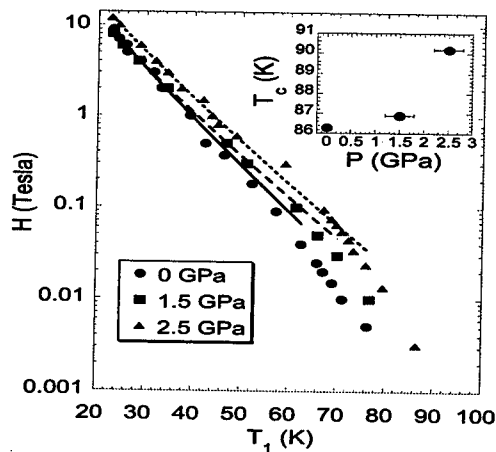


FIGURE 3. $\text{Bi}_2\text{Sr}_2\text{CaCu}_2\text{O}_8$ irreversibility lines at various pressures. The data are fit by an exponential function at high fields. The inset shows T_c as a function of pressure.

CONCLUSIONS

By measuring the third harmonic of the ac susceptibility, we have shown that pressure affects the irreversibility line significantly. The results for $\text{YBa}_2\text{Cu}_3\text{O}_{7-\delta}$ demonstrate that an increase in the interplanar coupling causes a shift in the depinning line to higher temperatures. In $\text{Bi}_2\text{Sr}_2\text{CaCu}_2\text{O}_8$, the results at high fields are consistent with surface barriers dominating the vortex dynamics. In this material too, the effect of decreasing the interplanar spacing is to shift the irreversibility line to higher temperatures.

REFERENCES

1. Y. Yeshurun and A.P. Malozemoff, *Phys. Rev. Lett.* **60**, 2202 (1988).
2. David R. Nelson, *Phys. Rev. Lett.* **60**, 1973 (1988).
3. M.P.A. Fisher, *Phys. Rev. Lett.* **62**, 1415 (1989).
4. D.R. Nelson and H.S. Seung, *Phys. Rev. B* **39**, 9153 (1989).
5. M.P.A. Fisher, *et al.*, *Phys. Rev. B* **40**, 546 (1989).
6. G. Blatter, *et al.*, *Rev. Mod. Phys.* **66**, 1125 (1994).
7. D.A. Farrell *et al.*, *Phys. Rev. Lett.* **63**, 782 (1989).
8. D.T. Fuchs, *Phys. Rev. Lett.* **80**, 4971 (1998).
9. B. Khaykovich, *Phys. Rev. Lett.* **76**, 2555 (1996).
10. K. Kishio, *et al.*, *Proceedings of the 7th International Workshop on Critical Currents in Superconductors* edited by H.W. Weber (World Scientific, Singapore, 1994), p.339.
11. Zhi-Xiong Cai, *et al.*, *Physica C* **299**, 91 (1998).
12. M.P. Raphael, M.E. Reeves, E.F. Skelton, *Rev. Sci. Inst.* **80**, 4971 (1998).
13. C.C. Kim, *et al.*, *Rev. Sci. Inst.* **65**, 992 (1994).
14. C. Kendziora, *et al.*, *Phys. Rev. B* **45**, 13025 (1992).
15. T. A. Vanderah, *et al.*, *Journal of Crystal Growth* **118**, 385 (1992).
16. R. Liang, *et al.*, *Phys. Rev. B* **50**, 4212 (1994).
17. M. Konczykowski, *et al.*, *Phys. Rev. B* **43**, 13707 (1991).
18. L. Burlachkov *et al.*, *et al.*, *Phys. Rev. B* **50**, 16770 (1994).
19. V. N. Kopylov, *et al.*, *Physica C* **170**, 291 (1990).
20. A. Schilling, *et al.*, *Phys. Rev. Lett.* **71**, 1899 (1993).
21. C. Bernhard, *et al.*, *Phys. Rev. B* **52**, R7050 (1995).
22. J. S. Olsen, *et al.*, *Physica Scripta* **44**, 211 (1991).
23. C. Kendziora, *et al.*, *Physica C* **257**, 74 (1996).

Phaseseparation in overdoped $\text{Y}_{1-0.8}\text{Ca}_{0-0.2}\text{Ba}_2\text{Cu}_3\text{O}_{6.96-6.98}$

J. Röhler^{*1}, C. Friedrich^{*}, T. Granzow^{*}, E. Kaldis[†], and G. Böttger[†]

^{*}Universität zu Köln, D-50937 Köln, Germany

[†]ETH Zürich, CH-8093 Zürich, Switzerland

Abstract. The dimpling in the CuO_2 planes of overdoped $\text{Y}_{1-y}\text{Ca}_y\text{Ba}_2\text{Cu}_3\text{O}_{6.96-6.98}$, ($y = 0.02-0.2$) has been measured by x-ray absorption-fine-structure spectroscopy (Y-K EXAFS). A step-like decrease around 12% Ca indicates a percolation threshold for distorted sites of 5 cells, and thus phase segregation. We conclude the charge carriers added by substitution of Y^{3+} by Ca^{2+} to be trapped at the Ca sites and their *nn* environment.

INTRODUCTION

The unusual metallic properties of the high T_c cuprate superconductors are difficult to reconcile with a homogenous electronic state. Since inhomogeneities in the electronic structure may lift the translational invariance of the underlying lattice, it is suggesting to measure both, the atomic structure using short-range (or local) structural probes, and the average crystallographic structure using diffraction techniques [1]. Anomalous atomic displacements may be then extracted from careful comparisons between the local and the crystallographic structure.

The anomalous electronic structure of the cuprate superconductors is frequently discussed in terms of dynamic inhomogeneities, for instance a mixture of microscopically segregated phases. The notorious nonstoichiometry of all known superconducting cuprates, even their optimum doped phases, causes many static inhomogeneities thus adding a constraint to the analysis of anomalous atomic displacements.

Advantageously the metallic CuO_2 -planes of the cuprate superconductors are the structurally most perfect blocks. Thus significant structural anomalies in the planes can be safely related to nontrivial electronic inhomogeneities. We have recently shown that upon oxygen doping of $\text{YBa}_2\text{Cu}_3\text{O}_x$ the locally measured spacing between the $\text{Cu}2$ and $\text{O}2,3$ layers ("dimpling") in the CuO_2 -planes keeps track of the planar hole concentration [1]. The data from Y K-edge EXAFS comprise the

¹⁾ Corresponding author: abb12@rs1.rz.uni-koeln.de

atomic structure of the 8 next neighbored CuO_2 -plaquettes, and thus the effective charge in only 32 Cu2-O23 bonds. Oxygen doping for $x \rightarrow x_{opt}=6.92$ has been found to increase the dimpling, in other words: the increasing number of oxygen holes bends the Cu2-O23 bonds out-of-plane towards the Ba-layer. At the onset of the overdoped regime, $x \simeq 6.95$, the dimpling and thus also the number of holes exhibits a sharp maximum [3]. A concomitant displacive transformation of the crystallographic structure however seems to block a further increase of the dimpling. Although further doping from $x \simeq 6.95 \rightarrow 7$ increases the nominal hole concentration, the dimpling starts to decrease.

In this contribution we report on Y *K*-EXAFS measurements of the dimpling in a series of overdoped compounds, $\text{YBa}_2\text{Cu}_3\text{O}_{6.96-6.98}$, additionally overdoped by substitution of Y^{3+} with 2-20% Ca^{2+} .

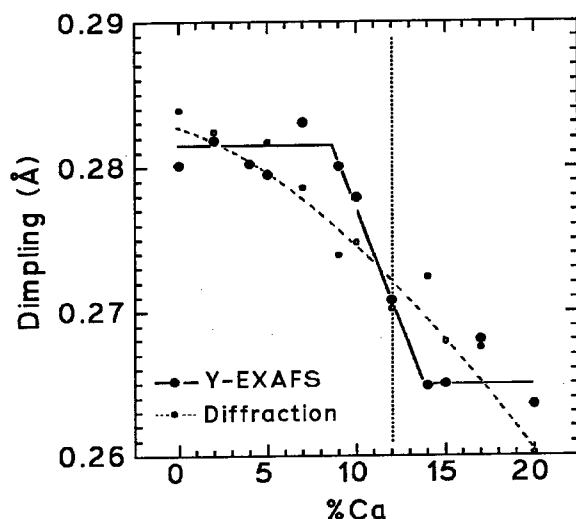


FIGURE 1. Dimpling of the CuO_2 -planes in $\text{Y}_{1-y}\text{Ca}_y\text{Ba}_2\text{Cu}_3\text{O}_{6.96-6.98}$ as a function of Ca concentration. Large full circles (thick drawn out line): data from Y-EXAFS at 25 K. Thin open circles (thin dashed line): data from neutron diffraction at 5 K [2]. For convenience the latter are offset by +0.01 Å.

EXPERIMENTAL DETAILS

The polycrystalline samples were from the same batches studied previously by diffraction with x-rays and neutrons, and by magnetometry [2]. Up to 20% Ca could be homogeneously solved in $\text{YBa}_2\text{Cu}_3\text{O}_x$ while the oxygen content was kept at the highest numbers possible: $x = 6.96 - 6.98$, i.e. surprisingly always < 7.00 . Ca EXAFS of the same samples confirmed that calcium has replaced yttrium ($> 97\%$),

and not barium. The EXAFS spectra ($T = 20 - 60K$) were recorded at the European Synchrotron Radiation Facility (ESRF) using the double crystal spectrometer at BM29. Details of the spectroscopic technique and of the data analysis are given in [1].

RESULTS

Fig.1 exhibits the dimpling of the CuO_2 -planes in $\text{Y}_{1-y}\text{Ca}_y\text{Ba}_2\text{Cu}_3\text{O}_{6.96-6.98}$ ($T = 25\text{ K}$) for $y = 0.02 - 0.2$ as extracted from the Y EXAFS (large full circles, drawn out line). Comparison is made with the results from neutron diffraction (small circles, dashed line) by Böttger *et al.* [2]. From the Y EXAFS the dimpling is found independent on the Ca concentration up to 9% ($0.281(2)\text{ \AA}$), then undergoes a step-like decrease by about 0.015 \AA , and flattens around $0.265(4)\text{ \AA}$ for 14-20 % Ca. The position of the step may be located around 12% Ca (dotted vertical line). The discontinuous behaviour of the dimpling from the Y EXAFS is at variance with the continuous behaviour obtained from the refinement of the average crystallographic structure [2]. For better comparison the diffraction data are offset by $+0.01\text{ \AA}$ showing that both methods yield the same overall variations, and that the discontinuity from the EXAFS work is clearly outside the scatter of the data points from the diffraction work.

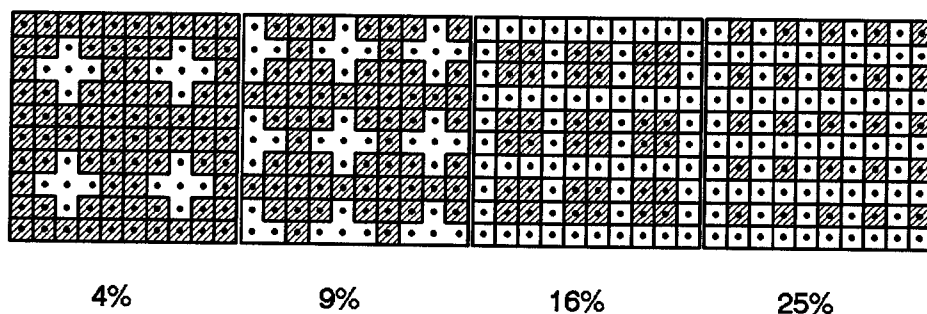


FIGURE 2. Square lattices of Cu_2 with Y/Ca (dots) in their centers. Increasing concentrations (from left to right) of ordered Ca substitute Y. The divalent Ca impurities are assumed to be screened only by the $nn\text{ Y}^{3+}$. The thus locally distorted areas appear as white crosses starting to percolate somewhere between 9% and 16%Ca. The remaining undistorted Y-cells are hatched.

DISCUSSION

The step-like variation of the dimpling with increasing Ca concentration points to a percolative transition induced by Ca doping. Fig. 2 exhibits a plausible scheme demonstrating the occurrence of percolative paths for concentrations around 16% Ca. Here it is assumed that the holes doped by Ca^{2+} are predominantly screened by

the nn Y cells thus creating a cross-like cluster of 5 distorted cells. It is suggesting that these holes are trapped and do not contribute to the density of the mobile carriers.

Considering the Ca impurities as percolating sites in a random process, the exact theory for a square 2-D lattice [4] predicts the critical percolation to occur for 59.2746%. Then straightforwardly the critical percolation for the cross-like clusters, each centered at a Ca impurity, is expected for $59.2746\%/5 \simeq 12\%$ Ca. We conclude that the observed step-like decrease of the dimpling around 12% Ca is connected to this percolation threshold.

The other way around: the observation of a percolation threshold at 12% Ca indicates the percolating sites to be 5 cells large. The solid solution thus segregates into two phases: *i.* the matrix of undistorted Y cells, and *ii.* distorted clusters at the Ca sites.

CONCLUDING REMARKS

We conclude that doping of $\text{YBa}_2\text{Cu}_3\text{O}_x$ with heterovalent cations substituting Y is electronically nonequivalent with oxygen doping in the chain layer. Thus generalized phase diagrams treating Ca^{+2} and O^{-2} dopants in $\text{Y}_{1-y}\text{Ca}_y\text{Ba}_2\text{Cu}_3\text{O}_x$ on an equal footing are questionable. In particular the superconducting transition temperature of dually doped $\text{Y}_{1-y}\text{Ca}_y\text{Ba}_2\text{Cu}_3\text{O}_x$ is not expected to match a parabolic behaviour T_c vs. hole concentration.

ACKNOWLEDGMENTS

Beamtime at the ESRF was under the proposals HS376 and HS 533. We thank S. Thienhaus for help during the data acquisition.

REFERENCES

1. Röhler, J., Loeffen, P. W., Müllender, S., Conder, K., and Kaldis, E., in *Workshop on High- T_c Superconductivity 1996: Ten Years after the Discovery*, Kaldis, E., Liarokapis, E., and Müller, K. A., eds., NATO ASI Series E343, Dordrecht, Kluwer, 1997, pp. 469–502.
2. Böttger, G., Mangelshots, I., Kaldis, E., Fischer, P., Krüger, Ch., and Fauth, F., *J. Phys: Cond. Matter* **8**, 8889 (1996).
3. Kaldis, E., Röhler, J., Liarokapis, E., Poulakis, N., Conder, K., and Loeffen, P. W., *Phys. Rev. Lett.* **79**, 4894–4897 (1997).
4. Stauffer, D., and Aharony A., *Perkolationstheorie: eine Einführung*, Weinheim, VCH, 1995, ch. 2, p. 18.

Vortex Motion in YBCO Thin Films

V. Shapiro, A. Verdyan, I. Lapsker, J. Azoulay

*Center for Technological Education,
Holon Institute of Technology Arts and Science,
P.O. Box 305, Holon 58102, Israel*

Abstract. Hall resistivity measurements as function of temperature in the vicinity of T_c were carried out on a thin films YBCO superconductors. A sign reversal of Hall voltage with external magnetic field applied along c axis have been observed upon crossing T_c . Hall voltage in the mixed state was found to be insensitive to the external magnetic field inversion. These effects are discussed and explained in terms of vortex motion under the influence of Magnus force balanced by large damping force. It is argued that in this model the flux-line velocity has component opposite to the superfluid current direction thus yielding a negative Hall voltage.

INTRODUCTION

The motion of vortices in high-temperature copper-oxide superconductors is responsible for a large variety of electrical and physical properties [1]. However the driving transverse force on the moving vortex and its direction of motion are intriguing issues [1]. Hall effect is one of the key tools through which it is used to understand and analyze the mixed state in high- T_c superconductors.

Hall voltage may be caused by charge carriers deflection due to Lorentz force thus being antisymmetric in the applied magnetic field, or by vortex motion, particularly in the mixed state of type II superconductors. In the second case any component of the vortex velocity \mathbf{V}_L along the transport current will produce a transverse electric field \mathbf{E} according to Josephson relation $\mathbf{E} = \mathbf{B} \times \mathbf{V}_L$, thus being symmetric [2] in the applied magnetic field \mathbf{B} . Early experiments [3] on high- T_c superconductors have shown an unexpected sign reversal of the Hall resistivity near T_c . The same anomalous behavior observed in low T_c elemental superconductors [4] whose electronic system are very different, strongly indicates that this phenomenon is a general feature of the vortex state. Therefore it has attracted much theoretical attention [5].

EXPERIMENTAL

All the films in this work were synthesized in a vacuum system by evaporation of pulverized stoichiometric mixture of Y, BaF₂ and Cu powder from a resistively heated tungsten boat onto a c oriented well polished MgO substrate. The deposited thin film

with typical thickness of $5 \cdot 10^{-5}$ cm was subsequently annealed in situ in oxygen atmosphere[6]. The films thus obtained were characterized by X-ray diffraction for c -axis orientation and those highly oriented with c -axis perpendicular to the surface were selected for measurements.

The longitudinal resistivity ρ_{xx} versus temperature shown for different values of magnetic fields B in fig. 1 displays the expected transition broadening (about 30 K) as compared to the one with zero magnetic field. Fig. 2 depicts a typical field cooled (f.c.) lateral experimental measured voltage U_{xy} vs. temperature in which the well known sign reversal anomaly near T_c is observed for both direct and reverse magnetic field direction. Note that there is almost no change when the magnetic field is reversed. Measurements were carried out for 0.5T 0.75T and 1T (see fig.2).

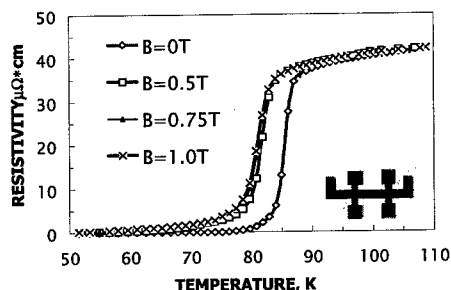


FIGURE 1. The longitudinal resistivity ρ_{xx} vs. temperature for different values of magnetic fields all of which are along C direction. Inset: multicontact configuration sample.

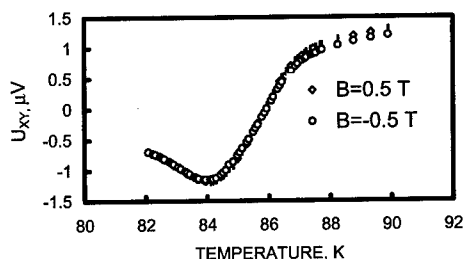


FIGURE 2. A typical lateral voltage vs. temperature for 0.5T and -0.5T.

Clearly the longitudinal voltage U_{xx} is insensitive to the inversion of the magnetic field direction, whereas the lateral voltage U_{xy} above T_c is expected to behave as a normal Hall voltage. However our lateral voltage U_{xy} measurements above T_c have shown clear insensitivity to the inversion of the magnetic field direction namely $U_{xy}(B)$ is very closed to $U_{xy}(-B)$ for $T > T_c$ (fig. 2) and also $U_{xy}(T) \ll U_{xx}(T)$ for $T > T_c$, it is therefore suggested that the experimental measured values $U_{xy}(T)$ above T_c are mainly the residual U_{xx} values caused by misalignment in the Hall contacts equipotentiality. We have therefore used the correction equation $U_H(T) = U_{xy}(T) - k \cdot U_{xx}(T)$ to eliminate this spurious signal where k assumed to be a temperature independent constant was found from the condition $U_H = 0$ at $T = T_c$.

RESULTS AND DISCUSSION

The Hall coefficient as a function of temperature was conventionally obtained by subtracting the Hall voltage values U_H for both magnetic field direction. The results summarized in fig. 3 showing the well known sign reversal are similar to those obtained by Hagen et al. [7]. Conventionally the symmetrical part is obtained by

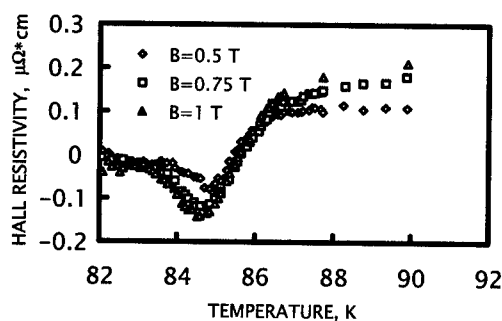


FIGURE 3. Hall coefficient as a function of temperature obtained by subtracting the Hall voltage values U_H for both magnetic field directions. This is an asymmetrical part in the magnetic field.

$[U_H(B) + U_H(-B)]/2$, however since $U_{xy}(B) = U_{xy}(-B)$ in the mixed state, the correction equation yields it directly. The results are shown in fig. 4. The motion of the flux

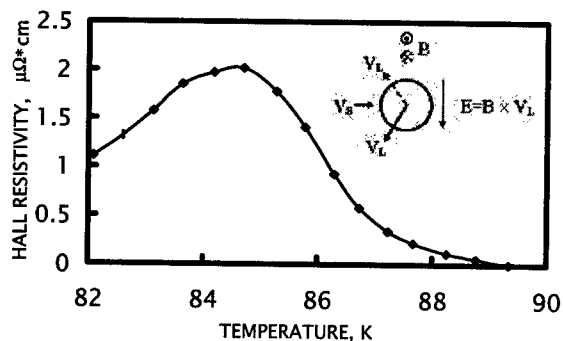


FIGURE 4. The symmetrical part of the resistivity ρ_{xy} vs. temperature. Inset: a schematic draw showing the symmetrical behavior of the electric produced by a vortex motion under Magnus force and a large drag force. Dotted lines depicts the reversal case.

vortices at a velocity V_L in superconductor through which flows a transport current density J and which is under a magnetic field B induces an electric field E according to Josephson relations $E = B \times V_L$ in which B and J are along z and x axes respectively.

Thus any V_L component perpendicular to the superfluid velocity V_s will induce a longitudinal voltage. Similarly a V_L component parallel or antiparallel to V_s will produce a transverse electric field positive or negative respectively (see insert in fig. 4). It is therefore argued that the flux motion in the mixed state has a nonzero component of its velocity in the antiparallel direction of V_s . In order to explain the normal Hall anomaly, Hagen et al. [8] have modified the Nozieres-Vinnen model by introducing a drag force to balance the Magnus force through which they were able to show that the equation of motion thus obtained for V_L is given by $V_L = C_1 V_s \times Z + C_2 V_s$, where C_1 and C_2 are friction factors. For large damping one gets $C_2 < 0$ and V_L will have an antiparallel component to V_s and therefore the Hall voltage will have its sign opposite to the one in the normal state. However it is quite clear that as long as V_L has antiparallel component to V_s no sign change in Hall voltage will be sensed when the magnetic field is inverted. In the Andreev reflection mechanism electrons are reflected at the grain boundaries interface between the normal core of the vortex and the superconducting environment of the vortex and a momentum of the order of twice the electron momentum is transferred to the lattice and the vortex acquire a momentum in the opposite direction of superfluid velocity V_s .

SUMMARY

The anomalous Hall effect and its insensitivity to the external magnetic field inversion for small fields were discussed in terms of directed motion vortices along certain channels. It was shown that in this model the flux-line will always have an antiparallel velocity component to the superfluid velocity thus yielding a negative Hall voltage and insensitivity to the magnetic field inversion.

ACKNOWLEDGMENTS

This work was supported by the Israeli ministry of Science.

REFERENCE

1. E.H.Brandt, Rep. Prog. Phys. 58,1465 (1995)
2. Ya.V.Kopelevich,V.V.Lemanov, E.B.Sonin and A.L. Kholkin, JETP Lett.,50,212 (1989)
3. M.Galfy and E.Zirngiebl, Solid State Commun.,68, 929 (1988)
4. N.Usui, T.Ogasawara, K.Yasukochi and S.Tamegai, J Phys. Soc. Jpn. 27, 574 (1969)
5. D.I Khomskii and A.Freimuth, Phys.Rev.Lett. 75, 1384 (1995)
6. Jacob Azoulay, J.Am.Ceram.Soc. 79,568 (1996)
7. S.J.Hagen, A.W.Smith, M.Rajeswari, J.L.Peng, Z.Y.Li, R.L.Greene, S.N.Mao, X.X.Xi, S.Bhattacharya, QiLi and C.J.Lobb Phys.Rev.B 47, 2, 1064 (1993)
8. S.J.Hagen, G.J.Lobb, R.L.Green, M.G.Forster and G.H.Kang, Phys.Rev. B41,11630 (1990)

Electronic Raman scattering in high- T_c superconductors

T. Strohm, M. Cardona, and A.A. Martin

Max-Planck-Institut für Festkörperforschung, Heisenbergstr. 1, D-70569 Stuttgart, Germany, E.U.

Abstract. We discuss some results of electronic Raman scattering in superconducting cuprates concerning the position of the superconductivity-induced pair-breaking peaks. In addition, the low-frequency behavior predicted by theory is compared to experimental results.

Theory of electronic Raman scattering. *Raman scattering* can be described by a process of second order in the vector potential of the radiation. The transitions leading to Raman scattering involve the destruction of an *incoming photon* of wavevector \mathbf{k}_L and polarization \mathbf{e}_L , followed by the creation of a *scattered photon* ($\mathbf{k}_S, \mathbf{e}_S$). The *relevant states* for the description of the electronic scattering process are composed of the state of the photon field and the state of the electron system in the crystal, $|i\rangle = |i_{ph}\rangle|i_{el}\rangle$ and $|f\rangle = |f_{ph}\rangle|f_{el}\rangle$ are the initial and final state describing the transition. The states of the (non-equilibrium) photon field are $|i_{ph}\rangle = |n_L, 0_S\rangle$ and $|f_{ph}\rangle = |n_L - 1, 1_S\rangle$. The electron system for $T = 0$ is in its ground state $|i_{el}\rangle = |GS\rangle$ while its final state $|f_{el}\rangle$ is arbitrary. The *translational symmetry* of the crystal allows the labeling of the single-particle wave functions as irreducible representations of the translation group, i.e. Bloch waves $\psi_{\mathbf{n}\mathbf{k}}(\mathbf{r}) = e^{i\mathbf{k}\mathbf{r}}u_{\mathbf{n}\mathbf{k}}(\mathbf{r})$, where $u_{\mathbf{n}\mathbf{k}}(\mathbf{r})$ is a lattice-periodic function for the wavevector \mathbf{k} .

The *Hamiltonian* that describes the coupling of the electrons to the photon field, $H = (\mathbf{p} - (e/c)\mathbf{A}(\mathbf{r}))^2/2m_0$, can be written as

$$H = H_0 + H_{Ap} + H_{A^2}, \quad H_{Ap} = -\frac{e}{m_0c}\mathbf{A}\mathbf{p}, \quad H_{A^2} = \frac{e^2}{2m_0c^2}\mathbf{A}^2. \quad (1)$$

The vector potential is $\mathbf{A}(\mathbf{r}) = \mathbf{A}_L(\mathbf{r}) + \mathbf{A}_S(\mathbf{r})$; for Stokes scattering we have

$$\mathbf{A}_L(\mathbf{r}) = A_L^- \mathbf{e}_L e^{+i\mathbf{k}_L \mathbf{r}}, \quad \mathbf{A}_S(\mathbf{r}) = A_S^+ \mathbf{e}_S e^{-i\mathbf{k}_S \mathbf{r}}, \quad (2)$$

and A_L^- and A_S^+ are proportional to the annihilation operator for the incoming and the creation operator of the scattered photon, respectively. The terms H_{A^2}

and H_{Ap} are of different order in \mathbf{A} and, in principle, must be treated separately: H_{A^2} in first order and H_{Ap} in second order perturbation theory. We shall introduce an *effective Hamiltonian* which includes both terms and has to be treated in first order perturbation theory only.

The transition amplitude given by the operator H_{A^2} is $r_0 \langle A_S^+ A_L^- \rangle \mathbf{e}_S^* \cdot \mathbf{e}_L \langle n_f \mathbf{k}_f | e^{i\mathbf{q}\mathbf{r}} | n_i \mathbf{k}_i \rangle$ where $\mathbf{q} \equiv \mathbf{k}_L - \mathbf{k}_S$ is the wavevector transferred to the electron system and r_0 is Thomson's electron radius. Since $v_F \ll c$, the optical transitions are nearly vertical, and the expectation value leads to the selection rule that only *intraband* transitions are induced by H_{A^2} .

The operator H_{Ap} produces Raman transitions in second order perturbation theory via *virtual transitions* to an intermediate state $|m\rangle$, and introduces *resonance effects*. Assuming $|m_{ph}\rangle = |n_L - 1, 0_S\rangle$ (at $T = 0$ the other option, $|m_{ph}\rangle = |n_L, 1_S\rangle$, is far off-resonance), the transition amplitude is given by the expression (we take $m_0 = 1, \hbar = 1$)

$$r_0 \langle A_S^+ A_L^- \rangle \frac{\langle n_f \mathbf{k} + \mathbf{q} | \mathbf{e}_S^* \cdot \mathbf{p} | n_m \mathbf{k} + \mathbf{k}_L \rangle \langle n_m \mathbf{k} + \mathbf{k}_L | \mathbf{e}_L \cdot \mathbf{p} | n_i \mathbf{k} \rangle}{\epsilon_{n_i \mathbf{k}} - \epsilon_{n_m \mathbf{k} + \mathbf{k}_L} + \omega_L + i0}. \quad (3)$$

The states $|n\mathbf{k}\rangle$ are Bloch states. Considering that $\mathbf{k}_i \approx \mathbf{k}_m \approx \mathbf{k}_f$ we conclude that even-parity virtual transition $|i\rangle \rightarrow |m\rangle$ are forbidden. This is especially true for the virtual intraband transition. The transition $|i\rangle \rightarrow |f\rangle$, though, may be an intraband transition involving two virtual interband transitions. The two contributions from first and second order perturbation theory can be lumped together into an *effective Raman Hamiltonian* that has the form

$$H_R = r_0 \langle 2A_S^+ A_L^- \rangle \mathbf{e}_S^* \cdot \hat{\gamma}_{\mathbf{k}} \cdot \mathbf{e}_L \quad (4)$$

and yields the total transition amplitude for Raman scattering by first order perturbation theory. The second rank tensor $\hat{\gamma}_{\mathbf{k}}$ is the dimensionless *Raman vertex*.

At this point we introduce the *effective mass approximation* [1]. The essential step in this approximation is to neglect the laser frequency ω_L in the denominator of (3). Using $\mathbf{k} \cdot \mathbf{p}$ -theory we express the Raman vertex in terms of the inverse effective mass:

$$\mathbf{e}_S^* \cdot \hat{\gamma}_{\mathbf{k}} \cdot \mathbf{e}_L = \sum_{i,j} \mathbf{e}_{S,i}^* \frac{\partial^2 \epsilon_{\mathbf{k}}}{\partial k_i \partial k_j} \mathbf{e}_{L,j}. \quad (5)$$

The accuracy of the off-resonance assumption implicit in the effective mass approximation is hard to verify. Calculations of scattering efficiencies without this approximation suggest that it is semiquantitatively correct for high- T_c superconductors when using ordinary laser frequencies [2]. The experiments described below also suggest that resonances, if any, are weak.

Using Fermi's Golden Rule, the transition rate for $|GS\rangle \rightarrow |f_{el}\rangle$ is found to be $\Gamma_{f_{el}} = 2\pi |\langle GS | H_R | f_{el} \rangle|^2 \delta(\delta E_{f_{el}} - \omega) \sim 2\pi |\langle GS | \gamma_{\mathbf{k}} | f_{el} \rangle|^2 \delta(\delta E_{f_{el}} - \omega)$, where $\gamma_{\mathbf{k}} = \mathbf{e}_S^* \cdot \hat{\gamma}_{\mathbf{k}} \cdot \mathbf{e}_L$ and $\delta E_{f_{el}}$ is the energy of the excitation $|f_{el}\rangle$, and $\omega = \omega_L - \omega_S$. For the

determination of the *Raman efficiency*, we sum over all final states with $\mathbf{k}_S \in d\Omega$ and $\omega_S \in d\omega$, normalize to the incoming laser power, and obtain

$$\frac{d^2 S}{d\Omega d\omega} = r_0^2 \frac{\omega_S}{\omega_L} \langle |\gamma_{\mathbf{k}}|^2 \delta(\epsilon_{\mathbf{k}} - \omega) \rangle \quad (6)$$

where $\langle \cdot \rangle$ represents a Brillouin zone (BZ) average per unit crystal volume and $\epsilon_{\mathbf{k}}$ is the energy of an electronic excitation with wavevector \mathbf{k} . This result is valid for a clean metal and does not take into account Coulomb screening. When considering the effect of impurities or the superconducting state, the equation above has to be generalized. The BZ average then becomes the imaginary part of the so-called *Raman susceptibility*, a quantity represented in diagrammatic perturbation theory by a polarization loop with the Raman vertex playing the role of the vertex in the diagram [3,1]. The BZ-average in (6) can often be replaced by a simpler Fermi surface (FS) average because the δ -function is only nonzero near the FS [1].

The extension to the non-clean or the superconducting case can be formally easily performed using diagrammatic perturbation theory. As a result, the BZ average in (6) must be replaced by $\langle |\gamma_{\mathbf{k}}|^2 \Lambda_{\mathbf{k}}(\omega) \rangle$, where the kernel $\Lambda_{\mathbf{k}}(\omega)$ is the imaginary part of the Tsuneto-function $\lambda_{\mathbf{k}}(\omega)$ [3,1] in the superconducting state, and may be modeled by the function $-\delta(\epsilon_{\mathbf{k}})(\omega, /(\omega^2 + \gamma^2))$ in the non-clean metal [4].

Thus far the effect of *Coulomb screening* has not been considered. Using the RPA and the limit $\mathbf{q} \rightarrow 0$, it can be seen [5] that the inclusion of screening involves the replacement of the BZ average in (6) by the expression

$$\langle |\gamma_{\mathbf{k}}|^2 \Lambda_{\mathbf{k}}(\omega) \rangle - \frac{|\langle \gamma_{\mathbf{k}} \Lambda_{\mathbf{k}}(\omega) \rangle|^2}{\langle \Lambda_{\mathbf{k}}(\omega) \rangle} \quad (7)$$

The screening has two important consequences. The kernel $\Lambda_{\mathbf{k}}(\omega)$ has the full symmetry of the crystal point group. Therefore the screening term vanishes identically for non-fully symmetric components of the Raman vertex, such as B_{1g} and B_{2g} in a crystal of D_{4h} symmetry. For the A_{1g} component, it does not. In this case, a \mathbf{k} -independent component of the A_{1g} vertex is screened completely.

The numerical calculation. For the superconducting state, calculations of the Raman efficiency have been performed for the compounds $\text{YBa}_2\text{Cu}_3\text{O}_7$ (Y-123) and $\text{YBa}_2\text{Cu}_4\text{O}_8$ (Y-124) [1]. They use a full BZ integration with the effective mass Raman vertex obtained from the LDA-LMTO band structure [6]. The gap function was assumed to have $d_{x^2-y^2}$ symmetry, the same for all electronic bands. A Fermi surface (FS) integration was shown to yield results similar to those of the BZ integration.

In the discussion of the results for the Y-123 system, we use the irreducible representations of the tetragonal D_{4h} point group (Fig. 1). Then, B_{1g} corresponds to the (xy) scattering configuration. The definition of the B_{1g} and A_{1g} components of the Raman efficiency is more delicate in the presence of a chain-related orthorhombic distortion: both components transform in the same way under the operations of the D_{2h} point group. We will use the approximate relations $I_{B_{1g}} = I_{(x'y')}$ and

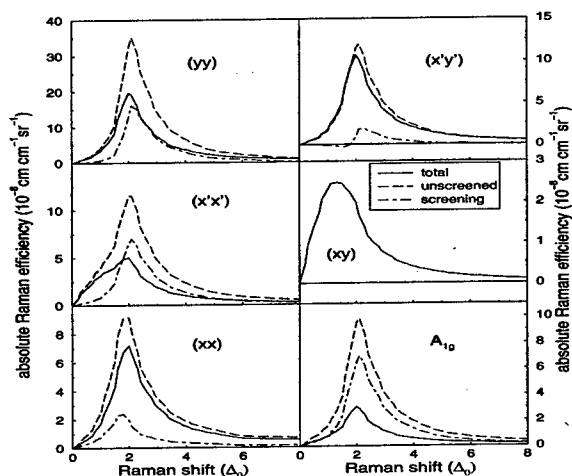


FIGURE 1. Scattering efficiencies calculated for Y-123 using BZ integration and an LMTO-LDA band structure. Each of the six panels contains the total absolute efficiency for electronic scattering and its two constituents, the unscreened and the screening part that follow from Eq. (7).

$I_{A_{1g}} = I_{(x'x')} - I_{(xy)} = (I_{(xx)} + I_{(yy)})/2 - I_{(x'y')}$. The A_{2g} component vanishes for the non-resonant case because, in the effective mass approximation, the Raman tensor is symmetric.

Figure 1 shows that the A_{1g} component is screened by a factor of 0.3. This reduction may be larger if only one CuO_2 plane is present [4,7]. The screening preserves the shape of the spectrum. In particular, the position of the A_{1g} peak remains nearly the same. The B_{1g} component (D_{4h} notation), which is not orthogonal to the fully symmetric representation in this orthorhombic case, is also screened, but only weakly. Since the B_{2g} (D_{4h}) component does not contain fully symmetric parts, it is not screened even in the orthorhombic case.

The calculated peak positions are nearly the same ($\approx 2\Delta_0$) for the A_{1g} and B_{1g} Raman components, the one for the B_{2g} component is $\approx 35\%$ lower ($\approx 1.3\Delta_0$). The fact that the B_{1g} component peaks at $2\Delta_0$ is expected, because the B_{1g} component of the Raman vertex is large in ,X directions where the gap is $2\Delta_0$. For the unscreened A_{1g} component this argument also holds, especially for two or more CuO_2 planes per primitive cell. However, the result that the screening does not alter the peak position is nontrivial. The lower peak position of B_{2g} is due to the vanishing of the B_{2g} Raman vertex along the ,X and ,Y directions.

The A_{1g} problem. The experimental results [4] are shown in Fig. 2 in terms of the *absolute* Raman efficiencies. Care has been taken to use the correct prefactor in (6), so as to be able to compare the absolute values of the peak intensities for the different components of the Raman efficiency. They are given for $A_{1g} : B_{1g} : B_{2g}$ by

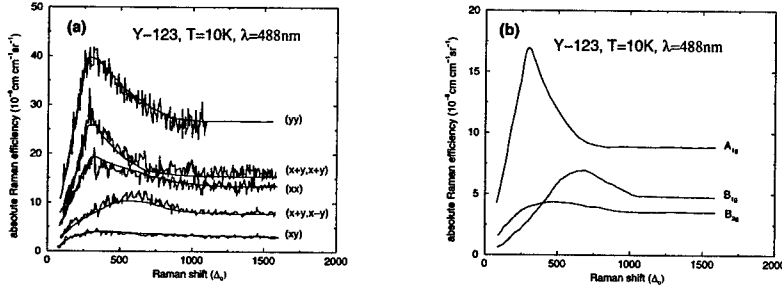


FIGURE 2. (a) Experimental Raman scattering efficiencies for Y-123. The vertical scales represent absolute Raman efficiencies, measured at $T = 10$ K and with an exciting laser wavelength of $\lambda = 488$ nm. (b) The A_{1g} component is plotted together with the quasitetragonal B_{1g} and B_{2g} components corresponding to D_{4h} symmetry, obtained from linear combinations of the D_{2h} components in (a) [4].

3 : 11 : 3 in the calculation, and by 18 : 12 : 4 (the units are $10^{-8} \text{ cm cm}^{-1} \text{ sr}^{-1}$) in the experiment. With the exception of the A_{1g} component, the matching is striking.

Concerning the measured peak positions, Y-123 gives $700 \text{ cm}^{-1} : 400 \text{ cm}^{-1}$ for the $\omega_{\text{peak}}(B_{1g}) : \omega_{\text{peak}}(B_{2g})$ ratio, which agrees with the calculated ratio $2\Delta_0 : 1.3\Delta_0$. But the A_{1g} components differ with respect to both, the peak height and the peak position. Another difference between calculated and measured spectra is the behavior for Raman shifts much larger than $2\Delta_0$. The calculated spectra vanish due to the fact that the density of pair breaking excitations vanishes for $\omega \gg 2\Delta_0$, where the density of electronic excitations resembles that of the normal state, which is zero in the clean limit. The experimental results show a constant Raman efficiency for $\omega \gg 2\Delta_0$, the same as in the normal state. Our description of the superconducting state, however, does not include “dirty limit” scattering as does that of the normal state [8].

Attempts to solve the A_{1g} problem. Krantz *et al.* [4] suggested that the screening may be lowered considerably in systems with multiple Fermi surface sheets [7]. Devereaux *et al.* [9], however, argue that this effect should be weak. Another suggestion [4] involves different gaps on two main FS sheets, e.g. a constant s -wave gap on the odd sheet and a d -wave gap on the even sheet. Another proposal by Devereaux *et al.* [3] suggests that the screening is responsible for shifting the A_{1g} peak down to lower frequencies. This idea was underpinned by a calculation that turned out to be numerically incorrect [10]. We have calculated the screened A_{1g} Raman efficiency in a 2D model with cylindrical Fermi surface and using the Raman vertex $\gamma_\varphi = \sqrt{2/(1+\alpha^2)} \cdot (\cos 4\varphi + \alpha \cos 8\varphi)$. The results are shown in Fig. 3: there is almost no shift of the A_{1g} peak position except for large values of $|\alpha|$. It can be also shown [11] that even the B_{1g} peak position shifts when using large values of $|\alpha|$: the conjecture depends critically on the value of α

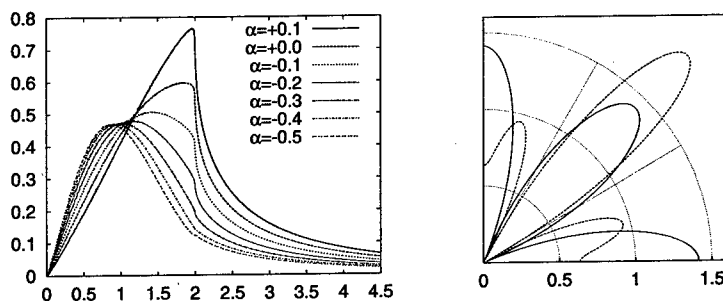


FIGURE 3. Left panel: The screened A_{1g} Raman efficiency for the Raman vertex $\gamma_\varphi = \sqrt{2/(1+\alpha^2)} \cdot (\cos 4\varphi + \alpha \cos 8\varphi)$ in units of ω/Δ_0 . The solid line corresponds to $\alpha = +0.1$, the others to $\alpha = 0, \dots, -0.5$. Right panel: The Raman vertex γ_φ as function of φ illustrating the origin of the peak shift. The solid line corresponds to $\alpha = -0.5$, the dashed one to $\alpha = 0$.

which in our *ab initio* calculations cannot be changed. Reference [12] suggests that the calculated B_{1g} peak shifts to slightly higher frequencies because of vertex corrections to the B_{1g} Raman vertex. However the calculations also contained an error [13] which invalidates their conclusions.

Doping dependence. More recent work sheds some light on the “ A_{1g} ” problem by measuring the peak positions as a function of doping for different compounds. It has been suggested that

1. for *underdoped* systems, only the B_{2g} seems to be related to pair breaking excitations. The B_{1g} component loses weight at low frequencies already at temperatures much higher than T_c [14–16]. The A_{1g} peak becomes very weak.
2. for *overdoped* systems, the A_{1g} , B_{1g} , and B_{2g} components all show a clear spectral redistribution at T_c , and *peak at approximately the same frequency* [15,17].

These facts suggest that the “ A_{1g} -problem” may be instead a “ B_{1g} -problem”, the latter component being unrelated to pair breaking excitations except for materials more doped than optimally. At this meeting, M. Klein has suggested that in the latter case the Raman spectra peak slightly below $2\Delta_0$ because of final state interactions.

Low-frequency behavior and orthorhombicity. General asymptotic power laws govern the low-frequency behavior of the Raman efficiency near $T = 0$ [3,18]. For components of the efficiency with different symmetry than the gap function, the Raman efficiency is linear in the Raman shift. For the component with the same symmetry, the additional zeroes of the mass vertex at the zeroes of the gap imply two additional powers of the frequency and makes it cubic in the Raman shift. Hence, for tetragonal $d_{x^2-y^2}$ -wave superconductors, the A_{1g} and B_{2g} components show a linear low-frequency behavior, and the B_{1g} Raman efficiency becomes cubic for low ω .

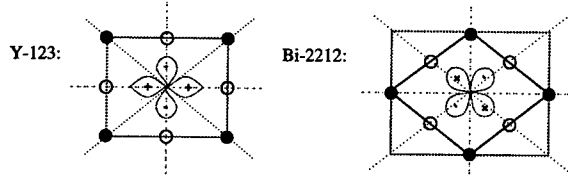


FIGURE 4. The two possibilities of deforming a tetragonal crystal (D_{4h} point group) into an orthorhombic one (D_{2h} point group) in the case of high- T_c cuprates.

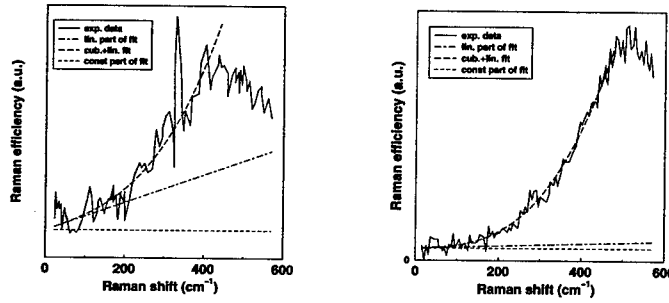


FIGURE 5. Low-frequency B_{1g} behavior of Y-123 (left panel, [19]) and Bi-2212 (right panel, [20]) and fits with $C + \alpha\omega + \beta\omega^3$. For Bi-2212 (but not for Y-123), $\alpha \approx 0$.

The orthorhombic distortion of the tetragonal CuO_2 cell can happen in the two different ways (Fig. 4) found for the Y-123 and $\text{Bi}_2\text{Sr}_2\text{CaCu}_2\text{O}_8$ (Bi-2212) systems, respectively. The distortion alters the symmetry of the $d_{x^2-y^2}$ -like gap function in Y-123, but not in Bi-2212. Thus, we expect the low- φ Raman efficiency of Y-123 to show a linear component that should be absent for Bi-2212. This is indeed the case as shown in Fig. 5 through a fit of $C + \alpha\omega + \beta\omega^3$ to the Raman efficiency.

The orthorhombic distortion allows for an s -wave component of the gap function in addition to the $d_{x^2-y^2}$ -wave component. Using the results of the $\alpha\omega + \beta\omega^3$ fit, and the mass vertex obtained from the LDA-LMTO band structure, the respective strength of the s - and $d_{x^2-y^2}$ -wave components can be estimated. This estimate [18] yields a value of $r = -0.31$ for the parameter r in the gap function $\Delta_\varphi = \Delta_0 \cdot [\cos(2\varphi) + r]$. For Bi-2212 (Fig. 5), and also for tetragonal Hg-1223 [11], we found $r \approx 0$.

The linear term in the B_{1g} -like response need not arise from a (Y-123)-like orthorhombic component. It can also arise from impurity scattering [21]. The fact that it is absent for Bi-2212 but not for Y-123 in Fig. 5 suggests that for these optimally doped crystals impurity scattering does not play an important role. We show in Fig. 6 the B_{1g} spectrum of an overdoped (through $\text{Y}^{3+} \rightarrow \text{Ca}^{2+}$ substitution) Y-123 sample. The presence of a strong linear term for $\omega \rightarrow 0$ is also observed in

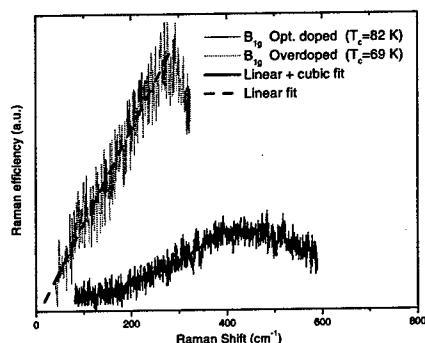


FIGURE 6. The low-frequency part of the Raman efficiency in quasitetragonal B_{1g} configuration for optimally doped and overdoped $Y_{0.8}Ca_{0.2}Ba_2Cu_3O_{7-\delta}$ at $T = 10$ K.

overdoped Bi-2212 [22].

REFERENCES

1. T. Strohm and M. Cardona, Phys. Rev. B **55**, 12725 (1997).
2. S.N. Rashkeev and G. Wendin, Phys. Rev. B **47**, 11603 (1993).
3. T. P. Devereaux and D. Einzel, Phys. Rev. B **51**, 16336 (1995).
4. M. Krantz and M. Cardona, J. Low Temp. Phys. **99**, 205 (1995).
5. M.V. Klein and S.B. Dierker, Phys. Rev. B **29**, 4976 (1984).
6. O. K. Andersen *et al.*, Phys. Rev. B **49**, 4145 (1994).
7. M. Kang *et al.*, Phys. Rev. B **56**, R11427 (1997).
8. M. Krantz, I. Mazin, and M. Cardona, Phys. Rev. B **51**, 5949 (1995).
9. T.P. Devereaux *et al.*, Phys. Rev. B **54**, 12523 (1996).
10. T. P. Devereaux and D. Einzel, Phys. Rev. B **54**, 15547 (1996).
11. M. Cardona, T. Strohm, and X. Zhou, Physica C **282-287**, 2001 (1997).
12. D. Manske *et al.*, Phys. Rev. B **56**, R2940 (1997).
13. T. Strohm, D. Munzar, and M. Cardona, Phys. Rev. B **58**, 1043 (1998).
14. R. Hackl, in: *The Gap Symmetry and Fluctuations in High- T_c Superconductors* (Plenum Press, New York, 1998).
15. R. Nemetschek *et al.*, Phys. Rev. Lett. **78**, 4837 (1997).
16. X.K. Chen *et al.*, Phys. Rev. B **56**, R513 (1997).
17. C. Kendziora, R.J. Kelley, and M. Onellion, Phys. Rev. Lett. **77**, 727 (1996).
18. T. Strohm and M. Cardona, Solid State Commun. **104**, 223 (1997).
19. R. Hackl *et al.*, Phys. Rev. B **38**, 7133 (1988).
20. T. Staufer *et al.*, Phys. Rev. Lett. **68**, 1069 (1992).
21. T.P. Devereaux, Phys. Rev. Lett. **21**, 4313 (1995).
22. K.C. Hewitt *et al.*, Phys. Rev. Lett. **78**, 4891 (1997).

Experimental Evidence for Topological Doping in the Cuprates

J. M. Tranquada

Physics Department, Brookhaven National Laboratory, Upton, NY 11973-5000

Abstract. Some recent experiments that provide support for the concept of topological doping in cuprate superconductors are discussed. Consistent with the idea of charge segregation, it is argued that the scattering associated with the "resonance" peak found in $\text{YBa}_2\text{Cu}_3\text{O}_{6+x}$ and $\text{Bi}_2\text{Sr}_2\text{CaCu}_2\text{O}_{8+\delta}$ comes from the Cu spins and not from the doped holes.

INTRODUCTION

One of the striking features of the layered cuprates is the coexistence of local antiferromagnetism with homogeneous superconductivity. After recognizing that the superconductivity is obtained by doping holes into an antiferromagnetic (AF) insulator, the simplest way to understand the survival of the correlations is in terms of spatial segregation of the doped holes [1]. If the segregated holes form periodic stripes, then time-reversal symmetry requires that the phases of the intervening AF domains shift by π on crossing a charge stripe [2-4]. This topological effect is quite efficient at destroying commensurate AF order without eliminating local antiferromagnetism [5].

The clearest evidence for stripe correlations has been provided by neutron and x-ray scattering studies of Nd-doped $\text{La}_{2-x}\text{Sr}_x\text{CuO}_4$. Much of this work, together with related phenomena in hole-doped nickelates, has been reviewed recently [6,7] and some further details are given in [8-10]. In the Nd-doped system, the maximum magnetic stripe ordering temperature corresponds to an anomalous minimum in the superconducting T_c . This fact has caused some people to argue that stripes are a special type of order, unique to certain cuprates, that competes with superconductivity. However, there has been a significant number of recent papers that provide experimental evidence for stripe correlations in other cuprates. Some of these are briefly discussed in the next section.

One corollary of the stripe picture is that the dynamic spin susceptibility measured by neutron scattering and nuclear magnetic resonance (NMR) comes dominantly from the Cu spins in instantaneously-defined AF domains and not directly from the doped holes. This has implications for the interpretation of features such

as the "resonance" peak found in $\text{YBa}_2\text{Cu}_3\text{O}_{6+x}$. Some discussion of this issue is presented in the last section.

EVIDENCE SUPPORTING STRIPES

In $\text{La}_{2-x}\text{Sr}_x\text{CuO}_4$, long-range AF order is destroyed at $x \geq 0.02$; however, a recent muon-spin-rotation (μSR) study by Niedermayer *et al.* [11] (presented at this conference) shows that the change in local magnetic order is much more gradual. At $T \leq 1$ K, the average local hyperfine field remains unchanged even as LRO disappears, and it decreases only gradually as x increases to ~ 0.07 . In particular, local magnetic order is observed to coexist with bulk superconductivity.

In contrast, Wakimoto *et al.* [12] have shown, using neutron scattering, that the static spatial correlations change dramatically as x passes through 0.05. The magnetic scattering near the AF wave vector is commensurate for $x \leq 0.04$, and incommensurate for $x \geq 0.06$, consistent with stripes running parallel to the Cu-O-Cu bonds. The scattering is also incommensurate at $x=0.05$, but with the peaks rotated by 45° compared to the case for $x \geq 0.06$, suggesting the presence of diagonal stripes, as in $\text{La}_{2-x}\text{Sr}_x\text{NiO}_4$ [6].

Local magnetic inhomogeneity at $x = 0.06$, consistent with a stripe glass, is confirmed by a ^{63}Cu and ^{139}La NMR/NQR study by Julien *et al.* [13]. One particularly striking observation is a splitting of the ^{139}La NMR peak for $T < 100$ K, in a manner very similar to that observed below the charge-stripe-ordering temperature in $\text{La}_{1.67}\text{Sr}_{0.33}\text{NiO}_4$ [14]. Another feature noticed by Julien *et al.* [13] is a loss of ^{63}Cu NQR intensity at low temperature. Independently, Hunt *et al.* [15] have investigated this intensity anomaly in a number of systems, including Nd- and Eu-doped $\text{La}_{2-x}\text{Sr}_x\text{CuO}_4$, and shown that the intensity loss correlates with the charge-stripe order parameter observed by neutron and x-ray diffraction [6]. Their results imply that static charge-stripe order occurs in $\text{La}_{2-x}\text{Sr}_x\text{CuO}_4$ for $x \leq 0.12$. This result is quite compatible with recent neutron-scattering work that shows static incommensurate magnetic order at $x = 0.12$ ($T \leq 31$ K) and $x = 0.10$ ($T \leq 17$ K), but not at $x = 0.14$ [16].

Static stripes are not restricted to Sr-doped La_2CuO_4 . Lee *et al.* [17] have demonstrated that incommensurate magnetic order occurs, with an onset very close to T_c (42 K), in an oxygen-doped sample with a net hole concentration of ~ 0.15 . Furthermore, the Q dependence of the magnetically-scattered neutron intensity indicates interlayer spin correlations very similar to those found in undoped La_2CuO_4 , thus showing a clear connection with the AF insulator state.

Stripe spacing, which is inversely proportional to the incommensurability, varies with doping. Yamada *et al.* [18] have shown that, for a number of doped La_2CuO_4 systems with hole concentrations up to ~ 0.15 , T_c is proportional to the incommensurability. Recently, Balatsky and Bourges [19] have found a similar relationship in $\text{YBa}_2\text{Cu}_3\text{O}_{6+x}$, in which the incommensurability is replaced by the Q width of the magnetic scattering about the AF wave vector. Indications that the magnetic

scattering might be incommensurate were noted some time ago [20,21]; however, it is only recently that Mook and collaborators [22,23] have definitively demonstrated that there is a truly incommensurate component to the magnetic scattering in underdoped $\text{YBa}_2\text{Cu}_3\text{O}_{6+x}$. They have also shown that the modulation wave vector is essentially the same as in $\text{La}_{2-x}\text{Sr}_x\text{CuO}_4$ with the same hole concentration.

As discussed by Mook [24] and by Bourges [25], there is also a commensurate component to the magnetic scattering in $\text{YBa}_2\text{Cu}_3\text{O}_{6+x}$. This component, which sharpens in energy below T_c , is commonly referred to as the "resonance" peak. It has now been observed in an optimally doped crystal of $\text{Bi}_2\text{Sr}_2\text{CaCu}_2\text{O}_{8+\delta}$ by Fong *et al.* [26]. This observation demonstrates a commonality, at least among the double-layer cuprates studied so far. Of course, the significance of the resonance peak itself depends on the microscopic source of the signal, and this is the topic of the next section.

MAGNETIC SCATTERING COMES FROM COPPER SPINS

Comparisons of the spin-fluctuation spectra in un- and optimally-doped $\text{La}_{2-x}\text{Sr}_x\text{CuO}_4$ [27] and in un- and under-doped $\text{YBa}_2\text{Cu}_3\text{O}_{6+x}$ [28–30] show that, although doping causes substantial redistributions of spectral weight as a function of frequency, the integrated spectral weight (over the measured energy range of 0 to ~ 200 meV) changes relatively little. The limited change in spectral weight is most easily understood if the magnetic scattering in the doped samples comes from the Cu spins in magnetic domains defined by the spatially segregated holes.

The spin fluctuations in $\text{YBa}_2\text{Cu}_3\text{O}_{6.5}$ look very similar to overdamped spin waves [29]. With increasing x , the spin fluctuations measured at low temperature gradually evolve into a peak that is sharp in energy [24,31]. The intensity of this resonance peak has a well defined dependence on the component of the scattering wave vector perpendicular to the CuO_2 planes, Q_z . If d_\perp is the spacing between Cu atoms in nearest-neighbor layers, then

$$I(Q_z) \sim \sin^2(\tfrac{1}{2}Q_z d_\perp). \quad (1)$$

(It should be noted that the spacing between oxygen atoms in neighboring planes is significantly different from the Cu spacing, and is incompatible with the observed modulation [20].) It so happens that this response is precisely what one would get for Cu spin singlets formed between the layers [32]. Thus, both the evolution of the resonance peak with doping and the Q_z dependence of its intensity suggest that the scattering is coming from antiferromagnetically coupled Cu spins.

Is commensurate scattering compatible with stripe correlations? In order to observe incommensurate peaks, it is necessary that there be interference in the scattered beam between contributions from neighboring antiphase magnetic domains. If the spin-spin correlation length along the modulation direction becomes

smaller than the width of two domains, then the scattering from the neighboring domains becomes incoherent, and one observes a broad, commensurate scattering peak. To the extent that singlet correlations form within an individual magnetic domain, the coupling between domains will be frustrated. If the charge stripes in nearest neighbor layers align with each other, then the magnetic domains will also be aligned, and the magnetic coupling between them should enhance singlet correlations. Thus, the weak interlayer magnetic coupling in bilayer systems may enhance commensurate scattering and the spin gap relative to the incommensurate scattering that dominates at low energies in $\text{La}_{2-x}\text{Sr}_x\text{CuO}_4$.

If the resonance peak is associated with the spin fluctuations in itinerant magnetic domains, then it is not directly associated with the superconducting holes. Instead, it corresponds to the response of the magnetic domains to the hole pairing. The temperature and doping dependence of the resonance peak indicates that the Cu spin correlations are quite sensitive to the hole pairing.

ACKNOWLEDGMENTS

While I have benefited from interactions with many colleagues, I would especially like to acknowledge frequent stimulating discussions with V. J. Emery and S. A. Kivelson. Work at Brookhaven is supported by the Division of Materials Sciences, U.S. Department of Energy under contract No. DE-AC02-98CH10886.

REFERENCES

1. V. J. Emery and S. A. Kivelson, this proceeding; cond-mat/9902077.
2. O. Zachar, S. A. Kivelson, and V. J. Emery, *Phys. Rev. B* **57**, 1422 (1998).
3. J. Zaanen and O. Gunnarsson, *Phys. Rev. B* **40**, 7391 (1989).
4. S. R. White and D. J. Scalapino, *Phys. Rev. Lett.* **80**, 1272 (1998).
5. A. H. Castro Neto and D. Hone, *Phys. Rev. Lett.* **76**, 2165 (1996).
6. J. M. Tranquada, in *Neutron Scattering in Layered Copper-Oxide Superconductors*, edited by A. Furrer (Kluwer Academic, Dordrecht, 1998), pp. 225-260.
7. J. M. Tranquada, *J. Phys. Chem. Solids* **59**, 2150 (1998).
8. J. M. Tranquada, N. Ichikawa, and S. Uchida, cond-mat/9810212.
9. J. M. Tranquada, N. Ichikawa, K. Kakurai, and S. Uchida, *J. Phys. Chem. Solids* (in press).
10. N. Ichikawa, Ph.D. thesis, University of Tokyo (submitted).
11. C. Niedermayer, C. Bernhard, T. Blasius, A. Golnik, A. Moodenbaugh, and J. I. Budnick, *Phys. Rev. Lett.* **80**, 3843 (1998).
12. S. Wakimoto, R. J. Birgeneau, Y. Endoh, P. M. Gehring, K. Hirota, M. A. Kastner, S. H. Lee, Y. S. Lee, G. Shirane, S. Ueki, and K. Yamada, cond-mat/9902201.
13. M.-H. Julien, F. Borsa, P. Carretta, M. Horvatić, C. Berthier, and C. T. Lin, (preprint).
14. Y. Yoshinari, P. C. Hammel, and S.-W. Cheong, cond-mat/9804219.

15. A. W. Hunt, P. M. Singer, K. R. Thurber, and T. Imai, (preprint).
16. G. Aeppli, T. E. Mason, S. M. Hayden, H. A. Mook, and J. Kulda, *Science* **278**, 1432 (1997).
17. Y. S. Lee, R. J. Birgeneau, M. A. Kastner, Y. Endoh, S. Wakimoto, K. Yamada, R. W. Erwin, S.-H. Lee, and G. Shirane, cond-mat/9902157.
18. K. Yamamoto, T. Katsufuji, T. Tanabe, and Y. Tokura, *Phys. Rev. Lett.* **80**, 1493 (1998).
19. A. V. Balatsky and P. Bourges, cond-mat/9901294.
20. J. M. Tranquada, P. M. Gehring, G. Shirane, S. Shamoto, and M. Sato, *Phys. Rev. B* **46**, 5561 (1992).
21. B. J. Sternlieb, J. M. Tranquada, G. Shirane, M. Sato, and S. Shamoto, *Phys. Rev. B* **50**, 12915 (1994).
22. H. A. Mook, P. Dai, S. M. Hayden, G. Aeppli, T. G. Perring, and F. Doğan, *Nature* **395**, 580 (1998).
23. P. Dai, H. A. Mook, and F. Doğan, *Phys. Rev. Lett.* **80**, 1738 (1998).
24. H. A. Mook, this proceeding.
25. P. Bourges, this proceeding; cond-mat/9902067.
26. H. F. Fong, P. Bourges, Y. Sidis, L. P. Regnault, A. Ivanov, G. D. Gu, N. Koshizuka, and B. Keimer, *Nature* (in press); cond-mat/9902262.
27. S. M. Hayden, G. Aeppli, H. A. Mook, T. G. Perring, T. E. Mason, S.-W. Cheong, and Z. Fisk, *Phys. Rev. Lett.* **76**, 1344 (1996).
28. S. Shamoto, M. Sato, J. M. Tranquada, B. J. Sternlieb, and G. Shirane, *Phys. Rev. B* **48**, 13817 (1993).
29. P. Bourges, H. F. Fong, L. P. Regnault, J. Bossy, C. Vettier, D. L. Milius, I. A. Aksay, and B. Keimer, *Phys. Rev. B* **56**, R11 439 (1997).
30. S. M. Hayden, G. Aeppli, P. Dai, H. A. Mook, T. G. Perring, S.-W. Cheong, Z. Fisk, F. Dogğan, and T. E. Mason, *Physica B* **241-243**, 765 (1998).
31. L. P. Regnault, P. Bourges, and P. Burlet, in *Neutron Scattering in Layered Copper-Oxide Superconductors*, edited by A. Furrer (Kluwer Academic, Dordrecht, 1998), pp. 85-134.
32. Y. Sasago, K. Uchinokura, A. Zheludev, and G. Shirane, *Phys. Rev. B* **55**, 8357 (1997).

Quasiparticle properties of d -wave superconductors in the vortex state

I. Vekhter*, J. P. Carbotte[†], P. J. Hirschfeld[‡], and E. J. Nicol* ¹

*Department of Physics, University of Guelph, Guelph, Ont. N1G 2W1, Canada

[†]Department of Physics, McMaster University, Hamilton, Ont. L8S 4M1, Canada

[‡]Department of Physics, University of Florida, Gainesville, FL 32611, USA

Abstract. We review recent progress in the understanding of the quasiparticle properties of d -wave superconductors in a magnetic field within a semiclassical treatment. We demonstrate that there exists quantitative agreement between theory and experimental data on $\text{YBa}_2\text{Cu}_3\text{O}_{7-\delta}$ (YBCO) for the field applied along the c -axis. We suggest that the field dependence of the NMR magnetization in the regime where the single relaxation time approximation breaks down can be used as a probe of the quasiparticle properties. We also show that for the field applied in the a - b plane the density of states and thermodynamic properties depend on the angle between the applied field and the order parameter nodes, resulting in fourfold oscillations of the electronic specific heat and anisotropy of the thermodynamic coefficients. We argue that this anisotropy can serve as a test of gap symmetry in the bulk, and as a further probe of the nodal quasiparticles.

INTRODUCTION

Soon after the discovery of the high temperature superconductors it was established that their thermal and transport properties in the normal state cannot be understood in the framework of the conventional Fermi liquid picture. On the other hand the experimental data in the superconducting state of these materials lend support to a BCS-like approach, and indicate the existence of a condensate with a highly anisotropic order parameter, commonly believed to have a d -wave symmetry, and well-defined quasiparticle excitations above it. This suggests that it is important to understand whether all aspects of the low temperature behavior of the cuprates can be explained by "conventional" physics, or whether some of the non-Fermi liquid properties survive deep in the superconducting state.

Some of the most revealing information about the quasiparticle excitations at low energies can be obtained from the analysis of the vortex state properties. Theoretical approaches to the vortex state are largely based on a result by Volovik [1]

¹⁾ Supported in part by NSERC of Canada (JPC and EJN), CIAR (JPC), NSF/AvH Foundation (PJH), and the Cottrell Scholar Program of Research Corporation (EJN).

who has showed that in a superconductor with lines of nodes in the energy gap the thermodynamic and transport properties are dominated by the extended quasiparticle states, rather than states in the vortex cores. These extended states exist in the bulk for quasiparticles with momenta nearly aligned with the nodal directions. Simon and Lee [2] showed that as a consequence of the Dirac-like spectrum of the nodal quasiparticles the thermal and transport coefficients exhibit scaling with a variable T/\sqrt{H} . The scaling implies that the quasiparticles can be probed either with temperature or with the applied field. Consequently the analysis of the properties of the mixed state provides a testing ground for the separation of qualitatively new physics from the not yet fully explored effects arising from the interplay between well-defined quasiparticles and an unconventional order parameter.

FORMALISM

In the semiclassical approach the energy of a quasiparticle with momentum \mathbf{k} is shifted due to circulating supercurrents. For experimentally accessible magnetic fields the superflow is well approximated by the velocity field around a single vortex, $\mathbf{v}_s(\mathbf{r}) = \hbar\hat{\beta}/2mr$, where r is the distance from the center of the vortex, and $\hat{\beta}$ is a unit vector along the current. Kübert and Hirschfeld [3] proposed to incorporate the Doppler shift, $\delta\omega_{\mathbf{k}}(\mathbf{r}) = \mathbf{v}_s \cdot \mathbf{k}$, into the BCS Green's function with a d -wave gap, $\Delta = \Delta_0 \cos 2\phi$, to compute physical quantities (see also Ref. [4]). These quantities now depend on the real space coordinate \mathbf{r} , and have to be averaged over a unit cell of the vortex lattice, which can be approximated by a circle of radius $R = a^{-1}\sqrt{\Phi_0/\pi H}$, where Φ_0 is the flux quantum, and $a \sim 1$ is a geometric constant. This method provides a simple one parameter description of the vortex state.

RESULTS

Magnetic field perpendicular to the layers

Within this approach the effect of a magnetic field $\mathbf{H}||c$ is described by a new energy scale, the typical Doppler shift

$$E_H = \frac{a}{2}v_f\sqrt{\frac{\pi H}{\Phi_0}}. \quad (1)$$

This energy can be estimated by taking $v_f \simeq 1.2 \cdot 10^7$ cm/s [5,6], which yields $E_H \approx 18aK\sqrt{H}$, Tesla.

The low temperature behavior of the thermal and transport coefficients is determined by the competition between E_H , temperature T , and the impurity bandwidth γ . In the clean limit, $\gamma \ll E_H, T$, the ratio T/E_H plays the role of the scaling variable, and when either T or E_H becomes smaller than γ , scaling is obeyed only approximately or breaks down altogether [3]. The "dirty Doppler shift" theory

[3,7], in which the scatterers are assumed to be in the unitarity limit, and in which the physical nature of the impurity scattering is assumed to be the same in the vortex state as with no applied field, has been successful in analyzing the experimental data on the field dependence of the specific heat. [3,8,9] It also agreed quantitatively with recent experiments on the field dependence of the electronic thermal conductivity $\kappa(H)$ in YBCO [6,7]. At the same time the existence of a plateau in $\kappa(H)$ [10] does not find a natural explanation within this approach, and may hint at qualitatively new physics (although it has been suggested that the phenomenon can be explained by including the scattering of quasiparticles from a disordered vortex lattice into a semiclassical analysis [11]).

It is therefore important to compare the results of other experiments with the predictions of the theory. In the clean limit such comparison allows for an estimate of E_H . Recently, the field dependence of the penetration depth at $T = 0$ obtained from the μ SR measurements on YBCO [12] have been compared with the predicted change in superfluid density, $\delta n_s/n_s = 4E_H/(\pi\Delta_0)$. [13] In that analysis a BCS-like relationship between Δ_0 , the upper critical field, H_{c2} , and the coherence length ξ_0 was used, leading to $H_{c2} \sim 88a^2$ Tesla. Without these assumptions, taking $\Delta_0 \simeq 200$ K [6], we obtain $E_H \simeq 27K\sqrt{H, \text{Tesla}}$. The magnitude of E_H can also be inferred from the critical value of the scaling variable $z = T/\sqrt{H}$ at which a crossover from the low- T , high-field regime to the temperature dominated behavior occurs. In the scaling of the specific heat it has been found that $z_c = 6.5 \text{ K}/T^{-1/2}$, [14] yielding $E_H \simeq 30K\sqrt{H, \text{Tesla}}$, close to the value obtained from the μ SR experiments, and in agreement with our estimates.

Among further experimental possibilities the analysis of the NMR magnetization can be especially instructive since such measurements are always done in a magnetic field. It has been pointed out that since the spin-lattice relaxation rate depends on the density of states and becomes a local quantity in the presence of a magnetic field, [13,15] the decay of the average magnetization, $M(t) \propto \int_{\text{cell}} \exp(-t/T_1(\mathbf{r}))$, cannot be described by a single relaxation rate [13], and it is the decay of $M(t)$ that has to be analysed [15]. As we show in Fig.1 for a spin-1/2 system, while for strong fields $M(t)$ is clearly not exponential, it is possible to describe the magnetization decay in a fixed field by an effective relaxation time, which would provide a fit to the experimental data over about two decades in $M(t)$. For $E_H \leq T$

$$\frac{1}{T_1} \simeq \frac{1}{T_1^{H=0}} \left[1 + \frac{3E_H^2}{\pi^2 T^2} \ln \left[4\eta \frac{T}{E_H} \right] \right], \quad (2)$$

where

$$\frac{1}{T_1^{H=0}} = \frac{\pi^2}{3} \frac{1}{T_c} \frac{T^3}{T_c \Delta_0^2}, \quad (3)$$

T_1^c is the relaxation rate at T_c , and $\eta \sim 1$ is weakly time dependent. As we show in Fig.1, Eq.(2) describes the decay quite well even for $E_H = T$. The field dependent part of the effective relaxation rate varies linearly in TH in this regime,

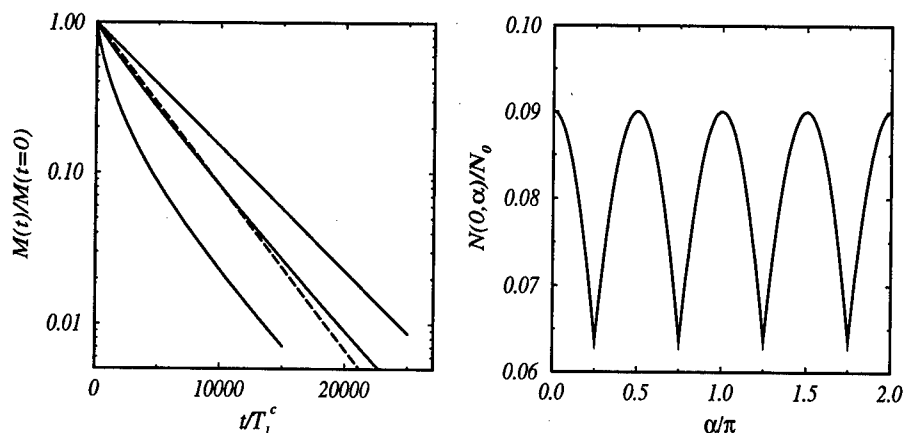


FIGURE 1. Left: NMR magnetization for $T = 0.03\Delta_0$ and (top to bottom) $E_H = 0, 0.03\Delta_0, 0.1\Delta_0$. Dashed line: approximate expression of Eq.(2) for $E_H = 0.03\Delta_0$. Right: Density of states $N_0(\alpha) = N(0, \alpha)/N_0$ for $\mathbf{H} \parallel ab$ and $E_H^{ab} = 0.1\Delta_0$.

and it still describes the short-time ($t \ll T_1^{H=0}$) relaxation for higher fields, when $E_H \gg T$, and the decay is manifestly non-exponential. At longer times, $t \geq T_1^{H=0}$, a full numerical evaluation is needed. We note that at higher temperatures there are additional contributions to the relaxation rate due to, for example, thermal vibrations of the vortices, which have to be included in the analysis. [15]

Magnetic field parallel to the layers

We have recently extended the same approach to the case when the applied field is parallel to the ab plane in not too anisotropic high- T_c materials, such as YBCO [16,17]. The energy scale associated with the Doppler shift for such an arrangement is given by $E_H^{ab} = \sqrt{\lambda_{ab}/\lambda_c} E_H$, where λ_{ab} (λ_c) is the in-plane (c-axis) penetration depth. Then for YBCO near optimal doping $E_H^{ab} \approx 6 - 8 K \sqrt{H, \text{Tesla}}$. While no experimental data exist which allow a direct determination of this scale, its magnitude can be inferred from the scaling of the specific heat anisotropy, $\delta C \equiv C(\mathbf{H} \parallel c) - C(\mathbf{H} \parallel ab)$ [18], which gives $E_H^{ab} \leq 4 K \sqrt{H, \text{Tesla}}$ [17]. The $T \ll E_H^{ab}$ regime has not been achieved in Ref. [18], and the data can only indicate the upper limit for E_H^{ab} , which is within a factor of 2 of our estimate.

For high fields, $T \ll E_H$, the thermal and transport properties depend sensitively on the angle α between \mathbf{H} and the crystalline axis. [16,17] The anisotropy is related to the vanishing Doppler shift for the quasiparticles moving parallel to the field, so that for the field along the nodal direction, $\alpha = \pi/4$, only two of the four gap nodes contribute to the residual density of states (DOS) $N(0, \alpha)$. Consequently the

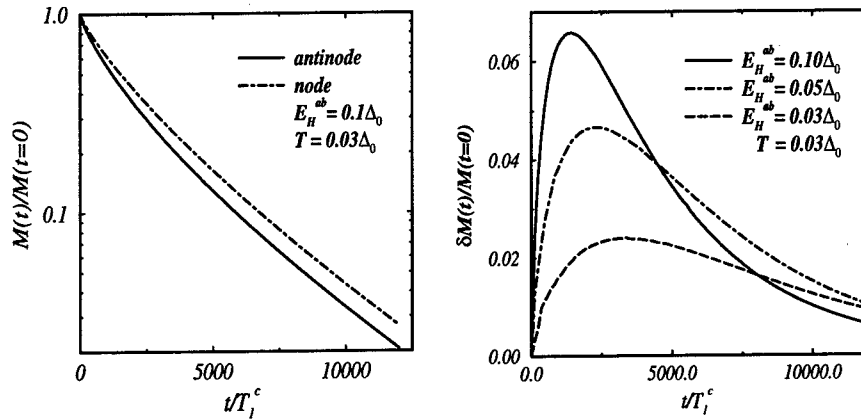


FIGURE 2. NMR magnetization for $\mathbf{H}||ab$ (left); NMR magnetization anisotropy $\delta M(t)$ (right).

DOS has a minimum for $\mathbf{H}||node(n)$, and a maximum for $\mathbf{H}||antinode(an)$,

$$\frac{N(0, \alpha)}{N_0} = \frac{2\sqrt{2}E_H^{ab}}{\Delta_0\pi} \max(|\sin \alpha|, |\cos \alpha|), \quad (4)$$

where N_0 is the normal state DOS. [16,19] For the same reason the dependence of $N(\omega, \alpha)$ is linear, in ω , for $\mathbf{H}||n$ with a slope of one half its value in the zero field DOS. In contrast, for $\mathbf{H}||an$, $N(\omega)$ is quadratic in ω [16].

The anisotropy in the DOS is accessible via measurements of the specific heat, which exhibits fourfold oscillations, see Fig.1. The amplitude of these oscillations in YBCO at low temperature is estimated to be $\delta C/T \simeq 0.11 - 0.19\sqrt{H}$, Tesla mJ/mol K², and therefore within experimental resolution for fields $H \sim 8 - 20$ Tesla. Because of the linear growth of the DOS in the nodal direction, the amplitude is reduced sharply with increased T , and in moderate fields it can disappear for $T \geq 2 - 3$ K [17]. The anisotropy in the DOS leads to the anisotropy of other properties. The change in the superfluid density at $T \ll E_H^{ab}$ is given by

$$\delta n_s \approx \begin{cases} \eta_1 \sqrt{H} + \eta_2 T^2 / \sqrt{H} & \text{for } \alpha = 0; \\ \eta_1 \sqrt{H} / \sqrt{2} + \eta'_2 T & \text{for } \alpha = \pi/4, \end{cases} \quad (5)$$

where η_1 , η_2 , and η'_2 are coefficients, and the linear, in T , term is field independent with $\eta'_2 = \eta(H = 0)$. This quantity can be inferred from the change in the penetration depth as measured by the μ SR or from the optical conductivity measurements, although in both these cases a better understanding of the role played by the non-local effects is needed [20]. The NMR relaxation rate would provide another sensitive test of our predictions: for $\mathbf{H}||an$ the effective relaxation rate is greater than for $\mathbf{H}||n$, see Fig.2, left, although in both cases the decay is non-exponential, as for $\mathbf{H}||c$. Experimentally it is easier to detect the magnetization

anisotropy, $\delta M(t) \equiv M(\alpha = 0, t) - M(\alpha = \pi/4, t)$ which we show in Fig. 2, right. The anisotropy is most prominent in the field dominated regime, $T \ll E_H$, where at present we do not have analytic results. The peak occurs in the region where $M(t)$ is non-exponential and broadens as the deviations from the exponential behavior become less significant. We expect to be able to report on this behavior in more detail in the near future.

SUMMARY

A one parameter description of the vortex state in the semiclassical approach captures the essential physics and provides a description of unconventional superconductors in the vortex state. We find a semi-quantitative agreement between theoretical predictions and experimental results for $\mathbf{H} \parallel c$. We also find anisotropy in the properties of the vortex state for the field $\mathbf{H} \parallel ab$ and suggest that it can be used to map out the position of the gap nodes in the bulk and to further probe the nodal quasiparticles.

REFERENCES

1. G. E. Volovik, JETP Lett. **58**, 469 (1993).
2. S. H. Simon and P. A. Lee, Phys. Rev. Lett. **78**, 1548 (1997).
3. C. Kübert and P. J. Hirschfeld, Sol. St. Comm. **105**, 459 (1998).
4. Yu. S. Barash, V. P. Mineev, A. A. Svidzinskii, JETP Lett. **65**, 638 (1997).
5. P. A. Lee and X.-G. Wen, Phys. Rev. Lett. **78**, 4111 (1997).
6. M. Chiao *et al.*, cond-mat/9810323.
7. C. Kübert and P. J. Hirschfeld, Phys. Rev. Lett. **80**, 4963 (1998).
8. K. A. Moler *et al.*, Phys. Rev. Lett. **73**, 2744 (1994); Phys. Rev. **B 55**, 3954 (1997).
9. R. A. Fisher *et al.*, Physica C **252**, 237 (1995).
10. K. Krishana *et al.* Science **277**, 83 (1997).
11. M. Franz, cond-mat/9808230.
12. J. Sonier *et al.*, Phys. Rev. B **55**, 11789 (1997).
13. I. Vekhter, J. P. Carbotte, E. J. Nicol, Phys. Rev. B **59**, 1417 (1999).
14. D. A. Wright *et al.*, Phys. Rev. Lett. **82**, in press.
15. R. Wortis, Ph.D. thesis, UIUC, 1998; R. Wortis *et al.*, unpublished.
16. I. Vekhter, P. J. Hirschfeld, J. P. Carbotte, and E. J. Nicol, cond-mat/9809302.
17. I. Vekhter, P. J. Hirschfeld, J. P. Carbotte, and E. J. Nicol, cond-mat/9811315, to appear in Proceedings of PPHMF-III.
18. B. Revaz *et al.*, Phys. Rev. Lett. **80**, 3364 (1998).
19. G. E. Volovik, unpublished; in K. A. Moler *et al.*, J. Phys. Chem. Solids **56**, 1899 (1995).
20. I. Kosztin and A. Leggett, Phys. Rev. Lett. **79**, 135 (1997).

Observations of YBCO superconductors under a low-temperature scanning electron microscope

A.Vyas, C.C.Lam, P.C. W. Fung*, S.H.Li, H.S. Lam

Department of Physics and Materials Science, City University of Hong Kong, Hong Kong, China.

* Department of Physics, University of Hong Kong, Hong Kong, China.

Abstract. Microscopic analyses have been performed on YBCO superconductors with Ca-doping and Gd-doping as a function of temperature by employing a low-temperature scanning electron microscope (LTSEM). On lowering temperature of the sample from 300 K to 90 K, the brightness of the SEM image changes due to the change in resistance of the sample. For the underdoped cuprates $Y_{1-x}Ca_xBa_2Cu_3O_{7-\delta}$, with $x = 0.2$, the pseudo gap in the normal state is opened at a temperature T^* which far below the critical temperature T_c of the superconductor. The opening of the pseudo gap has directly been observed under LTSEM (temperature fluctuating in the range of ± 5 K). At temperature T^* the formation of quasi-particles takes place, thus a sudden brightness change in the SEM image is observed. The results of these measurements are compared with the four-point probe measurement. It is proved that the data of these two measurements are quite in agreement with each other.

INTRODUCTION

It is well known that the brightness of the morphological image of a specimen observed under scanning electron microscope (SEM) depends on the secondary electron yield (SEY) scattered off that material [1-2]. Considering a primary electron beam in the SEM perpendicular to the surface of the superconductor, the SEY of the superconductor should vary when it changes from normal to superconducting state. We expect that such a variation in the SEY will reflect in the brightness of SEM image as mentioned above. Therefore, when the morphological image of a YBCO superconductor is observed under LTSEM from room temperature to its critical state, we can expect that there should be variation in the brightness of the material. Such experiment is performed to study carefully the following points: (1) a "brightness change" phenomenon exists in our

sample due to the resistance change on lowering the temperature; and (2) there is a significant "brightness change" in the SEM image at temperature T^* . In other words the brightness of the SEM image should vary at T^* due to the formation of quasi-particles.

EXPERIMENT

The LTSEM observation was carried out with a model: Polaron LT 4700. The LTSEM for this investigation has been proved to be efficient for studying the microcharacterization of YBCO superconductors [3-5]. A freshly fractured YBCO sample was observed at temperatures from 300 K to 90 K. On reducing the temperature from 300 K to a temperature slightly higher than T^* , the brightness of the SEM image changed very slightly. Across the temperature T^* , we observed the morphological image for particle of the superconducting phase. A sudden drop in the brightness of such particle occurred. From the result of the resistance vs temperature we can plot a relationship between $\ln \left[\frac{1}{\rho(T)} - \frac{1}{\rho_n(T)} \right]$ vs. $\frac{1}{T}$, as shown in fig. 1. From this figure, we

can see the temperature which corresponds to T^* is the temperature at which the resistivity begins to deviate from the linear relationship with the temperature. This temperature can be explained as the starting temperature for the formation of quasi particles that take place during the lower temperature. As the temperature is further reduced, the more quasi-particles are formed. The formed quasi-particles seem to contribute less resistivity to the ceramic material. Owing to this reason, therefore the SEY is reduced. In other words, the brightness of the morphological image for the particles of the superconducting phase, which reflects the scattering events are significantly reduced. This phenomenon can be seen from figs. 2(a) to 2(d). This formation of quasi-particles indicates that a pseudo-gap is being opened at the temperature T^* .

Similar phenomenon is also observed in the Gd-doped YBCO samples under LTSEM. For this system, we have measured the intensity for SEY. Results are shown in fig. 3. Again, these results show that at the temperature T^* , there is a significant reduction in the secondary electron yield intensity.

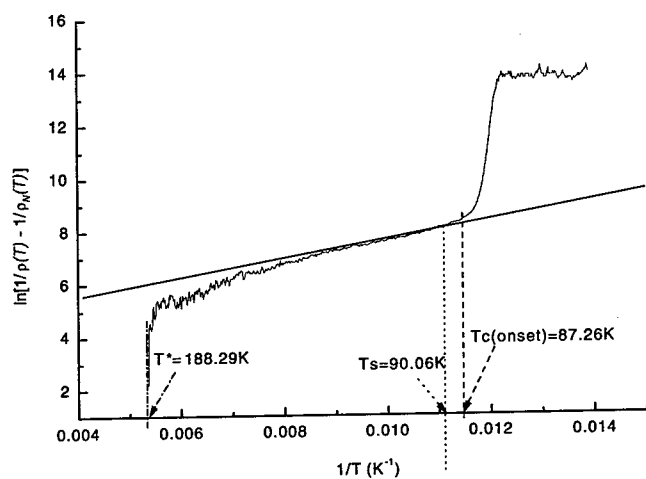


FIGURE 1. Relationship between $\ln[1/\rho(T) - 1/\rho_N(T)]$ vs $1/T$.

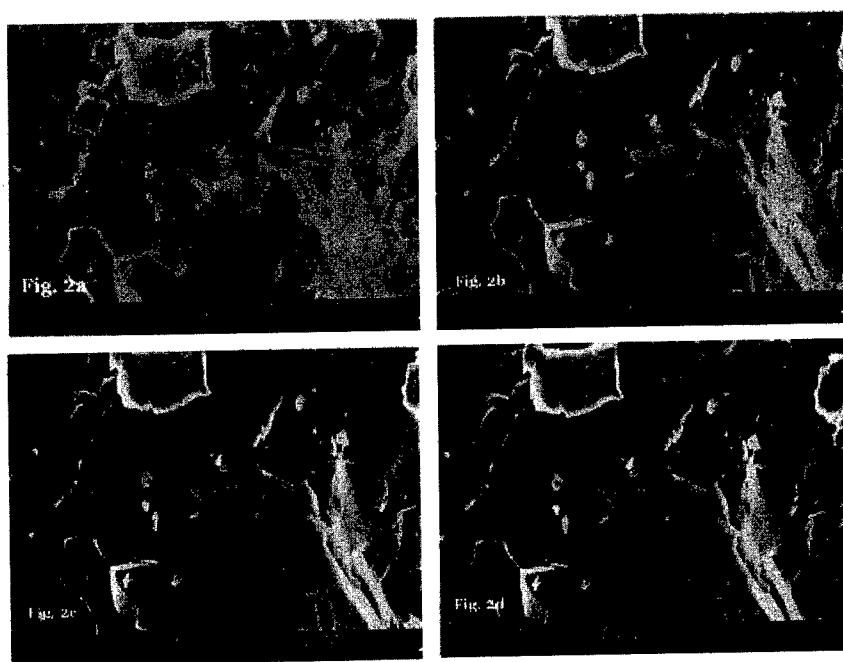


FIGURE 2. SEM micrograph of the Ca(x=0.2) doped YBCO a) T=300K, b) T=195K, c) T=183K, d) T=175K

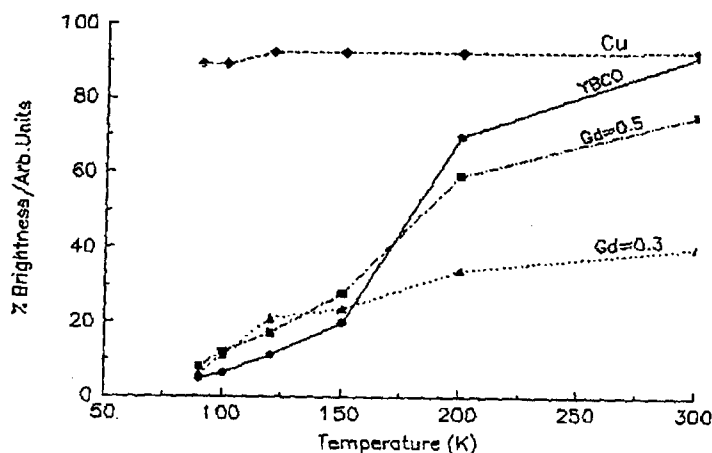


FIGURE 3. Variation in the brightness percentage versus temperature for Cu and Gd doped YBCO samples

CONCLUSION

We have investigated the quasi-particles formation effect during the lowering temperature from 300 K to the critical temperature of the ceramic superconductors of Ca-doped and Gd-doped YBCO. The reduction in the SEY was observed significantly at T^* . This reduction in the SEY indicates that there is reduction in the resistivity for the normal state materials. This phenomenon, namely the reduction in the intensity of the SEY, can be related to the formation of some quasi-particles, which is started from T^* . The data of T^* observed under LTSEM are in agreement with the resistivity versus T measurement. This investigation will be useful in understanding the mechanism of the high temperature superconductivity.

REFERENCES

1. Dale E. Newbury et al. *Advanced scanning electron microscopy and X-Ray Microanalysis* (1986).
2. Klaus Wetzig et al. *In Situ Scanning Electron Microscopy in Materials Research* (1995).
3. P. C. W. Fung, J. C. L. Chow, *J. Superconductivity* **36**, 14 (1994).
4. S. Uchida, *Physica C* **282-287**, 12-18 (1997).
5. H. Ding et al., *Nature* **382**, 51 (1996).

Quasiparticle Tunneling and Andreev Reflection Study of the Pairing Symmetry in $\text{YBa}_2\text{Cu}_3\text{O}_{7-\delta}$

J. Y.T. Wei¹, N.-C. Yeh¹, D. F. Garrigus², M. Strasik² and R. P. Vasquez³

¹*Department of Physics, California Institute of Technology, Pasadena, CA 91125*

²*Boeing Phantom Works, Seattle, WA 98124*

³*Center for Space Microelectronics Technology, Jet Propulsion Laboratory, California Institute of Technology, Pasadena, CA 91109*

Abstract. We report on two tunneling experiments studying the pairing symmetry in $\text{YBa}_2\text{Cu}_3\text{O}_{7-\delta}$ ($T_c=90\text{K}$) at 4.2K. First, directional tunneling and point-contact spectroscopy measurements were made on the {100}, {110} and {001} faces of single crystal samples. The conductance spectra showed either quasiparticle tunneling, Andreev-reflection or zero-bias peak characteristics, depending on the junction orientation and impedance. Quantitative spectral analysis using the generalized Blonder, Tinkham and Klapwijk theory indicated a predominantly $d_{x^2-y^2}$ pairing symmetry, with less than 5% s -wave component in either the $d+s$ or $d+is$ scenario. Second, scanning tunneling spectroscopy was performed on epitaxial superconductor/ferromagnet heterostructures comprising $\text{YBa}_2\text{Cu}_3\text{O}_{7-\delta}$ and $\text{La}_{0.7}\text{Ca}_{0.3}\text{MnO}_3$. Quasiparticle tunneling and zero-bias peak characteristics observed on the cuprate were consistent with d -wave pairing symmetry, which appeared to be invariant under a spin-polarized quasiparticle current injected from the manganite, up to at least $7 \times 10^3 \text{A/cm}^2$.

DIRECTIONAL TUNNELING & POINT-CONTACT SPECTROSCOPY ON $\text{YBa}_2\text{Cu}_3\text{O}_{7-\delta}$ SINGLE CRYSTALS

The issue of pairing symmetry has remained central in the field of high-temperature superconductivity (1). For $\text{YBa}_2\text{Cu}_3\text{O}_{7-\delta}$ (YBCO), phase-sensitive experiments involving pair tunneling in the CuO_2 plane have demonstrated $d_{x^2-y^2}$ symmetry (2,3), while Josephson-junction experiments perpendicular to the CuO_2 plane have indicated the presence of an s -wave order parameter (4). A more recent Josephson-junction experiment has shown evidence for a mixed $d+s$ symmetry in YBCO (5), while another study involving planar-junction quasiparticle tunneling has suggested broken time-reversal symmetry, such as in the $d+is$ or $d+id'$ scenario (6,7).

Although *qualitatively* addressing the issue of pairing symmetry, these results have provided little information on the magnitudes of the component order parameters. In principle, quasiparticle tunneling and Andreev reflection could be used to map out the order parameter anisotropy, by directionally measuring the superconducting density of states (DOS). In the conventional picture involving *s*-wave pairing, the tunneling conductance dI/dV for a high-impedance junction is proportional to $E/(E^2 - \Delta^2)^{1/2}$, where E is the quasiparticle energy and Δ is the gap function representing the order parameter (8). A low-impedance point-contact junction, on the other hand, is known to exhibit enhanced (ideally double) subgap dI/dV as a result of the time-reversed retroreflection (Andreev reflection) of incident quasiparticles upon combining into Cooper pairs (9). Both types of spectral behavior can be described by the standard theory of Blonder, Tinkham and Klapwijk (BTK), using a single parameter Z to represent the junction impedance (10). In each case, however, the dI/dV spectrum is sensitive only to the magnitude and not the phase of Δ .

Generalization of the BTK formalism for *d*-wave pairing indicates a complex spectral dependence on both junction orientation and impedance, as a direct result of the order parameter phase. Recent theoretical studies (11,12) have shown that the *d*-wave phase sign change about its nodal axes ($k_x = \pm k_y$) allows constructive interference between Andreev-reflected electrons and holes at the junction, and thus the formation of resonant *surface* states which could prevent direct tunneling into the *bulk* states. For a model {110} tunnel junction, these Andreev-bound surface states are nearly degenerate at $E=0$, giving rise to a zero-bias conductance peak (ZBCP). The ZBCP is expected to diminish for either large junction misorientation from the nodal axes or high junction transmission, as the surface states become less robust, suggesting that the bulk *d*-wave quasiparticle DOS may nonetheless be probed by either reducing the junction impedance or orienting the junction normal to either the (100) or (001) axis. A detailed spectral analysis could then be made to assess the purity of the *d*-wave order parameter, in particular the amount of *s*-wave component present.

To study these issues *quantitatively*, we have performed directional tunneling and point-contact spectroscopy on the {100}, {110} and {001} faces of YBCO single crystals. The twinned crystals were grown by a crystal-pulling technique followed by extensive oxygen annealing, showing $T_c \approx 90\text{K}$ with $\sim 1\text{K}$ transition in both electrical resistivity and magnetic susceptibility (13). Samples with {100}, {110} and {001} faces were oriented, cut, polished, reannealed and bromine-etched before being measured (14). The tunneling and point-contact spectroscopy measurements were performed with a cryogenic scanning tunneling microscope (STM) at 4.2K in 1 μTorr ultrapure helium, with the sample biased relative to a Pt-Ir tip. Details of the experimental setup and technique are given elsewhere (14,15). The tunneling and point-contact junctions were $\sim 10\text{M}\Omega$ and $\sim 100\Omega$ respectively, the latter being larger than typical point-contact impedances, but well in the Knudsen regime (contact radius $<$ mean free path) to assure ballistic transmission with negligible local heating (16).

The dI/dV data are plotted after background normalization as circles in the figures. Figure 1(a) is for a {110} STM junction, showing a pronounced ZBCP; the left inset is for a {100} point-contact junction, showing an Andreev-reflection plateau with an asymmetric inflection near zero-bias. Figure 1(b) is for a {001} STM junction, showing a distinct quasiparticle tunneling gap with broadened and asymmetric edges. Very similar gap structures have been seen by STM on $\text{Bi}_2\text{Sr}_2\text{CaCu}_2\text{O}_{8+\delta}$ (17) and $\text{HgBa}_2\text{Ca}_{n-1}\text{Cu}_n\text{O}_{2n+2+\delta}$ (15). Also noteworthy are the spectral kinks at $\sim \pm 38\text{mV}$, which have been seen by STM on as-grown YBCO crystals (18).

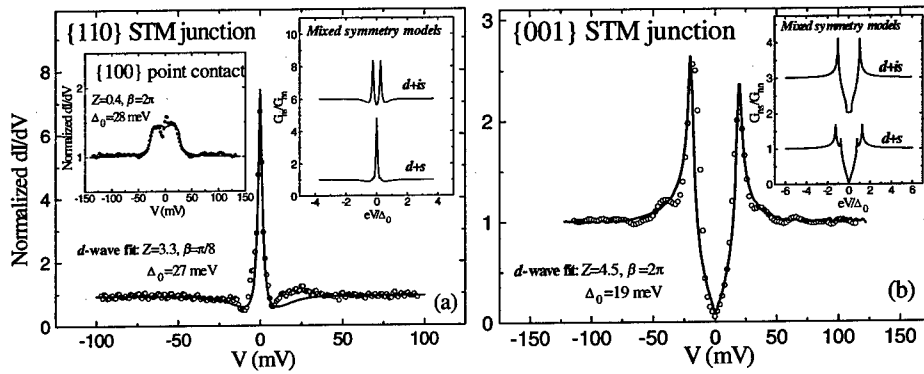


FIGURE 1. Normalized conductance spectra taken on YBCO at 4.2K. (a) is for a {110} STM junction, showing a zero-bias peak; left inset is for a {100} point-contact, showing an Andreev-reflection plateau. (b) is for a {001} STM junction, showing a quasiparticle tunneling gap. The data are given as open circles and the d -wave fits by solid curves. The right insets give the $d+s$ and $d+is$ simulations.

To explain the spectral data, we use the generalized BTK theory (11,12) to express the normal/superconductor (NS) junction conductance:

$$G_{NS} = G_{NN} \iint e^{-\beta^2 k_i^2} d^2 k_i \int dE_k [1 + A(E_k, \Delta_k, Z) - B(E_k, \Delta_k, Z)] \partial f(E_k - eV) / \partial eV \quad (1)$$

where A and B are the phase-dependent Andreev-reflection and normal-reflection probabilities from Ref.(12), f is the Fermi-Dirac function and G_{NN} is the normal-state junction conductance. Anisotropies in both Δ_k and E_k are incorporated by the integration over transverse momenta k_i (19), weighted by a Gaussian cone of width β with the proviso that the band structure implicit in E_k affect only B and not A , since the latter entails the formation of Cooper-pairs and not quasiparticles (20). The d -wave gap-function $\Delta_k = \Delta_0(\cos k'_x - \cos k'_y) / 2 \approx \Delta_0 \cos(2\theta')$ is used, with θ' defined relative to (100). The quasi two-dimensional (2D) band structure of YBCO is modelled by the tight-binding dispersion $\xi_k = -2t(\cos k'_x + \gamma \cos k'_y) + 4t'(\cos k'_x \cos k'_y) - \mu$, with

$t=185\text{meV}$, $t'=30\text{meV}$, $\gamma=1.02$ and $\mu=0.51\text{eV}$ (21), through the relation $E_k^2 = \xi_k^2 + \Delta_k^2$. The tunneling cone width is approximated by $\beta=\pi/8$ and $\beta=2\pi$ for the STM *tunnel* and *point-contact* junctions respectively (14), except for the {001} STM case which has only transverse final states because of the quasi-2D band structure and thus a flat tunneling cone ($\beta=2\pi$) (15).

Spectral fits of the *d*-wave BTK model to our data are shown as solid curves in the figures. In Fig.1(a), the ZBCP for the {110} STM junction is successfully fitted with $Z=3.3$ and $\Delta_0=27\text{meV}$, as a clear manifestation of the Andreev-bound surface states induced by the *d*-wave. In the left inset of Fig.1(a), the plateau behavior for the {100} point-contact junction is well reproduced, apart from the asymmetric zero-bias inflection, by using $Z=0.4$ and $\Delta_0=28\text{meV}$ in a *d*-wave averaging ($\beta=2\pi$) of ordinary Andreev reflection. In Fig.1(b), the enhanced peak structure for the {001} STM junction can be interpreted as a spectral convolution of the *d*-wave quasiparticle DOS, which gives a V-shaped gap broadening, and the quasi-2D normal-state DOS, which has a logarithmic singularity near the Fermi level (15). In this latter fit, $Z=4.5$ and $\Delta_0=19\text{meV}$ were used, and the Fermi level was doped 10meV away from the DOS singularity to account for the peak-height asymmetry.

To assess the amount of *s*-wave present in YBCO, we analyzed the mixed symmetry *d+s* and *d+is* scenarios represented respectively by the gap functions $\Delta_k=\Delta_0\cos(2\theta')+\Delta_1$ and $\Delta_k=\Delta_0\cos(2\theta')+i\Delta_1$. The corresponding spectral simulations are shown in the right insets of Fig.1, using $\Delta_1/\Delta_0=0.25$ and the same *Z* parameter as in each main panel for comparison, and neglecting band-structure effects for simplicity. For the {110} STM junction in Fig.1(a), *d+is* splits the ZBCP into broken time-reversal symmetry pairs separated by $2\Delta_1$, while *d+s* has little effect. For the {001} STM junction in Fig.1(b), *d+is* flattens out the gap-bottom while *d+s* splits the gap-edges by $2\Delta_1$, neither feature being apparent in our data. From our measurement resolution (1meV) and our fitting results for Δ_0 , we estimate an upper bound of 5% *s*-wave relative to the predominant *d*-wave in either the *d+s* or *d+is* scenario.

SCANNING TUNNELING SPECTROSCOPY ON EPITAXIAL $\text{YBa}_2\text{Cu}_3\text{O}_{7-\delta}$ FILM UNDER QUASIPARTICLE SPIN-INJECTION

Recent transport experiments on epitaxial cuprate/manganite heterostructures have shown that the superconducting critical current I_c in the high- T_c cuprate can be suppressed by a current injected from the lattice-matched ferromagnetic manganite (22-24). The effect is believed to be due to dynamic magnetic pair-breaking in the superconducting cuprate by a non-equilibrium distribution of spin-polarized quasiparticles injected from the half-metallic manganite. More recently, Yeh *et al.* have carried out a pulsed-current study of this phenomenon to minimize the spurious effects of Joule heating, verifying the I_c -attenuation near T_c for spin-polarized injection and the absence of this attenuation for unpolarized injection (25).

To see how the high- T_c order parameter is affected by quasiparticle spin-injection, we have performed scanning tunneling spectroscopy on heterostructures of $\text{YBa}_2\text{Cu}_3\text{O}_{7-\delta}$ /yttria-stabilized-zirconia/ $\text{La}_{0.7}\text{Ca}_{0.3}\text{MnO}_3$ (YBCO/YSZ/LCMO) at 4.2K. The samples were 100nm/2nm/100nm in thickness and $6\times 6\text{mm}^2$ (YBCO= $6\times 2\text{mm}^2$) in size, and grown by pulsed laser deposition on (100) LaAlO_3 substrates. The surface morphology indicated predominantly c -axis epitaxy, with some ab -plane outgrowth. Resistivity measurements showed the LCMO layer to have a colossal magnetoresistivity peak near its Curie temperature $T_M\approx 260\text{K}$ and the YBCO layer to have $T_c\approx 87\text{K}$ with $\approx 1\text{K}$ transition (25). Critical current density of the YBCO layer was determined by pulsed-current measurement to be $J_c\approx 5\times 10^4\text{A/cm}^2$ (25). Details of the experimental setup and technique are published elsewhere (26).

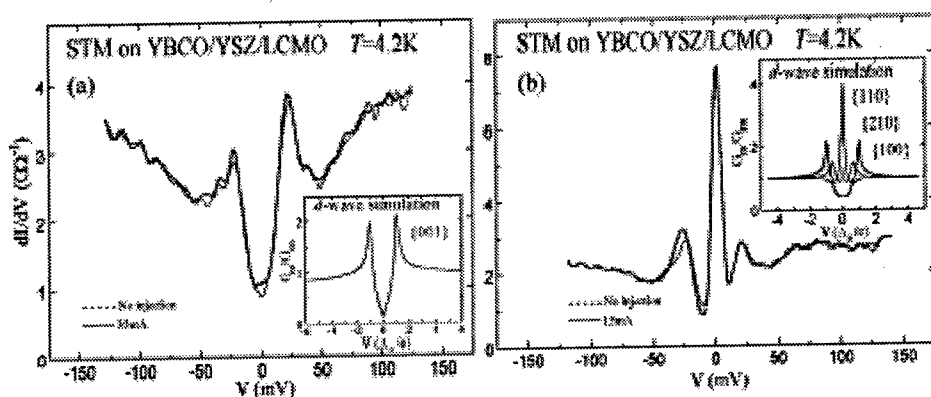


FIGURE 2. STM tunneling spectra taken on an epitaxial YBCO/YSZ/LCMO heterostructure at 4.2K. (a) is the predominant type, showing a distinct gap structure. (b) shows the type with a zero-bias peak. The spectra taken under quasiparticle spin-injection are given as solid curves, and data taken without injection as dashed curves. The insets show the d -wave simulations for various junction orientations.

Two types of tunneling dI/dV spectra were observed on the YBCO layer at 4.2K. Figure 2(a) plots the predominant type, showing a distinct gap structure with finite midgap conductance, asymmetric peaks, linear spectral background and a kink structure at $\pm 38\text{mV}$ (c.f. Fig.1(b)). The dashed curve is for 0mA and the solid curve for 35mA ($7\times 10^3\text{A/cm}^2$) injection. Considerable spectral broadening was seen at higher injections (up to 70mA) although negligible sample heating was detected, suggesting a non-equilibrium quasiparticle distribution (26). The observed gap structure can be attributed to c -axis tunneling, as shown in the inset by the d -wave BTK simulation (Eqn.1) using $Z=4$ and $\Delta_0=19\text{meV}$ with optimal doping. Figure 2(b) shows the other type of tunneling spectra observed, with a pronounced ZBCP structure. The dashed curve is for 0mA and the solid curve for 15mA ($3\times 10^3\text{A/cm}^2$) injection. Little spectral variation was seen, even at higher injections (up to 35mA),

apart from some minor broadening. The ZBCP can be compared with the {110} single-crystal data (Fig.1(a)) and attributed to tunneling in the *ab*-plane, as illustrated in the inset by the *d*-wave BTK simulations (Eqn.1) using $Z=2$ and $\Delta_0=19\text{meV}$ for the various junction orientations. Note that a *split* ZBCP would be expected for *broken time-reversal symmetry* of the *d*-wave pairing, such as with a complex *d+id'* order parameter (7), or by the exchange scattering which introduces finite pair-lifetime ($\Delta_k \rightarrow \Delta_k + i\Gamma_{ex}$) in a magnetic pair-breaking scenario (27). The absence of such ZBCP splitting in our tunneling data indicates the *d*-wave pairing symmetry in YBCO to be invariant under a spin-polarized quasiparticle current, up to at least $7 \times 10^3 \text{A/cm}^2$.

ACKNOWLEDGEMENTS

This work is supported by NSF #DMR-9705171, NASA/OSS, the Packard Foundation and the DRDF fund at the Jet Propulsion Laboratory. Laboratory assistance by L. Hedges, N. Asplund, L. Yi, K. Vakili and C.-C. Fu was greatly appreciated.

REFERENCES

1. For a review, see Annett, J. F., *et al.*, J. Low Temp. Phys. **105**, 473 (1996).
2. Tsuei, C. C., *et al.*, Phys. Rev. Lett. **73**, 593 (1994).
3. Wollman, D. A., *et al.*, Phys. Rev. Lett. **71**, 2134 (1993).
4. Sun, A. G., *et al.*, Phys. Rev. Lett. **72**, 2267 (1994).
5. Kouznetsov, K. A., *et al.*, Phys. Rev. Lett. **79** (1997).
6. Covington, M., *et al.*, Phys. Rev. Lett. **79**, 277 (1997); Fogelstrom, M., *et al.*, *ibid* **79**, 281 (1997).
7. Balatsky, A. V., Phys. Rev. Lett. **80**, 1972 (1998).
8. Wolf, E. L., *Principles of Electron Tunneling Spectroscopy*, Oxford University Press, U. K. (1985).
9. Andreev, A. F., Sov. Phys. JETP **19**, 1228 (1964).
10. Blonder, G. E., Tinkham, M., Klapwijk, T. M., Phys. Rev. B **25**, 4515 (1982).
11. Hu, C.-R., Phys. Rev. Lett. **72**, 1526 (1994).
12. Tanaka, Y. and Kashiwaya, S., Phys. Rev. Lett. **74**, 3451 (1995).
13. Strasik, M. and Garrigus, D. F., unpublished.
14. Wei, J. Y. T., *et al.*, Phys. Rev. Lett. **81**, 2542 (1998).
15. Wei, J. Y. T., *et al.*, Phys. Rev. B **57**, 3650 (1998).
16. Deutscher, G. and Noziers, P., Phys. Rev. B **50** (1994).
17. Renner, Ch., *et al.*, Phys. Rev. Lett. **80**, 149 (1998); DeWilde, Y., *et al.*, *ibid* **80**, 153 (1998).
18. Maggio-Aprile, I., *et al.*, Phys. Rev. Lett. **75**, 2754 (1995).
19. DeWilde, Y., *et al.*, Phys. Rev. Lett. **72**, 2278 (1994).
20. Hoevers, H. F. C., Ph. D. thesis, University of Nijmegen, The Netherlands (1992).
21. Markiewicz, R. S., J. Phys. Chem. Solids **58**, 1179 (1997).
22. Vas'ko, V. A., *et al.*, Phys. Rev. Lett. **78**, 1134 (1997).
23. Chrissey, D. B., *et al.*, IEEE Trans. Appl. Supercond. **7**, 2067 (1997).
24. Dong, Z. W., *et al.*, Appl. Phys. Lett. **71**, 1718 (1997).
25. Yeh, N.-C., *et al.*, submitted to Phys. Rev. Lett. (1998).
26. Wei, J. Y. T., *et al.*, J. Appl. Phys. **85** (1999).
27. Abrikosov, A. A. and Gor'kov, L. P., Sov. Phys. JETP **12**, 1243 (1961).

RELATED COMPOUNDS THEORY

Possibility of High Temperature Superconductivity in C_{36} and $C_{24}N_{12}$ Solids

Marvin L. Cohen

*Department of Physics, University of California, and
Materials Sciences Division, Lawrence Berkeley National Laboratory
Berkeley, CA 94720-7300*

Abstract. Some preliminary discussion is presented concerning predicting superconductivity in general and the properties of existing fullerene superconductors. This is followed by a consideration of the likelihood of superconductivity in C_{36} solids. Our present knowledge about C_{36} and the similar molecule $C_{24}N_{12}$ is reviewed along with the relevant arguments used as a basis for suggesting that these systems are good candidates for superconductivity at relatively high temperatures.

INTRODUCTION

It took 46 years to achieve a successful theory of superconductivity (1) after the discovery (2) of the phenomenon. Now it is generally accepted that the so-called conventional superconductors such as Pb, Hg, or Al are well understood using this BCS theory. In contrast, the high temperature superconducting oxides (HTSO) have been around (3) since 1986, and there is still no consensus regarding the underlying theory. At this point, only the HTSO systems are superconducting above liquid nitrogen temperatures, while the so-called conventional superconductors have much lower transition temperatures.

The purpose of this work is to consider the possibility of superconductivity in fullerene systems at high temperatures assuming the BCS theory based on overlapping pairs of electrons where the pair binding is caused by electron-lattice interactions. Although this goal appears to be a straight-forward application of proven theory, even when the BCS theory is an appropriate description of a superconductor, a calculation of the transition temperature T_c is still difficult. In fact, an early criticism of the BCS theory itself was the fact that predicting T_c was very difficult because of the exponential dependence of T_c on the pairing interaction. If calculating T_c or predicting new superconductors using BCS theory had been the only criteria for establishing its validity, it would have taken much longer to demonstrate the correctness of the BCS description of the superconducting state and the mechanism responsible for superconductivity.

PREDICTING SUPERCONDUCTING TRANSITION TEMPERATURES

In principle, it was not the theory of superconductivity itself which needed refinement to compute accurate T_c 's, although extensions of the theory were important. The problem in evaluating T_c was principally limited by not having a sufficiently precise theoretical description of the normal state properties of solids. Now, the so-called "standard model of solids" (4) which is applicable to a wide variety of metals, semiconductors, and insulators allows calculations of electronic properties and electron-lattice interactions. A popular form of this approach (4) involves pseudopotentials and density functional theory, the pseudopotential density functional method (PDFM).

Although the Coulomb repulsion parameter, μ or μ^* , is normally left as a scaling parameter, in recent years even it has been evaluated from first principles for special cases (5).

Calculating T_c requires good descriptions of the phonon spectrum, electron-phonon spectral function $\alpha^2F(\omega)$, and the electronic band structure. The outputs of the full calculations can be characterized by the electron-phonon coupling parameter λ , μ^* , and an appropriate average phonon frequency $\langle\omega\rangle$. These parameters can then be used in a BCS, McMillan (6), or Kresin-Barbee-Cohen (7,8) type expression for T_c , or Eliashberg (9) theory can be used directly. In early predictions of T_c , experimental input was used to make the estimates. Superconducting degenerate semiconductors (10) were particularly useful systems to study in this way because the band parameters had been measured. Examples (11,12) include GeTe, SnTe, and SrTiO₃. Here, BCS theory could be employed with good estimates of normal state parameters. Later, theoretical work on high pressure phases of Si not only correctly predicted (13) superconductivity in ph and hcp metallic Si, it could predict the existence of high pressure phases and their electronic and vibrational properties. Successful results for GaAs (14), Nb₃Nb (15), and S (16) at high pressures are further examples. There were also several "after the fact" calculations for known superconductors which gave excellent agreement with experiment using first principles theory. However, these calculations tend to be less effective in convincing skeptics about the robustness of the theory than the ones above where theory preceded experiment.

After the discovery (17) of superconductivity in C₆₀ systems, there was concern about whether BCS theory was appropriate for these materials. In fact, there was concern about whether the "standard model" could be applied to these systems and whether band theory was appropriate. It was argued that strong electron correlation would not only invalidate the band model, but it might also lead to an electronic mechanism for pairing and superconductivity. The consensus now appears to be that both band theory and the usual BCS approach are sufficiently robust to account for the observed properties of M₃C₆₀ (where M represents an alkali metal). Band calculations (18) including quasiparticle "GW" corrections give results consistent with optical and photoemission experiments. And superconducting and normal state transport properties (19) such as resistivity are consistent with an electron-phonon mechanism both for scattering and for electron-electron pairing even for T_c in the 20-40 K range.

CALCULATIONS FOR FULLERENES

The contrast between the T_c of intercalated graphite and M_3C_{60} immediately attracted the attention of theorists because of the two orders of magnitude increase in T_c for the C_{60} systems. Analysis of the characteristic parameters λ , μ^* , and $\langle\omega\rangle$ led to the conclusion that of the three it was an increase in λ that was primarily responsible for the increase in T_c . Specifically, it has been proposed (20) that the increase in the electron-phonon matrix element V_{ep} results from the curvature change in going from graphite to C_{60} . The expression for V_{ep} has the form

$$V_{ep} = \sum_{\alpha} \frac{1}{M\omega_{\alpha}^2} \frac{1}{g^2} \sum_{i,j=1}^g |\langle i | \epsilon_{\alpha} \cdot \nabla V | j \rangle|^2 \quad (1)$$

where ϵ_{α} is the polarization vector, V is the electron-ion potential, i and j label electronic states, ω_{α} is the phonon frequency, and g is the degeneracy of the electronic states. For a phonon with polarization which causes distortions perpendicular to the graphite sheet, the matrix elements between even or odd states vanish because the ∇V term is odd under reflection. The curvature allows the σ and π (or σ^* and π^*) electronic states to mix and allows even terms in the change in the potential resulting in non-zero values for V_{ep} . Calculations of V_{ep} by various authors (21,22) yield consistent results for K_3C_{60} .

Hence, the general picture for superconductivity in the M_3C_{60} systems is one in which the outermost valence electrons donated by the metal atoms form a nearly free electron sea of charge which interacts with the vibrations of the C_{60} molecule. Although intermolecular vibrations contribute to the electron-phonon induced pairing, it is the intramolecular vibrations which dominate. Clearly, the Coulomb parameter μ^* which has the form

$$\mu^* = \frac{\mu}{1 + \mu \ln \frac{\langle\omega\rangle}{E_F}} \quad (2)$$

will differ from its value in common metals because of the small ratio of $\langle\omega\rangle$ to the Fermi energy E_F and the more localized nature of the bands. Arguments related to strong peaks in the density of states causing enhancement of λ or μ are usually weak because the same peaks arise in the screening functions and cancel out the enhancements. Other characteristics which add credence to the electron-intramolecular phonon model for pairing is the near constancy of the pressure dependence of T_c (23) and the absence of an isotope effect for the alkali metal atom (24). At first, a range of isotope effect parameters were measured for the carbon atom, but now the results appear consistent with the standard theoretical model.

Moving from C_{60} to tubes, one can again state that currently the "standard model" is generally accepted as appropriate for describing the electronic and structure properties of carbon nanotubes. In fact, it has been used successfully to predict (25,26,27) the existence of $B_xC_yN_z$ compound nanotubes. At present, however, superconductivity in tubes has not been observed. Theoretical investigations (28) based on models for tubes

suggest modest T_c 's. For example, these studies argue that if a generic electron-phonon pairing potential U is broken into a flat component U_{flat} appropriate for graphite and a curved contribution, then the total U should scale approximately with the radius of curvature for balls and tubes as follows:

$$U_{\text{ball}} = U_{\text{flat}} + U_{\text{curve}} \left(\frac{R_0}{R} \right)^2 \quad (3)$$

and

$$U_{\text{tube}} = U_{\text{flat}} + \frac{1}{4} U_{\text{curve}} \left(\frac{R_0}{R} \right)^2 \quad (4)$$

where U_{curve} is the curvature contribution corresponding to a ball of radius R_0 . Using Eq. (4) and arguments about appropriate densities of states and phonon frequencies, T_c (R) can be computed (28) for tubes. The curve asymptotically goes to the T_c value for intercalated graphite at large R and increases to modest T_c 's below $R \sim 10 \text{ \AA}$.

An interesting variation on the idea of starting with a graphite sheet and investigating the effects of curvature is to begin with a monolayer sheet of carbon atoms with the graphite hexagons replaced by five-fold and seven-fold rings. The proposal (29) that a system of this type could be made predicts that this pure carbon planar system is a metal. This is the case even though it might be expected that the reduction in symmetry going from an all hexagon arrangement to a plane of heptagons and pentagons would change the graphite sheet band structure from semimetal to insulating since, in a graphite sheet, the π and π^* bands touch at the Fermi surface at a point in the Brillouin zone. The finite density of states at E_F and the fact that one expects comparable parameters to the fullerene superconductor suggests that this system would be a superconductor, but no enhancement in T_c is expected from bending the "5-7" sheets into tubes because of the σ - π mixing arguments. However, deviations from sp^2 bond angles in the plane increase the electron-phonon interaction compared to graphite, and doping effects may be interesting leading to an MC_4 type system for alkali metals.

C₃₆ AND C₂₄N₁₂

Studies of mass spectra of carbon clusters have demonstrated the sensitivity of the results to experimental conditions. It is possible to have varying ratios of abundance. The large C₆₀ and C₇₀ peaks initially focused research on these systems. However, motivated by the arguments above regarding curvature, it is reasonable to search for smaller molecules in this class since roughly speaking they will have higher curvature when forming a solid and then doped. Two interesting candidates are C₃₂ and C₃₆. Here, we focus on C₃₆ and also briefly consider the analogous compound molecule C₂₄N₁₂.

Using Euler's arguments, C₃₆ will have 12 pentagons. Since the regions of the molecules near the pentagons are more chemically reactive than those near the hexagons, C₃₆ will be proportionally more reactive than C₆₀. In fact, it is suggested that while C₆₀ is van der Waals-like, C₃₆ may be a more covalent-like molecule when thought of as a component in forming clusters or solids.

There are many choices for the structural arrangement of the atoms in C₃₆. An energetically favorable arrangement is the D_{6h} structure which is also conducive for forming crystals. In this arrangement, there is a hexagon on the "top" (and "bottom")

caps of the molecule with 6 pentagons forming below (and above) the caps yielding the 12 required by Euler. These caps fit together with an additional 6 hexagons around the "belly" of the molecule. The result is a "football" shaped molecule which would be expected to stack differently when forming a solid than the more spherical C_{60} molecule. The pseudopotential density functional method (PDFM) was used (30) to calculate equilibrium geometries, total energies, electronic charge densities, and electron affinities for C_{36} and N-substitutional doping. For the N-doped cases, the changes in bond lengths and in particular the substantial shortening of the sp^2 c-c bond when it is trapped between four nitrogens is explained in terms of an inhibition of the carbon π bonds to forming sp^2 networks.

Relying on the results of the PDFM, which suggest that the D_{6h} symmetry for the C_{36} molecule is a good candidate structure, various stacking sequences become possible. Unlike the C_{60} case, where the more spherical molecules are expected and found to stack in ABC close packing of van der Waals spheres (leading to an fcc lattice), the C_{36} molecules stacked this way would lead to a rhombohedral arrangement. Another similar stacking sequence (ABAB) leads to a crystal with hexagonal symmetry which appears to have lower energy than the rhombohedral case. However, studies of the differences in the ease of dimerization of C_{36} molecules suggest (31) other arrangements with even lower energy involving the stacking of planes of hexagonal arrangements of well-separated or bonded C_{36} molecules. For C_{60} , dimers are formed after being photoexcited and the solid forms require pressure to polymerize. However, alkali doped C_{60} polymerizes spontaneously. The situation for C_{36} is different. The PDFM calculations indicate that C_{36} may have spontaneous polymerization without doping and doping may inhibit this effect.

Using the above arguments, a likely candidate for the crystal structure of C_{36} molecules in the solid form is a structure formed by stacking hexagonal planes of bonded C_{36} molecules in an AB stacking sequence called (31) S2-AB. The electronic structure of this arrangement and the expected changes arising from Na and K doping leading to Na_2C_{36} and K_2C_{36} have been examined (31) in some detail. The experimental situation is progressing (32,33) in this area, but definitive results on the molecular and crystal structure are not yet available.

Returning to the question of superconductivity, the first attempt to estimate T_c would be to invoke the curvature arguments presented earlier. These estimates were done first (34) for K_3C_{60} with Eq. (3) as a model yielding $U_{total} \approx 1.1 + 140/N$ eV-atom (normalized to one atom with the density of states universally proportional to the volume). This leads to $\lambda \approx 0.3$ for doped graphite in the $N \rightarrow \infty$ limit and $U \approx 57$ meV - C_{60} and $\lambda \approx 1$ for the C_{60} system. For C_{36} , this formula gives $U \approx 140$ meV - C_{36} in reasonable agreement with the *ab initio* results discussed below. It should be emphasized that this estimate is based on simple scaling arguments and as the *ab initio* results demonstrate there are many subtle contributions to the increase in λ in going from the K_3C_{60} like system to C_{36} based solids.

The estimates (21) of the electron-phonon properties and T_c 's were made using *ab initio* theory based on the PDFM, but for computational convenience the D_{6h} molecules were assumed to be in a rhombohedral lattice. If the model appropriate to C_{60} with nearly free electrons interacting with intraball vibrations is applicable to the C_{36} case, then structural changes are not critical. However, the studies of N_2C_{36} and K_2C_{36} do suggest possible variations in this model with some covalency. At this point, the assumption of the C_{60} like model is useful for estimating changes.

Even though there is excellent agreement between the current electron-phonon coupling calculations for the C_{60} case, it is still more prudent to assume that ratios of calculated parameters between C_{60} and C_{36} are more predictive than absolute calculations for the C_{36} system since the M_3C_{60} materials are known superconductors. Hence, for estimating T_c , the density of states at E_F , $N(0)$, is assumed to be comparable to the C_{60} case. Also, the estimate (21) of $\mu^* \approx 0.25$ using experimental data on M_3C_{60} is assumed to be appropriate. These values yield a $T_c = 18$ K for K_3C_{60} . If the PDFM calculational approach is used for C_{36} in the same way as for C_{60} and the above $N(0)$ and μ^* parameters are assumed, then the solution of the Eliashberg (9) equations yield $T_c(C_{36}) \approx 6T_c(C_{60})$.

SUMMARY AND CONCLUSIONS

The general goal presented here is to explore systems in addition to the copper oxides which have the potential of exhibiting superconductivity above the boiling point of nitrogen. Since the fullerenes do have relatively high T_c 's, they appear to be a good family of materials to explore. After a description of the current status of calculating and predicting T_c for materials, a description of the nanotube and C_n molecules was presented. The focus on C_{36} as a prototype suggests that simple estimates based on scaling and *ab initio* theory give values of T_c in the range of temperatures near the boiling point of nitrogen. Because of the chemical changes resulting in shortened bonds in going from C_{36} to $C_{24}N_{12}$, it is expected that metallic solids based on the latter molecule may yield even higher T_c 's.

ACKNOWLEDGMENTS

I would like to thank Dr. Jeffrey C. Grossman for helpful discussions and Professor Vincent H. Crespi for a preprint of his work. This work was supported by National Science Foundation Grant No. DMR-9520554 and by the Director, Office of Energy Research, Office of Basic Energy Sciences, Materials Sciences Division of the U.S. Department of Energy under Contract No. DE-AC03-76SF00098.

REFERENCES

1. Bardeen, J., Cooper, L. N., and Schrieffer, J. R., *Phys. Rev.* **108**, 1175 (1957).
2. Kamerlingh Onnes, H., *Akad. Van Wetenschappen* (Amsterdam) **14**, 113 (1911).
3. Bednorz, J. G. and Müller, K. A., *Z. Phys. B* **64**, 189 (1986).
4. Cohen, M. L., *Physica Scripta* **T1**, 5 (1982).
5. Lee, K.-H., Chang, K. J., and Cohen, M. L., *Phys. Rev. B* **52**, 1425 (1995).
6. McMillan, W. L., *Phys. Rev.* **167**, 331 (1968).
7. Krezin, V. Z., *Bull. Am. Phys. Soc.* **32**, 796 (1987).
8. Bourne, L. C., Zettl, A., Barbee III, T. W., and Cohen, M. L., *Phys. Rev. B* **36**, 3990 (1987).

9. Eliashberg, G. M., *JETP* **11**, 696 (1960).
10. Cohen, M. L., *Phys. Rev.* **134**, A511 (1964).
11. Cohen, M. L., Tung, Y., and Allen, P. B., *J. Phys. (Paris)* **29**, 163 (1968).
12. Schooley, J. F., Hosler, W. R., and Cohen, M. L., *Phys. Rev. Lett.* **12**, 474 (1964).
13. Chang, K. J., Dacorogna, M. M., Cohen, M. L., Mignot, J. M., Chouteau, G., and Martinez, G., *Phys. Rev. Lett.* **54**, 2375 (1985).
14. Chen, A. L., Lewis, S. P., Su, Z., Yu, P. Y., and Cohen, M. L., *Phys. Rev. B* **46**, 5523 (1992).
15. Pickett, W. E., Ho, K. M., and Cohen, M. L., *Phys. Rev. B* **19**, 1734 (1979).
16. Zakharov, O., and Cohen, M. L., *Phys. Rev. B* **52**, 12572 (1995).
17. Hebard, A. F., Rosseinsky, M. J., Haddon, R. C., Murphy, D. W., Glarum, S. H., Palstra, T. T. M., Ramirez, A. P., and Kortan, A. R., *Nature* **350**, 600 (1991).
18. Shirley, E. L., and Louie, S. G., *Phys. Rev. Lett.* **71**, 133 (1993).
19. Cohen, M. L. and Crespi, V. H., in Billups, W. E., and Ciufolini, M. A. (Eds.), *Buckminsterfullerenes*, New York: VCH Publishers, 1993, p. 197.
20. Martins, J. L., *Europhys. News* **23**, 31 (1992).
21. Côté, M., Grossman, J. C., Cohen, M. L., and Louie, S. G., *Phys. Rev. Lett.* **81**, 697 (1998).
22. Antropov, V. P., Gunnarsson, O., and Liechtenstein, A. I., *Phys. Rev. B* **48**, 7651 (1993).
23. Crespi, V. H., and Cohen, M. L., *Phys. Rev. B* **53**, 56 (1996).
24. Burk, B., Crespi, V. H., Zettl, A., and Cohen, M. L., *Phys. Rev. Lett.* **72**, 3706 (1994).
25. Rubio, A., Corkill, J. L., and Cohen, M. L., *Phys. Rev. B* **49**, 5081 (1994).
26. Miyamoto, Y., Rubio, A., Cohen, M. L., and Louie, S. G., *Phys. Rev. B* **50**, 4976 (1994).
27. Miyamoto, Y., Rubio, A., Louie, S. G., and Cohen, M. L., *Phys. Rev. B* **50**, 18360 (1994).
28. Benedict, L. X., Crespi, V. H., Louie, S. G., and Cohen, M. L., *Phys. Rev. B* **52**, 14935 (1995).
29. Crespi, V. H., Benedict, L. X., Cohen, M. L., and Louie, S. G., *Phys. Rev. B* **53**, R13303 (1996).
30. Grossman, J. C., Côté, M., Louie, S. G., and Cohen, M. L., *Chem. Phys. Lett.* **284**, 344 (1998).
31. Grossman, J. C., Louie, S. G., and Cohen, M. L., to be published.
32. Piskoti, C., Yarger, J., and Zettl, A., *Nature* **393**, 771 (1998).
33. Collins, P. G., Grossman, J. C., Côté, M., Ishigami, M., Piskoti, C., Louie, S. G., Cohen, M. L., and Zettl, A., *Phys. Rev. Lett.* **82**, 165 (1999).
34. Crespi, V. H., to be published.

Electronic Characteristics of Quasi-2D Metallochloronitrides: Na_xHfNCl ($T_c=25$ K)

R. Weht, A. Filippetti, and W. E. Pickett

Department of Physics, University of California, Davis CA 95616

Abstract. Local density functional results are presented for the electron-doped metallochloronitrides $A_x\text{ZrNCl}$ and $A_x\text{HfNCl}$, $A=\text{Li}$ or Na , which superconduct up to 25K. The alkali non-stoichiometry is treated in a virtual crystal approximation. The electronic structure is strongly two dimensional, especially in the conduction band region occupied by the carriers, because the states are formed from the in-plane orbitals d_{xy} , $d_{x^2-y^2}$ of the metal ion and the p_x, p_y orbitals of the N ion. We predict a change of behavior at a doping level of $x=0.3$.

INTRODUCTION

High temperature superconductivity (HTS) in the layered cuprates continues to puzzle even after a dozen years of intense scrutiny. Even outside of the class of HTSs, however, the appearance of high T_c (in the pre-cuprates sense) also is baffling. The highest T_c is achieved in the fullerenes, with $T_c=40$ K reported, [1] which are three dimensional (3D) materials with, however, a great deal of zero dimensional (cluster) character. $T_c \sim 35$ K is achieved in $\text{Ba}_{1-x}\text{K}_x\text{BiO}_3$, also a 3D system, with only some flat portions of Fermi surface to bring in questions of low dimensionality. There is not yet any clear theoretical accounting for the magnitude of T_c in these two systems [2,3] although some phonon modes in the fullerenes are strongly coupled to the conduction electrons. The A15 superconductors (T_c up to 23 K) present a class in which the relatively high value of T_c is understood in terms of strong electron-phonon coupling and a high density of states (DOS) $[N(E_F)]$ at the Fermi level E_F . [4]

A new, 2D material has recently been added to the list of (non-HTS) superconductors with unusually high T_c . Yamanaka *et al.* [5] discovered superconductivity up to 12 K in Li-doped ZrNCl , and up to 25.5 K in Na-doped HfNCl . [6] Shamoto *et al.* [7,8] have reproduced the superconductivity and determined the crystal structure of superconducting materials using synchrotron X-ray diffraction data. We provide here the first calculation of the electronic structure of this system, considering in particular variation with doping level.

DESCRIPTION OF CALCULATIONS

Electronic Structure Methods

We have applied the local density approximation [9] using two methods: the linearized augmented plane wave (LAPW) method [10] for the bands and density of states (DOS) that we show, and the plane wave ultrasoft pseudopotential method [11] for the phonon frequencies. Both methods produced essentially the same band structures.

To account for the doping we have used a virtual crystal treatment. For example, for x fractional occupancy of a site by Na (ten core electrons and one valence electron), that site is fully occupied by a nucleus of charge $10+x$ with the corresponding number of electrons. As expected, Na is ionized with the electrons going into bands that are primarily metal d bands, so the virtual crystal treatment should be reasonable. We will find that it is important to treat this charge self-consistently, because non-rigid-band behavior appears not far from the region of immediate interest.

Structure

We have used the structures of Shamoto *et al.* [7,8] for these materials. Because a Cl-HfN-HfN-Cl slab is only weakly coupled to its neighboring slabs, we expect that the stacking sequence (for example, whether hexagonal or rhombohedral) is not important, and indeed that was found to be the case. One such structure is shown in Fig. 1, and the slab structure is the same for Hf and Zr, with only the stacking sequence varying with doping. [12]

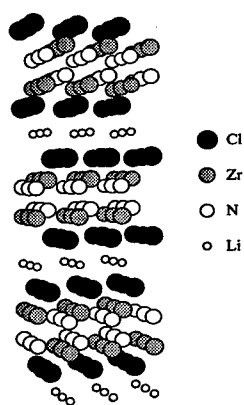


FIGURE 1. Rhombohedral structure of Li_xZrNCl determined by Shamoto *et al.* [7,8] The stacking along c can change with doping, but the basic slab structure is unchanged with doping. Li sites are only fractionally occupied

DISCUSSION OF RESULTS

The band structures are strongly two dimensional, so we discuss only the in-plane dispersion here. The undoped compounds have a band gap of 1.7-1.8 eV, between valence bands that are $2p$ states of Cl and N, and conduction states that are mostly Hf or Zr. Thus the formal ionic description $(\text{Hf,Zr})^{4+}\text{N}^{3-}\text{Cl}^-$ is reasonable, but obscures the strong metal-N hybridization.

In Fig. 2 the band structure of $\text{Na}_{0.25}\text{HfNCl}$ is shown along the hexagonal symmetry directions. Only a single band is occupied by the doped carriers, and the band structure is very similar to that of the undoped compound, *i.e.* a rigid band picture is good. The projected DOS of Fig. 3 illustrates several things: (1) the occupied band is a hybridized planar band of Hf $d_{xy}, d_{x^2-y^2}$ and N p_x, p_y character; (2) Hf d_{xz}, d_{yz} and N p_x character do not appear until the band flattening 0.3

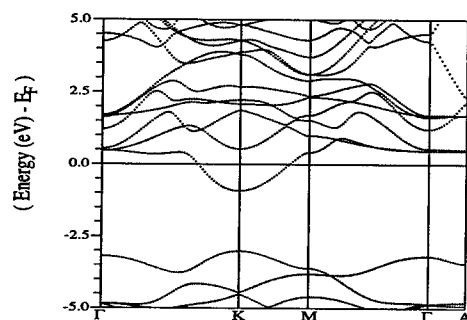


FIGURE 2. Plot along symmetry lines of the band structure of $\text{Na}_{0.25}\text{HfNCl}$. Points are $\Gamma = (0, 0, 0)$, $K = (2/3, 1/3, 0)$, $M = (1/2, 0, 0)$, $A = (0, 0, 1/2)$, in units of the hexagonal reciprocal lattice vectors. The lack of dispersion along Γ -A of the lower conduction bands reflects the strong 2D character of the important conduction band.

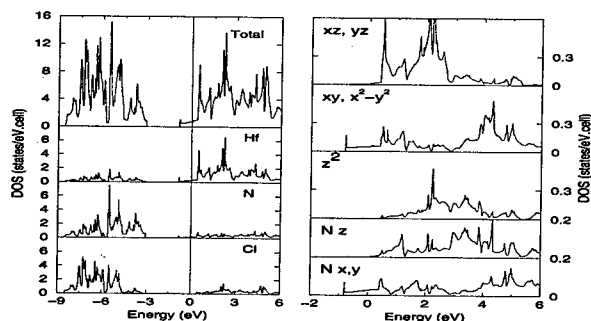


FIGURE 3. Atom (left panel) and orbital (right panel) projected DOS for $\text{Na}_{0.25}\text{HfNCl}$. In the right panel only the conduction bands are pictured.

eV above E_F in Fig. 2; (3) the Hf d_{z^2} character is higher still. This behavior is completely different from what Woodward and Vogt [13] calculated for a bilayer structure reported by Juza and collaborators, [14] in which two Hf ions are bonded across the bilayer, rather than the Hf-N bonding across the bilayer as in the structure determined by Shamoto. Thus electrons are not doped into a very flat band, which almost certainly would be strongly correlated, but rather into a broad band with a light mass $m^* \approx 0.6m$.

The other material parameters we obtain (for $x=0.25$) are

- Fermi velocity $v_F = 3 \times 10^7$ cm/s
- Drude plasma energy $\Omega_p = [4\pi e^2 N(E_F) v_{F,x}^2]^{1/2} = 1.5$ eV
- Gap $2\Delta \approx 3.5 k_B T_c \approx 7.5$ meV
- Coherence length $\xi = \frac{\hbar v_F}{\pi \Delta} \approx 180$ Å
- London penetration depth $\Lambda = \frac{c}{\Omega_p} = 1300$ Å
- $\kappa = \Lambda/\xi = 7 \rightarrow$ Type II superconductor.

In Fig. 4 we present the Fermi surface for $x=0.25$ doping level. It consists of threefold distorted circles at the zone corner (K) points. There are two inequivalent such points, each with mean radius $k_F = \frac{2}{9} \frac{\pi}{a}$. On-Fermi-surface scattering processes will be dominated by (1) small $Q \leq 2k_F$ intraband scattering, and (2) large $Q \sim K$ interband scattering. [Note that the vector connecting two neighboring zone corners K is also the vector K.]

We have calculated the frequencies of the three fully symmetric (A_{1g}) Raman active vibrational modes of pristine ZrNCl and HfNCl at the zone center, corresponding to modulation of the internal coordinates $z_{Zr/Hf}$, z_N , z_{Cl} . The frequencies are 586, 334, and 202 cm^{-1} and 604, 368, and 191 cm^{-1} respectively for the two compounds. The highest frequency is almost pure N motion.

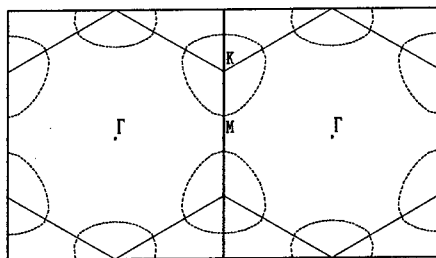


FIGURE 4. Plot of the distorted circular Fermi surface of $Na_{0.25}HfNCl$ shown in two hexagonal Brillouin zones. The surface is centered at the zone corner point K; since there are two such inequivalent points, there are two Fermi surfaces.

DOPING

As these systems are studied further, the question of the effect of doping will be very important. We have performed virtual crystal calculations for several doping levels, with results for $x = 0.25, 0.35$ and 0.45 shown in Figure 5. There are continuous rigid-band-like changes up to just above $x = 0.30$, above which bands with different character (specifically, out of plane orbitals) begin to become occupied. At this point in doping the properties should show a change in slope (plotted versus x). At $x=0.35$ E_F coincides with a band that is very flat band along Γ -K and has a small mass along Γ -M as well, *i.e.* a peak in the density of states. This range of doping should prove very interesting, and whether T_c rises or falls will reveal important characteristics of the pairing mechanism.

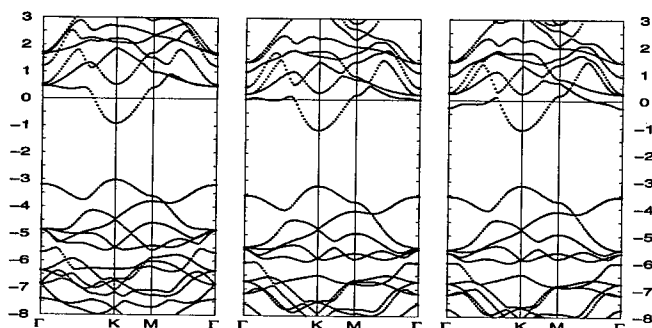


FIGURE 5. Band structure plots of Na_xHfNCl , for $x=0.25, 0.35$, and 0.45 (left to right). Around $x=0.35$ the Fermi level enters a region where the bands have different character, and already the conduction band dispersion is visibly non-rigid-like. At $x=0.45$ there is a large Fermi surface centered at Γ as well as the ones at K.

SUMMARY AND ACKNOWLEDGMENTS

It is surprising that such low mass, low DOS materials such as those described here can superconduct up to 25 K. Since there is no indication, experimentally or theoretically, of strong correlation effects in the range of doping reported by the superconductors, a possible candidate for pairing mechanism could be phononic. Given the 2D character and the strong nesting that might introduce characteristics of 1D behavior, purely electronic pairing mechanisms should also be considered. Given the apparent extreme two dimensionality of the crystal, it will be important to establish that coherent supercurrent actually will flow perpendicular to the layers.

We are indebted to R. Seshadri for many communications on the ZrNCl system, to comments from D. J. Scalapino, and to S. Shamoto for communication of unpublished work including structural data. This research was supported by Office

of Naval Research Grant No. N00014-97-1-0956 and National Science foundation Grant DMR-9802076.

REFERENCES

1. S. C. Erwin and W. E. Pickett, *Science* **254**, 842 (1991); S. C. Erwin, in *Buckminsterfullerines*, edited by W. E. Billups and M. A. Ciufolini (VCH Publ., Cambridge, U.K., 1993), 217.
2. O. Gunnarsson, *Rev. Mod. Phys.* **69**, 575 (1997).
3. V. Mereghalli and S. A. Savrasov, *Phys. Rev. B* **57**, 14453 (1998).
4. B. M. Klein and W. E. Pickett, in *Superconductivity in d- and f- Band Metals*, edited by W. Bckel and W. Weber (Kernforschungszentrum, Karlsruhe, 1982), 97.
5. S. Yamanaka, H. Kawaji, K. Hotehama and M. Ohashi, *Adv. Mater.* **8**, 771 (1996).
6. S. Yamanaka, K. Hotehama and H. Kawaji, *Nature* **392**, 580 (1998).
7. S. Shamoto, T. Kato, Y. Ono, Y. Miyazaki, K. Ohoyama, M. Ohashi, Y. Yamaguchi and T. Kajitani, *Physica C* **306**, 7 (1998).
8. S. Shamoto, T. Kato, Y. Ono, Y. Miyazaki, K. Ohoyama, M. Ohashi, Y. Yamaguchi and T. Kajitani, *J. Phys. Chem. Solids* (1998, in press).
9. D. M. Ceperley and B. J. Alder, *Phys. Rev. Lett.* **45**, 566 (1980), as parametrized by J. P. Perdew and Y. Wang, *Phys. Rev. B* **45**, 13244 (1992) or by Vosko, Wilk and Nusair, *Can. J. Phys.* **58**, 1200 (1980).
10. P. Blaha, K. Schwarz, and J. Luitz, WIEN97, Vienna University of Technology, 1997. Improved and updated version of the original copyrighted WIEN code, which was published by P. Blaha, K. Schwarz, P. Sorantin, and S. B. Trickey, *Comput. Phys. Commun.* **59**, 399 (1990). The sphere radii used in fixing the LAPW basis were chosen to be 2.00 a.u for Hf(Zr), Cl, and alkali atoms, and 1.90 for N. Local orbitals (Zr 3s, 3p; Hf 3s, 3p, 4f; N and Cl 2s) were added to the basis set for extra flexibility and to allow semicore states to be treated within the same energy window as the band states. The LAPW plane wave cutoff corresponded to energy of 17.7 Ryd.
11. D. Vanderbilt, *Phys. Rev. B* **32**, 8412 (1985); K. Laasonen, A. Pasquarello, R. Car, Changyol Lee, and D. Vanderbilt, *Phys. Rev. B* **47**, 10142 (1993). More discussion of the method, and an example of the use of the N pseudopotential, is given by A. Filippetti, W. E. Pickett and B. M. Klein, *Phys. Rev. B* (in press) [cond-mat/9808266].
12. For $\text{Na}_{0.29}\text{HfNCl}$ the structure is rhombohedral $R\bar{3}m$ (#166), with $a=3.5892$ Å, $c=29.722$ Å. Internal coordinates for the atoms (each in 6c sites) are $z_{\text{Hf}}=0.2083$, $z_{\text{N}}=0.1368$, $z_{\text{Cl}}=0.3944$. Na was refined in the 3a site at the origin. $\text{Li}_{0.16}\text{ZrNCl}$ is isomorphous, with $a=3.60$ Å being slightly larger.
13. P. M. Woodward and T. Vogt, *J. Solid State Chem.* **138**, 207 (1998).
14. V. R. Juza and J. Heners, *Z. Anorg. Allg. Chem.* **332**, 159 (1964); V. R. Juza and H. Friedrichsen, *ibid.* **332**, 173 (1964).

p-wave superconductivity in Sr_2RuO_4

H. Won^a, K. Maki^b, E. Puchkaryov^b & G. F. Wang^b

^a *Department of Physics and IRC, Hallym University
Chuncheon 200-702, South Korea*

^b *Department Physics & Astronomy, University of Southern California
Los Angeles, CA 90089-0484*

Abstract. The superconductivity in both Sr_2RuO_4 and Bechgaard salts is most likely of p-wave. Here we review the effect of impurity scattering and the features of the vortex state in p-wave superconductors. There are striking similarities between those properties in p-wave superconductors and the ones in d-wave superconductors.

I INTRODUCTION

The confirmation of d-wave superconductivity in the hole doped high T_c cuprate superconductors has naturally strong repercussion [1,2]. We believe now the majority of heavy fermion superconductors and organic superconductors are unconventional. That is they are of non-s-wave pairing and originated from magnetic interaction (i.e exchange of paramagnon and/or antiparamagnon) [3,4]. In this background the discovery of p-wave superconductivity in Sr_2RuO_4 [5] and Bechgaard salts [6] will be no big surprise. We shall review here how p-wave superconductivity in Sr_2RuO_4 and Bechgaard salts is established. Then we go on to describe the effect of impurity scattering [7] and the upper critical field in the vortex state [8,9].

Sr_2RuO_4 is a perovskite and has the same crystal structure as La_2CuO_4 [5]. However unlike La_2CuO_4 , Sr_2RuO_4 is metallic and behaves like standard Fermi liquid below 20K, though the system is very anisotropic. Further it becomes superconducting with $T_c=1.2\sim 1.5\text{K}$. The strong sensitivity of T_c to the impurity concentration is well documented [10]. In particular the superconductivity disappears when the electron mean free path within the a-b plane becomes shorter than about one micron.

The growing evidence indicates the superconductivity is of p-wave. The Knight shift in NMR experiments indicate clearly the spin triplet pairing in Sr_2RuO_4 [11] very similar to the A phase in superfluid ^3He where now the \vec{d} vector is parallel to the c axis. Further T_1^{-1} in NMR does not exhibit the Hebel-Slichter peak but

drops precipitously at $T=T_c$ [12]. This behavior can be only interpreted in terms of isotropic p-wave pairing and strong paramagnon contribution [13].

The third piece of evidence is the electronic specific heat which behaves like that for a s-wave superconductors if we subtract a T-linear term as in the normal state [14,15]. In earlier experiments the coefficient of this additional T-linear term γ_0 was somewhat larger than $\frac{1}{2}\gamma_N$ where γ_N the same coefficient in the normal state. This leads to the proposal of non-unitary p-wave state [16]. However, since the most recent data [15] indicates $\gamma_0 \leq \frac{1}{4}\gamma_N$, the non-unitary state is untenable. Therefore we adapt here the three orbital band model proposed by Agterberg *et al* [17], where it is assumed that the superconductivity resides principally in the γ band. Although superconductivity in the α and β band is not unknown, we neglect at the present moment completely the superconductivity in the α and β band for simplicity [9]. Of course we may need to consider the contribution from the α and β band as well in the future. So in the following we concentrate to the superconductivity in the γ band only. Then the superconducting order parameter is given by

$$\vec{\Delta}(\vec{k}) = \Delta \hat{d} e^{\pm i\phi}, e^{\pm i\phi} = \hat{k}_1 \pm i\hat{k}_2 \quad (1)$$

where \hat{d} is the unit vector presenting the spin component [18] and \vec{k}_1 and \vec{k}_2 are the quasi-particle moment within the a-b plane.

There is the convincing evidence that the same superconducting order parameter applies to Bechgaard salts as well [6,9].

II IMPURITY SCATTERING

In the absence of impurity scattering and in the absence of magnetic field, the thermodynamics of isotropic p-wave superconductivity is identical to the one in an s-wave superconductor. Also even in the presence of impurity, if the impurity scattering is weak we can describe many features of p-wave superconductors in the term of Abrikosov-Gor'kov theory [19] (i.e. magnetic impurity in s-wave superconductors). Therefore we consider the impurity scattering in the unitarity limit; the resonance scattering on the Fermi surface [7]. Then the renormalized frequency in the quasi-particle Green function is given by

$$\tilde{\omega} = \omega + \Gamma \frac{\sqrt{\tilde{\omega}^2 + \Delta^2}}{\tilde{\omega}} \quad (2)$$

where $\Gamma = n_i \pi N_0$ and n_i is the impurity concentration and N_0 is the quasi-particle density of states in the normal state per spin. See Ref[20] for an earlier analysis of Eq.(2).

Then the gap equation is given by

$$\lambda^{-1} = \frac{2\pi T}{\Delta} \sum_n' \frac{1}{\sqrt{1+u^2}} \quad (3)$$

where λ is the dimensionless coupling constant and the sum over the Matsubara frequency has to be cut off at $\omega_n = E_c$. Then putting $\Delta \rightarrow 0$, Eq(3) reduces to the well-known Abrikosov-Gor'kov formula

$$-\ln\left(\frac{T}{T_c}\right) = \psi\left(\frac{1}{2} + \frac{\Gamma}{2\pi T_c}\right) - \psi\left(\frac{1}{2}\right) \quad (4)$$

where $\psi(z)$ is the di-gamma function and T_c (T_{c0}) is the superconducting transition temperature in the presence(absence) of impurities. T_c vanishes at $\Gamma = \Gamma_c = \frac{1}{2}\Delta_{00}$, where Δ_{00} is the superconducting order parameter at $T=0K$ and in the absence of impurities. At $T=0K$ Eq(3) simplifies also and we obtain

$$-\ln\left(\frac{\Delta}{\Delta_{00}}\right) = \ln(C_0 + \sqrt{1 + C_0^2}) - \zeta(C_0^{-1} - \arctan(C_0^{-1})) \quad (5)$$

where $\zeta = \Gamma/\Delta$ and C_0 is defined as $C_0 = \frac{\tilde{\omega}}{\Delta}|_{\omega=0}$ or

$$C_0 = \left(\zeta\left(\sqrt{1 + \frac{\zeta^2}{4}} + \frac{\zeta}{2}\right)\right)^{\frac{1}{2}} \quad (6)$$

Here Δ is the order parameter at $T=0K$ but in the presence of impurities. Finally the residual density of states(i.e. the quasi-particle density of states on the Fermi surface) is given by

$$N(0)/N_0 = \frac{C_0}{\sqrt{1 + C_0^2}} = \sqrt{\frac{\zeta}{\frac{1}{2}\zeta + \sqrt{1 + \frac{\zeta^2}{4}}}} \quad (7)$$

Figure 1 shows T_c/T_{c0} , Δ/Δ_{00} and $N(0)/N_0$ as function of Γ/Γ_c . The similarity of these behaviors with the ones in the d-wave superconductors [21] is very striking. It is more so, since the quasi-particle density of states in the p-wave superconductors is

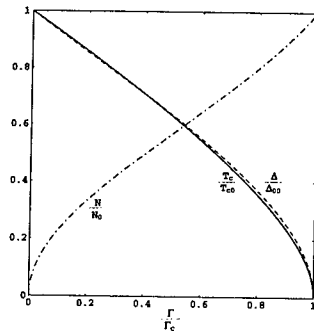


FIGURE 1. T_c/T_{c0} , Δ/Δ_{00} and $N(0)/N_0$ as function of Γ/Γ_c

very different from the one in d-wave superconductors . Figure 2 shows the density of states for a few Γ/Δ values. For a small amount of impurities a small island of the density of states develops around $E=0$. This island expands with Γ/Δ and finally it merges with the main part when $\Gamma/\Delta \simeq 0.38$. Also this low energy island controls both the low temperature and the low frequency response of the system.

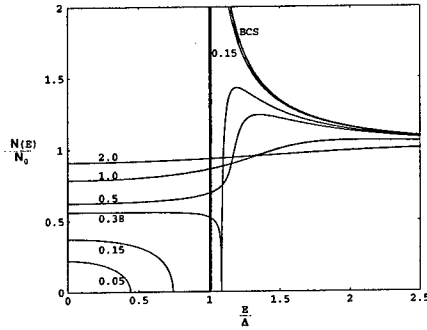


FIGURE 2. the density of states for a few Γ/Δ values

III UPPER CRITICAL FIELD FOR $\vec{B} \parallel \vec{c}$

The upper critical field in the presence of impurities is determined by [8,9]

$$-\ln t = \int_0^\infty \frac{du}{\sinh u} [1 - \exp(-\rho u^2 - \nu u) (1 + 2C\rho u^2)] \quad (8)$$

$$-C \ln t = \int_0^\infty \frac{du}{\sinh u} \{C - \exp(-\rho u^2 - \nu u) [\rho u^2 + C(1 - 4\rho u^2 + 2\rho^2 u^4)]\} \quad (9)$$

where $t = T/T_{c0}$, $\rho = v_F^2 e H_{c2}(T) / 2(2\pi T)^2$, $\nu = \Gamma/\pi T$. Here we took $\Delta(\vec{r}, \vec{k})$ given by

$$\Delta(\vec{r}, \vec{k}) \propto (e^{i\phi} + C(a^+)^2 e^{-i\phi})|0\rangle \quad (10)$$

and $|0\rangle$ is the reference Abrikosov state for an s-wave superconductor

$$|0\rangle = \sum_n C_n e^{inky} e^{-eB(x - \frac{nk}{2eB})^2} \quad (11)$$

and a^+ is the analog to the raising operator in a harmonic potential. The upper critical field and the coefficient C are obtained for a few Γ 's and shown in Fig. 3 and Fig. 4 respectively.

In particular at $T=0K$ Eq(8) and (9) reduces to

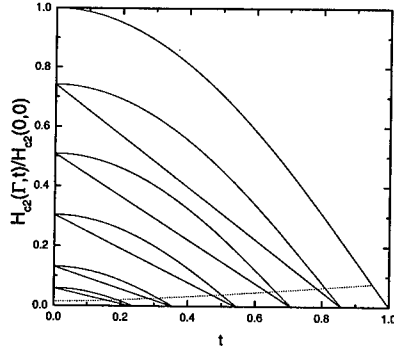


FIGURE 3. The upper critical field $h(\Gamma, t) = H_{c2}(\Gamma, t) / H_{c2}(0, 0)$ versus t . From up to down for $\Gamma/\Gamma_c = 0, 0.2, 0.4, 0.6, 0.8$ and 0.9 . The dot line represents the transition temperature from square vortex lattice to hexagonal one for different Γ

$$-\frac{1}{2} \ln\left(\frac{H_{c2}(\Gamma, 0)}{H_{c2}(0, 0)}\right) = \int_0^\infty \frac{du}{u} e^{-u^2} (1 - e^{-xu}) + C(0) - 2C \int_0^\infty du u e^{-u^2 - xu} \quad (12)$$

$$C = -(1 - X) + \sqrt{\frac{1}{2} + (1 - X)^2}, \quad X = \frac{\frac{1}{2} \int_0^\infty du u^3 e^{-u^2 - xu}}{\int_0^\infty du u e^{-u^2 - xu}} \quad (13)$$

and $C(0) = \frac{1}{2}(\sqrt{3} - 1)$, $x = \nu/\sqrt{\rho} = 2\sqrt{2}\Gamma(v_F^2 e H_{c2}(T))^{-\frac{1}{2}}$. Both $(T_c/T_{c0})^2$ and $H_{c2}(\Gamma, 0)/H_{c2}(0, 0)$ are shown in Figure 5 as function of Γ/Γ_c . It is remarkable that the relation

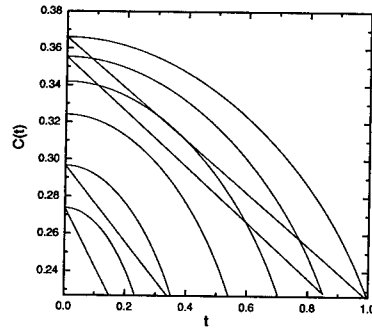


FIGURE 4. The coefficient C versus t . From up to down for $\Gamma/\Gamma_c = 0, 0.2, 0.4, 0.6, 0.8$ and 0.9 .

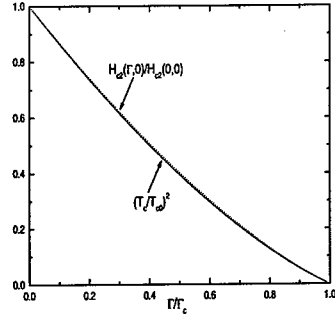


FIGURE 5. $(T_c/T_{c0})^2$ and $H_{c2}(\Gamma, t)/H_{c2}(\Gamma, 0)$ as function of $t'=T/T_c$

$$\frac{H_{c2}(\Gamma, 0)}{H_{c2}(0, 0)} = \left(\frac{T_c}{T_{c0}}\right)^2 \quad (14)$$

is obeyed with high accuracy (within 5% error). This relation has been discovered in a recent study of $H_{c2}(\Gamma, T)$ for $\vec{B} \parallel \vec{c}$ [22]. This implies that if we define the coherence length $\xi(T)$ by $H_{c2}(\Gamma, T) = \phi_0/2\pi\xi^2(T)$ we will obtain

$$\xi(\Gamma, 0) = 0.1473v_F/T_c \quad (15)$$

Figure 6 shows $H_{c2}(\Gamma, T)/H_{c2}(\Gamma, 0)$ versus T/T_c . As is readily seen the curves collapse to almost a single curve. We believe these are the hallmark of unconventional superconductors.

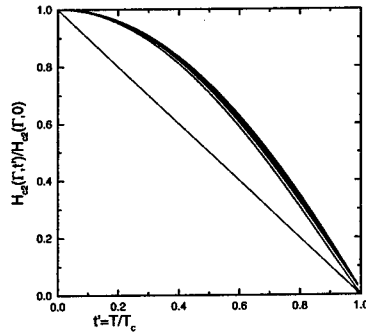


FIGURE 6. $H_{c2}(\Gamma, T)/H_{c2}(\Gamma, 0)$ versus T/T_c for several Γ s

IV SQUARE VORTEX LATTICE

The coefficient C determined in the preceding section plays the crucial role in the stability of the square vortex lattice [23]. Studying the Abrikosov parameter β_A we find that the square vortex lattice is realized when $C \geq 0.243$. Therefore in the vicinity of $B=H_{c2}(T)$ the square vortex lattice should be realized for $t \leq 0.95$. Indeed such a square lattice is seen by small angle neutron scattering in the majority of B-T phase diagram [24]. Further the observed vortex lattice is aligned parallel to the a-b axis, while p-wave superconductors described here do not contain the orientation energy. We believe the orientation of the vortex lattice arises from a small tetragonal distortion of the Fermi surface of the γ band from circle [25]. Further such a small distortion of Fermi surface is required to describe an extremely small a-b anisotropy in upper critical field recently observed in Sr_2RuO_4 [9,26]. Further the vortex lattice phase in Sr_2RuO_4 is very similar to the one predicted for d-wave superconductors [27] except here the vortex lattice is aligned parallel to the a-b axis while in d-wave superconductors it is aligned in the four diagonal directions.

V CONCLUDING REMARKS

We have reviewed a few aspects of p-wave superconductivity in Sr_2RuO_4 and Bechgaard salts, though some crucial experiments in Bechgaard salts are still missing. To our surprise we have discovered a number of parallelism between p-wave superconductivity and d-wave superconductivity, which are not found in s-wave superconductivity. It appears to the wonderland of unconventional superconductivity is waiting us for fresh exploration.

VI ACKNOWLEDGMENTS

We have benefitted from discussion with Daniel Agterberg. The present work is supported by National Science Foundation under grant number DMR95-31720. One of us(H.W) acknowledges the support from Hallym University through the 1997 research fund.

REFERENCES

1. Tsuei C. C and Kirtley J. R. (1997) *Physica C* **282-287** 4
2. Van Harlinger D. J.(1997) *ibid* 128.
3. Maki K. and Won H. (1996) *J. Phys. (Paris)* **6** 2317
4. Won H. and Maki K. (1999) in "Symmetry and pairing in superconductors" M. Ausloos and S. Kruchinin, (eds), Kluwer, Dordrecht.
5. Maeno Y. (1997) *Physica C* **282-287** 206

6. Maki K., Puchkaryov E. and Won H. (1999) *Synth. Metals* (in press).
7. Maki K., Puchkaryov E. (1999) *Europhys. Lett* **45** 263.
8. Wang G. F. and Maki K. (1999) *Europhys. Lett* **45** 71.
9. Maki K., Wang G. F. and Won H. (1999) *J. Superconductivity* (in press).
10. Mackenzie A.P., Haselwimmer R.K.W., Tyler A.W., Lonzarich G. G., Mori Y., and Nishizaki S. (1998) *Phys. Rev. Lett.* **80** 161.
11. Ishida K., Mukuda H., Kitaoka Y., Asayama K., Mao Z. Q., Mori Y. and Maeno Y. (submitted to *Nature*).
12. Kitaoka Y., Ishida K., Asayama K., Ikeda S., Nishizaki S., Maeno Y., Yoshida K. and Fujita T., (1997) *Physica C* **282-287** 210.
13. Puchkaryov E. and Maki K. (1999) in preparation
14. Nishizaki S., Maeno Y., Farmer S., Ikeda S. and Fujita T. (1998) *J.Phys. Soc. Jpn* **67** 560.
15. Nishizaki S., Mao Z. Q. and Maeno Y. (private communication).
16. Sigrist M. and Zhitomirsky M.E. (1996) *J.Phys. Soc. Jpn* **67** 3452
17. Agterberg D.F., Rice T.M. and Sigrist M. (1997) *Phys. Rev. Lett.* **78** 3374.
18. See for example Vollhardt, D. and Wölfle, P. (1990) "Superfluid Phases in ^3He " (Francis-Taylor, London)
19. Abrikosov A.A. and Gor'kov L.P. (1961) *Soviet Phys. JETP* **12** 5788.
20. Buchholtz L.J. and Zwicknagl G. (1981) *Phys. Rev. B* **23** 5788.
21. Sun Y and Maki K. (1995) *Phys. Rev. B* **53** 6059.
22. Mao Z. Q., Mori Y. and Maeno Y. *Phys. Rev. B* (submitted).
23. Wang G. F., Puchkaryov E. and Maki K. (1999) in "Material Science, Fundamental Properties and Future Electronic Applications of High T_c Superconductors" edited by S.-L. Drechsler, T. M. Mishonov, Kluwer, Dordrecht.
24. Riseman T.M., Kealey P.C., Forgan E.M., Mackenzie A.P., Galvin, L.M., Tyler A.W., Lee, S. L., Ager, C., Paul D., Mukuda H., Aegerter C. M., Cubitt, R., Mao Z. Q., Akima, S., and Maeno Y. (1998) *Nature* **396** 242.
25. Shiraishi J. and Maki K. (in preparation).
26. Mao Z. Q., Maeno Y., Ando, T., Ishiguro T., Sigrist M. and Oguchi T. *Phys. Rev. Lett.* (submitted).
27. Shiraishi J., Kohmoto M. and Maki K. (1998) *Europhys. Lett* **44** 367; (1999) *Phys. Rev. B* (in press).

RELATED COMPOUNDS EXPERIMENT

X-ray Scattering Studies of Charge Stripes in Manganites and Nickelates

C.-H. Du*, Y. Su*, P. D. Hatton*, S. Brown[†], and S.-W. Cheong[†]

*Department of Physics, University of Durham, Durham DH1 3LE, U. K.

*XMaS CRG, ESRF, 38043 Grenoble, France

[†] Bell Laboratories, Lucent Technologies, Murray Hill, NJ 07974-0636, USA

[†] Department of Physics & Astronomy, Rutgers University, Piscataway, NJ 08854, USA

Abstract. Using synchrotron x-ray scattering on single crystals of $\text{Nd}_{1/2}\text{Sr}_{1/2}\text{MnO}_3$ and $\text{La}_{5/3}\text{Sr}_{1/3}\text{NiO}_4$, we have demonstrated the existence of charge stripe structures in both compounds. In $\text{Nd}_{1/2}\text{Sr}_{1/2}\text{MnO}_3$ charge ordered satellite reflections were located at positions $(h/2 \ 0 \ l)$, $h = \text{odd}$ and $l = \text{even}$. In addition we have also observed some weak reflections at other positions $(h/2 \ k \ l/2)$ and $(h/2 \ 0 \ l/2)$, $h \ \& \ l = \text{odd}$ and $k = 1$. The result is in accord with the CE-type antiferromagnetic structure as reported by neutron powder diffraction. The transition was observed to be at a transition temperature $T_{\text{CO}} \approx 159 \text{ K}$ and to be strongly first order in nature. By contrast, studies of $\text{La}_{5/3}\text{Sr}_{1/3}\text{NiO}_4$ showed a second order transition at $T_{\text{CO}} \approx 240 \text{ K}$. This produced charge stripe satellites with a wavevector $q = (h \pm 2\epsilon \ 0 \ l)$, $h = \text{even}$ and $l = \text{odd}$. Critical exponents of the transition were obtained and show that the system is in the 2D universality class. The two dimensional nature of the charge stripes is clearly shown in their markedly different correlation lengths at low temperatures e.g. $\xi_a \approx 110 \text{ \AA}$, $\xi_b \approx 130 \text{ \AA}$, whilst ξ_c is only about 17 \AA . These results demonstrate clearly that the charge stripes are themselves two dimensional in character.

INTRODUCTION

Charge and spin ordering in direct space in manganites, and nickelates have recently attracted considerable attention for both fundamental physics as well as possible device applications. Manganites are synthesised by doping divalent alkaline ions in the cation site of manganese perovskites, namely $\text{R}_{1-x}\text{A}_x\text{MnO}_3$ where $\text{R} = \text{La, Pr, and Nd}$, and $\text{A} = \text{Ca, Sr, and Ba}$, and have been demonstrated to exhibit colossal magnetoresistance (CMR) under the application of a magnetic field. Undoped RMnO_3 is an antiferromagnetic (AFM) insulator, but with carrier doping of divalent A elements in R sites, the system becomes a ferromagnetic (FM) metal with the observed CMR in the composition range $0.2 < x < 0.5$.

Despite the demonstrations of charge ordering and spin ordering in colossal magnetoresistance oxides and in nickelates by neutron scattering, x-ray scattering has the merits of superior spatial resolution and direct probing of the charge density modulation. In this article we report x-ray scattering studies which show that the charge stripes are 2 dimensional and highly disordered above the transition temperature and that they are quenched below the transition temperature T_{CO} [1].

Single crystalline samples of $\text{Nd}_{1/2}\text{Sr}_{1/2}\text{MnO}_3$ (NSMO) and $\text{La}_{5/3}\text{Sr}_{1/3}\text{NiO}_4$ (LSNO) were grown using the floating zone method at Bell Laboratories, and LSNO had been

previously characterised by neutron scattering [2]. The crystals were first examined and oriented in our laboratory using a rotating anode source with graphite crystals as monochromator and analyser. The synchrotron experiment on the crystal NSMO was performed at station 16.3 at Daresbury Laboratory, and further studies on LSNO were carried out on the beamline XMaS at the ESRF. Both stations are equipped with multi-axis diffractometers which allow the measurements to be performed along any direction in reciprocal space.

$\text{Nd}_{1/2}\text{Sr}_{1/2}\text{MnO}_3$

$\text{Nd}_{1/2}\text{Sr}_{1/2}\text{MnO}_3$ is orthorhombic at room temperature with lattice parameters $a=5.434 \text{ \AA}$, $b=7.634 \text{ \AA}$, $c=5.477 \text{ \AA}$. The magnetic transport properties of $\text{Nd}_{1/2}\text{Sr}_{1/2}\text{MnO}_3$ show a transformation from a paramagnetic state to a ferromagnetic metallic state at about 250 K, followed by a transition into a charge ordered antiferromagnetic insulating state around 160 K [3]. The structure does not change until $T \approx 160 \text{ K}$ at which the charge-ordered state appears. The charge ordered pattern

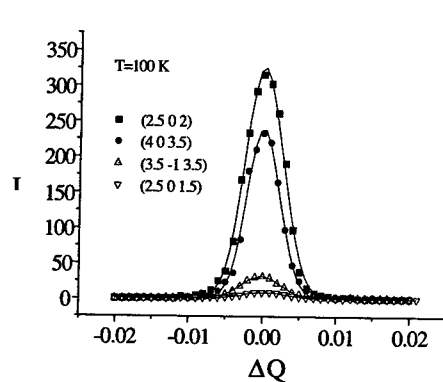


FIGURE 2. Longitudinal scans through the satellite reflections in a single crystal $\text{Nd}_{1/2}\text{Sr}_{1/2}\text{MnO}_3$ at $T=100 \text{ K}$. The squares and circles are the charge ordering peaks, and the triangles are from scattering from positions in reciprocal space associated with spin ordering.

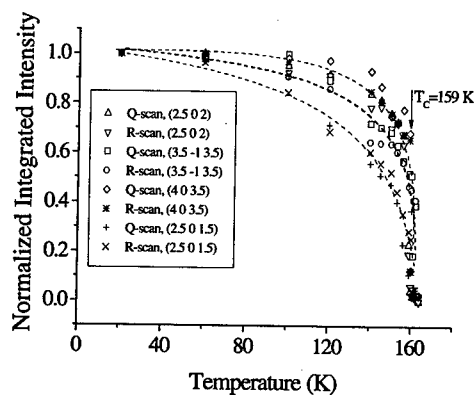


FIGURE 1. Temperature dependence of the integrated intensities of satellites reflections as measured in $\text{Nd}_{1/2}\text{Sr}_{1/2}\text{MnO}_3$. Q-scans indicate the scans along the longitudinal direction, and R-scans for the transverse direction. The dashed lines are only a guide to the eye.

of Mn^{3+} and Mn^{4+} is alternating in the ac plane, doubling the unit cell along the a - and c -axis and resulting in Bragg reflections at positions with wavevectors $\vec{q} = \pm \frac{n}{2} \vec{h}$ or

$\pm \frac{n}{2} \vec{l}$, $n = \text{odd}$. Longitudinal scans through the satellite reflections are shown in Fig. 1.

Both charge ordering reflections of (2.5 0 2) and (4 0 3.5) show nearly identical widths, indicating a long-range ordered structure at low temperatures. The evolution of the integrated intensities of both reflections with temperature also shows identical behaviour, i.e. a first order phase transition with a transition temperature $T \approx 159$ K (see figure 2). In addition we also observed some weak satellite reflections at positions of $(h/2 \ k \ l/2)$ and $(h/2 \ 0 \ l/2)$, h and $l = \text{odd}$, and $k=1$. $\text{Nd}_{1/2}\text{Sr}_{1/2}\text{MnO}_3$ undergoes a structural phase transition at $T \approx 160$ K into the CE-type charge ordered antiferromagnetic state [3,4]. The charge ordered peaks have been observed as above, and the magnetic reflections have also been probed at positions, such as $(1/2 \ 1 \ 1/2)$ and $(1/2 \ 1 \ 3/2)$, by neutron scattering. Surprisingly, the positions of those weak reflections observed in this study agree with that probed by neutron scattering. Due to the relative insensitivity of magnetic ordering to x-rays, it is unclear if these weak satellite reflections are caused by the spin ordering in the antiferromagnetic phase. Figure 2 displays the temperature dependence of the integrated intensities, the order parameter, of satellite reflections. It is clear that the intensities of the charge ordering peaks remain 80% of that at low temperatures at close to the transition temperature $T \approx 159$ K, but those weak reflections only have about 30% for (2.5 0 1.5) and 50% for (3.5 -1 3.5). However, the order parameters of those weak reflections seem to show a similar behaviour to that measured by neutron scattering [4], and further detailed studies on those weak reflections have been scheduled using the beamline *XMAS* at ESRF.

$\text{La}_{5/3}\text{Sr}_{1/3}\text{NiO}_4$

$\text{La}_{(2-x)}\text{Sr}_x\text{NiO}_4$ is isostructural with the high- T_C superconductors cuprates, $\text{La}_{(2-x)}\text{Sr}_x\text{CuO}_4$ and $\text{La}_{(2-x)}\text{Ba}_x\text{CuO}_4$, it thus provides a prototypical system in helping the understanding of the mechanism of high T_C superconductivity [5]. At doping levels of $x \approx 1/3$ and $1/2$ commensurate charge modulations have been observed by Chen *et al.* [6] using electron diffraction. Using neutron scattering the charge ordering and the spin ordering have been evidenced to be a common feature in nickelates [7]. Satellite reflections were observed at positions of $(h \pm 2\varepsilon \ 0 \ l)$, $\varepsilon \approx 1/3$, $h = \text{even}$ and $l = \text{odd}$, at low temperatures in accord with the neutron scattering studies [7]. In Sr-doped La_2NiO_4 (LSNO), the characteristic wavevector for the charge density modulation is $q_{CO} = (2\varepsilon \ 0 \ 1)$, and $q_{SO} = (1 + \varepsilon \ 0 \ 0)$ for the spin density modulation. The transition temperature for the formation of the charge ordering in $\text{La}_{5/3}\text{Sr}_{1/3}\text{NiO}_4$ was reported to be $T_{CO} \approx 240$ K as obtained by transport measurements [8], which is in agreement with our observation. Figure 3 shows a plot of the integrated intensity of charge ordering peak (4.66 0 5) versus temperature. Clearly, the data can be fitted to a power law

$I(t) \propto \left(\frac{T_{CO} - T}{T_{CO}}\right)^{2\beta}$, with $2\beta \approx 0.248 \pm 0.03$, and $T_{CO} \approx 240$ K, and shows the transition

to be second order in nature. As compared to the predicted exponents for 2D and 3D

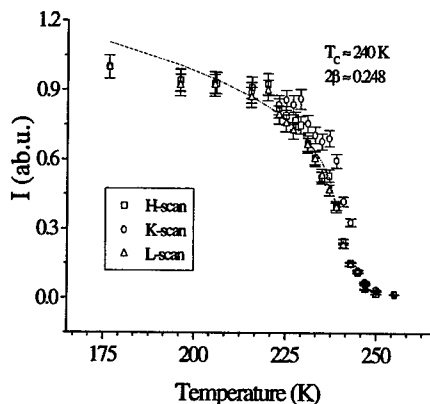


FIGURE 3. The evolution of the integrated intensity of the charge ordering peak (4.66 0 5) with temperature in a single crystal $\text{La}_{5/3}\text{Sr}_{1/3}\text{NiO}_4$. The solid line is the best fit to a power law $I(T) \propto \left(\frac{T_{\text{co}} - T}{T_{\text{co}}}\right)^{2\beta}$.

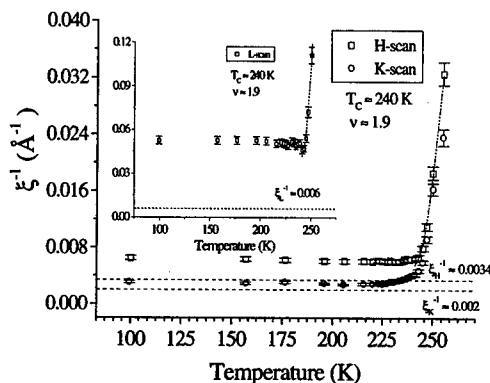


FIGURE 4. The evolution of the inverse correlation lengths of the charge stripe satellite (4.66 0 5) along the H, K, and L directions. The data can be fitted to a power law $\xi^{-1}(T) \propto \left(\frac{T - T_{\text{co}}}{T_{\text{co}}}\right)^\nu$. The dotted lines show the experimental resolution obtained from measurements of a Bragg peak. The inset shows the evolution and the best fit along the L direction.

models [1], the value of $2\beta \approx 0.25$ clearly demonstrates that the charge stripes in $\text{La}_{5/3}\text{Sr}_{1/3}\text{NiO}_4$ are in the 2D universality class.

In Figure 4, we display the evolution of the correlation lengths with temperature. Above the transition temperature $T_{\text{co}} \approx 240$ K, only very weak scattering is observed at the expected positions in reciprocal space. Such scattering is caused by critical scattering due to dynamic spatial fluctuations into the charge stripe phase. The size of these clusters varies with temperature and shows a marked divergence close to T_{co} . Fitting to the data of figure 5 to a power law for the inverse correlation length shows a unusual high exponent of $\nu \approx 1.9 \pm 0.1$ for the correlation length of charge ordering. we ascribe this behaviour to the effects caused by the randomly distributed strain energy [1]. At low temperatures, the charge stripes do not develop long-range order, like the Bragg reflections, as compared to the resolution limitations in the H, K, and L directions, indicating that the disordered charge stripes are quenched below the transition temperature. This quenched state can be explained to be caused by the pinning effect resulting from either the spins in the hole deficient regions or the defects induced by Sr dopants [2,10].

In summary, we have observed the charge ordered superstructures resulting from the formation of the charge stripes in both maganites and nickelates using high-

resolution synchrotron x-ray scattering. In $\text{Nd}_{1/2}\text{Sr}_{1/2}\text{MnO}_3$, the transition was observed to be first order with $T_{CO} \approx 159$ K, and the charge stripes developed to a long-range ordered state at low temperatures. By contrast, the charge stripes in nickelates display a more fascinating behaviour. Firstly, the charge stripes form very locally with lengths of only few unit cells along the H, K, and L directions respectively, resulting in an unusually high exponent of the correlation length. Upon cooling, the disordered charge stripes are quenched below the transition temperature $T_{CO} \approx 240$ K, i.e. charge stripes remain in the short-range ordered state. This transition was observed to be the second order, and the system is in the 2D universality class.

ACKNOWLEDGEMENTS

This work is financially supported by the Engineering and Physical Sciences Research Council. We gratefully acknowledge access to the XMaS facility during commissioning time. Comments and requests for the details are welcome to c.h.du@durham.ac.uk and p.d.hatton@durham.ac.uk.

REFERENCES

1. C.-H. Du, Y. Su, J. P. Allen, P. D. Hatton, S. Brown, W. G. Stirling, and M. J. Cooper, and S-W. Cheong, (submitted to Phys. Rev. Lett.)
2. S.-H. Lee, and S.-W. Cheong, Phys. Rev. Lett. **79**, 2514 (1997).
3. H. Kuwahara, Y. Tomioka, A. Asamitsu, Y. Moritomo, and Y. Tokura, Science, **270**, 961 (1995).
4. H. Kawano, R. Kajimoto, H. Yoshizawa, Y. Tomioka, H. Kuwahara, and Y. Tokura, Phys. Rev. Lett. **78**, 4253 (1997).
5. J. M. Tranquada, B. J. Sternlieb, J. D. Axe, Y. Nakamura, and S. Uchida, Nature **375**, 561, 1995; B. G. Levi, Physics Today, June, 19, 1998.
6. C.-H. Chen, S-W. Cheong, and A. S. Cooper, Phys. Rev. Lett. **71**, 2461 (1993).
7. J. M. Tranquada, D. J. Buttrey, V. Sachan, and J. E. Lorenzo, Phys. Rev. Lett. **73**, 1003 (1994); J. M. Tranquada, D. J. Buttrey, and V. Sachan, Phys. Rev. B **54**, 12318 (1996).
8. S-W. Cheong, H. Y. Hwang, C. H. Chen, B. Batlogg, L. W. Rupp, Jr., and S. A. Carter, Phys. Rev. B **49**, 7088 (1994).
9. M. F. Collins, "Magnetic Critical Scattering", (Oxford University Press, 1989)
10. S. A. Kivelson, E. Fradkin, and V. J. Emery, Nature **393**, 550 (1998); Physica C **209**, 597 (1993).

Electron-Lattice Interactions in Nickel-Oxide Perovskites

J.B. Goodenough⁺, J.-S. Zhou⁺, and B. Dabrowski^{*}

⁺Texas Materials Institute, ETC 9.102
University of Texas at Austin, Austin, TX 78712-1063

^{*}Department of Physics, Northern Illinois University, DeKalb, IL 60116

Abstract. The AMO₃ perovskites containing a first-row transition-metal atom M allow study of the cross-over from localized to itinerant electronic behavior in a single-valent MO₃ array dominated by (180° - ϕ) M-O-M interactions. The LnNiO₃ perovskites with Ln a lanthanide have one electron per low-spin Ni(III) in a narrow σ^* band that approaches cross-over from the itinerant-electron side. Transport measurements are reported that add to the mounting evidence for a heterogeneous electronic transition in the perovskites rather than the homogeneous transition assumed in conventional treatments of the Mott-Hubbard transition.

INTRODUCTION

In 1965, it was demonstrated that single-valent LaNiO₃ is metallic and Pauli paramagnetic [1], which established that the AMO₃ perovskites containing a transition-metal atom M from the first long period may be either magnetic insulators with localized dⁿ configurations or Pauli paramagnetic metals in which the d electrons occupy itinerant-electron states [2]. Localized-electron behavior is found where the intraatomic electron-electron coulomb energy U separating a filled dⁿ and an empty dⁿ⁺¹ configuration on an M atom is larger than the interatomic M-O-M interaction energies that give rise to a band of itinerant-electron states of width W. The energy U increases as W decreases; and above a critical ratio (U/W)_c, a semiconductive state with localized electrons is stabilized relative to a metallic state with itinerant electrons. A systematic study of the Mott-Hubbard transition in perovskites has been plagued by lattice instabilities at the cross-over. In this paper, we report a study of the approach to cross-over from the itinerant-electron side in the single-valent LnNiO₃ family where Ln is a lanthanide and the NiO₃ array contains a single electron per low-spin Ni(III) in an orbitally twofold-degenerate, antibonding σ^* band. The data indicate the Mott-Hubbard transition is first-order and, in the perovskite structure, is characterized by a heterogeneous electronic state with strong coupling of electrons to cooperative fluctuations of the equilibrium Ni-O bond lengths.

In the AMO₃ cubic-perovskites, a measure of the mismatch of the equilibrium (A-O) and (M-O) bond lengths is the deviation from unity of the tolerance factor

$$t \equiv (A-O)/\sqrt{2}(M-O) \quad (1)$$

that may be calculated for room temperature and ambient pressure from the sums of tabulated ionic radii. The LnNiO_3 perovskites accommodate a $t < 1$ by cooperative rotations of the $\text{NiO}_{6/2}$ corner-shared octahedra about either the cubic [111] or [110] axis to give, respectively, rhombohedral $R\bar{3}c$ or orthorhombic $Pbnm$ distortions of the NiO_3 array. The bending angle ϕ of the $(180^\circ - \phi)$ Ni-O-Ni bonds increases with decreasing t and increases discontinuously on changing from $R\bar{3}c$ to $Pbnm$ symmetry.

Whereas rhombohedral LaNiO_3 remains metallic, the orthorhombic LnNiO_3 exhibit a weakly first-order transition from a semiconductive phase below T_i to a metallic phase above T_i [3], Fig. 1. Below a $T_N \leq T_i$, an antiferromagnetic order consisting of alternating ferromagnetic and antiferromagnetic Ni-O-Ni interactions [4] has been interpreted [5] to reflect stabilization of coexisting charge-density and spin-density waves (CDW/SDW). T_i increases dramatically with decreasing t ; hydrostatic pressure P decreases T_i : $dT_i/dP = -6.1$ and -9.2 K/kbar, respectively, for NdNiO_3 and PrNiO_3 [6,7]. Neutron-diffraction data [8] for PrNiO_3 and NdNiO_3 have shown that the (Ni-O) bond length is identical and temperature-independent in the metallic phase of both compounds, but it increases discontinuously by 0.0035 \AA on cooling through T_i . Normally, the (A-O) bond is more compressible than the (M-O) bond, but a $dt/dP > 0$ is possible where two phases of different equilibrium (M-O) bond length coexist. The pressure data together with Fig. 1 have suggested a $dt/dP = 0.0004/\text{kbar}$ on the assumption that T_i depends only on the bending angle ϕ . We may expect that T_i occurs at a critical bandwidth, and even with the conventional tight-binding bandwidth

$$W_b \sim \epsilon_\sigma \lambda_\sigma^2 \cos \phi \quad (2)$$

for a homogeneous system, pressure changes not only ϕ , but also the covalent-mixing parameter λ_σ . Substitution of ^{18}O for ^{16}O in NdNiO_3 increases T_i by 10.3 K without introducing any change in either λ_σ or ϕ [9], which raises questions about the applicability of equation (2). However, if the electronic system is heterogeneous, containing two fluctuating phases of different (Ni-O) equilibrium bond length as a $dt/dP > 0$ implies, then strong electron coupling to lattice fluctuations could give a single-valent bandwidth

$$W_\sigma \approx W_b \exp(-\lambda \epsilon_{sc}/\hbar \omega_0) \quad (3)$$

analogous to the mixed-valent polaron bandwidth derived by Holstein [10]. In equation (3), ϵ_{sc} is the stabilization energy of a strong-correlation fluctuation in a Fermi-liquid sea and $\lambda \sim \epsilon_{sc}/W_b$ is an electron-lattice coupling parameter.

In order to probe the adequacy of equation (2) and the inequivalence of hydrostatic pressure and chemical variation of t , we have measured the resistivity $\rho(T)$ and thermoelectric power $\alpha(T)$ under different hydrostatic pressures of four compositions

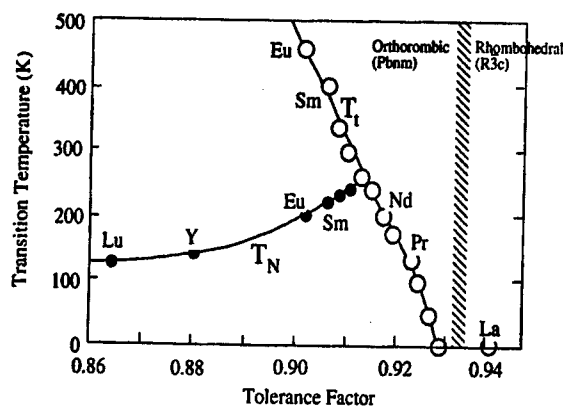


Fig.1 The I-M transition temperature T_I and Néel temperature T_N for the LnNiO_3 perovskite family (adapted from [3])

that span the critical portion of Fig. 1: LaNiO_3 , PrNiO_3 , NdNiO_3 , and $\text{Sm}_{0.5}\text{Nd}_{0.5}\text{NiO}_3$. Moreover, we contrast the $\rho(T)$ and $\alpha(T)$ curves for one composition at atmospheric pressure with another having the same T_I under hydrostatic pressure. If the bandwidth is $W = W_b$, compositions with the same T_I should have similar transport properties.

EXPERIMENTAL DATA

Our experiments used ceramic samples that were synthesized under 600 bar oxygen pressure at 1080°C. Powder x-ray diffraction showed that all samples were single-phase. The oxygen content in all samples was determined to be 3.00 ± 0.01 by thermogravimetric analysis in 50-50 H_2 -Ar atmosphere. The transport measurements were made under pressure as described elsewhere [11]. Fig. 2 shows $\rho(T)$ and $\alpha(T)$ under different hydrostatic pressures for the four samples. Fig. 3 compares high-pressure data with atmospheric-pressure data having an equivalent T_I , and Fig. 4 compares the variation of T_I and the resistivity at 15 K for PrNiO_3 . We discuss four aspects of these data.

1. Comparisons of LaNiO_3 and PrNiO_3 . Fig. 2(a) shows the $\rho(T)$ and $\alpha(T)$ data for rhombohedral LaNiO_3 under pressures $P < 14$ kbar. The $\rho(T)$ curves are similar to those reported by others [12,13]; the temperature dependence is typical of a Fermi liquid, but $\rho(T)$ is too high and pressure-dependent for a conventional metal. This observation prompts comparison with the system $\text{Sr}_{1-x}\text{Ca}_x\text{VO}_3$ where photoemission spectroscopy has revealed the coexistence of incoherent (strong-correlation) and coherent (Fermi-liquid) states with a progressive transfer of spectral weight from coherent to incoherent states as the π^* band was narrowed by substitution of Ca^{2+} for Sr^{2+} ions [14]. As shown in Fig. 5, the Brinkman-Rice [15] expression $m^* = m/[1 - (U/U_c)^2]$ for the enhancement of the effective mass breaks down where the homogeneous electronic system becomes heterogeneous [11]. The heterogeneity of the $\text{Sr}_{1-x}\text{Ca}_x\text{VO}_3$ system reflects the lattice instability encountered at the cross-over from itinerant to localized electronic behavior. Measurement of $\alpha(T)$ for CaVO_3 gave

two characteristic features of a heterogeneous electronic phase for $U/U_c \leq 1$ [11]: the low-temperature phonon-drag enhancement ($T_{\max} \approx 70$ K) is suppressed, but it increases with pressure, and an increase in $|\alpha(300 \text{ K})|$ with pressure signals an increase in m^* . These two features can be seen in the $\alpha(T)$ data for LaNiO_3 , Fig.2(a). Therefore the two-phase condition that equation (3) apply is fulfilled already in LaNiO_3 , and W_b can only become narrower on substitution of a smaller Ln^{3+} ion for La^{3+} .

Fig. 2(b) shows the $\rho(T)$ and $\alpha(T)$ data for orthorhombic PrNiO_3 under pressure $P < 15$ kbar. At atmospheric pressure, the first-order insulator-metal (I-M) transition at $T_N = T_i \approx 130$ K in the $\rho(T)$ curve is reflected in the sharp increase in $|\alpha(T)|$ at T_i . Between 2.7 and 4.7 kbar, the low-temperature ($T \leq 50$ K) $\rho(T)$ curve changes from a semiconductive to a metallic temperature dependence; and with increasing pressure $P \geq 4.7$ kbar, the jump in $\rho(T)$ and $|\alpha(T)|$ at T_i decreases with T_i , disappearing above 13 kbar even though a weakly first-order transition is retained at $T_i \approx 80$ K, Fig. 4. These unusual data suggest that an increase in the Fermi-liquid volume under pressure creates a Fermi-liquid phase percolating through the CDW/SDW phase.

Fig. 3(a) shows that PrNiO_3 under a pressure of 14.9 kbar is converted completely to the disordered metallic phase; but comparison with LaNiO_3 at atmospheric pressure shows that reduction of the equilibrium (Ni-O) bond length has lowered $\rho(T)$.

2. Evolution of $\rho(T)$ and $\alpha(T)$ with t and P . Figs. 2(b) and (c) show that PrNiO_3 and NdNiO_3 , each with $T_N = T_i$, show similar changes of $\rho(T)$ and $\alpha(T)$ under pressure. However, NdNiO_3 has the higher T_i . Moreover, a somewhat smaller thermal hysteresis at T_i signals that the first-order character of the transition decreases with increasing T_i as is made even more evident in Fig. 2(d) for $\text{Sm}_{0.5}\text{Nd}_{0.5}\text{NiO}_3$, which has $T_N < T_i$. The change from a weakly first-order to a second-order transition at $T_i > T_N$ also indicates an order-disorder transition occurs at T_i .

3. Comparisons for same T_i . NdNiO_3 has a $T_i \approx 135$ K under a pressure of 15 kbar; it is nearly the same as the T_i found for PrNiO_3 at atmospheric pressure, Fig. 3(b). However, the jump in $\rho(T)$ on cooling through T_i is four orders of magnitude in PrNiO_3 , but only two in NdNiO_3 under 15 kbar. The jump in $\alpha(T)$ at T_i is also smaller in NdNiO_3 and the metallic temperature dependence of $\rho(T)$ below 50 K contrasts with the semiconductive dependence in PrNiO_3 . In Fig. 3(c), the $\alpha(T)$ curve for NdNiO_3 at atmospheric pressure does not change sign on cooling through T_i whereas it does in $\text{Sm}_{0.5}\text{Nd}_{0.5}\text{NiO}_3$. Moreover, the first-order transition in NdNiO_3 contrasts with the smooth transition in $\text{Sm}_{0.5}\text{Nd}_{0.5}\text{NiO}_3$. Thus Fig. 3 demonstrates not only that hydrostatic pressure is not equivalent to a change of ϕ with t , but also that W_b is not described by equation (2) since for the same bandwidth, corresponding to the same T_i , the transport properties at ambient pressure are different from those under hydrostatic pressure. However, since a shorter equilibrium (Ni-O) bond length under

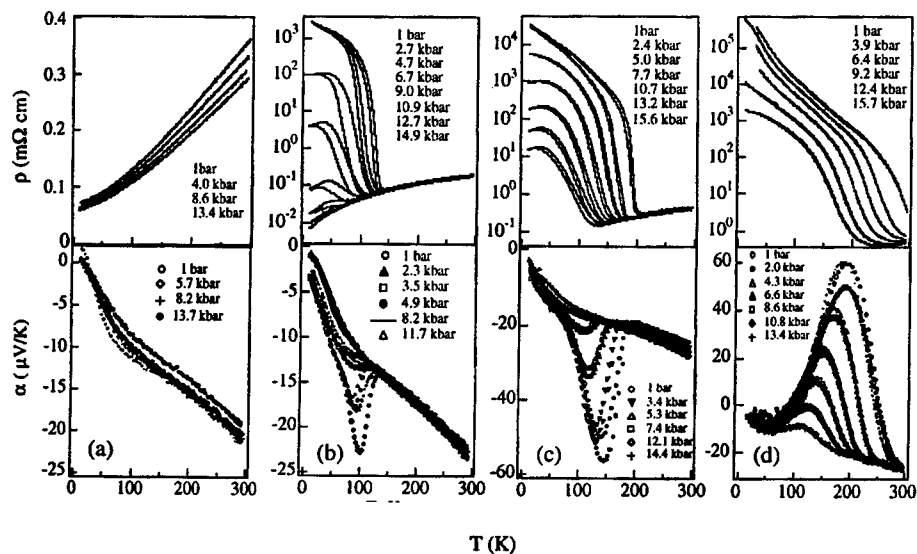


Fig. 2. The resistivity $\rho(T)$ and thermoelectric power $\alpha(T)$ under different hydrostatic pressures for (a) LaNiO_3 , (b) PrNiO_3 , (c) NdNiO_3 , and (d) $\text{Sm}_{0.5}\text{Nd}_{0.5}\text{NiO}_3$.

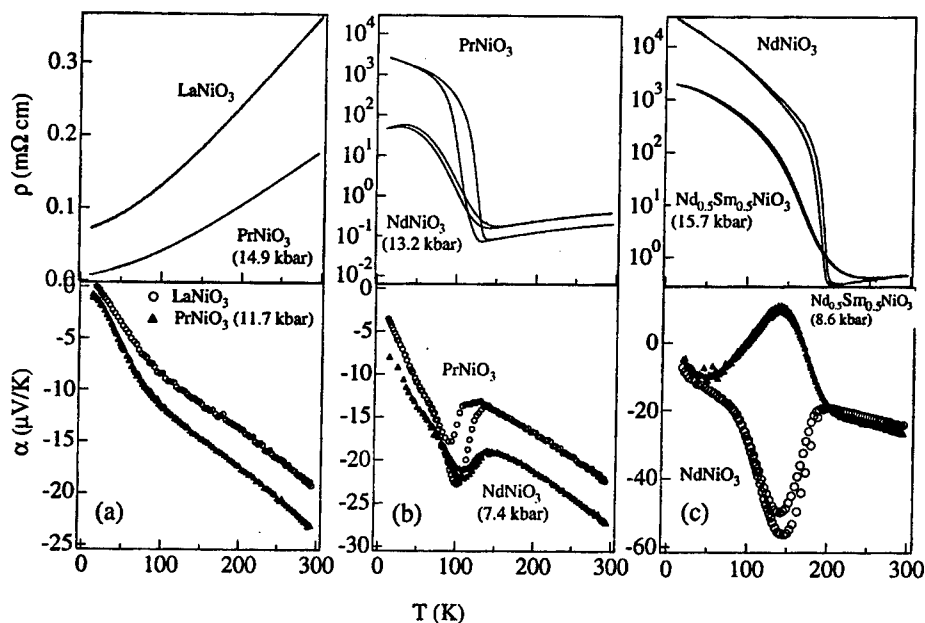


Fig. 3. Comparisons of the resistivity $\rho(T)$ and thermoelectric power $\alpha(T)$ for two compounds with the same T_c , one at atmospheric pressure and the other under hydrostatic pressure.

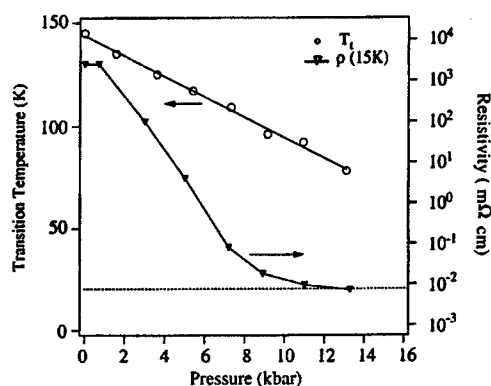


Fig.4 Variation with pressure of T_i and resistivity at 15 K for PrNiO_3 .

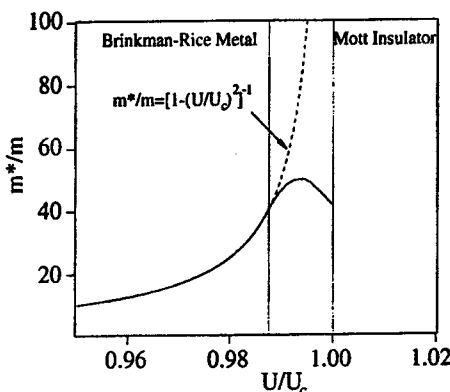


Fig.5 Schematic variation of normalized effective mass versus normalized Hubbard energy

pressure would increase ω_0 , the W_0 of equation (3) would be compatible with these data as well as with the shift of T_i with $^{18}\text{O}/^{16}\text{O}$ isotope exchange.

4. Pressure dependence above and below T_i . Above T_i , the $\rho(T)$ and $\alpha(T)$ curves are all similar, but $|\alpha(300 \text{ K})|$ increases with pressure, which is consistent with placement of the compounds in the two-phase region of Fig. 1 where $U/U_c \rightarrow 1$. From Fig. 2, the pressure dependence of $\rho(T)$ above T_i is seen to be insignificant compared to the enormous pressure dependence below T_i . Pressure not only stabilizes the high-temperature phase having the smaller volume; it also reduces the long-range order below T_i by transferring spectral weight from the strong-correlation to the fermi-liquid volume, thereby introducing a fermi-liquid phase that percolates through the CDW/SDW long-range-ordered phase.

We thank the NSF and the TCSUH for financial support.

REFERENCES

1. J.B. Goodenough and P.M. Raccach, *J. Appl. Phys.* **36**, 1031 (1965)
2. J.B. Goodenough, *J. App. Phys.* **37**, 1415 (1966)
3. J.B. Torrance, *et al*, *Phys. Rev.* **B45**, 8209 (1992)
4. J.L. García-Muñoz, P. Lacorre, and R. Cywinski, *Phys. Rev.* **B51**, 15197 (1995)
5. J.B. Goodenough, *J. Solid State Chem.* **127**, 126 (1996)
6. X. Obradors, *et al*, *Phys. Rev.* **B47**, 12353 (1993)
7. P.C. Canfield, *et al*, *Phys. Rev.* **B47**, 12357 (1993)
8. J.L. García-Muñoz, *et al*, *Phys. Rev.* **B46**, 4414 (1992)
9. M. Medarde, *et al*, *Phys. Rev. Lett.* **80**, 2397 (1998)
10. T. Holstein, *An. Phys. (Paris)* **8**, 325 (1959)
11. J.-S. Zhou and J.B. Goodenough, *Phys. Rev.* **B54**, 13393 (1996)
12. K. Streedhar, *et al*, *Phys. Rev.* **B46**, 6382 (1992)
13. X.Q. Xu, *et al*, *Phys. Rev.* **B48**, 1112 (1993)
14. K. Morikawa, *et al*, *Phys. Rev. Lett.* **74**, 2539 (1995).
15. W.F. Brinkman and T.M. Rice, *Phys. Rev.* **B2**, 4302 (1970)

Electronic Raman scattering in the perovskite manganese oxides

H.L. Liu,¹ S. Yoon,¹ S.L. Cooper,¹ S-W. Cheong,² and P.D. Han³

¹ *Department of Physics and Frederick Seitz Materials Research Laboratory,
University of Illinois at Urbana-Champaign, Urbana, Illinois 61801*

² *Bell Laboratories, Lucent Technologies, Murray Hill, New Jersey 07974*
and *Department of Physics and Astronomy, Rutgers University, Piscataway, New Jersey 08855*

³ *Department of Material Science and Engineering and Frederick Seitz Materials Research
Laboratory,
University of Illinois at Urbana-Champaign, Urbana, Illinois 61801*

Abstract. We present an electronic Raman scattering study of the colossal magnetoresistance manganese perovskites as a function of temperature, magnetic field, symmetry, and doping. The low-frequency electronic Raman spectrum of these materials exhibits a distinctive change through the paramagnetic insulator / ferromagnetic metal transition, characterized by a transformation from a diffusive scattering response to a flat continuum response. We also find that the magnetic-field dependence of electronic Raman scattering in the manganese perovskites is both highly anisotropic and indicative of an inhomogeneous ferromagnetic phase.

INTRODUCTION

The diversity of electronic and magnetic properties in the perovskite manganese oxides $R_{1-x}A_x\text{MnO}_3$ (R and A being trivalent rare-earth and divalent alkaline-earth ions, respectively) has received a great deal of attention in recent years [1-3]. In the doping range $0.2 < x < 0.5$, the perovskite manganites undergo a paramagnetic (PM) insulator to a ferromagnetic (FM) metal phase transition upon cooling, and exhibit colossal magnetoresistance (CMR) near the Curie temperature. These phenomena have been described within the framework of the double exchange (DE) mechanism [4] augmented by strong Jahn-Teller (JT) lattice distortions [5], although there remains some disagreement as to the significance of JT effects in these systems [6].

In this paper, we study the electronic Raman scattering response of these materials as a function of temperature, magnetic field, symmetry, and doping. Raman spectroscopy is a unique and effective tool for studying the metal-insulator (MI) transition and CMR effect in the manganese perovskites, as it allows one to obtain

direct information about the temperature- and field-dependencies of the electronic scattering rate associated with *different* scattering channels.

EXPERIMENTAL

The samples used in our study were a floating-zone-grown $\text{Pr}_{0.63}\text{Sr}_{0.37}\text{MnO}_3$ ($T_c \sim 300$ K) single crystal and a flux-grown $\text{Pr}_{0.7}\text{Pb}_{0.21}\text{Ca}_{0.09}\text{MnO}_3$ ($T_c \sim 145$ K) single crystal. The Raman spectra were measured with 6471 Å photons from a Kr^+ laser (~ 5 mW) by focusing to a 50 μm diameter spot on the ab plane of the crystal surface, and the backward scattering light was collected and dispersed by a modified subtractive triple spectrometer equipped with a liquid-nitrogen-cooled charge-coupled device detector. The crystals were mounted in a continuous helium flow optical cryostat, which was installed in the bore of a superconducting magnet. The applied magnetic field was normal to the ab plane of the sample surface. The magnetic-field spectra were obtained in (RCP,LCP) and (LCP,LCP) geometries, where RCP and LCP are right and left circularly polarized, respectively. These geometries allowed us to selectively probe either B_{1g} (RCP,LCP) or A_g (LCP,LCP) symmetries, where B_{1g} and A_g are the singly degenerate irreducible representations of the manganite space group $D_{2h}^{16}\text{-Pnma}$.

RESULTS AND DISCUSSION

The zero-field Raman scattering spectra of the $T_c \sim 300$ K sample are shown in Fig. 1(a) as a function of temperature. The 330-K B_{1g} spectrum is composed of an electronic background and three broad phonon bands. As no Raman active modes are expected in the cubic perovskite structure, these phonons are activated due to the distortions of Mn-O octahedra [7]. Notably, the two high-frequency Mn-O modes exhibit a dramatic narrowing through the MI transition, reflecting an abrupt decrease in these distortions at T_c [7]. In this paper, we focus primarily on the temperature- and field-dependencies of the low-frequency electronic Raman response, which is associated with scattering from conduction electrons [7]. When the temperature is lowered from 330 K, the electronic Raman scattering contribution in both B_{1g} and A_g symmetries exhibits a distinctive change from a diffusive response in the PM insulator phase to a flat continuum response in the FM metallic state, illustrating the sensitivity of the electronic Raman response to the MI transition in the manganese perovskites.

We have fit the B_{1g} spectra with the collision-limited model [8], which was previously applied to the analysis of electronic Raman spectra of heavily doped semiconductors [9] as well as strongly-correlated metals [10]. In this model, the Raman scattering intensity is given by [8]

$$S(\omega) \sim [1 + n(\omega)] \frac{B_L \omega \Gamma_L}{\omega^2 + \Gamma_L^2}, \quad (1)$$

where the quantity $[1+n(\omega)] = [1 - \exp(-\hbar\omega/k_B T)]^{-1}$ is the Bose-Einstein thermal factor, B_L is the symmetry-dependent amplitude, which is related to the square of Raman scattering vertex γ_L associated with scattering channel L , and Γ_L is the carrier scattering rate in channel L . A fit of this model to the 330-K Raman spectrum is shown by a dashed line in Fig. 1(a). In the high-temperature PM phase, we obtain a relatively good quality fit to the data using Eq. 1 and a ω -independent scattering rate, $\Gamma_{B_{1g}} = 125 \text{ cm}^{-1}$, to describe the electronic response, and three Lorentzian oscillators to account for the phonon contributions. However, below T_c , satisfactory fits to the flat continuum spectra require a ω -dependent Γ , *e.g.*, $\Gamma(\omega) = \Gamma_0 + \alpha\omega^2$, where the parameter α reflects electron correlation effects [10]. For example, fits to the 5-K data of Fig. 1(a) (dotted-dashed line) yield values of

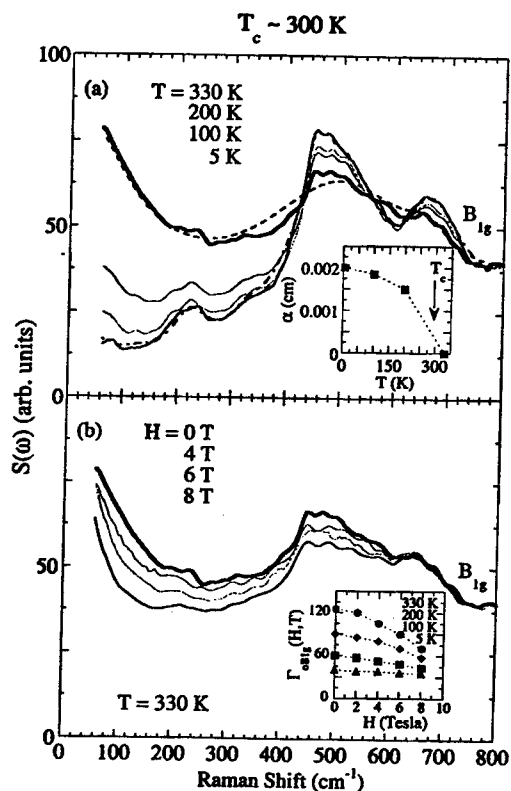


FIGURE 1. (a) The measured zero-field B_{1g} Raman scattering spectra of the $T_c \sim 300 \text{ K}$ sample at several temperatures. The dashed (330 K) and dotted-dashed (5 K) lines are fits to the data using a collision-limited model (Eq. 1). The inset shows the fitted values of α as a function of temperature for $H = 0 \text{ T}$. (b) The B_{1g} -symmetry Raman spectra of the $T_c \sim 300 \text{ K}$ sample at 330 K and as a function of magnetic field. The inset shows the temperature- and field-dependent scattering rate $\Gamma_0(H, T)$, obtained by fitting the data to the scattering response in Eq. 1.

$\alpha = 2.0 \times 10^{-3}$ cm and $\Gamma_0 = 40$ cm $^{-1}$. The complete temperature-dependence of α for $H = 0$ T is shown in the inset of Fig. 1(a), illustrating that the dramatic effect of the PM insulator / FM metal transition on the electronic Raman response is primarily attributable to an abrupt increase in electronic correlations, *i.e.*, α . A similar change in the electronic Raman response due to increased electronic correlations was also observed as a function of doping in the band-filling-controlled metals $\text{Sr}_{1-x}\text{La}_x\text{TiO}_3$ [10], and as a function of temperature in the low T_c CMR material EuB_6 [11].

Figure 1 (b) illustrates the magnetic field-dependence of the Raman spectra for the $T_c \sim 300$ K sample in B_{1g} scattering geometries. Remarkably, near T_c the B_{1g} -symmetry electronic Raman scattering intensity exhibits a substantial suppression with increasing magnetic field below 600 cm $^{-1}$. By contrast, there is very little field-dependence associated with either the A_g -symmetry electronic scattering response or the phonons. We have also used Eq. 1 to fit the field-dependent B_{1g} Raman response. While it is found that there may be a small variation in B_L and α with increasing field, the best fits are obtained by assuming that the dominant effect of the magnetic field is to decrease the static contribution of the scattering rate $\Gamma_{0B_{1g}}$ (see inset of Fig. 1 (b)), which can be related to the dc magnetoresistivity according to the relationship, $\rho(H, T) = 4\pi\Gamma_{0B_{1g}}(H, T)/\omega_{pD}^2$, where ω_{pD} is the Drude plasma frequency. Note that the small influence of magnetic field on the parameter α implied by these fits reflects the fact that the system is far from a magnetic-field-induced metal-insulator transition at the temperatures investigated. As seen in the inset of Fig. 1(b), the size of the field-dependent $\Gamma_{0B_{1g}}$ is highest near T_c , and there is a decreasing field effect for $T < T_c$. By $T \sim 5$ K, there is no discernible field-dependence. Thus, within the context of the DE model, the strong field-dependence of the B_{1g} electronic Raman response can be simply interpreted as due to a decrease in spin scattering, and a concomitant increase in (e_g) carrier mobility, caused by increased alignment of the Mn spins upon applying a magnetic field. However, there are several important respects in which the DE model cannot fully explain our field-dependent Raman data. For example, in Fig. 2 we plots the temperature-dependence of the fractional change in the integrated electronic scattering intensity at $H = 8$ T, $\Delta I(H = 8\text{T})/I(0\text{T})$, for both $T_c \sim 300$ K and $T_c \sim 145$ K samples. It can be seen in Fig. 2 that the field-dependence of the B_{1g} electronic scattering response persists at temperatures for which the magnetoresistance, $-\left[\rho(H = 5\text{T}) - \rho(0\text{T})\right]/\rho(0\text{T})$, is nearly zero. Notably, the persistent field-dependence of the B_{1g} electronic Raman response below T_c is further evidence that the FM phase of the manganese perovskites is inhomogeneous, possibly comprised of coexisting metallic regions and localized states in the form of remnant small polarons. This picture is also supported by extended x-ray absorption fine-structure [12], muon spin relaxation measurements [12], field-dependent thermoelectric power [13], and temperature-dependent Raman scattering [7], all of which report evidence for the presence of localized states even in the FM phase of the CMR manganese perovskites.

In summary, the temperature- and field-dependent Raman scattering spectra of the manganese perovskites were investigated. The low-frequency electronic Raman spectrum in the paramagnetic-insulating phase of these materials is characterized by a diffusive Raman scattering response, while a nearly flat continuum response is observed in the ferromagnetic-metallic state. We also find that the B_{1g} -symmetry electronic scattering intensity is significantly reduced with applied magnetic field near T_c , in a manner reminiscent of the dc magnetoresistivity. The strongly field-dependent scattering rate in the B_{1g} channel is consistent with a highly field-dependent mobility along the Mn-O bond direction, as expected in the double exchange mechanism. In addition, we observe a field-independent A_g electronic scattering contribution, and a substantial field-dependence in the B_{1g} electronic scattering response for $T \ll T_c$, which suggest that the ferromagnetic phase is inhomogeneous, perhaps consisting of both metallic and insulating contributions.

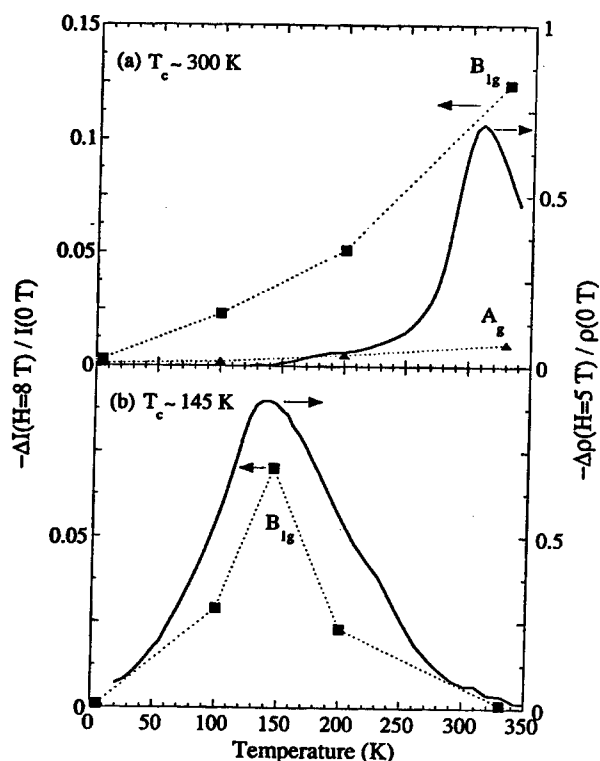


FIGURE 2. The temperature-dependence of the fractional change in integrated electronic spectral weight at $H = 8$ T of two samples for different scattering geometries. Shown for comparison are the temperature-dependence of the negative magnetoresistance ratio at $H = 5$ T (solid lines).

ACKNOWLEDGEMENTS

We are indebted to G. Blumberg for technical help and appreciate valuable discussions with M.B. Salamon. This work is supported by the Department of Energy under Grant No. DEFG02-96ER45439.

REFERENCES

1. P. Schiffer *et al.*, Phys. Rev. Lett. **75**, 336 (1995).
2. C.H. Chen and S-W. Cheong, Phys. Rev. Lett. **76**, 4042 (1996).
3. A.P. Ramirez *et al.*, Phys. Rev. Lett. **76**, 3188 (1996).
4. C. Zener, Phys. Rev. **82**, 403 (1951); P.W. Anderson and H. Hasegawa, *ibid.* **100**, 675 (1955); J. Goodnough, *ibid.* **100**, 564 (1955); P.-G. de Gennes, *ibid.* **118**, 141 (1960).
5. A.J. Millis, P.B. Littlewood, and B.I. Shraiman, Phys. Rev. Lett. **74**, 5144 (1995); A.J. Millis, B.I. Shraiman, and R. Mueller, *ibid.* **77**, 175 (1996); A.J. Millis, Nature **392**, 147 (1998).
6. C.M. Varma, Phys. Rev. B **54**, 7328 (1996).
7. S. Yoon *et al.*, Phys. Rev. B **58**, 2795 (1998).
8. M. Cardona and I.P. Ipatova, in Elementary Excitations in Solids edited by J.L. Birman, C.Sébenne and R.F. Wallis (Elsevier Science Publ., Amsterdam, 1992), p. 237; A. Zawadowski and M. Cardona, Phys. Rev. B **42**, 10732 (1990); A. Virosztek and J. Ruvalds, *ibid.* **45**, 347 (1992).
9. M. Chandrasekhar, M. Cardona, and E.O. Kane, Phys. Rev. B **16**, 3579 (1977); G. Contreras, A.K. Sood, and M. Cardona, *ibid.* **32**, 924 (1985).
10. T. Katsufuji and Y. Tokura, Phys. Rev. B **49**, 4372 (1994).
11. P. Nyhus *et al.*, Phys. Rev. B **56**, 2717 (1997).
12. R.H. Heffner, M.F. Hundley, and C.H. Booth (unpublished).
13. M.F. Hundley *et al.*, Appl. Phys. Lett. **67**, 860 (1995); M. Jaime *et al.*, *ibid.* **68**, 1576 (1996); T.T.M. Palstra *et al.*, Phys. Rev. B **56**, 5104 (1997).

Local Lattice Effects in Oxides

Despina Louca and George H. Kwei

Los Alamos National Laboratory

Condensed Matter and Thermal Physics Group,

MST 10, MS K764, Los Alamos, NM 87545

Abstract. Neutron diffraction measurements were used to investigate the local atomic structure of manganese and cobalt oxides. Static Jahn-Teller (JT) distortions present in the lightly doped perovskite manganates were found in metallic compositions as well. The cooperativeness of the distortions is however lost as the doping is increased. In the two-layer manganates, the existence of a local JT effect helps explain the similarities in the properties between cubic and layered systems. In the cobalt system, the coupling strength of the lattice to the e_g states during the thermal activation from the ground, low-spin (LS) state to an excited, intermediate (IS) or high-spin (HS) states for Co in LaCoO_3 changes as a function of temperature. The introduction of extra carriers by doping of $\text{La}_{1-x}\text{Sr}_x\text{CoO}_3$ stabilizes the IS JT states, populated at a rate proportional to the charge density. The JT distortions induced in this system are dynamic in nature if compared to the ones in the manganates.

INTRODUCTION

Cobalt and manganese oxides have been interesting to study as their magnetic ordering and transport properties can change with temperature, pressure, charge carrier density and applied magnetic field. More recently, the interest was renewed in this class of materials due to the colossal magnetoresistance (CMR) effect in the manganese oxides which is associated with a large drop in the resistivity under an applied field. Although cobalt oxides do not exhibit the CMR effect in spite of their high metallicity, they show very similar transitions in their properties. This motivated us to investigate a possible mechanism that might commonly be present in these two classes of oxides.

The lattice degree of freedom has been suggested to contribute significantly to the mechanism that brings about the CMR phenomenon as well as the various transitions in the properties (1). In this paper, we present evidence pointing towards a one-to-one correspondence

between the local atomic structural distortions and the transitions in the magnetic and transport properties (2-4). It is the aim to show that understanding the microscopic lattice changes under the experimental conditions is a step towards understanding the physical properties in this class of oxides.

EXPERIMENT

The pulsed neutron diffraction measurements collected in the time-of-flight (TOF) mode were performed at the Intense Pulsed Neutron Source (IPNS) of the Argonne National Laboratory. Data were collected at temperatures ranging from 10 K to 350 K. They were corrected for absorption, incoherent scattering, multiple scattering and inelastic scattering (Placzek correction) to obtain the structure function, $S(Q)$, ($Q = 4\pi\sin\theta/\lambda$, where Q is the momentum transfer, θ is the diffraction angle and λ is the wavelength of a neutron) up to Q_{\max} of 35 \AA^{-1} . The high- Q portion of the data is particularly important in this study because it carries information regarding small local displacements of atoms. The PDF, $\rho(r)$, is calculated by Fourier transforming the structure function, $S(Q)$, in the following way:

$$\rho(r) = \rho_0 + \frac{1}{2\pi^2 r} \int_0^\infty Q[S(Q) - 1] \sin(Qr) dQ \quad (1)$$

where ρ_0 is the average atomic number density of the sample. The PDF is a real space representation of atomic pair-density correlations (5). The PDF analysis has been used for the studies of glasses, liquids as well as other crystalline materials, and it has been proven effective and reliable in determining the local atomic structure. The PDF analysis takes into account the full structural information including the diffuse scattering intensity up to high values of Q . It can describe periodic as well as aperiodic structures accurately, and this technique can provide information regarding any local deviations from their average crystallographic structure.

RESULTS AND DISCUSSION

A. $\text{La}_{1-x}\text{Sr}_x\text{CoO}_3$

The ground state electronic spin configuration of Co in the parent compound, LaCoO_3 , is the low-spin (LS) ($t_{2g}^6 e_g^0$) state. A broad transition in the magnetic susceptibility observed at ~ 100 K corresponds to the thermal activation to an excited state which could be either a high-spin (HS) ($t_{2g}^4 e_g^2$) or an intermediate spin (IS) ($t_{2g}^5 e_g^1$) configuration. The low temperature crystal structure is rhombohedral with $R\bar{3}C$ symmetry (6). With the e_g orbitals empty, the directional Coulomb repulsion between the Co and O atoms is minimal and the CoO_6 octahedra are almost symmetric where the Co-O bond distances are quite similar. The nature of the transition from the LS state was investigated by studying the temperature dependence of the Co-O bond.

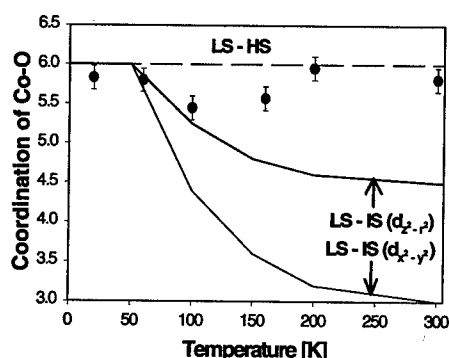


FIGURE 1. The local coordination number of Co as a function of temperature for LaCoO_3 . The distortions strongly couple to the LS-IS transition up to 100 K where the expected change in the local environment is taken from ref. (7) (solid lines). Above 100 K, a mixed spin state is present, gradually converting to the HS configuration (9).

Integration of the area under the first PDF peak provides the first coordination shell for Co. In an ideal octahedral environment without any distortions, it is 6. As the e_g orbital is thermally populated, the CoO_6 octahedral environment is modified depending on the coupling strength of the e_g to the lattice. In the weak coupling limit, an IS transition looks structurally similar to an HS state because the atomic distortions are small. In the strong coupling limit, however, the IS state has a single occupancy of the e_g orbitals resulting in a JT active mode, whereas the HS is not e_g JT-active. Population of a single level in the e_g orbitals will be reflected as a split in the Co-O distances to short and long. The ratio of short and long bonds will depend on the orbital that actually becomes occupied. On the other hand, the HS transition produces distortions that are associated with small displacements of the oxygen atoms (8) and almost no split of the Co-O bondlengths. The lines of Fig. 1 represent the effective coordination resulting from the two types of transitions. The results correspond to an LS \rightarrow IS

transition up to 100 K, with d_{z^2} orbital occupancy. Deviations from the LS-IS strong coupling limit are observed from 100 - 300 K which suggest the activation to both HS and IS states.

With the introduction of Co^{4+} sites through Sr doping, the local atomic structure changes. The percentage of CoO_6 sites in the IS state is determined by calculating the number of short Co-O bonds and subtracting that number from 6, the total number of bonds in the octahedron (4). This gives an estimate of the number of sites with JT distortions, Fig. 2, which increases

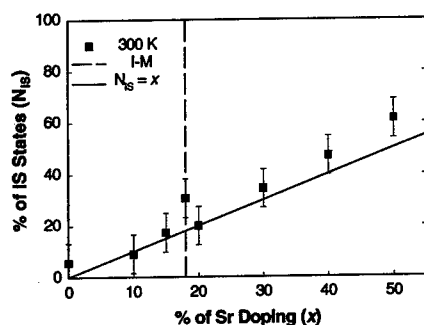


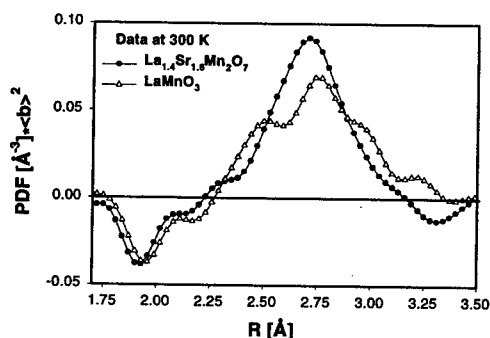
FIGURE 2. The percent of IS sites formed as a function of doping. At 300 K, the number of IS sites is linearly proportional to x where the system is a paramagnetic insulator.

almost linearly with the charge concentration in the paramagnetic insulating phase, at a rate that is almost equal to x (solid line). This represents an increase in the population of the JT-active IS states due to the straightening of the Co-O-Co bonds with doping. The IS state appears for different reasons with temperature (in LaCoO_3) than with doping. As a function of temperature, the higher entropy of the higher spin states drives the transition, while as a function of doping, the increase in the average Co-O bondlength reduces the crystal field splitting and shifts the balance towards the higher spin states.

B. $(\text{La/Sr})_{n+1}\text{Mn}_n\text{O}_{3n+1}$

The CMR effect is exhibited both by the perovskite as well as the layered manganese oxides. While the double exchange (DE) interaction was the proposed mechanism used to explain the spin-to-charge coupling in these materials, it is now an established fact that the lattice plays an important contribution in the microscopic functionalities of these materials. We established that a local Jahn-Teller (JT) distortion of similar magnitude as the one present in the perovskite manganites is found in the two-layer materials as well. This is demonstrated by

the PDF's of the local structure of the pure perovskite LaMnO_3 (Fig. 3), compared to



$\text{La}_{1.4}\text{Sr}_{1.6}\text{Mn}_2\text{O}_7$ ($x = 0.30$). Due to the cooperative JT phenomena in LaMnO_3 , the first peak

FIGURE 3. The local structure of the layered compound, $\text{La}_{1.4}\text{Sr}_{1.6}\text{Mn}_2\text{O}_7$, is compared to the one obtained for pure LaMnO_3 at 300 K. The PDF's have been renormalized with the average scattering length. The first peak in the PDF is the Mn-O peak and is negative because the neutron scattering length for manganese is negative.

in the PDF which corresponds to the MnO_6 octahedron splits into two at 1.95 and at 2.15 Å. For comparison, the same peak in the layered material also splits into two, strongly suggesting that local JT effects are most likely present in this system as well.

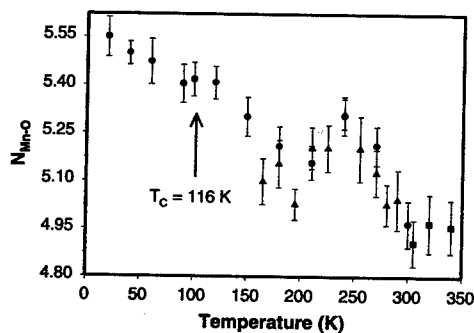


FIGURE 4. The number of short Mn-O bonds, $N_{\text{Mn-O}}$, increases by lowering the temperature.

The temperature dependence of the Mn-O correlations is determined from the changes of the octahedral environment. As the peak at 1.95 Å is clearly defined we integrated the area under this peak which corresponds to the number of short bonds, $N_{\text{Mn-O}}$ within the octahe-

dron. In the absence of any JT distortions, $N_{\text{Mn-O}}$ is 6. From the data it is seen that at room temperature, about 50 % of the sites have the JT distortion. Thus 50 % of the sites form polarons, a fraction that is higher than the 30 % single-site small polarons expected from the charge concentration. With cooling, more sites become undistorted giving rise to structural uniformity in the metallic state. In addition, the changes observed around 250 K suggest a change in the rate of polaron formation at temperatures away from the ferromagnetic transition. This might correspond to an increase in the transport in the ab-plane, prior to any transport commencing along the c-axis. This could also indicate a crossover from small to large polarons (10).

CONCLUSION

The evidence provided above showed how local lattice effects can be measured in a unique way using powder neutron diffraction, especially the PDF technique. This has allowed us to identify the true nature of the polarons in a variety of complex oxides, and has helped to establish the connection between local distortions and metal-insulator/magnetic phase transitions. This work will be extended to include dynamical local effects.

ACKNOWLEDGMENTS

The authors would like to acknowledge valuable discussions particularly with H. Röder, J. L. Sarrao, T. Egami, J. B. Goodenough, A. R. Bishop, J. D. Thompson, J. F. Mitchell, E. L. Brosha, M. Hundley, C. H. Booth, B. Dabrowski, R. H. Heffner and S. Trugman. Work at the Los Alamos National Laboratory is performed under the auspices of the U.S. Department of Energy under contract W-7405-Eng-36. The IPNS is supported by the U.S. Department of Energy, Division of Materials Sciences, under contract W-31-109-Eng-38.

REFERENCES

1. Röder, H., Zang, J., and Bishop, A.R., Phys. Rev. Lett. **76**, 1356-1359 (1996).
2. Louca, D., Egami, T., Brosha, E.L., Röder, H., Bishop, A.R., Phys. Rev. B **56**, 8992-8995 (1997).
3. Louca, D., Kwei, G.H., Mitchell, J.F., Phys. Rev. Lett. **80**, 3811-3814 (1998).
4. Louca, D., *et al.*, submitted Phys. Rev. Lett. (1998).
5. Toby, B.H. and Egami, T., Acta Crystall. A **48**, 336-346 (1992); Egami, T. and Billinge, S.J.L., Prog. Mater. Sci. **38**, 359-424 (1994).

6. Megaw, H.D. and Darlington, C.N.W., *Acta Crystall. A* **31**, 161-173 (1975); Thornton, G., *et al.*, *J. Solid State Chem.* **61**, 301-307 (1986); Petrov, A. N., *et al.*, *Solid State Ionics* **80**, 189-199 (1995).
7. Saitoh, T., *et al.*, *Phys. Rev. B* **55**, 4257-4266 (1997).
8. Bersuker, I.B., *Electronic Structure and Properties of Transition Metal Compounds* (John Wiley & Sons, Inc., New York, 1996), 279.
9. Asai, K., *et al.*, *J. Phys. Soc. Japan* **67**, 290-296 (1998).
10. Röder, H., private communication.

Measurement of the spin-polarization of LaSrMnO

M. S. Osofsky,¹ B. Nadgorny,¹ R. J. Soulen, Jr.,¹ P. Broussard,¹ M. Rubinstein,¹ J. Byers,^{1,2} G. Laprade,³ Y. M. Mukovskii,⁴ D. Shulyatev,⁴ and A. Arsenov⁴

¹*Naval Research Laboratory, Washington, D.C. 20375*

²*George Washington University, Washington, DC*

³*INSA, Toulouse, France*

⁴*Moscow State Steel and Alloys Institute, Moscow, Russia*

Abstract. A new method for determining the transport spin-polarization, point contact tunneling from a low temperature superconductor into a ferromagnet, is used to determine the spin polarization of several LaSrMnO thin films and crystals. The Andreev reflection process and its utility in measurements of spin-polarization are described. Preliminary results for the spin polarization of LSMO are presented.

INTRODUCTION

The doped manganates have generated a great deal of interest recently due to their peculiar magnetic and transport properties. Specifically, when appropriately doped and annealed there exists a Curie temperature where the samples undergo a paramagnetic to ferromagnetic transition which is nearly coincident with a transformation from activated to metallic or nearly metallic resistivity. One of the most studied of these materials is $\text{La}_{0.7}\text{Sr}_{0.3}\text{MnO}_3$ (LSMO).

It is generally believed that these materials are double exchange ferromagnets[1,2] and that the conduction electrons are 100% spin polarized below the Curie temperature. Such materials are of considerable interest for fundamental studies of spin polarized transport and as critical components in a new class of electronic devices[3]. In fact, the low temperature (4K) performance of ferromagnet/insulator/ferromagnet (FIF) tunneling devices, fabricated using LSMO as the ferromagnetic layers indicates that these oxides are indeed highly spin-polarized[4,5].

A new technique[6,7], based on the suppression of Andreev scattering, has been developed for determining the spin polarization of a ferromagnet. Soulen, *et al.*[6] have shown that a modified Blonder-Tinkham-Klapwijk (BTK)[8] analysis of point-contact tunneling conductance data of a low temperature superconductor into a ferromagnet (or vice versa) can be used to determine the ferromagnet's transport spin polarization. This method has the advantage of being versatile, allowing the study of films, foils or crystals of virtually any metallic material without the necessity of forming planar tunnel junctions. The results for conventional ferromagnets have been confirmed

by Upadhyay, *et al.*[7] who observed the suppression of Andreev reflection in microlithographically fashioned SF junctions.

ANDREEV REFLECTION

Andreev reflection is a process that occurs at a normal metal/superconductor interface in which normal current converts into supercurrent[9]. Figure 1 illustrates the process. In figure 1a, a spin-up electron approaches the interface. Since the superconductor has a gap, Δ , there are no available single particle states within Δ of the Fermi energy and the electron cannot enter the superconducting condensate. The only way for the "up" electron to enter is as part of a Cooper pair. This can happen only if a "down" electron also enters the superconductor from the normal metal. For this to occur, a hole-with momentum and spin opposite that of the down electron-must be reflected back into the normal metal. Figure 1b shows a simplified energy diagram representing the availability of states in the down band for an unpolarized normal metal. These holes add to the transport current and thus double the conductance, dI/dV , for voltages less than Δ (figure 2). In the 100% spin-polarized case (Fig. 1c) the Andreev process is suppressed by the lack of states near the Fermi energy in the "down" band. Thus the conductance is suppressed to zero for $V < \Delta$. The expected normalized conductance spectra at $T=0$ K are shown in figure 2. The curves broaden at higher temperatures.

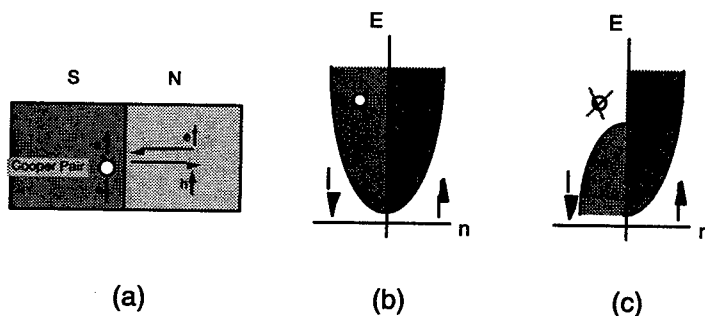


FIGURE 1. Schematic diagram of Andreev reflection at a normal metal/superconductor interface. a) An electron propagates across the interface creating a Cooper pair in the superconductor and a hole which is reflected into the normal metal. b) Density of states diagram showing the availability of states in the "down" band for an unpolarized normal metal. c) Density of states diagram showing that there are no holes available for Andreev reflection in a 100% spin-polarized normal metal.

CONDUCTANCE MEASUREMENTS

The probes for this study were fabricated by mechanically polishing a Nb rod to a sharp point using sandpaper. The tip was attached to a drive shaft which was vertically positioned above the sample. The shaft was driven by a micrometer mechanism capable of moving the point linearly by 100 nm per revolution. The measurements were made using a conventional four-terminal arrangement while the point contact and sample were immersed in a liquid helium bath at either 4.2 K or 1.5 K. The dI/dV data was obtained by standard AC lock-in techniques at a frequency of 2 kHz[6]. Figure 3 shows a schematic diagram of the experimental apparatus. The point contacts were formed by forcing the superconducting Nb tip into the LSMO samples. Details of the point contact conductance measurements are presented elsewhere[6].

Several thin film and crystal manganates were studied. Crystals of $\text{La}_{0.7}\text{Sr}_{0.3}\text{MnO}_3$ were grown by a floating zone technique, which has been described in a previous report[10]. Thin films of $\text{La}_{0.7}\text{Sr}_{0.3}\text{MnO}_3$ were grown by off-axis sputtering using composite targets of LSMO material mounted in a copper cup. The substrates were (100)-oriented neodymium gallate (NdGaO_3) silver-pasted onto a stainless steel substrate holder that was radiatively heated from behind by quartz lamps. Although there was no direct measurement of the holder temperature for the samples prepared for this study, previous runs (under nominally the same conditions) using a thermocouple clamped onto the front surface of the holder indicated a temperature of 670° C. The LSMO target was dc-sputtered in a sputter gas composed of 80% Ar and 20% O_2 (as measured by flow meters) and at a total pressure of 100 mTorr. These conditions gave deposition rates of approximately 17-50 nm/hr, with film thicknesses being typically 100 nm. After deposition, the samples were cooled in 100 Torr of oxygen. Similar growth conditions have been reported for LCMO films[11].

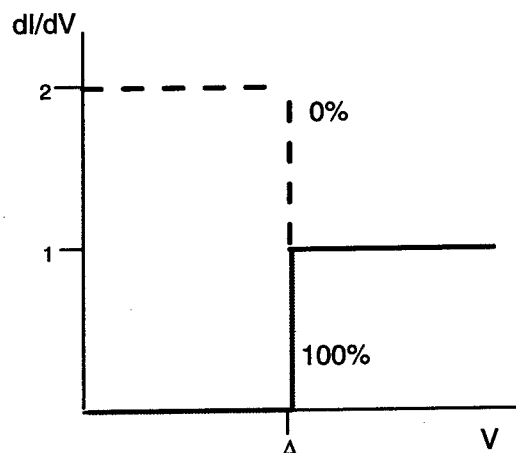


FIGURE 2. Expected normalized conductance for unpolarized and 100% spin-polarized normal metals at $T=0$ K.

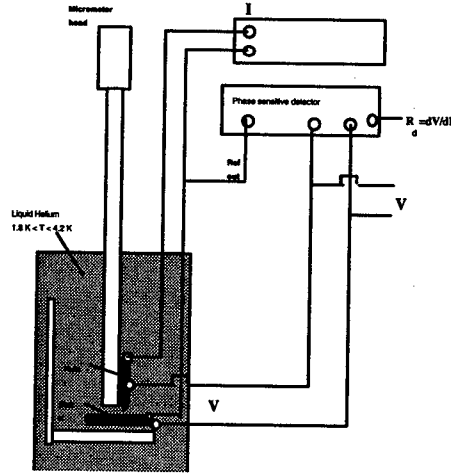


FIGURE 3. Schematic diagram of the apparatus.

Figure 4 shows the results for the Nb point into a $\text{La}_{0.7}\text{Sr}_{0.3}\text{MnO}_3$ thin film taken at 1.5 K. The spin-polarization can be calculated from the conductance curves using a modified BTK theory[6,8]. At $T=0$ this theory yields:

$$\frac{1}{G_n} \frac{dI}{dV} = 2(1 - P_c) \quad (1)$$

for $V < \Delta$ where G_n is the normal conductance (for $V > \Delta$) and

$$P_c = \frac{N_\uparrow(E_F)v_{F\uparrow} - N_\downarrow(E_F)v_{F\downarrow}}{N_\uparrow(E_F)v_{F\uparrow} + N_\downarrow(E_F)v_{F\downarrow}} \quad (2)$$

where $N_\uparrow(E_F)$ and $N_\downarrow(E_F)$ are the density of states of the up and down bands respectively and $v_{F\uparrow}$ and $v_{F\downarrow}$ are the Fermi velocities for the up and down bands respectively.

The polarization of the samples can be estimated from the conductance values at $V=0$ using eq. 1. This analysis shows that the spin-polarization of the film is approximately 80%.

These results show that though the spin-polarization of LSMO is high, it is not 100%. Factors such as surface morphology and paramagnetic impurities could be responsible for the lower values of spin polarization that were obtained.

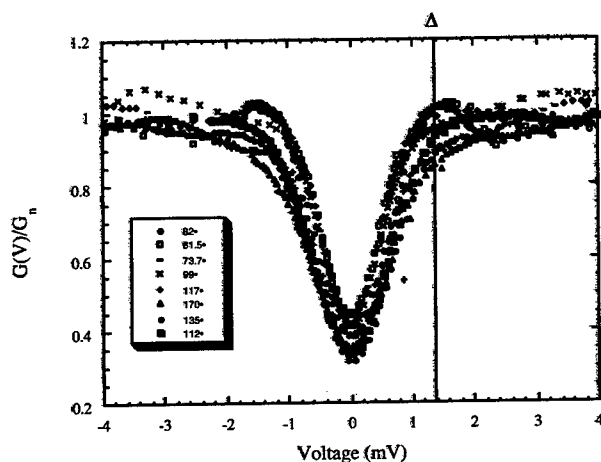


FIGURE 4. Nb point into $\text{La}_{0.7}\text{Sr}_{0.3}\text{MnO}_3$ thin film at 1.5 K for several junction resistances. The energy gap of Nb, 1.4 mV, is indicated by Δ .

ACKNOWLEDGMENTS

This work was supported in part by the Office of Naval Research under Contract No. N0001496WX20507 and DARPA under ARPA order #B118/98. B. N. was supported under an ASEE fellowship. We also acknowledge T. Clinton, G. Prinz, S. Wolf, G. Deutscher, I. Mazin, M. Johnson, and K. Hathaway for useful conversations and J. Claassen for technical assistance.

REFERENCES

1. C. Zener, *Phys. Rev.* **82**, 403 (1951).
2. P. W. Anderson and H. Hasegawa, *Phys. Rev.* **100**, 675 (1955).
3. G. Prinz, *Physics Today* **48**, 58 (1995).
4. Y. Lu *et al.*, *Phys. Rev. B* **54**, 8357 (1996).
5. J. Z. Sun *et al.*, *Appl. Phys. Lett.* **70**, 1769 (1997).
6. R. J. Soulen, Jr., J. M. Byers, M. S. Osofsky, B. Nadgorny, T. Ambrose, S. F. Cheng, P. R. Broussard, C. T. Tanaka, J. Nowak, J. S. Moodera, A. Barry, and J. M. D. Coey, *Science* **282**, 85 (1998).
7. S.K. Upadhyay, A. Palanisami, R. N. Louie, and R. A. Buhrman, *Phys. Rev. Lett.* **81**, 3247 (1998).
8. G. E. Blonder, M. Tinkham, and T. M. Klapwijk, *Phys. Rev. B* **25**, 4515 (1982).
9. A. F. Andreev, *Sov. Phys. JETP* **19**, 1228 (1964).
10. M. Balbashov, S. G. Karabashov, Y. M. Mukovskii, and S. A. Zverkov, *J. Cryst. Growth* **167**, 265 (1996).
11. P.R. Broussard, S.Q. Qadri, V.M. Browning and V.C. Cestone, *Appl. Surf. Sci.* **115**, 80 (1997).

Anomalous Linear Resistivity from ~ 1 to 10^3 K in $\text{Sr}_2\text{RuO}_{4-\delta}$

Davor Pavuna, László Forró and Helmuth Berger

*Department of Physics, Ecole Polytechnique Federale de Lausanne,
CH - 1015 Lausanne, Switzerland*

Abstract. We discuss striking, linear resistivity in single crystals of $\text{Sr}_2\text{RuO}_{4-\delta}$ that persist over three decades of temperature, up to ~ 1050 K, while the superconductivity remains confined < 1 K. This suggests that linear resistivity is not an exclusive feature of the N- state of high- T_c cuprates, but rather of all layered oxides, especially perovskites, possibly even independently of the magnitude of T_c .

INTRODUCTION

It was the discovery of superconductivity < 1 K in the Sr_2RuO_4 compound that has renewed the interest in ruthenates, especially as it is the first copper free layered perovskite superconductor^{1,2}. It is well established that layered copper perovskites, in addition to high critical temperatures, also exhibit rather anomalous normal state properties³⁻⁵. One such 'anomaly' is the linear temperature dependence of resistivity: for example, the $\text{Bi}_2\text{Sr}_2\text{CuO}_6$ ($T_c \sim 8$ K) and $\text{La}_{2-x}\text{Sr}_x\text{CuO}_4$ ($T_c \sim 30$ K) exhibit linear resistivity up to 700 K⁴ and 1100 K³, respectively. The understanding of electronic properties of high- T_c cuprates still presents a major challenge, despite a remarkable progress in both, sample preparation and advanced experimental techniques. However, there are also many superconducting oxides with rather low- $T_c < 15$ K: for example, doped SrTiO_{3-x} , K_xWO_3 , LiTi_2O_4 , $\text{Ba}(\text{PbBi})\text{O}_3$. So, given recent enhanced interest in ruthenates it is timely to consider electronic characteristics and transport of all of these oxides.

Here we discuss resistivity of single crystals of $\text{Sr}_2\text{RuO}_{4-\delta}$, grown by the flux technique. The measured temperature dependence of Hall coefficient is rather similar to the results reported for other cuprates⁶. However, the electrical resistivity is strikingly linear up to ~ 1050 K while superconductivity remains confined below 1 K. As shown in Figure 1, our single crystals show no saturation even at low temperatures thereby clearly contradicting the conventional metallic transport picture. As the temperature dependence

of resistivity of our $\text{Sr}_2\text{RuO}_{4-\delta}$ crystals closely resembles data reported for other slightly underdoped, oxygen-depleted cuprates, especially LSCO, our result is a direct extension of initial reports on anomalous linear resistivities of superconducting cuprates.

RESULTS AND DISCUSSION

Structurally the metallic Sr_2RuO_4 belongs to the same tetragonal K_2NiF_4 family as the aforementioned $\text{La}_{2-x}\text{Sr}_x\text{CuO}_4$ superconductor, in contrast to the ferromagnetic SrRuO_3 that has nearly cubic perovskite structure¹¹. Both compounds have been extensively studied by a variety of techniques⁷⁻⁹ and recent quantum oscillations studies in the normal state of Sr_2RuO_4 show the form of the quasiparticle spectrum that may be consistently interpreted in terms of a two-dimensional Fermi liquid⁹. The anomalous transport properties of cuprates have been extensively discussed in the literature^{3-5,10-13}. Transport and electronic properties of ferromagnetic SrRuO_3 single crystals were discussed at length elsewhere¹¹ so here we concentrate only on the linear resistivity in $\text{Sr}_2\text{RuO}_{4-\delta}$. Our Hall effect measurements have been reported elsewhere⁶.

Detailed sample preparation was discussed elsewhere⁶; there is less than 1ppm Pt or other impurities in our samples. Here we note that our growth technique is different from that used by Maeno et al^{1,2} and MacKenzie et al^{9,15}. Their pristine samples were grown by the state-of-the-art zone melting, a technique that enables the growth of very clean crystals i.e. the degree of growth induced disorder is much smaller than in our case, with 'residual' resistivities of ~ 1 and $\sim 50 \mu\Omega\text{cm}$, respectively. This, as we shall see, has important consequences for understanding and discussion of our results.

For simplicity we refer to our samples as $\text{Sr}_2\text{RuO}_{4-\delta}$, and henceforth introduce the growth induced disorder into the chemical formula. The degree of uncertainty in the exact content and distribution of oxygen is given by the ' $4-\delta$ ', as is often done in the case of layered oxides. Obviously, there are other sources of disorder in our $\text{Sr}_2\text{RuO}_{4-\delta}$ samples; this is also true for $\text{La}_{2-x}\text{Sr}_x\text{CuO}_4$ superconductors or any K_2NiF_4 type compound, in general. Aforementioned simplification does not alter our results but simplifies the discussion and conclusions.

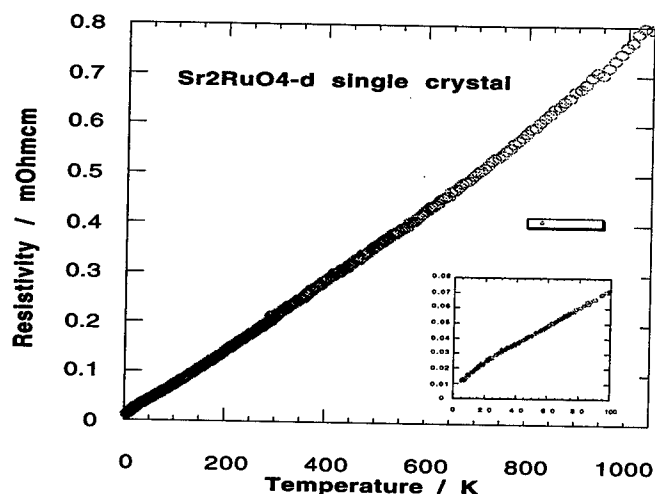


FIGURE 1. Striking linear resistivity over three decades of temperature in disordered $\text{Sr}_2\text{RuO}_{4-\delta}$ grown by the flux technique. Resistivity below 100K is shown in the insert.

Figure 1 shows the temperature dependence of resistivity $\text{Sr}_2\text{RuO}_{4-\delta}$ single crystal up to 1050K. As discussed at length elsewhere⁶, we emphasize the lack of saturation at low temperatures, apparently in contrast to the results from references 1, 9 and 15. However, as we already mentioned, this difference is mainly due to higher disorder in our samples, due to unavoidable differences in sample preparation and detailed treatment during and after the growth. Our inferred residual resistivity is $\sim 50 \mu\Omega\text{cm}$ (vs $\approx 1 \mu\Omega\text{cm}$ in high- T_c cuprates³). However, nowadays we know and therefore argue that this is not a unique feature of the high- T_c cuprates only.

Our linear resistivity down to low temperatures does not contradict the results and conclusions of MacKenzie et. al. who have measured T^2 dependence of the ab-plane resistivity¹⁵. Their transport results, and comprehensive study of magneto-oscillatory phenomena in the normal state⁹, show that their pristine crystals behave as a rather convincing example of the Landau-Fermi liquid metal, in this case the Sr_2RuO_4 single crystal grown by zone melting technique. Our results show that even in the case of such a clean metallic oxide one can increase/induce additional 'residual' scattering and consequently observe the resistive behavior that is usually measured in somewhat in Cambridge crystals) and consequently we estimate our elastic mean free path to be very short: only of the order of $\approx 1\text{nm}$. This is important as it probably implies that by introducing growth-induced disorder (and especially oxygen vacancies), the consequent

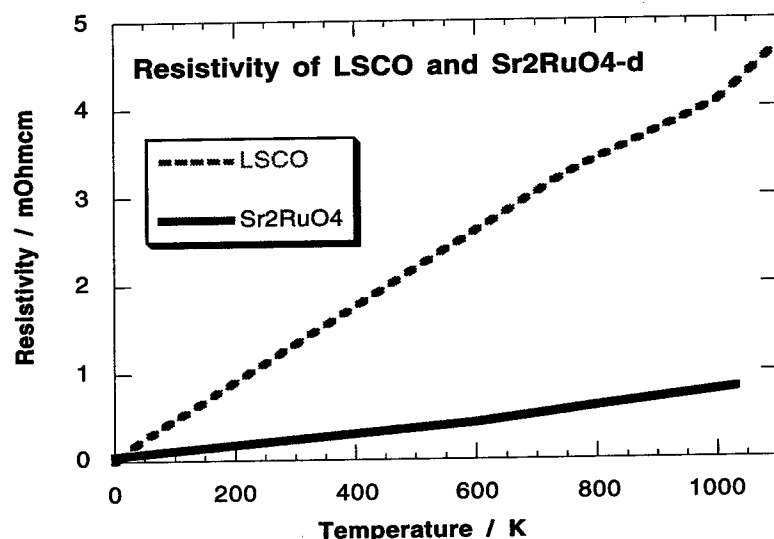


FIGURE 2. Linear resistivity of $\text{Sr}_2\text{RuO}_{4-\delta}$ single crystals grown by the flux technique⁵ compared to resistivity of LSCO high- T_c cuprate ceramic sample³.

scattering seems to effectively 'induce' linear resistivity behavior even at low temperatures. At present it is not clear whether this linearity simply 'masks' the Fermi-liquid T^2 -term that may remain 'hidden' underneath the disorder scattering; further studies are needed to clarify this point. The slope above 750K could be fitted with a power of 1.08; even in this range it is practically linear. We note that such linear $\rho(T)$ behavior in $\text{Sr}_2\text{RuO}_{4-\delta}$ up to $\sim 10^3\text{K}$ closely resembles the linear resistivity reported³ for single CuO_2 -layer superconducting $\text{La}_{2-x}\text{Sr}_x\text{CuO}_4$ ($T_c \sim 30\text{K}$): linear from $\sim 40\text{K}$ to 1100K (see Figure 2). Our result can therefore be considered as an extension of initial reports on anomalous linear resistivities 'underdoped' (and intrinsically somewhat disordered) HTSC cuprates. In the language of the well established HTSC phase diagram, the resistivity of our samples resembles behavior previously seen in cuprates close to optimum doping, or slightly 'underdoped'³, while the samples of MacKenzie et al⁹ behave more like 'overdoped' cuprates¹⁵. Similar, more 'conventional' metallic behavior, with T^2 behavior at low temperatures, was also measured in electron doped superconductors, for example in $\text{Nd}_{2-x}\text{Sr}_x\text{CuO}_4$ compound¹².

At present we are unaware of any model that specifically predicts or can convincingly account for essentially linear behavior of resistivity over three decades of temperature although most theories of HTSC, presented also elsewhere in this volume, discuss linear resistivity¹⁶. In our view, our result provides yet another puzzle to our present understanding of transport and N- state of layered oxides and suggests that anomalies, like linear resistivities exist also in low- T_c layered oxides and possibly even in non-superconducting phases, and that the presence of CuO_2 planes is evidently vital for truly high T_c 's (of $>50\text{K}$) as these are, so far, observed only in cuprates.

It is striking to see any physical quantity exhibit linear behavior over three decades of temperature. For example, ohmic junctions show linear I-V response but only over a limited range. We were not able to find in literature other examples of physical quantities that show essentially straight line response at very low and at rather high temperatures. In the simplest approximation it means that the electron scattering gives this linear resistivity over the energy range of $\approx 1\text{meV}$ up to $\approx 0.1\text{eV}$ which is again striking and requires an in-depth theoretical analysis; this certainly cannot be understood in terms of the conventional transport theory of metallic solids.

Finally, we note that the reflectance, ellipsometric and Raman spectra obtained by Bozovic et al¹⁴ on thin films of isotropic metallic oxides $\text{Ca}_{0.5}\text{Sr}_{0.5}\text{RuO}_3$ and $\text{La}_{0.5}\text{Sr}_{0.5}\text{CoO}_3$ closely resemble the spectra of high- T_c cuprates thus indicating that the 'anomalous' dielectric response could not be the sole root of high temperature superconductivity¹⁴. Most likely one needs a thorough understanding of all layered oxides in order to understand the N- and S- state anomalies of high- T_c cuprates.

CONCLUSIONS

In conclusion we have measured linear resistivity behavior that persists up to $\sim 10^3\text{K}$ in single crystals of $\text{Sr}_2\text{RuO}_{4.8}$ perovskite, in which the superconductivity remains confined $< 1\text{K}$. We observe no saturation at low temperatures that contradicts conventional metallic transport picture. Given rather high residual resistivity of our samples we argue that the conventional low temperature T^2 term, if present, is probably masked by the disorder scattering. As the temperature dependence of resistivity of our $\text{Sr}_2\text{RuO}_{4.8}$ crystals closely resembles data reported for other slightly underdoped, oxygen-depleted cuprates, especially LSCO, our result is a direct extension of initial reports on anomalous linear resistivities in superconducting cuprates. However, nowadays we know and therefore argue that this is not a unique, characteristic feature of the high- T_c cuprates only. Hence

we conclude that i) the linear non-Fermi liquid resistivity behavior exists also in non-cuprate perovskites, and ii) such behavior is not an exclusive signature of the unusual normal state of high- T_c cuprates but rather of layered oxides in general, and iii) possibly even independently of the existence of (high temperature) superconductivity in such layered oxides. Further studies, and especially in-depth theoretical analysis, are needed to account for such unusual resistivity behavior over three decades of temperature.

ACKNOWLEDGEMENTS

We gratefully acknowledge many discussions with numerous colleagues worldwide and the support from the EPFL and the Swiss National Fonds for Scientific Research.

REFERENCES

1. Y. Maeno et al, Nature **372**, 532 (1994)
2. D.H. Lu et al, Phys. Rev. Lett. **76** (25) 4845 (1996)
3. M. Gurvitch and A.T. Fiory, Phys. Rev. Lett. **59** (12) 1337 (1987)
4. S. Martin et al, Phys Rev Lett **60**, 2194 (1988)
5. see reviews by P. Allen et al, in *Physical Properties of High-Temperature Superconductors vol. I*, ed. D.M. Ginsberg, World Scientific, 1989, 213; N.P. Ong, ibid vol II, 459 (1990); N.P. Ong, Science **273**, p.321 (1996) and references therein
6. H. Berger, L. Forro, D. Pavuna, Europhysics Letters **41** (5), 531 (1998)
7. Tamio Oguchi, Phys Rev B **51** (2) 1385 (1995)
8. David J. Singh, Phys Rev B **52** (2) 1358 (1995)
9. A. P. Mackenzie et al, Phys. Rev. Lett. **76** (20) 3786 (1996)
10. N.P. Ong, Phys Rev B **43**, 193 (1991)
11. P.B. Allen et al, Phys. Rev. B **53** (8) p.4393 (1996)
12. W. Sadowski et al, J. of Less Common Metals **165**, 824 (1990)
13. D. M. Newns et al, Comm. Cond. Matt. Phys. **15** (5&6), 273 (1992)
14. I. Bozovic et al, Phys. Rev. Lett. **73** (10) 1436 (1994)
15. A.P. Mackenzie et al, Phys Rev B **54** (10) 7425 (1996)
16. see contemporary theoretical approaches elsewhere in this volume

Charge, Spin, and Lattice Excitations in Double-layer Manganites

D. B. Romero,^(1,2) Y. Moritomo,⁽³⁾ J. F. Mitchell,⁽⁴⁾ and
H. D. Drew⁽²⁾

⁽¹⁾ NIST-Optical Technology Division, Gaithersburg, MD 20899

⁽²⁾ Physics Dept., Univ. of Maryland, College Park, MD 20742

⁽³⁾ CIRSE and Dept. of Appl. Phys., Nagoya Univ., Japan

⁽⁴⁾ Mat. Science Div., Argonne Nat. Lab., Argonne, IL 60439

Abstract. A Raman-scattering investigation of the double-layer manganites, $\text{La}_{2-2x}\text{Sr}_{1+2x}\text{Mn}_2\text{O}_7$ ($x = 0.4, 0.5$), revealed signatures of a) charge stripe formation and melting, b) small polaron formation, and c) anisotropic quasiparticle dynamics in the ferromagnetic-metallic state. These observations and their implications are discussed in this work.

INTRODUCTION

The double-layer manganites, $\text{La}_{2-2x}\text{Sr}_{1+2x}\text{Mn}_2\text{O}_7$ where x is the doping level, are ideal systems to study the effects of electron-electron and electron-phonon interactions on the electron kinetic energy in low-dimensional systems. Their transport and magnetic properties are highly anisotropic [1], an indication of quasi-two dimensional behavior. Electron-diffraction studies [2] of half-filled ($x = 0.5$) doped compounds reveal an ordering of the Mn^{3+} and Mn^{4+} ions below a temperature around 200 K. However, it was shown recently that this charge-ordered phase does not survive at low temperatures [3]. Thus, the ground state of these charge-ordered insulators is still undetermined. For the pseudo-cubic manganite compounds such as $\text{La}_{1-x}\text{Sr}_x\text{MnO}_3$, there is accumulating evidence for the dominant role of Jahn-Teller small polarons in their magneto-transport properties [4]. In contrast, the tetragonal crystal field in the layered manganites can split the degenerate Mn e_g orbitals which could preclude the formation of polarons via the Jahn-Teller mechanism. Consequently, one can ask whether polarons are formed in the layered manganites and do they influence the insulating character of these compounds. Lastly, the nature of the ferromagnetic-metallic state is relatively unexplored.

To address the above issues, Raman investigation was carried on single crystals of the double-layer manganites with $x = 0.4$ and 0.5 over a wide range of temperatures ($T = 5$ K to 350 K) and magnetic fields ($H = 0$ T to 7.5 T). $\text{La}_{1.2}\text{Sr}_{1.8}\text{Mn}_2\text{O}_7$

($x = 0.4$) exhibits the phenomenon of colossal magneto-resistance (CMR) [1]. Its ground state is a ferromagnetic-metal. It becomes a paramagnetic-insulator above the Curie temperature $T_C \simeq 120$ K. For $\text{La}_1\text{Sr}_2\text{Mn}_2\text{O}_7$ ($x = 0.5$), the ground state is believed to be a charge-ordered antiferromagnetic insulator [5]. The low-energy excitations in both compounds are elucidated in this work.

OPTICAL PHONONS

The body-centered-tetragonal crystal structure [$I4/mmm(D_{4h}^{17})$] of the double-layer manganites is shown in Fig. 1(a). The typical polarization dependence of the room-temperature Raman spectra for these compounds is shown in Fig. 1(b) for $\text{LaSr}_2\text{Mn}_2\text{O}_7$. The sharp peaks are the optic phonons which are identified by their corresponding atomic vibration. This identification was derived from a group-theoretical analysis that predicted ($4A_{1g} + B_{1g} + 5E_g$) Raman-active phonons [6]. The in-plane E_g vibrations are not observed in the spectra in Fig. 1(b). On account of the symmetry of the site they occupy in the crystal structure of Fig. 1a, the $4A_{1g}$ phonons correspond to the symmetric c -axis vibrations of the (La,Sr), Mn, equatorial O_{xy} , and apical O_z atoms. They are observed, respectively, at 180 cm^{-1} , 244 cm^{-1} , 453 cm^{-1} , and 577 cm^{-1} in the xx , $x'x'$, and zz spectra, in accord with the Raman-selection rules. The only allowed B_{1g} phonon involving the c -axis out-of-phase vibrations of the O_{xy} atoms is seen at 326 cm^{-1} in the xx and $x'y'$ spectra.

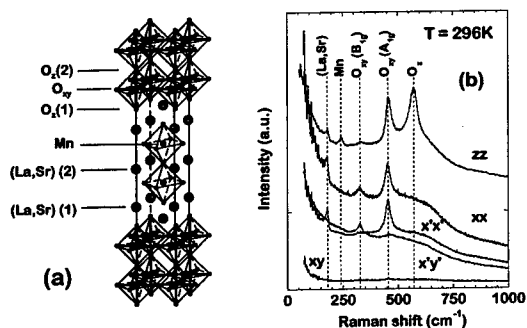


FIGURE 1. (a) Crystal structure and (b) typical room-temperature polarized Raman spectra of double-layer manganites shown here for $\text{LaSr}_2\text{Mn}_2\text{O}_7$.

CHARGE ORDERING

$\text{LaSr}_2\text{Mn}_2\text{O}_7$ becomes a charge-ordered antiferromagnetic insulator below the temperature $T_{co} \simeq 210$ K [2]. This transition is characterized by abrupt changes in the transport and magnetic properties of this compound. A direct evidence for the charge ordering is given by the observation by electron-diffraction studies [2] of superlattice peaks for $T < T_{co}$. The analysis of these extra diffraction peaks suggested that an alternating pattern of the Mn^{3+} and Mn^{4+} atoms along the Mn-O_{xy} bonds is formed in the charge-ordered state.

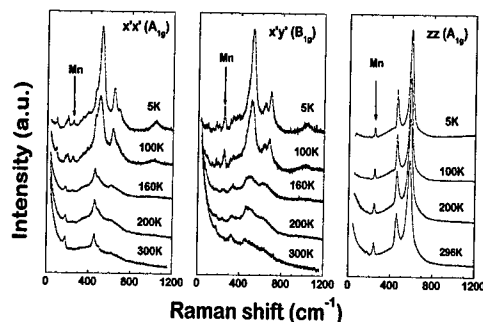


FIGURE 2. Evidence for symmetry breaking due to charge ordering in the MnO_2 plane in $\text{LaSr}_2\text{Mn}_2\text{O}_7$

The Raman signature for the charge ordering in $\text{LaSr}_2\text{Mn}_2\text{O}_7$ is presented in Fig. 2. In addition to the phonons associated with the tetragonal crystal structure, new features are observed below T_{co} . The Mn peak near 244 cm^{-1} which should be present only in the xx , $x'x'$, and zz spectra appears in the $x'y'$ as well. In addition, three strong peaks develop between 400 cm^{-1} to 800 cm^{-1} at $T = 5$ K. These results indicate that a structural-symmetry breaking has occurred in the charge-ordered phase. These new spectral features are absent in the zz spectra, suggesting that charge ordering is confined to the MnO_2 planes.

Recently, it was observed that the superlattice peaks observed near T_{co} in $\text{LaSr}_2\text{Mn}_2\text{O}_7$ disappear when $T \ll T_{co}$ [3]. This observation implies that the charge ordering pattern formed just below T_{co} does not survive in the low-temperature ground state of this compound. From the Raman point of view, no Raman-active phonons are associated with such a pattern because the Mn^{3+} , Mn^{4+} , and O_{xy} atoms occupy sites with inversion symmetry. Since new Raman features emerge below T_{co} , a different charge-ordered structure is formed at temperatures far below T_{co} . There is evidence in the pseudo-cubic manganites for the formation of Jahn-Teller stripes [7]. In this case, the stripes consist of square unit cells in which

the Mn^{4+} atom is at the center while the Mn^{3+} atoms occupy the corners of the square. The O_{xy} atoms are located along the diagonals halfway between the Mn^{3+} and Mn^{4+} sites. In this model, phonons of A_{1g} and B_{1g} symmetry are allowed for each of the Mn^{3+} and O_{xy} vibrations due to the lower symmetry of their sites in the one-dimensional stripe formed from this unit cell. The observation of a B_{1g} Mn phonon in the $x'y'$ spectra in Fig. 2 at $T \ll T_{\infty}$ is consistent with this picture. Two of the peaks at 521 cm^{-1} , 636 cm^{-1} , and 694 cm^{-1} in Fig. 2 could account for the O_{xy} phonons in the stripe phase. However, the selection rules for the A_{1g} and B_{1g} modes are not strictly obeyed by these phonons suggestive of a symmetry that is lower than a square unit cell.

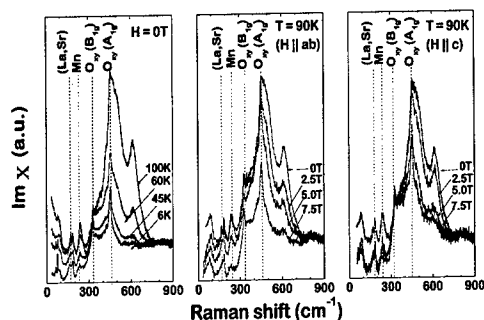


FIGURE 3. Evidence for the persistence of charge ordering in the colossal magnetoresistance compound $\text{La}_{1.2}\text{Sr}_{1.8}\text{Mn}_2\text{O}_7$.

Similar Raman features persists in the CMR compound $\text{La}_{1.2}\text{Sr}_{1.8}\text{Mn}_2\text{O}_7$ as illustrated in Fig. 3. The charge-stripe features disappear upon entry into the ferromagnetic-metallic state, either by lowering the temperature or by increasing the magnetic field. Note that only the phonons related to the tetragonal structure remains in this state. Because of the similar effects of the temperature and magnetic field, the suppression of the charge stripes is a consequence of the polarization of the Mn spins.

METAL-INSULATOR TRANSITION

In $\text{La}_{1.2}\text{Sr}_{1.8}\text{Mn}_2\text{O}_7$, the melting of the charge-stripe phase provides a signature of the insulator to metal transition at $T_C \simeq 120 \text{ K}$. In the metallic state, the ferromagnetic alignment of the Mn spins leads to the delocalization of the e_g electrons via the double-exchange mechanism which inhibits charge ordering. Additional signatures of the metal-insulator transition was also observed in tetragonal lattice anomalies [6] and in electronic Raman scattering.

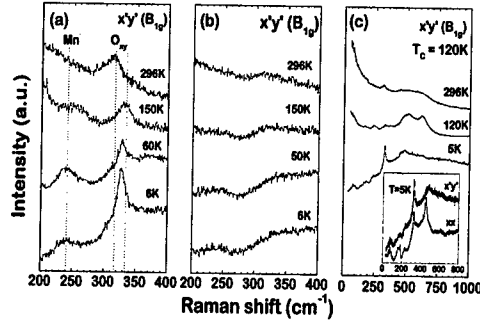


FIGURE 4. Signatures of the metal-insulator transition from (a) Lattice anomalies in $\text{La}_{1.2}\text{Sr}_{1.8}\text{Mn}_2\text{O}_7$ and their absence in $\text{Nd}_{1.2}\text{Sr}_{1.8}\text{Mn}_2\text{O}_7$ (b). (c) Electronic Raman scattering in $\text{La}_{1.2}\text{Sr}_{1.8}\text{Mn}_2\text{O}_7$.

1. Phonon Anomalies

The temperature dependence of the B_{1g} O_{xy} phonon in $\text{La}_{1.2}\text{Sr}_{1.8}\text{Mn}_2\text{O}_7$ is depicted in the $x'y'$ spectra of Fig. 4(a). This phonon is broad and weak for $T > T_C$. It evolves into a strong and asymmetric peak at $T = 6$ K, a typical Raman signature of a phonon coupled to a broad electronic continuum. The B_{1g} O_{xy} phonon displays an anomalous frequency shift as a function of temperature that resembles the non-linear T -dependence of the resistance [6]. As illustrated in Fig. 4(b), these effects are not observed in the antiferromagnetic insulator $\text{Nd}_{1.2}\text{Sr}_{1.8}\text{Mn}_2\text{O}_7$. Furthermore, the B_{1g} Mn phonon attributed to charge-stripe formation is not observed in this compound. This result is consistent with the interpretation discussed above since charge ordering does not occur in $\text{Nd}_{1.2}\text{Sr}_{1.8}\text{Mn}_2\text{O}_7$.

To digress briefly, the difference in the transport properties of $\text{La}_{1.2}\text{Sr}_{1.8}\text{Mn}_2\text{O}_7$ and $\text{Nd}_{1.2}\text{Sr}_{1.8}\text{Mn}_2\text{O}_7$ can be understood qualitatively in terms of their electronically-active e_g orbitals. The change from a metallic to an insulating ground state when $R = \text{La}$ is replaced by $R = \text{Nd}$ in $\text{R}_{1.2}\text{Sr}_{1.8}\text{Mn}_2\text{O}_7$ was attributed to the chemically-induced variation of the e_g electron orbital character from $d_{x^2-y^2}$ in $\text{La}_{1.2}\text{Sr}_{1.8}\text{Mn}_2\text{O}_7$ to $d_{3z^2-r^2}$ in $\text{Nd}_{1.2}\text{Sr}_{1.8}\text{Mn}_2\text{O}_7$ [8].

The anomalous behaviors of the B_{1g} O_{xy} phonon in $\text{La}_{1.2}\text{Sr}_{1.8}\text{Mn}_2\text{O}_7$ is attributed to its coupling to the in-plane ($d_{x^2-y^2}$) charge fluctuations. In this picture, such coupling is inhibited in $\text{Nd}_{1.2}\text{Sr}_{1.8}\text{Mn}_2\text{O}_7$ due to the out-of-plane ($d_{3z^2-r^2}$) character of the e_g orbitals. Recall that the B_{1g} O_{xy} phonon involves the out-of-phase c-axis vibrations of the O_{xy} atoms. This implies that the coupling of this phonon to the in-plane charge fluctuations must be mediated by an external mechanism. A possible mechanism is their coupling via a c-axis crystal electric field [6]. The

formation of small polarons can give rise to such electric field.

2. Electronic Raman Scattering

Raman scattering by the e_g electrons is observed in the double-layer manganites. In the paramagnetic-insulating state of $\text{La}_{1.2}\text{Sr}_{1.8}\text{Mn}_2\text{O}_7$, there is a quasielastic scattering feature as shown in Fig. 4(c) due to the diffusive motion of the charges and/or spins. This quasielastic peak develops into a nearly flat electronic continuum on entry into the ferromagnetic-metallic state (i.e. $T \simeq T_C$). At $T = 5$ K, the continuum is suppressed at low frequencies. The suppression is anisotropic. In the inset of Fig. 4(c), the decrease in the scattering intensity is linear below $\simeq 450$ cm^{-1} in the $x'y'$ spectrum while in the xx spectrum it is nearly zero below $\simeq 300$ cm^{-1} rising abruptly to a constant value. These results suggest an anisotropic quasiparticle dynamics. The transformation of the quasielastic scattering above T_C to an electronic continuum below T_C was also observed in the pseudo-cubic manganites [9]. However, the low-frequency suppression was not reported in these compounds which hints at the role of the quasi-2D nature of $\text{La}_{1.2}\text{Sr}_{1.8}\text{Mn}_2\text{O}_7$.

CONCLUSION

The main conclusions of the present work are: 1) The ground state of the charge-ordered layered manganites is characterized by the formation of one-dimensional stripe phases. The stripe correlations persist in the paramagnetic-insulating state of the CMR compounds, 2) Lattice anomalies due to polaron formation play a role in the transport properties of the layered manganites and, 3) The ferromagnetic-metallic state manifests an unusual anisotropic quasiparticle dynamics that is a hallmark of strongly-interacting electrons in quasi-2D systems.

We thank Dr. R.U. Datla for his interest in and support of this work. JFM acknowledges the support of the U.S. Department of Energy, Office of Basic Energy Sciences - Materials Sciences Division, under Contract No. W-31-109-ENG-38.

REFERENCES

1. Y. Moritomo *et al.*, *Nature* **380**, 141 (1996).
2. J. Q. Li *et al.*, *Phys .Rev. B* **57**, R3205 (1998).
3. T. Kimura *et al.*, *Phys .Rev. B* **58**, 11801 (1998).
4. C. H. Booth *et al.*, *Phys .Rev. Lett.* **80**, 853 (1998).
5. Y. Moritomo *et al.*, *Phys .Rev. B* **56**, R7057 (1997).
6. D. B. Romero *et al.*, *Phys .Rev. B* **58**, R14737 (1998).
7. S. Mori, C. H. Chen, and S. W. Cheong, *Nature* **392**, 473 (1998).
8. Y. Moritomo *et al.*, *Phys .Rev. B* **56**, 7057 (1997).
9. S. Yoon *et al.*, *Phys .Rev. B* **58**, 2795 (1998).

Universal Behavior of Magnetization Curves in Rb_3C_{60} Fullerene

Ming-Fong Tai¹, Jen-Bin Shi² and Chien-Jang Wu³

¹Department of Physics, National Chung Cheng University, Chia-yi 621, Taiwan, R.O.C.

²Department of Electronic Engineering, Feng-Chia University, Taichung 407, Taiwan, R.O.C.

³Department of Electro-optics Engineering, National Huwei Institute of Technology, Taiwan, R.O.C.

Abstract. The superconducting Rb_3C_{60} fullerene crystals with a transition temperature of 30.5 ± 0.2 K were well prepared. We found that the magnetization curves, $-4\pi M(H)$, in a wide H - T region can be represented to an universal temperature-independent curve with the scaling factor $\sqrt{2}H_c(T)$. This scaling behavior is consistent with the prediction of Ginzburg-Landau theory and Hao-Clem variation model. The thermodynamic critical fields H_c at various temperatures were precisely determined from the $-4\pi M(H)$ curves according to the theoretical fitting of Hao-Clem model. Temperature dependence of thermodynamic critical field $H_c(T)$ in $10 \text{ K} \leq T \leq 30 \text{ K}$ is in good agreement to the two-fluid model and BCS theory. However, the best fit is the power-law relation of $H_c(T) = H_c(0) * [1 - (T/T_c)]^\beta$, where $H_c(0) = 2344 \pm 19$ Oe, $T_c = 29.62 \pm 0.07$ K, and $\beta = 0.8682 \pm 0.008$.

INTRODUCTION

In Ginzburg-Landau (GL) theory, the temperature dependence of a superconductor can be contained in the scaling factors, such as $\sqrt{2}H_c(T)$ and $\lambda(T)$. Thus most of physical quantities in their dimensionless form are independent on T , and the only parameter intrinsic to sample is Ginzburg-Landau parameter, $\kappa = \lambda\xi$ (1-5). Many studies on the temperature- and field-dependence of magnetic properties and the superconducting parameters for superconducting fullerenes have been reported (6-10). However, very little discussion focused on detailed description of the magnetic characteristics and their scaling behavior for this family. In this report, we observed the scaling effect of magnetization curves in a rather broad H - T range than those in high- T_c cuprate oxides. Based on our experimental data and the Hao-Clem variation model (2,4), the thermodynamic critical fields at various temperatures are well determined.

EXPERIMENTS

The Rb_3C_{60} crystals were obtained by doping Rb metal with stoichiometric amount into C_{60} crystals. Details on the sample preparation of Rb_3C_{60} crystals were describes

elsewhere (9,10). All magnetic data as functions of temperature and field were performed using two commercial Quantum Design SQUID magnetometers equipped with superconducting magnets of 1 T and 7 T, respectively. The zero-field-cooled magnetization, M_{ZFC} , was measured as a function of temperature in several magnetic fields from 10 Oe to 1 T. Magnetic hysteresis loops, $M(H)$, between -5 T and 5 T were carried out at various temperatures from 5 K to 30 K with an interval of 2.5 K.

RESULTS AND DISCUSSION

According to the GL theory (1), as the temperature dependence is included in the scaling factors, *e.g.* $\sqrt{2}H_c(T)$ and $\lambda(T)$, then most of physical quantities in their dimensionless form are independent upon T , and the only intrinsic parameter is Ginzburg-Landau parameter, $\kappa = \lambda\xi_c$. For the Rb_3C_{60} crystals the temperature-independent curves of $-4\pi M' = -4\pi M/\sqrt{2}H_c(T)$ versus $H' = H/\sqrt{2}H_c(T)$ for $10 \text{ K} \leq T \leq 25 \text{ K}$ shown in Fig. 1(a) are obtained from the half-loops of the measured hysteresis curves, $M(H)$, for $H \geq 0$. Here, $H_c(T)$ is properly extracted according to such a condition of making these $-4\pi M'(H')$ curves in enough high fields to collapse onto a single curve based on the theoretical fitting of the Hao-Clem model (2,3).

For extremely type-II superconductors the contribution of the vortex core energies F_{core} to the magnetization are significant and cannot be ignored in intermediate or high fields. Hao and Clem (2) considered not only the electromagnetic energy of flux vortex F_{em} , but also the core energy F_{core} in the calculation of the total free energy of a superconductor. They put these energy terms arising from suppression of the order parameter into the GL-like equation, then numerically derived the related equations in the intermediate field regime.

They calculated the reversible magnetization of type-II superconductor in dimensionless units which length ρ , magnetic field H , and free energy F are normalized by penetration depth λ , $\sqrt{2}H_c$, and $H_c^2/4\pi$, respectively. Thus, the dimensionless magnetization $-4\pi M'(H')$ is obtained from the calculation of the Ginzburg-Landau free energy. The Hao-Clem theory has proven to be remarkably successful in describing the thermodynamic properties of discovered extremely type-II superconductors, including the high- T_c cuprate oxides and the low- T_c superconductors (3-5). Successful application of the Hao-Clem model to the experimental $M(H)$ data allows the GL parameter κ and the thermodynamic critical field H_c to be determined as fitting parameters to a variational solution for the extremely type-II superconductor.

The relation of $-4\pi M$ versus H' at various temperatures can also be constructed from a set of data $[H_i, -4\pi M_i]$ with $i=1, 2, 3, \dots$ at a fixed temperatures extracted from the $M_{ZFC}(T)$ curves in various fields. If the proper H_c values are used, then the curves of $-4\pi M'$ vs H' obtained from $M_{ZFC}(T)$ curves shall also fall into an universal curve. For $24 \text{ K} \leq T \leq 29 \text{ K}$ the data of $M(H)$ are extracted from our measured $M_{ZFC}(T)$ curves in various external fields from 10 Oe to 1 T. Thus selecting a proper $H_c(T)$ and drawing the relation of $-4\pi M'$ versus H' . As shown in Fig. 1(b), all curves for the selected temperatures are collapsed onto a single curve again. This result indicates that

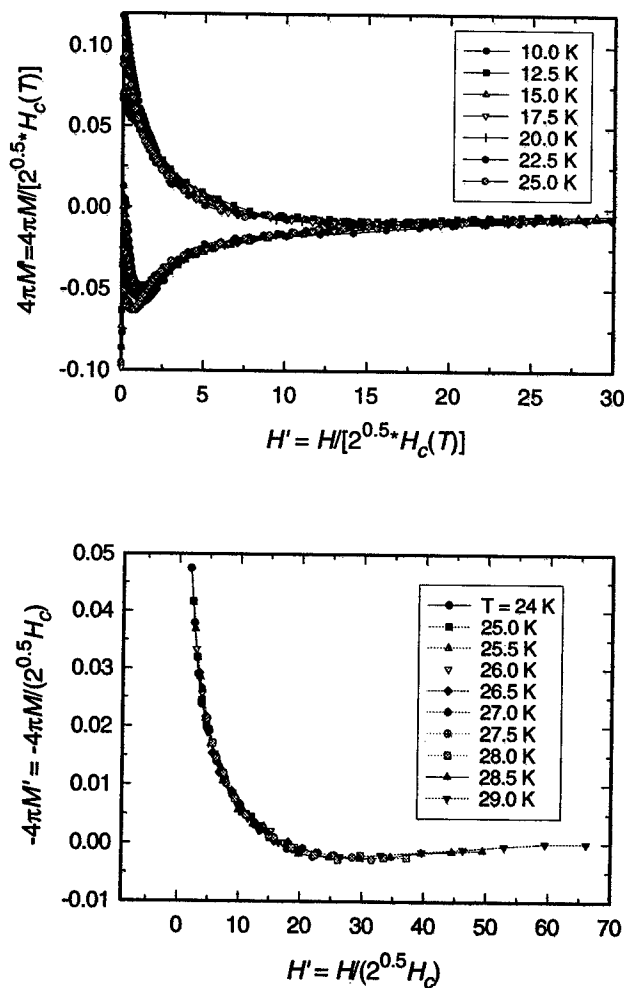


FIGURE 1. (a) $-4\pi M'$ vs H' for $10 \leq T \leq 25$ K, (b) $-4\pi M'$ vs H' for $24 \leq T \leq 29$ K.

$-4\pi M'$ vs H' curves in this temperature range also exhibit the temperature-independent universal feature.

Fig. 2 shows the temperature dependence of the thermodynamic critical field, $H_c(T)$, obtained from the theoretical analysis of Hao-Clem model. Here, $H_c(T)$ in $10 \text{ K} \leq T \leq 25 \text{ K}$ and $24 \text{ K} \leq T \leq 29 \text{ K}$ were determined from the above analyses based on the data in Fig. 1(a) and Fig. 1(b), respectively. These values are compared with those previously reported (6-8). For $T \geq 12.5 \text{ K}$, $H_c(T)$ can be well fitted to various formulas and models as shown by the various curves in Fig. 2. For the fit to the two-fluid model, $H_c(T) = H_c(0)[1 - (T/T_c)^\alpha]$, where $H_c(0) = 2066 \pm 35 \text{ Oe}$, $T_c = 29.96 \pm 0.07 \text{ K}$, and $\alpha = 1.398 \pm 0.04$. For the fit to the BCS relation based on the Hao-Clem model,

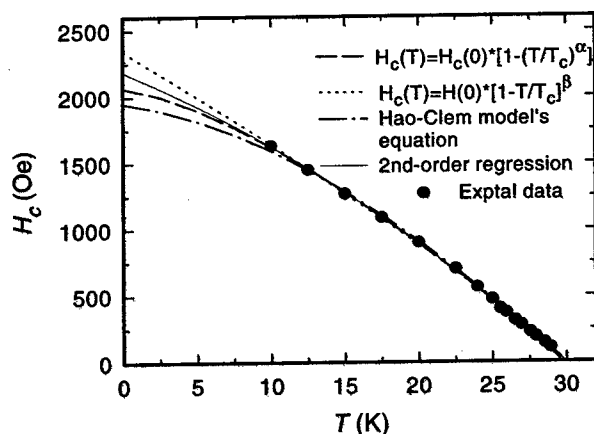


FIGURE 2. Temperature dependence of thermodynamic critical field $H_c(T)$ obtained from the theoretical fitting of Hao-Clem model. The various lines represent the temperature dependencies fitted to various model.

$$H_c(T) = H(0) \left\{ 1.7367 \left[1 - \frac{T}{T_c} \right] \left[1 - 0.2730 \left(1 - \frac{T}{T_c} \right) - 0.0949 \left(1 - \frac{T}{T_c} \right)^2 \right] \right\}$$

where $H_c(0) = 1777 \pm 11$ Oe and $T_c = 29.74 \pm 0.07$ K. However, the best fit is the power-law relation of $H_c(T) = H_c(0) * [1 - (T/T_c)]^\beta$, particularly for $T < 12.5$ K. Here, the best fitting parameters are $H_c(0) = 2344 \pm 19$ Oe, $T_c = 29.62 \pm 0.07$ K, and $\beta = 0.8682 \pm 0.008$.

In addition of H_c most of the superconducting parameters, such as the Ginzburg-Landau parameter κ , the upper and lower critical fields H_{c2} , H_{c1} , the penetration depth λ , and the coherence length ξ can also be derived by the Hao-Clem theoretical fitting to the measured magnetization data below T_c . For our sample of crystals Rb_3C_{60} , these superconducting parameters derived by this variation model will be reported elsewhere.

In summary, we measured the temperature and field dependence of magnetization in Rb_3C_{60} crystals, and found that the magnetization curves with the scaling factor of $\sqrt{2}H_c$ exhibit the universal behavior in a wide H - T range. Using the Hao-Clem model, the thermodynamic critical fields in $10 \text{ K} \leq T \leq 30 \text{ K}$ were determined. $H_c(T)$ well obeys the power-law relation in the above temperature range.

ACKNOWLEDGMENTS

This work was supported by the National Science Council, Taiwan, R.O.C. under grant No. NSC-87-2112-M-194-022.

REFERENCES

1. Tinkham, M., *Introduction to Superconductivity*, New York: McGraw-Hill Press, 1980.
2. Hao, Z., and Clem, J. R., *Phys. Rev. Lett.* **67**, 2371 (1991); Hao, M., *et al.*, *Phys. Rev. B* **43**, 2844 (1991).
3. Kim, M. S., Lee, S. I., Yu, S. C., and Hur, N. H., *Phys. Rev. B* **53**, 9460 (1996).
4. Kim, M. S., Bae, M. K., Lee, W. C., and Lee, S. I., *Phys. Rev. B* **51**, 3261 (1995).
5. Sok, J., Chen, W., Suh, B. J., Gohng, J., Schwartzkopf, L. A., and Dabrowski, B., *Phys. Rev. B* **51**, (1995).
6. Buntar, V., and Weber, H. W., *Supercond. Sci. Technol.* **9**, 599 (1996).
7. Politis, C., Buntar, V., Krauss, W., and Gurevich, A., *Europhys. Lett.* **17**, 175 (1992).
8. Buntar, V., Sauerzopf, M. F., Weber, H. W., Fischer, J. E., Kuzmany, H. and Haluska, M., *Phys. Rev. B* **56**, 14128 (1997).
9. Tai, M. F., Sung, C. M., Lee, M. W., and Shi, J. B., *Physica C* **272**, 131 (1996).
10. Lee, M. W., Shi, J. B., and Chen, C. S., *Japn. J. Appl. Phys.* **36**, 105 (1997).

Interlayer magnetoresistance peak in the ET-based organic superconductors

Fulin Zuo

Abstract. We report interlayer magnetoresistance studies in the ET-based organic superconductors. For field perpendicular to the planes, the magnetoresistance displays a peak as a function of field and temperature. By studying the magnetoresistance peak as a function of superconducting transition, we find the magnetoresistance peak is intrinsic to the layered structure.

Interlayer transport in layered systems such as the highly anisotropic high temperature cuprates and the organic superconductors, is of current interest. It is important for several reasons. First, what is the role of interlayer coupling on the superconducting transition temperature [1]? Second, what is the nature of the charge transport, is it coherent or incoherent [2,3]?

The questions remain unresolved in the cuprates. Depending on the doping level, the c-axis (perpendicular to the CuO layers) transport changes from metallic to semiconducting. For example, for optimally doped cuprates, it usually displays a linear or power-law temperature dependence and it becomes nonmetallic at low temperatures for the underdoped [4]. However, for the $\text{Bi}_2\text{Sr}_2\text{CaCu}_2\text{O}_8$, even at optimal doping, the c-axis resistivity exhibits a semiconducting temperature dependence in the normal state, while the in-plane resistivity is metallic with the resistivity decreasing with decreasing temperature [6–10]. At low temperatures (below the zero field transition temperature), the interlayer magnetoresistance displays a pronounced peak as a function of temperature and field [5,11–13]. For underdoped $\text{YBa}_2\text{Cu}_3\text{O}_{6+x}$ and $\text{La}_{2-x}\text{Sr}_x\text{CuO}_4$, the magnetoresistance displays a pronounced peak as a function of field. Two possible models have been proposed. In one model the peak is a result of a competition between the Josephson and the quasiparticle tunneling [6,9]. The other model suggests the peak is due to a density of state fluctuation contribution to the c-axis transport [14,15]. While both models can semi-quantitatively describe the experimental results, the mechanism remains controversial.

Organic superconductors, especially the $\kappa\text{-(BEDT-TTF)}_2\text{X}$ [bis(ethylenedithio) tetrathiafulvalene, abbreviated as ET] family with X being $\text{Cu}[\text{N}(\text{CN})_2]\text{Br}$, $\text{Cu}[\text{N}(\text{CN})_2]\text{Cl}$, and $\text{Cu}(\text{SCN})_2$, have shown recently physical properties very similar to the high temperature cuprates including unconventional metallic properties [16]. The $\kappa\text{-(ET)}_2\text{X}$ consists of the conducting cation layer (ET) sandwiched between

the insulating anion layers (X). ET is a large planar molecule and the different possible packing patterns are denoted by different Greek letters. In the κ phase, the ET molecules form a dimer, with each dimer contributing one electron to the anions. Because of the layered structure, the κ -(ET)₂X salts have shown similar anisotropic transport properties [17,18] as the cuprates with a typical resistivity anisotropy $\frac{\rho_{\perp}}{\rho_{\parallel}} \sim 10^3$. Furthermore, the κ -(ET)₂X salts share a very similar phase diagram with the cuprates if the pressure is replaced by doping. In other words, the system can transform between unconventional metal, magnetic insulator, and a superconductor, by changing the pressure, temperature and the anion [16].

Studies of interlayer transport in the κ -(ET)₂X have revealed an interesting magnetoresistance peak as a function of field for temperatures near and below the transition temperature [19–25]. However, there are several important differences between the organic superconductors and the cuprates. One is the temperature dependence of the normal state resistance. While the cuprates typically have semi-conducting temperature dependence for the c-axis, the interlayer resistance in the organics is metallic near the transition temperature. Another major difference is the observation of a large negative magnetoresistance as a function of field in the organic compounds. Several models have been proposed to qualitatively describe the peak, such as the magnetic impurity scattering [25], vortex-lattice interaction [21], a similar mechanism as in the cuprates, involving pair and quasiparticle tunneling has been proposed by several groups [20–22]. However, a quantitative agreement between the model and the experiment is lacking [26].

We have undertaken careful studies of interlayer magnetoresistance in several compounds [21] including the κ -(ET)₂Cu[N(CN)₂]Br, κ -(ET)₂Cu(SCN)₂ salts, the all-organic β'' -(ET)₂SF₅CH₂CF₂SO₃ and the κ -(ET)₂I₃. In the κ -(ET)₂Cu[N(CN)₂]Br system, the peak has been studied as a function of transition width [23]. The peak width increases and the peak height decreases with increasing transition width. For samples with transition width greater than 2K, the peak effect disappears completely.

For high quality samples, the magnetoresistance peak was observed for all four systems which had different superconducting transition temperatures. The peak field decreases drastically with increasing anisotropy for the same reduced temperature $\frac{T}{T_c}$. The results suggest that the appearance of the peak correlates with the coupling between the layers.

Shown in figure 1 is a plot of the normalized resistive transition of four samples. The transition widths increases from about 0.2K to over 2K corresponding to sample 1 to 4. The quality of samples has drastic effect on the field dependence of the magnetoresistance at temperatures below the superconducting transition. Shown in figure 2 is an overlay of magnetoresistance as a function of field at temperatures at or close to 6K and 7K. Clearly, figure 2(a) displays sharp peak with peak field at around 3.5T and 2.5T for 6K and 7K, respectively. With increasing transition width, the peak broadens up and disappears completely for sample 4, where magnetoresistance increases continuously with field.

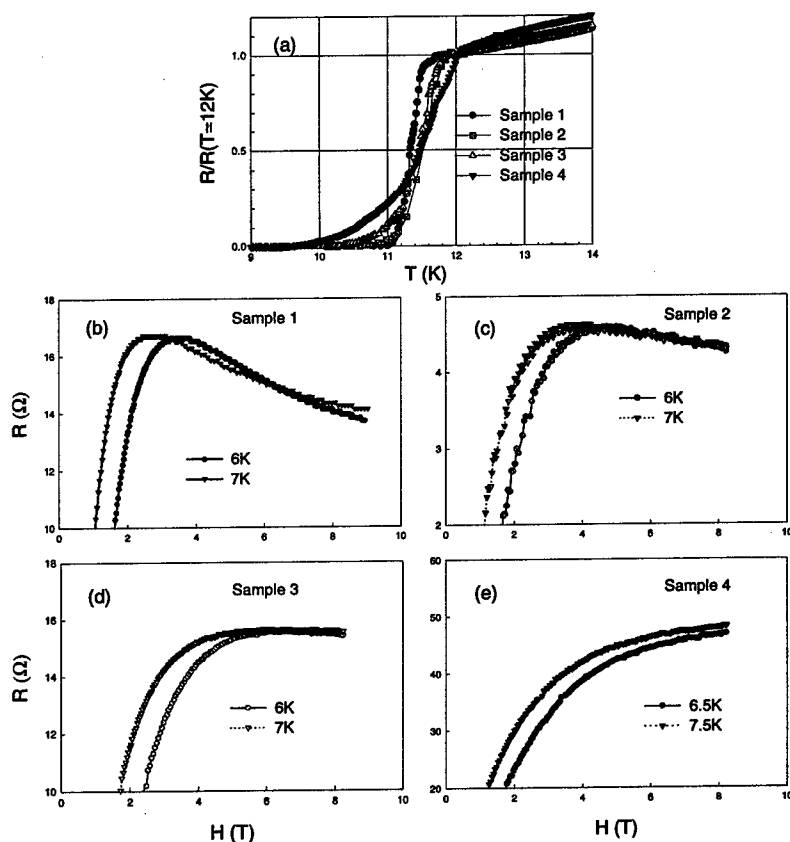


Fig. 1 (a) Normalized resistive transition for four samples. Fig. 1(b) through (e) are magnetoresistance as a function of field at different temperatures for sample 1 to 4.

The transition width dependence of the magnetoresistance peak is consistent with an earlier study where it has been shown with increasing sample quality, the interlayer peak remains while the in-plane magnetoresistance peak disappeared. The disappearance is associated with the mixing of the interlayer component in the in-plane measurements [20].

To test the magnetoresistance peak is intrinsic to the layered system, interlayer transport has been carried out in several systems with different chemical anions and superconducting transition temperatures. Shown in Figure 2(a) is a plot of the interlayer magnetoresistance as a function of field at high temperatures for an all-organic β'' -(ET)₂SF₅CH₂CF₂SO₃. Clearly, the magnetoresistance has a pronounced peak as a function of field at temperatures below T_c . The peak field

is very small compared with that of $\kappa-(\text{ET})_2\text{Cu}[\text{N}(\text{CN})_2]\text{Br}$. At low temperatures, as shown in figure 2(b), the magnetoresistance peak remains until 0.5K, below which the magnetoresistance is monotonic with field. It should be noted that the disappearance of the magnetoresistance peak is not unique to the β'' $-(\text{ET})_2\text{SF}_5\text{CH}_2\text{CF}_2\text{SO}_3$, similar field dependence has been observed in all other systems studied at low temperatures.

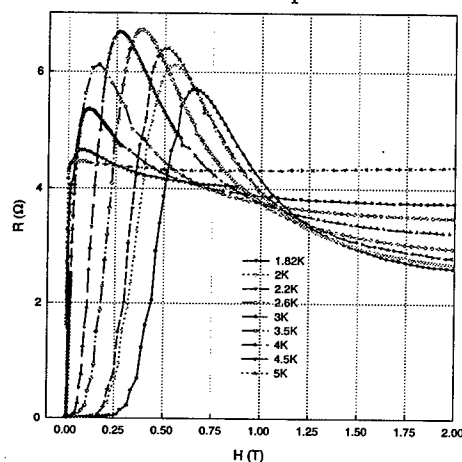


Fig. 2(a) Magnetoresistance as a function of field at high temperatures.

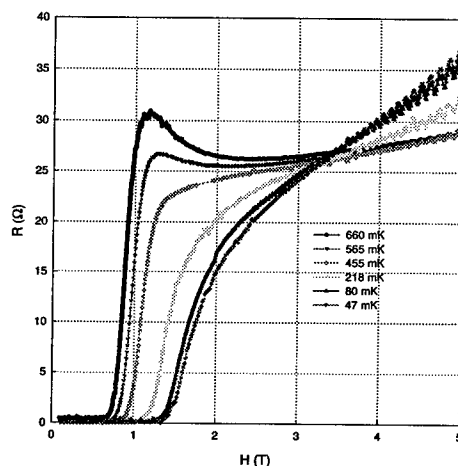


Fig. 2(b) Magnetoresistance as a function of field at low temperatures.

Figure 3 compiles the magnetoresistance peak field as a function of temperature for the four systems studied. With decreasing T_c , the H_{peak} decreases drastically. For example, the peak field for the Br salt is generally over an order of magnitude large than that of I_3 salt if compared in the reduced temperature scale. Nevertheless, the observation of the magnetoresistance peak in all systems studied suggests the universality of the field dependence of the interlayer transport in the layered compounds.

The dissipation mechanism in the interlayer direction in the mixed state remains controversial. Two approaches are known to give rise to a peak in the interlayer resistivity as a function of temperatures. One of them models the resistivity peak as a result of fluctuations above the mean field transition temperature [14,15]. Of the four possible fluctuation contributions to the interlayer resistivity, fluctuations in the density of state (DOS) and the regular Maki-Thompson term contribute to an increasing resistivity with decreasing temperatures. By choosing suitable parameters, the model can fit reasonably the temperature dependence of the resistivity before the peak for the cuprates. However, the model does not include critical fluctuations nor contributions from the vortices (for $T > T_{peak}$) and thus the field dependence of the peak temperature $T_{peak}(H)$. A more widely adopted approach,

discussed in the following, emphasizes the nature of Josephson coupling between the superconducting layers, especially at low magnetic fields. The peak in the resistivity comes when the Josephson coupling dominates the interlayer transport. The model can describe semi-quantitatively the field and temperature dependence of the interlayer transport at $H < H_{peak}$.

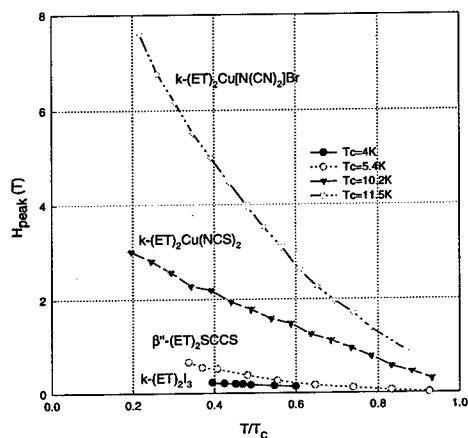


Fig. 3 Peak field versus the reduced temperature for all four samples.

In the case of $\text{Bi}_2\text{Sr}_2\text{CaCu}_2\text{O}_8$, dissipation mechanism for $H \parallel J \parallel c$ was first proposed by Briceño *et al* [6]. In this model, current moving parallel to the c axis is taken to pass through a narrow superconducting channel of area $A \approx \frac{\Phi_0}{H}$ between the densely packed vortices. Here Φ_0 is the flux quantum. Dissipation occurs through thermodynamic fluctuations which cause the phase of the superconducting order parameter in the c direction to jump by 2π . Assuming fluctuations in each channel are independent, the dissipation in the c direction can be modeled by a long, narrow Josephson junction at finite T [27]. The resistance of the weak link is given approximately by $R = R_n [I_0(\hbar I_c / 2ekT)]^{-2}$, where R_n is the normal state resistance, \hbar is the Planck's constant, I_c is the critical current, e is the charge of an electron, and I_0 is the modified Bessel function. Since the normal state resistance is activated in this direction, a peak is expected in the junction resistance at $T < T_c$. A similar approach which models the c axis conduction as a stack of Josephson tunnel junctions has been proposed by Gray *et al* [7]. For an intermediate Josephson coupling, the junction conductance is the sum of the quasiparticle conductance Y_{ss} and pair conductance Y_p , i.e. $Y = Y_{ss} + Y_p$. Since the quasiparticle conductance Y_{ss} is thermally activated $Y_{ss} \sim \exp[-\Delta(T, H)/kT]$, and the pair conductance $Y_p \sim [I_0(\hbar I_c / 2ekT)]^2 - 1$, a distinct peak in $R(T)$ arises naturally. While the field dependence of the critical current I_c is somewhat controversial [8], a recent study on thin mesa of a $\text{Bi}_2\text{Sr}_2\text{CaCu}_2\text{O}_8$ found $I_c \propto 1/H$ [28].

A similar model has been proposed to explain the magnetoresistance peak in the

organic superconductors [20,22,23]. To analyze the data quantitatively, consider the charge transport through a Josephson junction of area $a^2 \approx \frac{\Phi_0}{H+H_0}$ between the densely packed vortices, H_0 being a fitting parameter to take into account of effects of pinning and lattice rigidity [9]. The junction resistance due to thermal fluctuations of the phases is given by $R(H) = R_n [I_0(\frac{E_J}{2kT})]^{-2}$, where $E_J = \frac{\hbar I_c}{e} = \frac{\pi \hbar \Delta(T)}{2e^2 R_n} \tanh[\frac{\Delta(T)}{2kT}]$ is the Josephson coupling energy, R_n is the junction resistance in the mixed state. Because I_c is proportional to the junction area, E_J is also. It is natural to define an intrinsic Josephson coupling energy $e_J = \frac{E_J}{a^2}$, such that $R(H) = R_n [I_0(\frac{e_J \Phi_0}{(H+H_0)2kT})]^{-2}$. If $E_J \gg kT$, the junction resistance can be reduced to [9] $R(H) = R_n \exp[-\frac{e_J \Phi_0}{(H+H_0)kT}]$. Shown in Figure 4 is a plot of the magnetoresistance as a function of field at various temperatures for a κ -(BEDT-TTF)₂Cu(SCN)₂. The solid lines are fits to the stacked Josephson junction model. Clearly, the data can be reasonably well fitted over a large resistance range. The inset shows the temperature dependence of the fitted Josephson coupling energy e_J . e_J increases with decreasing temperature.

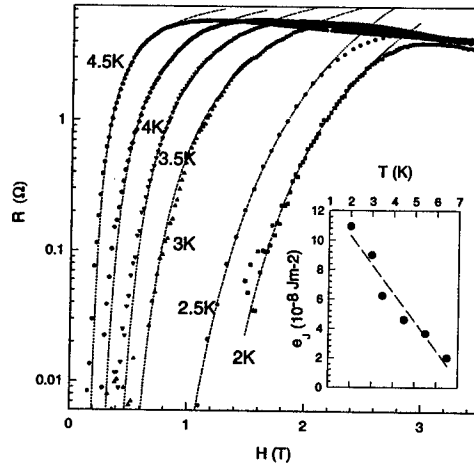


Fig. 4 Magnetoresistance as a function of field at various temperatures for SCN salt. The lines are fits to the stacked Josephson junction model. The inset show the temperature dependence of the coupling energy.

While the low field magnetoresistance can be described well with the stacked Josephson junction model, a mechanism with large negative magnetoresistance has to be invoked to explain the peak. One such model is the fluctuation contribution to the interlayer transport near the superconducting transition. Contrary to the conventional wisdom, the positive contribution to the fluctuation conductivity in

the interlayer direction is weak due to the hopping or tunneling nature of the quasiparticle propagation. Rather, the fluctuation conductivity is dominated by the negative contribution due to the decreases of density of state of quasiparticles [14,15].

The negative magnetoresistance can also arise from other interactions. For example, it has been proposed that the negative magnetoresistance in the underdoped cuprates is related to the presence of pseudogap in the oxygen deficient $\text{YBa}_2\text{Cu}_3\text{O}_{6+x}$ [12]. Indeed, DC magnetic susceptibility as well as NMR relaxation measurements suggest strongly the presence of a pseudogap near 50K in the ET based compounds [29]. However, the fact that negative magnetoresistance disappears a few degrees above the superconducting transition argues against the role of pseudogap formed at much higher temperature.

Negative magnetoresistance due to the vortices in the mixed state has also been suggested. For example, thermal fluctuation of the vortices can introduce extra scattering to the charge transport. With increasing field or decreasing temperature, the thermal fluctuation is suppressed and vortices are more rigid or lattice-like, resulting in the negative magnetoresistance. Nevertheless, one would not expect the negative magnetoresistance to persist well above the upper critical field.

Presence of magnetic impurities can also give rise to the peak effect. It has been suggested that the $\kappa\text{-(ET)}_2\text{Cu[N(CN)}_2\text{]Br}$ may contain traces of Cu^{++} ions [25]. With increasing field, the effect of magnetic moment scattering is reduced. However, the absence of negative magnetoresistance in the normal state suggests against the magnetic impurity model. Furthermore, the observations of the peak in the β'' - $(\text{BEDT-TTF})_2\text{SF}_5\text{CH}_2\text{CF}_2\text{SO}_3$ and $\kappa\text{-(ET)}_2\text{I}_3$ where no Cu^{++} is present contradicts the model of magnetic impurities scatterings.

In summary, interlayer transport measurements on several ET based organic superconductors reveal an universal magnetoresistance peak at temperatures below the superconducting transition. At very low temperatures, the magnetoresistance peak disappears. The peak field increases with increasing superconducting transition temperature or decreasing anisotropy. The magnetoresistance peak is mostly likely due to the density of state fluctuation of quasiparticles.

The work is supported by NSF grant No. DMR-9623306 and the petroleum research fund ACS-PRF 33812-AC5. The samples are provided by Dr. John A. Schlueter from Argonne National Laboratory. Part of the work is in collaboration with Dr. Jochen Wosnitza from Universität of Karlsruhe and Dr. James Brooks from the National High Magnetic Field Laboratory at Tallahassee, Florida.

REFERENCES

1. S. Chakarvarty and P.W. Anderson, *Phys. Rev. Lett.* **72**, 3859 (1994).
2. A.G. Rajo and K. Levin, *Phys. Rev. B* **48**, 16861 (1993).
3. N. Kumar and A.M. Jayanavar, *Phys. Rev. B* **45**, 5001 (1992).
4. T. Ido, S. Uchida, *Nature* **350**, 596 (1991).

5. K. Takenaka, K. Mizuhashi, H. Tagagi, and S. Uchida, *Phys. Rev. B* **50**, 6534 (1994).
6. G. Briceño, M.F. Crommie, and A. Zettl, *Phys. Rev. Lett.* **66**, 2164 (1991); *Physica C* **204**, 389 (1993).
7. K.E. Gray and D.H. Kim, *Phys. Rev. Lett.* **70**, 1693 (1993).
8. J.H. Cho, M.P. Maley, S. Fleshler, A. Lacerda, L.N. Bulaevskii, *Phys. Rev. B* **50**, 6493 (1994).
9. J.D. Huttinger, K.E. Gray, B. W. Veal, A.P. Paulikas, P. Kostic, B.R. Washburn, W.C. Tonjes and A.C. Flewelling, *Phys. Rev. Lett.* **74**, 4726 (1994).
10. A.S. Nygmatulin, A.A. Varlamov, D.V. Livanov, G. Balestrino and E. Milani, *Phys. Rev. B* **53**, 3557 (1996).
11. K. Nakao, K. Takamuku, K. Hashimoto, N. Koshizuka, and S. Tanaka, *Physica B* **201**, 262 (1994).
12. Y.F. Yan, P. Matl, J.M. Harris, and N.P. Ong, *Phys. Rev. B* **52**, R751 (1995).
13. Y. Ando, G.S. Boebinger, A. Passner, N.L. Wang, C. Geibel, and F. Steglich, *Phys. Rev. Lett.* **77**, 2065 (1996).
14. L.B. Ioffe, A.I. Larkin, A.A. Varlamov and L. Yu, *Phys. Rev. B* **47**, 8936 (1993).
15. A.A. Varlamov, G. Balestrino, E. Milani and D.V. Livanov, *Advance in Physics*, in press.
16. R.H. McKenzie, *Science* **278**, 820 (1997).
17. G. Saito, H. Yamochi, T. Nakamura, T. Komatsu, T. Ishiguro, Y. Nogami, Y. Ito, H. Mori, K. Oshima, *Synth. Metals* **41-43**, 1993 (1991).
18. L.I. Buravov, N.D. Kushch, V.A. Merzhanov, M.V. Osherov, A.G. Khomenko, E.B. Yagubskii, *J. Phys. I France* **2** 1257 (1992).
19. T. Ishiguro, H. Ito, Yu. V. Sushko, A. Otsuka, G. Saito, *Physica B* **197**, 563 (1994).
20. H. Ito, T. Ishiguro, T. Komatsu, G. Saito, H. Anzai, *Physica B* **201**, 470 (1994).
21. F. Zuo, J.A. Schlueter, M.E. Kelly, J.M. Williams, *Phys. Rev. B* **54**, 11973 (1996); *ibid. Physica C* **282**, 1901 (1997).
22. S. Friemel, C. Pasquier, and D. Jerome, *Physica C* **292**, 273 (1997).
23. F. Zuo, X. Su, P. Zhang, J.A. Schlueter, M.E. Kelly, J.M. Williams, *Phys. Rev. B* **57**, R5610 (1998).
24. X. Su, F. Zuo, J. Schlueter, J.M. Williams, *Phys. Rev. B* **59**, 4376 (1999).
25. C.H. Mielke, N. Harrison, D.G. Rickel, A.H. Lacerda, R. M. Vestal, L. K. Montgomery, *Phys. Rev. B* **56**, R4309 (1997).
26. F. Zuo, J. Schlueter, J.M. Williams, unpublished.
27. V. Ambegaokar and B.I. Halperin, *Phys. Rev. Lett.* **22**, 1364 (1969).
28. M. Suzuki, T. Watanabe, and A. Matsuda, *Phys. Rev. Lett.* **81**, 4248 (1998).
29. A. Kawamoto, K. Miyagawa, Y. Nakazawa and K. Kanoda, *Phys. Rev. Lett.* **74**, 3455 (1995).

AUTHOR INDEX

A

Abascal, C., 237
 Aksay, I. A., 207
 Alloul, H., 161
 Altshuler, E., 237
 Anderson, P. W., 3
 Arai, M., 172
 Arsenov, A., 407
 Ashkenazi, J., 12
 Awana, V. P. S., 176
 Azoulay, J., 324

B

Balzarotti, A., 26
 Bennington, S. M., 172
 Berger, H., 304, 412
 Bernhard, C., 201, 292
 Bianconi, A., 180
 Blackstead, H. A., 187, 191, 195
 Blasius, T., 201, 292
 Blumberg, G., 272
 Bobroff, J., 161
 Bolz, U., 201
 Bossy, J., 207
 Böttger, G., 320
 Bourges, P., 207
 Broussard, P., 407
 Brown, S., 383
 Budnick, J. I., 292
 Buffeteau, B., 310
 Byers, J., 407

C

Calemczuk, R., 310
 Carbotte, J. P., 288, 341
 Cardona, M., 328
 Castellani, C., 114
 Chen, Q., 22, 57
 Cheong, S.-W., 383, 394
 Christensen, S., 304
 Cini, M., 26
 Cohen, M. L., 359

Cohn, J. L., 213
 Cooper, S. L., 394

D

Dabrowski, B., 388
 de Lima, O. F., 176
 Demler, E., 30
 Demsar, J., 219
 Dennis, K. W., 310
 Deutscher, G., 225
 Di Castro, C., 114
 Dolgov, O. V., 63
 Dow, J. D., 187, 191, 195
 Drew, H. D., 418
 Du, C.-H., 383

E

Egami, T., 231
 Eisenmenger, J., 201
 Emery, V. J., 37
 Endoh, Y., 172, 231

F

Felner, I., 191
 Filippetti, A., 366
 Fisher, R. A., 310
 Fleck, M., 45
 Flores, L. E., 237
 Fong, H. F., 207
 Forró, L., 412
 Frazer, B., 304
 Friedrich, C., 320
 Fung, P. C. W., 347

G

Garrett, A., 172
 Garrigus, D. F., 351
 Gatt, R., 304
 Golnik, A., 201, 292

Gonzales, J. L., 237
 Goodenough, J. B., 388
 Granzow, T., 320
 Grilli, M., 114
 Grioni, M., 304
 Guptasarma, P., 272
 Gusakov, V. E., 49

H

Han, P. D., 394
 Hanaguri, T., 253
 Hargreaves, T. E., 310
 Haskel, D., 241
 Hatton, P. D., 383
 Hinks, D. G., 272
 Hirschfeld, P. J., 341

I

Ivanov, A. S., 207

J

Jackson, D. D., 191
 Jankó, B., 22, 57
 Jaya, N. V., 265

K

Kabanov, V. V., 219
 Kaldis, E., 320
 Kato, M., 53
 Keimer, B., 207
 Kelley, R. J., 304
 Kendziora, C., 314
 Kirtley, J. R., 247
 Kishio, K., 253
 Kitazawa, K., 253
 Kivelson, S. A., 37
 Klein, M. V., 272
 Kleiner, R., 304
 Klemm, R. A., 259
 Kosztin, I., 22, 57
 Kresin, V., 153
 Kulić, M. L., 63

Kumar, R. S., 265
 Kuščer, D., 284
 Kusko, C., 69
 Kwei, G. H., 400

L

Lam, C. C., 347
 Lam, H. S., 347
 Lanzara, A., 180
 Laprade, G., 407
 Lapsker, I., 324
 Latyshev, Y. I., 268
 Leiderer, P., 201
 Levin, K., 22, 57
 Li, S. H., 347
 Lichtenstein, A. I., 45
 Lin, C. T., 201
 Liu, H. L., 272, 394
 Louca, D., 400

M

Maekawa, S., 130
 Mahajan, A., 161
 Maki, K., 53, 372
 Malik, S. K., 176
 Marcenat, C., 310
 Margaritondo, G., 304
 Markiewicz, R. S., 69, 75
 Marsiglio, F., 126
 Martin, A. A., 328
 Mazin, I. I., 79
 McCallum, R. W., 310
 McQueeney, R. J., 231, 278
 Mendels, P., 161
 Mertelj, T., 284
 Mihailovic, D., 219, 284
 Milius, D. L., 207
 Misra, S., 304
 Mitchell, J. F., 418
 Moler, K. A., 247
 Moodenbaugh, A., 292
 Moritomo, Y., 418
 Mößle, M., 304
 Mukovskii, Y. M., 407
 Müller, P., 304

N

Nadgomy, B., 407
 Nagai, S., 130
 Narlikar, A. V., 176
 Natarajan, S., 265
 Nicol, E. J., 288, 341
 Niedermayer, C., 201, 292
 Nishijima, T., 172
 Noda, C., 237
 Nohara, M., 247
 Norman, M. R., 298

O

O'Connor, A. S., 310
 Oleś, A. M., 45
 Onellion, M., 304
 Osofsky, M. S., 407
 Ovchinnikov, Yu., 153

P

Pairor, P., 136
 Panas, I., 85
 Pavuna, D., 412
 Peña, R., 110
 Peter, M., 90
 Petrov, Y., 231
 Phillips, J. C., 104
 Phillips, N. E., 310
 Pickett, W. E., 141, 366
 Polinger, V., 241
 Pooke, D. M., 201
 Puchkaryov, E., 372
 Pulling, D. B., 191

Q

Quesada, D., 110

R

Raphael, M. P., 314
 Reeves, M. E., 314
 Regnault, L. P., 207

Rieck, C. T., 259
 Röhrer, J., 320
 Romero, D. B., 418
 Rubinstein, M., 407
 Runge, B.-U., 201

S

Saini, N. L., 180
 Sarrao, J. S., 278
 Sasagawa, T., 253
 Scharnberg, K., 259
 Schiessling, J., 201
 Schilling, A., 310
 Schmauder, T., 304
 Seibold, G., 114
 Sekar, A., 265
 Shafranjuk, S. E., 118
 Shapiro, V., 324
 Shi, J.-B., 424
 Shibata, Y., 130
 Shick, A. B., 141
 Shimoyama, J., 253
 Shiohara, Y., 172
 Shirane, G., 231
 Shulyatev, D., 407
 Sidis, Y., 207
 Sinha, K. P., 122
 Skelton, E. F., 314
 Soulen, Jr., R. J., 407
 Stefanucci, G., 26
 Stern, E. A., 241
 Strasik, M., 351
 Strohm, T., 328
 Su, Y., 383

T

Tai, M.-F., 424
 Tajima, S., 172
 Takagi, H., 247
 Takahashi, M., 172
 Tallon, J. L., 201
 Tanaka, K., 126
 Tohyama, T., 130
 Tomimoto, K., 172
 Trallero-Giner, C., 110
 Tranquada, J. M., 336

V

Vasquez, R. P., 351
Vaughn, M. T., 69, 75
Vekhter, I., 288, 341
Verdyan, A., 324
Vobornik, I., 304
Vyas, A., 347

W

Walker, M. B., 136
Wang, G. F., 372
Weger, M., 90
Weht, R., 141, 366
Wei, J. Y. T., 351
Weng, Z. Y., 147
Wolf, S., 153
Won, H., 372

Wu, J.-B., 424

Y

Yamashita, T., 268
Yeh, N.-C., 351
Yelon, W. B., 176
Yethiraj, M., 231
Yoon, S., 394
Yoshinari, Y., 161

Z

Zagar, K., 219
Zhang, S.-C., 30
Zhou, J.-S., 388
Zuo, F., 429
Zwick, F., 304